

AD-A261 116

(2)



# MINUTES OF THE TWENTY-FIFTH EXPLOSIVES SAFETY SEMINAR

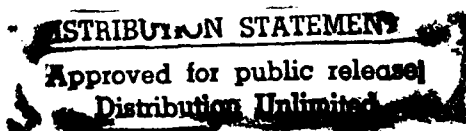
## VOLUME IV



DTIC  
ELECTED  
FEB 18 1993  
S E D

Anaheim Hilton Hotel  
Anaheim, California  
18-20 August 1992

93-03080  
632/28



Sponsored By  
Department of Defense Explosives Safety Board  
Alexandria, Virginia

95

**MINUTES OF THE  
TWENTY-FIFTH EXPLOSIVES SAFETY SEMINAR**

**VOLUME IV**

**Anaheim Hilton Hotel**

**Anaheim, California**

**18 - 20 August 1992**

**Sponsored by**

**Department of Defense Explosives Safety Board**

**Alexandria, Virginia**

**Approved for public release; distribution unlimited.**

## PREFACE

This Seminar is held as a medium by which there may be a free exchange of information regarding explosives safety. With this idea in mind, these minutes are being provided for your information. The presentations made at this Seminar do not imply indorsement of the ideas, accuracy of facts presented, or any product, by either the Department of Defense Explosives Safety Board or the Department of Defense.

Accession For	
NTIS CRA&I	<input checked="" type="checkbox"/>
DTIC TAB	<input type="checkbox"/>
Unannounced	<input type="checkbox"/>
Justification .....	
By .....	
Distribution /	
Availability Codes	
Dist	Avail and / or Special
A-1	

DAVID K. WALLACE  
Captain, USN  
Chairman

DTIC QUALITY INSPECTED 3

## **TWENTY-FIFTH DDESB EXPLOSIVES SAFETY SEMINAR**

### **TABLE OF CONTENTS**

#### **VOLUME IV**

<b>PREFACE .....</b>	iii
----------------------	-----

#### ***AMMUNITION HAZARD ASSESSMENT***

*Moderator: Ron Derr*

<b>Think Before Testing! .....</b>	1
Marc Défourneaux and Patrick Kernen	

<b>Simple Analytical Relationships for Munitions Hazard Assessment .....</b>	19
Andrew C. Victor	

<b>A Hardened, Self-Recording Instrumentation Device for Explosives Storage Safety Research .....</b>	63
L. Kim Davis	

<b>Safety Considerations in Storing Liquid Gun Propellant XM46 .....</b>	77
Janet S. Gardner	

#### ***BLAST RESISTANT STRUCTURES***

*Moderator: Bill Keenan*

<b>High Explosive Material Testing Laboratory Scale Model Test .....</b>	81
B. Louise Bolton, Richard V. Browning, and Larry W. Berkbigler	

<b>Approximate Analysis and Design of Conventional Industrial Facilities Subjected to Bomb Blast Using the P-i Technique .....</b>	111
Kirk A. Marchand, Charles J. Oswald, Dale Nebuda, and John Ferritto	

<b>Applications of Finite Element Technology to Reinforced Concrete Explosives Containment Structures .....</b>	133
T. A. Shugar, T. J. Holland, and L. J. Malvar	

<b>Time Dependent Stress and Strain Distribution in a Blastloaded Steelplate .....</b>	161
Gerhard H. Guerke	

*FRAGMENTS*  
*Moderator: Phillip Howe*

<b>Trials to Determine the Consequences of the Accidental Ignition of Stacks of Hazard Division 1.2 Ammunition .....</b>	179
Michael J. Gould and W. D. Houchins	
<b>Deflagrating Munitions and the Mass Detonation Hazard .....</b>	203
M. Chick, T. J. Bussell, D. McQueen, and L. McVay	
<b>Fragmentation Characteristics of Horizontally Stacked Bombs .....</b>	217
Frank McCleskey	

*HAZARD DIVISION 1.3 TESTS*  
*Moderator: Mel Hudson*

<b>Large Class 1.3 Rocket Motor Detonation Character .....</b>	225
Claude Merrill	
<b>Scaling Studies of Thermal Radiation Flux From Burning Propellants .....</b>	233
J. Edmund Hay and R. W. Watson	
<b>Hazards of Altitude Testing at AEDC .....</b>	269
Paul K. Salzman	

*BLAST RESISTANCE*  
*Moderator: John Hayes*

<b>Summary of Changes and Availability of the Revised TM5-1300 NAVFAC P-397, AFM 88-22--Design of Structures to Resist the Effects of Accidental Explosions .....</b>	281
Paul M. LaHoud	
<b>Constructibility Problems in Blast Resistant, Reinforced Concrete Structures .....</b>	299
Darrell D. Barker and Mark G. Whitney	
<b>Mitigation of Confined Explosion Effects by Placing Water in Proximity of Explosives .....</b>	311
William A. Keenan and Phillip C. Wager	

*EXPLOSIVES TESTING AND THE ENVIRONMENT*  
*Moderator: Rick Adams*

<b>Safety First: Environmental Compliance and Approvals for Large-Scale Explosive Safety Tests .....</b>	341
Carl C. Halsey, William T. Eckhardt, and Robin M. Hoffman	

***EXPLOSIVES TESTING AND THE ENVIRONMENT (Continued)***

<b>ESQD Arcs for Maritime Prepositioning Ships</b> .....	351
Michael M. Swisdak, Jr.	
<b>Evaluation of Trench Storage of Ammunition Trucks</b> .....	375
L. Kim Davis	
<b>Hazards from Underwater Explosions</b> .....	391
Michael M. Swisdak, Jr. and Paul E. Montanaro	

***HAZARD DIVISION 1.6***  
*Moderator: Earl Smith*

<b>Extremely Insensitive Detonating Substance Tests</b> .....	409
Kenneth J. Graham	
<b>Classification Tests for Assignment to Hazard Class/Division 1.6:</b>	
<b>SNPE Two Years Experience</b> .....	419
Jean Isler	
<b>What Q/Ds for H.D. 1.6?</b> .....	443
Jacques C. Besson	
<b>Sensitivity and Performance Evaluation of a 1.6 Candidate</b>	
<b>Explosive--AFX-770</b> .....	455
Larry Pitts, John Corley, Greg Glenn, Elton Grissom, and Stephen Struck	

***EXPLOSION CONTAINMENT TESTING***  
*Moderator: John Eddy*

<b>Shrapnel Protection Testing in Support of the Proposed Site 300</b>	
<b>Contained Firing Facility</b> .....	471
Charles F. Baker, John W. Pastrnak, and Larry F. Simmons	
<b>"Firebox"--An Environmentally Sound Test Enclosure</b> .....	505
Derek W. Erdley	
<b>Design of the M-9 Firing Facility Containment Vessel for</b>	
<b>Los Alamos National Laboratory</b> .....	511
Michael A. Polcyn, Edward D. Esparza, and Mark G. Whitney	
<b>Design of a Large Door for an Explosion-Containment Structure</b> .....	531
David A. Parkes and Harold D. Laverentz	

**SAFE SEPARATION DISTANCES**  
*Moderator: Phil McLain*

<b>Reduction of Hazard Zones by Uncoupling Between Munitions</b> .....	541
Maurice C. Chizallet	
<b>Safe Separation Distance of 81mm Mortars by Analogy to the M374 Series Testing</b> .....	555
Joseph P. Caltagirone	
<b>An Innovative Approach to Assess Quantity-Distance</b> .....	573
Khosrow Bakhtar	

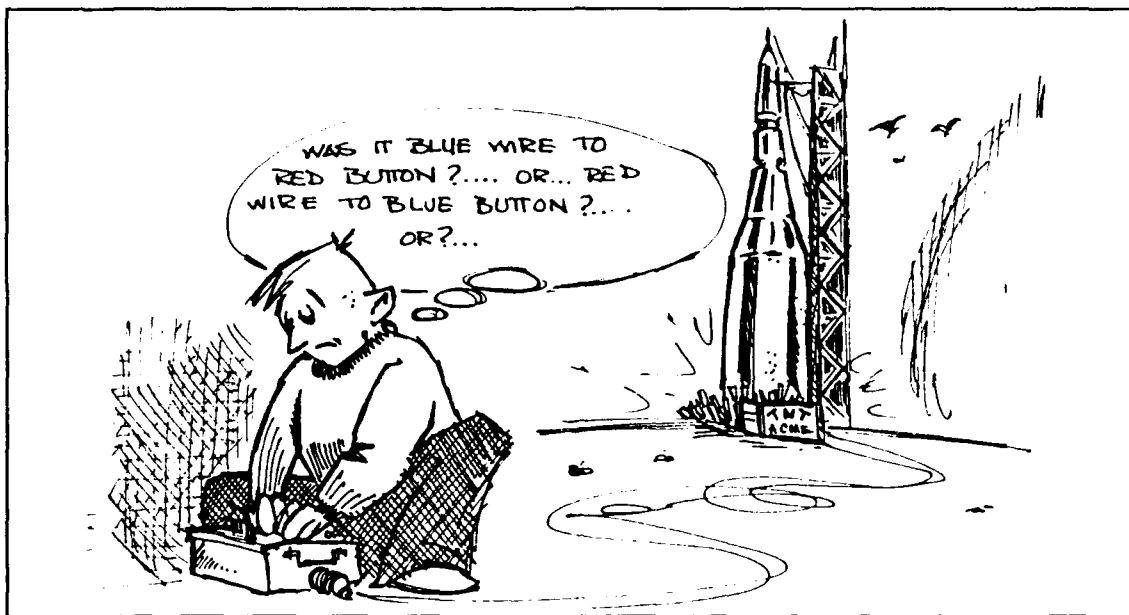
***CLOSING REMARKS***

<b>Chairman, Department of Defense Explosives Safety Board</b> .....	599
Captain David K. Wallace	
<b>Chairman, Explosives Storage and Transport Committee, United Kingdom</b> .....	601
Dr. John Connor	

***INDEXES***

<b>Table of Contents--Volume I</b> .....	607
<b>Table of Contents--Volume II</b> .....	611
<b>Table of Contents--Volume III</b> .....	615
<b>Author Index</b> .....	619
<b>Attendee List</b> .....	623

# THINK BEFORE TESTING!



Presented at the  
25th DoD Explosives Safety Seminar  
Anaheim, CA 1992

by

Marc Défourneaux

Patrick Kernen

NATO Insensitive Munitions Information Center (NIMIC)  
NATO Headquarters, B-1110 Brussels, Belgium

**Abstract:**

For a long time now experts on energetic materials and munitions have been using experimental tests to evaluate the vulnerability of such materials or munitions, or at least their sensitivity to various stimuli. Yet those tests are far from being representative of the scenarios of accidental or combat stimuli, and the interpretation of them itself sometimes needs to be treated cautiously, given the important decisions that may be made as the results of these trials, for the design of insensitive munitions.

A study of many examples, such as bullet impact and cook-off, enables a critical evaluation of those tests and suggests that they be conducted in a more scientific purpose by coupling them with mathematical modelling. It concludes by advocating international co-operation, as the recent NIMIC workshop shows the way, on modelling the tests and their experimental adaptation to the requirements of the models.

## **I. INTRODUCTION**

Nobody can deny the necessity of assessing the vulnerability of ammunition before delivery to any of the armed Services. The accidents that occurred on the Forestal in 1967, and more recently the gigantic explosion in Vladivostok and the incidents after "Desert Storm", remind us of this.

Two approaches have been attempted to predict this vulnerability versus accidental or war stimuli, such as bullet or fragment impact, fuel fire, shaped charge jet or sympathetic detonation:

- on the one hand, tests on whole munitions, costly therefore few, but unavoidable at the time when scientific generic tests and mathematical models did not exist;
- on the other hand, small scale tests set up by research centers in order to assess a given parameter and with the objective of avoiding full scale tests.

As part of the latter, measurements made within or outside the munitions tested, laboratory tests on energetic materials and small scale tests have highlighted such features as the lower vulnerability to bullet impact of cast cured plastic bonded explosives (PBXs), the influence of the explosives grain size, or the beneficial effect of buffer materials or of some particular warhead designs (e.g. dual) to prevent sympathetic detonation. They have brought a major contribution to the munition science, particularly in the last five to ten years, and this will increase in the future since measurements and computer science will be more and more efficient. They will be more and more used as input data for the mathematical modeling of the vulnerability of munitions.

On the other hand, during the last ten years, international groups within NATO and the UN have endeavored to standardize the former category of tests, i.e. tests on the munitions themselves, assumed to be representative of stimuli such as fuel fire and bullet impact. These tests are often effected as the final step in the development of a warhead, a rocket motor or a whole munition, and they are considered by some procurement authorities and program managers as sort of a Bible since they have the authority of official approval.

Questions can be raised about their representative value, their reproducibility and their trustworthiness, given the important decisions that may be made as the result of these trials. These questions, indeed, naturally came out on occasion of the first scientific workshop organized by NIMIC on the topic of vulnerability of munitions to impacts.

The joint knowledge and experience of the specialists who met at this workshop enabled a critical analysis of "go-no go" experimental tests, as the result of various examples examined. This helped to establish the necessity for performing an operational and functional analysis of munitions, and for coupling experimental testing with mathematical modeling.

## **II. CRITICAL EVALUATION OF EXPERIMENTAL TESTING**

Since energetic materials have first been used, various random accidents or externally induced incidents have made the world community aware of:

- a number of primary threats (shock wave, bullet impact, fire, etc.) that may cause accidental explosion of a munition;
- the additional threat of sympathetic propagation of explosive initiation from one munition to others.

In order to study these threats and their effects through other than undesirable and sporadic accidents, all the world's experts have considered it necessary to define simplified scenarios representing those accidents and to simulate them on demand. As mathematical modeling techniques developed only recently, everyone logically began by resorting to experiment for these simulations, trying to define tests as representative as possible of real scenarios.

But real scenarios may be highly diverse, with the result that defining a simplified scenario presupposes a choice, and defining the test with precision entails the even more restrictive choice of a particular geometrical configuration.

An example will illustrate these concepts:

- a bullet impact on a munition is a threat;
- real scenarios may include the impact of bullets of various calibers, at various velocities, from various angles of incidence and at various points on the munition;
- the simplified scenario involves choosing one type of bullet and one impact velocity;
- the test is carried out in a particular configuration, by selecting the angle of incidence and point of impact on each particular munition (or munition component).

Everyone agrees on the nature of the threats to be taken into account (e.g. bullet impact), but there is no such unanimity concerning the choice of simplified scenarios, still less on a precise definition of the tests. Indeed, NATO did standardize the simplified scenarios and define the reaction levels to be considered (I through V), but was not always very specific in the description of the configurations.

In order to clarify these statements, a number of particular examples are given in annex. They prove that it may be very dangerous to draw conclusions from standardized pass/fail tests, particularly as far as IM design is concerned. These tests, indeed, can highlight neither threshold effects nor margins. Moreover, even replacing a single test or a couple of tests with a set of similar tests would not substantially raise the degree of confidence of a result: applying the probability formulas would show that, if one wanted to be nearly sure of a non violent result, the number of tests to be carried out should be very large, hence costly.

The aim of this paper is to examine how these tests might be made more useful and fruitful. (1)

### **III. STANDARDIZATION AND GENERAL USE OF TESTS**

One of the drawbacks of standardized tests is the number of degrees of freedom left in the procedure, so the same test on the same munition can result in a different trial depending on the test center where it takes place. But this may even occur within the same center, e.g. according to whether a bullet remains stable or not within the target.

Yet, even assuming that standardization is sufficiently advanced to eliminate all these divergences, is it justified for all that? Standardization, indeed, is not an end in itself, and if one wants particular tests to be withdrawn in favor of a universal test, it is essential to prove that the latter is better than the others. In the absence of an unobjectionable answer to this question, it will always be difficult to eliminate the specific tests that have been conducted for years in national test centers, for a variety of reasons:

- political and psychological reasons, each center preferring its own test;
- financial reasons, everyone wishing to take advantage of past expenditure;
- and even scientific reasons, since withdrawing a test means withdrawing the corresponding results, therefore emptying data banks.

### **IV. FUNCTIONAL ANALYSIS OF AMMUNITION**

Yet how can it be proven that one test is better than another? And admitting it is actually better to simulate a particular configuration, what general conclusions can be drawn? For what is important, ultimately, is not how a munition behaves in a given test, but how it would behave in the scenario one wishes to simulate.

Simulation of a complete scenario is hard to envisage by purely experimental means, as shown in some examples. It is therefore necessary to make a functional analysis of the munition (e.g. consider separately HEs used as a booster or as a main charge) as well as a geometrical analysis (as shown in the case of a shaped charge or a cluster munition), that is to divide a given munition into homogeneous sub-elements, each one with a different vulnerability level. Vulnerability studies carried out on each of them (by means of experiment and modeling) will then help the designer of a munition to assess its hazard level for a given stimulus.

This approach has already been adopted by battle tank and aircraft designers, who are not in favor of destroying thousands of targets to reproduce every angle and location of impact. Based on this approach, NIMIC recently asked the Dutch establishment TNO to check whether one of its models could be applied to munitions.

## **V. PURPOSE AND OBJECTIVES OF TESTS**

Examination of the common tests reveals various possible purposes, which may be grouped under two headings:

- technical characterization of an energetic material, with no attempt to deduce directly conclusions relating to real scenarios;
- prediction of the behavior of a munition or munition component in a real scenario.

In both cases the ambitions of the tests may vary widely. In the first case they may range:

- from a simple check to ensure reproducibility of the energetic material tested, e.g. for the acceptance or rejection of a manufacturing batch,
- to a truly scientific test intended to go further into the understanding of phenomena associated with the initiation and the normal or accidental functioning of the energetic materials, given their geometry and containment.

In the second case, the scope of the test may range:

- from mere comparison of various munitions or different variants of a single munition (e.g. using different energetic materials) in a particular configuration of a particular scenario;
- to general prediction of the behavior of real munitions in all possible configurations of operational scenarios.

Obviously, the more ambitious the test (or series of tests), the more complex and expensive it will be. The problem is that one is always tempted to go for the quickest direct solution, because it is apparently the cheapest. Now, the real costs have to be compared between

- a test which appears simple but that provides little information (the cost/efficiency ratio then approaches infinity), and
- a well instrumented test, more expensive but productive.

## VI. FROM EXPERIMENTAL TESTING TO MATHEMATICAL MODELING

At the workshop organized in June 1992 by NIMIC on the vulnerability of munitions to impacts, 40 specialists of the five NIMIC participating countries confirmed that the interpretation of "go-no go" tests could be misleading, as opposed to scientifically usable (i.e. well instrumented) tests which make it possible to answer the questions raised within the hazard tree established for a stimulus. Only such scientific tests can provide input data for the mathematical modeling of munition sub-elements, hence their interest, even if their ambition were limited to that purpose.

The following experimental devices and methods have been carried out in the last 10 years by those who fund or carry out tests, although most of them are not being currently used for the purpose of modeling

- ionization gauges;
- flash X-rays (measuring bow shocks and internal damage during shaped charge impacts);
- velocity strips;
- fiber optics (measuring temperatures and velocities of luminous events);
- carbon resistor pressure gauges;
- manganin stress compensated pressure gauges;
- piezo pins (measuring bow shocks and reaction propagation);
- temperatures (internally in target material);
- burst gauges;
- external overpressure gauges;
- LASER Doppler interferometry measuring propagation velocities;
- internal shear;
- internal damage;
- delay time to detonation.

This does not mean that all the results of non instrumented tests carried out in the past must be disregarded: an analysis of these extensive data bases available all over the world is necessary before deciding that they are useless, as far as modeling is concerned.

Within the workshop mentioned above, the working group on the experimental characterization concluded that the following parameters or measurements constitute necessary input data for vulnerability mathematical modeling. These scientific tests and corresponding measurements are still to be devised, for most of them:

- ignition;
- pressure-time map of the internal charge;
- location of the ignition site;
- internal temperatures;
- localized shear;
- causes of ignition for explosives, including the burn to violent reaction process;
- sensitivity versus damage (vivacity, specific surface, porosity, density variation).

So, most of the experimental tests need to have their aim limited: the trials must be usable, i.e. they must be conducted under conditions such that their scientific outputs be transferable to other configurations, or even other scenarios. In order to make such a transfer, one must combine experiment with computation, i.e.

- build a mathematical model in which experimental measurements can be used as input data;
- reciprocally, organize the test and experiment plans so as to measure the parameters actually needed to operate the mathematical model.

## **VII. THE ADVANTAGE OF MATHEMATICAL MODELING**

The development of various mathematical models, particularly to simulate mechanical aggressions such as impacts, represents a major step towards a better understanding of the phenomena involved. In the case of bullet penetration, for example, the models have demonstrated that the critical part of the phenomenon was not necessarily the impact itself, and that the conditions for initiation of the energetic material (i.e. the buildup of high pressures and temperatures, and their permanence during a sufficient time) could appear at other points in the munition.

They have also explained the criticality (from the safety point of view) of the central bore-hole in a rocket motor, and accounted for the apparent paradox that a slow bullet may be more dangerous than a fast bullet in such a rocket motor, within a given range of diameters (SNPE).

The NAWC-developed FRAGMAP code, for instance, can be an essential tool in a whole program for the evaluation of munition vulnerability to all likely kinds of fragment hazards (fragments as available from warhead arena tests), and discusses other factors that should be considered in order to estimate the probability for a munition to detonate in response to fragment impact.

None of these phenomena could have been understood from the present purely experimental tests. Modeling therefore represents a very significant progress, which must be continued and which must definitely be the subject of international cooperation. Indeed, such a cooperation is:

- easy, because the subject is scientific and not industrial and commercial;
- desirable, because it is a vast undertaking which cannot be successfully concluded by a single team.

The workshop sponsored by NIMIC highlighted several possible cooperative efforts.

#### **VIII. SCIENTIFIC EVOLUTION OF THE TESTS**

Most of the standardized tests presently carried out, and some of the scientific ones, have been defined without any modeling purpose. In particular, in those dealing with whole munitions, more importance is given to the reproducibility of the test procedure (which is not always satisfactory, e.g. in the case of the bullet impact) or to the perfunctory observation of a reaction, if any. But this simple characterization is not sufficient to enable an efficient coupling between testing and modeling.

It must be recognized that such a coupling is difficult when the tests are carried out on real munitions (or munition components):

- because, in general, these are entirely enclosed, which makes it difficult to make internal measurements;
- and because their geometrical complexity may complicate the design of the mathematical models.

As a result, the users of the models carry out specific experiments for their own use, giving mathematical feasibility priority over strict realism, since the realism will then be reconstructed by the model. This consideration of feasibility (both mathematical and experimental) leads to carrying out the experiments:

- on mockups representing munition components, but with a simple geometry adapted both to modeling and to the implementation of measuring equipment, as listed in Part VI;
- with modes of aggression that are also simplified, for the same reasons;
- possibly replacing the energetic material with an inert material with equivalent mechanical properties in certain tests, in order to be able to obtain the necessary displays and measurements without risk.

Mathematical modeling must be improved, too. For instance, the details of all phenomena occurring in sympathetic detonation phenomena are still difficult to model. Also in bullet impacts, most hydrocodes are used in axysymmetrical 2-

D configurations, so they do not take into account the possible tumbling of the bullets and deviations of their trajectories in the target after impact. It is well known, though, from wound ballistics studies, that any trajectory can occur, even a U-turn.

In this case it might be preferable to replace the bullet impact with a sphere impact (whose interpretation would be less subject to doubt), or with the impact of a projectile specially designed to ensure its stability. True, such a test would apparently be less realistic, but what significance can one attach to the realism of a test that simulates only one specific configuration of one specific scenario, while introducing a margin of uncertainty that may entirely distort the result?

#### **IX. VULNERABILITY AND OPERATIONAL SCENARIOS**

We concluded earlier that, whatever test is considered, a purely experimental simulation of all possible configurations of a scenario would be financially out of reach. This being so, even if using numerical methods rather than experimental methods, simulating all possible configurations of even a simple scenario (and still more a compound one) may also involve considerable expenditure. However, not all configurations are equally important, and one must take into account their probability of occurrence in the real scenario. One must therefore identify:

- firstly, the technical scenario simulated by a test;
- secondly, the position of that technical scenario within an operational scenario over the whole life cycle.

Therefore, prior to coupling experiment and modeling in the "technical" tests, an operational research phase must be conducted to assess the probability of occurrence of the various types of aggression and of the various configurations, as well as the severity of the consequences in the event of an explosive reaction. The results of this operational research phase may differ widely from one service to another. For instance, sympathetic detonation constitutes a major risk in a ship's magazine, but whether this occurs or not makes little difference inside a tank, where the detonation - or even mere combustion - of a single munition is enough to cause unacceptable damage.

This whole method (operational model + breakdown of the target into elementary units + technical study) has been used for many years for land vehicles and aircraft. It has sometimes led to pointless refinements and excessive calculation time, but this should not be the case for munitions:

- because munitions are simpler objects, both geometrically and functionally;

- because one should benefit, in their case, from experience gained elsewhere, particularly of excesses to be avoided.

Halfway between the vulnerability of a single munition and that of a tank, it may be interesting to utilize these methods to study the vulnerability of a group of munitions (e.g. packed for logistic transport) in order to optimize the geometrical arrangement of the munitions and the position of shieldings, if any.

#### X. CONCLUSIONS

The current practice of conducting purely experimental tests is inadequate to evaluate the vulnerability of munitions to accidental or deliberate threats. And even if it only pretends to measure sensitivities (in terms of explosiveness) and not vulnerabilities (in the operational sense), it leads to making experiments which are often costly, yet poorly exploited, sometimes even inexploitable for lack of adequate understanding of the phenomena involved (or, worse, incorrectly interpreted).

In order to maximize the benefit of the existing tests, one should at least make an effort to understand these phenomena through mathematical models, in conjunction with the measurement of experimental parameters selected for their representative value and not for their accessibility. Major progress has been recently achieved in modeling, especially with the establishment of experimenting plans based on the requirements of the models, so as to achieve the reciprocal linking of experiment and calculation. This progress has brought a major contribution to the understanding of phenomena, but it has not been able to capitalize most of the existing tests, which are too empirical to be scientifically re-used. One must therefore go further and design experimental tests more scientifically so that, when coupled with mathematical models, they can correctly predict the behavior of ammunition.

The empirical nature of existing tests was acceptable - and even inevitable - when these tests were first designed, but the scientific environment has changed since then, and it must be utilized. This is an economically costly and scientifically difficult task, but it is all the more suited to international co-operation for that. The path to such co-operation was opened up a long time ago by those who managed to define jointly standard tests. We should now continue down that path for less normative and more scientific purposes, but with the same ambition. The NIMIC workshop was the first step.

## E X A M P L E S

### # 1 - Threshold Velocity in Bullet Impact

In order to select low sensitivity explosives, the French Ministry of Defense carried out vulnerability testing (2) on 3-liter analogs of munitions (Fig. 1). The plot describes 12.7mm (0.5") bullet impact trials, the targets being these analogs loaded with a melt cast explosive and different cast cured PBXs (Fig. 2). For two of these PBXs, it evidences the existence of two bullet velocity thresholds, one between 400m/s and 600m/s, the other between 600m/s and 800m/s. A violent reaction occurred between these two thresholds, but neither below nor - more surprisingly - above.

The reason for this is that, at 600m/s, the bullet stops within the target, hence releases all its energy in the HE. So this particular velocity is more dangerous than higher ones, which was at first sight unexpected.

The same phenomenon may occur in a real munition with a larger caliber and a different confinement, so carrying out one or two impact tests at 870m/s, as required by the standardized test, will not help discovering these two thresholds, if they exist. It would then be particularly misleading to conclude, on the basis of this single standardized test, that "Munition X does not react violently to bullet impact", then accept it and store it in the magazines of a nuclear-powered aircraft-carrier.

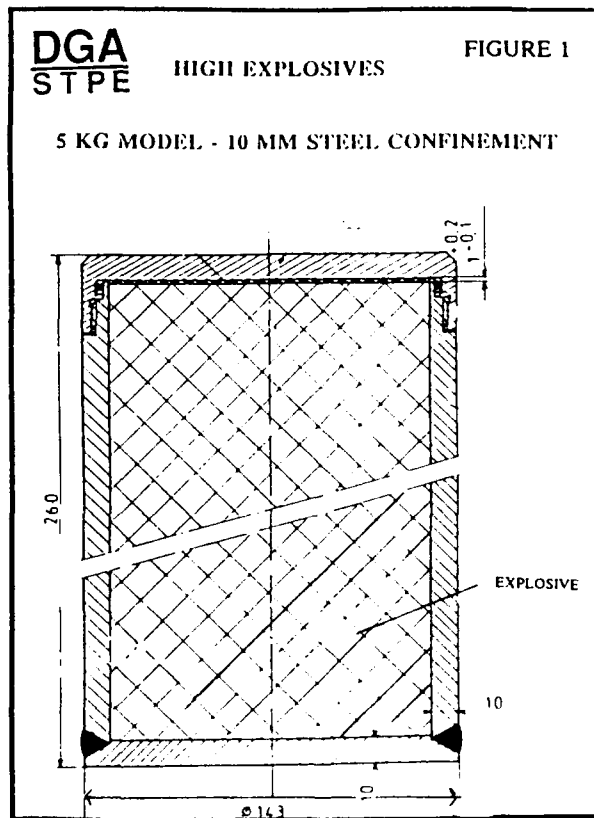


FIGURE 2

**VULNERABILITY TEST RESULTS**  
 (According to NATO Reaction Descriptions - type I to V)  
**HIGH EXPLOSIVES**  
 (3 LITERS - 10 MM STEEL MODEL)

0.50 Cal. BULLET IMPACT TEST (1 SHOT)

	400 M/S	600 M/S	800 M/S	1000 M/S	1200 M/S
OC101	II	II	II	IT	II
→ HTPB/RDX	IV	II	IV	IV	IV
HTPB/Al/RDX	N.R.	N.R.	V	IV	IV
HTPB/APV/ Al/RDX	IV	IV	V	IV	
→ PB/IMX	IV	II	IV	IV	IV

2

**# 2 - Bore Effect in Bullet Impact**

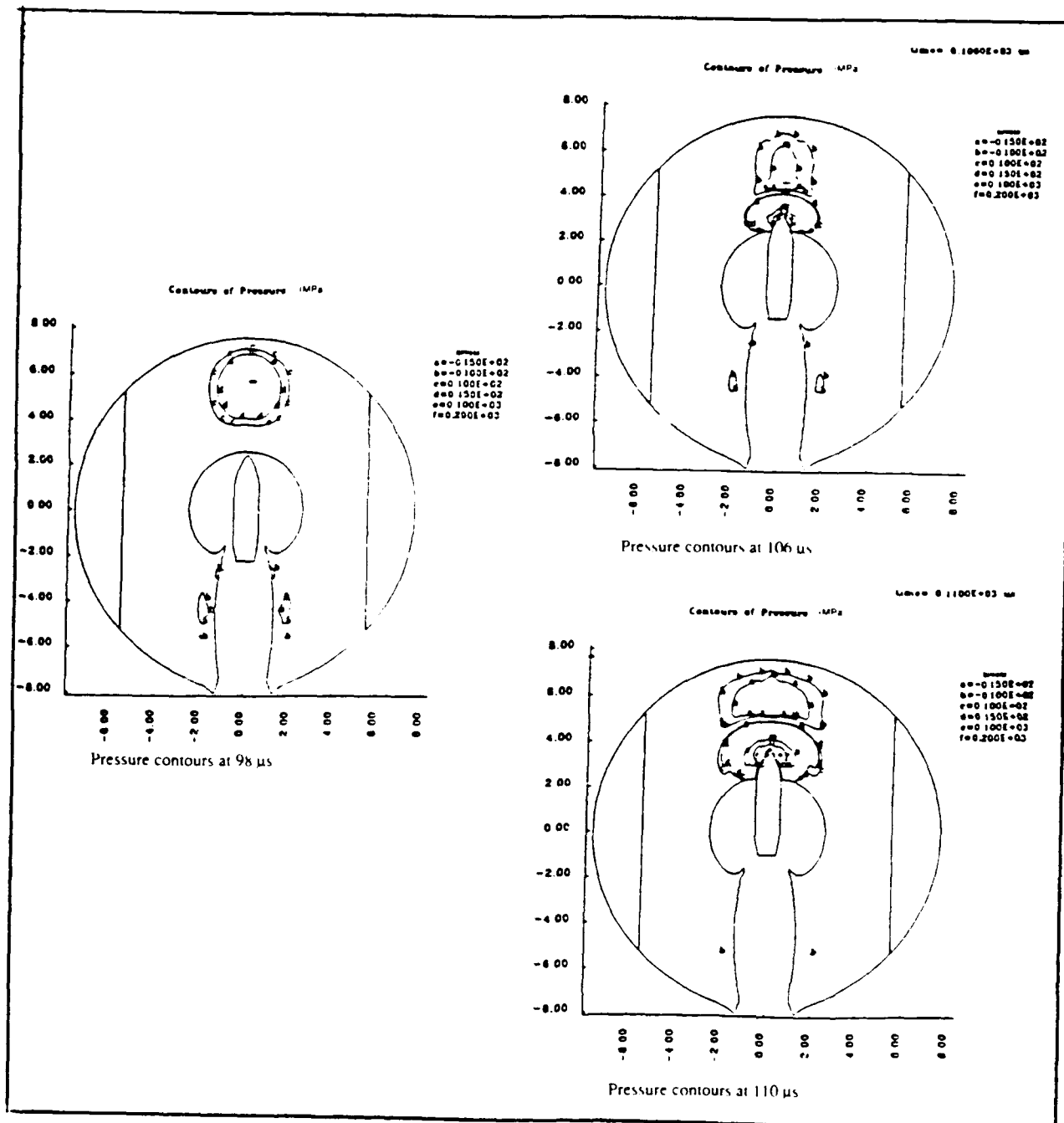
In the final stage of predevelopment studies for a French missile, a standardized bullet impact test was carried out on the rocket motor with an inner borehole. Surprisingly enough for the designers, who had planned one single test, a detonation occurred despite the low sensitivity of the rocket propellant (nitramite G or XLDB) when tested in similar diameters, but without a borehole. Further studies then showed that, for some given webs (i.e. wall thicknesses), and for some given impact velocities, the shock waves produced by the impact focused on the other side of the bore (Fig. 3), thus damaging the material prior to impact (cracking, disruption due to high strains), and might sometimes lead to violent reactions, up to detonation. This delayed detonation was called the "bore effect" (3).

A whole testing campaign was necessary to explain this phenomenon when it occurs, i.e. within a certain range of bore diameters. As in the previous example, this is more likely to appear at low impact velocities, since at high impact velocities, focusing occurs only after the bullet has reached the second section of the propellant. Therefore, had the initial test been satisfactory from the point of view of the designer (i.e. no violent reaction), the rocket motor and the missile would be in use in the Air Force as such, perhaps endangering aircraft.

FIGURE 3

Identification and Validation of the "Bore Effect"  
Scenario/Numerical Modelling

SNPE

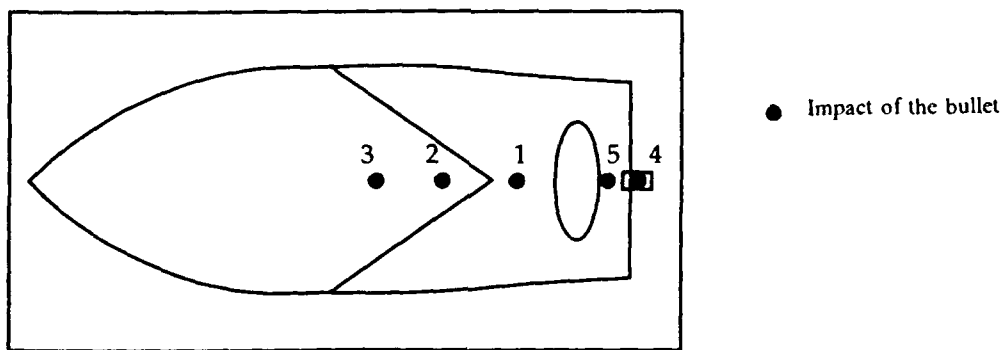


### **# 3 - Location of the Bullet Impact**

This bore effect may also appear when shooting at the base of a shaped charge, e.g. that of the HOT antitank missile (Fig. 4), whereas common sense would lead to estimating this location of the impact less dangerous than shooting at the solid section of the HE, across a diameter in order to get the longest possible path. This would not be the worst-case configuration either, since shooting off-diameter would produce an unsymmetry, and this might de-stabilize the bullet and make it tumble, hence make it release its whole energy within the explosive instead of passing through.

Anyhow, the worst-case configuration normally requires to hit the most sensitive material within the warhead, which means the booster and the detonator. But doing this systematically would totally hinder any progress achieved on the main explosive on the way to insensitive munitions.

Another case of ambiguity on the location of the impact is a cluster munition, e.g. a mine-dispensing system such as the MLRS phase 2 munition (Fig. 5). The choice of the impact area is much broader (gas generator, rocket propellant, pyrotechnics, main or booster charge, main mine charge) than assumed in the requirements for the vulnerability studies of this system, undertaken in view of its storage and use procedures in the British Army (4).



The outcome of the trial can depend on the location of the impact

**FIGURE 4 "HOT" SHAPED CHARGE SCHEMATIC**

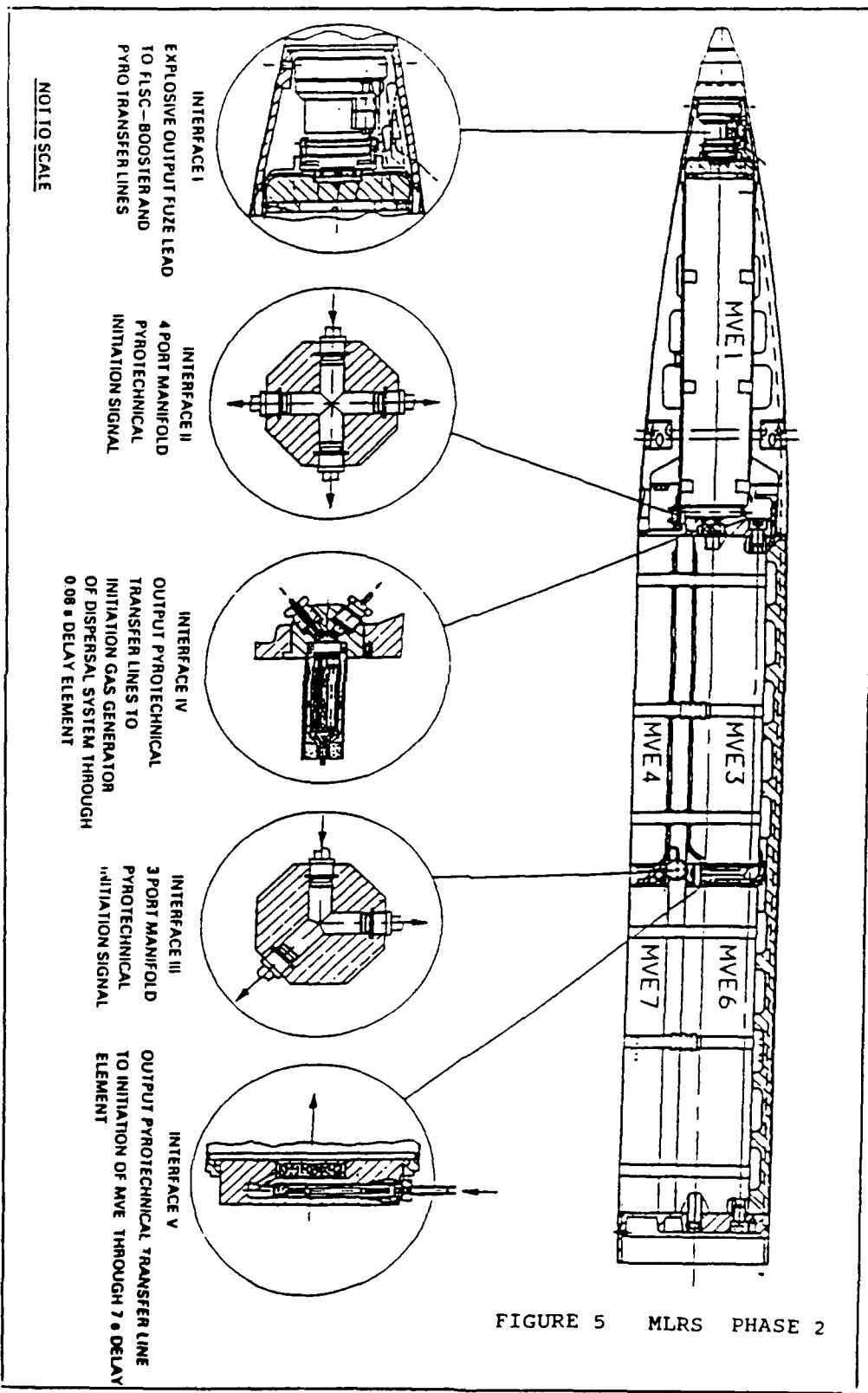


FIGURE 5 MLRS PHASE 2

#### # 4 - Fuel Fire

The standardized fuel fire test on a munition requires a minimal flame temperature, so this temperature is systematically measured. But this data is of little interest for the prediction of the reactivity of the energetic material, hence of the behavior of the munition. Indeed, let us assume that a missile warhead is normally stored with its booster (e.g. a missile warhead). If the test is nevertheless conducted without this booster, which is in principle the most sensitive element, and if the result is satisfactory, it is rather unusual that another test be carried out, either on the whole warhead or, better, on the booster element alone, by submitting it to the temperature history it would have faced if tested within the main charge.

It is often concluded that "Warhead X does not react violently to fire". This sort of assumption has already led to the design of warheads where the main charge was a cast cured PBX and the booster a pressed PBX, more sensitive to fire and impacts. So two separate tests should normally be conducted:

- the first one on a warhead without its booster, but making temperature measurements in the location of this booster;
- the second one on the booster alone submitted to the temperature history thus measured, as described above.

This is the only way of knowing the real cause, location and propagation of an event, particularly when it leads to a detonation where nothing can be retrieved for examination.

#### # 5 - Multiple Stimuli

The phenomena are more complicated yet in the case of multiple stimuli, or stimuli depending on several parameters, for example sympathetic detonation. French studies have highlighted that ONTA-based (i.e. NTO-based) cast cured PBXs were remarkably insensitive to sympathetic detonation, even in stacks of nine 40-kg test stores very close to each other (Fig. 6). But what would happen with a still higher confinement or a still more important number of targets, or, conversely, with dual explosive warheads (Fig. 7) whose outer layer would be still more insensitive? (5,6)

Anyhow, there again, "common sense" is not always the answer: a US mathematical model has explained why, in a stack storage configuration (Fig. 8), a sympathetic detonation is more likely to be transmitted diagonally rather than to the adjacent munition. (7)

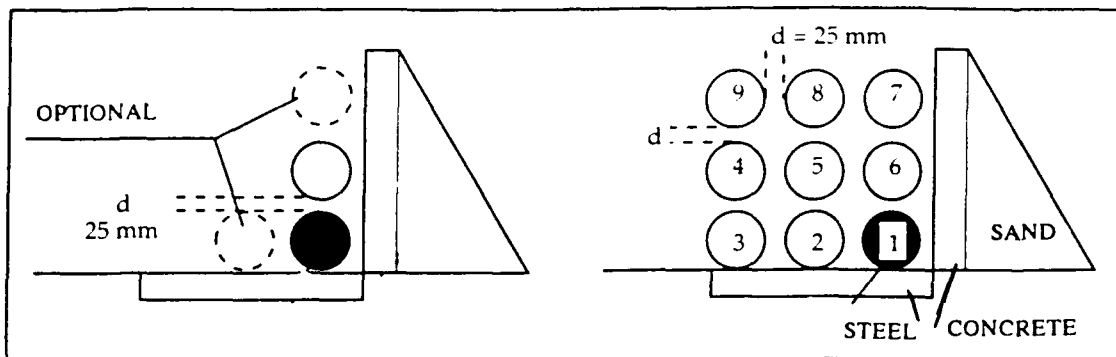


FIGURE 6 DONOR-RECECTOR CONFIGURATION (SNPE)

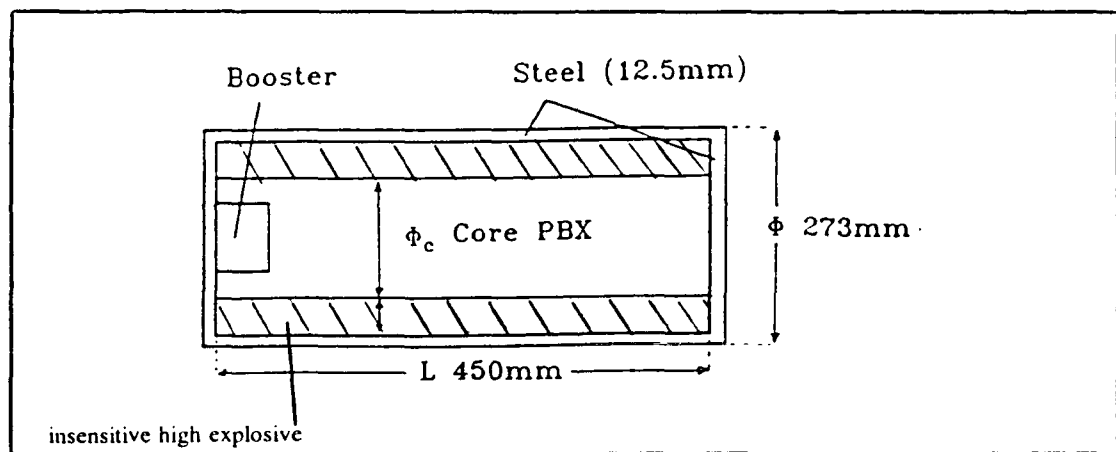


FIGURE 7 DUAL EXPLOSIVES WARHEAD

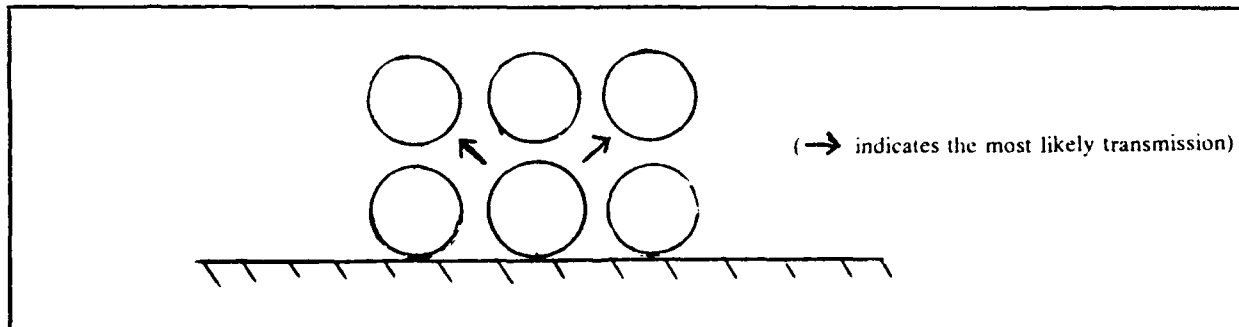


FIGURE 8 SYMPATHETIC DETONATION OF 500 LB BOMBS

As far as multiple impacts are concerned, the NIMIC workshop evidenced the major dependence of reactivity of an explosive on its physical damage. If a first projectile fractures the explosive without initiating it, but is followed by a second projectile, the behavior of this material under the second impact will depend on the degree of fracture due to the first impact (i.e. on the physical and mechanical properties of the material impacted), and also on the trajectory of the new projectile and the delay after the first one. The standardized test, as required by MIL-STD 2105A, can obviously not analyze all these sequences 1st impact/fracture/2nd impact.

### References

- (1) - M. DEFOURNEAUX - "Development of a Methodology for Evaluating the Vulnerability of Munitions" - NIMIC Report, Feb. 1992.
- (2) - J.M. DECORE, P. LAMY, B. SAINJON - "French Policy of Providing Industry with Gun Propellants, Rocket Propellants and High Explosives for Reduced Sensitivity Ammunition"- AGARD IM Conference, Bonn (Germany), Oct. 1991.
- (3) - J. BRUNET, S. HAMAIDE, B. NOUGUEZ, F. PITIOT - "Bullet Impact Behavior of Solid Propellant Grains" - AGARD IM Conference, Bonn (Germany), Oct. 1991.
- (4) - "MLRS Phase 2" - Ordnance Board Proceedings.
- (5) - J. ISLER, B. NOUGUEZ - "Insensitive Warhead Concepts"- ADPA Insensitive Munitions Technology Symposium, Williamsburg (VA, USA), June 1992.
- (6) IMAD Quarterly Reports.
- (7) G. GLENN - "Sympathetic Detonation Predictive Methods for Mk82 General Purpose Bombs" - ADPA Insensitive Munitions Technology Symposium, Williamsburg (VA, USA), June 1992.

## **SIMPLE ANALYTICAL RELATIONSHIPS FOR MUNITIONS HAZARD ASSESSMENT**

Andrew C. Victor  
Victor Technology  
Ridgecrest, California



Paper prepared for 1992 DDESB Explosives Safety Seminar, 18-20 August 1992, Anaheim, California.

VICTOR TECHNOLOGY  
712 N. Peg Street, Ridgecrest, CA 93555 (619) 375-2375

## **SIMPLE ANALYTICAL RELATIONSHIPS FOR MUNITIONS HAZARD ASSESSMENT**

Andrew C. Victor  
Victor Technology  
Ridgecrest, California

### **ABSTRACT**

This paper presents simple analytical relationships that can be used for credible prediction and assessment of munition behavior in hazard scenarios and tests. The methods have been used for predicting munition response to impact/shock and thermal several threats for Inensitive Munitions (IM) Threat Hazard Assessments and for proposing modifications to some of the IM test requirements. Unfortunately, no methods are yet available for predicting a priori the ultimate violence of reactions that may occur following ignition-to-burning of encased energetic material. Nevertheless, the simple methods in this paper, when used to predict the onset of reaction, can be valuable in system safety programs for hazard analysis and risk assessment of items containing energetic materials as well as for rocket motor and ordnance item preliminary design studies. The paper includes all equations and supporting data needed to make the calculations described for a number of energetic materials. Comparisons with data show the broad validity of the simple methods described.

### **INTRODUCTION**

The U.S. armed services have a chain of documents defining procedures for demonstrating compliance of munitions with IM requirements.<sup>1-13</sup> These documents are linked or are being linked to the NATO requirements to enhance commonality and interoperability. The primary feature of these requirements is compliance with full-scale munition testing procedures and results, which are fully described elsewhere. However, many additional tests are required at component and energetic material (EM) levels as well for "classification" and "qualification" of energetic materials and items.<sup>14-18</sup> In the U.S., all these requirements fall under system safety program requirements.<sup>19</sup>

The author's experience gained by managing a large program in insensitive munitions R&D (U.S. Navy IMAD Propulsion Project, 1984-1989) and subsequently participating in industrial efforts to develop proposals for weapons development programs to meet DOD IM requirements has helped highlight needs for expeditious analytical methods for preliminary munition design that includes consideration of explosive hazards.

It is the author's experience that the initial hazard assessments and test plans (including IM Threat Hazard Assessment (IMTHA), IM Test Plan, and Hazard Assessment Test Report, are typically contractually scheduled early in munition development programs and require information not readily available at the time they must be prepared. With enough money spent up front, adequate characterization data for the energetic materials in the munition (qualification) will be available – and it is often from these data that we must draw the information for use in the initial safety documents. Subsequently the system safety program will have the test data from the preliminary design tests to include in its documents (if indeed program scheduling has permitted such tests). The final hazard assessments will then have the advantage of more complete testing and design refinement, and at that time there will be more system-level data. But even at that final stage, analytical relationships are necessary to tie all the information together to provide reasonable inputs for the hazard assessment and classification required by the system safety program.

### **SCOPE**

This paper presents some analytical relationships the author has found useful for estimating technical input on explosive safety, hazards, and classification used in the initial phases of munition development.

The scope of the phenomena considered includes the seven basic IM test areas that are closely related to tests used to meet other classification requirements:

- Fast Cookoff
- Slow Cookoff
- Bullet Impact
- Fragment Impact
- Sympathetic Detonation
- Shaped Charge Jet Impact
- Spall Impact

At the proposal phase, a contractor will naturally concentrate on these seven IM test areas only as minimally specified by DOD requirements.<sup>11</sup> (This also seems to be a predilection of many Government weapon program managers for the obvious reasons that it conserves resources for more traditional uses, it seems to meet the requirements – if not the intent of DOD IM policy, and better approaches, although proposed, have not yet been implemented<sup>78</sup>.) Therefore, development programs focus on creating munition designs to pass the required tests.

Alternate or additional tests that simulate other possible threats may be suggested at the proposal phase usually only if there is serious doubt that the basic tests can be passed. However, to justify any alternate tests it is necessary to demonstrate threat feasibility (and if possible, probability) with a preliminary IMTHA. An adequate IMTHA describes the nature and probability of the alternate threats, the design of alternate corresponding tests, and the expected responses (and their probabilities) of the munition design to both the basic tests and the alternate tests. It does not require much imagination to visualize the scope of the prior test effort that would have been required to provide such an IMTHA with any degree of certainty, and to realize that it would be prohibitively expensive and untimely in today's development environment.

Into this data vacuum it is necessary to introduce analytical methods for estimating the IM behavior of a proposed design in the preliminary IMTHA. The reliance on such methods will be lessened if data from more pre-proposal R&D are available on the proposed design concept or by analogy and extrapolation from similar design concepts. In the future, as appropriate scientific studies are completed and complementary analytical techniques evolve, engineering approaches to IM design will become more refined and systematized through experience. Even in that optimistically envisioned future, simple methods will have an important part to play.

What is a proposal team to do in the current environment? The simple methods described in this paper can be very helpful in supporting required analyses. Admittedly, these methods do not advance the state-of-the art. Also, where they are phenomenological rather than basic scientific models, they often cannot be extrapolated reliably beyond the range of inputs on which they are based. Even where the methods do not predict the violence of munition reactions, they are useful for estimating the pre-reaction behavior of preliminary design concepts and the efficacy for risk reduction of various munition design approaches.

What kinds of questions can be answered with the methods given here? A few examples follow.

- What warhead case design/explosive combination optimizes kill probability and resistance to shock-to-detonation transition (SDT)?
- What is the probability that a particular warhead design will pass the IM fragment-impact test requirement?
- What is the expected fragment velocity from a particular warhead design? How can one predict this for a basically untested explosive?
- Will a warhead or rocket motor design resist sympathetic detonation in one-on-one configurations?
- How can one approximate the effects of a warhead stack on the sympathetic detonation response?
- What is the fast cookoff time for rocket motors or warheads with specific case, liner, insulator designs and specific energetic materials?
- What is the expected behavior of a warhead or rocket motor in a slow cookoff or intermediate cookoff test or scenario?
  - What is the maximum tolerable external temperature?
  - What is the expected time to reaction?
  - What is the internal temperature pattern and how will different energetic components be affected?
  - Are munition-scale thermal test results consistent with laboratory-scale test data?

Although much of what follows has been published elsewhere, its assembly here in one place should be useful as a brief compendium.

## IMPACT INITIATION OF REACTIONS

This section presents calculation methods for initiation of detonation and ignition in munitions subject to impact by bullets, warhead fragments, and shaped charge jets. Also provided are methods for estimating the velocities, size distributions and spatial distributions of fragments from threat warheads.

## DETONATION BEHAVIOR OF EXPLOSIVES

Simple methods for calculating the detonation behavior of explosives are available. With these methods, one can obtain results comparable in quality to those obtained with the Tiger or BKW codes, and useful in the absence of laboratory data.

### Detonation Pressure

The Kamlet-Jacobs formula<sup>20</sup> gives the detonation pressure in an explosive ( $P_d$ ) as:

$$P_d = 1.558 \rho_0^2 N M^{1/2} Q^{1/2}, \text{ GPa}, \quad (1-1)$$

where:  $N$  = moles of detonation product per gram of explosive. (~0.03)

$M$  = average molecular weight of detonation product gas. (~30)

$Q$  = chemical energy of detonation reaction, cal/g. (~1,000 cal/g)

If one has trouble estimating values for  $N$ ,  $M$ , or  $Q$  needed in equation (1-1), the detonation pressure can be estimated from the calculated propellant specific impulse ( $I_{sp}$ ) of the explosive formulation by the method of Gill, Asaoka, and Baroody (GAB):<sup>21</sup>

$$P_d = 4.44 \rho_0^2 (0.009807 [I_{sp}^{1000}]_{14.7}) - 2.1, \text{ GPa}. \quad (1-2)$$

( $I_{sp}$  in lb-sec/lb as obtained from PEP or NASA/Lewis codes with combustion and exit pressures as shown in psia.)

For a wide but reduced variety of explosives the GAB formula may be simplified to:

$$P_d = 4.44 \rho_0^2 (0.009807 [I_{sp}^{400}]_{14.7}), \text{ GPa}, \text{ which is in the same form as equation (1-1)}. \quad (1-3)$$

### Detonation Velocity

The detonation velocity ( $D$ ) can be approximated by Jacobs formula:<sup>20</sup>

$$D = (0.809/\rho_0 + 1.052) P_d^{1/2}, \text{ km/s}. \quad (1-4)$$

Walker<sup>22</sup> has described a method for estimating detonation velocity on the basis of the Hugoniots of the explosive's constituent elements and the measured or calculated detonation pressure.

$$D = \Sigma_e (U_{se} [W_e / \Sigma_e W_e]) (1 + f(P_d)), \text{ km/s} \quad (1-5)$$

where:  $W_e$  = formula weight of element =  $M_e \times n_e$ , for example, for  $C_6H_6N_6O_6$ ,

$n = 6$  for each element.

and

$$\begin{aligned} f(P_d) &= 2.0286(-3) + 2.231(-3) P_d + 9.6429(-6) P_d^2 - 4.1667(-7) P_d^3 \\ U_s(C) &= 4.5319 + 0.11651 P_d + 1.0717(-4) P_d^2 - 1.5162(-5) P_d^3 \\ U_s(H) &= 5.976 + 0.35362 P_d + 1.6859(-3) P_d^2 - 5.0439(-6) P_d^3 \\ U_s(N) &= 1.2364 + 0.51667 P_d + 1.5555(-2) P_d^2 - 1.9072(-4) P_d^3 \\ U_s(O) &= 2.7904 + 0.18343 P_d + 1.9501(-2) P_d^2 - 1.045(-5) P_d^3 \end{aligned}$$

It is conceivable that other elements could also be used in the Walker formulation; and for those elements that do not completely react to form gaseous products some approach involving partition of energy might be used to obtain good calculated values of detonation velocity.

### Heats of Detonation and Explosion

Baroody and Peters<sup>23</sup> have published a method based on  $I_{sp}$  calculations for calculating explosive heats of explosion and heats of detonation. This method is summarized in Figure 1, which also shows the calculated results obtained for two

densities of HMX explosive and an unmetallized composite rocket propellant. This method can be used to obtain reasonable values of Q for use in equation (1-1).

### Section Summary

With the data generated by the preceding equations, one can calculate the detonation pressure ( $P_d$ ) and the detonation velocity (D) for an explosive if its chemical formulation and density are known. With this information, one can proceed to estimating warhead performance.

## WARHEAD BEHAVIOR OF EXPLOSIVES FOR IM CONSIDERATIONS

The warhead behavior of explosives involves the acceleration of metal as in case fragmentation and shaped charge jet generation, and the generation of blast shock waves and overpressures and impulse in air and water (wherein gas bubble energy is also of interest). Our primary interest, from the IM standpoint, is the calculation of fragment velocities and sizes that may be important in fragment impact and sympathetic detonation scenarios.

### Fragment Velocity

The maximum velocity of metal fragments in the detonation of a cased explosive is approximated by the Gurney formulas. For cylindrical warheads, the initial elastic-plastic expansion of the case occurs as it expands from its original radius to about 1.2 times that radius. At the end of this phase the case radial velocity is about 60% of the calculated "Gurney velocity". The maximum velocity (as calculated by the Gurney formula) is that achieved at the end of fragment acceleration, with the fragments at a radius of about 1.6 to 1.8 times the initial warhead radius.<sup>24</sup> (It should be noted that lower values of the "Gurney constant" are often used to represent these lesser amounts of expansion.) The simplest expression of the Gurney formula for symmetrical configurations is:

$$V_{\text{gurney}} = \sqrt{\{2E / (\mu + n/n + 2)\}} \quad (2-1)$$

where:  $\mu = M/C$ , and  $M$ = mass of metal in "warhead case" and  $C$ = mass of explosive charge.

$\sqrt{2E}$  = "Gurney constant" in units of m/s or ft/s.

Values of  $n$  are 1 for a flat sandwich of explosive between two equivalent flat metal plates, 2 for a cylinder, and 3 for a sphere.

For an exploding cylindrical warhead with partial additional circumferential confinement, such as a bomb stored in a stack (typical of the sympathetic detonation stack test), it is reasonable to substitute a reduced value for the effective case mass,  $M_j$ . This will result in a calculated higher fragment velocity. For example, a 2/3 reduction (i.e.,  $M_j = M/3$ ) appears to be consistent with Lundstrom's calculations of the effects of stack confinement and fragment focusing in sympathetic detonation stack tests.<sup>25</sup> Another factor, with confinement effects, is that the donor case appears to be focused into a planar shape, so that the problem appears as a large impacting flyer plate upon a cylindrical charge (see Appendix D).

In addition, formulas for unsymmetrical sandwiches<sup>26</sup> are useful for flyer-plate warhead-booster performance calculations. Equation (2-2) may be used for an "open faced sandwich", with metal on only one face, although other formulas have been proposed as well.<sup>81</sup>

$$V_{\text{gurney}} = \sqrt{\{2E / \{ \mu + ((1+2\mu)^3 + 1)/(6(1+\mu)) \} \}} \quad (2-2)$$

For an unsymmetrical sandwich with metal mass of  $N$  on one face and  $M$  on the other:

$$V_M = \sqrt{\{2E / (1 + A^3)/(3[1+A]) + A^2 N/C + M/C\}} \quad (2-3)$$

and  $V_N = A V_M$

where  $A = (1 + 2[M/C]) / (1 + 2[N/C])$ .

The Gurney constant,  $\sqrt{2E}$ , can be approximated by the simple expression:

$$\sqrt{2E} = 0.338 D, \text{ km/s} \quad (2-4)$$

or by the equation of Kamlet and Finger<sup>27</sup>:

$$\sqrt{2E} = 2330 r_0^{-0.6} P_d^{1/2}, \text{ m/s (with } P_d \text{ in kbar} = 0.1 \text{ GPa}) \quad \text{or} \quad (2-5)$$

$$= 887 r_0^{0.4} (N M^{1/2} Q^{1/2})^{0.5}, \text{ m/s}$$

For a cylindrical warhead, the appropriate Gurney formula is applicable only for the cylindrical portion, and the values of  $M$  and  $C$  used must be adjusted to eliminate end effects. A recent Russian paper<sup>67</sup> published expressions applicable to the ends of cylindrical warheads. Equation (2-6) is derived from that work.

$$V_{\text{end}} = \sqrt{(d M V_{\text{gurney}} / 4 L m)} \quad (2-6)$$

- where:  $d$  = warhead diameter.  
 $M$  = mass of warhead cylinder case section.  
 $L$  = warhead cylinder length.  
 $m$  = mass of warhead case end section.

#### Fragment Size Distribution

The Mott equation is used to estimate the size distribution of fragments from a warhead:

$$N(m) = N_0 \exp(-m/a)^{1/2} = \text{total number of fragments of mass greater than } m. \quad (2-7)$$

- where:  $a = 1/2$  average fragment mass in grams  
 $N_0 = M/(2a) = \text{total number of fragments (M is total mass of fragments)}$   
 $a = B (t_0 [d_i + t_0]^{3/2}/d_i) (1 + \mu/2)^{1/2}$   
where:  $B = \text{a constant } \sim 338.1/P_d \text{ (in Kbar)}$   
 $t_0 = \text{casing thickness, inches}$   
 $d_i = \text{internal diameter of cylindrical case, inches.}$

The formulas in this section [(2-1) through (2-5) and (2-7)] are in common use, and are frequently modified to extend their useful range.<sup>28,73</sup> For sympathetic detonation predictions, the calculated fragment size distribution may be irrelevant, and for an unconfined donor-acceptor surface separation distance ( $x$ ) of one munition diameter ( $d$ ) or less, one could assume the impact by a cylindrical surface of radius  $x+d/2$  and thickness  $t/(x+d/2)$ , where  $t$  is the original donor case thickness. There are reasons to believe this approach may have some validity out to values of  $x < 3d$ . With confinement effects the donor case appears to be focused into a plane, and the problem may appear as a large impacting flyer plate upon a cylindrical charge.

#### Fragment Spatial Distribution

The spatial distribution of fragments about a detonating cylindrical warhead is not uniform.<sup>24,29-31</sup> Naturally fragmenting metal warhead cylinders typically fracture into 20 to 23 initial radial bands; therefore, the typical band width (peak to peak or valley to valley) about the cylinder axis varies between 15 and 18 degrees. These bands break up further during subsequent expansion into the ultimate fragment size distribution given by the Mott distribution. However, the number of fragments per angle increment may vary by as much as a factor of 4 or 5 between the peaks and valleys caused by the initial fracture. Sewell<sup>30</sup> gives a rule of thumb that the number of initial fracture sites is given by equation (2-8).

$$F = V_c / (2u_{pc}), \text{ number of fracture sites} = \text{number of axial fragment bands.} \quad (2-8)$$

- where:  $V_c = \text{initial circumferential velocity of inner wall} = 2\pi(\text{radial velocity}).$  The radial velocity is approximated by the sweeping wave pressure divided by the wall acoustic impedance. For steel and a typical explosive this radial velocity would be about  $(20-\text{GPa})/(45.2-\text{GPa/mm}/\mu\text{s}) = 0.442-\text{mm}/\mu\text{s}.$   
 $u_{pc} = \text{critical particle velocity. For typical warhead-case steel, } u_{pc} \text{ for shear is } 200 \text{ ft/s or } 0.061 \text{ mm}/\mu\text{s.}$

With these input values,  $F = 22.8.$

The azimuthal (polar) distribution of fragments is limited to a fan with small angular dispersion as shown in Figure 2. For single-end initiation, the peak angular fragment density is angled from the normal ( $90^\circ$ ) by an amount that can be approximated by one-half the Taylor angle,<sup>26</sup> or about  $5^\circ$ :

$$(\sin^{-1} |q/2|) \approx 0.6 V_{\text{gurney}} / 2D. \quad (2-9)$$

### Section Summary

Fragment velocities, size distribution, and spatial distribution can be estimated with the equations given in this section and the explosive behaviors calculated in the previous section. With this information, one can generate threat parameters relevant to IMTHA fragment impact and sympathetic detonation scenarios.

## SHOCK INITIATION OF DETONATION

Probably more effort has been devoted to analysis of shock initiation of detonation in explosive materials than to any other IM related phenomenon. This is probably due to the relative accessibility of the phenomenon to high-speed computer-based hydrodynamic calculations (hydrocode) as well as to the importance of the phenomenon both for safety and performance issues.

In the absence of a hydrocode capability, or with insufficient time to use it adequately, there are still many simple, yet useful, calculations that can be made. The shock sensitivity plane (SSP) displays both wedge test results (Pop plots) and the results of hydrocode calculations by Lundstrom<sup>32</sup> to provide a very accessible framework for such analyses. The ordinate of the SSP, shown in Figure 3, is the shock pressure ( $P_1$ ) entering an explosive in the wedge test that exactly results in a one-centimeter ( $x = 1 \text{ cm}$ ) run distance to detonation. The abscissa ( $S$ ) is the slope of the Pop plot of  $\log P$  vs.  $\log x$ :  $[S = \log x / (\log P_1 - \log P)]$ , or  $x = (P_1/P)^S \text{ cm}$ . Each explosive is assumed to have an exactly linear Pop plot, and this results in a single point for each explosive in the SSP. Lundstrom obtained the curves in the figure corresponding to the various test results with reactive-hydrocode calculations for specific explosive properties as defined in the SSP. Any explosive point that lies above the line corresponding to a particular test will not detonate in that test, whereas, any explosive that lies below the test curve will detonate. Some explosive and propellant values are shown in Figure 3 to aid in practical use of the figure as it stands.

The author has found that the following analytical relationships agree quite well with the SSP. For example, the functional relationship between an explosive's critical diameter ( $D_c$ ), the Pop plot slope,  $S$ , and the SSP pressure,  $P_1$ , defined above is given quite well by equation (3-1). The more cumbersome relationship of equation (3-2) fits the SSP curves for the NOL Large Scale Gap Test (LSGT).

$$\begin{aligned} \log P_1 &= 1.9123 + 0.04173 S + 0.1108 (\log D_c / \log S), \text{ Kbar} \\ \log D_c &= 9.025 (\log S (\log P_1 - 1.9123 - 0.04173 S)), \text{ cm} \end{aligned} \quad \text{or} \quad (3-1)$$

$$\log P_1 = A - B \log (\log S) \quad (3-2)$$

where:  $A = 1.9454 - 0.0259 G - 0.1466 G^2$   
 $B = 0.42227 + 0.12673 G - 0.36195 G^2 + 0.15377 G^3$ , where  $G = \text{PMMA gap thickness, inches}$

Equation (3-2) fits all the card gap curves in Figure 3 well except for that corresponding to zero (0) cards. It is reasonable that this is the point at which the relationship fails, since any material that does not detonate in a card gap test of a given size is not following the same relationship as those that do. Figure 4 shows the results of calculations with equations (3-1) and (3-2) for comparison with Figure 3. There is some question about the validity of values of  $D_c$  shown in Figure 3 for some non-ideal explosives due to the rate equations used in the hydrocode that generated the results.<sup>70</sup> For example,  $D_c$  for Destex has been variously reported at values of 6, 10 and 38 mm.

Both critical diameter and NOL LSGT tests are required for qualification of energetic materials. It is obvious from Figure 3 that there is some orthogonal relationship (i.e., they intersect) between card gap values and critical diameter (except for those corresponding to the highest values of  $P_1$ ). Therefore, it should be possible to convolve the results of card gap and critical diameter measurements into a corresponding point in the SSP. Equations (3-1) and (3-2) may aid the task by solving for  $P_1$  and  $S$  for measured pairs of  $D_c$  and card gap thickness values.

The critical impact velocity ( $V_{det}$ , lowest impact velocity (flat-on-flat) that will cause an SDT reaction) for explosives was investigated by several different curve-fitting approaches. The results of both approaches are given by equation (3-3) for "chunky" or cylindrical-rod steel impactors of diameter,  $d$ . Because of impedance matching effects, results will have some dependence on the shock Hugoniots of the impactor and unreacted explosive materials.

$$V_{det} = P_1 e^{at} / (44 |d/6|^{1/(2S)}), \text{ km/s} \quad (d \text{ in mm} > D_c) \quad \text{or} \quad (3-3a)$$

$$V_{det} = 10^A e^{at} / 10(B \log d) \quad (3-3b)$$

where:  $A = .6663 - .346 S + 0.007462 P_1$   $(d \text{ in mm} > D_c)$

$$B = 1.0663 - .346 S$$

$t$  = case thickness, mm

$a$  = an effective attenuation coefficient that depends on the case material,  $a = 0.073$  for steel,  
 $a=0.04$  for Al,  $a = 0.08$  for Plexiglass (PMMA). Attenuations may be combined for  
lined cases. See Appendix C for additional treatment.

The attenuation coefficient in equation (3-3) is an artifice that nevertheless can be used to account for non-planar shock wave effects that occur on propagation through cases thicker than about one fragment radius. Using impedance matching techniques, as shown in Appendix A, the matched pressure into the explosive (ignoring attenuation effects) can be calculated both for bare and covered (cased) explosives. Effects of some material impedance mismatches actually increase the sensitivity of an explosive in a thin cases. For example, as Appendices A and C show, for a steel impactor upon a thin aluminum case, the matched pressure into the explosive is actually greater than with the bare explosive. This has been confirmed by experiment.<sup>37</sup> Therefore, for situations of marginal sensitivity to shock initiation, selection of case and liner materials can be critical. However, with reasonably thick cases ( $t>d/2$ ), the effect is probably overwhelmed by the effects of release waves combining with the primary shock.

Equations (3-3a) and (3-3b) become less applicable toward the right side of the SSP. Equation (3-3b) fits nearly perfectly to data for explosives PBX-9404, Comp B, and Destex for  $d>D_c$  but its validity beyond that range of explosives is unknown. Equation (3-2a) fits all data less accurately. These equations were based on experiments involving planar geometry and would have to be modified to include curvature effects for typical munitions.

For  $d < D_c$ , equation (3-4) was obtained by fitting data for Comp B and Destex. However, there is very little work reported in this regime, particularly for explosives with relatively large critical diameters, and the equation should therefore be used only with extreme caution.

$$V_{det} = \exp(0.6 S D_c/d) e^{at}, \text{ km/s} \quad (\text{for } d \text{ in mm} < D_c) \quad (3-4)$$

The lack of a term in equation (3-4) related to  $P_1$  is initially disturbing until one realizes that the region of applicability (i.e.,  $d < D_c$ ) is a function of  $P_1$ . The values given by equations (3-3) and (3-4) are based on a limited number of curve fits to SSP results. This problem can be treated with more basic approaches, as shown in Appendix C, similar to those of Greene<sup>33</sup> and James,<sup>34</sup> or of course, with hydrocodes.

For impacts by spherically tipped (instead of flat tipped) projectiles with sphere-tip radius equal to rod radius, a rough rule of thumb obtained from the work of James and Hewitt<sup>35</sup> is that about a 50% to 100% higher impact velocity is required to initiate detonation than with flat-tipped projectiles:

$$V_{det(sph)} = G V_{det(flat)}, \quad (3-5)$$

where  $G$  ranges between about 1.4 (tungsten) and 1.8 (steel) and depends on the impactor material as well as on the explosive material, impactor and case dimensions, and impact velocity. The experimentally-based work of Liddiard and Roslund<sup>36</sup> indicates the factor in equation (3-5) is in the same range as their results. Their work is recommended as an alternate method of calculating. A future step in these studies will be to relate the constants in the Liddiard, Roslund report to the SSP. (Sewell's relationship that can be expressed as  $d_{sph} = d_{flat} (0.4393 V_i - 0.060814 V_i^2 - 0.00029359 V_i)^3$  in equation (3-3), seems to give values of  $d_{sph}$  for low  $V_i$  that are lower than reported data.)<sup>79</sup> Ferm and Ramsay<sup>82</sup> give  $d_{sph} = (2x + d_{cr}) (1 + (c_0/V_i)^2)^{1/2}$  (See Appendix C and reference 82).

For rods with the spherical tip radius greater than the rod radius,  $V_{det(sph)}$  is lower and approaches, with increasing sphere radius, the value for a flat-tipped rod. The relationship of  $V_{det(sph)}$  to the relative radii of the rod and sphere is given by equation (3-6), which is also applicable with some amount of protective case on the explosive, provided the value of  $V_{det(flat)}$  also applies to the cased explosive.

$$V_{det(sph)} = V_{det(flat)} \times 10^{(0.2785 r_{rod}/r_{sphere})} \quad (3-6)$$

For cone-tipped projectiles, James' recent work shows a dependence of  $V_{det}$  on cone angle,  $\eta$ .<sup>37</sup> As a rough rule of thumb, equation (3-7) gives the relationship of increasing  $V_{det}$  as a function of decreasing cone angle (where a flat surface has a 180° cone angle).

$$V_{det(cone)} = V_{det(flat)} (1 + 0.0183 [180 - \eta]), \text{ for } \eta \text{ between } 180^\circ \text{ and } 120^\circ. \quad (3-7)$$

Equation (3-7) is also applicable with some amount of protective case on the explosive.

For oblique impacts of flat-faced projectiles, a rule-of-thumb used by Sewell<sup>38</sup> is that the critical impact velocity,  $V_{det}$ , is increased by about 61 m/s for every one-degree increase of obliquity.

$$V_{det(obl)} = V_{det(flat)} + 61\alpha, \text{ m/s, where } \alpha \text{ is the angle of obliquity in degrees.} \quad (3-8)$$

For side-on impacts against cylindrical munitions, the effect of this trend alone can be expressed as a probability less than unity of SDT given a randomly located impact of a specific size projectile at a specific velocity. This is because at most fragment impact velocities (for example the 2,530 m/s "unaimed" IM fragment impact test) there may be a large invulnerable area that can result in hits that do not cause SDT. For example, consider a fragment impact scenario against a cylindrical munition for which the fragment velocity is equal to  $V_{det(obl)}$  as calculated by equation (3-8) for a = 20°. For impacts at all angles greater than 20° off the cylinder normal (assuming flat projectile face normal to direction of travel), the target will not detonate by an SDT mechanism; since  $\sin 20^\circ = 0.34$ , this represents a 66% probability that a single randomly located impact on the cylinder will not cause a detonation by SDT. This isn't as good as it sounds, since with only 3 such impacts on the cylinder, the detonation probability rises to 96%. Sewell<sup>46</sup> suggests that if the angle of obliquity (or for pointed impactors, the cone angle of equation (3-7)) exceeds the minimum jetting angle for the impacting materials, the impulsive load follows dynamic pressure relations (of equation (4-4)) rather than shock wave equations. The critical angle range for jet formation for steel upon steel impacts is given by equation (3-9).<sup>71,76</sup>

$$\tan^{-1}(5.945/V_i) > 0_j > \sin^{-1}(0.864/V_i), \text{ degrees, with } V_i = \text{impact velocity in km/s} \quad (3-9)$$

where  $0_j$  is the angle the projectile surface tangent makes with the target surface.

Johansson and Persson<sup>39</sup> show a relatively small effect of obliquity upon bare explosive for angles up to 8°. At larger angles of obliquity an abrupt increase in critical impact velocity commences.

If the explosive is cased in a warhead or rocket motor, as is the usual situation of IM interest, applicability of equations (3-3) and (3-4) to closely related data should be checked before using them. For impactors of diameter less than the explosive's critical diameter (such as the IM test fragment (2,530 m/s) or a shaped charge jet), SDT can apparently occur with very high impact velocities, although there are speculations that a shear heating and ignition mechanism could be operating (see next section).<sup>47</sup> Chick<sup>74</sup> cited an empirical observation that prompt surface impact (SDT) initiation of bare explosives can occur with shaped charge jet impact for ratios of  $D_c/d < 5$ . For this situation, equation (3-10) can be used to obtain the critical jet impact velocity.

$$V_{ji}^2 \rho d = \text{a constant, where } \rho = \text{jet density} \quad (3-10)$$

Chick ascribes initiation occurring when  $D_c/d > 5$  to the bow wave of the penetrating shock. It is also possible for shear heating effects to operate in this second situation.<sup>47</sup> For this situation, equation (3-11) can be used to obtain the critical jet velocity for bow wave initiation. Data reviews can be used to obtain values of the constants for particular materials.

$$V_{jb}^2 d \rho^{1/2} = \text{a constant} \quad (3-11)$$

### Section Summary

The minimum fragment impact velocity  $V_{det}$  that will initiate SDT reaction of an explosive can be estimated by the equations given in this section. The equations given apply only to "rod" or "chunky" fragments. (The shorter duration shocks caused by flyer plate impacts (generally of radius more than six times thickness)<sup>34</sup> require higher shock pressures (higher velocity) to cause SDT.) With these equations one may now estimate probabilities of SDT given impact by the fragments generated in the previous section. Other factors that decrease fragment velocity and spread the fragment pattern and otherwise reduce the chances of an impacting fragment detonating a munition were given by Wagenhals, et al<sup>40</sup> and are summarized in Figure 5. Drag data on warhead fragment shapes are available for application to problems of this type.<sup>65,69</sup> An orthogonal relationship between card gap test results and critical diameter exists that may permit generation of SSP loci for energetic materials on the basis of those two common tests without the need to perform wedge tests in all cases.

### **OTHER REACTION MODES INITIATED BY IMPACT**

SDT initiation modes for cased explosives may be envisioned as occurring in the time frame prior to projectile perforation of the case. Other impact initiation modes than SDT are too complicated for simple analysis. Specifically, at this time a priori prediction of reaction violence is not possible. The mechanisms by which these modes occur are not known with certainty, and analytical and experimental research in these areas is ongoing. The basic mechanisms, as currently envisioned, are:

1) XDT, by which damaged explosive can be initiated by lower impulsive loads than required for SDT, with the damage appearing as voids from structural failure of the explosive due to physical damage by the current load or shock effects of the current load that cause tension failure. (Preshocking can also reduce an explosive's SDT sensitivity by compression and presumably reducing the concentration of hot spot sites.) Fairly small void volumes (a few percent) can cause significant increases in an explosive's SDT sensitivity. (Increased shock sensitivity caused by prior damage would logically be classified as an SDT, however, with a different locus on the SSP.) Apparent XDT mechanisms in bullet impact tests against rocket motors and rocket motor simulants have been reported to be influenced slightly by the nature of the motor case and greatly by the bore dimensions of the propellant grain.<sup>41,42</sup> No analytical model for this phenomenon is presented here.

2) DDT, by which ignition and burning of the explosive creates pressure that compresses the explosive and at the same time builds the pressure to a level with a rate that forms a shock wave. DDT generally requires a substantial initial void volume.

3) All other mechanisms of impact-induced reactions lead initially to propellant burning. Then, depending upon a number of factors, the reaction (1) may continue to completion as burning, (2) may increase in violence to cause a case burst with some projection of debris (what is referred to as "deflagration" in reference 11), (3) may consume explosive at a nearly sonic rate causing an explosion, or (4) may build to a detonation as in a DDT.

The first requirement for these mechanisms to occur is penetration of one wall of the munition case. More often, perforation is required since this leaves the projectile with some excess kinetic energy after penetrating the case wall. Perforation is defined as complete penetration without plugging. (There have been only a few examples of initiation of serious reactions by projectiles that did not have sufficient energy for case penetration.) Figure 6 is a "phase diagram" of the various phenomena that may occur upon projectile impact.<sup>43</sup> The tip shape of the projectile has only a small effect on the perforation-ballistic limit for normal impact. For complete perforation, the ballistic limit of conically tipped projectiles is slightly larger than for flat faced projectiles. Also, rounded or conically tipped projectiles will have a greater tendency to ricochet at oblique impact angles, particularly when the impact obliquity angle exceeds the tip half-angle.<sup>44</sup> The ballistic limit of a steel case can be calculated approximately by the equation<sup>45</sup>:

$$V_{50} = C \{4 \rho t A / (\pi m \cos \theta)\}^{1/6}, \text{ m/s} \quad (4-1)$$

where:  $C = 332.43 + 171.06 B - 14.286 B^2 - 3.1111 B^3$

$B = \text{BHIN}/100$  (BHIN = Brinell hardness number).

$\rho$  = projectile density.

$t$  = case thickness, cm.

$A$  = projected frontal area of projectile,  $\text{cm}^2$ .

$m$  = projectile mass, grams.

$\theta$  = angle of obliquity of impact. For a cylindrical target it is the tangent angle at the impact point.

This equation applies for a blunt projectile and a steel case that is thick enough that the bracketed term in equation (4-1) is always greater than 0.125. For other case materials than steel the equation may become more complicated and the cited reference<sup>45</sup> should be used.

For harder aluminum alloy case materials, the ballistic limit equation is given approximately by equation (4-2).

$$V_{50} = \{190 [4 \rho t A / (\pi m \cos q)]^{1.75} + 120\}, \text{ m/s} \quad (4-2)$$

If the ballistic limit is exceeded, the projectile moves into the case material with an initial residual velocity given by equation (4-2):

$$V_r = (V_i^2 - V_{50}^2)^{1/2} (1 + \rho_c t / \rho_p l) \quad (4-3)$$

where:  $V_i$  = initial projectile velocity

$l$  = length of impactor

$t$  = thickness of case

$\rho_c$  = density of case material

$\rho_p$  = density of projectile material

Ignition of the energetic material will occur by a combination of heat from the case debris and projectile after their violent impact and heat generated by shear heating as these items move through the energetic material. The least damage that can be caused to the energetic material is the hole through which the metallic intruders have moved. It is more common to have severe breakup of the energetic material due to these intruders. This generates increased surface area that can burn following ignition and result in a very rapid pressure rise.

Sewell and Graham<sup>46</sup> use equation (4-4) to calculate the dynamic pressure generated as a projectile penetrates explosive.

$$P_{dyn} = 1/2 r_e V_r^2 C_D \times 10^{-9} \quad (4-4)$$

where:  $P_{dyn}$  is in GPa if the explosive density,  $r_e$ , is in kg/m<sup>3</sup>, and is  $V_r$  in km/s.

$C_D$ , the drag coefficient = 2.68 for velocities of interest:  $V_r > 100$  m/s or  $C_D = 1.8$  for  $V_r < 100$  m/s.<sup>46</sup>

This dynamic pressure is then combined with the work of Frey<sup>47</sup> to obtain a temperature in the shear-heated explosive based on an assumed shear heating mechanism. If one assumes the shear velocity is equal to the projectile residual velocity, equation (4-5) approximates temperature rise as a function of residual velocity. This may be used, if the "ignition temperature" of the energetic material is known, to make a first approximation to the lowest residual velocity that might cause ignition.

$$T = 25 + 0.4 V_r + 0.003 V_r^2, ^\circ\text{C} \text{ with } V_r \text{ in m/s} \quad (4-5)$$

Any temperature rise due to shear heating competes with cooling thermal conductivity and phase change effects. Nevertheless, equation (4-5) gives as a rough approximation, 350 m/s as an approximate minimum residual velocity required to ignite more sensitive energetic materials. (It must be recognized that the concept of an "ignition temperature", being a dimensional balance between a source temperature, heat loss by conduction and phase change, and exothermic decomposition, must be used cautiously. The methods used in this paper's section on slow cookoff can be used to estimate an ignition temperature for appropriate shear-layer thicknesses with known durations of heat addition.) Melting of the energetic material will absorb heat and increase the velocity required for ignition. Heating of the projectile during case penetration and hot spall will tend to reduce the velocity required for ignition.

Sewell and Graham<sup>46</sup> also proposed calculations of case confinement effects, including projectile induced venting, on reaction buildup (specifically, by the buildup of internal pressure). To make such calculations in a meaningful way one must also know the burning-rate slope vs. pressure for the contained energetic material and the surface area of the burning portion as a function of time. For very rapid reactions, the dynamic confinement conditions of the reacting region, rather than the static conditions given by measurable case burst pressure are critical.

Recent work<sup>48</sup> reports a relationship between response of munitions to the bullet impact test (0.50-caliber) and response of the energetic materials to friability (shotgun and relative quickness - pressure rise rate) tests and hot ball ignition (800°C).<sup>18</sup> The results show absence of reaction or only mild combustion in bullet impacts up to 1,140 m/s for explosives whose laboratory tests give 0.5 MPa/ms quickness and no ignition with the hot ball test. Combustion and

give 0.5 MPa/ms quickness and no ignition with the hot ball test. Combustion and deflagration reactions in bullet impact were reported corresponding to pressure rise rates of 3 to 7 MPa/ms and ignition occurring with the hot ball. With hot ball ignition, materials with quickness of about 8 to 20 MPa/ms showed mostly deflagrations with one reaction ranked an explosion (HMX/polyurethane (PU) at a projectile impact velocity of 1,140 m/s) in the bullet impact test, and for quickness above 24 MPa/ms a mix of explosions and detonations. Comp B explosive detonated in all its bullet impact tests at velocities above 740 m/s and had a quickness of 114 MPa/ms.

Ammonium perchlorate (AP) containing materials have a shock-to-ignition threshold considerably lower than their threshold for detonation. Some iron-containing burning-rate catalysts can greatly reduce the ignition temperature as well as the friction sensitivity of AP. For some other energetic materials, the thresholds for shock ignition and SDT seem to be quite similar.<sup>34,49</sup> Figure 7, taken from the work of Anderson and Louie shows a relationship between detonation and ignition thresholds for a material comprised of 75% HMX and 25% PU.

Liddiard's results on low level shock-induced ignition in water-attenuated shock-ignition tests<sup>80,46</sup> tend to follow a  $P^n t =$  constant relationship, with  $t$  between 5 and 50  $\mu\text{s}$  and  $n$  between 0.7 and 2.6. In general, the percentage standard deviation of the constant for a specific explosive is between 10% and 25% over the entire range of data. For TNT-based explosives,  $n$  tends to be about 2 (1.7 to 2.6), indicative of a critical energy relationship; for plastic-bonded explosives,  $n$  tends to be about 1 (0.7 to 1.6), indicative of a critical impulse relationship. However, there are exceptions, for example, for the two data points for PBXC-117 explosive at  $P=7.8$  and 10.1 kbar,  $n=2.2$ ; and two of the eight data points for PBX-9404-03 show considerable irregularity, although they have little influence on the average value of  $n = 1.5$ . The one fairly stable factor in the water-attenuated tests is that the minimum shock pressure that will cause ignition in a large number of explosives is about  $5 \pm 2$  kbar (there are some exceptions apparent in the data).

The effect of multiple bullet impacts on a cased energetic material can be significant, as shown in Figure 8, which is taken from the work of Milton and Thorn.<sup>50</sup> All of the propellants tested by Milton and Thorn contained RDX or HMX, and were shock detonable if struck hard enough. Also, Milton and Thorn found .223-caliber bullets more effective in causing violent reactions than .50-caliber bullets. A possible reason for this is that the hyperdamaged zone for the .50-caliber bullets may have been larger than the propellant samples themselves. When the first bullet grazed the edge of the grain bore, more propellant was damaged and the probability of a closely placed second bullet causing a very violent reaction was increased. Although it is premature to use this work to generate analytical relationships, it is clear that if a bullet impacts a region damaged (but not "destroyed") by a previous bullet the reaction will often increase in violence, presumably because of the increased sensitivity and surface area of the damaged energetic material.

### Section Summary

Projectiles with insufficient energy to initiate prompt detonation of a munition can still cause reactions that range in violence from burning through deflagration, explosion and detonation. From a simple analytical standpoint, it is possible to do little more than estimate the perforation of the case and ignition by shear heating. Parametric studies can be done involving as variables, burning rate vs. pressure, case vent area, and burning surface area. Such studies can be used to estimate the case vent and energetic material damage conditions that will permit pressure buildup to levels that cause hazardous case bursts; in fact, such studies have been done.<sup>51</sup> One must always be aware that stimuli or environmental conditions like confinement may be outside the range of available data. A protocol for assessment of the many effects related to impact initiation is in preparation.<sup>74</sup>

## THERMAL THREATS

Exposure to high temperatures will initiate reaction in energetic materials. Two heating rate regimes are of concern, (1) rapid heating by flame impingement directly on munitions, and (2) slower heating as might occur in an area subject to heating, but without direct flame impingement on munitions. The first of these conditions is exemplified by the IM fuel-fire fast cookoff test (FCO)<sup>1,11</sup> or the wood-based bonfire test.<sup>14</sup> At such heating conditions, bare munitions are brought to ignition in about one to five minutes, depending on design details and specific test-fire conditions. The second condition is tested, in extremis, by the IM slow cookoff test (SCO) at a heating rate of  $6^\circ\text{F}/\text{hr}$  ( $3.3^\circ\text{C}/\text{hr}$ ). Assessment of threat conditions indicates a wide range of possible intermediate heating rates, with  $50^\circ\text{F}/\text{hr}$  ( $27.8^\circ\text{C}/\text{hr}$ ) being a reasonable estimated likely minimum heating rate under shipping or storage conditions.<sup>52,53</sup> In this section, simple analytical methods for calculating cookoff behavior are presented.

## FAST COOKOFF

The most important thing one can do to analyze the fast-cookoff problem of a munition exposed to direct flame impingement is a heat transfer analysis. The reason for making this statement is the presumption that if the energetic material, exposed to the rapidly rising temperature of a flame impinging on its case, gets hot enough to ignite, it will.

Fifteen years ago Vetter<sup>54</sup> proposed using pyrolyzable outgassing liners to build up decomposition gas pressure, collapse the grain (for star perforated propellant grains) and expose the case for a short time to direct flame heating with no radial backwall heat conduction path. Vetter demonstrated the feasibility of this approach with stress analyses. This model was further presumed to be correct on the basis of previous and subsequent test results, and was subsequently proved by IMAD tests that used real time X-ray (side view) and video cameras (longitudinal view through the nozzle).<sup>66</sup> Pakulak has reported the use of outgassing liners in warheads with violence reducing effects when combined with stress risers or other mechanical case venting mechanisms.<sup>55</sup> Although these approaches do not yield easily to simple analyses, it is possible to calculate generated gas pressure at temperature from the liner material and apply the calculated pressure to heated case burst or explosive ejection calculations.

For heat transfer analyses, simple one-dimensional cylindrical analysis will be adequate (if applicable to the munition geometry) for metal cased munitions, if there are no other heat paths from the munition case to the interior of the propellant (for example, metal bulkheads) and no important end heating effects. Non-metal cases, such as fiber/epoxy composites, will experience charring, burning, and other physical changes that obviate the use of a simple heat-transfer calculation.

The most critical factor in a heat transfer calculation simulating a fast-cookoff heating scenario is the selection of the proper heat flux to the munition. Measurements at Sandia National Laboratories<sup>56</sup> determined a maximum heat flux in large hydrocarbon pool fires of about 160 KW/m<sup>2</sup>. The decrease in heat flux as the surface temperature of the heated cylinder rises can be approximated by equation (5-1) for surface temperatures up to about 1350°F. These values are consistent with those measured at the Naval Weapons Center in the late 1970s (6 - 10 BTU/in<sup>2</sup>-sec). In open propane burner tests, the heat flux values are about one-half the magnitude of those in liquid hydrocarbon fuel fires.

$$Q = 0.75 (156 - (T_s/100)^2), \text{ KW/m}^2 \quad \text{or} \quad (5-1)$$
$$Q = 0.062 (156 - (T_s/100)^2), \text{ BTU/sec-ft}^2$$

where:  $T_s$  = munition surface temperature in Kelvins (K), ( $K = ({}^\circ F - 32)/1.8 + 273.15$ )  
 $R_O$  = outer radius of munition

The numbers in equation (5-1) can be increased for larger or hotter fires, or decreased for smaller or less sooty fires. This heat flux is many times greater than would be obtained by assuming an initial heat flux from an outer wall at the nominal flame temperature (1500°F) flowing to an inner wall at ambient temperature (for example, 70°F), and that is why this factor is so critical.

Because the thermal conductivity of the metal case is at least 100 times higher than that of the liner or energetic material immediately in contact with its inner surface, as a first approximation, the case wall temperature rise can be approximated by the ignoring heat flux from its backwall ( $Q_{\text{liner}}$ , which ranged from < 2% to 7% of the influx). Ignoring the backwall heat flux in equation (5-2) reduces calculated time to cookoff by about 3%.

$$T_{\text{ave}} = T_{\text{ave}(t-\Delta t)} + (Q' - Q_{\text{liner}}) \Delta t / (C_p c_{\text{case}} \pi \rho (R_O^2 - R_i^2)) \quad (5-2)$$

where:  $T_{\text{ave}}$  = average case wall temperature. The subscript,  $(t-\Delta t)$ , represents condition at previous time step.  $T_s = T_{\text{ave}} + \Delta T/2$ , see equations (5-1) and (5-3).  
 $R_O$  = outer case wall radius.  
 $R_i$  = inner case wall radius.  
 $Q' = 2\pi R_O Q$  (assuming unit length cylinder)  
 $C_p c_{\text{case}}$  = specific heat of case  
 $\Delta t$  = time step used in step-by-step calculation.

The temperature gradient through the case wall is given by the usual cylindrical heat flow equation:

$$\Delta T = Q' \ln (R_0 / R_i) / 2\pi k_{\text{case}} \quad (5-3)$$

where:  $k_{\text{case}}$  = thermal conductivity of case.

The heat flux through the liner/insulator is calculated by:

$$Q_{\text{liner}} = 2\pi k_{\text{ins}} \Delta t (T_{\text{ave}} - \Delta T / 2 - T_{\text{liner}}(t-\Delta t)) / \ln (R_i / R_p) \quad (5-4)$$

where:  $k_{\text{ins}}$  = thermal conductivity of liner.

$T_{\text{liner}}(t-\Delta t)$  = temperature of inner surface of liner or outer propellant/explosive surface.

$R_p$  = radius of inner liner surface or outer propellant/explosive surface.

Finally, the propellant/explosive surface temperature is approximated by considering Arrhenius kinetics and using the method of Appendix B, although in the earliest runs ignition was postulated to occur (instantly) upon reaching energetic material surface temperatures greater than some value (both 550 and 980°F were used).

Although the approach is quasi-steady state, the problem is stable enough to give a solution. A spreadsheet has the advantage that numerical instabilities can be spotted immediately and bootstrapped across. The problem can be set up on spreadsheet and run, all in a fraction of an hour. The values used in these calculations are shown in Table I. I have found that these equations are solved reasonably well with a spreadsheet using 1-second steps.

Figure 9 shows the results of some fast cookoff calculations with the spreadsheet. The results show calculated energetic material "surface" temperature vs. time. All these calculations were for 8-inch diameter cylindrical munition cases including AP/HIPB composite propellant b (from Table II) in cases with 0.1 inch aluminum, 0.1 inch steel, and 0.5 inch steel wall thicknesses, each with 1/8 and 1/4 inch of insulation/liner, and PBXN-109 explosive (also from Table II) in a 0.5 inch thick case with 1/8 inch liner. The calculated cookoff times are reasonably consistent with data.<sup>57</sup>

When a similar calculation was attempted with a composite case, such a large temperature gradient built up through the case wall that it was obvious the case would be destroyed by the fire before conducted heat could ignite the energetic material. It is clear therefore, that a more complicated procedure is needed for composite case fast-cookoff analysis.

Table I. Thermal Properties Used in Fast Cookoff Heat Transfer Calculation\*

Material	$k$ (BTU/hr-ft-°F)	$C_p$ (BTU/lbm-°F)	$\rho$ (lb/ft <sup>3</sup> )
Aluminum	130	0.21	169
Steel	25	0.11	490
Insulation	0.1	0.2	100
Propellant	0.1	0.2	110

\* "English" units used because of availability of data tables.

There is currently no a priori method for calculating the violence level to be expected in a fast cookoff reaction. If all pertinent parameters (material condition, vent area to burning surface area, thermal parameters, burning rate and slope, case strength at all locations, etc.) are known, or can be reasonably estimated, such a calculation could be attempted - but it would involve a fairly large effort, in the context of this paper. Reaction violence cannot be calculated in a simple way with the present state of the art.

### Section Summary

Simple one-dimensional quasi-static heat transfer calculations can be used to estimate fast cookoff times of cylindrical ordnance with metal cases. However, modern, low conductivity composite cases cannot be analyzed in the same way. The most critical parameter for the analysis is the heat flux to the ordnance submerged in a jet-fuel fire. Good values for material thermal

## SLOW COOKOFF

From the perspective of preparing IMTHAs and IMTPs, there are two pertinent questions concerning slow cookoff analysis. First, how will the munition react in the standard IM SCO test (heating rate, 6°F/hr), and second, what other heating rates are of operational importance, and how will the munition react at those heating rates?

From the perspective of IM preliminary design, the question of how design variables will affect the heat flow, total cookoff time, and the ignition site are important. Of course, the ideal solution would also predict reaction violence and its dependence on design variables, but that is currently beyond even the most sophisticated analytical methods. Simple methods for predicting slow cookoff reaction violence will not be available until more complex methods have succeeded and the important physical parameters are identified and routinely measured and reported.

The primary equation of thermal decomposition and heat transfer applicable to predicting thermal explosion is equation (6-1), the Frank-Kaminskii differential equation. For materials that undergo physical changes, it may be necessary to include appropriate changes in density and thermal conductivity (and even Z and E) during the calculation. For materials that melt, it may be necessary to include a convection term in the heat transfer calculation.

$$-\lambda \nabla^2 T + r C_p (dT/dt) = r Q Z w \exp(-E/RT) \quad (6-1)$$

(The Laplacian operator  $\nabla^2$ , in the special cases of spheres, infinitely long cylinders, and infinite slabs, reduces to  $\nabla^2 T = (\partial^2 T / \partial x^2) + (m \partial T / \partial x)$ .)

where:  
λ = thermal conductivity, cal/s-cm °C  
T = temperature, K  
ρ = density, g/cm<sup>3</sup>  
C<sub>p</sub> = specific heat, cal/g-K  
Q = heat of reaction, cal/g  
Z = collision number, sec<sup>-1</sup>  
w = mass fraction of undecomposed energetic material, = 1 for 0<sup>th</sup> order solution.  
E = activation energy, cal/mole  
R = gas constant, 1.987 cal/mole-K  
m = shape factor: 0 for slabs, 1 for cylinders, and 2 for spheres.

Table II gives values of the constants in equation (6-1) for a number of energetic materials.

When the reaction heating term (the right side of equation (6-1)) is zero, the equation is the well known heat flow equation. Because equation (6-1) is not solvable in closed form, it is common practice to solve it for the limiting adiabatic boundary condition,  $\partial T / \partial t = 0$ . This defines the critical temperature, T<sub>cr</sub> in equation (6-2). If the exposure temperature is less than T<sub>cr</sub>, self-heating ignition will never occur.

$$T_{cr} = E / (R \ln ((a^2 \rho Q Z w) / (T_{cr}^2 \lambda \delta R))) , \text{ Kelvins, K} \quad (6-2)$$

where:  
a = slab half-thickness or cylinder or sphere radius.  
δ = shape factor (0.88 for slabs, 2 for cylinders, and 3.32 for spheres).

Note that the unknown variable, T<sub>cr</sub>, appears on both sides of the equation. Equation (6-2) can be quickly solved iteratively on a pocket calculator; it is helpful to note that the left side of the equation is relatively insensitive to the guessed value of T<sub>cr</sub> on the right side. A 20 K error in T<sub>cr</sub> on the right side leads to an error of only about 1 K on the left. If an energetic material is exposed to a temperature greater than T<sub>cr</sub> it will eventually cook off. The time to cookoff can be calculated from equation (6-3).

Table II. Thermal Phenomena: Critical Temperatures\* and Parameter Values for Explosives.

Explosive	T <sub>cr</sub> (°C)	$\rho$ (g/cm <sup>3</sup> )	Q (cal/g)	Z (s <sup>-1</sup> )	E (kcal/m)	$\lambda \times 10^4$ (cal/g/s/K)	C (cal/g/K)	T <sub>d</sub> °C**
HMX	253	1.81	500	5 (19) #	52.7	7.0	.27	287
RDX	215	1.72	500	2.015 (18)	47.1	2.5	.27	204
TNT	287	1.57	300	2.51 (11)	34.4	5.0	.36	300
PETN	200	1.74	300	6.3 (19)	47.0	6.0	.25	202
TATB	331	1.84	600	3.18 (19)	59.9	10.0		384
DATB	320	1.74	300	1.17 (15)	46.3	6.0	.23	
NQ	200	1.63	500	2.84 (7)	20.9	5.0	.3	
HNS	320	1.65	500	1.53 (9)	30.3	5.0	.4	
N-109		1.68	525	1.023 (14)	36.5	13.0	.34	
NC		1.5	500	8.46 (18)	48.5	3.0	.31	
AP/HTPB <sup>a</sup>		1.806	500	1.29 (10)	32.8	12.7	.31	
AP/HTPB <sup>b</sup>		1.715	300	1.35 (8)	27.0	7.5	.29	

\* Lowest experimental values for "a" between 0.003 and 0.039 slab cm thickness.

# Numbers in parentheses are powers of ten.

\*\* T<sub>d</sub> represents deflagration point or ignition temperature (shown for comparative information only).

<sup>a,b</sup> Typical values for two different (AP/HTPB) reduced smoke composite propellants.

$$t_{co} = (\rho C a^2 / \lambda) F_n \quad (6-3)$$

where:  $F_n = 10^{lc}$

$lc = -0.008511 - 0.0173 v - .0061754 v^2 + 4.0756 \times 10^{-5} v^3$ , for a cylinder geometry.

$v = E / ((1/T_{cr}) - (1/T))$ , where T is the environmental temperature.

For a sphere, the value of F<sub>n</sub> is about 1/2 as large, and for a slab about 2.5 times larger.

Equations (6-2) and (6-3) are readily set up in the memory of an inexpensive pocket calculator for solutions within a minute of problem definition.

Solution of equation (6-1) with the SINDA finite difference code (one-dimensional spherical geometry) and RDX parameters given in Table II is compared in Figure 10 with measured values.<sup>59</sup> The agreement is virtually perfect. The results of quasi-static spreadsheet calculations of time to cookoff for an 8-inch diameter cylinder of RDX are shown in Figure 11 for a wide range of heating rates and initial soak temperatures; the same results were obtained with the SINDA code. These results are remarkably consistent with measured cookoff times for ordnance of similar size. The result is relatively automatic, since when thermal explosion occurs in the calculation it "blows up" the computer run. The spreadsheet solution of the slow cookoff problem uses equations (5-3), (5-4), and (6-1) with the RDX values from Table II, and the cylindrical item divided into 10 calculation shells of equal thickness. Calculated thermal profiles for the RDX problem are shown in Appendix B along with more explanation of the calculation. Calculations with a reduced-smoke propellant were similarly successful. The method has also been used to successfully model reduced smoke propellants in the NWC 25°F/hr Slow Cookoff Visualization (SCV) Test (190 gram, 2-inch long cylindrical sample [Table II<sup>a</sup>] in glass tube: measured cookoff time and temperature: 7.88 hrs/436°F; calculated: 7.55 hrs/438°F) and 18°F/min differential thermal analysis (DTA) test (0.5 gram spherical sample [Table II<sup>b</sup>]: measured cookoff time and temperature: 23 min/494°F; calculated: 23.5 min/503°F). The problem is relatively unstable and calculational time steps must be selected appropriately depending on heating rate, physical dimensions, density, and heat transfer parameters of the materials and the various interfaces involved. Spreadsheets requiring 2Mbytes of memory are not uncommon. The spreadsheet method fails for very small samples in which thermal gradients cannot be approximated linearly in reasonable time step sizes.

There are no currently available simple methods for calculating the violence of slow cookoff reactions. Recent research indicates the importance of energetic material type, condition, and dynamic confinement at the instant of ignition.<sup>60-64</sup> When calculation methods become available they will operate in the microscale regime of time steps comparable to those required in reactive hydrocode calculations of SIDI and in DDT analyses.

### Section Summary

Simple hand analysis of the slow cookoff problem is limited to simple symmetric shapes of the type that were published over 30 years ago involving constant boundary temperatures. Modern computers, using finite-difference codes can be used to readily solve problems with varying boundary temperatures to predict time to cookoff. Quasi-static solutions of symmetric shapes (slabs, cylinders and spheres) obtained with desktop computer spread sheets may give the same results as the finite difference codes. There are no a priori methods for predicting the violence of the slow cookoff reaction. These same comments apply as well to intermediate cookoff heating rates (greater than 6°F/hr).

### **PROJECTION OF FRAGMENTS BY REACTING MUNITIONS**

To meet the U.S. Navy's IM requirements, a munition must react no more violently than burning in the fast cookoff, slow cookoff, bullet impact, and fragment impact tests.<sup>11</sup> The burning reaction is defined as one with no fragments that cause fatal wounds to humans or "hazardous fragments" at distances less than 50 feet from the test item.<sup>11</sup> A hazardous fragment is defined, as it generally is in safety standards, as one having less than 58 ft-lb of energy.<sup>14</sup> If a test result fails to meet this requirement, the reaction is usually ranked a "deflagration." It can be very important to program offices and contractors that the Government evaluators use a consistent ranking method to evaluate IM tests.

The evaluation of fragment hazard has often been done by mapping the final location of reaction debris found on the ground surrounding the test item. It is then not uncommon to find that a reaction has been ranked a deflagration if any debris is found outside a circle of 50-feet radius. Sometimes, the video record is also studied, and if any debris is seen moving more than 50 feet from the test item following the munition reaction, a reaction may be ranked a deflagration even if no debris has been found beyond 50 feet.

This situation bothered me. It seemed obvious that some debris could travel more than 50 feet from the test item and yet not constitute a hazardous fragment at 50 feet. It is not at all difficult, given a specific fragment, to calculate its trajectory and its energy at every range. However, a general relationship, while perhaps not quite as accurate as such individual calculations, would be very helpful to rationalize the judgement of fragment hazard. Such a relationship follows.

The maximum range to which an object subject to a one-time initial velocity can travel is given approximately (within the ranges of interest for IM evaluation) by a generalized relationship between non-dimensional maximum range ( $R'$ ) and non-dimensional initial velocity ( $V'$ ).<sup>68</sup>

$$V' = 0.10606 + 1.7593 R' + 1.2609 R'^2 + 0.45671 R'^3, \text{ "English" (slug, ft, sec) units} \quad (7-1)$$

where:  $V' = \log(r_{\text{air}} C_D A_D V_0^2 / Mg)_{\text{air}}$

$R' = \log(r_{\text{air}} C_D A_D R_{\max} / M)$

$C_D$  = drag coefficient

$A_D$  = area for drag calculation,  $\text{ft}^2$ .

$M$  = mass of debris projectile, slugs.

$\rho_{\text{air}} = 0.0024 \text{ slug}/\text{ft}^3$

$g$  = acceleration due to Earth's gravity,  $32 \text{ ft}/\text{s}^2$

The velocity at 50 feet can be approximated by equation (7-2).<sup>69</sup>

$$V_{50} = V_0 \exp(-\rho_{\text{air}} C_D A_D 50 / 2 M) \quad (7-2)$$

Figure 12 shows the results of such calculations for six debris projectiles: (1) a 2-lb nozzle, both end and side-on, (2) a 0.01-lb (70 grain) chunky fragment, (3) a 0.1-lb chunky fragment, (4) a 1-lb chunky fragment, (5) a 16-square-inch area thin case fragment (0.12 lb-wt), and (6) a 1-square inch area thin case fragment (.0075 lb-wt). The values of drag coefficients<sup>65,69</sup> used in the calculations are shown on the figure. What Figure 11 shows, in brief, is that only the 2-lb nozzle, thrown end-on is a "hazardous fragment" at 50 feet, if its maximum trajectory distance is 50 feet. The same nozzle, thrown side-on can travel a 65-foot horizontal distance to have been a "hazardous fragment" at 50 feet. All the other debris fragments may have maximum horizontal trajectory distances in excess of 100 feet and still pass the hazardous fragment criterion (< 58 ft-lb) at 50 feet.

An evaluation technique that is able to measure the debris initial velocities,  $V_0$ , and relate them to specific debris projectile masses and shapes found in the later mapping process would form a better basis for compliance with published requirements<sup>11</sup> than the current approach.

#### Section Summary

It takes more than debris mapping or estimation of fragment range and velocity from video-tape records to determine whether or not a munition has ejected "hazardous fragments." In order to create a technically and contractually solid basis for IM requirements, the Government should either change the published requirement for debris energy to define measurable variables, or adopt an evaluation approach that accounts for realistic trajectory phenomena.

#### SUMMARY

This paper presents simple analytical methods for estimating values of parameters important for evaluating the IM and other hazard behaviors of munitions. While these methods are no substitute for laboratory and field testing or for state-of-the-art (and hopefully, new near-future) computer-based analyses, they provide virtually instant values for preliminary design purposes. Under the pressure of proposal preparation and for use in preliminary hazard assessments and test plans, methods of this simplicity can be invaluable. Many other relationships of similar simplicity are available and under continuing study by the author.<sup>36,77,78</sup> Simple techniques based on laboratory data are also available.<sup>72,75</sup>

#### REFERENCES

1. McQuaide, P.B., "Test and Evaluation of Insensitive Munitions," *Test and Evaluation of the Tactical Missile, AIAA Progress in Astronautics and Aeronautics, Volume 119*, pp. 203-232, 1989.
2. Naval Surface Warfare Center, Accident Incident Data Bank, NSWC, Dahlgren, Virginia.
3. Naval Weapons Station, *Explosive Incident Summaries*, NWS, Yorktown Virginia, prepared for Deputy Commander for Weapons and Combat Systems, Naval Sea Systems Command (an example document), June 1984.
4. Bentley, R. "Peacetime Stimuli Potentially Hazardous to Air Force Munitions," 1990 Joint Government/Industry Symposium on Insensitive Munitions, ADPA, White Oak, Maryland, 13-14 Mar 1990.
5. The Joint Chiefs of Staff, "Memorandum of Agreement on Establishment of a Joint Requirement for Insensitive Munitions," Washington, D.C., 3 Sept 1987.
6. NATO Insensitive Munitions Information Center (NIMIC), NATO Headquarters, B-1100 Brussels, Belgium. Quarterly newsletter available: Naval Sea Systems Command, attn: NIMIC NFPO, SEA-661, Washington, DC 20362-5101.
7. Advisory Group for Aerospace Research and Development, *Hazard Studies for Solid Propellant Rocket Motors*, AGARDograph, AGARD, Neuilly sur Seine, France, 1990.
8. North Atlantic Treaty Organization, *NATO Standardization Agreement, Principles and Methodology for the Qualification of Explosive Materials for Military Use*, NATO AC/310 Working Group, STANAG 4170.
9. Chief of Naval Operations, "U.S. Navy Insensitive Munitions Policy," OPNAVINST, 8010.13B, 27 June 1989.
10. Naval Sea Systems Command, "U.S. Navy Insensitive Munitions Requirements," NAVSEAINST 8010.5B, 5 Dec 1989.
11. Military Standard, "Hazard Assessment Tests for Non-Nuclear Ordnance," MIL-STD-2105A(NAVY), 8 Mar 1991.
12. Department of Defense, "Department of Defense -- Ammunition and Explosive Safety Standards," DoD-6055.9 ASD(M,I, and L), July 1984.
13. North Atlantic Treaty Organization, "Guidance on the Assessment of the Safety and Suitability for Service of Munitions for NATO Armed Forces," NATO-AOP-15, Mar 1985.
14. Department of Defense, "Department of Defense - Explosives Hazard Classification Procedures," Army, TB 700-2, Navy NAVSEAINST 8020.8, Air Force TO 11A-1-47, Defense Logistics Agency DLAR 8220.1, Dec 1989.
15. Naval Sea Systems Command, "Qualification of Energetic Materials," NAVSEAINST 8020.5B, 16 May 1988.

16. Military Standard, "Qualification Procedures for Explosives (High Explosives, Propellants, and Pyrotechnics)," MIL-STD-1751(A), proposed draft, 1 Feb 1990. (Pending completion and approval.)
17. Naval Ordnance Systems Command, "Safety and Performance Tests for Qualification of Explosives," NAVORD OD 44811, 1 Jan 1972.
18. North Atlantic Treaty Organization, *Manual of Tests for the Qualification of Explosive Materials for Military Use*, NATO-AOP-7, Feb. 1988, also see AOP-7, Annex-1, July 1989.
19. Department of Defense, "Military Standard, System Safety Program Requirements," DoD-MIL-STD-882B, March 1984.
20. Lawrence Livermore National Laboratory, *LLNL Explosives Handbook*, Livermore, California, UCRL-52996 Change B, January 1985.
21. R. Gill, L. Asaoka, and E. Baroody, On Underwater Detonations, 1. A New Method for Predicting the CJ Detonation Pressure of Explosives," *J. Energetic Materials*, 5, pp.287-307, 1987.
22. F.E. Walker, "Calculation of Detonation Velocities from Hugoniot Data" *Propellants, Explosives, Pyrotechnics*, 15, pp. 157-160, 1990.
23. E. Baroody and S. Peters, *Heat of Explosion, Heat of Detonation, and Reaction Products: Their Estimation and Relation to the First Law of Thermodynamics*, Indian Head, Maryland, NOS, HTTR 1340, May 1990.
24. J. Pearson, *A Fragmentation Model for Cylindrical Warheads*, China Lake, Calif, NWC TP 7124, December 1990.
25. E. Lundstrom, *Advanced Bomb Family Sympathetic Detonation Analysis*, China Lake, Calif., NWC TP 7120, March 1991.
26. W.P. Walters and J.A. Zukas, *Fundamentals of Shaped Charges*, John Wiley & Sons, New York, 1989.
27. M. Kamlet and M. Finger, "An Alternate Method for Calculating Gurney Velocities," *Combustion and Flame*, 34, pg. 213-214, 1979.
28. See recent issues of the journal *Propellants, Explosives, Pyrotechnics* for articles by Hirsch, Held, etc.
29. J.S. Rinehart and J. Pearson, *Behavior of Metals Under Impulsive Load*, American Society for Metals, Cleveland, Ohio, 1954.
30. R.G.S. Sewell, *Fragmentation of Uncontrolled Cylinders*, COMARCO, Ridgecrest CA, September 1987.
31. J. Pearson, *A Fragmentation Model Applied to Shear-Control Warheads*, China Lake, Calif, NWC TP 7146, May 1991.
32. E. Lundstrom, "Shock Sensitivity Testing and Analysis for a Minimum Smoke Propellant," 1990 JANNAF Propulsion Systems Hazards Subcommittee Meeting, Albuquerque, New Mexico, CPIA Publ. 562, March 1991.
33. L. Green, "Shock Initiation of Explosives by Impact of Small Diameter Cylindrical Projectiles," *Seventh Symposium (International) on Detonation*, White Oak, Maryland, NSWC, pp. 273-277, June 1981.
34. H.R. James, "Critical Energy Criterion for the Shock Initiation of Explosives by Projectile Impact," *Propellants, Explosives, Pyrotechnics*, 13, pp. 35-41, (1988).
35. H.R. James and D.B. Hewitt, "Critical Energy Criterion for the Initiation of Explosives by Spherical Projectiles," *Propellants, Explosives, Pyrotechnics*, 14, pp. 223-233, (1989).
36. T. Liddiard and L. Roslund, *Fragment Impact Sensitivity of Explosives*, White Oak, Maryland, NSWC TR 89-184, September 1991.
37. H.H. James, P.J. Haskins, and M.D. Cook, "Effect of Case Thickness and Projectile Geometry on the Shock Initiation Threshold for a Given Explosive," *Inertious Munitions*, AGARD Conference Preprint 511, Neuilly sur Seine, France, AGARD, October 1991.
38. R.G.S. Sewell, COMARCO, Inc., Private communication.

39. C.H.Johansson and P.A. Persson, *Detonics of High Explosives*, Academic Press, Inc., Orlando, Florida, 1981.
40. M. Wagenhals, E. Lundstrom, R. Heimdal, R. Randolph, and T. Boggs, "Which Threat? Which Response? or Determining Vulnerability of Weapons to Real World Ballistic Impact Hazards," 1988 JANNAF Propulsion Systems Hazards Subcommittee Meeting, Los Angeles, Calif., CPIA Publ. 477, March 1988.
41. J. Brunet, S. Hamaide, B. Nouguez, and F. Pitiot, "Bullet Impact Behavior of Solid Propellant Grains," *In insensitive Munitions*, AGARD Conference Preprint 511, Neuilly sur Seine, France, AGARD, October 1991.
42. S.A. Finnegan, J.C. Schultz, J.K. Pringle, and A.J. Lindfors, "The Relationship Between Ballistic Impact Damage and Violent Reaction in Cased Propellant," 1991 JANNAF Propulsion Systems Hazards Subcommittee Meeting, Albuquerque, New Mexico, CPIA Publ. 562, March 1991.
43. M.E. Backman and W. Goldsmith, "The Mechanics of Penetration of Projectiles into Targets," *Int. J. Engng Sci.*, **16**, pp. 1-99, 1978.
44. Naval Weapons Center, *Effect of Projectile Nose Shape on Ballistic Limit Velocity, Residual Velocity, and Ricochet Obliquity*, by T. Ipson, R. Recht, and W. Schmeling, Denver Research Institute for NWC, China Lake, Calif., NWC TP 5607, December 1973.
45. JTCG/ME, *Penetration Equations Handbook for Kinetic Energy Penetrators*, 61 JTCG/ME-77-16, 1977.
46. R.G.S. Sewell, K.J. Graham, "Fragment Initiation of Cased Explosives," in *Air Weaponry Technology Program for Strike Warfare, FY 1983, Second Quarterly Report, Volume 4, Warheads*, NWC TP 6350-6, Volume 4, China Lake, Calif., NWC, 1983.
47. R.B. Frey, "The Initiation of Explosive Charges by Rapid Shear," *Seventh Symposium (International) on Detonation*, White Oak, Maryland, NSWC, pp. 36-42, June 1981.
48. J. Isler, P. Gimenez, and S. Hamaide, "Experimental Addressing of Energetic Materials for IM Applications," Joint Int. Symp. on Compatibility of Plastics and Other Materials with Explosives, Propellants, Pyrotechnics and Processing of Explosives, Propellants and Ingredients, ADPA, San Diego, Calif. April 1991.
49. W.H. Andersen and N.A. Louie, "Projectile Impact Ignition Characteristics of Propellants, I. Deflagrating Composite Propellants," *Combustion Science and Technology*, **20**, pp. 153-160, 1979.
50. Milton, R.W. and Thorn L.B., "Propellant Reactions and Damage Caused by Multiple Bullet Impact," 1991 JANNAF Propulsion Systems Hazards Subcommittee Meeting, Albuquerque, New Mexico, CPIA Publ. 562, March 1991.
51. D.E. Cantey, *In sensitive High Explosive Munition Redesign Study, Technical Report*, Contract No. F08635-87-C-0225, Sunnyvale, Calif., LMSC-F230369, January 1990.
52. Naval Weapons Center, *Analysis of Heating Rates for the In sensitive Munitions Slow Cookoff Test*, by Fontenot, J. S., and Jacobson, M., China Lake, Calif., NWC, NWC TM 6278, July 1988.
53. A. Victor, IM Threat Hazard Assessment Reports on the ABF, AIWS, and ARS, Victor Technology, 1991.
54. R.F. Vetter, *Reduction of Fuel Fire Cook-off Hazard of Rocket Motors*, China Lake, Calif., NWC TP 5921, June 1977.
55. J.M. Pakulak, "ABF Cookoff," ABF Technology Transfer Conference, San Diego, Calif., 2-4 April 1991.
56. J.J. Gregory, N.R. Keltner, and R. Mata, Jr., "Thermal Measurements in Large Pool Fires," *Transactions of the ASME*, **111**, pp. 446-454, May 1989.
57. J.S. Fontenot, *Summary Report of In sensitive Munitions Testing of Bombs, Rockets, and Missiles*, Naval Weapons Center, China Lake, Calif., NWC TP 7077, January 1991.
58. H. Bazaki and N. Kubota, "Friction Sensitivity Mechanism of Ammonium Perchlorate Composite Propellants," *Propellants, Explosives, Pyrotechnics*, **16**, pp. 41-47, 1991.
59. J. Zinn and C.L. Mader, "Thermal Initiation of Explosives," *J. Applied Physics*, **31**, pp. 323-328, 1960.

60. R.D. Skocypec, et al, "An Evaluation of Cookoff: Status and Direction," 1991 JANNAF Propulsion Systems Hazards Subcommittee Meeting, Albuquerque, New Mexico, CPIA Publ. 562, March 1991.
61. G.A. Butcher, "Propellant Response to Cook-off as Influenced by Binder Type," 1990 JANNAF Propulsion Systems Hazards Subcommittee Meeting, Laurel, Maryland, CPIA Publ. 538, April 1990.
62. G.A. Butcher, "Propellant Response to Cook-off as Influenced by Binder Type, II: Effects of Confinement" 1990 JANNAF Propulsion Systems Hazards Subcommittee Meeting, Albuquerque, New Mexico, CPIA Publ. 562, March 1991.
64. A. Dieder and A. Victor, "Propellant and Rocket Motor Behavior in Low Heating Rate Thermal Environments, (U), 1989 JANNAF Propulsion Systems Hazards Subcommittee Meeting, San Antonio, Texas , CPIA Publ. 509, Feb 1989. CONFIDENTIAL (Unclassified - Public Release version available from the Naval Air Warfare Center, Weapons Division, China Lake, Calif.)
65. P. Daniels, J.W. McDonald, and V.K. Morgan, *Subsonic Transonic, and Supersonic Drag Categories of Warhead Fragments*, Dahlgren, Virginia, NSWC TR 81-112, May 1981.
66. Naval Weapons Center, *A Study of Rocket Motors and Large-Scale Hazards Testing for the Insensitive Munitions Advanced Development (IMAD) Propulsion Program*, by J.W. Farmer, R.W. Pritchard, and L.M. Davis, China Lake, Calif., NWC, NWC TP 6840, August 1988.
67. V.A. Odintsov, "Expansion of A Cylinder with Bottoms Under the Effect of Detonation Products." *Combustion, Explosion, and Shock Waves*, 27, pp. 94-97, 1991.
68. U.S. Department of Energy, *A Manual for the Prediction of Blast and Fragment Loading on Structures*, Amarillo, Texas, U.S. DOE Albuquerque Operations Office, DOE/TIC-11268, pg. 6-54, Change 2 - 1 April 1982.
69. U.S. Army Materiel Command, *Engineering Design Handbook, Design for Control of Projectile Flight Characteristics*, AMCP 706-242, pg. 4-6, September 1966.
70. E. Lundstrom, Naval Air Warfare Center, China Lake, California, Private Communication, January 1992.
71. S. Carpenter, *High Energy Forming*, Denver Research Institute, Report No. AMMRC CTR 74-69, Nov. 1974.
72. J.M. Pakulak, Jr. *Simple Techniques for Predicting Sympathetic Detonation and Fast and Slow Cookoff Reactions of Munitions*, Naval Weapons Center, China Lake, Calif., NWC TP 6660, June 1988.
73. T. Zulkowski, *Development of Optimum Theoretical Warhead Design Criteria*, Naval Weapons Center, China Lake, California, NWC TP 5892, December 1976.
74. T.L. Boggs and C.W. Dickinson (Ed), *The Hazards of Energetic Materials and Their Relation to Munitions Survivability*, The Technical Cooperation Program (TTCP) Subgroup W Action Group(WAG)-11, Summary Report of Workshop held at The Naval Weapons Center, China Lake, California, March 1990 .
75. P.M. Howe, *The Response of Munitions to Impact*, Ballistic Research Laboratory, Aberdeen, Maryland, ARBRL-TR-02169, June 1979.
76. R.G.S. Sewell *Effects of Velocity and Material Properties on Design Limits for Linear Shaped Charges*, Naval Ordnance Test Station, China Lake, California, NOTS TP 3894.
77. M. Kornhauser, *Engineering Methods of Calculating Munition Sensitivity to Impact by Bullets and Fragments*, 3C Systems, Inc., Wynnewood, Pennsylvania, SBIR Contract N00024-87-C-5163, July 1987.
77. M. Kornhauser, *Engineering Methods of Calculating Sympathetic Detonation of Shielded and Unshielded Munitions*, 3C Systems, Inc., Wynnewood, Pennsylvania, SBIR Contract N00024-87-C-5162, July 1987.
78. JANNAF, Propulsion Systems Hazards Subcommittee, Safety and Hazard Classification Panel, Meeting of 13-14 November 1991, as described in minutes by JANNAF Itr, WBR-BLW-JEC/CTII-24-91 of 28 January 1992.
- 79 R.G.S. Sewell, "Fragment Impact Response of Warheads," in *JTCG Surface Target Survivability Meeting*, Eglin AFB, Florida, January 1975.

80. T.P. Liddiard and J.W. Forbes, *A Summary Report of the Modified Gap Test and the Underwater Sensitivity Test*, Naval Surface Warfare Center, Silver Spring, Maryland, NSWC TR 86-350, March 1987.
81. M. DeFourneaux, "Energy Transfers in Explosive Propulsion," UCRL-Trans-10778, October 1974 of pp. 723-930 of *Sciences et Techniques de l'Armement*, vol. 47, No. 3 (1973).
82. E.N. Ferm and J.B. Ramsay, "Spherical Projectile Impact on Explosives," 9th Symposium on Detonation, paper No. 41, pp. 662-665, U.S. Government Printing Office, August 1989.

A	B	C	D	E	F	G	H	I	J	K	L
<b>Barrody &amp; Peters calculation of Heats of Detonation and Explosion, IJTR 1340, 7 May 1990.</b>											
for HMX explosive											
Density	Enthalpy (cb)	Enthalpy (ex)	Heat Content	Enthalpy (cb-ex)	Hdet cal/g	Hdet cal/cc	Enth exhi 14.7psi	Heat Content	Enthalpy (cb-ex)	Hexpl, cal/g	Hexpl, cal/cc
1.9	6.054	-132.32	140.779	-1383.7	1525	2896.89	-74.735	529.234	-807.89	1337	2541
1.899	6.1	-132.3	140.788	-1384	1525	2895.27	-74.66	530	-807.6	1338	2540
For AP/HIPB (R6/14) Reduced Smoke Propellant											
1.806	-51.59	-171.17	189.78	-1195.8	1386	2502.36	-121.41	524.42	-698.2	1223	2208
B=chamber enthalpy at 1000 psi											
C= exhaust enthalpy at 0.0017 psi											
D=heat content for exhaust condition (0.0017 psi)											
E=(C-B)*1000/gfw, cal/g											
F=E*D, cal/g											
G=F*A, cal/cc											
H-exhaust enthalpy at 14.7 psi											
I=heat content at exhaust condition (14.7 psi)											
J=(H-B)*1000/gfw, cal/g											
K=J*I, cal/g											
L=K*A, cal/cc											

Figure 1. Calculating Heats of Detonation and Explosion with PEP Code.<sup>23</sup>

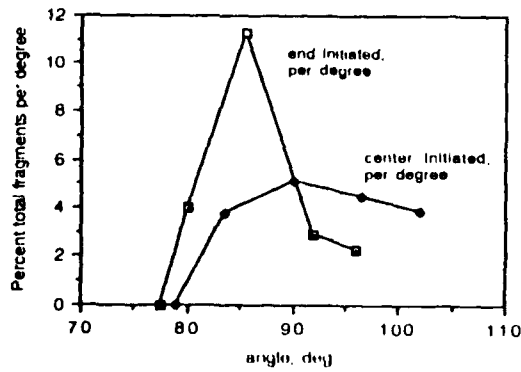


Figure 2a. Azimuthal Differential Percentage Fragment Spatial Distribution, per degree for end- and center-initiated cylindrical warheads.

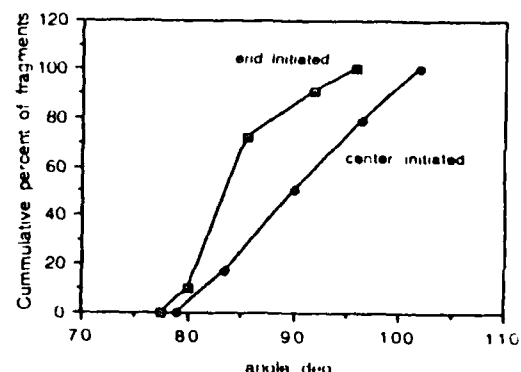


Figure 2b. Azimuthal Cumulative Percentage Fragment Spatial Distribution, per degree for end- and center-initiated cylindrical warheads.

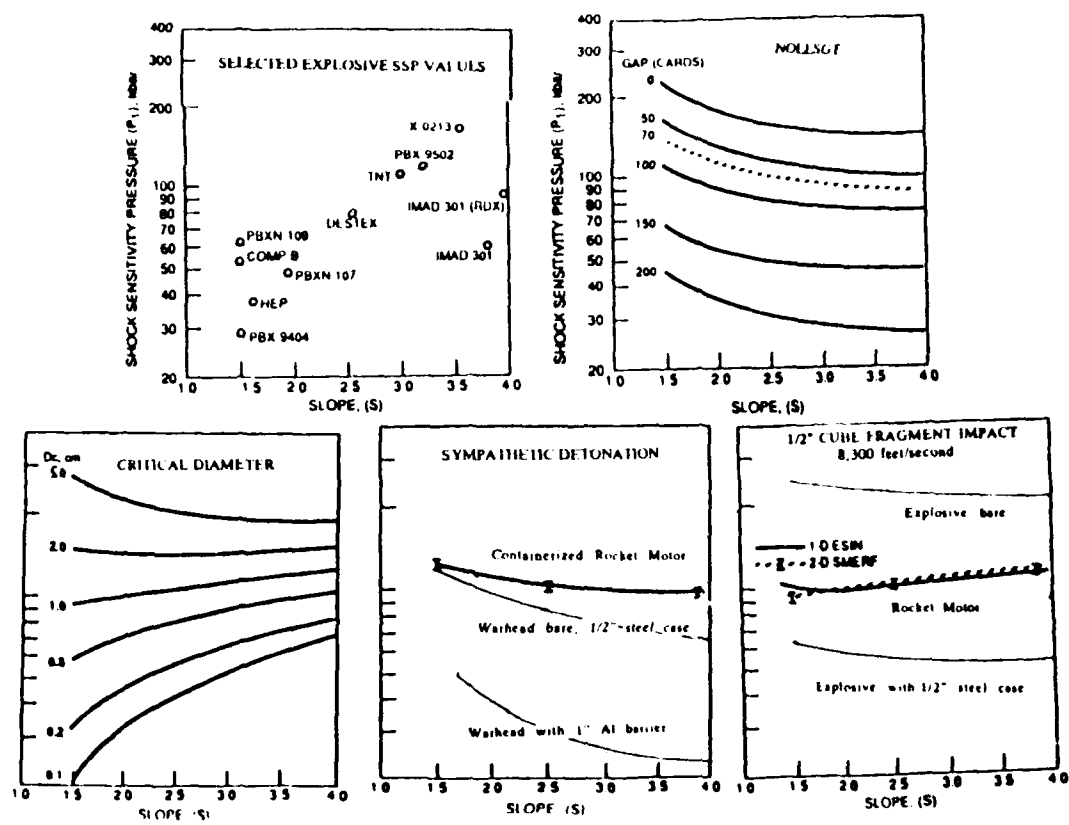
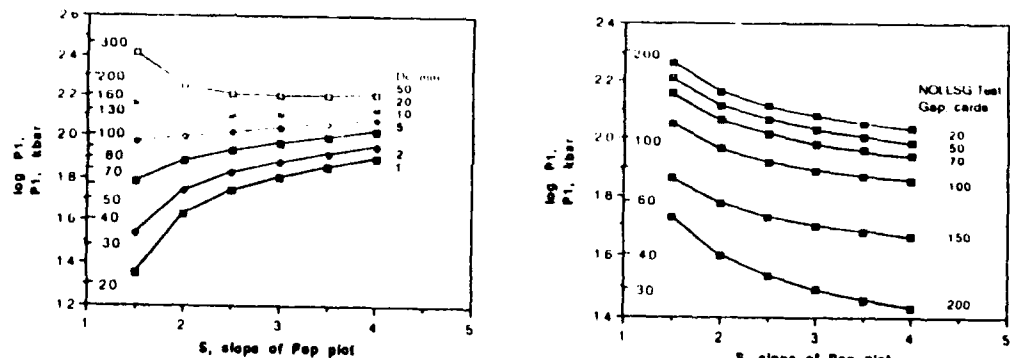


Figure 3. Shock Sensitivity Plane (SSP) Presentation of SDT Phenomena.<sup>32</sup>



a. Critical Diameter Calculated by Equation (3-1).

b. NOL LSGT Results Calculated by Equation (3-2).

Figure 4. Shock Sensitivity Plane Showing Results of Algebraic Calculations

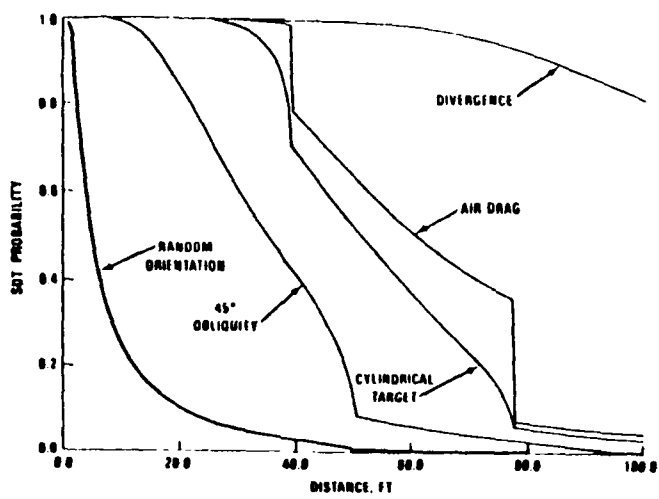


Figure 5. Reduction of Probability of Warhead SDT Due to Degradation of Fragment Hazard Threat by Effects of Randomness.<sup>40</sup>

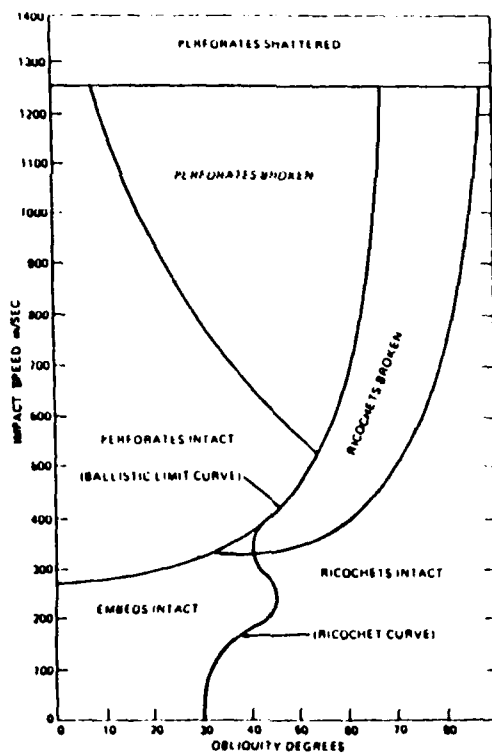


Figure 6. Phase Diagram of Projectile Impact Phenomena

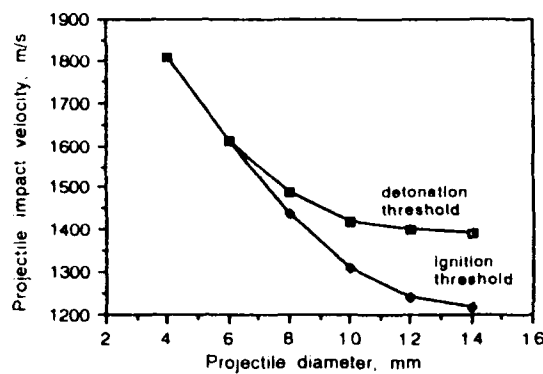


Figure 7. Effect of Impact Velocity and Projectile Diameter (Brass) on Ignition and Detonation Thresholds for a 75% HMX/25% Polyurethane propellant.

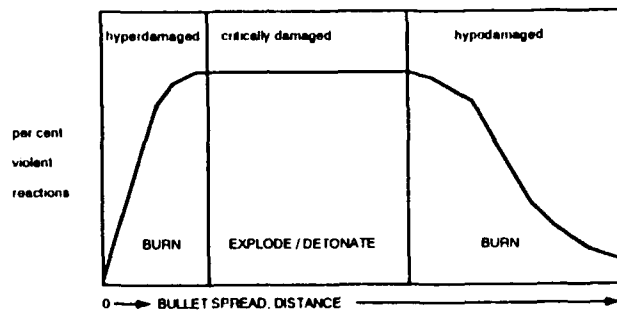


Figure 8. Effect of Multiple Bullet Spatial Distribution on Reaction Violence.<sup>50</sup>

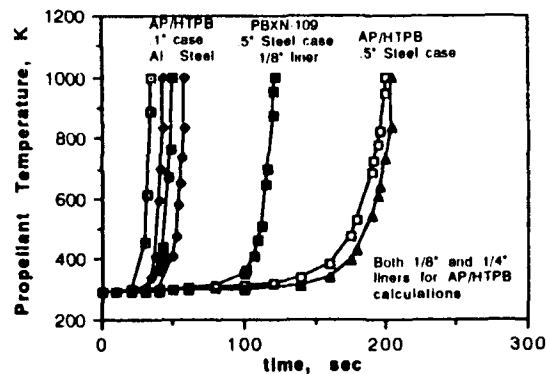


Figure 9. Results of Fast Cookoff Spreadsheets Calculations for AP/HTPB Propellant in 0.1-inch Thick Aluminum and Steel Cases and 0.5-inch Thick Steel Cases with 1/8 and 1/4- inch Liners, and PBXN-109 Explosive in 0.5-inch Thick Steel Case with 1/8-inch Liner.

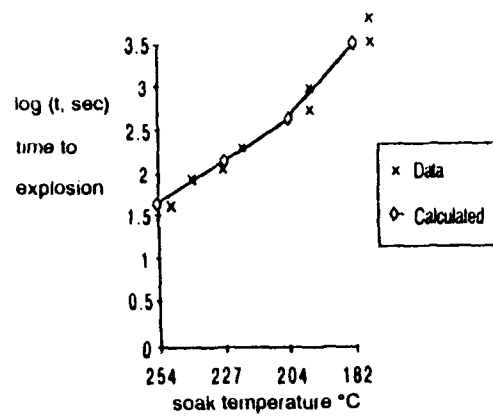


Figure 10. Comparison of Data and SINDA Calculation for 1-inch radius RDX Spheres with Initial Temperature,  $T_0 = 25^\circ\text{C}$ .

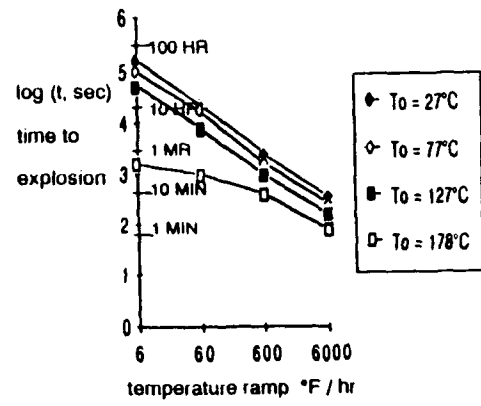


Figure 11. Calculated (Spreadsheet and SINDA) Time to Cookoff for RDX Cylinders of 8-inch Diameter, for Four Initial Soak Temperatures.

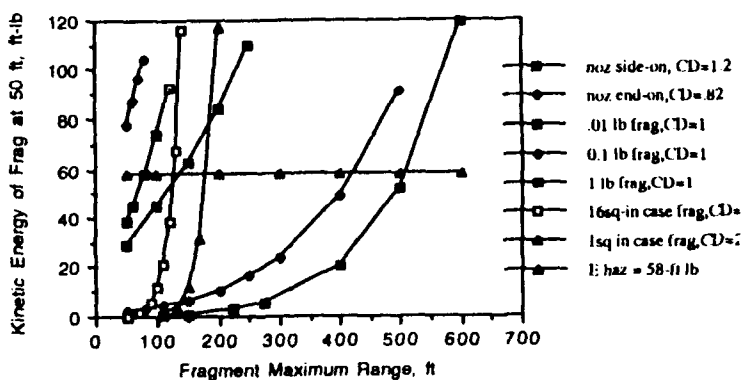


Figure 12. Plot of Kinetic Energy of Debris Fragments at 50 Feet from Test Item vs. Maximum Trajectory Range of Fragment.

**APPENDIX A**  
**IMPEDANCE MATCHING CALCULATIONS FOR**  
**IMPACT PROBLEMS**

The conservation equations for the "jump conditions" for shock wave transfer across a material discontinuity are:

$$\text{MASS} \quad V/V_0 = \rho_0/\rho = (u_s - u_p)/u_s \quad (\text{A-1})$$

$$\text{MOMENTUM} \quad P - P_0 = \rho_0 u_p u_s = \rho_0 u_p (c_0 + s u_p) \quad (\text{A-2})$$

$$\text{ENERGY} \quad E - E_0 = 1/2 (P + P_0)(V_0 - V) \quad \text{or,} \quad u_p = \sqrt{[P(1/\rho_0 - 1/\rho)]} \quad (\text{A-3})$$

where: the subscript 0 refers to the unshocked material.

$\rho$  = material density.

$u_s$  = shock velocity.

$u_p$  = particle velocity, material velocity in direction of shock wave.

P = pressure.

V = specific volume.

E = energy.

$c_0$  = sonic velocity in unshocked material.

s = coefficient for calculation of  $u_s = c_0 + s u_p$ , these parameters are published, <sup>A-1</sup> some are shown in Table A-1.

The acoustic impedance of a material is defined as  $\rho_0 c_0$ . At a material free surface, the free surface velocity is equal to twice the particle velocity (i.e.,  $v_{fs} = 2 u_p$ ).

The equation of state (EOS) or Hugoniot for materials is defined by these equations and can be presented in two orthogonal dimensions such as P vs. V, P vs.  $u_p$ , or  $u_s$  vs.  $u_p$ , etc. Impedance matching calculations can be done graphically in the P vs.  $u_p$  plane. Figure A-1 shows shock Hugoniots for several materials relevant to IM problems. Values of the parameters of the conservation equations for some materials are shown in Table A-1.

**Table A-1. Shock Properties of Selected Materials**

Material	$\rho, \text{g/cm}^3$	$c_0, \text{km/s}$	s
Tungsten	19.224	4.029	1.237
Titanium	4.527	5.037	0.955
Steel	7.89	4.58	1.49
Aluminum	2.785	5.328	1.338
Copper	8.93	3.94	1.489
PMMA (Plexiglass)	1.186	2.654	1.488
Water	.998	1.647	1.921
Polyurethane	1.265	2.486	1.577
Polyrubber	1.01	0.852	1.865
Comp B	1.715	3.03	1.73
Nitroguanidine	1.71	2.72	1.5
PBXN-109	1.66	1.75	2.78
PBXN-110	1.657	3.70	1.905
PBXN-107	1.63	2.449	2.019
PBX 9404	1.84	2.43	2.57
Pressed TNT	1.54	2.08	2.44
Destex	1.694	2.31	1.83

<sup>A-1</sup> S.P. Marsh, *LASL Shock Hugoniot Data*, University of California Press, Berkeley, Calif., 1980.

The one-dimensional impedance matching calculation can be done graphically as shown in Figure A-2 and given by equation (A-4). The intersection of the Hugoniot curve for the target (in this case, Plexiglass) and the "mirror image" or "reflection" Hugoniot curve for the impactor (in this case, aluminum) is found in  $(P, u_p)$  coordinates intersecting the abscissa at the velocity of the impactor (the free surface velocity). The intersection of the point where the reflected impactor Hugoniot curve crosses the target Hugoniot curve gives the matched pressures and particle velocities in both materials. The intersection of the aluminum Hugoniot curve and its mirror image curve defines the matched pressure and particle velocity for a problem in which an aluminum projectile impacts an aluminum case. Since this analogy applies to any impact of identical materials, that step can be left out of problems involving impacts of steel projectiles on steel cases, which can thus be treated as steel impacting directly on the next layer of liner or energetic material.

$$P_1 = P_2 = \rho_1 u_{s1}(u - u_p) = \rho_2 u_{s2} u_p, \quad (u_{s1} = c_{01} + s_1 u_p) \quad (A-4)$$

Problem Statement: 1 km/s Al plate hitting plexiglass.

Match conditions:  $u_p = 0.784$  km/s,  $P = 3.8$  GPa.

Plexiglass free surface velocity = 1.57 km/s ( $2u_p$ ).

A more general problem would involve an impactor of material (1) a munition case of material (2) and an internal load of energetic material (3), as in Figure A-3 and equations (A-5) and (A-6). One can also envision a fourth material, a liner or insulator between the case and the energetic material, as in Figure A-4. The problem shown graphically in Figure A-3 involves three materials: steel impactor, aluminum case, and Comp-B explosive load. On the graph of Figure A-3, the positions are labeled for the solutions to the variables defined in the following equations:

$$P_1 = P_2 = \rho_1 u_{s1}(V_i - u_{p1}) = \rho_2 u_{s2} u_{p1}, \quad (A-5)$$

where the subscripts 1 = Steel, 2 = Aluminum, 3 = Comp B.

$$P_3 = r_3 u_{s3} u_p = r_2 u_{s2}(V_2 - u_p), \quad V_2 = 2u_p \quad (A-5)$$

where:  $V_i = 2.53$  km/s impactor velocity.

$$u_{p1} = 1.7249 \text{ km/s}, \quad P_1 = 36.68 \text{ GPa}$$

$$u_p = 2.1664 \text{ km/s} \quad P_3 = 25.18 \text{ GPa}$$

The solutions can be found quadratically or by setting the equations up on a spreadsheet – which can be manipulated to give both solution points and a plot of the problem, as shown in Figures A-2, A-3, and A-4. It is interesting to note that the aluminum case actually increases the shock pressure into the explosive over what it would be if struck directly by the steel impactor. This is consistent with measured data. (See reference 37 of the main text.)

If the impactor velocity is known, as in the problems shown here, the matched pressures into the case and explosive can be found. Alternatively, if the pressure into the explosive ( $P_3$ ) is known, or can be calculated, as from  $V_{det}$  using equation (3-3) or (3-4) of the main text of this paper, the other variables can be worked through to find the impactor velocity.

For two- and three-dimensional geometries, a rarefaction wave starting at the boundary of the impactor/target surface proceeds into the shocked target material at the sonic velocity of the shocked material, which is approximately:

$$c_s = (u_s - u_p)(u_s + s u_p)/u_s. \quad (A-7)$$

For thin material layers, the shock strength can be treated as constant in the shocked cone of decreasing diameter until the diameter becomes smaller than the critical diameter of the explosive within. Thereafter attenuation approximations can be applied as suggested by Greene,<sup>33</sup> Lundstrom's 1-D ESIN code,<sup>32</sup> or the exponential term in equation (3-3). See Appendix C for discussion and application of these shock-wave approaches.

For impactors with cone angles,  $\theta$ , of 90 degrees or greater, the radial contact velocity of the impactor boundary ( $v_r = V_i \tan(\theta/2)$ ) exceeds the impact velocity and an approximately spherical shock wave will progress into the target.<sup>37</sup> For spherically tipped impactors, the radial contact velocity ( $v_r = V_i \sqrt{(2R/V_i t - 1)}$ , averaged over contact time, and  $dv_r/dt$  gives the instantaneous change in  $v_r$ ) varies with sphere penetration, and is enormous (infinite at  $t=0$ ) during the initial contact period. Material distortion during penetration modifies these relationships.

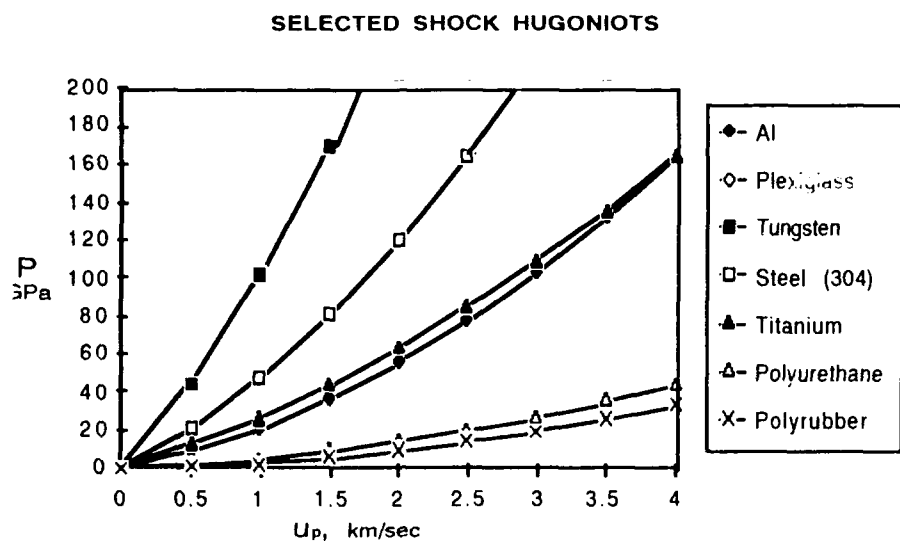


Figure A-1. Shock Hugoniots for Selected Materials

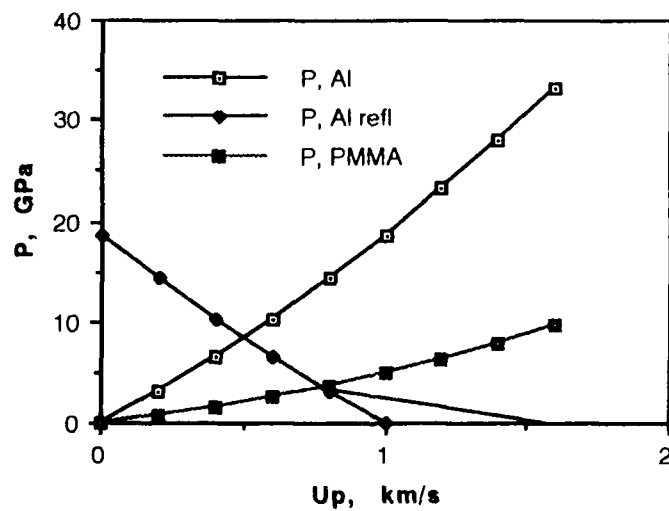


Figure A-2. Impedance Matching for Aluminum Impactor and Plexiglass Target For Impactor Velocity of 1 km/s.

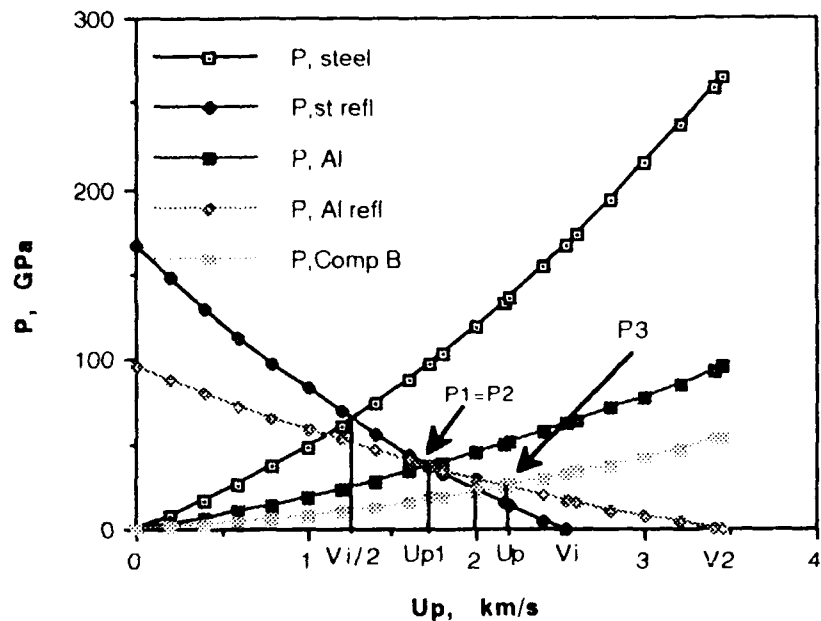


Figure A-3. Impedance Matching Display for Steel Impactor, Aluminum Case, and Comp-B Internal Explosive For Impactor Velocity of 2.53 km/s.

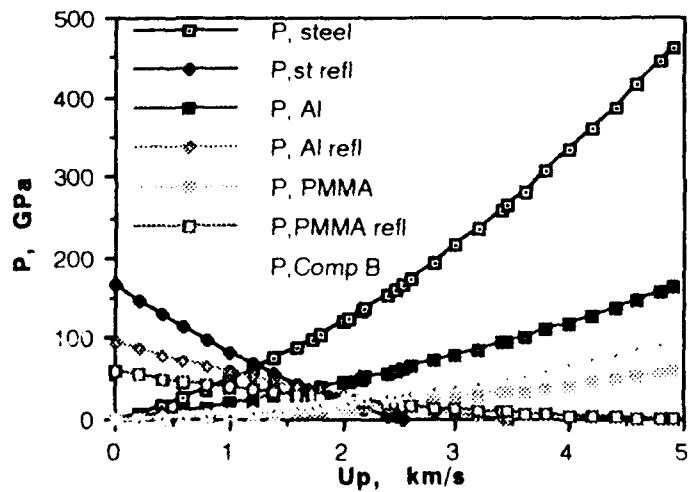


Figure A-4. Impedance Matching Display for Steel Impactor, Aluminum Case, PMMA liner, and Comp-B Internal Explosive For Impactor Velocity of 2.53 km/s.

## APPENDIX B

### THERMAL PROFILES CALCULATED WITH SPREADSHEET SLOW COOKOFF PROGRAM

The method was developed on an EXCEL spreadsheet on a MACINTOSH SE/30 computer with a math coprocessor and 8 Mbytes of RAM. The calculation uses the steady-state heat flow equations for cylindrical geometry. The following logic is followed.

1. The ordnance cylinder is subdivided into a number of concentric radial shells, and the initial temperature at each shell interface is input.
2. The outer wall temperature is set by raising it at the desired heating rate.
3. The heat flow through each shell of energetic material is calculated. In the same calculation, shell self-heating due to energetic material decomposition is calculated. This resets the temperature at the inner wall of the shell. The calculation moves inward to the next shell. The outer boundary temperature is assumed to be independent of any internal heating. However, each shell is subject to radial heat flow from either direction.

The basic equations solved in each cell are shown below, with the spatial index, n, given to the shell volume heat flow being calculated and to its outer boundary temperature. The time index, k, applies to the time step being calculated.

$$Q_n = \pi((t_k - t_{(k-1)}) (2k(T_{nk} - T_{(n+1)(k-1)})) / \ln(R_n/R_{(n+1)}) + \rho Q Z (R_n^2 - R_{(n+1)}^2) \exp(E/(R(T_{nk} + T_{(n+1)(k-1)})/2))$$

$$T_{(n+1)} = T_n + Q_n / (\pi \rho C_p (R_n^2 - R_{(n+1)}^2))$$

For calculations with a reduced smoke propellant (86% ammonium perchlorate, 14% HTPB) the following values of the parameters were used.

$$k = 0.00127 \text{ cal/cm-sec-}^\circ\text{C}, \text{ thermal conductivity}$$

$$\rho = 1.806 \text{ g/cm}^3, \text{ propellant density}$$

$$Q = 500 \text{ cal/g, related to heat of explosion}$$

$$Z = 10^{10.11} \text{ sec}^{-1}, \text{ rate constant ("preexponential term")}$$

$$C_p = 0.32 \text{ cal/g-}^\circ\text{C}$$

$$E = 32.8 \text{ kcal/mole, activation energy}$$

$$R = 1.987 \text{ cal/g-}^\circ\text{C-mole, gas constant}$$

$Q$  was taken as the value midway between 1/3 and 1/2 the calculated heat of explosion<sup>72</sup> for a propellant containing 86% ammonium perchlorate (AP) and 14% HTPB. Heat of explosion was calculated using the method of Baroody and Peters.<sup>23</sup> E and Z were selected from among many different published values for AP.

Toaster Oven Test<sup>64</sup> simulation was done with the Pyrex glass containment cylinder and inner air space between the container and the propellant (before propellant expansion) included in the calculation. The Toaster Oven simulation included modification of the heat flow equation to include convection effects from oven temperature air to the outer glass surface and from the inner glass surface to the air space between the glass and propellant. For the Toaster Oven simulation, the following additional values physical properties used were:

$$k = 0.0124 \text{ cal/cm-sec-}^\circ\text{C, glass thermal conductivity}$$

$$\rho = 2.17 \text{ g/cm}^3, \text{ glass density}$$

$$h = .0002 \text{ cal/cm-sec-}^\circ\text{C, air convection coefficient}$$

In addition, the heat equation was modified for the experimental results NWC obtained that show propellant volumetric expansion of 38% starting at a propellant temperature of 349°F and continuing until the propellant was at 409°F. This was simulated by assuming that all expansion occurred when the propellant was at 349°F (450K). Upon this expansion, density

and thermal conductivity of the propellant were reduced to the following values, and the propellant was assumed to come into contact with the Pyrex cylinder wall:

$$k = 0.0008 \text{ cal/cm-sec-}^{\circ}\text{C}, \text{ thermal conductivity of expanded (foamed) propellant.}$$

$$\rho = 1.2 \text{ g/cm}^3, \text{ density of expanded (foamed) propellant.}$$

The Toaster Oven Test is run with an initial accelerated heating rate intended to bring it within about 6 hours (150°F) of cookoff reaction at the subsequent heating rate of 25°F/hr. In the calculation, a heating rate of 194.4°F/hr was used for the first hour followed by 25°F/hr to reaction.

The calculated time to reaction was 7.55 hours with an oven temperature at ignition of 438°F.

The measured time to reaction was 7.88 hours with an oven temperature at ignition of 436°F.

Calculations were also made for several motor geometries containing this and another reduced smoke propellant.

Figures B-1, B-2, and B-3 were obtained from the spreadsheet slow cookoff analysis of 8-inch diameter RDX cylinders with a 1-cm (.3937 inch) diameter central bore. The RDX thermal parameters of Table II were used. The outer temperature is given by  $T_0$  and the other stations, through  $T_9$  represent radial increments of 1.016 cm (0.4 inch), with the final station,  $T_{10}$ , at .5 cm radius. The calculations are shown for heating rates of 6°F/hr, 21°F/hr, and 24°F/hr. These two higher heating rates are interesting because it is in the range of these heating rates that the calculated cookoff point moves from the inner to the outer shell of RDX. At 21°F/hr the calculated ignition point is at shell 9 and at 24°F/hr it is at shell 2. Sample dimensions and thermal conductivity are critical parameters for this effect.

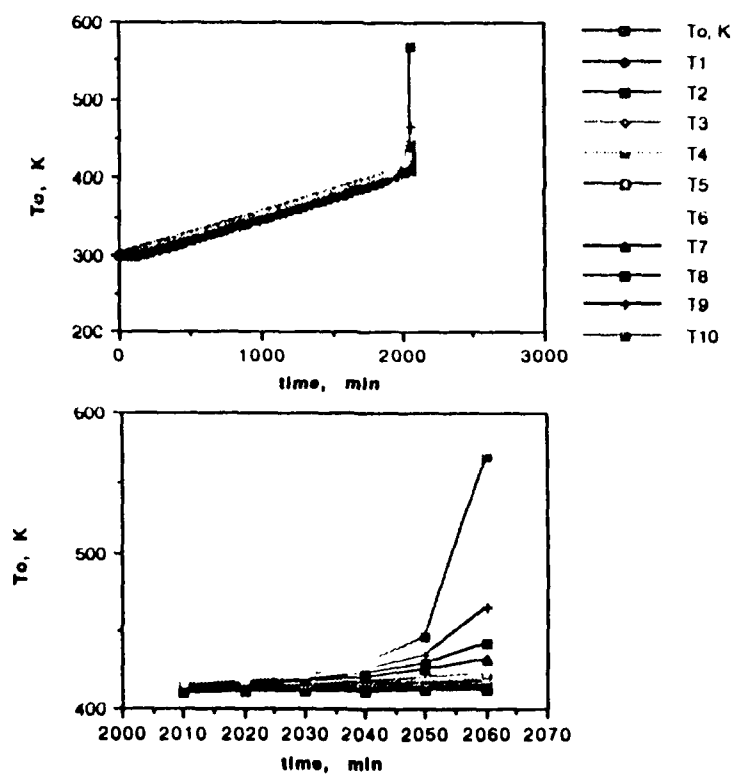
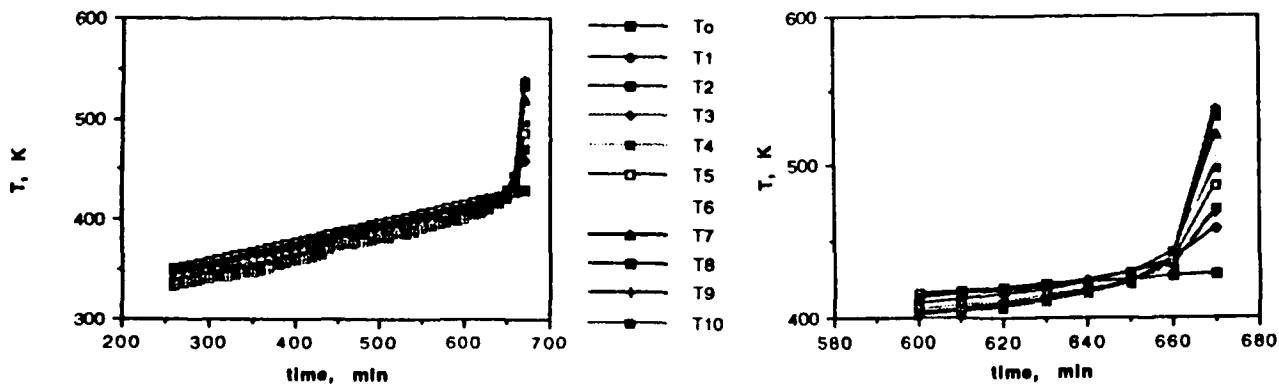
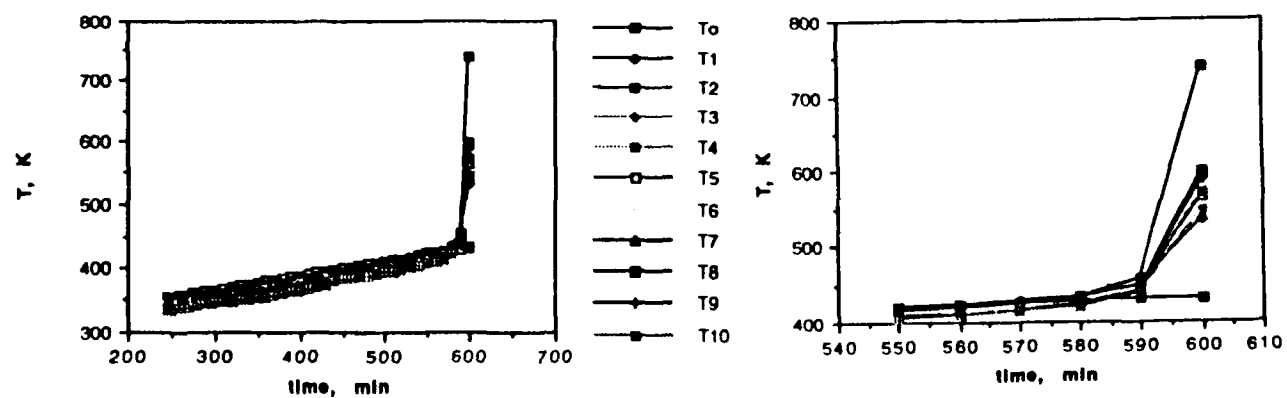


Figure B-1. Calculated Thermal Profiles for 8-inch Diameter RDX Cylinder at Slow Cookoff Heating Rate of 3.3K/hr (6°F/hr) with Spreadsheet Cookoff Program.



**Figure B-2. Calculated Thermal Profiles for 8-inch Diameter RDX Cylinder at Intermediate Cookoff Heating Rate of 11.67 K/hr (21°F/hr).**



**Figure B-3. Calculated Thermal Profiles for 8-inch Diameter RDX Cylinder at Intermediate Cookoff Heating Rate of 13.3K/hr (24°F/hr).**

## APPENDIX C

### SDT CALCULATIONS USING SHOCK RELATIONS

In the main text, equations (3-3) and (3-4) were given for simple calculations of critical impact velocity for detonation for right circular cylindrical impactors larger and smaller than explosive critical diameter, respectively. Figure C-1\* compares data and calculations (using equations (3-3b) and (3-4)) for critical impact velocity values for the three explosives PBX-9404, Comp B, and Destex. The agreement is excellent. However, since the equations used are based on curve fitting to data or to the results of more sophisticated calculations, it is not surprising that the equations are inapplicable in certain regions of the shock sensitivity plane (Figure 3). Specifically, equation (3-3b) fails for explosives with values of POP plot slope (S) greater than 3. To overcome this problem, a more fundamental approach is required. This Appendix presents more basic equations for calculating SDT. Since these equations are based on shock wave propagation, they should be applicable over a wider range of explosive types.

The method used here to predict shock initiation limits by projectile impact is a modification of approaches by James,<sup>34</sup> Green,<sup>33</sup> and Lundstrom.<sup>25</sup> Lundstrom's shock sensitivity plane (SSP) in Figure 3 is used as a data source. All calculations were made for projectiles shaped as right circular cylinders impacting upon plane explosive or case surfaces.

Two different methods are used to calculate shock initiation of detonation:

- 1) The shock wave responsible for initiating detonation is reduced in diameter by lateral release waves as it progresses through the case and explosive. During this process, the shock wave pressure does not change. This method can only be used if the impactor diameter is larger than the explosive critical diameter and at least about twice the case thickness.
- 2) The shock wave is assumed to expand in area as it progresses through the case and explosive. During this expansion, the shock pressure decreases proportionally to the increase in the wave diameter.<sup>33</sup> The expanded wave is then used as the basis for calculating shock initiation. This method is only needed if the projectile diameter is too small or the case is too thick to use method 1).

#### Method for Impactors Larger than Explosive Critical Diameter and Thin-Wall Case

From the SSP, the relationship of run distance (X) to shock pressure (P) is obtained from equation (C-1).

$$X = 10 \cdot (P_1/P)^S, \text{ with pressures in GPa.} \quad (\text{C-1})$$

Critical diameter ( $d_{cr}$ ) can be obtained either from equation (3-1) or by direct measurement. The latter is preferable. The shock jump relations are given by equations (A-1) through (A-3), and the approximate value of sonic velocity in a shocked explosive ( $c_s$ ) is given by equation (A-7). The material property constants  $\rho_0$ ,  $c_0$ , and  $s$  that are required to specify the Hugoniot equation of state for a number of materials are given in Table A-1.

The following steps comprise the calculation:

1. A value of  $P=P_e$  (shock pressure at the explosive surface, GPa) is selected, and the corresponding run distance is calculated from equation (C-1).
2. The particle velocity,  $u_{pe}$ , and shock velocity,  $u_{se}$ , in the explosive for pressure  $P_e$  are calculated from equation (A-2). The velocity of sound in the shocked explosive,  $c_{se}$ , is calculated from equation (A-7).
3. The diameter of the corresponding shock at the surface of the explosive,  $d_e$ , that will cause of a pressure wave of diameter  $d_{cr}$  at a depth X in the explosive is calculated using equation (C-2). Figure C-2 shows the geometry underlying equations (C-2) and (C-5).

$$d_e = 2X \tan(\theta) + d_{cr}, \text{ where } \theta = \cos^{-1}(u_{se}/c_{se}); \quad (\text{Green}^{33} \text{ uses } \tan \theta = 1.) \quad (\text{C-2})$$

\* The prefix C is used for all equations and figures in this Appendix. Other prefixes refer to other Appendices or main text.

There is reason to think that the argument of  $\cos^{-1}$  in equation (C-2) can be better expressed by the term  $[(u_{se} - u_{pe})/c_{se}]$  to represent the motion of the release wave in the shocked material superimposed on the particle velocity. However, a better fit to the data for explosives PBX-9404 and Comp B is obtained with the equation as given. Green's assumed value of  $\theta = 45$  degrees is in reasonable agreement with the values calculated using the shock and sonic velocities over a reasonable shock pressure range.

4. The corresponding impact velocity for a projectile (impactor) of material i is calculated by equation (C-3).

$$V_e = u_{pe} + P_e / (\rho_i u_{si}), \text{ where: } u_{si} = co_i + s_i u_{pe} \quad (C-3)$$

For uncovered explosives PBX-9404, Comp B, and Destex, the calculation with these equations is compared with data in figure C-3. The calculated results appear quite good. Some improvement in the agreement for Destex is obtained if a larger value of  $d_{cr}$ , corresponding to measured values, is used in equation (C-2).

At this point it is relevant to note Ferm and Ramsay's equation<sup>82</sup> (C-4) for the diameter of a sphere that will shock initiate detonation at the same impact velocity,  $V_e$ , as the cylindrical impactor of diameter  $d_e$ . If case parameters are substituted for explosive parameters in equation (C-4), the method also seems to work for sphere impacts on cased explosives.

$$D_{sph} = (2X + d_{cr}) (1 + (c_{oe}/V_e)^2)^{1/2} = (2X \tan \theta + d_{cr}) (1 + (c_{oe}/V_e)^2)^{1/2} \quad (C-4)$$

#### Method for Impactors Smaller than Explosive Critical Diameter or Thick-Wall Cases

Method 2) for calculating shock initiation by impactors smaller than critical diameter follows the appropriate geometry of figure C-2 for expanding waves. The method used here for uncovered explosives defines  $\theta$  in the same way as equation (C-2). The results using this assumption were compared with Green's<sup>33</sup> assumption and virtually no difference in plots of  $V_i$  vs.  $d_i$  was found. The basic assumptions of the method are as follows:

- The shocked diameter ( $d_e$ ) on the explosive surface is too small to calculate initiation of the explosive by method 1).
- The shock wave pressure into the explosive is assumed to decrease uniformly with distance from the explosive surface to a depth,  $X$ , that corresponds to the run distance for the surface shock pressure,  $P_e$ . The equivalent pressure,  $P_{eq}$ , at the depth  $X$  is inversely proportional to the diameter increase in the shock wave. The shock wave equivalent diameter at this depth is given by  $D_{eq}$ .
- The new values,  $P_{eq}$  and  $D_{eq}$  are used to calculate run distance,  $X_{eq}$ , by method 1) to a critical diameter of propellant,  $d_{cr}$ , deeper in the explosive.

In order to use this method to determine values of critical impact velocity, it is necessary to start from the inside, i.e., at the inner  $d_{cr}$  position and work outward to the explosive surface, as follows.

1. Solve the following equations for a wide range of  $P_{eq}$  values. This is easily done by setting up a solution matrix in a desktop computer spreadsheet.

2. Calculate  $X_{eq} = (P_i/P_{eq})^S$  for these values of  $P_{eq}$ , also calculate  $u_{peq}$ ,  $u_{seq}$ , and  $c_{seq}$ . (C-5)

3. Calculate  $D_{eq} = d_{cr} + 2 X_{eq} \tan \theta_{eq}$ , where  $\theta_{eq} = \cos(u_{seq}/c_{seq})$ . (Green<sup>33</sup> uses  $\theta_{eq} = 45$  degrees) (C-6)

4. Calculate  $P_e = P_{eq} D_{eq}/d_e$ . For each  $P_e$ , calculate  $u_{pe}$ ,  $u_{se}$ , and  $c_e$ . (Shock pressure at explosive surface) (C-7)

This step should be more complicated than this simple calculation indicates. If shock pressure is assumed to attenuate with depth, the corresponding velocities in the unreacted explosive will also change. This results in variations of  $\theta$  with depth in equation (C-6) that can only be calculated with a stepped or differential approach. This difficulty alone recommends Green's approach for quick calculations.

5. Calculate  $X = (D_{eq} - d_e)/(2 \tan \theta)$  for each  $P_e$ , where  $\theta$  is defined by equation (C-2). (C-8)

(Greene<sup>33</sup> effectively uses  $\tan \theta = \sqrt{2}/2$  in this step.)

This step must be done for a range of  $d_e$  values for each initial value of  $P_{eq}$ .

6. Calculate impact velocity on bare explosive,  $V_i = u_{pe} + P_e / (\rho_i u_{si})$  for all selected values of  $d_e$  (C-9)

This will provide a number of different values of  $V_i$ , corresponding to the initially selected values of  $P_{eq}$ . The desired solution of  $V_i$  vs.  $d_e$  corresponds to the minimum value of  $V_i$  for each value of  $d_e$ . This will generally correspond to an initially selected value of  $P_{eq}$  in the range of 4 to 20 GPa, depending on the explosive being studied. As a rough rule of thumb, the minimum value of  $V_i$  for each value of  $d_e$  will occur for  $P_{eq} = 2 P_1$ .

Figure C-4 compares calculated values and data over the impactor size range surrounding the explosive critical diameter. Green's simple assumptions about the shock spreading angle seem to be completely adequate for explosive PBX-9404.

The method described by equations (C-5) through (C-9) gives an excellent fit to PBX-9404 data, but poorer fits to Comp B and Deslex. Green's simple assumption of a 45 degree expansion angle seems to give a generally better fit for all three explosives. These methods calculate the critical (minimum) impact velocity at each impactor diameter that will cause shock initiation. It is obvious, but not trivial, that for a given impactor diameter, initiation will occur for any higher velocity, or for a given velocity, initiation will occur for any greater impactor diameter. This point is important when the results obtained above are used as the basis for calculating shock initiation of cased explosives.

#### Method for Covered or Cased Explosives

For more practical scenarios the explosive will be covered or cased by a material designated by the subscript c. In these scenarios, an impactor of diameter  $d_i > d_e$  (where  $d_e$  is determined as described above) will generally be required to cause SDT. However, there are exceptions; for example, thin aluminum cases, because of acoustic impedance coupling, actually decrease the critical impact velocity or impactor diameter required to initiate a detonation. This is born out in the calculation as well as by measured data.

For cased explosives, one might propose to use either method 1) or 2) to determine the  $V_i$  vs.  $d_i$  locus of impacts on the case that will give the  $V_i$  vs.  $d_e$  locus determined above for impacts on bare explosive. However, cursory examination of the equations indicates that method 2) will fail to give a positive (real) value of  $d_i$  for small values of  $d_e$  or for thick cases. Therefore, method 1) is recommended as a first approach for calculating the shock in the case. The loci of the  $V_i$  vs.  $d_e$  pairs is exactly as given by equations (C-1) through (C-9).

#### Method 1) for Thin Cases

For the cased explosive, the conservation jump conditions as discussed in Appendix A, give:

$$\rho_e u_{se} u_{pe} = \rho_c u_{sc} (2 u_{pc} - u_{pe}) = P_e \quad (C-10)$$

$$\rho_i u_{si} (V_i - u_{pe}) = \rho_c u_{sc} u_{pe} = P_i \quad (C-11)$$

Arranging terms, one obtains the easily solved quadratic for  $u_{pc}$ :

$$2 s_c u_{pc}^2 + (2 c_{sc} - s_c u_{pe}) u_{pc} - (c_{sc} u_{pe} + P_e/\rho_c) = 0 \quad (C-12)$$

$u_{sc}$  and  $u_{si}$  are easily obtained across the projectile-case matched conditions (as discussed in Appendix A),

$$u_{sc} = c_c + s_c u_{pc}$$

$$u_{si} = c_j + s_j u_{pc}$$

and the impactor velocity is given by equation (C-13)

$$V_i = u_{pc} + P_i / (\rho_i u_{si}) \quad (C-13)$$

The impactor diameter required at the outer case wall to give the conditions already calculated in the explosive is

$$d_i = d_e + 2 t_c \tan(\cos^{-1}(u_{sc}/(u_{sc} + s_c u_{pc}))), \text{ where } t_c \text{ is the case thickness, mm} \quad (C-14)$$

Figure C-5 shows resulting calculations for the explosive PBX-9404. The curves of  $V_i$  vs.  $d_i$  appear to become vertical at some case thickness. This is interpreted to mean that this initiation mechanism ceases to apply with "thick" cases (greater than about one-half the projectile diameter). What actually happens, is that the diameter of the transmitted shock becomes

smaller than the critical diameter at the explosive surface. This results in the interesting relationship calculated between critical detonation velocity and case thickness for fixed projectile diameter (13.15 mm in this case) with PBX-9404 shown in figure C-6a. This is reasonably good relative agreement with James<sup>37</sup> data for PE4 explosive, as shown in figure C-6b. To the right of the region shown in figure C-6b the data move on to regimes of greater case thickness, where the measured behavior of critical impact velocity vs. case thickness diverges considerably from the calculation. The data show somewhat discontinuous behavior in moving to these regimes. It is reasonable to assume that in these regimes a different mechanism is causing the transition to detonation. One possibility is that the mechanism may be related to that which causes detonation upon impact by high-velocity projectiles that are smaller than  $d_{cr}$ . Another possibility is that expanding shock waves in the thicker cases are responsible for initiating detonation.

#### Method for Thick Cases or Small Impactors

There is a definite limit to the use of method 1) for calculating critical impact velocity for covered explosives. First of all, the method fails to compute for  $t > 0.5 d_i$ , and the results begin to diverge from data for  $t > 0.4 d_i$ . In applying method 2), one must be careful to use reasonable values of the spreading angle  $\theta$  in the case material. If one assumes that  $\tan \theta = \sqrt{2}/2$ , no reasonable answers are readily obtained for case thicknesses,  $t$ , greater than about  $0.75 d_i$ . In applying method 2) to case attenuation effects it is quickly seen that the results are proportionally dependent on the assumed shock wave spreading angle, and gross errors may be made with no other indication than that the calculated critical impact velocities seem unreasonably low.

I have chosen instead to apply the results published recently by Heimdal and Dimarahan.<sup>C-1</sup> These results are based upon SMERF hydrocode calculations involving PBXN-107 explosive and steel and titanium coverplates of thicknesses ranging from zero to the impactor diameter, and extrapolated in the original paper to  $1.2 d_i$ . I found their results fit simple exponential equations very well, which when applied to PBX-9404 explosive agreed with equation (C-3) out to  $t = 0.4 d_i$  and generally agree with the data of James out to about  $t=d_i$  (which is as far as James' data go). The critical impact velocity equations in terms of the critical impact velocity on bare explosive,  $V_e$ , for right circular cylindrical steel impactors upon steel, aluminum, and titanium cases are as follows:

$$\begin{aligned} \text{Steel} \quad V_i/V_e &= 0.949 \cdot \exp(1.035(t/d_i)) \\ \text{Aluminum} \quad V_i/V_e &= 0.814 \cdot \exp(0.9051(t/d_i)) \\ \text{Titanium} \quad V_i/V_e &= 0.902 \cdot \exp(0.869(t/d_i)) \end{aligned} \quad (\text{C-15})$$

In figure C-7a calculations with equation (C-15) for aluminum and steel cases are compared with the results of equation (C-14), as plotted in figure C-6. In figure C-7b the equation (C-15) calculations are compared with James' data for covered PE4 explosive. The agreement is generally good. Although the finer details of James' experimental data are not reproduced, the general trends of the data are carried in the equations out to the limit of the data ( $t = 12\text{mm} = 0.91 d_i$ ).

It seems, from the comparisons in figure C-7, that equation (C-15) can replace method 1) for thin cases. Its applicability for very small impactors and for  $t/d_i > 1$  is not known, as these situations were outside the scope of the studies from which the equation was derived.

Recent work by Hudson on hydrocode energy flux analysis of various projectile shapes and case materials also provides a basis for setting up simple equations for calculations of this type.<sup>C-2</sup> Experimental data from high-velocity impact tests are also available for a range of explosives, case materials, and impactor shapes.<sup>C-3</sup>

Hancock, et al's data for steel cylinder and sphere impact on aluminum covered PBXN-110 explosive is fit well by equation (C-16) based upon other equations generated in this paper, as clearly shown in figure C-8. The author of the present paper is continuing to explore these simple methods and relating them to published experimental and hydrocode studies.

$$D_{\text{sph}} = d_i (1 + (c_{\text{oc}}/V_i)^2)^{1/2} \quad (\text{C-16})$$

C-1 O.E.R. Heimdal and L.F. Dimarahan, "Study of Impact Induced Detonation for Steel and Titanium Covered PBXN-107," 1992 JANNAF Propulsion Systems Hazards Subcommittee Meeting, NSWC, Silver Spring, Maryland, 27 April-1 May 1992, Vol. I, pp. 251-258, CPIA Publ. 582.

C-2 L.C. Hudson, III, "Energy Flux Analysis of Various Projectile Impacts," Ininsensitive Munitions Technology Symposium, 15-18 June 1992, Williamsburg, Virginia.

C-3 P. Hancock, J. O'Connor, P. Spahn, and W. Wilson, "Fragment Impact Studies for Explosives, Cases, and Liners," ibid.

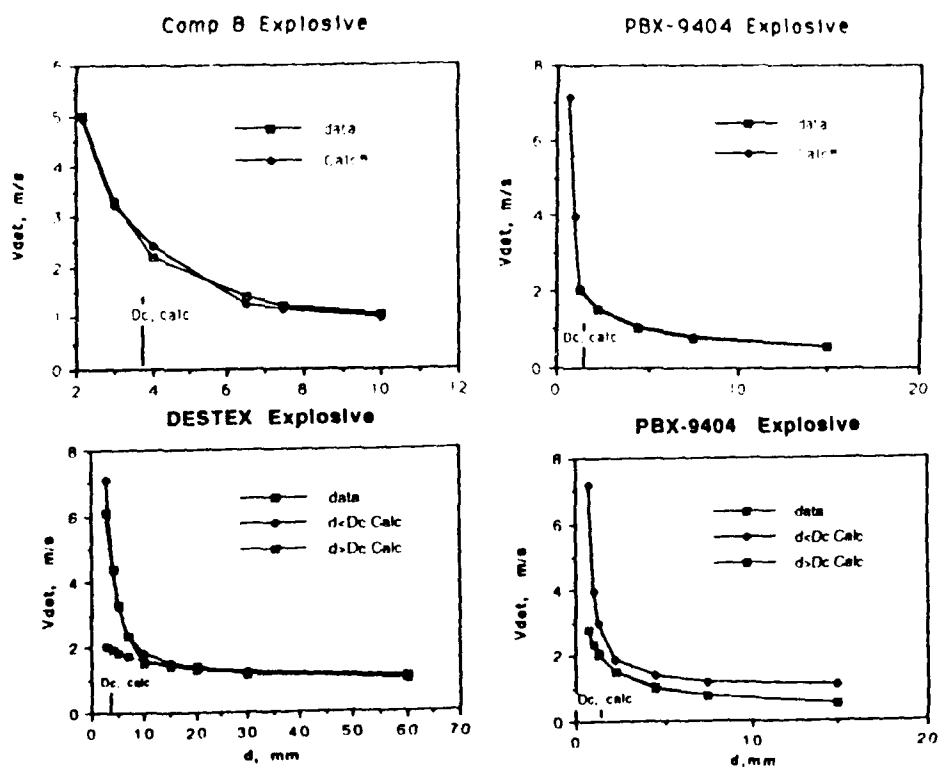


Figure C-1. Critical Impact Velocities Calculated with Equation (3-3b).

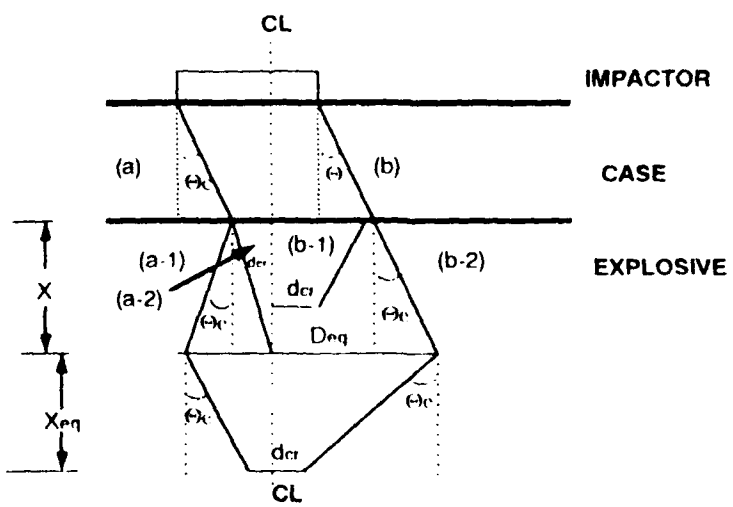


Figure (C-2) Geometry of Shock Initiation Calculations

- (a) Lateral release Wave in Case; (a-1) Expanding Wave in Explosive; (a-2) Lateral Release Wave in Explosive
- (b) Expanding Wave in Case; (b-1) Lateral Release Wave in Case; (B-2) Expanding Wave in Explosive

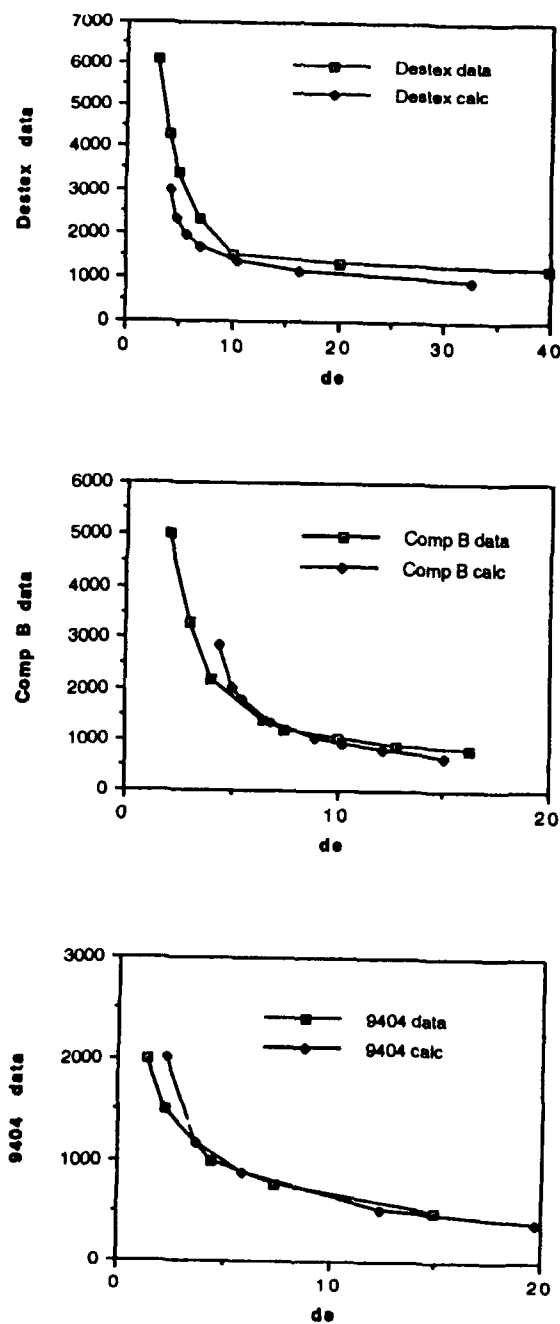


Figure C-3. Calculated Critical Impact Velocities Calculated using Shock Relations for  $d_c > d_{cr}$  on Bare Explosives.

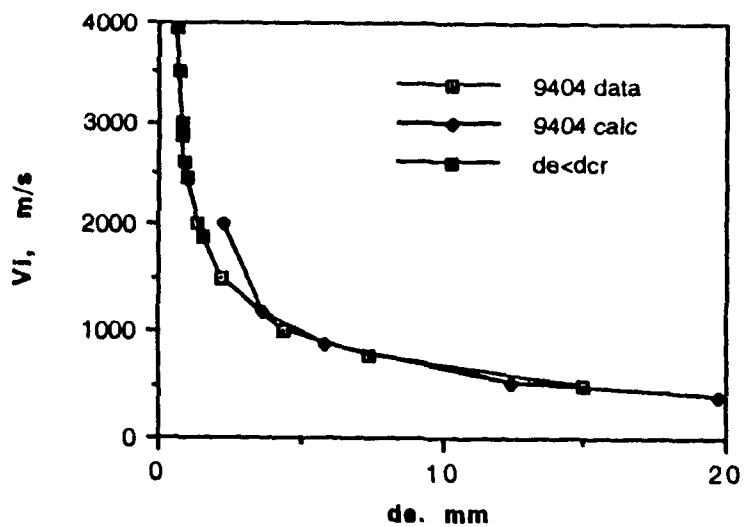


Figure C-4. Bare PBX-9404: Critical Impact Velocities Calculated using Shock Relations for  $d_{cr} > d_e > d_{cr}$ .

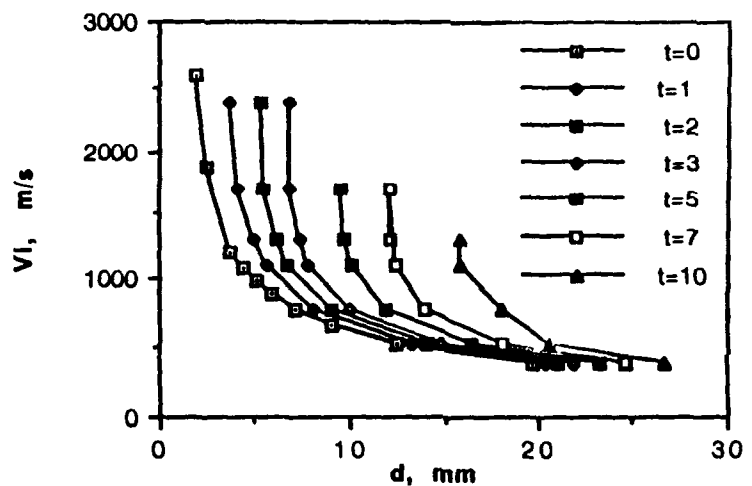
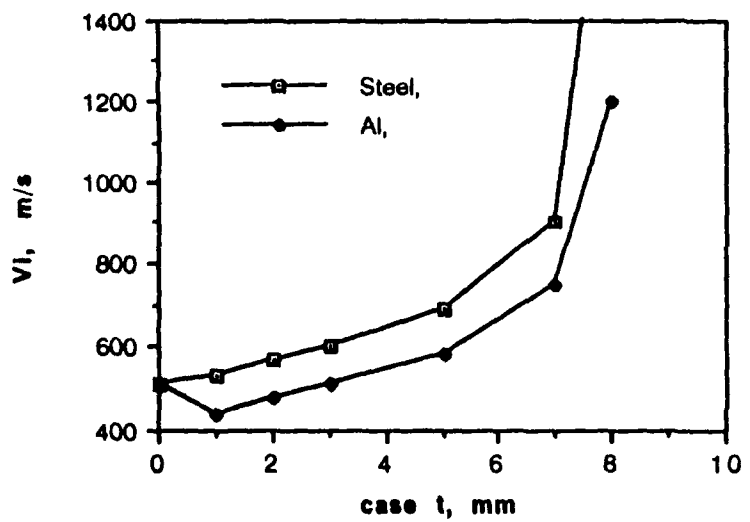
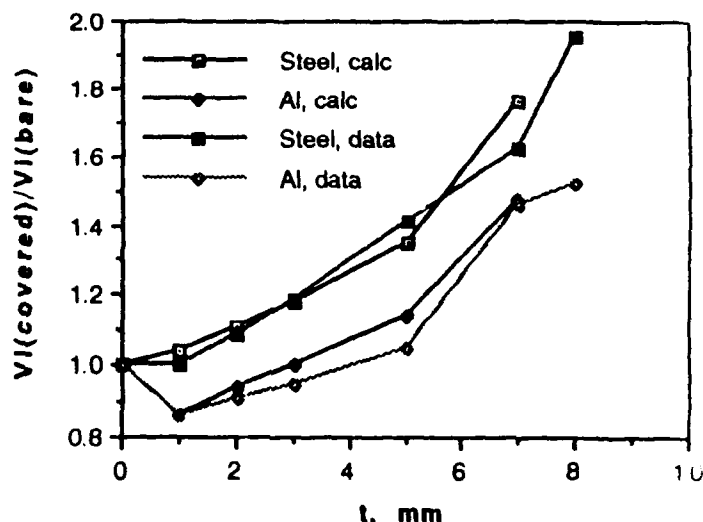


Figure C-5. Critical Impact Velocities for Cased PBX-9404 using Method 1).

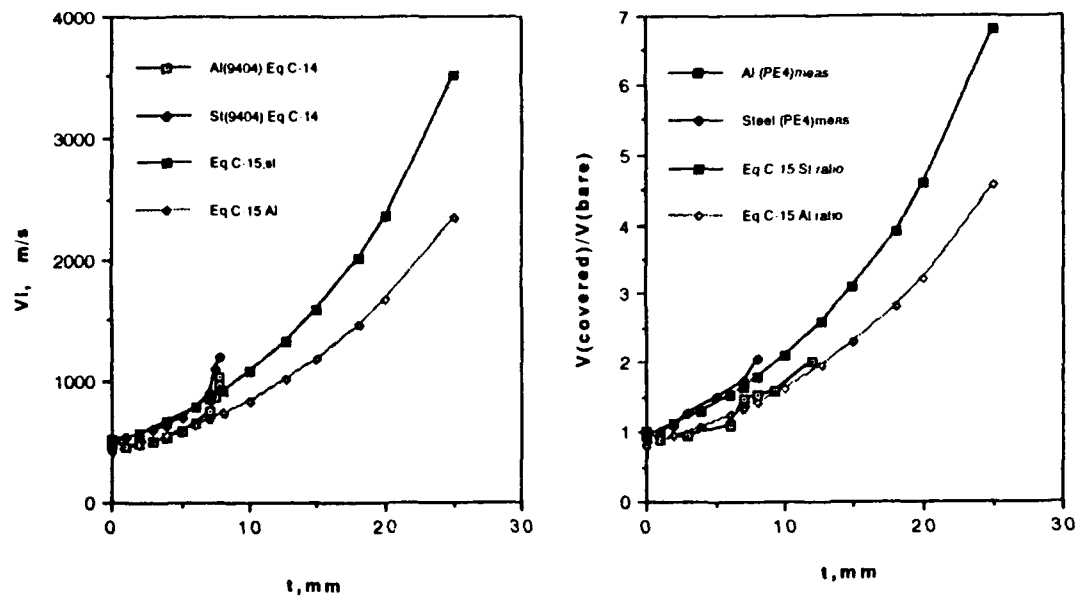


(a) Calculated using method 1



(b) Calculation Compared with data for PE4 Explosive.

Figure C-6. Critical Impact Velocities of 13.15 mm Steel Impactor on Steel and Aluminum Cased PBX-9404.



a. Comparison of Eqs. (C-15) and (C-14)

b. Comparison of Eq. (C-15) and James' PE4 Data.

Figure C-7. Critical Impact Velocities of 13.15 mm Steel Impactor on Steel and Aluminum Cased PBX-9404. Results of Exponential Equation (C-15) for Steel and Aluminum Covers.

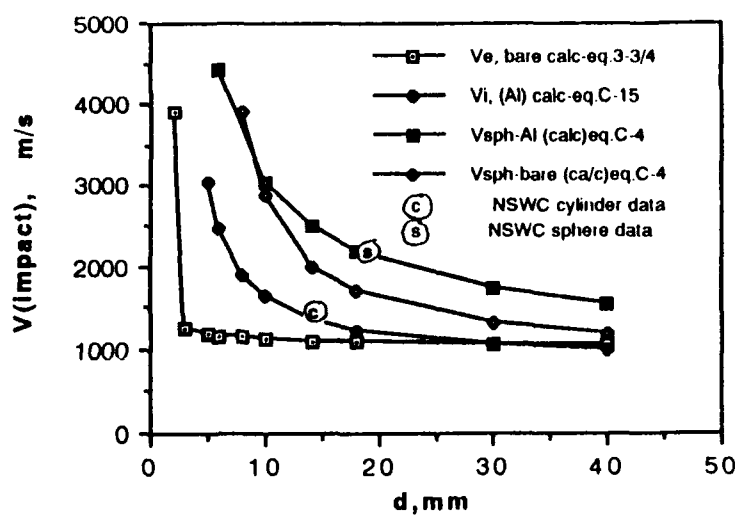


Figure C-8. Comparison of Calculated and Measured Steel Cylinder and Sphere Critical Impact Velocities for PBXN-110 Explosive Covered with 1/4-inch (6.35 mm) Aluminum Sheet. ( $S=1.5$ ,  $P_1 = 41.53$  kbar)

## APPENDIX D

### SYMPATHETIC DETONATION CALCULATIONS

The method of Ferm and Ramsay<sup>82</sup> as exemplified in equation (C-16) can be expanded to explore sympathetic detonation (SD) problems involving cylindrical donors and acceptors. The key assumption in developing this approach is that a shock wave is introduced into the acceptor by a cylindrical or plane impactor. Release waves are assumed to originate on the surface of the acceptor case at the location where the phase velocity of the leading surface contact point is equal to the bulk velocity of sound,  $c_0$ , on the case surface. The examples given in this section are for similar donor and acceptor geometries, however, the method was derived for the more general case of non similar geometries. For one-on-one SD configurations, the donor case is assumed to expand as a growing cylinder with velocity,  $V_D$ , given by equation (D-1). For stack geometries with confinement of the expanding donor case metal, the impacting case is assumed to distort to a planar shape due to confinement effects<sup>32</sup> on the expanding gas, however, for simplification, and consistent with hydrocode calculations,<sup>D-1</sup> the velocity of the plane impactor is assumed to follow equation (D-1). Figure D-1 shows the form taken by equation (D-1),

$$V_D/V_{\text{Gurney}} = 1.2 \sqrt{[(L)/R]} \quad \text{for } L < 0.7 R; \quad \text{for } L > 0.7 R, V_D = V_{\text{Gurney}} \quad (\text{D-1})$$

where:

$V_D$  = Velocity of donor case at position L.

L = Distance donor case has moved from its original position or equatorial distance between donor and acceptor cases.

R = Original outer radius of donor case.

$V_{\text{Gurney}}$  = Gurney velocity of donor explosive as given by equation (2-1).

For values of  $L < 0.7R$ , in equation (D-1) the value of  $V_D$  should continue to increase during impact with the acceptor case. However, since this adds considerable complexities to simple calculations it was ignored in the derivations for this paper. It will result in fairly large errors using equation (D-3) for SD geometries in which the donor and acceptor are in contact or fairly close together.

The solutions involve circular geometry as shown in equations (D-2) and (D-3). The plane impactor velocity in equation (D-2) is generally taken to equal the Gurney velocity.

For the situation of a plane impacting on the cylindrical acceptor case, equation (D - 2) applies.

$$\begin{aligned} S^2 &= R^2 \theta^2 = \theta^2(Y^2 + X^2) \\ 2S \frac{dS}{dt} &= \theta^2(2Y \frac{dY}{dt} + 2X \frac{dX}{dt}) + 2\theta \frac{d\theta}{dt}(Y^2 + X^2) \approx 2R\theta c_0 \\ \frac{dX}{dt} &= V_i \\ d_i / D_A &= .707 V_i / c_0 \end{aligned} \quad (\text{D - 2})$$

For expanding donor cylinder geometry, equation (D - 3) applies.

$$Y^2 = (R_D + L)^2 - (X - R_A - (R_D + L))^2 \quad (\text{D - 3})$$

$$\frac{dX}{dt} = 1.2 \frac{V_G(R_A + L)}{(2R_A + L)} \sqrt{\frac{L}{R_A}}, \text{ for } L/R < .7; \quad \frac{dX}{dt} = \frac{V_G(R_A + L)}{(2R_A + L)}, \text{ for } L/R > .7.$$

$$d_i / D_A = 1.2 \frac{V_G(R_A + L)}{(2R_A + L)c_0} \sqrt{\frac{L}{2R_A}}, \text{ for } L/R < .7; \quad d_i / D_A = .707 \frac{V_G(R_A + L)}{(2R_A + L)c_0}, \text{ for } L/R > .7.$$

$D_A = 2R_A$ , and L is as defined in equation (D-1).

---

<sup>D-1</sup> J.G. Glenn, M. McCormick, and M.E. Gunger, "Sympathetic Detonation Predictive Methods," Insensitive Munitions Technology Symposium, 15-18 June 1992, Williamsburg, Virginia.

The solutions to equation (D-3) as given by  $d_i$  represent the effective shock width on the acceptor surface. The value of  $d_i$  can be worked back through the methods of Appendix C to obtain loci of SD explosives in the shock sensitivity plane (SSP) of figure 4 in the main text. The results of a worked example for an AFX-1100 filled Mk83 bomb case are shown in figure D-2.

Further development of this method is possible. The following limitations should be noted at this genesis: (1) as noted earlier,  $dX/dt$  would be more accurately given in equation (D-3) for  $L/R < .7$  if  $L$  were allowed to grow during the impact, (2) the effect of the cylindrical geometry is ignored in working back through the methods of Appendix C. Lundstrom's hydrocode calculations have shown surface reflection effects on shock propagation and SDT in cylindrical warheads.<sup>D-2</sup>

E. Lundstrom, *Advanced Bomb Family Sympathetic Detonation Analysis*, NWC TP 7120, March 1991.

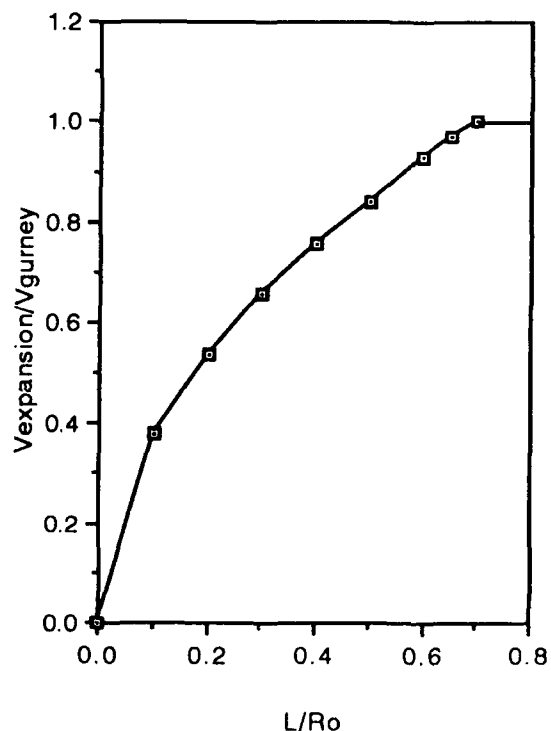


Figure D-1. Velocity of Case Expansion from Eq. (D-1).

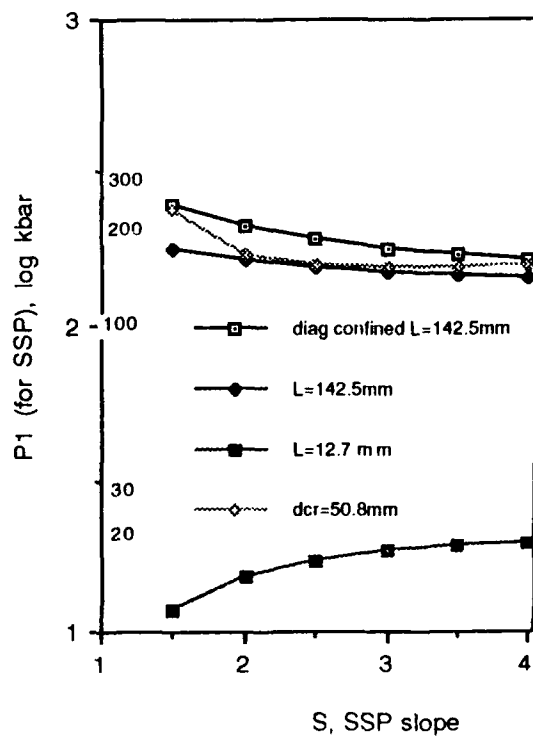


Figure D-2. Shock Sensitivity Plane (SSP) Showing Threshold Line for Sympathetic Detonation with Mk83 Bomb containing AFX-1100 Explosive ( $\sqrt{2E} = 2 \text{ km/s}$ ) ( $d_{\text{cr}} = 50.8 \text{ mm}$  shown too).

**A HARDENED, SELF-RECORDING INSTRUMENTATION  
DEVICE FOR EXPLOSIVES STORAGE SAFETY RESEARCH**

**Twenty-Fifth DOD Explosives Safety Seminar**

**Anaheim Hilton Hotel, Anaheim, CA**

**18-20 August 1992**

by

**L. K. Davis**

**Explosion Effects Division**

**Structures Laboratory**

**U.S. Army Engineer Waterways Experiment Station**

**Corps of Engineers**

**3909 Halls Ferry Road**

**Vicksburg, MS 3980-0631**

## **A HARDENED, SELF-RECORDING INSTRUMENTATION DEVICE FOR EXPLOSIVES STORAGE SAFETY RESEARCH**

by

L. K. Davis

U.S. Army Engineer Waterways Experiment Station  
3909 Halls Ferry Road, Vicksburg, Mississippi 39180-6199

### **BACKGROUND**

Over the last several decades, research on explosives storage safety has been a subject of steadily increasing interest, not only in the U.S., but in many countries around the world where significant amounts of military ammunition must be stored in areas surrounded by encroaching civil development. This research normally is performed (a) to refine the definitions of hazardous areas (Quantity-Distances, or Q-D's), or (b) to develop improved storage methods which will reduce the hazards produced by an accidental explosion.

Many explosive tests have been conducted to simulate accidental explosions, and to measure the blast and shock effects for specific test conditions. Until recently, the primary areas of interest for such measurements were at distances where the blast and shock levels are near the threshold for damage to surrounding structures. Additional measurements are made at closer distances mainly to establish attenuation rates of the blast and shock, as a function of distance.

Within the last few years, however, it has become increasingly important to record more intense levels of blast effects, very near the explosion source. Such data are needed to develop better understandings of the explosion process (for example, the propagation of a detonation from one unit of munitions to another), or to evaluate the performance of storage structure configurations, barriers, or other concepts designed to contain, reduce, or simply survive the intense blast effects from an accidental explosion.

The Explosion Effects Division of the Waterways Experiment Station (WES) has specialized for many years in the measurement of blast, shock, and other effects of explosions. In 1986, WES made airblast and ground shock measurements for a U.S. Air Force test simulating an accidental detonation of 28 MK-84 bombs in an earth-covered magazine, or "igloo." Hardened blast pressure gages were installed inside the igloo to help evaluate the performance of "buffer" walls in limiting the propagation of the explosion.

Although the gages were able to record peak pressures in excess of 103 MPa (15,000 psi), the pressure records ended only a few milliseconds after the peak reading, due to destruction of the gage cables by the explosion.

From this test and similar experiments, it was evident that a measurement technique was needed which would not only allow the sensor to survive intense explosion loads, but would also enable the recording system to survive long enough to capture complete records of the explosion effects. To achieve this capability, WES began development of a hardened, self-recording measurement package which would eliminate the need for cables connecting the sensor to a remote recording unit.

### HDAS DESCRIPTION

The product of this development effort was the Hardened Data Acquisition System, or HDAS. The basic HDAS module is a miniature, solid-state device containing an instrumentation amplifier, an auxiliary gain amplifier, an 11-bit flash analog-to-digital converter, a 128 kiloword (16-bit word) memory, and an output interface (Reference 1). The module is encapsulated in an epoxy/glass microbead matrix to provide shock hardening. Together with a shock-hardened 10.5-volt battery power supply, the complete unit measures only 15 cm long, 6.5 cm wide and 4 cm thick (see Figure 1).

The data sample rate is adjustable from 1 MHz down to less than 10 kHz, with associated recording times of 120 msec to 12 seconds, respectively. The recorder can be activated either by a small, expendable cable connection, or by an internal shock-sensitive switch. Data is recorded in a continuous loop mode after the device is activated. The internal battery allows the data to be stored for five months or more. After the unit is recovered following a test, it can be connected to a portable computer and a plotter to immediately produce finished plots of the data record. Filtering, baseline correction, and single and double integration can also be performed within a very few minutes, as desired.

### TEST RESULTS

Over the last few years, WES has used the HDAS system on a wide variety of explosives safety tests -- sometimes successfully; sometimes not. As with any complex, developmental device, unexpected problems occur that must be solved in a careful, deliberate process. This paper describes some of the successes, and some of the problems, that have been experienced with HDAS.

The first use of HDAS on an explosion test was in 1988 (Reference 2), in a project sponsored by the KLOTZ Club, which simulated an accidental detonation of 20,000 kg of explosives in a shallow underground magazine (Figure 2). Standard, hard-wired gages were used to measure the detonation pressures in the chamber, the short

access tunnel, and the outside area. Two HDAS gages were installed in the floor of the tunnel entrance. As expected, the standard gages inside the chamber and tunnel recorded only the first few milliseconds of pressure, before destruction of the gage cables. The detonation produced a large crater, extending beyond the tunnel entrance. After some hours of digging, the HDAS units were located in the crater rubble. The top of the gage located 1 m outside the tunnel entrance had originally been installed with its top surface projecting about 1 cm above the concrete floor of the tunnel entrance (due to a construction error). As a result, the intense "plasma" of detonation gases going out of the tunnel (before the chamber cover was blown away) eroded the metal cover of the unit, burning up the pressure gage after about 20 msec. The second HDAS unit was properly installed flush with the surface, and was undamaged. As can be seen in Figure 3, it produced a complete record of the pressure history.

In 1990, the United Kingdom and Australia jointly conducted a test at Woomera, Australia, involving the detonation of 75,000 kg of explosives to evaluate the survivability of a new design for an earth-covered magazine, called a "Spantech" structure (Reference 3). HDAS units were used to record the internal pressures in the donor magazine (Figure 4), as well as the pressure loads on adjacent Spantech structures, and in the free-field around the test. Good records were obtained from all of the HDAS units outside the donor magazine, and from units on the side walls in the interior of the donor structure. As shown in Figure 5, the measured interior pressure reached 72 MPa (10,500 psi).

The interior gages near the top of the donor structure were thrown several thousand metres by the explosion. Several were never found; those that were found survived the detonation itself, but were destroyed by their impact with the ground due to an inadequate design of the protective canisters containing the HDAS units.

In later Spantech tests, HDAS units with redesigned canisters were placed on top of the donor magazine to measure the initial, or "break-away", motions of the structure. The canisters were again thrown several thousand metres, but those that were located survived the impact and produced good motion data (Figure 6).

Also in 1990, WES conducted a series of experiments for the U.S. Army Program Manager for Ammunition and Logistics (PM/AMMOLOG) to evaluate the effectiveness of parking ammunition trucks in shallow, covered trenches, as an expedient method for reducing the blast and debris hazards from an accidental explosion of an ammo truck at a temporary field storage site (Reference 4). One of these tests involved the detonation of an unprotected ammo truck (parked in the open) containing 1,500 kg (net explosive weight) of 155-mm projectiles and propellant canisters, to provide control data on the blast pressure and debris hazard from such an accident.

To measure the initial velocities of debris thrown out by the explosion, HDAS units containing accelerometers were installed inside empty 155-mm projectiles, and placed around the live ammunition (Figure 7). The instrumented projectiles were separated from the live rounds by a single layer of sandbags, to prevent their destruction by the detonation. Unfortunately, a single layer of sandbags was not enough. While the instrumented projectiles were not destroyed, they were deformed enough to crush the HDAS units inside.

On the third experiment in this series, two ammo trucks were parked rear end-to-rear end in a single covered trench, with a 1.5-m thick sand wall between them. The purpose was to prove that an accidental explosion of one ammo truck would not propagate to the other, even when the trucks were confined by the trench walls and cover. HDAS units were again installed in empty projectiles, and placed on the top and rear of the acceptor truck to measure the blast pressure environment from the detonation of the donor truck (Figure 8). These units survived the detonation, and produced complete pressure histories (Figure 9).

One of the most recent attempts to use the HDAS system was in support of the U.S. Navy's program to develop an advanced design of an earth-covered magazine, called the High Performance Magazine, or HPM. The HPM concept is based on limiting the total amount of explosives involved in an accident, by using barrier walls between individual storage bays within a magazine. The barrier walls must be thick enough to prevent a detonation in one bay from propagating to adjacent bays, yet small enough to allow an efficient volume of munitions to be stored in the magazine.

In a recent series of experiments by the U.S. Naval Civil Engineering Laboratory, different barrier designs were tested to evaluate their effectiveness in preventing the propagation of a detonation from one stack of bombs to another. In small-scale tests using 155-mm projectiles to model the acceptor bombs, HDAS units were used to measure the acceleration of the acceptor rounds impacted by the barrier material. The donor in this test was an MK-82 bomb. Figure 10 shows such a measurement for an acceptor round located 15 cm behind a 1-m thick sand wall, which was 1.0-m from the donor bomb. The HDAS unit record a peak acceleration of about 750 g's, and a peak velocity of about 10.5 m/sec induced in the acceptor projectile by the impact of the well. Unfortunately, a number of the HDAS units in this test failed to operate properly, possibly due to an electromagnetic pulse induced in the HDAS trigger circuit by the detonation. The pulse apparently caused the HDAS memory to stop recycling before the arrival of the shock wave.

## CONCLUSIONS

The HDAS system shows great promise as a revolutionary technique for investigating intense explosion environments that current instrumentation systems cannot survive. The HDAS concept is still in the developmental stage, however. Although HDAS units have been used to make measurements of explosion effects that would have been impossible with normal instrumentation methods, several problems have been encountered with HDAS use in very severe explosion environments.

The most important problems to date are the HDAS units' vulnerability to crushing forces, being lost (i.e., not found after a test), and the recent case of electromagnetic interference. The crushing problem has largely been solved by redesign of the protective containers. An effort is also underway at WES to develop a miniature radio transmitter that can be included in HDAS packages used on large explosive tests. The transmitter should allow the HDAS units to be found up to several kilometers away after the test. A prototype transmitter has been designed, and preliminary experiments have confirmed its ability to survive high levels of detonation shock.

When the current work to overcome the operational problems described here is complete, the HDAS system will be turned over to the private sector for commercial production. At that time, it will become widely available as, we hope, a significant new tool for explosives safety research.

## ACKNOWLEDGEMENT

The analysis presented herein was performed by the U.S. Army Engineer Waterways Experiment Station. We gratefully acknowledge permission from the Chief of Engineers and the test sponsors to publish this paper.

## REFERENCES

1. Franco, Raphael A., Jr. and Ingram, James K; "HDAS, A Miniature, Self-Contained, Super-Hardened, Digital Data Acquisition System (module);" "Paper No. 78, DNA Conference on Instrumentation for Nuclear Weapons Effects Testing," June 1989, Monterey, CA.
2. Joachim, Charles E.; "Shallow Underground Tunnel/Chamber Explosion Test Program;" TR SL-90-10, August 1990; US Army Engineer, Waterways Experiment Station, Vicksburg, MS.
3. Ingram, James K. and Franco, Raphael A., JR.; "Test Results form HDAS Autonomous Digital Data Acquisition System Performance on the Joint UK/Australian Stocked Fragmentation Trials, Phase-4, Stage-1 Test"; (in publication); US Army Engineer, Waterways Experiment Station, Vicksburg, MS.
4. Davis, L. K., et. al.; "Evaluation of the Trench Storage Concept for Field Storage of Ammunition Trucks;" (in publication); US Army Engineer, Waterways Experiment Station, Vicksburg, MS.

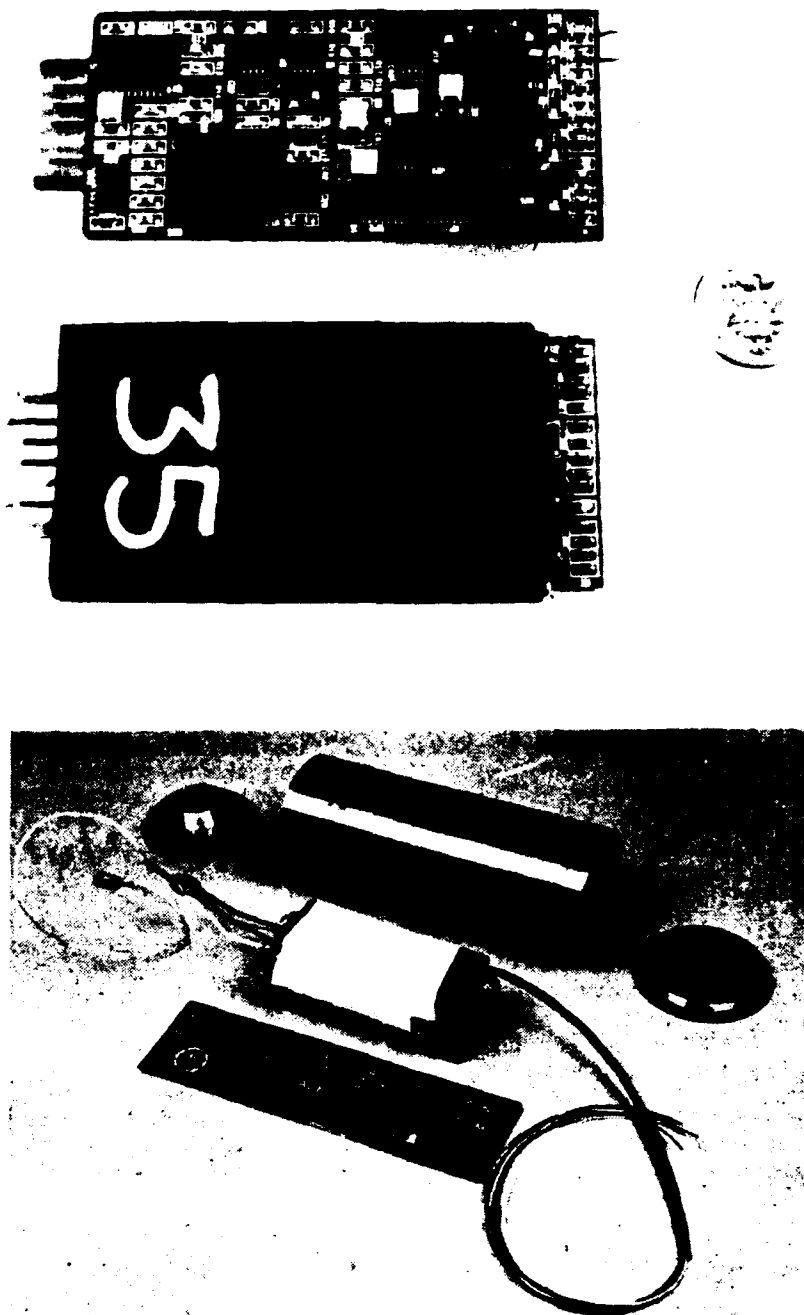


Figure 1. HDAS circuit board before and after encapsulation in epoxy case (top), and mated with batteries prior to insertion with sensors in protective canisters (bottom).

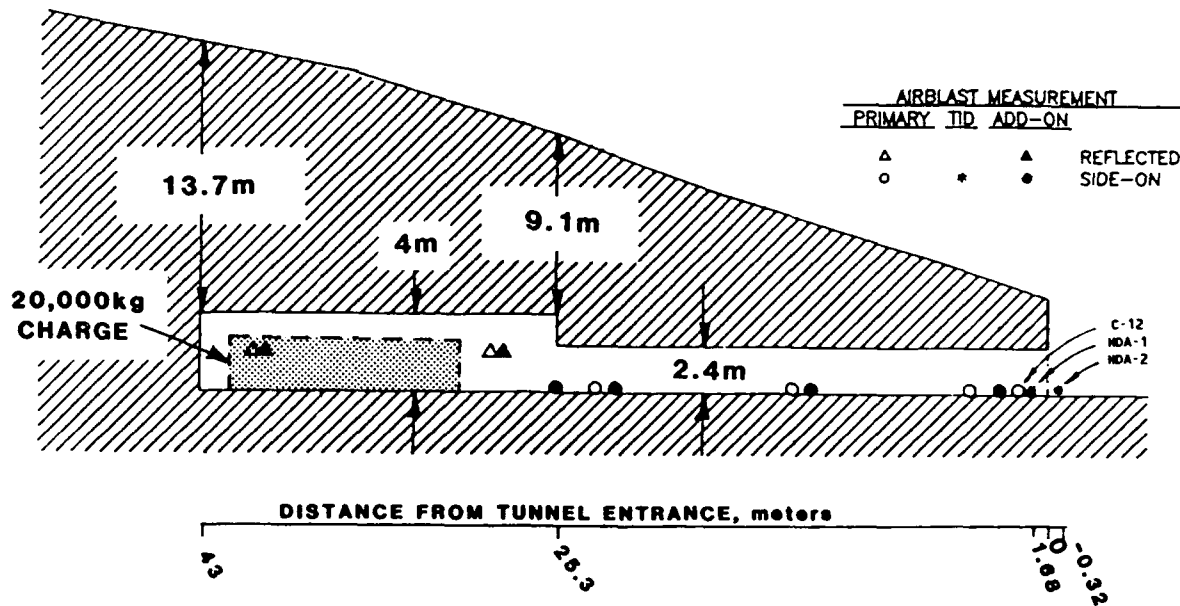


Figure 2. Elevation view of 1988 Klotz Club magazine test, showing locations of standard pressure gages (circles and triangles) and HDAS units (HDA-1 and -2).

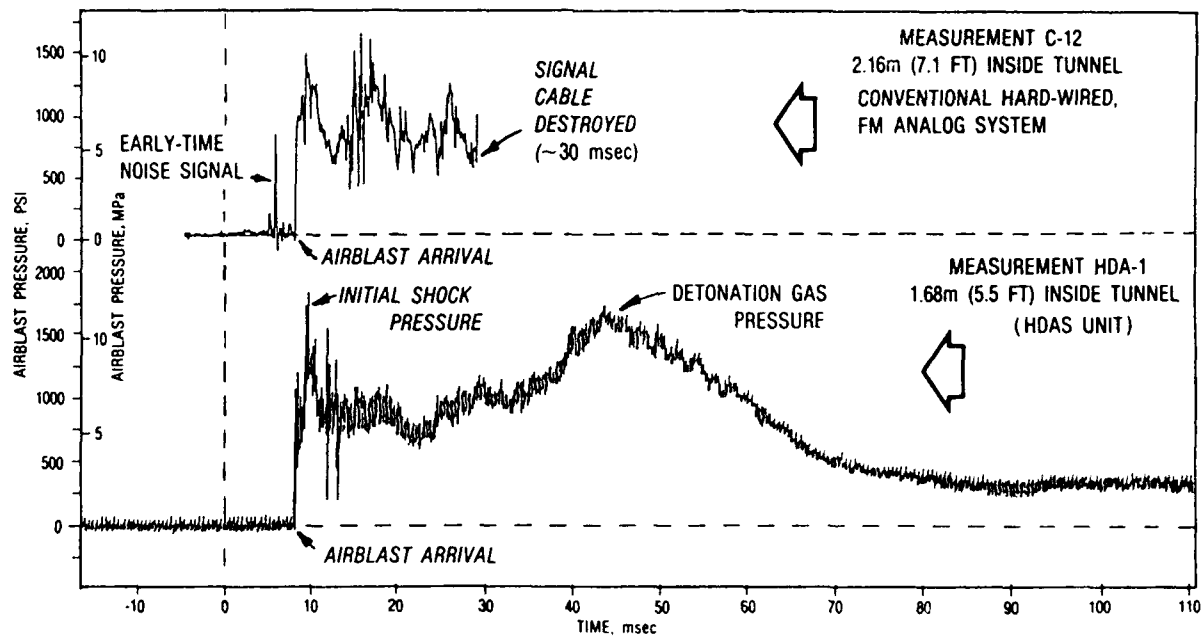


Figure 3. Comparison of pressure histories recorded by pressure gage (top) and HDAS unit, for 1988 Klotz magazine test.

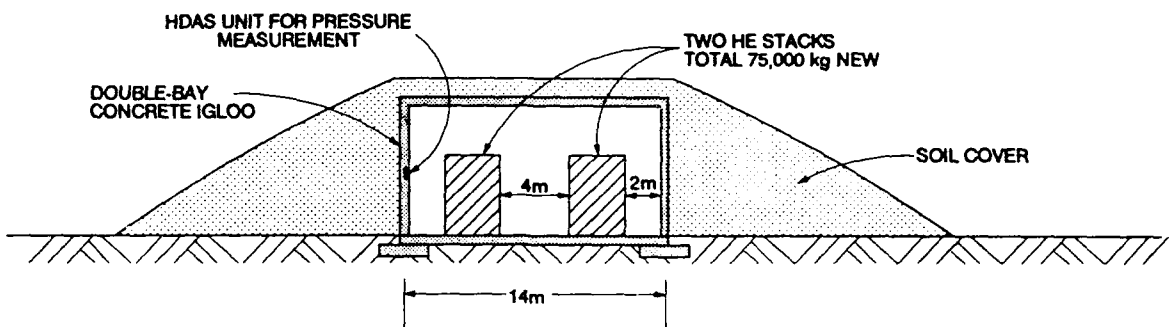


Figure 4. HDAS unit location to measure internal blast pressure from destructive test of a donor igloo magazine at Woomera, Australia.

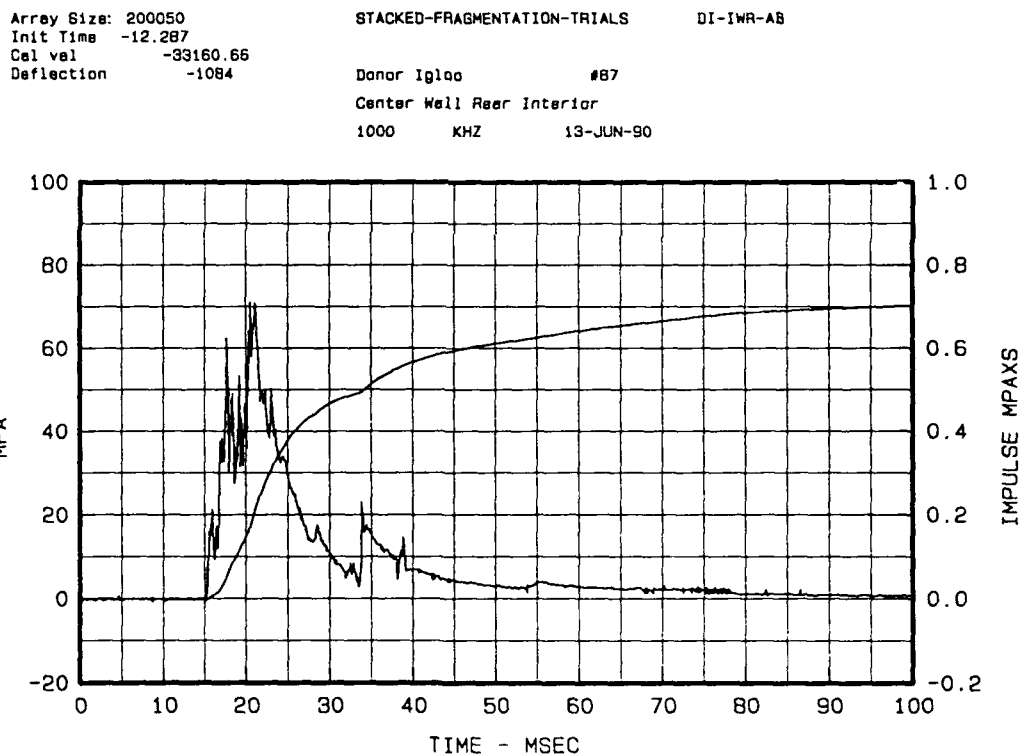


Figure 5. Blast pressure and impulse histories recorded by HDAS unit shown in Figure 4.

Array Size: 300050  
Cal val -131038.61  
Deflection -778

SPANTECH

AUG\_89

SA-1

HDAS

500

KHZ

21-NOV-91

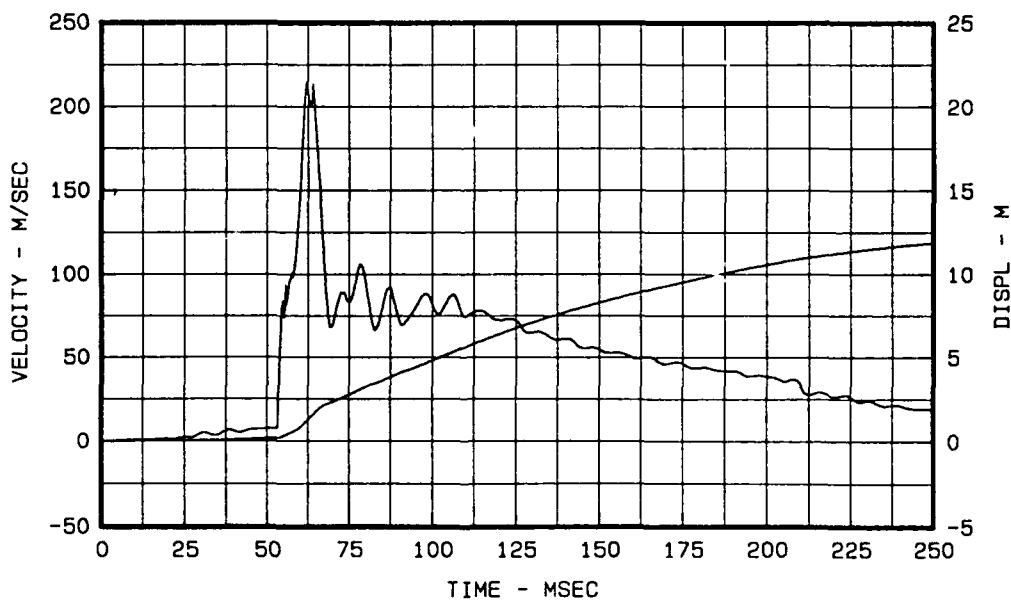
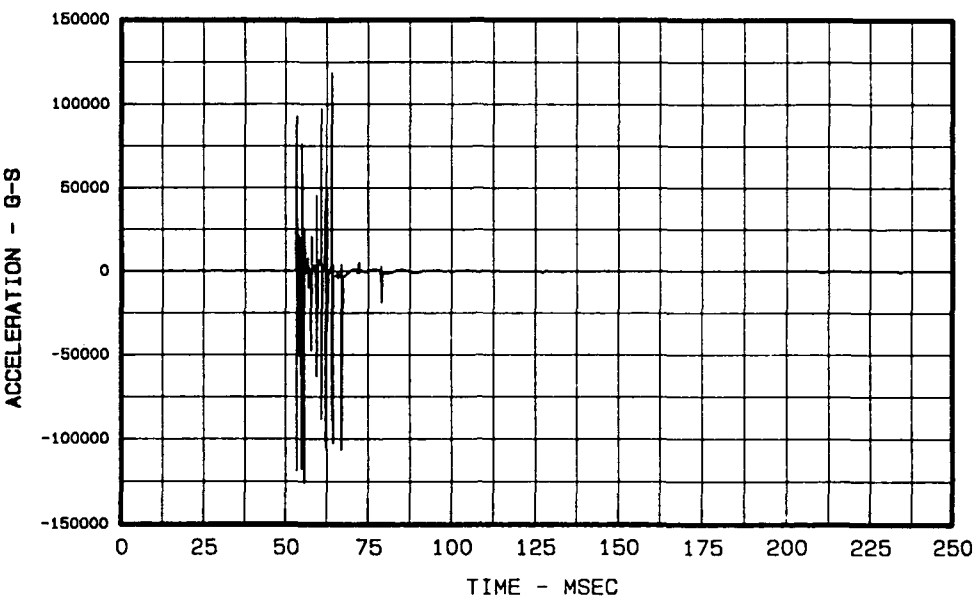


Figure 6. Records obtained by HDAS accelerometer units installed in top of Spantech concrete igloo to measure initial debris velocities for structure breakup by detonation of 75,000 kg of explosives. Acceleration record (top) was integrated to produce velocity and displacement histories.

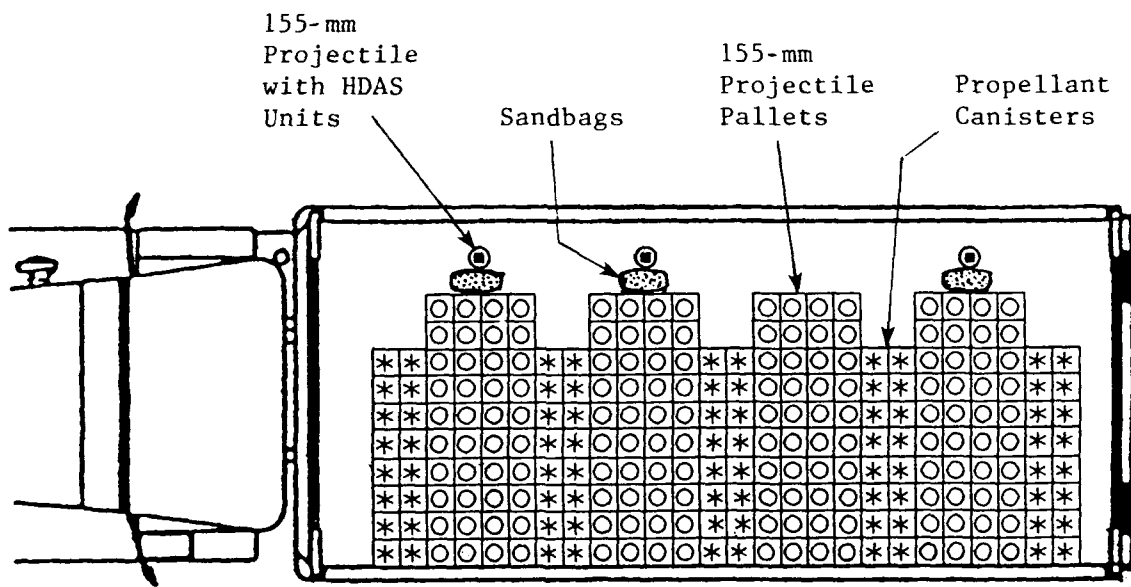
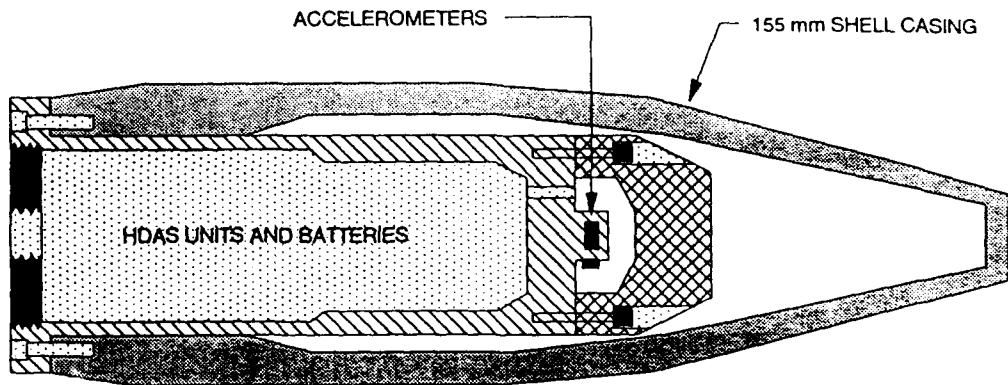


Figure 7. Installation of HDAS units with accelerometers in empty 155-mm projectiles (top) and placement of HDAS-instrumented projectiles on truckbed with Unit Basic Load of 155-mm ammunition.

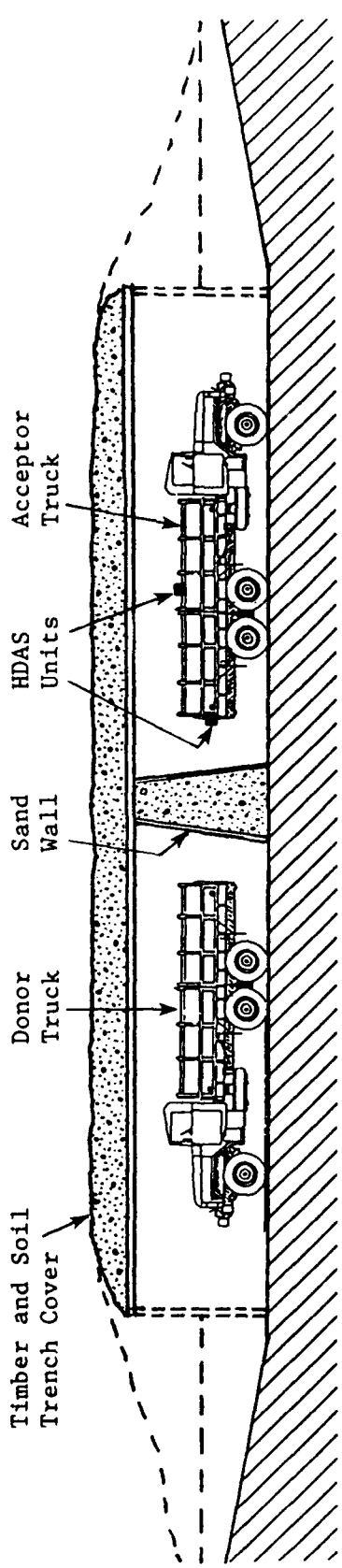


Figure 8. Locations of HDAS units used to measure blast pressures in Acceptor truck bay from detonation of Donor truck (Two-Truck Trench Test).

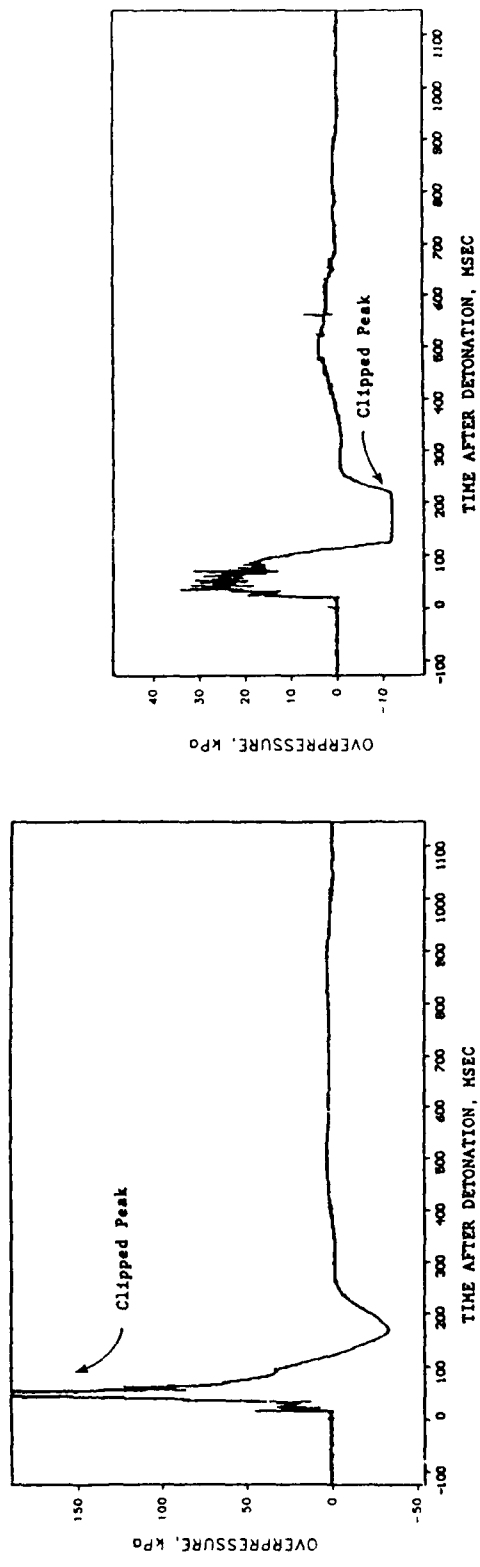


Figure 9. Blast pressure histories recorded by HDAS units for Two-Truck Trench Test; at rear of Acceptor truck (left) and on top of acceptor ammo load (right).

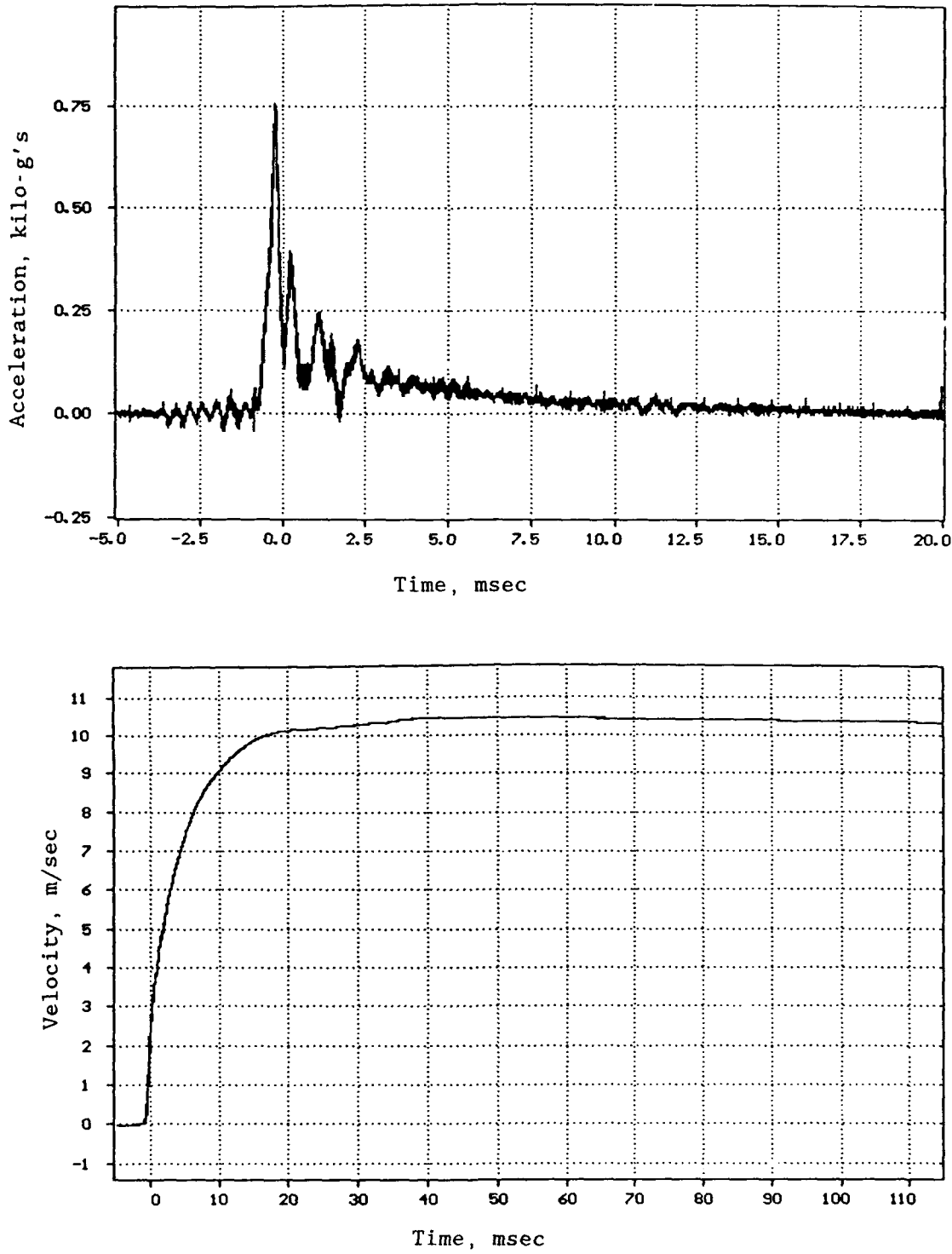


Figure 10. HDAS-recorded acceleration (top) and velocity of acceptor (inert 155-mm) projectiles induced by impact of sand wall between projectiles and donor detonation of a MK-82 GP bomb.

## **SAFETY CONSIDERATIONS IN STORING LIQUID GUN PROPELLANT XM46**

by J.S. Gardner

**U.S. Army ARDEC  
Picatinny Arsenal, N.J.  
07806-5000**

### **INTRODUCTION**

The U.S. Army is currently developing a regenerative liquid propellant gun for artillery application. The liquid propellant XM46 (LP) is composed of 60% Hydroxyl Ammonium Nitrate (HAN), 20% Triethanol Ammonium Nitrate (TEAN), and 20% water. Since this is the first time that a liquid gun propellant is being planned for field use, it is important to investigate the conditions and environment for safely storing the LP. This paper will discuss some of the considerations necessary for storing XM46.

### **STORAGE COMPATIBILITY GROUP ASSIGNMENT**

One major consideration for storing the LP is determined by its storage compatibility group assignment (SCG) given by its hazard classification. Liquid propellants have historically had their own classification and SCG assignment, however these hazard groupings (4 total) are designated by description in DARCOM 385-100 and not by rigorous testing. The LP XM46 is a monopropellant which did not fit any of these liquid hazard groupings. Therefore the tests required for solid propellant classification described in the Army TB 700-2 were modified for liquid propellant testing and then conducted on XM46 (ref 1). These tests resulted in a 1.3 interim hazard classification for the LP, but since there was no designation of liquid propellants for any of the storage compatibility groups in TB 700-2, the XM46 was given a compatibility group C which is the same as that for solid propellants. However, since liquid propellants have never been stored with solid propellants, the safety community requested that compatibility tests be conducted on solid propellants contaminated with XM46. Since there are no formal compatibility tests for an SCG assignment (assignment by description), the tests were developed independently and then reviewed by the local (ARDEC) Safety Office. The tests were the same as the interim hazard classification tests described in TB 700-2 but were conducted on solid propellants immersed in the LP for at least 3 weeks. These propellants passed all of the tests except for the Thermal Stability test, which indicates that a solid propellant cookoff is possible if contaminated with LP. As a result, the SCG for the LP was changed to group L, which simply states that any material in this group will be stored alone.

The next revision of Army TB 700-2 will be modified for interim hazard classification testing of liquid propellants, but the Storage Compatibility Group descriptions still do not include liquid propellants. It is recommended that a new SCG be developed which is designated specifically for liquid gun propellants, and that formal compatibility tests be developed for assigning new liquid propellants into the appropriate SCG.

### MATERIAL COMPATIBILITY

The decomposition temperature of neat XM46 is approximately 125°C, but it can be lowered if it degrades or becomes contaminated. Transition metals, for example, are known to accelerate the decomposition of HAN and lower the decomposition temperature of the LGP. Since the possibility of a spill in the magazine or storage site always exists, it is necessary to determine the compatibility of the LP with anything it may contact. This would include magazine construction materials, pallet and container materials, clothing and cleanup materials. Some of the materials necessary for compatibility tests are given below:

<u>Construction Materials</u>	<u>Packaging Materials</u>	<u>Cleanup Materials</u>
Concrete	Polyethylene	Rags
Wood (Softwoods)	Low Carbon steel	Rubber gloves
Pine	Paints (MSD 171)	Clothing
Nails	Plastic	Absorbent Mat'l's
	Fiberboard	

The compatibility tests to be developed will require analyzing the integrity of the material after LP contamination and also to analyze the sensitivity of the LP. This is designed to identify any materials which should not contact the LP or to identify the hazards which may occur in case of a spill.

### ENVIRONMENTAL PROTECTION

Another important consideration for storing the LP is to protect the environment in the case of a large scale spill. The storage facility may need to be bermed so that any size spill can be contained in the magazine and thereby preventing contamination to the outside environment.

### LONG TERM STORAGE

#### Temperature

It is also necessary to determine the maximum and minimum ambient temperature conditions required for safe long term storage. The XM46 does not freeze above -50 C, which is considered to be the coldest storage condition for propellants, and since degradation is decreased at lower temperatures, it is therefore anticipated that cold temperature storage should be safe.

However, since the LP does decompose more rapidly at elevated temperatures, it is essential to determine the kinetic rates of decomposition as a function of temperature and contamination, and also to determine the ignition temperature of the LP as a function of degradation. Current accelerated aging studies of the LP will eventually answer these questions (ref 2) and their results will be incorporated into the surveillance procedure for monitoring the stability of the LP during long term storage.

### Packaging

Another major factor in the long term storage of the LP is its container. It is very important to design a container which is compatible with the LP at the entire storage temperature range of -50°C to 65°C. Since metal contamination can increase LP decomposition, the material in contact with the LP must be non-metallic. However, not all plastic materials are compatible with the LP and other plastics may not maintain its integrity at the required temperature extremes. They may become brittle and break at low temperatures or become soft and pliable at elevated temperature. At the present time, high density polyethylene is the preferred material, but additional compatibility and temperature testing with the LP is required before the final material is chosen.

In addition to the container compatibility, it is also important to incorporate pressure relief features into the container so that any gaseous degradation can be vented thereby avoiding a container explosion from pressure build-up.

### REFERENCES

1. Seals, W.O., Herrera, W., and Grelecki, C., Hazard Classification of Liquid Propellants, 1990 JANNAF Propulsion Meeting
2. Tutt, G & Gardner, J.S. , "Modeling the Storage Degradation Kinetics of Liquid Propellant -XM46" 2nd ADPA Predictive Surveillance Symposium, Nov 13-14, 1991

# **High Explosive Material Testing Laboratory**

## **Scale Model Test**

by

B. Louise Bolton, Richard V. Browning,  
and Larry W. Berkbigler

### **ABSTRACT**

An experimental study of the personnel protective capability of a proposed high explosive material test laboratory using a one-eighth-scale model is summarized. Various configurations of the scale model were tested against internal blast loading over a range of scaled explosive charge weights. Pressures and resulting impulses were measured at pertinent locations on the model. The experimental results are compared with standard blast loading calculation methods. This study provides data for developing guidelines to protect personnel in typical high explosive test facilities.

---

## **1. INTRODUCTION**

A new High Explosive Material Test Laboratory specifically designed for materials property testing work on high explosive materials was configured with eight relatively small testing bays in order to separate different testing functions. Although the use of small, separate bays was done to enhance operational safety, there is a side effect of increasing pressure loadings on bay walls and building occupants outside a bay in the event of an accidental detonation.

Early calculations done using simple methods in design handbooks, such as Baker, Cox, Westine, Kulesz, and Strehlow (1983), indicated that using desirable HE loads in the working bays resulted in pressures close to the allowable 5 psi in the hallway outside the bays. To obtain more accurate values of pressures, an overstrong scale model of a bay pair was designed and constructed of aluminum plate. This model could be viewed as one end of the building or as a bay pair from the middle of the building. The overly strong model provides accurate scaled measurements of initial pressure loads in corridors, adjacent bays, and the immediate surroundings. It also allows for experimentation with simple modifications, such as alternate blow-out-wall (BOW) and bay door arrangements. It does not provide any information about the structural response of the building; it addresses only the blast pressure-induced structural loads. The scale model results will be used to calibrate the design handbook methods and provide reference values for interpolation to allowable HE loads. Additional tests are planned on the actual building to provide a final confirmation of the pressure levels expected in accidental situations.

The selection and arrangement of pressure gauges were based on recent experience in explosive effects testing, (Berkbigler and Walker, 1990), and earlier tests on scale buildings, (Anderson, 1969). The pressure gauges were arranged to measure the maximal effective pressure (referred to as "overpressure" in the rest of this report). DOE 6430.1A (1989) defines the maximal effective pressure as "the highest of (1) the peak incident pressure, (2) the incident plus dynamic pressure, or (3) the reflected pressure." The peak positive incident pressure is defined by DOE 6430.1A (1989) as "the almost instantaneous rise from the ambient pressure caused by a blast wave's pressure disturbance." The incident plus dynamic pressure (caused by particle flow) is the pressure of the blast wave once the wave continues past the tip of the probe. The reflected pressure is the pressure of the blast wave after it has been reflected off a solid surface. The peak positive incident pressure was measured only in the loaded bay because the blast wave was reflected many times before reaching the other pressure gauges.

## 2. DESCRIPTION OF THE MODEL

The model was a 1/8 scale of a bay pair of the proposed building. A hall and an instrument room were included in the model. The floor plan of the proposed building is shown in Figure 2.1. The model's roof was made of a steel plate with lead bricks for weight and was removable for easy access to the instrumentation. The model was made from 1/2-in. welded aluminum plate. The bay walls in the proposed building will be made from 12-in.-thick reinforced concrete. Because the wall thickness was not scaled exactly (the model walls should be 1 1/2 in. thick at 1/8 scale), the model's floor plan was not quite to scale, but sufficiently accurate. The floor plan of the model is shown in Figure 2.2. A photograph of the model is shown in Figure 2.3. The model had no permanent front wall or hallway door, so different blow-out walls and attenuator doors could be tested and the instrumentation and charge could be easily accessed. The blow-out walls and attenuator doors will be described in Sections 4.3 and 4.4.

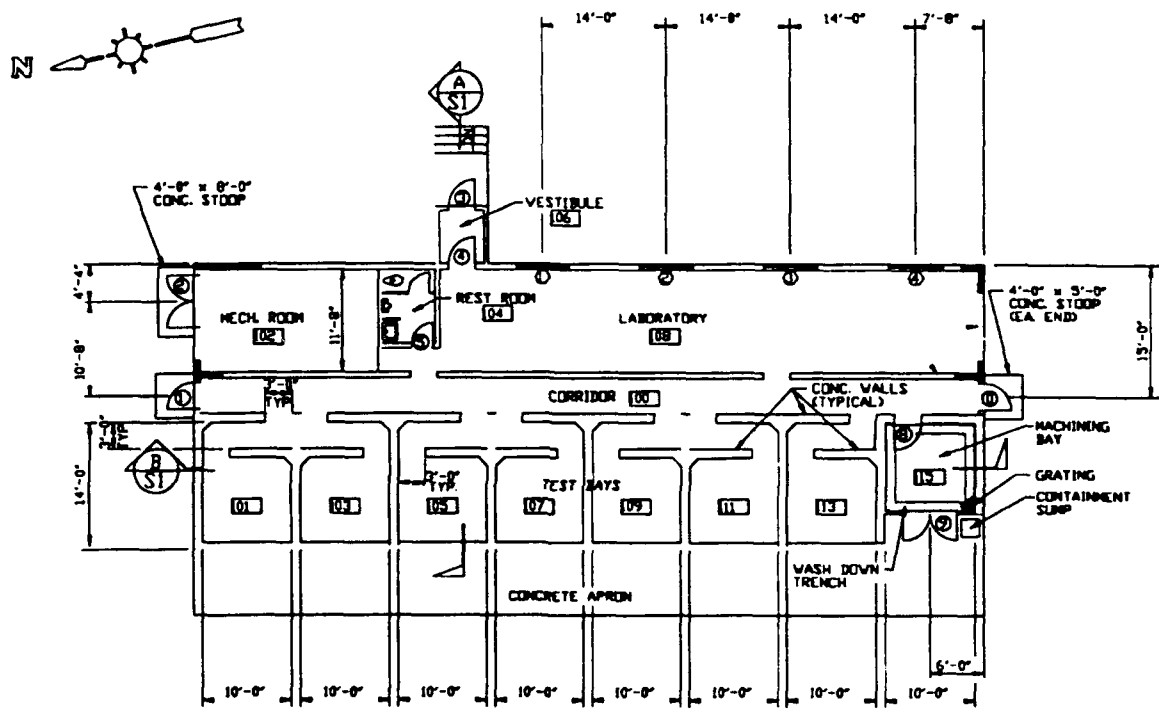


Figure 2.1. Floor plan of the proposed High Explosive Material Test Laboratory.

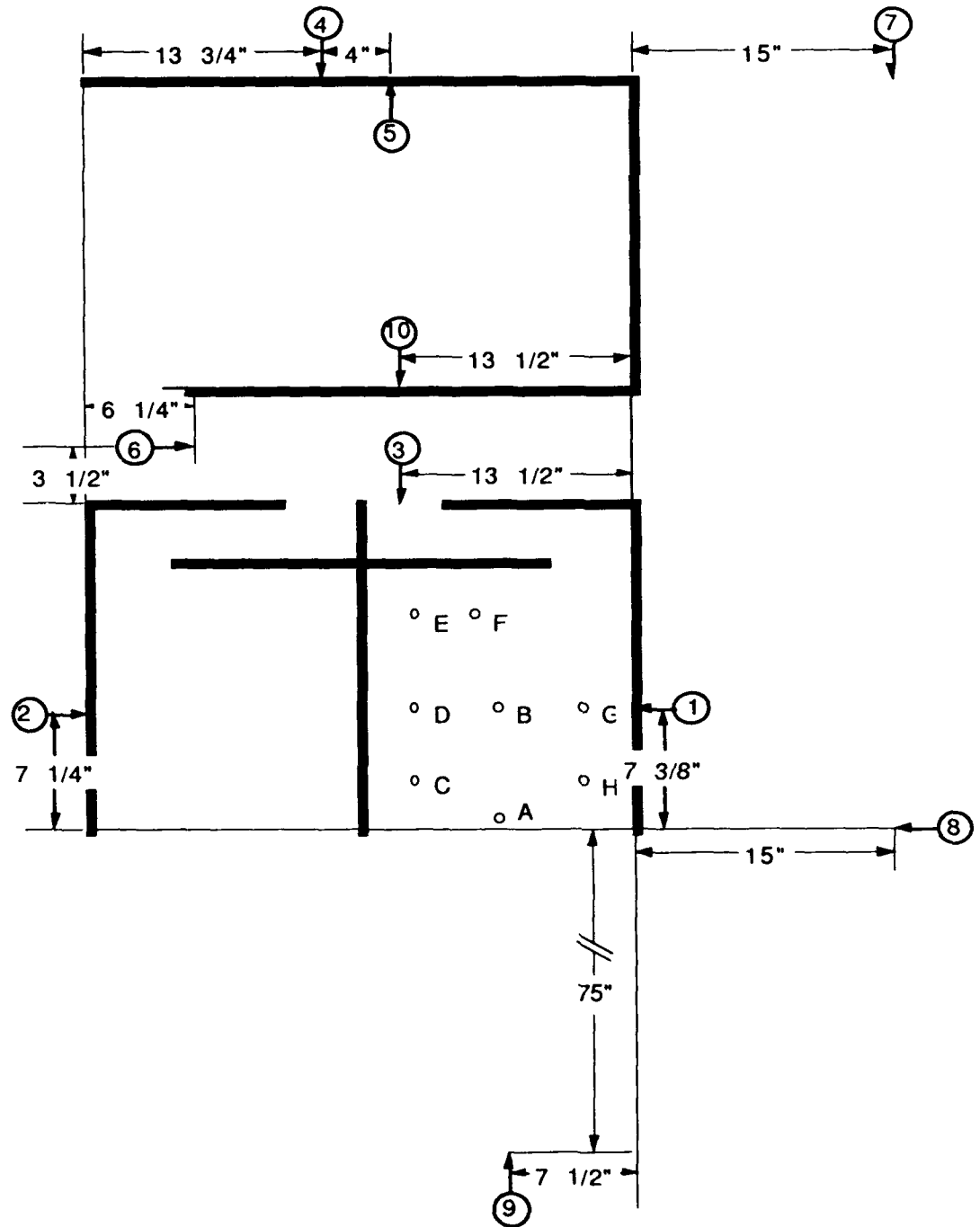


Figure 2.2. Floor plan of the model showing pressure gauge locations 1 through 10 and charge locations A through H.



Figure 2.3. Photograph of the model.

### 3. MODEL INSTRUMENTATION

#### 3.1. Description of pressure gauges

Three types of piezoelectric (PE) pressure gauges with internal amplifiers were used in the tests: PCB models 102M141, 102M156, and 102M160. These pressure gauges are designed to measure pressures normal to the blast wave. We plan to test the gauges further to find their response to off-axis pressure waves. Table 3.1 gives the pressure range, sensitivities, the discharge time constant, and bandwidth of each gauge. Table 3.2 gives the gauge assignment and gauge operating range for each channel by test. Model 102M160 became available for use only after test 22. Models 102M141 and 102M156 were used because of their availability even though their pressure range was higher than desired.

Gauge - PCB model	Pressure Range (psi)	Sensitivity (mv/psi)	Discharge time constant (sec)	Bandwidth (Hz)
102M141	1000	5	100	0.0016 - 100k
102M156	5000	1	500	0.0003 - 100k
102M160	200	30	1	0.16 - 100k

Table 3.1. The pressure range, sensitivity, discharge time constant, and bandwidth for each gauge.

	Tests 1-5	Tests 6-22	Tests 23-29	Test 30
Ch No.	Gauge / Operating Range (psi)			
1	102M156 / $\pm$ 350	102M156 / $\pm$ 350	102M156 / $\pm$ 350	102M156 / $\pm$ 700
2	102M141 / $\pm$ 20	102M141 / $\pm$ 20	102M160 / $\pm$ 20	102M160 / $\pm$ 80
3	102M141 / $\pm$ 20			
4	102M141 / $\pm$ 20			
5	102M141 / $\pm$ 20			
6	102M141 / $\pm$ 20			
7	102M141 / $\pm$ 20			
8	102M156 / $\pm$ 200	102M156 / $\pm$ 100	102M156 / $\pm$ 100	102M156 / $\pm$ 100
9	102M141 / $\pm$ 20	102M141 / $\pm$ 20	102M160 / $\pm$ 20	102M160 / $\pm$ 40
10	N.A.*	102M141 / $\pm$ 20 *	102M141 / $\pm$ 20	102M141 / $\pm$ 20

\*Channel 10 was not used in tests 1 through 7.

Table 3.2. The gauge assignment and gauge operating range for each channel by test.

All gauges were supplied with manufacturer's calibration sheets; the calibration values were used as exact gauge sensitivities. Before each event, each pressure gauge was checked using a compressed air "puff" (of about 15 psi) as a stimulus. The pressure gauges were located as shown in Figure 2.2.

### 3.2 Description of recording system

The NOMADD digital recording system was used for these events. All recording equipment was housed in the bunker at K-Site, which was located about 100 feet from the model. Nine analog data channels were used for the first 7 events, and 10 channels were used for the remaining 23 events. The NOMADD system also used several other types of channels for housekeeping and setup purposes.

#### 3.2.1. Cabling

The analog signals were carried from the model to the bunker by one overall-shielded 150-foot cable that contained 20 twisted/shielded pairs. At the model, each channel was terminated in an 8-pin connector and each gauge was wired to a mating 8-pin connector.

#### 3.2.2. Signal conditioners

Ectron 755 signal conditioning amplifiers were used for each data channel. They supplied excitation current to the gauges and the gain needed for the recording system channel.

For the PE pressure gauges on these tests, a 10-mA current source was used with a high pass filter having approximately a 40 sec. time constant. That time constant was

short enough to eliminate dc drifts in the gauges, while still being long enough to minimize filter roll-off errors during measurement periods.

The amplifier has a maximum bandwidth of dc to 100 kHz, a filter stage that can limit the bandwidth to lower ranges, and a maximum usable gain of 2000. The filter was set to 100 kHz for these tests.

The Ectron 755 also has a voltage calibration capability. Under computer control, the amplifier input can be switched between the gauge signal and a calibration source. Before each event, a programmable precision calibration source was connected to each amplifier's input. The calibration source was first set for zero and then for half-scale level. At each setting, the channel output was recorded and saved. When the finished data file is made, each channel's calibration information is used to correct the data for zero and gain errors in the recording system channel.

### **3.2.3. Recorders**

The amplifiers' outputs were recorded with Pacific 9820 transient digitizers. These recorders convert the data to 12-bit binary values at a maximum sample rate of 500 kilosample/sec. The sample rate for these tests was 500 kilosample/sec.

When the recorders are armed and triggered, they digitize and store data until they fill their local memories. For these events, 1 kilosample of data was saved for each channel before triggering and 15 kilosamples were saved after the trigger. After the recording is finished, the controlling computer reads the data from the digitizer local memory and stores it on a disk. The digitizer's local memories are battery backed up and retain the data until it is overwritten.

### **3.2.4. Triggering**

The system trigger is considered zero time on data plots. Because reliable triggering is crucial, redundant schemes using conditioning equipment fabricated by the Analysis and Testing Group were used for these events. The first trigger source was a voltage pulse from the fire set, and the second was a flash detector. In all these events, the fire-set pulse provided the system trigger. The fire-set trigger pulse was optically isolated from the fire set. The flash detector was a United Detector Technology PIN 10 detector with no filter. It was set to provide a trigger at about twice the intensity of midday sun.

## **3.3. Data formats**

After an event, the digitizer data is stored in raw data files on a hard disk in binary format. Binary format allows the highest transfer speed and uses the least storage space. The data quick-look is done using the raw data files, and data is backed-up and transported on digital tapes in the binary format.

Later, the raw data is converted and saved as finished data files. The finished data files are ASCII coded to enhance transportability and readability. They are also plotted for end users who desire hard copies.

## 4. MODEL TESTING

We varied five factors for the scale model test:

1. Charge magnitude
2. Charge location
3. Blow-out-wall design and use
4. Attenuator door design and use
5. Room addition

These five factors were varied in each of the 30 tests, but the tests can be grouped into three main categories. Data from the first 7 tests and test 30 are questionable because of problems with the instrumentation; however, we will present these results for comparison purposes.

### 4.1. Charge magnitude

Five charge magnitudes were used: 100 mg (the 1E30 detonator was assumed to be equivalent to a 100 mg charge), 500 mg, 2.5 g, 2.7 g, and 25.5 g. The TNT equivalent HEs for the model and prototype are given in Table 4.1 below. Table 4.1 gives the charge magnitude for each test. Calculations for the conversion from the charge used and the TNT-equivalent HE are given in the Appendix.

Charge	Equivalent HE model	Equivalent HE prototype
100 mg	0.0002 lb	0.1 lb
500 mg	0.001 lb	0.5 lb
2.5 g	0.005 lb	2.4 lb
2.7 g	0.005 lb	2.6 lb
25.5 g	0.048 lb	24.7 lb

Table 4.1. Equivalent HE.

### 4.2. Charge location

The charge was placed at one of eight locations in the loaded bay as shown in Figure 2.2. Location A, positioned front center of the blow out wall, was used for 17 of the 30 tests. Locations B through G were used for the remaining 13 tests. We varied the location of the charge to see the effect of charge location on the pressures in the surrounding rooms.

#### 4.3. Blow-out-wall design and use

Various blow-out-wall designs were used on the front wall of the loaded bay and adjacent bay. We simulated the density of proposed blow-out walls (scaled as described in Appendix A) by using Styrofoam sheets, aluminum sheets, and a combination of Styrofoam and aluminum sheets. The blow-out walls were generally modeled to match only the simulated density of the proposed blow-out walls areal density although the aluminum-Styrofoam assemblies were not totally unrealistic. Table 4.2 gives the density of each blow-out wall. Table 4.3 gives the loaded-bay configuration, and Table 4.4 gives the visual results for each test.

Test Number	Material/ Dimension/ Weight/ Density	Prototype equivalent
4, 5, 10-17, 20-28	Styrofoam/ 32 in. x 24 in. x 1 in./ 0.845 lb/ 1.9 lb/ft <sup>3</sup> (0.03 g/cm <sup>3</sup> )	1.27 lb/ft <sup>2</sup>
6-9	Styrofoam strips/ 8 ea. - 4 in. x 24 in. x 0.5 in./ 0.055 lb/ 1.9 lb/ft <sup>3</sup> (0.03 g/cm <sup>3</sup> )	0.63 lb/ft <sup>2</sup>
18-19	Styrofoam/ 2 ea. - 16 in. x 24 in. x 1-in./ 0.423 lb/ 1.9 lb/ft <sup>3</sup> (0.03 g/cm <sup>3</sup> ) Aluminum/ 4 ea. - 32 in. x 24 in. x .005 in./ 4.7 lb/ 168.5 lb/ft <sup>3</sup> (2.7 g/cm <sup>3</sup> ) Total	1.27 lb/ft <sup>2</sup> 1.12 lb/ft <sup>2</sup> 2.39 lb/ft <sup>2</sup>
29-30	Aluminum/ 32 in. x 24 in. x .063 in./ 4.7 lb/ 168.5 lb/ft <sup>3</sup> (2.7 g/cm <sup>3</sup> )	7.07 lb/ft <sup>2</sup>

Table 4.2. Blow-out-wall density and prototype equivalent.

<b>Test Charge</b>		<b>Equiv. HE</b>	<b>Confinement/Mitigation</b>
1	Det. only (100 mg)	0.1 lb	None
2	Det.+ 2.7 g PBX-9407	2.6 lb	None
3	"	"	None
4	"	"	1-in. Styrofoam BOW, both bays
5	"	"	1-in. Styrofoam BOW, one bay
6	"	"	0.5-in. Styrofoam BOW, door, header
7	"	"	0.5-in. Styrofoam BOW, header
8	Det. only (1E30)	0.1 lb	0.5-in. Styrofoam Strips BOW on other bay reinforced with two angles. Vinyl door. Pos. A
9	1E30 Det. + 2.5 g	2.4 lb	0.5-in. Styrofoam Strips BOW on both bays. Vinyl door. Pos. A.
10	"	"	1-in. Styrofoam BOW on both bays. Two vinyl doors. Pos. A.
11	"	"	1-in. Styrofoam BOW on both bays. One vinyl door. Pos. G.
12	"	"	Same as above. Pos H.
13	"	"	Same as above. Pos C.
14	"	"	Same as above. Pos D.
15	"	"	Same as above. Pos. E.
16	1E30 Det. + 2.5 g	2.4 lb	Same as above. Pos. F.
17	"	"	Same as above. Pos. A.
18	"	"	1-in. Styrofoam "Slide Door" with 1-in. brace. (1) layer 0.005-in. Al on each side of 1-in. Styrofoam BOW. Pos. A.
19	"	"	Massive Styrofoam. One layer 0.005-in. Al on each side of 1-in. Styrofoam BOW. Pos. A.
20	1E30 Det. + 500 mg	0.5 lb	1-in. Styrofoam BOW, no attenuator doors. Pos. A.
21	"	"	Same as above. Pos. B.
22	"	"	Same as above. Pos. G.
23	"	"	Same as above. Pos. A.
24	"	"	Same as above. Pos. H.
25	"	"	Same as above. Pos. C.
26	"	"	Same as above. Pos. D.
27	"	"	Same as above. Pos. E.
28	"	"	Same as above. Pos. F
29	1E30 Det. + 500 mg	0.5 lb	0.063-in. Al BOW, no attenuator doors. 1-in Styrofoam building addition (2-ft. addition). Pos. A.
30	1E30 Det. + 25.5 g	24.7 lb	0.063-in. Al BOW, massive Styrofoam door. 1-in Styrofoam building addition (2-ft. addition). Pos. A.

Table 4.3. Summary of the loaded-bay configuration for each test.

TEST	VISUAL DAMAGE NOTES FROM VIDEO AND PHOTOS
1	No BOW.
2	No BOW, smoke.
3	No BOW.
4	One BOW covered both bays. The BOW blew straight out and up and broke into two pieces. The half piece in front of the adjacent bay dropped slowly to the ground and the other half broke up into two large pieces and several small pieces that were blown around. Explosion moved roof back.
5	One BOW covered the main bay and 1/3 of the adjacent bay. The explosion broke up the BOW into five big pieces and several small pieces
6	Two BOWs with four strips each. The strips were broken into many pieces in the main bay. The adjacent bay had two strips that remained attached and whole and two strips that were broken in half.
7	Two BOWs with four strips each. Main bay had one strip that was almost whole and three that were broken into pieces. Adjacent bay had one strip that stayed intact and attached, two strips that broke in half, and one strip that was blown apart and away.
8	No video.
9	Two BOWs with four strips each. All strips broke. Retaining bar in adjacent bay broke strips in half with top half of strips remaining attached. Pieces of the main bay blew out and back around the building.
10	One BOW, covering both bays, stayed in one piece after explosion.
11	Two BOWs. Main BOW blew apart; adjacent BOW separated from the building intact.
12	Two BOWs. Main BOW blew apart; adjacent BOW separated from the building intact.
13	Two BOWs. Main BOW blew apart; adjacent BOW separated from the building intact at a delayed time
14	Two BOWs. Both broke up. A large piece of the adjacent BOW still attached. Roof moved back approximately 3/4 in.
15	Two BOWs. Main BOW broke in several pieces, adjacent BOW broke in half down the center. Vinyl door damaged slightly, strips twisted.

Table 4.4. Summary of the visual results for each test.

TEST	VISUAL DAMAGE NOTES FROM VIDEO AND PHOTOS
16	Two BOWs. Main BOW blew off intact, adjacent BOW stayed together and slowly dropped to the ground. Roof moved back approximately 11/16 in.
17	Two BOWs. Bright flash. Main BOW blew off from bottom to top, could not see door remains. Adjacent BOW dropped slowly top first to the ground and remained intact.
18	Two BOWs. Bright flash. Main BOW blew off; top intact and bottom mangled. Adjacent BOW blew off, breaking far left corner.
19	Two BOWs. Bright flash. Main BOW torn apart and sheet separated from Styrofoam. Adjacent BOW fell slowly to ground intact.
20	Two BOWs. Smaller bright flash. Main BOW has small hole from charge. Adjacent BOW still attached.
21	Two BOWs. No flash. Main BOW blew off vertically, adjacent BOW still attached.
22	Two BOWs. No flash. Main BOW blew off vertically, adjacent BOW still attached.
23	Two BOWs. No flash. Main BOW blew off vertically, but not as fast or as far as BOW in tests 21 and 22. Adjacent BOW still attached.
24	Two BOWs. No flash. Main BOW broke in half (top/bottom) plus a few small pieces. Adjacent BOW still attached.
25	Two BOWs. Saw a flash. Main BOW broke in half (top/bottom) plus a few small pieces. Adjacent BOW dropped to ground intact.
26	Two BOWs. Saw a very small flash. Main BOW blown off intact. Adjacent BOW separated at sides from building.
27	Two BOWs. Very, very small flash. Main BOW blown off intact, adjacent BOW intact.
28	Two BOWs. No flash. Main BOW blown off intact, adjacent BOW separated slightly at sides but returned back to original place.
29	One BOW covered both bays. Building addition. BOW blown off bottom first, rest of building intact.
30	One BOW covered both bays. Building addition. flash larger than building. Building addition destroyed, roof blown off, BOW blown off and mangled.

Table 4.4. (cont.)

#### **4.4. Attenuator door design and use**

Various attenuator doors were installed in the doorway to the loaded bay in combination with the blow-out walls. Vinyl strips were used in tests 8 through 17, a massive Styrofoam door was used in tests 19 and 30, and a braced Styrofoam slide door was used in test 18 (see Figure 4.1). For the other 17 tests no attenuator door was used. A header was also installed in the doorway for test 6 and all tests following.

#### **4.5. Room addition**

A room addition, shown in Figure 4.1, was added to the scale model to better simulate a complete building. The scale model without the room addition had openings directly to the exterior, and we felt that these openings may have lowered the interior pressures. The addition was made from 1-in.-thick Styrofoam sheets held together with tape. The addition was used in tests 29 and 30. It survived test 29 with a 0.5-lb-equivalent charge substantially intact but was demolished by the 24.7-lb-equivalent charge of test 30.

#### **4.6. Test categories**

The 30 tests can be grouped into three main categories:

1. 1-in. Styrofoam blow-out wall and vinyl attenuator door with 2.4-lb-equivalent HE charge at seven locations (tests 11 through 17);
2. 1-in. Styrofoam blow-out wall and no attenuator door with 0.5-lb-equivalent HE charge at eight locations (tests 20 through 28);
3. Comparison of a variety of blow-out walls and attenuator doors with various charges at location A (tests 1 through 10, 17 through 20, 23, 29, and 30).

Note that category 3 does include a few tests from categories 1 and 2.

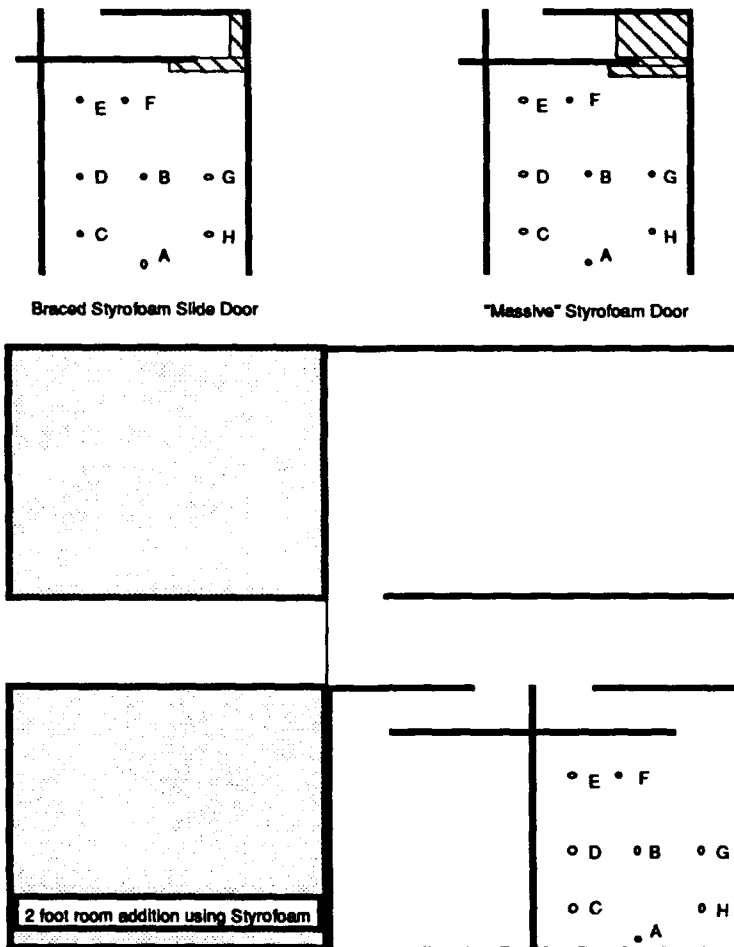
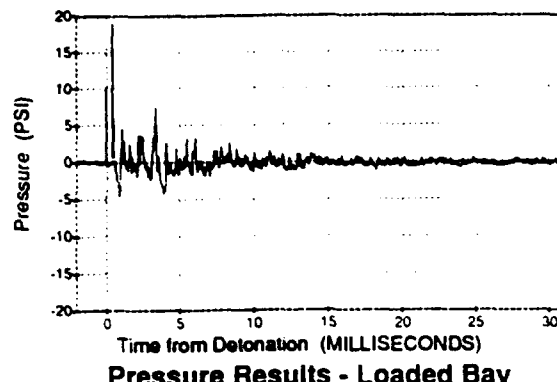


Figure 4.1. Attenuator door design and room addition.

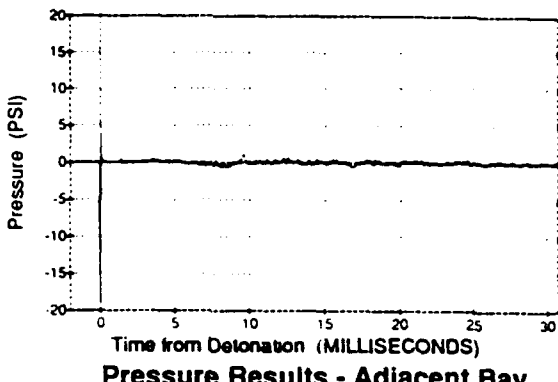
## 5. MODEL TEST RESULTS

### 5.1. Pressure time histories

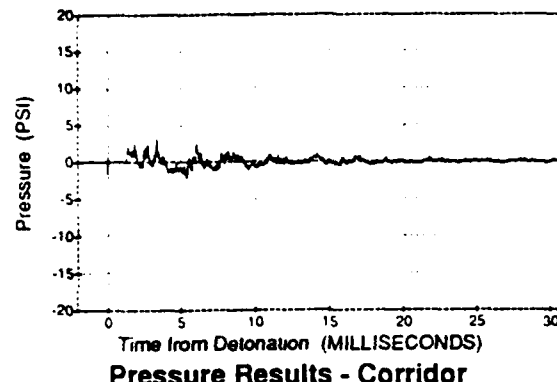
We obtained pressure time histories from the interior and exterior pressure gauges described in the Model Instrumentation Section. An example of pressure time histories for six sensor locations is shown in Figure 5.1. From this data, we read off the peak pressure. These peak pressures are summarized in Table 5.1.



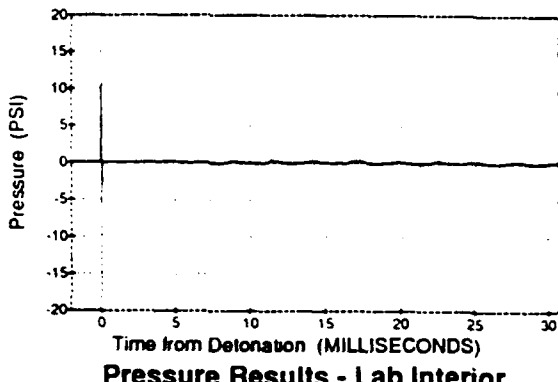
**Pressure Results - Loaded Bay**



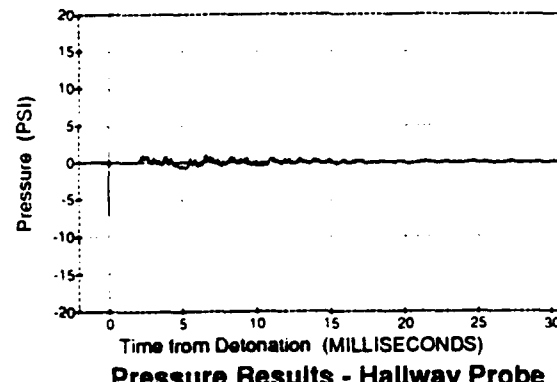
**Pressure Results - Adjacent Bay**



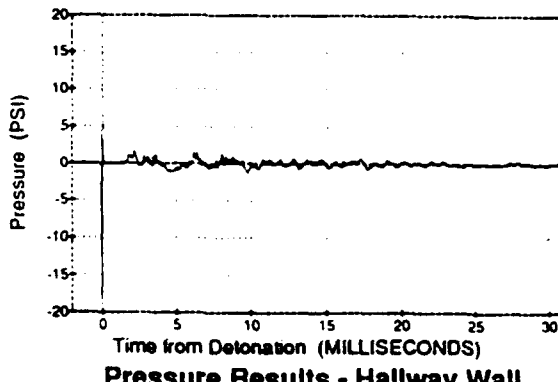
**Pressure Results - Corridor**



**Pressure Results - Lab Interior**



**Pressure Results - Hallway Probe**



**Pressure Results - Hallway Wall**

**Figure 5.1.** Example of time history pressure results for six sensor locations. Data from test 20. A 0.5-lb-equivalent HE charge was used at position A. Facility had a 1-in. Styrofoam blow-out wall and no attenuator doors.

Test	Loc	Ch. 1	Ch. 2	Ch. 3	Ch. 4	Ch. 5	Ch. 6	Ch. 7	Ch. 8	Ch. 9	Ch. 10
		Loaded Bay (psi)	Adjacent Bay (psi)	Corridor	Lab Interior (psi)	Rear Wall, Ex (psi)	Hallway Probe (psi)	Rear Corner, Ex (psi)	Front Corner, Ex (psi)	50 ft. from Bow (psi)	Hallway Wall (psi)
1	A	10	2.6 (noisy)	0.9 (noisy)	3.4 (noisy)	0.1 (flat)	0.6	0.2	1.3	0.5	N.A.
2	A	62	13.2 (noisy)	7.3 (noisy)	6.4 (noisy)	0.1	3.8	0.5	10.0	2.4	N.A.
3	A	95	9.2	11.1	3.4 (noisy)	0.6	4.1	1.4	10.0	2.2	N.A.
4	A	98	5.0	18.3	4.6 (noisy)	0.7	6.5	1.1	3.6	1.5	N.A.
5	A	74	5.6	15.1	1.8 (noisy)	0.5	6.4	0.3	3.8	1.4	N.A.
6	A	85	3.3	4.9	1.6 (noisy)	0.5	4.6 (flat)	0.7	5.7	bad data	N.A.
7	A	75	3.8	15.7	0.6	0.5	5.8	0.7	3.8	2.0	N.A.
8	A	12	0.5	1.2	0.2	0.0	0.5	0.1	1.4	0.6	0.5
9	A	83	3.5	5.8	1.9 (noisy)	0.5	2.4	0.5	5.0	1.6	4.7
10	A	85	5.1	6.6	1.3	0.6	2.4	0.5	3.2	1.3	3.9
11	G	276	2.8	7.9	0.8	0.7	5.6	1.1	6.2	2.7	6.0
12	H	117	2.1	8.0	0.6	0.6	3.1	0.8	5.9	1.3	4.8
13	C	55	5.8	6.7	0.6	0.5	2.7	0.7	4.1	2.0	5.2
14	D	68	3.5	8.6	0.7	0.8	3.5	0.8	7.6	1.7	6.2
15	E	140	2.1	5.8	0.6	0.5	3.3	0.9	7.1	2.3	4.1
16	F	49	2.7	7.1	0.6	0.5	5.6	1.0	4.0	2.3	6.6
17	A	54	5.0	6.0	0.5	0.5	3.1	0.6	4.5	1.2	3.6
18	A	57	7.5	5.3	2.4	0.5	3.1	0.5	3.3	2.7	3.7
19	A	52	4.1	0.9	0.8	0.5	0.9	0.5	3.8	1.3	1.0
20	A	20	1.2	3.3	0.5	0.1	1.2	0.1	0.9	0.5	1.7
21	B	42	0.7	3.5	0.5	0.2	1.8	0.2	1.4	0.4	1.8
22	G	55	0.8	4.3	0.4	0.1	1.8	0.3	1.2	0.4	2.4
23	A	29	1.1	2.7	0.5	0.1	1.2	0.1	1.1	0.6	1.8
24	H	44	0.8	3.9	0.5	0.1	1.7	0.2	2.5	0.7	1.9
25	C	19	1.9	3.9	0.5	0.1	1.7	0.1	0.8	0.6	2.3
26	D	25	1.0	3.1	0.5	0.2	1.9	0.2	1.2	0.4	2.1
27	E	32	1.0	3.3	0.6	0.2	1.3	0.3	1.0	0.5	1.6
28	F	30	0.8	3.5	0.5	0.2	1.4	0.2	1.0	0.3	1.4
29	A	26	1.2	3.9	0.4	0.2	1.4	0.2	1.2	0.4	2.6
30	A	320	18.4	19.7	6.2 (noisy)	5.0	20.2	4.0	32.9	27.0	19.8

Table 5.1. Pressure results from all sensors.

## 5.2. Impulse time histories

From the interior channels, we determined the resulting impulse time histories. Tabular results of the peak impulse are shown in Table 5.2. Impulse results were taken from tests 9 through 30.

Test	Ch. 1 Loaded Bay (psi-ms@ms)	Ch. 2 Adjacent Bay (psi-ms@ms)	Ch. 3 Corridor (psi-ms@ms)	Ch. 6 Hallway Probe (psi-ms@ms)	Ch. 10 Hallway Wall (psi-ms@ms)
9	N.A.	1.3 @ 3.7	2.5 @ 3.3	1.1 @ 4.2	2.0 @ 3.6
10	11.6 @ 2.8	1.2 @ 4.4	2.7 @ 3.6	1.2 @ 4.2	1.9 @ 3.6
11	14.0 @ 2.3	1.1 @ 4.5	6.9 @ 3.4	2.5 @ 3.5	4.6 @ 3.7
12	10.1 @ 2.7	1.0 @ 4.8	5.2 @ 3.4	1.8 @ 3.7	3.6 @ 3.4
13	9.7 @ 1.7	1.5 @ 4.3	4.0 @ 3.0	1.4 @ 3.9	2.7 @ 3.4
14	12.7 @ 2.6	1.5 @ 4.9	5.5 @ 3.5	1.9 @ 3.9	3.6 @ 3.5
15	17.1 @ 2.3	1.1 @ 4.6	5.9 @ 3.3	2.2 @ 3.7	3.8 @ 3.3
16	13.1 @ 2.4	1.4 @ 4.5	7.4 @ 3.3	2.8 @ 3.6	5.0 @ 3.5
17	8.5 @ 2.6	1.3 @ 4.8	3.3 @ 3.1	1.3 @ 4.0	2.3 @ 3.6
18	10.9 @ 3.1	1.8 @ 3.5	3.5 @ 3.8	1.4 @ 4.2	2.3 @ 3.8
19	11.8 @ 2.9	1.3 @ 4.4	0.7 @ 5.9	0.5 @ 5.2	0.6 @ 6.2
20	2.1 @ 3.4	0.3 @ 5.5	1.5 @ 3.9	0.5 @ 4.4	0.9 @ 3.9
21	3.9 @ 3.2	0.4 @ 5.2	1.9 @ 3.5	0.6 @ 4.1	1.1 @ 3.8
22	4.1 @ 3.2	0.5 @ 5.0	1.9 @ 3.9	0.7 @ 3.8	1.2 @ 3.4
23	2.3 @ 3.6	0.3 @ 5.6	1.3 @ 3.9	0.4 @ 4.1	0.8 @ 3.8
24	2.4 @ 3.2	0.5 @ 5.3	1.8 @ 3.8	0.7 @ 4.0	1.2 @ 3.6
25	3.8 @ 0.9	0.5 @ 4.9	2.1 @ 3.7	0.8 @ 4.5	1.5 @ 3.9
26	3.8 @ 1.1	0.5 @ 5.3	2.2 @ 3.8	0.7 @ 4.2	1.3 @ 3.8
27	3.9 @ 2.9	0.5 @ 5.3	2.1 @ 3.8	0.7 @ 4.1	1.4 @ 3.7
28	4.0 @ 3.7	0.5 @ 5.3	2.0 @ 3.9	0.7 @ 4.0	1.3 @ 3.5
29	4.1 @ 3.5	0.6 @ 5.8	2.7 @ 3.9	0.9 @ 4.3	1.6 @ 4.1
30	92.3 @ 3.4	9.0 @ 3.7	N.A.	N.A.	N.A.

Table 5.2. Tabular results of peak impulses at five interior locations.

## 5.3. Charge location comparison

We looked at the effect of charge location in the loaded bay on various interior locations by comparing the peak pressure and peak impulse as shown in Figures 5.2 and 5.3.

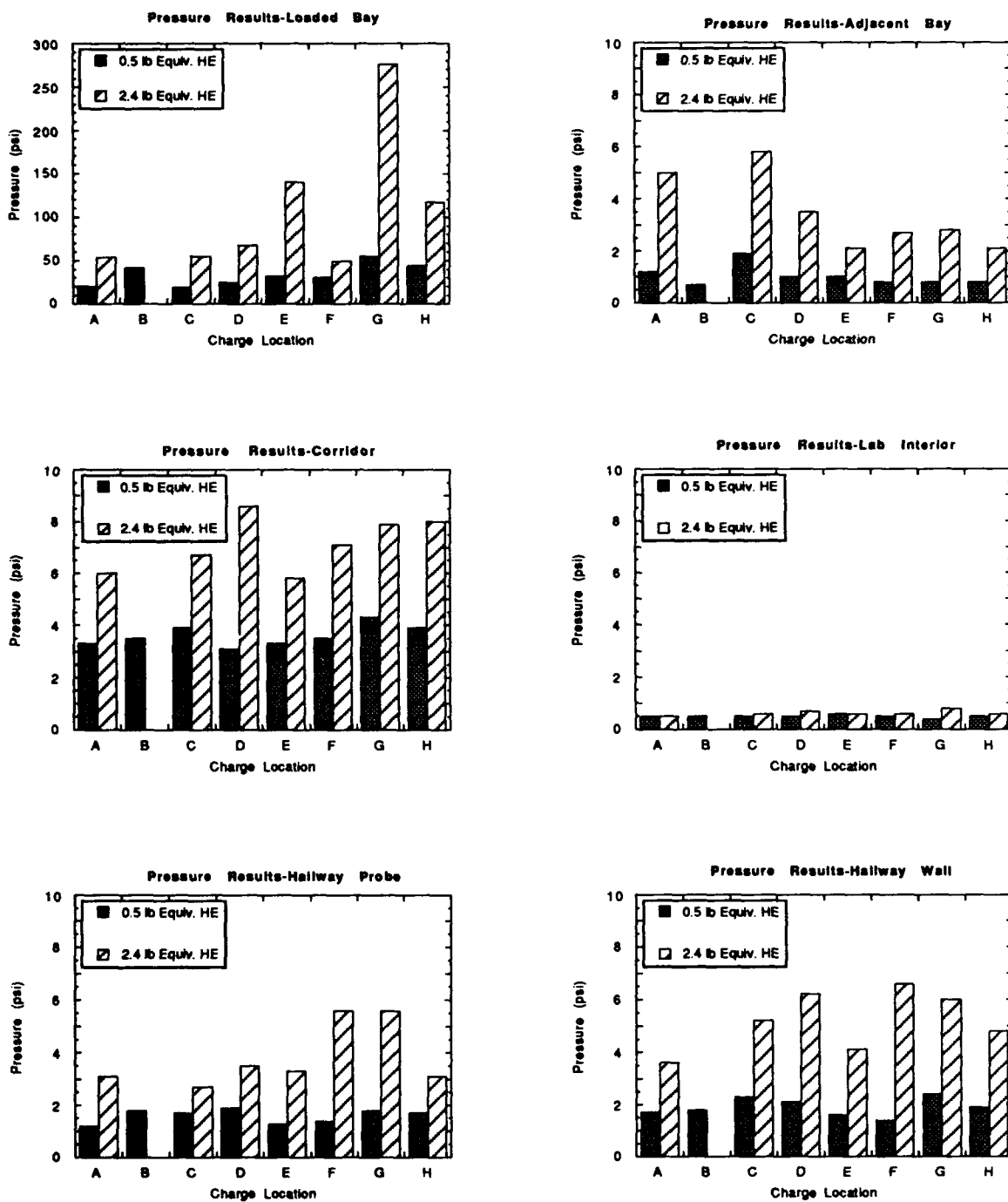


**Figure 5.2.** Comparison of 0.5-lb- and 2.4-lb-equivalent HE charge pressure results at six interior locations as a function of charge location. (Note the change in the pressure scale for the loaded bay.)

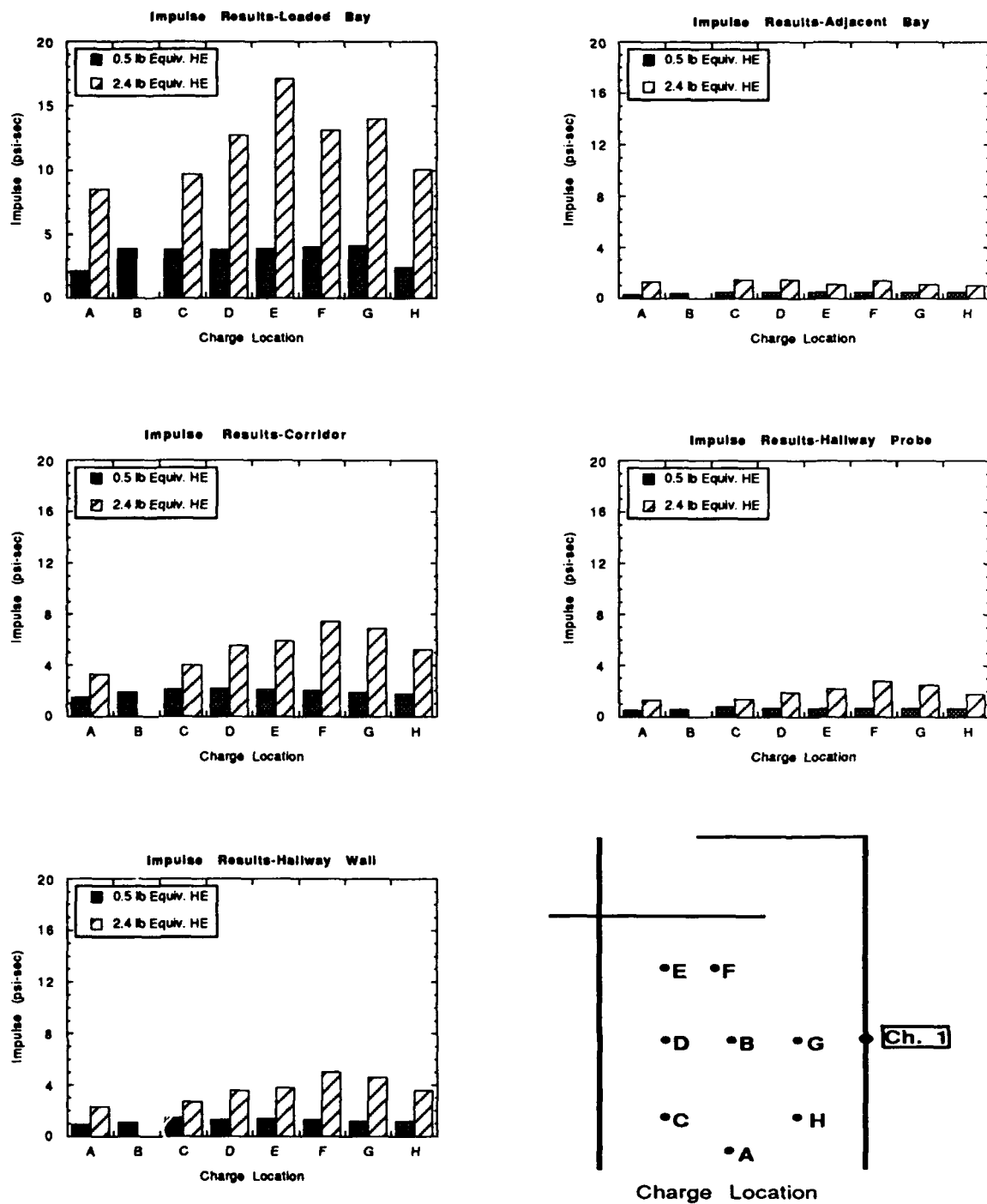


Figure 5.3. Comparison of 0.5-lb- and 2.4-lb-equivalent HE charge impulse results at five interior locations as a function of charge location.

#### **5.4. Scaled distance versus pressure**

In order to extrapolate pressure at various locations in the building, we compared our pressure and position data with two log-log plots found in Baker et al. (1983):

- 1) Side-On Blast Wave Properties for Bare, Spherical TNT at Sea Level (Figure A.1) and
- 2) Normally Reflected Blast Wave Properties for Bare, Spherical TNT at Sea Level (Figure A.2).

To compare our data with bare, spherical TNT log-log plots we normalized our charge weight to bare, spherical TNT at sea level. Because our charge was placed on the floor, we multiplied the charge weight by a factor of 2 to take into account the reflection off the hard surface (DOE/TIC-11268, 1980).

As a check on our arrival time data, we compared the measured distance between the charge and each pressure gauge, with distances based on blast arrival times. Blast arrival times were converted into scaled arrival times, as discussed in Appendix A. Scaled distance was read off the arrival time curve from the Side-On Blast Wave Properties for Bare, Spherical TNT at Sea Level log-log plot (Figure A.1). The measured distance between the charge and each pressure gauge was converted into a scaled prototype distance as discussed in Appendix A. The scaled distances were then plotted versus the peak pressure as shown in Figures 5.4 and 5.5. As a comparison, side-on and reflected pressures (adjusted for altitude) from the bare, spherical TNT plots (Figures A.1 and A.2) are also shown on the plot. There is scatter in the distance data in Figures 5.4 and 5.5 for each pressure gauge (channel) because of the different charge weights and charge locations.

A few discrepancies in the data will be discussed next. The scaled distance (based on arrival time) plot, Figure 5.5, does not have as many data points as the scaled measured distance plot because many arrival times were questionable for channels 4, 5, and 7. Channels 4 and 5 had low signal-to-noise ratios, possibly from wall vibrations, and channel 7 had problems from sunlight. Channel 4 recorded a frequency between 300 and 500 Hz, in the range of the natural vibration of 400 Hz for a plate clamped on all sides. Channel 5 had a frequency in the range of 1000 to 1500 Hz. Channels 4 and 5 were both located in the same wall but the mounting of channel 5's support inside the model makes the vibration approximation more difficult. Another factor in the low pressure readings for channels 4, 5, and 7 was the measurement limits of the pressure gauges. The pressure gauge, rated for 1000 psi and operated at  $\pm 20$  psi, was measuring pressures below 0.5 psi. Also some of channel 1 data is on the high side. This is probably because location of the charge relative to the pressure gauge in the loaded bay. Data from channel 9 was higher than the bare spherical TNT plots because of the effects of the blow-out wall delaying arrival times and/or increasing pressures.

The remaining data agrees well with the bare, spherical TNT pressure curves. This good agreement indicates that we can extrapolate peak pressure at various locations in the building.

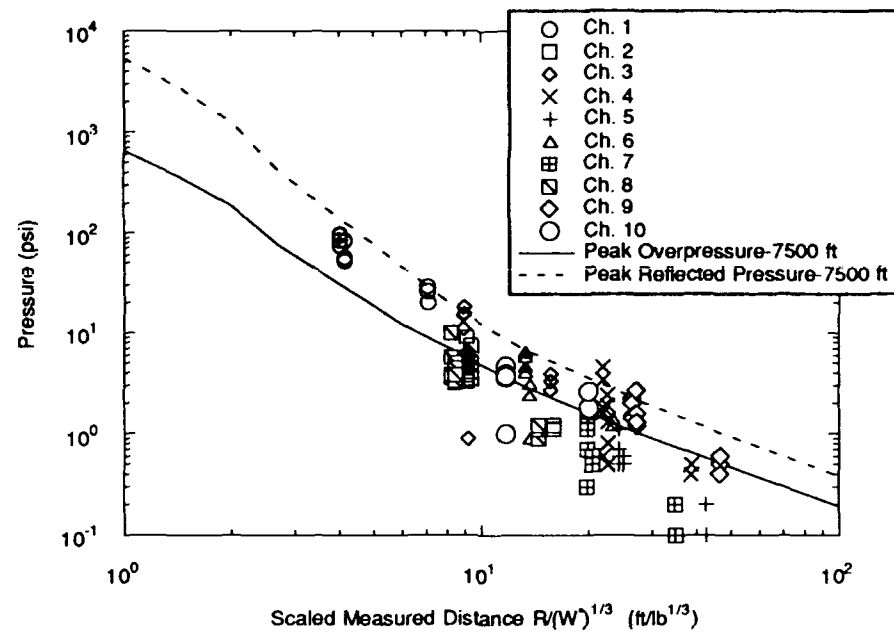


Figure 5.4. Scaled measured distance versus pressure for charge location A. As a comparison, side-on and reflected pressures (adjusted for altitude) from bare, spherical TNT charges (see Figures A.1 and A.2) are also shown on the plot.

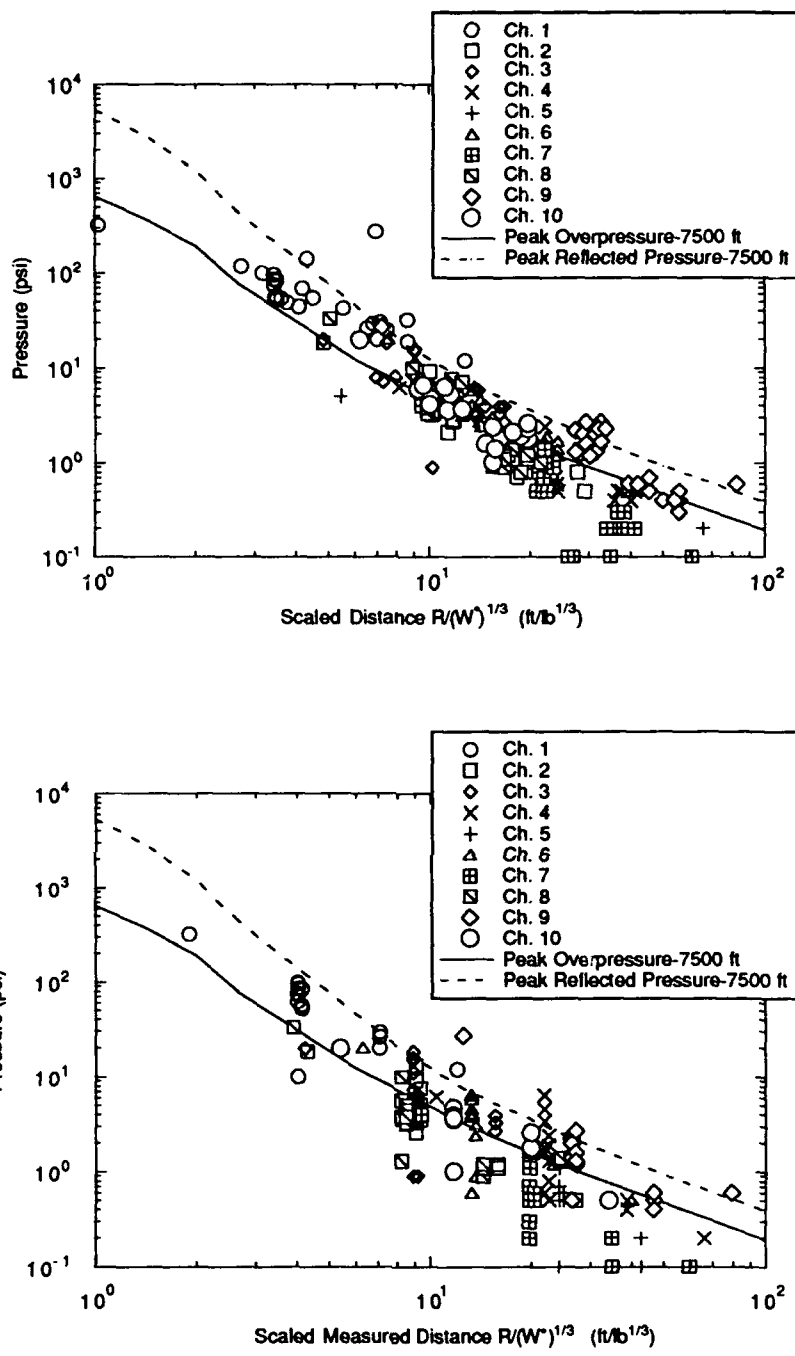
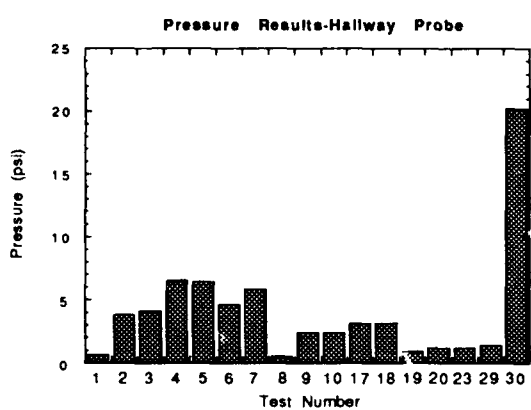
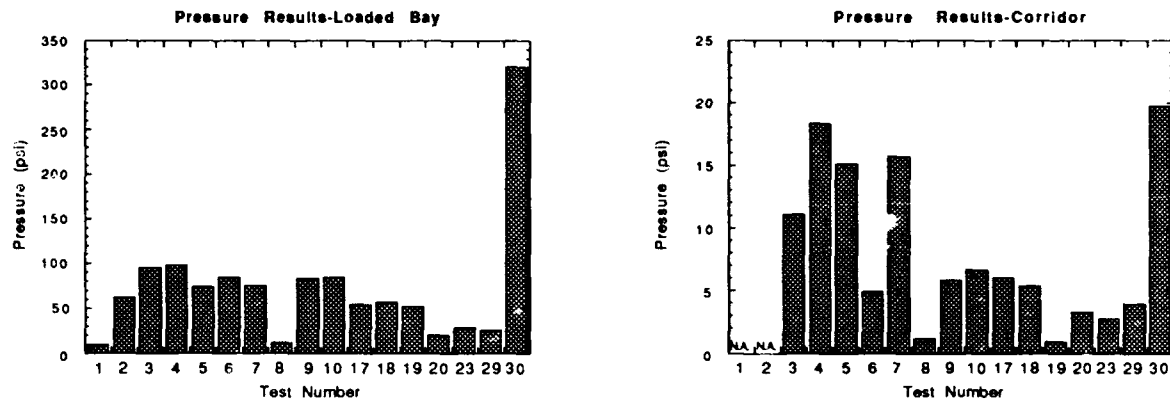


Figure 5.5. Comparison of scaled distance (based on arrival time) versus pressure (top plot) with scaled measured distance versus pressure (bottom plot).

## 5.5. Blow out wall and attenuator door comparison

As discussed in the Model Testing Section (Section 4), various blow-out walls (BOW) and attenuator doors were studied. A tabular summary of pressures and graphical peak pressures are shown in Figure 5.6 and Table 5.3.



Test	Test notes
1	det. only, no confinement.
2	2.6 lb, no confinement.
3	2.6 lb, no confinement.
4	2.6 lb, 1-in. BOW both bays.
5	2.6 lb, 1-in. BOW one bay.
6	2.6 lb, 0.5-in. BOW,door,header.
7	2.6 lb, 0.5-in. BOW,header.
8	det only, 0.5-in. Strips BOW, other bay reinforced. Vinyl door.
9	2.4 lb, 0.5-in. Strips BOW, both bays. Vinyl door.
10	2.4 lb, 1-in. BOW both bays. (2) Vinyl doors.
17	2.4 lb, 1-in. BOW both bays. (1) Vinyl door.
18	2.4 lb, 1-in. 'Slide' Door with 1-in. brace;(1) layer .005-in. Al on each side of 1-in. BOW.
19	2.4 lb, Massive Door (1) layer. .005-in. Al on each side of 1-in. BOW.
20	0.5 lb, 1-in. BOW, no att. doors.
23	0.5 lb, 1-in. BOW, no att. doors.
29	0.5 lb, .063-in. Al BOW, no att. doors. 1-in. Styrofoam Building Addition.
30	24.7 lb, .063-in. Al BOW, Massive door. 1-in. Styrofoam Building Addition.

Figure 5.6. Comparison of blow-out-wall and attenuator-door configurations at three interior locations. The charge was at location A for all tests. Test descriptions are given in the table.

Test	Ch. 1 Loaded Bay (psi)	Ch. 2 Adjacent Bay (psi)	Ch. 3 Corridor (psi)	Ch. 4 Lab Interior (psi)	Ch. 5 Rear Wall, Ex (psi)	Ch. 6 Hallway Probe (psi)	Ch. 7 Rear Corner, Ex (psi)	Ch. 8 Front Corner, Ex (psi)	Ch. 9 50 ft. from BOW (psi)	Ch. 10 Hallway Wall (psi)
1	10	2.6 (noisy)	0.9 (noisy)	3.4 (noisy)	0.1 (flat)	0.6	0.2	1.3	0.5	N.A.
2	62	13.2 (noisy)	7.3 (noisy)	6.4 (noisy)	0.1	3.8	0.5	10.0	2.4	N.A.
3	95	9.2	11.1	3.4 (noisy)	0.6	4.1	1.4	10.0	2.2	N.A.
4	98	5.0	18.3	4.6 (noisy)	0.7	6.5	1.1	3.6	1.5	N.A.
5	74	5.6	15.1	1.8 (noisy)	0.5	6.4	0.3	3.8	1.4	N.A.
6	85	3.3	4.9	1.6 (noisy)	1.1 (noisy)	4.6 (flat)	5.7	(bad data)	N.A.	
7	75	3.8	15.7	0.6	0.5	5.8	0.7	3.8	2.0	N.A.
8	12	0.5	1.2	0.2	0.0	0.5	0.1	1.4	0.6	0.5
9	83	3.5	5.8	1.9 (noisy)	0.5	2.4	0.5	5.0	1.6	4.7
10	85	5.1	6.6	1.3	0.6	2.4	0.5	3.2	1.3	3.9
17	54	5.0	6.0	0.5	0.5	3.1	0.6	4.5	1.2	3.6
18	57	7.5	5.3	2.4	0.5	3.1	0.5	3.3	2.7	3.7
19	52	4.1	0.9	0.8	0.5	0.9	0.5	3.8	1.3	1.0
20	20	1.2	3.3	0.5	0.1	1.2	0.1	0.9	0.5	1.7
23	29	1.1	2.7	0.5	0.1	1.2	0.1	1.1	0.6	1.8
29	26	1.2	3.9	0.4	0.2	1.4	0.2	0.4	0.4	2.6
30	320	18.4	19.7	6.2 (noisy)	5.0	20.2	4.0	32.9	27.0	19.8

Table 5.3. Pressure results from tests with charge at Position A.

## 6. SUMMARY AND CONCLUSIONS

Our results indicate that in order to maintain an interior maximum pressure less than 5 psi, a maximum 0.5 lb equivalent HE charge should be used in a building with no attenuator doors and a blow-out wall equivalent to 1 in. Styrofoam (1.27 lb/ft<sup>2</sup> density).

In comparing charge magnitude and charge location, we looked at the results from tests 11 through 28 where we had two charges, 0.5-lb and 2.4-lb-equivalent HE, and eight charge locations. The location of the 0.5-lb-equivalent HE charge had little effect on the pressures measured in the model as shown in Figure 5.2. The 2.4-lb-equivalent HE charge at locations D, F and G produced the largest pressure readings in the hallway. These three charge locations are adjacent to the doorway (location B was not used with the 2.4-lb charge.) Location A for both charges produced the lowest impulses outside the loaded bay as shown in Figure 5.3. For the 0.5-lb-equivalent HE charge, location C gave the highest impulse at all interior sensor locations but little variation in impulse was seen for locations C through H. For the 2.4-lb-equivalent HE charge, more variation in impulses was seen but they remained fairly consistent. Location F produced the highest impulses outside the loaded bay of the 2.4-lb-equivalent HE charge cases.

Our data was in good agreement with bare, spherical TNT data from Baker et al. (1983) as shown in Figures 5.4 and 5.5. A few discrepancies in the data were discussed in Section 5.4. Our data was from all test conditions, with and without blow out walls and attenuator doors. Also our data was obtained from a maze-like model, and the bare, spherical TNT data was from "unobstructed" tests. Even with these differences we believe that estimates of pressure at various locations in the model can be made from Figures 5.4 and 5.5.

We found that the pressure and impulse results varied considerably with different attenuator-door and blow-out wall designs, as shown in Figure 5.6 and Table 5.2. The pressure results from using different attenuator doors are given below in order of maximum pressure reduction in the hallway:

1. Massive Styrofoam door with approximately 600% reduction in pressure (test 19),
2. Slide door with approximately 200% reduction in pressure (test 18),
3. Vinyl door with approximately 200% reduction in pressure (test 17), and
4. No door (tests 4, 5, 7).

The various attenuator door options not only reduce the peak pressure but also reshape the pressure time histories by changing the peak impulse. The massive door as compared with the slide door reduces the peak impulse by five times in the corridor

and four times in the hallway wall as shown in Table 5.2 (tests 18 and 19). The massive door also delays the peak impulse by 40% in the corridor and hallway.

The results for the various blow-out walls indicate that the stronger, and more solid the blow-out wall, the higher the pressure in the hallway and corridor, Figure 5.6 (tests 20, 29). Test 20 with a 1-in. Styrofoam blow-out wall had 20% lower pressures and 50% lower impulses in the corridor than test 29 with a 0.063 in. aluminum blow-out wall. The 2-ft. building addition added in test 29 could account for some of the differences.

## APPENDIX. SCALING

The derivation of the scaling laws, based on the Buckingham Pi theorem, is presented in several references, for example, Kinney (1962); Baker, Westine, and Dodge (1973); and Anderson (1969). The scaling relations used in this report are given in Table A.1 below. They assume that air and detonation products can be treated as inviscid but compressible gases. Only inertial forces are considered. These scaling assumptions will lead to some situations that cannot be properly modeled. One situation is common combustion processes because gravity-forced convection effects are not scaled correctly.

Prototype		Model
length	$\Leftrightarrow$	length/8
force	$\Leftrightarrow$	force/64
pressure	$\Leftrightarrow$	pressure
time	$\Leftrightarrow$	time/8
impulse	$\Leftrightarrow$	impulse/8
mass	$\Leftrightarrow$	mass/512

Table A.1. Scaling conversions.

Calculations for the conversion from the charge used in the model and the TNT-equivalent HE at sea level are given in Equation A.1. This conversion takes into

consideration altitude differences,  $\frac{p}{p_0}$ ; heat of detonation differences,  $\frac{\Delta H_{9407}}{\Delta H_{TNT}}$ ; and scaling differences,  $L'$ :

$$(W_{eq})_{prototype} = \frac{p}{p_0} \cdot \frac{\Delta H_{9407}}{\Delta H_{TNT}} \cdot (L')^3 \cdot W_{9407} \quad (A.1)$$

Substitute pressure and temperature for density from the Ideal Gas Law:

$$PV = nRT$$

$$\rho = \frac{P}{RT}$$

Equation (A.1) now becomes

$$(W_{eq})_{\text{prototype}} = \frac{P}{P_0} \cdot \frac{T_0}{T} \cdot \frac{\Delta H_{9407}}{\Delta H_{\text{TNT}}} \cdot (L^*)^3 \cdot W_{9407}. \quad (\text{A.2})$$

As discussed in Section 5.4, the prototype charge equivalent HE was multiplied by a factor of 2 in order to compare our data with bare, spherical TNT, as shown in Figures A.1 and A.2. And we had to convert from actual distance and time to scaled distance and time to make a comparison. Equations A.3 and A.4 give the conversion from actual distance and time to scaled distance and time. The actual distance and time are from the model and had to be multiplied by the scale factor,  $L^*$ , so that the comparison would be in terms of the prototype:

$$(\text{scaled distance})_{\text{prototype}} = \frac{\left(\frac{P}{P_0}\right)^{1/3} \cdot L^* \cdot (\text{actual distance})}{\left(\frac{(W_{eq})_{\text{prototype}}}{W_0}\right)^{1/3}} \quad (\text{A.3})$$

and

$$(\text{scaled time})_{\text{prototype}} = \frac{\left(\frac{P}{P_0}\right)^{1/3} \cdot \left(\frac{T}{T_0}\right)^{1/2} \cdot L^* \cdot (\text{actual time})}{\left(\frac{(W_{eq})_{\text{prototype}}}{W_0}\right)^{1/3}}, \quad (\text{A.4})$$

where:

$(W_{eq})_{\text{prototype}}$  = equivalent weight of TNT for prototype (lb)

$W_{9407}$  = weight of 9407 in model (lb)

$W_0$  = 1 lb TNT

$\Delta H_{\text{TNT}}$  = heat of detonation for TNT ( $1.29 \frac{\text{kcal}}{\text{g}} \text{H}_2\text{O gas}$ )

$\Delta H_{9407}$  = heat of detonation for 9407 ( $1.46 \frac{\text{kcal}}{\text{g}} \text{H}_2\text{O gas}$ )

$\rho$  = air density during model test

$\rho_0$  = air density at sea level for TNT test

$P$  = air pressure during model test (579 mm Hg)

$P_0$  = air pressure at sea level for TNT test (760 mm Hg)

$T$  = air temperature during model test ( $527.69^{\circ}\text{R}$ )

$T_0$  = air temperature at sea level for TNT test ( $529.69^{\circ}\text{R}$ )

$$L^* = \frac{\text{prototype length}}{\text{model length}} = \frac{8}{1}$$

This form of blast scaling is the Hopkinson-Cranz or "cube-root" scaling with correction factors for altitude. The Hopkinson-Cranz law states that "self-similar blast waves are produced at identical scaled distances when two explosive charges of the same explosive but of different sizes are detonated in the same atmosphere" (DOE/TIC-11268, 1980).

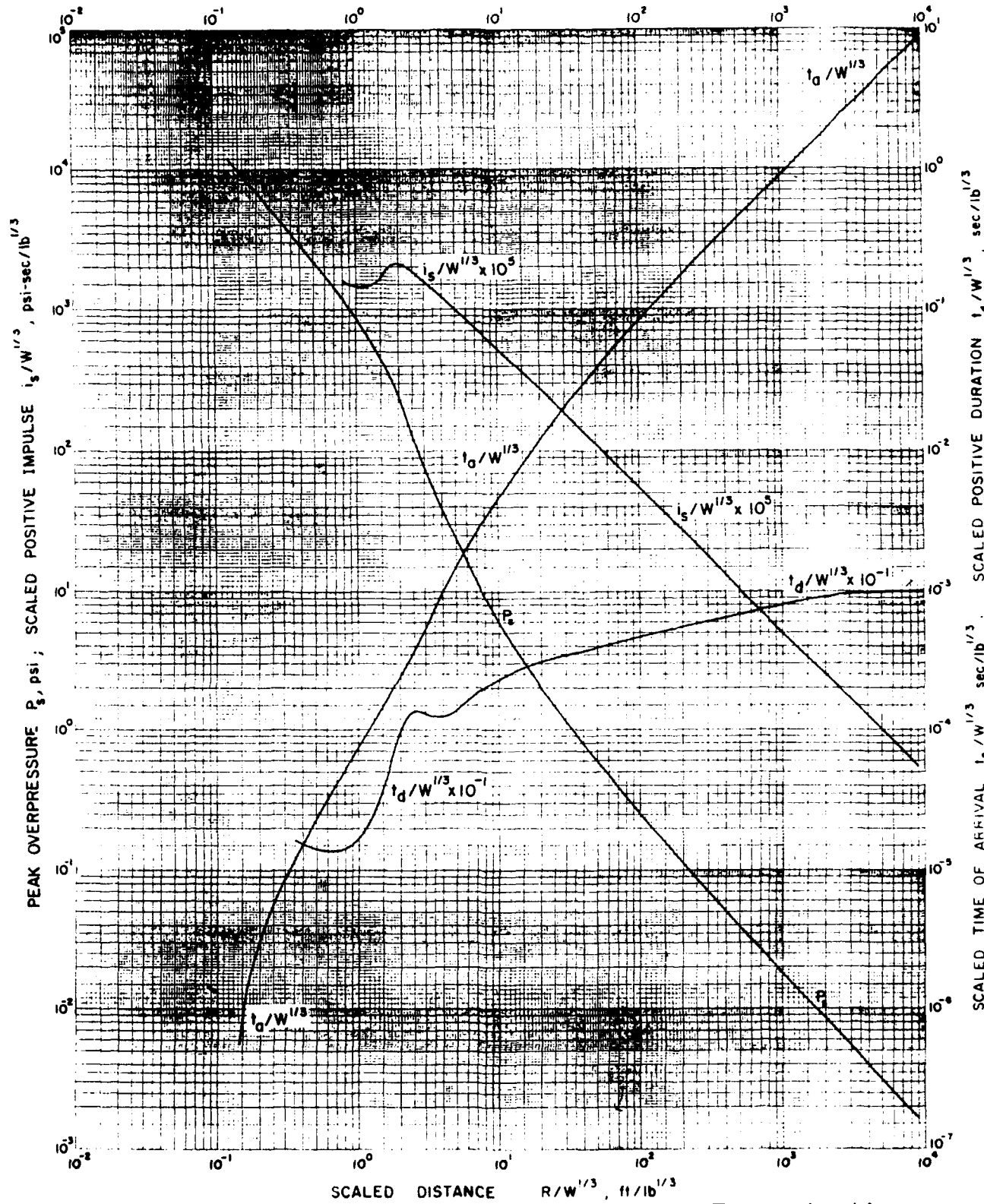


Figure A1. Side-on blast wave properties for bare, spherical TNT at sea level from Baker et al. (1983).

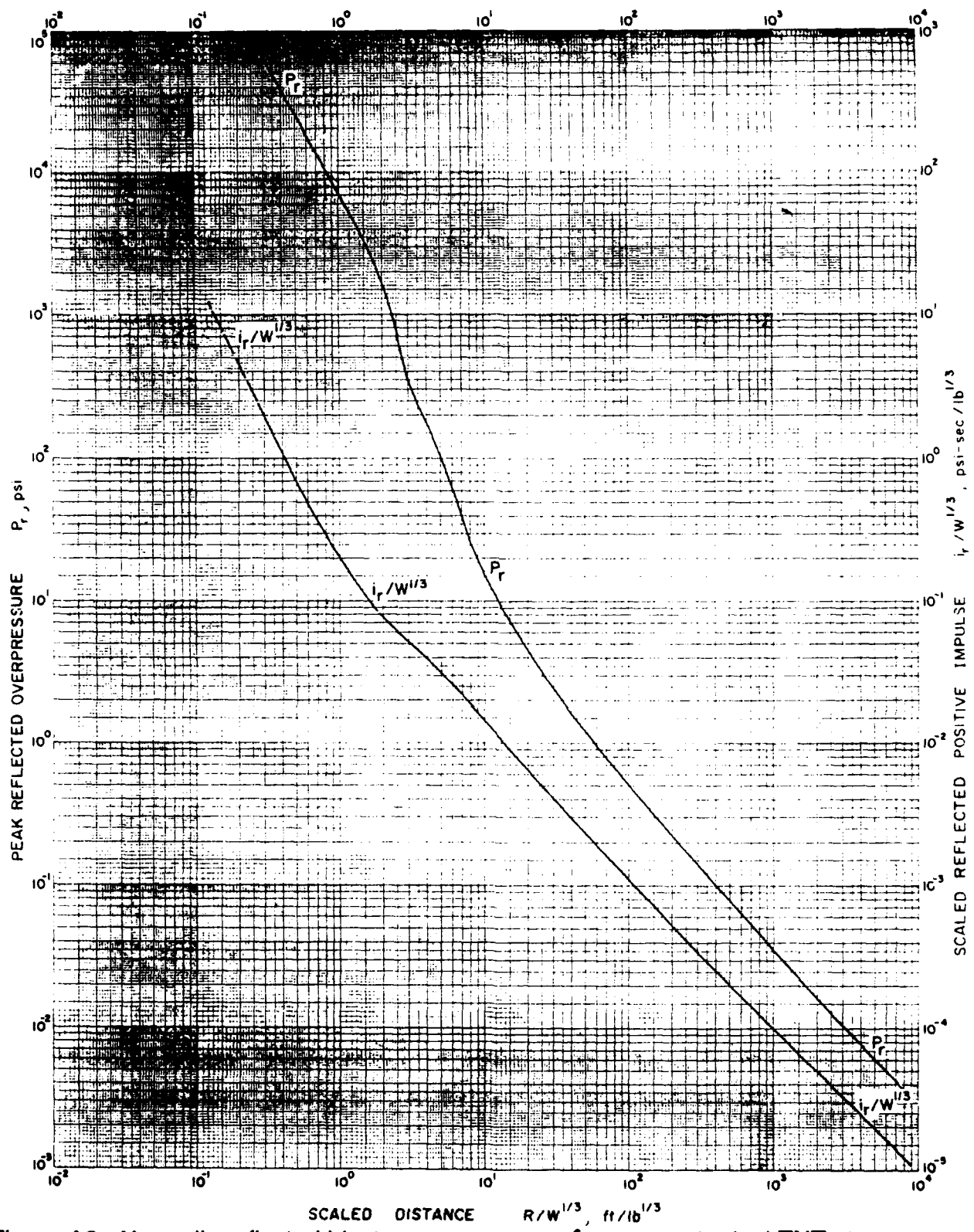


Figure A2. Normally reflected blast-wave properties for bare, spherical TNT at sea level from Baker et al. (1983).

*Approximate Analysis and Design of Conventional Industrial Facilities  
Subjected to Bomb Blast Using the P-i Technique*

by:

**Kirk A. Marchand**

**Charles J. Oswald**

**Southwest Research Institute, San Antonio, Texas, USA**

**Mr. Dale Nebuda**

**US Army Corps of Engineers Omaha District**

**Omaha, Nebraska, USA**

and

**Mr. John Ferritto**

**Naval Civil Engineering Laboratory**

**Port Hueneme, California, USA**

**ABSTRACT**

Efforts to characterize the response of complex structural systems to the intense transient loads generated by bomb blast can involve significant computational effort. Additionally, the practitioner must have a substantial amount of experience to interpret the results of these analyses. Unfortunately, when facilities are subject to terrorist attacks, sufficient time is often not available for detailed analysis.

Southwest Research Institute (SwRI), under contract to the US Army Corps of Engineers at Omaha and the Naval Civil Engineering Laboratory at Port Hueneme, California, has been developing simplified procedures for the prediction of damage to conventional buildings generated by airblast transient loads. In these methods component damage is first calculated for each component in the building using pressure-impulse curves (P-i curves). The P-i curves relate non-dimensional terms calculated using the component geometry, material strength, material stiffness, and boundary condition, and the peak applied blast pressure and impulse, to component damage. The P-i curves were developed theoretically using an energy approach and then shifted, where necessary, to match measured damage data. The theoretical curves are shifted to match damage data in regions where the damage is overpredicted.

In the second step of these procedures, building response is calculated by summing component damage. Several summation algorithms have been written which calculate percentage of overall damage to the building, the amount of reusable floor space, the repairability of the building, and the level of protection provided by the building for a given explosive threat.

## 1.0 Introduction

A general procedure for determining the vulnerability of common industrial buildings to explosion threats has been established and is outlined in this paper. This procedure is essentially a two-step process where, first, damage to each component in the building is determined using P-i diagrams, and then damage from all the components in the structure is summed to determine overall building damage. The key features of the procedure include the development of the P-i curves which correlate the blast load and component structural properties to component damage and the summing algorithms used to add up component damage and determine building response. The procedure has been programmed into a computer code, called BDAM, and the code has been used to calculate damage to a number of different buildings, considered "typical" of commonly constructed buildings, from a wide variety of explosive threats. The key features of the blast vulnerability analysis procedure are described in this paper and some results of damage calculated to common building types from given explosive threats are shown.

## 2.0 P-i Curve Use

The general procedure for determining building vulnerability that is outlined in this paper is based on the calculation of building member response using P-i curves. P-i curves, or pressure-impulse curves, are used in the procedure because they can be programmed easily into a computer code and because they were used in the initial work on this procedure to describe measured component response in terms of component properties and blast loading parameters. Work on simplified vulnerability analysis of industrial facilities began at SwRI several years ago with an effort sponsored by the Naval Civil Engineering Laboratory (NCEL) to develop a procedure which predicted damage for common construction components based on available data. P-i curves were chosen as the basic tool for this purpose. Damage data was plotted against theoretical P-i curves (developed using energy methods) and when the data did not agree with the curves, the curves were shifted, or "calibrated" to overlay the measured damage points as closely as possible. An ongoing effort at Southwest Research Institute (SwRI) is the improvement of the theoretical P-i curves to include all the types of strain energy that affect member response (such as compression and tension membrane action) so that damage data will match better with theoretical curves.

Figure 1 shows a typical P-i diagram which can be used to calculate the level of dynamic response in terms of level of protection for two-way concrete slabs (the relationship between level of protection and component response parameters such as ductility ratio is defined later in the paper). The protection levels shown in the margin of the diagram apply throughout the diagram between

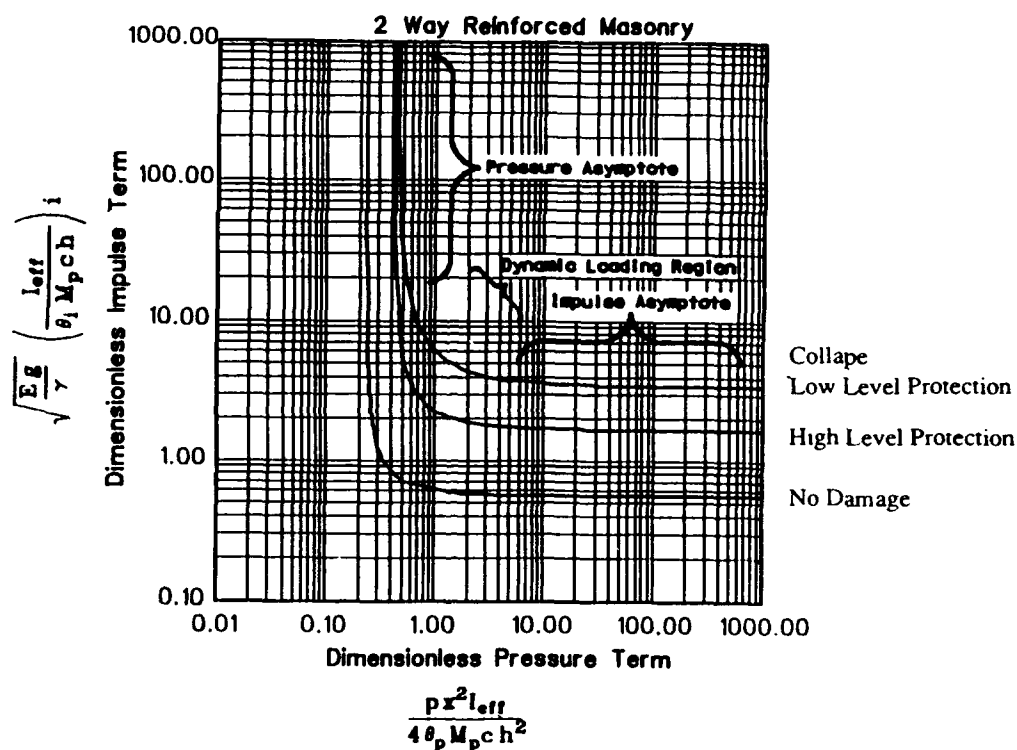


**Figure 1. Example P-i Curve**

the curves. The terms on each axis are made up of blast loading parameters, the peak pressure ( $p$ ) and the blast load impulse ( $i$ ), and slab structural parameters, such as the plastic moment capacity ( $M_p$ ) and characteristic span length ( $l$ ). The level of protection provided by the slab is determined by calculating the non-dimensional terms on either axis of the P-i diagram and reading the protection level off the diagram based on the location of the point defined by the two terms. In cases where detailed information about the structural parameters are unknown, approximations can be made. The curves assume a given shape of the blast load history, a right triangular load history for all the P-i curves used in the procedures discussed here, and are only valid for load histories with the assumed shape.

P-i curves are different from other similar tools used to calculate dynamic response to blast loads, such as time-stepping computer programs or other types of charts showing dynamic response, in that the portion of the dynamic response that is affected only by the peak load is separated from that which is independent of the peak load and only affected by the time integral of the applied load (the impulse). This is due to the manner in which loading history parameters and structural member geometry and physical property parameters are grouped into algebraic terms and plotted against each other to make up the P-i curves. Often, it is advantageous to the designer to know the extent to which impulse or the peak load affects member response since the effectiveness of various design strategies depends on the which loading parameters are controlling dynamic response. Another distinct feature of P-i diagrams is the simple shape of the response curves. This feature is advantageous to the implementation of P-i curves into computer codes since the response curves can typically be described with a single equation that connects the two asymptotic values.

Figure 1 shows these distinct features. The figure shows the two basic loading parameters, the peak pressure and the impulse, are separated into the two terms along the axes. In the portion of the curves which is perpendicular to the horizontal axis, the level of response (or protection) is controlled only by the horizontal axis term which indicates that, in this portion of the curves, response is controlled only by the peak load and not by the impulse. This is labeled as the quasistatic region in Figure 1. The opposite is true in the portions of the curves perpendicular to the vertical axis, which are labeled as the impulsive region. In the portions of the curves perpendicular to neither axis, the response is dependent to some extent on both loading parameters, and this region is labeled as the dynamic region in Figure 1. The simple shape of the response curves is also shown in the figure.

P-i curves based on damage data have been developed for a variety of structural components which are representative of those expected in common industrial buildings. Table 1, which is presented later in this paper, lists all these structural components. For some components no damage data from explosive loading was located in the literature and theoretical P-i curves are used. References 1 and 2 document this work.

The P-i curves assume a given type of structural response (e.g. flexural response, buckling). Some structural elements fall under more than one type of P-i diagram as more than one mode of failure is possible for these members. The components for which there is more than one failure mode include:

- Open web steel joists
- Exterior columns (all)
- Interior columns (all)

**Open Web Steel Joists** - Two modes of failure are possible: tension failure of the bottom cords and web buckling. P-i diagrams are provided for each failure mode. The user should calculate the protection level using each diagram and accept the lesser of the two values.

**Exterior Columns** - These elements can fail due to bending induced from exterior blast loading or by deformations due to frame sway of the structure. First, use the P-i diagram for a column in bending to obtain a protection level. Second, use the frame P-i diagram to obtain a protection level. Use the lesser level of protection provided.

**Interior Columns** - These elements can fail due to either buckling or frame sway. Since buckling is simply a fail/no fail condition, the P-i diagram for column buckling for dynamic axial loads is used first to determine if the element will fail or not. If it does not fail due to buckling, then the diagram for frame response is used to determine the protection level provided by the columns.

The following are a variety of comments concerning various structural components and how they are addressed in analysis.

**Non-Arched and Arched Sections** - P-i curves are provided for one-way masonry and two-way reinforced concrete components for both the non-arched (NA) and fully arched (FA) cases. Arching is the contribution of compressive membrane effects to the resistance of the section in flexure. Arching can be considered when the supporting structure of a component provides in-plane resistance, or resistance to in-plane translation during response. Specific cases include concrete frame structures with in-fill masonry walls (arched walls), or in-fill two-way concrete walls. When it is not apparent that arching can develop, the non-arched figures should be used. It is always conservative to use the non-arched case.

**Columns** - A structure can have interior and exterior columns. This guide considers response modes of buckling for interior columns, but not exterior columns. Exterior columns are loaded directly by the blast wave and can respond in bending. The damage caused by bending response is expected to cause more severe than that caused by buckling for most cases. It takes a relatively large load to induce buckling failure, and such a load will easily cause bending response failure in the column. The P-i diagrams are based on the assumptions that interior columns are unsupported over each story height and are not laterally loaded to a significant extent by any of the blast wave which "leaks" inside the building.

For structures which have moment resisting frames, the frame mode of response needs to be accounted for in the analysis. Both interior and exterior columns can contribute to the frame stiffness if they are moment resisting. Only those that are moment resisting should be included. Direction is given on the P-i diagrams on how to calculate the strengths and mass of framed structures.

**Doors, Windows, and Cement-Asbestos Corrugated Panels** - For these structural components, P-i diagrams are not provided since these elements are considered to be pressure sensitive only. The suggested failure criterion is 2.0 psi. Above this value, these elements are considered to have failed; below this value, they survive.

Finally, end conditions of components (i.e., "fixity") can be specified if not completely known using the guidance provided in Reference 4. Localized response experienced by structural elements due to very close-in or contact detonations is not considered by the P-i diagrams.

### 3.0 Component Damage Evaluation

Two different sets of categories have been used to describe the level of component and building response in blast vulnerability assessment projects at SwRI. In previous work performed by SwRI for the Naval Civil Engineering Laboratory (NCEL) (References 1, 2), four damage categories generally were defined for each structural element. They were:

*Slight Damage* -- damage level 0, (0% damage)

*Moderate Damage* -- damage level 0.3, (30% damage)

*Severe Damage* -- damage level 0.6, (60% damage)

*Failure* -- damage level 1.0

These damage levels corresponded to damage observed in tests used to adjust the theoretically determined energy solution curves or "P-i" curves. They are used to characterize component and building response in the blast vulnerability procedures developed for NCEL. The inputs required to analyze the blast damage to each component with P-i curves are explained in detail in the "Blast Vulnerability Guide" (1) developed for NCEL by SwRI. The guide provides easy-to-follow calculation procedures which allow engineers estimate blast damage to structural components using hand calculations for a wide range of explosive threats. Figure 2 shows a P-i diagram which describes the response of a wood roof subjected to blast loading in terms of the four damage levels shown above.

In subsequent work for the US Army Corp of Engineers at Omaha (COE), a different set of categories were used to define component damage in terms of component utility. For vehicle bomb and exterior attacks, the COE "Security Engineering Manual" (SEM)<sup>[3]</sup> defines three levels of protection.

They are:

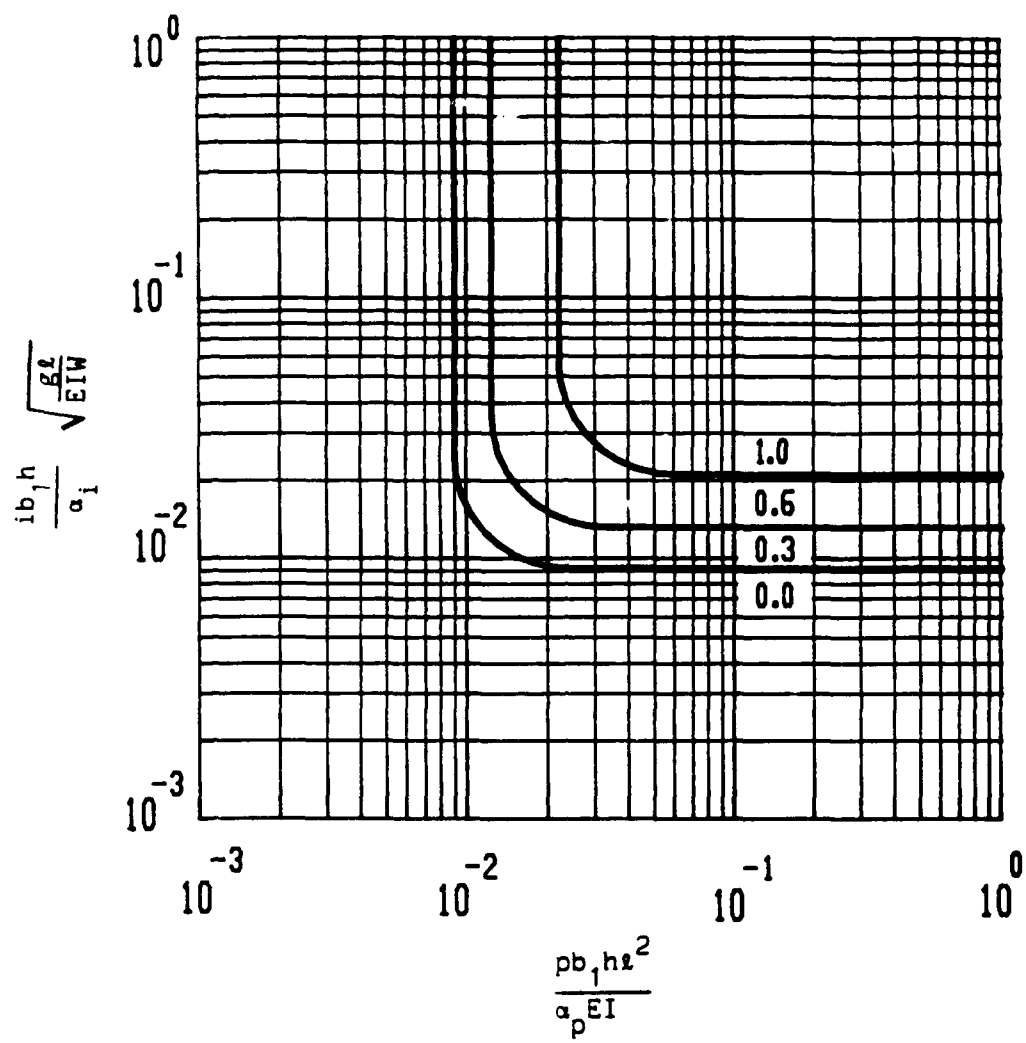
*Low Level of Protection* -- unrepairable structural components, a high level of damage without collapse

*Medium Level of Protection* -- repairable structural components, a significant degree of damage

*High Level of Protection* -- superficially damaged

The adjustment required to use the P-i curves developed for NCEL, which are based on the 30%, 60%, and failure damage levels, to define Low, Medium and High protection levels described in the SEM is based on component utility. Table 1 lists the 25 components which can be analyzed with P-i curves and indicates whether the component is judged to be repairable at a certain damage level. Note that the R's indicate a repairable component, while the U's indicate a component requiring replacement. This table was developed during work for NCEL because the Navy wanted building response described in terms of both damage level and reusability.

Particular attention was given to the fact that the steel components generally are shown to require replacement at the 30% damage level. As discussed in Reference 2 however, this requirement is more of a suggestion, since "(steel members) are relatively easily and inexpensively replaced;



**Boundary  
Conditions**

$\alpha_i$

$\alpha_p$

Simple-Simple	1.4610	8.0
Fixed-Simple	0.8944	8.0
Fixed-Fixed	0.3944	12.0

**Figure 2. Pressure-Impulse Relation for Wood Roofs Showing Response to Blast Loads in Terms of Damage Levels**

**Table 1. Repair/Replace Factors Recommended in the Reference 2**

Structural Component	Damage Level			
	0.0	0.3	0.6	1.0
R/C Beams	R	R	R	U
R/C One-Way Slabs	R	R	U	U
R/C Two-Way Slabs	R	R	U	U
R/C Exterior Columns (bending)	R	R	R	U
R/C Interior Columns (buckling)	R	R	R	U
R/C Frames	--	--	--	--
Prestressed/Post-tensioned planks	R	U	U	U
Steel Beams	R	U	U	U
Metal Stud Walls	R	U	U	U
Open Web Steel Joists (web failure)	R	U	U	U
Open Web Steel Joists (chord failure)	R	U	U	U
Corrugated Metal Deck	R	U	U	U
Steel Exterior Columns (bending)	R	R	U	U
Steel Interior Columns (buckling)	R	R	U	U
Steel Frames	--	--	--	--
One-Way Unreinforced Masonry	R	R	U	U
Two-Way Unreinforced Masonry	R	R	U	U
One-Way Reinforced Masonry	R	R	U	U
Two-Way Reinforced Masonry	R	R	U	U
Masonry Pilasters	R	R	U	U
Wood Stud Walls	R	R	U	U
Wood Roofs	R	R	U	U
Wood Beams	R	--	--	U
Wood Exterior Columns (bending)	R	--	--	U
Wood Interior Columns (buckling)	R	--	--	U

**Note:** R = repairable, U = unrepairable

hence, we chose to require replacement for damage levels of 0.3 and above." Thus, it could be interpreted that the steel components may *not* require replacement at the 30% level, but will require replacement at the 60% level.

These repair/replace suggestions were used to translate the P-i curves based on damage levels into curves corresponding directly to SEM protection levels. The following correlation was defined:

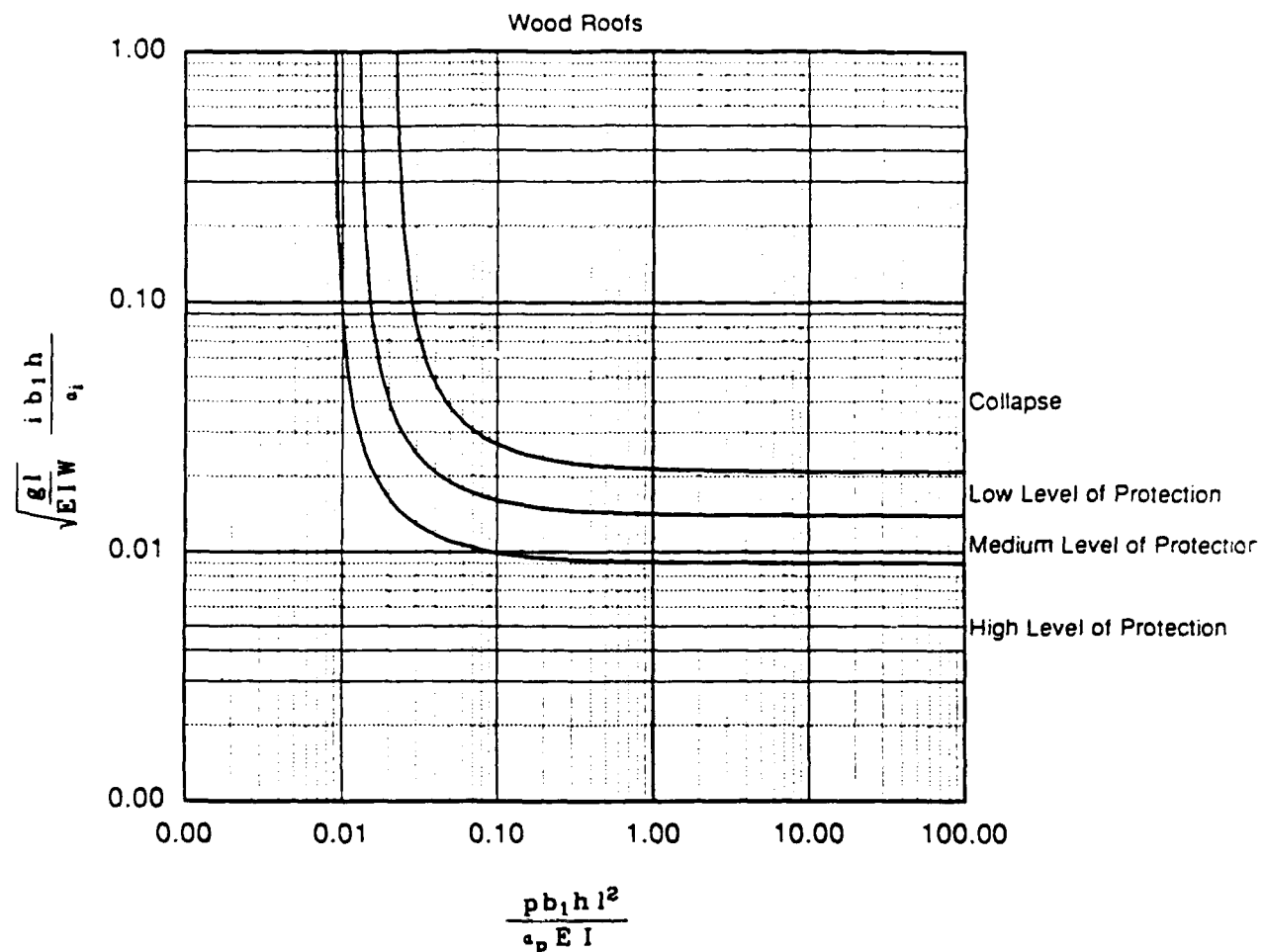
*Low Level of Protection* -- this level is indicated on the P-i curves by all values falling below and to the left of the threshold line dividing 60% damage and failure and above and to the right of the threshold line dividing 30% and 60% damage. The upper limit for a low level of protection generally corresponds with the 60% damage level.

*Medium Level of Protection* -- this level is indicated on the P-i curves by all values falling below and to the left of the threshold line dividing 30% damage and 60% damage and above and to the right of the threshold line dividing 0% and 30% damage. The upper limit for a medium level of protection generally corresponds with the 30% damage level.

*High Level of Protection* -- this level is indicated on the P-i curves by all values falling below and to the left of the threshold line dividing 0% damage and 30% damage. The upper limit for a high level of protection generally corresponds to the 0% damage level.

Figure 3 shows a P-i diagram which describes the response of a wood roof to blast loading in terms of the three protection levels shown above. Reference 4 shows the P-i curves which relate level of protection to the non-dimensional terms on the axes of the P-i diagrams. In this reference the inputs required to determine the level of protection provided by the structural components listed in Table 1 using the P-i curves developed at SwRI are explained in detail and easy-to-follow calculation procedures are provided which allow engineers to estimate blast damage to structural components using hand calculations for a wide range of explosive threats. There are numerous example problems. Default values which can be used as inputs when detailed structural information is not available are also listed.

In summary, two different approaches to characterize component damage have been used in the building blast vulnerability procedures developed at SwRI. Basically these two approaches are based on the same damage data and are equivalent to each other except for the nomenclature used to describe component response. Table 2 shows how the High, Low, and Medium protection levels used in work for the COE are defined in the more generally used response terms of deflection to length ratios ( $w/l$ 's) and ductilities ( $\mu$ 's). Since the level of protection terms used by the COE correlate closely with the percentage of damage terms used for NCEL, Table 2 also indicates the correlation between deflection values and ductilities and percentage damage levels shown at the top of this section.



Boundary Conditions	$a_i$	$a_p$
Simple-Simple	1.4610	8.0
Fixed-Simple	0.8944	8.0
Fixed-Fixed	0.8944	12.0

**Figure 3. Pressure-Impulse Relation for Wood Roofs Showing Response to Blast Loads in Terms of Level of Protection**

**Table 2. Comparison Between Protection Level and Deflection and Ductility Response Criteria**

Structural Component	Proposed Damage Criteria						Notes	
	High Protection Level		Medium Protection Level		Low Protection Level			
	$\mu$	w/l	$\mu$	w/l	$\mu$	w/l		
R/C Beam	1	.01	5	.02	20	.035		
R/C One-Way Slabs	1	.01	5	.02	20	.035	Same as R/C beam	
R/C Two-Way Slabs	1	.002	5	.008	20	.134	Both unarched (no compressive membrane effects) and arched (w/compressive membrane effects)	
R/C Exterior Columns (bending)	1	.01	5	.02	20	.035	Same as R/C beam	
R/C Interior Columns (buckling)	--	--	--	--	--	--		
R/C Frames	3	.02	6	.04	12	.08		
Prestressed/Post-tensioned T-beams and slabs	.2	--	.5	--	1	--		
Steel Beams	2	.0087	7	.033	15	.067		
Metal Stud Walls	2	.0087	7	.033	15	.067	Same as steel beams	
Open Web Steel Joists (web bending failure)	1	.0083	3.5	.017	6	.033	Same as steel beams	
Open Web Steel Joists (chord buckling failure)								

**Table 2. Comparison Between Protection Level and Deflection and Ductility Response Criteria (continued)**

Structural Component	Proposed Damage Criteria						Notes
	High Protection Level		Medium Protection Level		Low Protection Level		
	$\mu$	$w/l$	$\mu$	$w/l$	$\mu$	$w/l$	
Corrugated Metal Deck	2	.0087	7	.033	15	.067	Same as steel beams
Steel Exterior Columns (bending)	2	.0087	7	.033	15	.067	Same as steel beams
Steel Interior Columns (buckling)	--	--	--	--	--	--	
Steel Frames	3	.02	6	.04	12	.08	
One-Way Unreinforced Masonry (unarched)	1	--	1	--	1	--	Wall becomes unstable when deflection approaches the wall thickness
One-Way Unreinforced Masonry (arched)	.25	--	.5	--	1.0	--	
Two-Way Unreinforced Masonry	.1	--	.15	--	.25	--	All considered fully arched
One-Way Reinforced Masonry	1	--	5	--	20	--	Same as R/C beam
Two-Way Reinforced Masonry	1	--	5	--	20	--	Same as R/C slab
Masonry Plasters	1	--	5	--	20	--	Same as R/C beam
Wood Stud Walls	1	--	2.2	--	4.4	--	
Wood Roofs	2.0	--	2.8	--	4.4	--	
Wood Beams	1	--	1	--	4.4	--	
Wood Exterior Columns (bending)	1	--	1	--	4.4	--	
Wood Interior Columns (buckling)	--	--	--	--	--	--	

## **4.0 Building Vulnerability Assessment**

The preceding sections explain how component damage is calculated. This section describes how several measures of overall building response are calculated with the blast vulnerability procedures. Two separate types of summation algorithms for summing component damage and determining overall building response have been used because NCEL and the COE have used the blast vulnerability methods to assess blast damaged buildings for different end purposes. NCEL has been more concerned with overall, or average damage and the need for building repair or replacement, while the COE has been concerned with the level of protection provided by the most damaged portion of the building.

### **4.1 Building Damage Assessment Procedures Developed for NCEL**

Separate procedures to calculate the total building damage, a building reusability factor, and a building repairability factor for a given explosive threat were developed for NCEL. In these procedures the damage level of each component is first calculated as described in the preceding section, and then building response is determined using different summation algorithms. The procedure to calculate total building damage begins by weighting each component based on the importance of the component to the overall integrity of the building structure, and then summing the product of the damage level of each component multiplied by the weighting factor. This sum is divided by the weighted sum of all components corresponding to total building destruction. This fraction is the total building damage and it is usually expressed as a percentage. The summing algorithm used to determine building damage assumes that, if any component fails (100% damage), all members supported by this component also fail. This is referred to as cascading failure. Component weighting is determined primarily according to how other many members are supported by the component in question (e.g. columns are weighted more heavily than beams).

The results of an evaluation made using this procedure with the same charge weight at several standoffs can be used to determine building damage as a function of explosive separation distance and plotted as a "damage function" for that particular charge weight. Several damage functions can be plotted on the same graph. The explosive amounts which can be considered range from a few ounces of TNT for a typical hand grenade up to 4000 pounds for a large bomb.

The component damage levels are also used to determine the building reusability factor. This factor, which can be used to determine how much of the building is reusable prior to repair, is equal to the percentage of usable floor space in the damaged building. In this procedure it is assumed that floor space is nonreusable only if a component beside or over that area incurs 100% damage. Finally, the building repairability factor is calculated based on the calculated component damage levels and the assumed relationships between damage level and repairability in Table 1. The sum of all the weighting factors of all unrepairable components is divided by the sum of the

weighting factors of all components and this ratio is called the repairability factor. If the factor is greater than 0.5, rebuilding is recommended rather than repair. This factor provides a recommendation as to whether the building should be repaired or rebuilt for a given explosive threat.

Twelve building types considered to be representative of common industrial facilities were "designed" by SwRI so that the damage that was likely to be incurred by common buildings exposed to various explosive threats could be calculated. During subsequent work for the COE a thirteenth common building was added. These common buildings, each of which represent a "category" of buildings common to a naval or army base, are summarized in Table 3. Doors and windows in all buildings are assumed to be of standard construction. These non-hardened doors and windows are assumed to fail at low pressures.

Building damage functions (percent building damage plotted against standoff for a given explosive threat), building reusability functions, and building repairability functions were calculated for each common building in Table 3 and these functions are included in Reference 2. Figures 4, 5, and 6 show percent building damage, percent building reusability, and rebuild/repair plotted for three explosive threats at various standoffs to Building No. 6 in Table 3.

In order to automate the work involved in assessing building vulnerability to blast loading with these procedures, SwRI developed the computer program BDAM. The P-i curves and the summation algorithms that calculate each type of building response described above (damage, reusability, and repairability) are programmed into the code. Thus, the BDAM code automates the procedure of calculating component and building damage so the user can determine the vulnerability of a building if he/she is given the weight and location of the explosive and the structural characteristics of all components comprising the building as determined by on-site surveys and structural drawings. The final output of the BDAM code includes total building damage, repair/rebuild factors, and the percentage of usable area of the building. The code will also output a summary of the damage to each individual component. Details of the input and output to the code are included in Reference 5.

#### **4.2 Security Engineering Manual (SEM) Approach Developed for the COE**

Subsequent to the NCEL work, the US Army Corps of Engineers Omaha District (COE) contracted SwRI to improve the P-i curves for concrete and masonry components, to simplify the building damage summation procedure, and to redefine the building damage in terms of that described in their SEM as described in Section 2. Improvement of the P-i curves is an ongoing effort where new data is used as it becomes available to obtain better correlation between damage predicted by the P-i curves and measured values. Improvement efforts have also included a reformulation of the theoretical P-i curves for some components to include strain energy absorbed in response modes other than flexural response (e.g. compression membrane response) which has resulted in a better agreement between theoretical P-i curves and damage data for these components.

**Table 3. A Summary of Building Types and Categories**

Building No.	Category
1	One-story, large ( $> 6000 \text{ ft}^2$ ), reinforced concrete building.
2	One-story, small ( $< 6000 \text{ ft}^2$ ), reinforced concrete and reinforced masonry building.
3	One-story, small ( $< 6000 \text{ ft}^2$ ) unreinforced masonry building.
4	One-story, small ( $< 6000 \text{ ft}^2$ ), unreinforced clay brick building.
5	One-story, small ( $< 6000 \text{ ft}^2$ ), metal stud wall building.
6	Two-story, small ( $< 6000 \text{ ft}^2$ ), reinforced concrete building.
7	One-story, small ( $< 6000 \text{ ft}^2$ ), pre-engineered (Butler® type) building.
8	One-story, large ( $> 6000 \text{ ft}^2$ ) metal stud wall building.
9	Two-story, small ( $< 6000 \text{ ft}^2$ ), timber building.
10	One-story, large ( $> 6000 \text{ ft}^2$ ), tilt-up reinforced concrete building.
11	One-story, large ( $> 6000 \text{ ft}^2$ ), heavy timber building.
12	Two-story, large ( $> 6000 \text{ ft}^2$ ), steel frame building.
13	One-story, large ( $> 6000 \text{ ft}^2$ ), prestressed concrete (double "T") building.

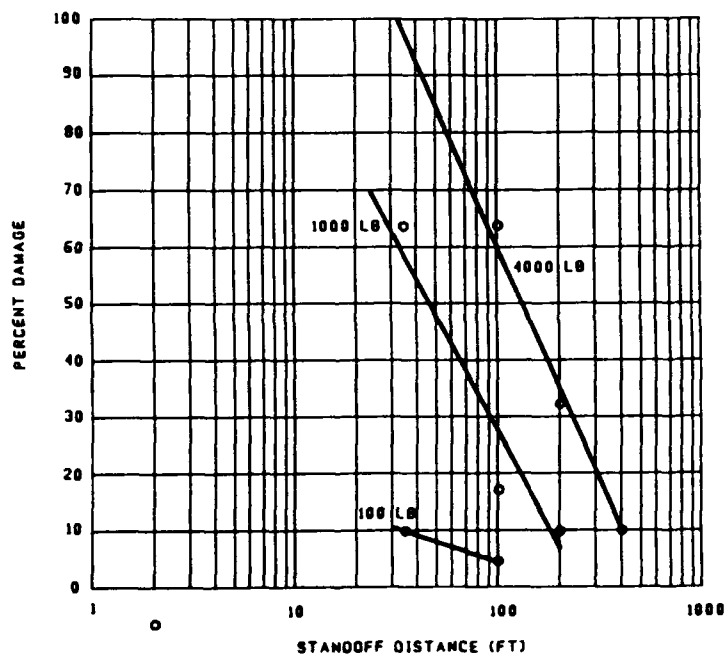


**Figure 4. Percentage Building Damage to Building No. 6 Calculated for Given Explosive Threats**

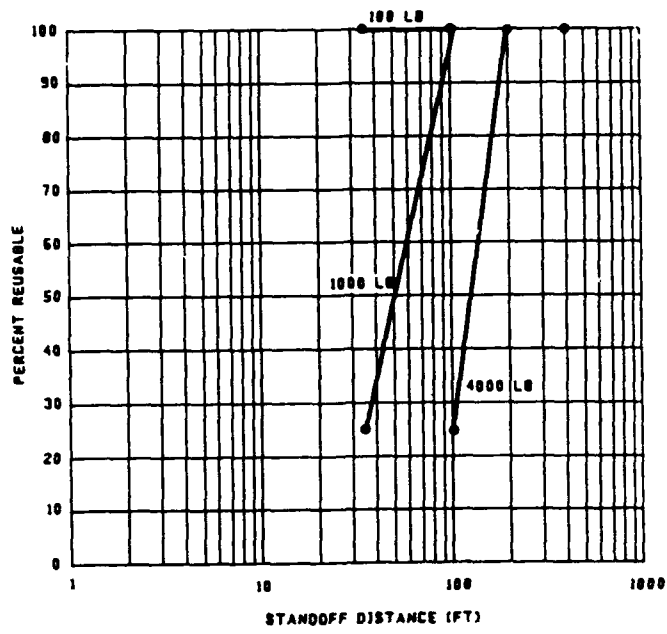


**Figure 5. Percentage of Reusable Floor Space in Building No. 6 Calculated for Given Explosive Threats**

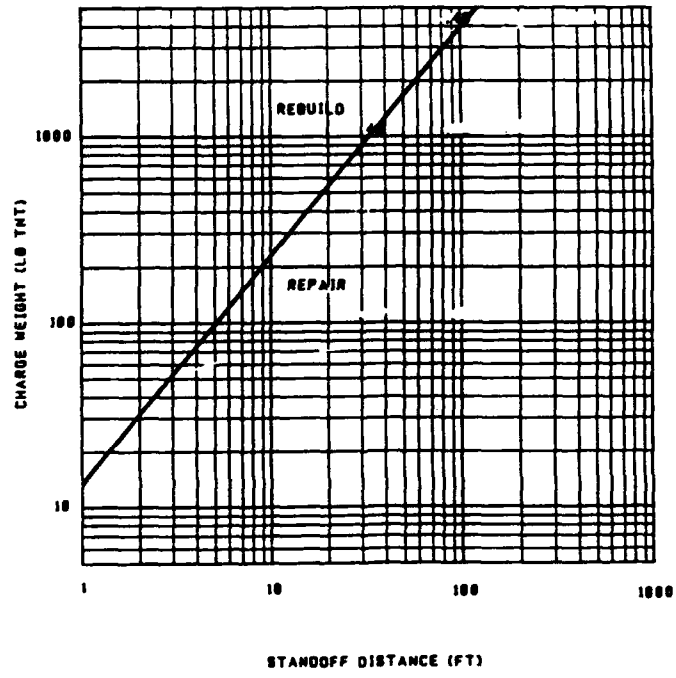


**Figure 6. Rebuild/Repair Relationship for Building No. 6 Calculated for Given Explosive Threats**

The method for determining building damage originally presented in the NCEL work was reviewed and determined not suitable for use when building response in terms of protection level provided. The criteria required by the SEM considers the damage of *any* component at a given protection level to determine the protection provided by the whole facility. Therefore, the summing algorithms used in the building damage procedures developed for NCEL were not applicable. The following definitions of building damage level were generated:

*Low Level of Protection* -- this level corresponds to a charge weight and standoff combination that generates damage no more severe than that associated with a low level of protection for any component anywhere in the facility. This excludes door and window components.

*Medium Level of Protection* -- this level corresponds to a charge weight and standoff combination that generates damage no more severe than that associated with a medium level of protection for any component anywhere in the facility. This excludes door and window components.

*High Level of Protection* -- this level corresponds to a charge weight and standoff combination that generates damage no more severe than that associated with a high level of protection for any component anywhere in the facility. This excludes door and window components.

The criteria and resulting curves were incorporated into two computer based algorithms. The first algorithm predicts *building damage* as described in Section 4.1. The second algorithm computes *building protection level* based on any component reaching a prescribed protection level (damage) at a particular standoff for a given charge weight. Buildings 1-13 in Table 3 were analyzed using these algorithms. Figure 7 shows a comparison between percentage building damage as calculated using the method described in Section 4.1 and protection level as prescribed in the SEM for Building No. 6 in Table 3.

The final product of this work for the COE was a set of building protection level curves. These curves are shown in Reference 4 for the thirteen typical structures in Table 3. They can be used for an estimate of structure protection level if the cases under study are of similar construction to one of the common building types. The accuracy in applying these curves depends directly upon how closely the structures in question compare with the structures represented by the curves. In general, if the dimensions (i.e., spans, roof height, column spacing) of the structure are within 25% of those described for each building type, and the materials (wall thickness, roof type, etc.) are similar (within 15% of thickness or depth) the protection level curves may be generally applied to similar buildings. Building plan dimensions are not as critical. A wide range of plan sizes and aspect ratios (length to depth ratios) can be analyzed with the curves.

The following steps can be taken to conduct an analysis using the building protection curves:

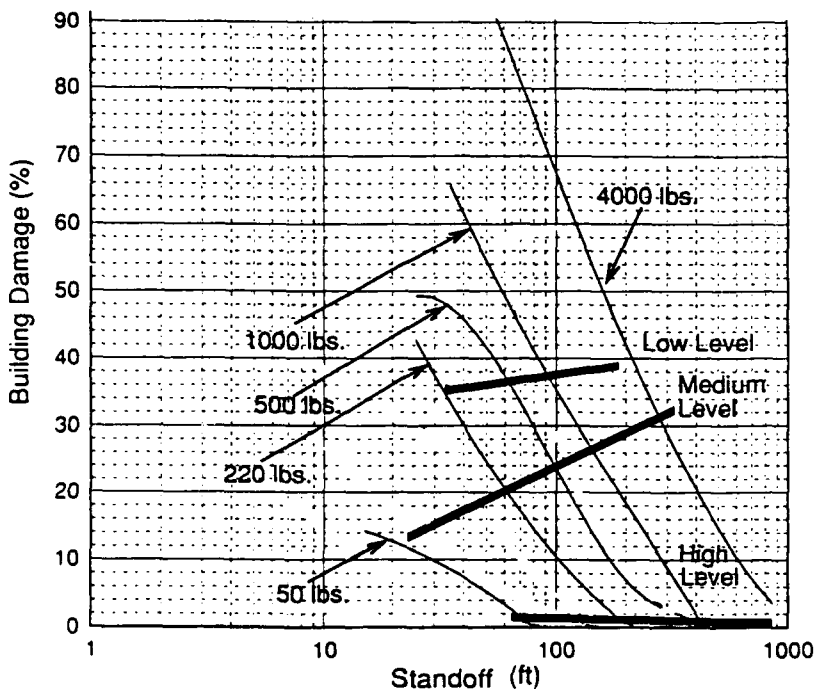


**Figure 7. Comparison of Percentage Building Damage to Building Level of Protection for Building No. 6 Subjected to Various Explosive Threats**

1. Select the analysis parameters. Determine three of the following four parameters.
  - desired level of protection
  - charge quantity
  - distance from weapon to structure (standoff)
  - orientation to structure (adjacent to long dimension or short dimension of the structure)
2. Define the building type to be analyzed.
  - determine which type closely represents the structure of interest
  - check to make sure story heights, spans, column/beam spacings are generally within 25% of "common" types and that thicknesses and depths are within 15% of "common" types
3. Determine the protection level provided or standoff required by entering the curves. Enter the curve with the appropriate charge weight on the vertical axis, and the

appropriate standoff on the horizontal axis. Read the protection level at the intersection of these lines. Points below and to the right of the low, medium and high curves correspond to protection levels at the indicated level or higher.

The protection level curves present the protection levels provided by the buildings described in Table 3 for different charge weights (TNT equivalent) and standoffs. A typical protection level curve is shown in Figure 8. The dashed lines indicate the protection level provided against an explosive charge placed at a standoff perpendicular to the center of the "short" side of the buildings, or 90° for the "long" side. The solid lines or 0° lines represent the protection level provided for a charge placed at a standoff perpendicular to the center of the building "long side".

The curves should be entered with the standoff in feet and the charge weight in pounds of TNT. The intersection of those points, then, indicates protection level provided. A point to the right and below a curve indicates a level of protection greater than that curve, but less than that of the curve further to the right. Conversely, a point to the left and above a curve indicates a protection level less than that of the curve, but greater than that of the curve to the immediate left. Points to the left of the low level of protection curve indicate structural failure.

On several of the plots the protection level curves do not extend down to lower standoffs. This indicates that the use of the respective Level of Protection (LOP) curve below that standoff is beyond the range of applicability of the analysis used to define the curve. In all cases, scaled standoffs of  $R/W^{1/3} = 3.0$  were defined as a lower limit, since response mode changes can occur for certain materials below that standoff. These response mode changes can mean that local breaching or panel shearing could occur at these low standoffs. If local breaching is not important to overall building or asset protection, the analyst can neglect this component response. If the desired or plotted point is in this regime, the protection level provided can be determined as the greater of the values obtained by either moving horizontally to the right along the same charge weight line or vertically up to the next LOP curve.

If the building to be analyzed cannot be compared well with those in Table 3, the level of protection can be calculated by first calculating the level of protection provided by each component in the building using the P-i curves in Reference 4 (see Figure 3 for an example). The use of these P-i curves requires knowledge of structural and geometry parameters describing each component and the peak pressure and impulse applied to each component. Considerable guidance in the calculation of each of these parameters is provided in Reference 4. Then, the level of protection provided by all the components is searched for the lowest level of protection. This lowest level of protection is the building level of protection for the given charge weight and standoff used to calculate the blast loads.

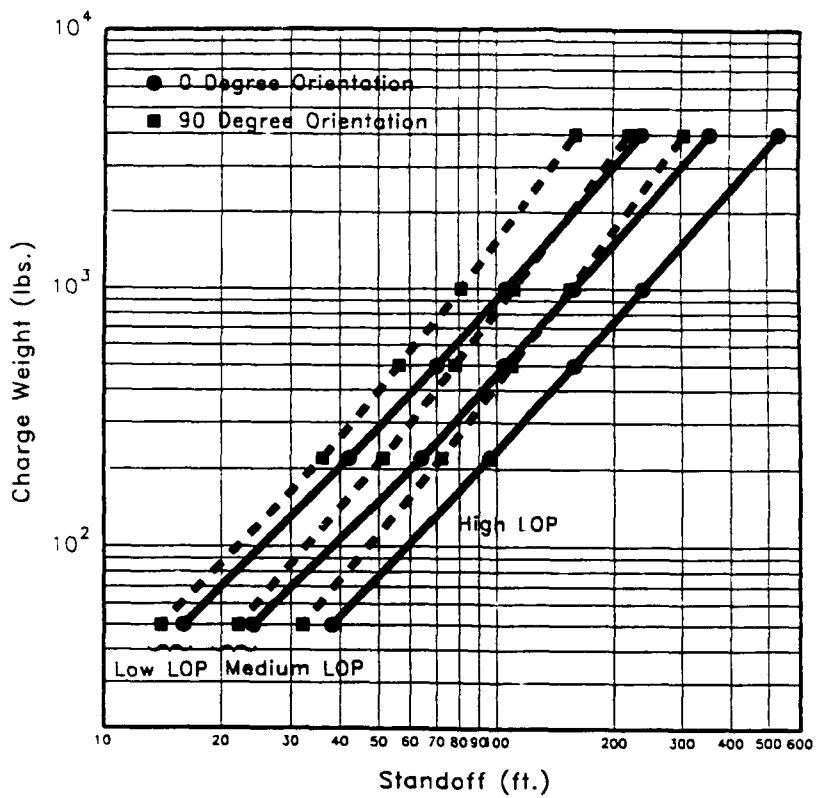


**Figure 8. Building No 7 (Small Pre-Engineered "Butler" Type Building)  
Protection Level Curves versus Charge Weight**

## 5.0 Future Developments

- First and most importantly--any future efforts must begin with additional literature searches to collect data for all components to be considered. In order to truly confirm the analytical resistance functions we postulate for the components--we must validate the predicted response with data for all components.
- Secondly, additional data must be acquired to validate building damage predictions. The most recent work for NCEL included some limited validation of building damage using WW II data that was not really sufficient in detail for analysis. Details of most of the attacks that have occurred over the last ten to twelve years in Britain and Ireland may be available. These documented "data points" should have sufficient detail for analysis.
- Third, we ought to look at the way we calculate collapse--and attempt to come up with a more realistic (in a structural sense) scenario for member collapse and subsequent loss of a building's usable space. There are data and reports available describing collapse. The thing to remember is that engineered structures retain an astonishing amount of load carrying capability even after the loss of "key" members because of strength in secondary structure and sheathing, etc.

- Fourth, response modes other than flexural should be investigated and included in the code or procedure capability. We should start by looking at buckling, shear and local shear (breach).
- BDAM or the code should also be modified to allow analysis or design of individual components. A tool might be developed that can be entered with standoff and charge weight, told what type of construction (concrete, steel frame and sheathing, wood, etc.) the designer wants, and the code will do preliminary sizing, etc.

## **6.0 Conclusions**

The work summarized in this paper demonstrates the usefulness of the P-i approach as a basic method for quickly assessing blast damage to relatively large buildings taking into account the blast response of each component. The P-i curve approach is flexible enough to be used to describe many types of components, ranging from open web steel joists to concrete slabs; many types of response, ranging from buckling to flexural response; and different types of building vulnerability assessment approaches, ranging from a level of protection assessment to a building damage assessment.

The usefulness of the P-i approach is considerably enhanced by the BDAM program developed at SwRI. This computer code reads a description of all the building components and the charge weight and charge locations of interest and quickly calculates damage to all components in the building based on the P-i curves which are programmed into the code and then sums component damage or level of protection according to the set of "rules", or algorithms which are programmed into the code. The code outputs both a detailed component-by-component summary of damage and simple plots which show the total building damage or level of protection as a function of charge weight and charge standoff. Work which is funded by the US Army Corp of Engineers at Omaha is currently underway at SwRI to reduce the effort involved in the input of typical buildings.

## **References**

1. Whitney, M.G., Ketchum, D.E. and Polcyn, M.A., "Blast Vulnerability Guide," Final Report, Prime Contract No. N00123-86-D-0299, Naval Civil Engineering Laboratory, October 1987.
2. Oswald, C.J. et al., "Blast Damage Assessment Procedures for Common Construction Categories," Final Report, Prime Contract No. N00123-86-D-0299, Naval Civil Engineering Laboratory, October 1987.
3. "Security Engineering Manual," US Army Corps of Engineers Missouri River Division-Omaha District Protective Design Center, January 1990.
4. Marchand, K.A., Cox, P.A. and Peterson, J.P., "Blast Analysis Manual Part I--Level of Protection Assessment Guide," Final report, Prime Contract No. DACW45-89-D-0139, US Army Corps of Engineers, Omaha District, PD-MCX, July 1991.
5. Polcyn, M. et al., "Users Manual for Blast Damage Assessment Model, BDAM," Final Report, Prime Contract No. N47408-91-D-1127, Naval Civil Engineering Laboratory, December 1991.

**APPLICATIONS OF FINITE ELEMENT TECHNOLOGY  
TO REINFORCED CONCRETE EXPLOSIVES CONTAINMENT STRUCTURES**

by

T. A. Shugar and T. J. Holland  
Naval Civil Engineering Laboratory  
Port Hueneme, CA 93043

and

L. J. Malvar  
University of California, Davis  
Davis, CA 95616

Paper Submitted to

Department of Defense Explosives Safety Board  
Twenty-Fifth Explosives Safety Seminar

Anaheim, California  
18-20 August 1992

## ABSTRACT

Two widely available general purpose computer programs for three-dimensional nonlinear dynamic finite element analysis were applied to three types of reinforced concrete structures of recent interest to Navy explosive safety: a novel cylindrical missile test cell concept, flat slabs with variable shear steel, and a soil-covered roof slab for a new high performance magazine concept. Results from codified single-degree-of-freedom (SDOF) methods for design of explosive safety structures were considered and compared with finite element technology. An overview of these baseline studies is presented.

A commercial implicit finite element program was used to analyze the cylindrical missile test cell. Three-dimensional model construction, nonlinear concrete material modeling, and dynamic response were emphasized. Support for embedded reinforcement modeling was found to be very useful in construction of the model so as to retain the inherent anisotropic behavior of the composite structure. Concrete material modeling capability was highly sophisticated, but problematical in application when substantial cracking accumulated in the dynamic response. Sufficient results were nonetheless obtained to demonstrate the value of computational structural dynamics technology in providing detailed understanding of the behavior of complex explosive safety designs.

An explicit finite element program was used to analyze the dynamic response of two flat slabs subjected to conventional blast pressure levels. Elasto-plastic models included in the material library were used to model the material behavior of concrete and steel. The rebar pattern was modeled via the discrete reinforcement method; no embeded modeling capability existed. Measured residual deflections from field tests were compared to calculations from both three-dimensional finite element models and codified SDOF methods. In these limited data, the codified SDOF method was prone to unconservative results, while the finite element method bracketed the measured residual displacements, and further, successfully calculated observed failure modes and the onset of buckling in the reinforcement.

The explicit finite element program was also applied in the analysis of the soil-covered roof slab design. In this case, the blast load pressures were an order magnitude higher, and the concrete material response included hydrodynamic behavior. The three-dimensional finite element model also included discrete reinforcement modeling and elasto-plastic behavior of the rebar. The dynamic response of the slab was calculated up to onset of a localized failure mode. This failure mode was consistent with initial field test observations of breach failure modes in scale models of slabs.

It is concluded that commercial or available general purpose finite element programs for nonlinear dynamic analysis of reinforced concrete structures merit wider recognition and application in analysis and design of explosive safety systems. However, these programs have definite strengths and weaknesses, and consequently proficiency in their application must be developed to exploit them as resources.

## **INTRODUCTION**

Traditional design of reinforced concrete structures to resist blast loads has been based on structural dynamics of elastic-plastic lumped parameter models of one or two degrees of freedom. These models are well explicated in the classical reference by Biggs (1964). In addition to this analytical technology, design procedures are also based on field testing experience accumulated in explosive safety engineering for the past quarter century. The combination of traditional structural dynamics and field test experience has led to a semi-empirical method for the design of explosive safety facilities as embodied by the standard Tri-Services guide, NAVFAC P-397 Design Manual (1991). However, this guide does not address modern computer methods in structural dynamics and finite element methods. It neither promotes nor precludes their use in the analysis and design of explosive safety facilities. Nonetheless, it is of interest to investigate how well these modern methods perform, and whether they merit further recognition in conjunction with codified procedures in explosive safety.

### **Objective**

The objective of this paper is to discuss the effectiveness of modern computational structural dynamics methods which have been applied to recent problems in naval explosive containment facilities constructed of reinforced concrete. The methods are embodied by two widely used general purpose, nonlinear dynamic, finite element computer programs. One is based on implicit and the other on explicit, temporal integration of the equations of motion. More detailed information on this subject is presented in a corresponding NCEL technical report (Shugar, et al., 1992).

### **Structural Analysis Models Studied**

The reinforced concrete structures studied include a novel missile test cell concept subjected to an internal blast load, flat slabs subjected to close in blast loads and a soil-covered roof slab subjected to an internal blast load which has been recently proposed for a high performance magazine concept.

The unique feature of the missile test cell analysis is the complexity of the steel reinforcement model which was constructed using the embedded reinforcement model method. In contrast to this method discrete reinforcement models were employed for the analysis of the flat slabs and the soil-covered roof slab, both of which have comparatively regular patterns of reinforcement. The missile test cell analysis was addressed with the implicit code, ABAQUS (1989), whereas the flat slabs and soil-covered roof slab were analyzed with the explicit finite element program, DYNA3D (Hallquist and Whirley, 1989). In general, implicit codes are suitable to analyses dealing with slow, sluggish dynamic loads, while the explicit codes are suitable to highly transient dynamic loads. On the other hand, reinforced concrete modeling capability is more substantial in ABAQUS than in DYNA3D. This is because the former supports modeling of complex reinforcement patterns, and because the concrete model is more sophisticated; it includes strain softening and orthotropic cracking behavior, for example.

The DYNA3D analysis of the flat slabs was noteworthy because some experimental data was available and was used to compare computed and measured dynamic response. Two slabs were studied, one with substantial shear steel reinforcement, and the other with no shear steel reinforcement. Further, comparisons included computed dynamic response as calculated according to the NAVFAC P-397 Design Manual.

The unusual feature of the soil-covered roof analysis was the magnitude of specified blast loads. These were an order of magnitude higher than in the missile test cell analysis. This necessitated an auxiliary study of DYNA3D material models available for concrete behavior in the hydrodynamic range, as well as in the shear deformation range. In addition to discussion of the dynamic response of the roof, an approach to computing fragment and debris distance is also discussed.

## **NONLINEAR DYNAMIC FINITE ELEMENT ANALYSIS OF REINFORCED CONCRETE MISSILE TEST CELL**

In this baseline study we addressed the problem of analyzing a reinforced concrete missile test cell (MTC) structure subjected to an internal blast load. The study employed ABAQUS Version 4.8, which is a general purpose implicit finite element program for static and dynamic analysis. The study featured accurate replication of three-dimensional geometry and composite structural behavior for a complex reinforced concrete design. Accurate modeling of an entire reinforced concrete structure was pursued, and how current technology addresses nonlinear material behavior such as cracking and crushing of concrete was studied.

Though the study included linear static analyses, eigenvalue analyses and linear dynamic analyses of the MTC, these and other results are generally omitted for brevity. The discussion given emphasizes the MTC model development, the nonlinear concrete material model, and the numerical results for the nonlinear dynamic response of the MTC wall.

### **Missile Test Cell Model Development**

Commercial computational methods that may be used for the analysis of a complex reinforced concrete missile test cell are limited to ones based on implicit temporal integration algorithms. This adversely impacts the requirement for computational efficiency. For large scale problems this may mean that the analysis will be prohibitive. Codes based on implicit temporal integration are technically capable of predicting high frequency response, and are capable of predicting both nonlinear material and nonlinear geometric behavior, but the required computational power can be prohibitive.

**Blast Load and Expected Structural Response.** To model the MTC so that its dynamic response can be accurately computed, the blast load should be determined as closely as possible. For purposes of this investigation, the MTC is presumed subjected to the two-phase design (internal) blast load graphed in Figure 1 which is based on an inadvertent detonation of a missile warhead.

The bilinear triangular pressure history shown is composed of an initial triangular shock pressure phase and a subsequent triangular gas pressure phase (Murtha and Dede, 1988). In this case, the pressure is further assumed uniformly distributed over all internal surfaces of the MTC. The shock pressure history includes a 2,560-psi peak pressure with a duration of 1.75 milliseconds and a specific impulse of 2,240 psi-ms.

The calculation of the gas pressure phase is based on containment of the products of detonation. This phase has a comparatively low magnitude, long duration triangular pressure history. The semi-empirical method used and the computer program developed for calculating the gas pressure loads are described by Tancreto and Helseth (1984). According to this methodology, the gas pressure history depends on the shock pressure and various geometric and physical properties of any venting mechanisms present. In the case of the MTC, a frangible circular aperture in the back wall constitutes a venting mechanism which is factored into the computation. The resulting gas pressure history shown has a peak value of 307 psi, a duration of 177 milliseconds, and a specific impulse of 27,155 psi-ms which is substantially larger than the specific impulse of the shock phase.

**MTC Configuration and Steel Reinforcement.** The MTC is fundamentally a reinforced concrete thick-wall cylinder with thick circular plate endwalls. The walls of the structure are 32 inches thick, and the inside chamber is approximately 20 feet in diameter and 30 feet in length. Regarding model construction, these simple geometrical aspects are deceiving because the geometrical complexity of the steel reinforcement is substantial. Modeling this complexity represented the major challenge to the development of the finite element model of the MTC for it was desired to retain, as closely as possible, the anisotropic behavior inherent in its composite design.

Description of the MTC steel reinforcement design is facilitated by subdividing it into three sections as shown in Figure 2; they include the cylinder, the front wall and the back wall. The geometrical patterns shown in these graphics are the result of an intermediate stage of the reinforcement modeling procedure which employed computer aided design software. This stage was necessary to clarify and define the reinforcement patterns from data taken directly from design drawings of the MTC.

The hoop and longitudinal steel reinforcements for the cylinder subsection, which are indicated in Figure 2a, are comprised of #11 bars. Groups composed of four concentric hoop bars are located at stations every 6-inches along the length of the cylinder. To each of the four hoop bars there corresponds a layer of longitudinal reinforcement. Each layer contains 156 longitudinal bars equally spaced about the circumference at intervals of 2.3 degrees.

The reinforcement design for the back wall of the MTC is shown in Figure 2b. It is composed of two identical layers of mutually orthogonal hoop and radial bars. One layer each is embedded just beneath the inside and outside concrete surfaces of the wall.

The front wall reinforcement design shown in Figure 2c is more complex since the aperture is rectangular instead of circular to provide for a blast resistant access door. The radial steel is similar to the radial steel in the back wall in that only every other bar extends from the outer perimeter to the aperture. The radial reinforcement consists of 156 #6 bars, and the hoop bars are #11 bars in both end walls.

In addition to the primary reinforcement described, the MTC design also included shear steel and diagonal bars, which for clarity are omitted in these graphics. For example, the shear steel consists of stirrup bars tying together the four concentric layers of primary bars in the cylinder wall. These stirrup bars are meant to confine the concrete to the hoop and longitudinal steel bars. The diagonal bars are #11 bars, and they were intended to reinforce the interface between the cylinder and the front and back walls. To this end, a pair of crossing diagonal bars were included at each of 156 uniformly spaced stations around the two perimeter interfaces between the cylinder and end walls.

**Three-Dimensional Finite Element Model.** The three-dimensional finite element model of the MTC is shown in Figure 3. One plane of symmetry is exploited due to symmetry of the structure and applied load. Eight-node brick elements in which the displacement fields are interpolated linearly were prescribed. Two elements were prescribed through the thickness of the wall. Earlier models were also developed with four elements through the thickness, and linear static runs indicated that the radial stiffness of the MTC model was the same for either model. The model possessed 1300 nodes or 3900 degrees of freedom. PATRAN Plus (1989), Release 2.4, was employed to generate the basic three-dimensional models. It has ABAQUS file format translators for basic mesh and surface load information, but it does not support the ABAQUS embedded reinforcement data files which describe the reinforcement model.

**Description of Embedded Element.** The steel reinforcement model is constructed by the embedded reinforcement model approach. The advantage of this approach is that it provides a reasonably accurate replication of the effect of reinforcement while being convenient and expedient to implement into an existing finite element model. No changes to the aforementioned finite element model (Figure 3) were required to introduce the reinforcement model, in spite of the complexity of the reinforcement patterns. A recent discussion of the embedded reinforcement modeling method is provided by Cervera, Hinton and Hassan (1989).

A sketch of an embedded element is shown in Figure 4. This element is typical of the cylindrical wall of the MTC model, so that principal directions are labeled hoop, longitudinal and radial. Two such elements, each 16 inches thick, model the wall through its thickness. There are four layers of steel reinforcement in the wall, of which two exist within each element. Shown here is the inner element with the bottom node lying in the internal cylindrical surface of the wall, and the top node lying in the middle surface of the cylindrical wall. The exact locations of the two inner layers of reinforcement relative to the middle surface are indicated. Each layer is a smoothed composition of bars running through the element. Moreover, a layer possesses an anisotropic or directed stiffness corresponding to the percentage and direction of the steel. This stiffness is superimposed on the otherwise isotropic stiffness of the parent concrete element.

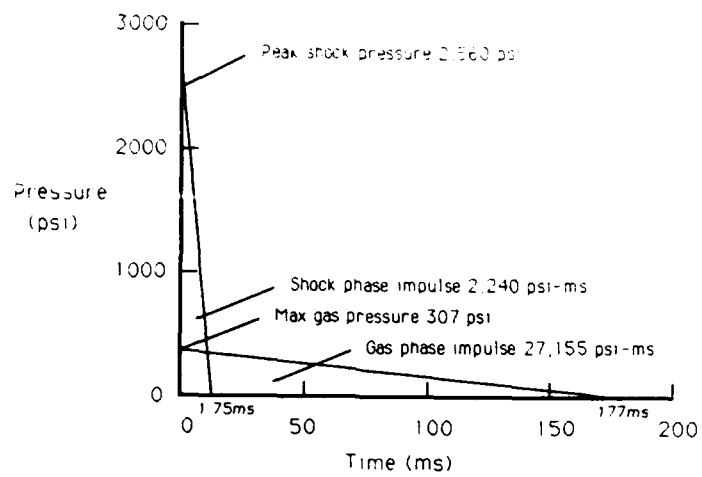


Figure 1. Assumed internal shock and gas pressure load for MTC.

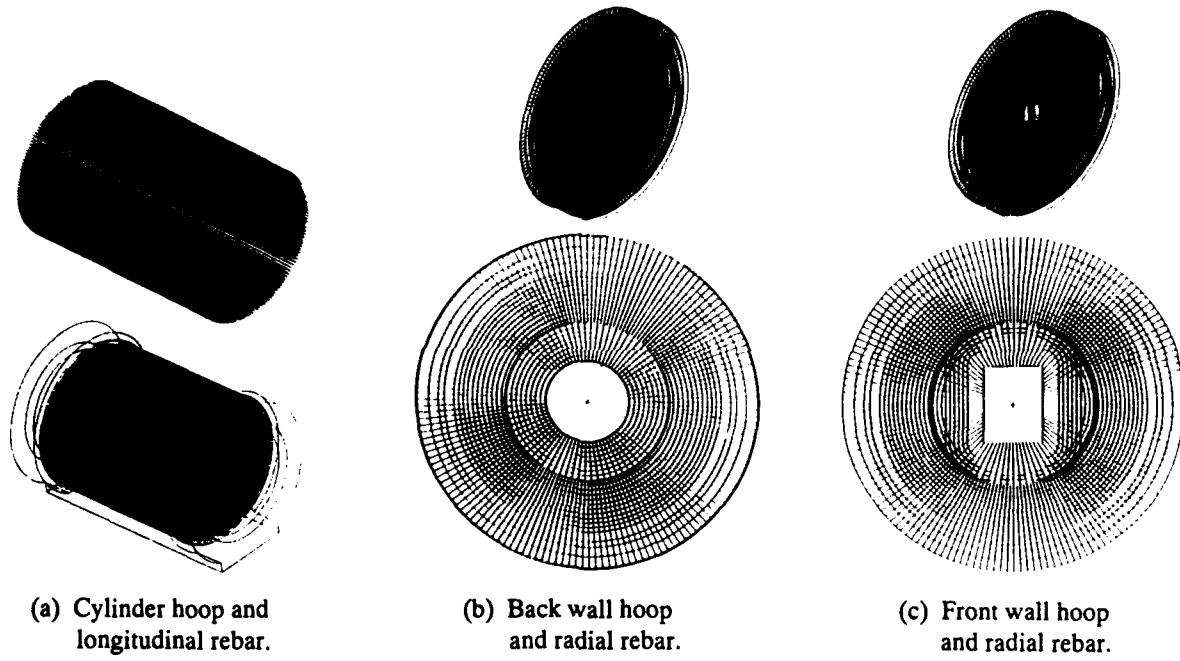


Figure 2. MTC primary rebar definition.

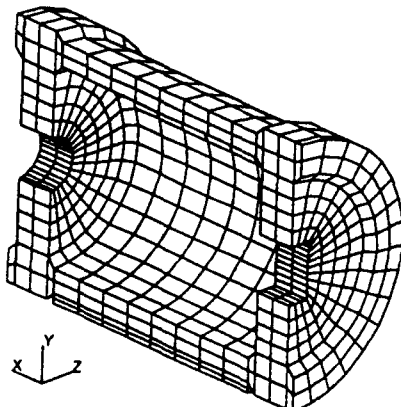


Figure 3. Three-dimensional finite element model for the MTC.

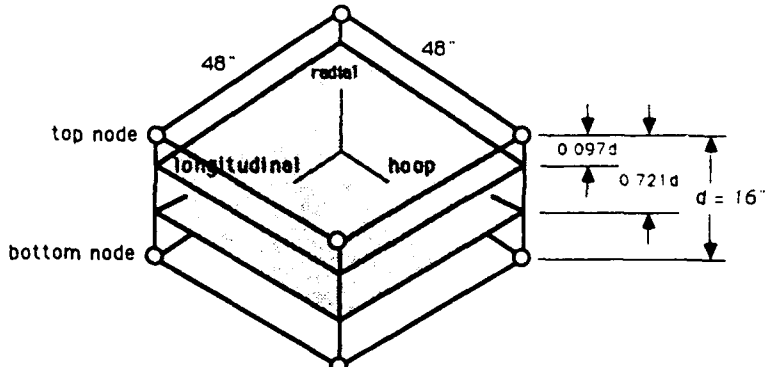


Figure 4. Typical embedded element for MTC model.

**Embedded Reinforcement Element Test.** Forces were applied to the nodes of a single embedded element (Figure 4) to demonstrate the anisotropy in load-deflection behavior due to the embedded steel reinforcement. The node forces were applied in the longitudinal, hoop and radial directions in separate tests. The applied nodal forces were uniform and predetermined such that without reinforcement, the plain concrete element would experience 1 psi axial stress in each case.

The numerical results of the three cases, with and without reinforcement present, are compiled in Table 1. The top and bottom node point displacements and element concrete stresses which were computed agree with the expected solution in the absence of the steel reinforcement. Comparison between these values and values computed with the reinforcement present demonstrated that the anticipated anisotropic behavior of the embedded reinforcement was present. The results showed that the steel reinforcement added more stiffness to the upper portion of the element in both the longitudinal and hoop directions, as would be expected from the placement of the two steel layers nearer the upper half of the element. Correspondingly, the element concrete stresses diminish below 1 psi in the longitudinal and hoop directions because the applied load is shared by the steel reinforcement. The element stiffness in the radial direction is otherwise insensitive to the longitudinal and hoop reinforcement.

Table 1. Embedded Element Behavior

Nodal Load Direction	Node Displacement (in. $\times 10^5$ )		Concrete Stress* (psi)	
	Without Steel Top/Bottom	With Steel Top/Bottom	Without Steel Top/Bottom	With Steel Top/Bottom
Longitudinal	1.600/1.600	1.261/1.317	1.000/1.000	0.800/0.810
Hoop	1.600/1.600	1.240/1.310	1.000/1.000	0.790/0.800
Radial	0.533/0.533	0.533/0.533	1.000/1.000	1.000/1.000

\*Concrete stresses are reported at the top and bottom Gauss points.

**MTC Reinforcement Model Description.** ABAQUS provides a graphics package for visual checking of the input data specifying the location of embedded reinforcement. Samples of these graphics for the MTC model are shown in Figure 5, in which the reinforcement model is shown located relative to the three-dimensional finite element mesh. A longitudinal vertical section through the MTC's steel rebar cage model is shown in Figure 5a. For clarity, it is only one element deep in the direction perpendicular to the section. The four nested layers of longitudinal steel running horizontally through the cylinder wall and terminating at the end walls, are clearly visible at both the top and bottom of the cylinder. The thinner vertical lines uniformly spaced in the section of the cylinder wall represent stirrups.

Design of haunches in a conventional sense aims to provide fixity against rotation to develop the strength in adjoining walls and slabs. These graphics show how the crossing pair of diagonal bars in the haunch design of the MTC are modeled in detail. Each bar is modeled individually. This capability demonstrates unprecedented potential for accurately modeling the dynamic anisotropic interaction between walls and slabs in corner regions of explosive safety facilities in a reasonably automated fashion. Design and analysis procedures in explosive safety typically ignore this interaction which nonetheless is important to the overall dynamic response of magazines or missile test cells.

In Figure 5b, multiple layers of hoop and radial steel through the wall thickness are shown for the back wall. A similar model of the front wall reinforcement had an elliptical rather than a circular hoop reinforcement pattern near the aperture.

### Nonlinear Concrete Material Model

The necessity of modeling nonlinear material behavior of concrete in explosive safety applications of finite element technology is apparent when it is considered that these structures are designed to sustain severe damage while containing or managing explosions. The anticipated extent of nonlinear material behavior might well vary with the particular facility, and modeling this behavior may be more important for some designs than for others. Compression behavior is important, for example, because compressive stresses equilibrate tension forces in steel rebar at cracked sections in flexure. Even if the compressive strength is not exceeded in such cases, the stress-strain behavior may well be nonlinear.

Moreover, failure of concrete in tension precipitates cracks which propagate and affect subsequent dynamic response. Nonlinear concrete material modeling is therefore primarily necessary for accurate determination of cracked surfaces and hence the structural modes which participate in the subsequent dynamic response of the structure.

Nonlinear concrete material models are generally very complex both theoretically and computationally. The overall complexity of modeling reinforced concrete is reduced somewhat by the strategy of modeling the reinforcement separately (e.g., using an appropriate reinforcement model) from modeling the concrete material behavior.

The interaction between reinforcement and concrete, known as bond-slip behavior, is rarely accounted for in today's technology. Bond-slip models are the subject of ongoing basic research at NCEL (Cox and Herrmann, 1992), as well as elsewhere. Such models have been used with embedded reinforcement models for steel, for example by Elwi and Hrudey (1989). However, the technique remains tentative and embryonic as the discussion by Pandey (1991) suggests. Schnobrich (1989) suggests that application of bond-slip models is currently prohibitive with large, nonlinear finite element analysis of reinforced concrete structures.

**Theoretical Aspects.** Theoretical complexity derives from the concepts of the theories of plasticity and continuum damage mechanics as applied to the failure of brittle materials. Such materials exhibit very different behavior for compression and tension loadings, and the material model is correspondingly very different for compression and tension stress-strain behavior. The ABAQUS concrete material model uses plasticity theory to describe crushing behavior and

damage mechanics for cracking behavior. These theories are combined to derive a constitutive, or stress-strain, law for overall material behavior. The constitutive law is ultimately expressed as a system of several nonlinear differential equations.

**Computational Aspects.** The constitutive law must be numerically integrated in a manner analogous to numerical integration of an initial value problem. Computational complexity derives from the algorithms used to integrate the system of equations along the stress-strain path at special points within each finite element known as stress points or Gauss points. For example, the nonlinear concrete material model implemented in ABAQUS, as described by Resende (1987, 1989), is over 4,000 lines of code in length. In an implicit nonlinear dynamic finite element analysis, this code sequence must be traversed for each Gauss point, within each element, for each iteration, within each load step, over the history of the dynamic response. For a single three-dimensional analysis using the MTC model, this could amount to over one million traverses of the material model loop. Clearly these analyses are not suited to personal computers, and require at least the use of very powerful workstations.

**Practical Aspects.** The ABAQUS nonlinear concrete model is limited to confining pressures below three to four times the concrete compressive strength. Hydrodynamic material models such as are available in DYNA3D offer an alternative in this regard when much higher pressures are encountered.

Furthermore, while the concrete material model handles severe loading, well beyond the elastic response, it is limited to relatively monotonic loads. The ABAQUS concrete material model should therefore be applicable to problems involving over pressurization of containment structures such as nuclear reactor containments or missile test cells since there is generally little interest in the response after only a very few cycles. Conversely, it is not suited to high performance magazine concepts wherein design pressures are of an order magnitude higher than the compressive strength, or to severe seismic loads where cyclic inelastic response with many cycles is important.

### **Nonlinear Dynamic Response of MTC Wall**

It was discovered that the nonlinear dynamic response of the MTC using the aforementioned three-dimensional model could not be computed satisfactorily due to the extreme sensitivity to cracking of the concrete material model. In the material model, cracks form when the direct stress exceeds the tensile strength of concrete. Secondary cracks form in planes orthogonal to the plane containing the initial or primary crack. At most we were able to simulate only the first 1.6 ms of the dynamic response before secondary cracking took place, which could not be handled by the material model. This deficiency is now documented in ABAQUS version 4.9.

**Simplified Model of the MTC Wall.** To determine further the cause of the difficulty, a simpler model of the MTC wall was constructed. This model consisted of a transverse section through the cylinder, and was formed directly from a ring of solid elements from the center of

the three-dimensional model. Plain strain conditions were imposed on this layer of elements, so that the dynamic response derived from this model would be strictly applicable to the wall of an infinitely long tube possessing the cross-section shape of the MTC.

Attempts to run the simplified model were successful, but not before many failed attempts occurred which were similar to those for the three-dimensional model.

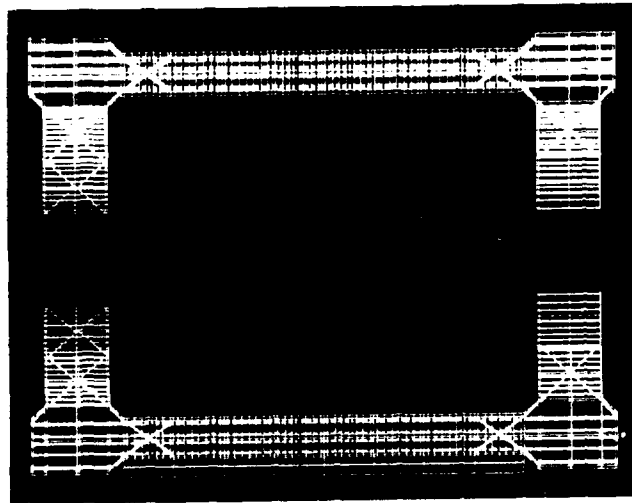
Post mortem data of failed runs indicated that primary radial cracks had formed in the wall in a rational manner, but that the directions of secondary cracks which also formed were arbitrary and meaningless. Furthermore, the occurrences of secondary cracks were correlated with occurrences of hashing in the reported hoop stress data in the MTC wall. The hashing, or occurrence of large spikes in the response, was spurious since subsequent to formation of radial cracks, the concrete hoop stress response should have diminished smoothly to zero with continued loading. It was found that boundary conditions at the base of the MTC induced high bending moment in the wall which caused severe cracking to occur, and this overburdened the concrete material model's capacity to handle cracking correctly. The difficulty was finally resolved when boundary conditions representing support at the base of the model were removed. Subsequent to that adjustment, the simplified model ran reasonably successfully.

Unfortunately, similar adjustment of the boundary conditions at the base of the three-dimensional MTC model did not noticeably improve subsequent simulation attempts. This model is more challenging to the concrete material model since the additional geometrical complexity induces severe stress concentrations, particularly at the interface between the cylinder and end walls, which leads to widespread cracking. These stress concentrations were clearly visible in the results of preliminary linear static runs with the three-dimensional model.

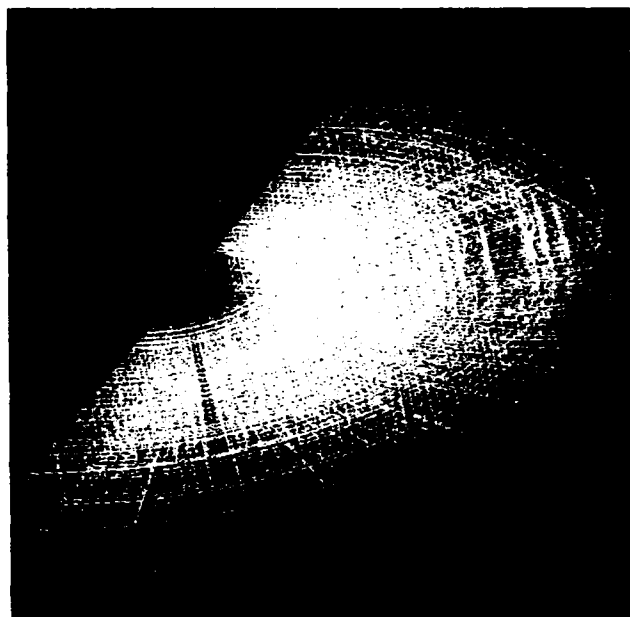
**Dynamic Response of the MTC Wall.** Using the unrestrained simplified model of the MTC wall, the nonlinear dynamic response was computed relative to the prescribed blast load (Figure 1). The simulation terminated after 30 ms. The displacement fields at three intermediate stages of the response are depicted in Figure 6 where the radial expansion of the wall and base are shown (exaggerated for clarity).

The nonlinear dynamic response at top dead center (TDC) of the wall is shown in Figure 7. The first peak occurred at 12 ms and the second peak occurred at about 28 ms as shown in Figure 7a. The second peak is slightly larger at 2.3 inches displacement on the cylinder inner radius.

The hoop stress response at TDC is shown in Figure 7b. These data are remarkable for they show the relationship between radial cracking of concrete and progressive transfer of hoop force to the steel reinforcement at this section. This information is important to a detailed understanding of how the MTC wall behaves in resisting load. It would otherwise be difficult to obtain this information experimentally in full scale or model field tests of any reinforced concrete structure or structural element subjected to severe blast loading. It typifies the potential contribution of modern computational structural dynamics methods in supplementing information gained from full scale or model tests in explosive safety research.

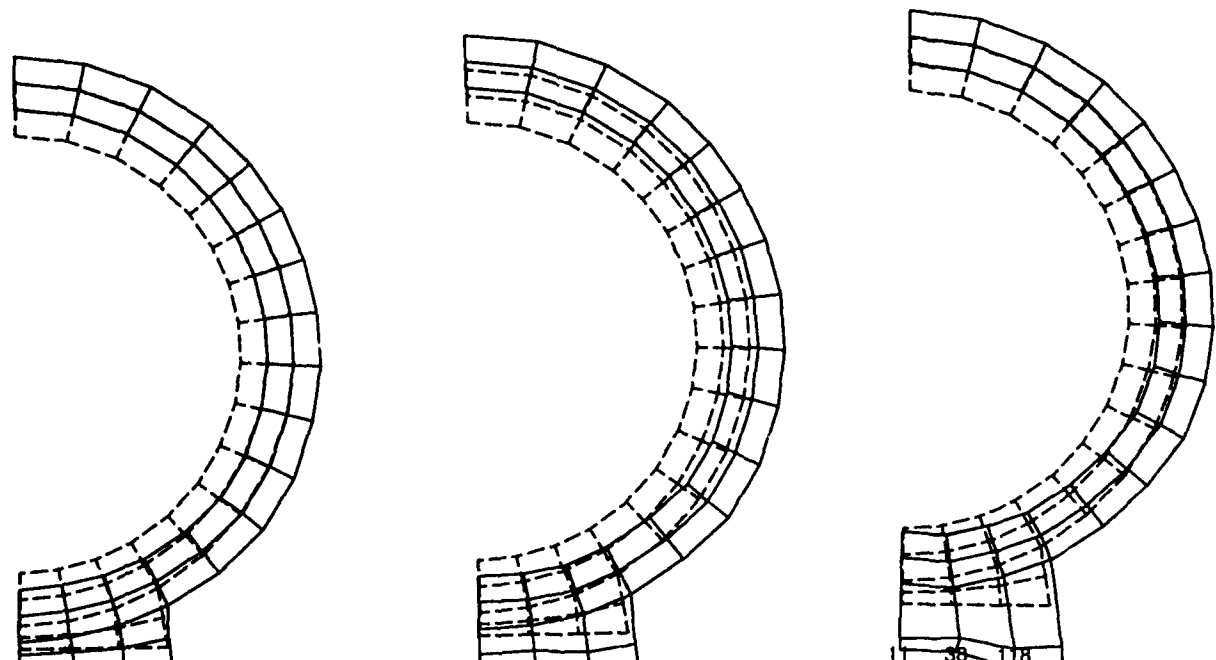


(a) Longitudinal section through cylinder.



(b) Isometric view of back wall model.

Figure 5. Embedded reinforcement model for MTC.

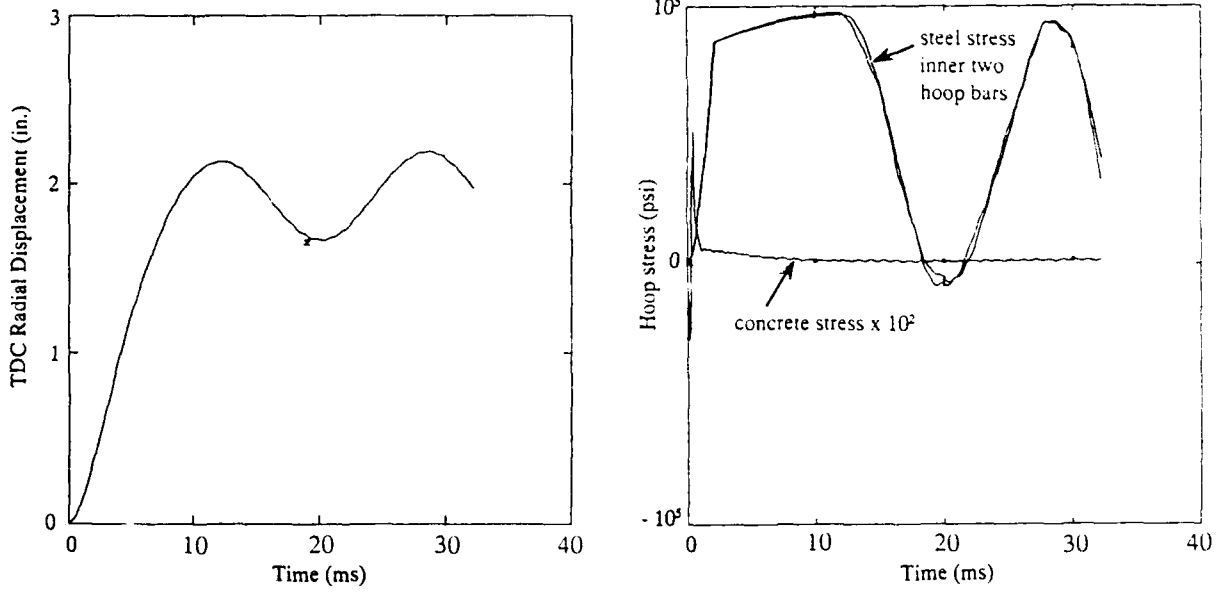


(a)  $t = 6.03$  ms

(b)  $t = 12.00$  ms

(c)  $t = 20.04$  ms

Figure 6. Dynamic response of MTC wall.



(a) Radial displacement response.

(b) Hoop stress response.

Figure 7. Dynamic response of MTC wall at TDC.

The aforementioned response results are from the inner finite element at TDC. Similar results also occurred for the outer element, thus indicating that the 32-inch wall was completely fractured at TDC. The peak tensile stress shown for the concrete is 540 psi, which was precisely the value prescribed in the material model for the tensile strength of concrete. The section completely cracks within the first millisecond, and data from other finite elements in the wall indicate that this response was also typical of most of the wall. That is, the concrete strength of the wall was not a factor after the first millisecond in resisting the residual gas pressure impinging on the wall.

The hoop steel reinforcement was seen to carry the load for the great majority of the dynamic response. These results tend to corroborate the assumption made in the MTC design that the concrete strength plays a negligible role in resisting internal blast loads and may be ignored (Ayvazyan et al., 1988).

The two inner layers of hoop reinforcing bars are shown to yield at the prescribed value of 86.7 ksi (Ayvazyan et al., 1988) within the first three milliseconds. Again these data were typical of the entire section and of most of the wall. Prescribed strain hardening of the bars was also evident in the response subsequent to yield until such time as the wall rebounded after 12 milliseconds had elapsed. Complete unloading of the hoop reinforcement was indicated, and in fact the bars momentarily experience compression before the second cycle of the response. These data warn that buckling of reinforcing bars designed primarily to resist tension forces is often a possibility due to rebound. A similar observation is made in the subsequent description of the computed dynamic response of reinforced concrete slabs.

## **NONLINEAR DYNAMIC FINITE ELEMENT ANALYSIS OF REINFORCED CONCRETE SLABS**

An assessment of explicit finite element methods using the program DYNA3D is carried out in this section. Data from blast tests of reinforced concrete slabs conducted by NCEL were used to evaluate the calculations of dynamic response from DYNA3D as well as from standard NAVFAC P-397 single-degree-of-freedom (SDOF) methods. It is shown that finite element technology can provide very detailed insight into the structural response as well as improved accuracy for close-in blast loads.

### **Slab Test Program Overview**

Dynamic blast load tests have been conducted on 12 two-way reinforced concrete slabs to verify shear reinforcement design criteria for NAVFAC P-397. Test results were reported by Tancreto (1988).

The test setup is shown in Figure 8. A 7.5 x 7.5 x 8 ft. deep cubicle was used to support the test slabs. The 10.5 x 10.5 ft. slabs (clear span 7.5 ft) had their outer 1.5 ft. edge clamped to the cubicle top.

Only slabs I and V were analyzed in the present study. Slab I had 1.06% (each way, each face) longitudinal steel (#2 deformed bars, yield stress 74.5 ksi) at d/2 spacing, W1 stirrups (yield stress 60 ksi) at d/2 spacing, a 4.5-in. thickness, and an effective depth  $d = 3.1$  in. Slab V was designed with no shear steel, had a longitudinal steel percentage of 0.31% with #2 bars at d spacing, a 6-in. thickness and a 4-in. effective depth.

Spherical Composition C4 explosives (60 lbs) were used to generate the blast loads (TNT equivalency by weight of 1.13). Scaled standoff distances were 0.69 and 1.1 ft/lb<sup>1/3</sup> for slabs I and V, respectively.

### **Finite Element Models of Slabs**

A three-dimensional nonlinear dynamic analysis of the two slabs was carried out using DYNA3D. In the finite element model, eight node solid elements and two node truss elements were used to represent the concrete slabs and steel bars, respectively. Representation of bars directly using truss elements is known as a discrete reinforcement model. Due to double symmetry, only 1/4 of the slabs was discretized as shown in Figure 9. The solid elements are 3x3 inches in plan with variable thickness. Four elements are used through the depth. Truss elements are located on the first layer in from each face. The steel area was lumped at 3 inches on center as dictated by the size selected for the solid elements.

To facilitate comparison to SDOF models the load was first assumed to be uniformly distributed. The corresponding idealized triangular load history decreased from 5,724 to 0 psi in 0.2 ms for slab I, and from 3,564 to 0 psi in 0.264 ms for slab V. A second round of analyses considered a non-uniform load distribution. Pressure load histories were obtained using the program SHOCK (NCEL 1988) in the absence of measured blast load data.

To verify the different material models available in DYNA3D for the behavior of concrete and steel, single elements were analyzed under tension and compression loads. From these tests, material models 3 and 16 were chosen as best suited for steel and concrete, respectively.

Concrete properties used were as follows: the modulus of elasticity was 4,000 ksi, Poisson's ratio was 0.2, and the dynamic compressive strength was 6,000 psi. A dynamic increase factor DIF of 1.25 to account for strain rate effects on strength was specified from NAVFAC P-397. The pressure versus volumetric strain graph for specifying the equation of state in DYNA3D material model 16 was used for concrete. For steel, the modulus of elasticity was 29,000 ksi, the Poisson ratio was 0.3, the dynamic yield stress was 97 ksi (DIF 1.3), and the dynamic ultimate stress was 102 ksi (DIF 1.05).

### **Results and Discussion of the Dynamic Response for the Slabs**

DYNA3D computations of the dynamic response, as well as design values from standard NAVFAC P-397 single-degree-of-freedom (SDOF) methods, are compared to limited experimental test data in the following.

**Experimental Results.** Measured maximum residual deflections were 8 and 8.3 inches at the center of slabs I and V, respectively. These deflections were measured after rebound, and are less than the maximum deflections reached during the tests. The deformed shapes, including yield line formations, were also apparent in Figure 10. For slab I, classical yield lines formed along the diagonals (Figure 10a). Slab V however exhibited a circular yield line about 9 inches from the sides (Figure 10b). During the rebound phase buckling of the lower reinforcement at the center of both slabs was observed.

**SDOF Predictions.** Design deflections, which included membrane action, were found using SDOF modeling procedures from NAVFAC P-397 using the computer program SOLVER (Holland, 1989). The results were 5.5 and 6.1 inches for the centers of slabs I and V, respectively.

Using the simplified procedure in NAVFAC P-397, employing a constant plastic resistance function, and design values for both steel and concrete, maximum deflections were calculated again yielding 6.8 and 6.9 inches for slabs I and V, respectively. These values are closer to measured residual values and represent an upper bound for SDOF predictions. Figure 11 shows the dynamic response data for the slabs.

In all cases, SDOF calculations of maximum response were less than the measured residual deflections. Although maximum predictions are only 15% off, they are unconservative. This could be due to the fact that the SDOF model was employed assuming an equivalent uniform load distribution which is not as severe as assuming a non-uniform load distribution.

**DYNA3D Predictions.** Figure 11 also shows the dynamic response of both slabs using DYNA3D. Experimental residual deflections fall between the residual deflection values predicted by the uniform and non-uniform load cases, the former being unconservative and the latter being conservative.

Computed displacement fields at specific times are shown in Figure 12. Figure 12a shows the deformed shape of slab I at peak displacement under uniform and non-uniform loads. Classical yield lines for this slab are indicated by the greater deflections along the diagonals. Figure 12b shows the deformed shape of slab V at 50 ms (displacements enhanced for clarity). Experimental yield line patterns for slab V were circular, and the finite element model also computed a circular localized deformation for this case.

Figure 13 shows a typical stress-time history of a bar located at center bottom of slab V. Initially, both top and bottom steel bars go into compression (less than 16 ksi for all cases) for a very short time while the shock load is still being applied. Later both top and bottom steel go into tension reaching yield stress, indicating that membrane action is taking place. During rebound, top and bottom bars unload and go into relatively high compression. In practice, these high compression stresses will not be reached because the bars are usually not braced against buckling. Buckling of the lower bars was discovered in photographs of the tested slabs as a result of analysis of these finite element data. However, beyond the indication of potential buckling in bars the finite element simulation was not necessarily accurate because it did not account for buckling phenomena.

**Summary of Alternative Methods.** In the case of close-in explosions it appears from these results that SDOF design criteria predictions can be unconservative unless the non-uniformity of the load is some how accounted for when computing the dynamic response. DYNA3D predictions with uniform and non-uniform loading, using material model 16, provided lower and upper bounds for the measured residual deflections. Dynamic responses from DYNA3D with uniform loading assumed were in reasonably close agreement with results from SDOF models. In addition, the finite element models provided an efficient and accurate way to obtain detailed information on the nonlinear dynamic response and structural behavior of flat slabs, including yield line pattern, concrete and rebar stress histories, and prediction of the potential for reinforcement buckling.

## **NONLINEAR DYNAMIC FINITE ELEMENT ANALYSIS OF A SOIL-COVERED REINFORCED CONCRETE ROOF**

The explicit finite element code DYNA3D was evaluated for a problem involving much higher blast loading pressures. A soil-covered reinforced concrete slab represents the roof of a proposed high performance magazine concept, currently being developed at NCEL, consisting of several adjacent cells for efficient explosives storage.

The objective of the numerical analysis is to determine the dynamic behavior of the roof slab due to a very high pressure (up to 24 ksi) explosion in one of the cells. This study also included examination of computed initial debris velocities of concrete fragments emanating from the failed slab.

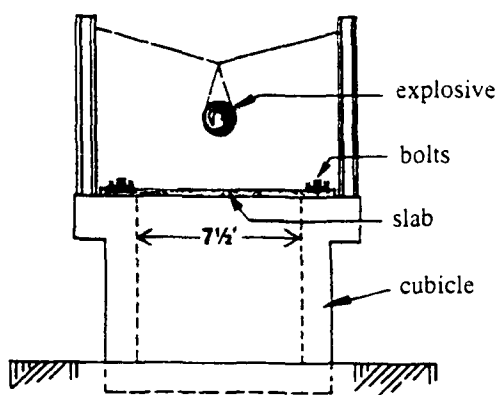


Figure 8. Slab test set-up.

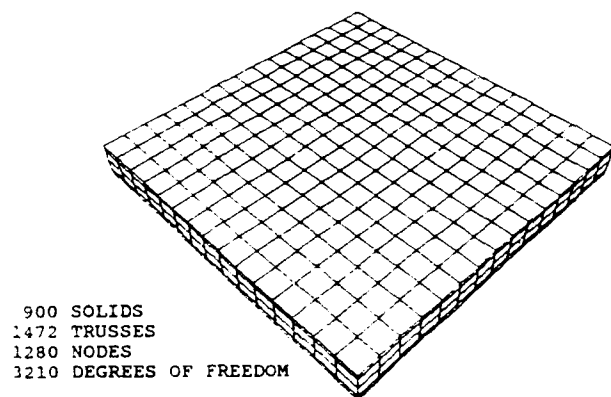
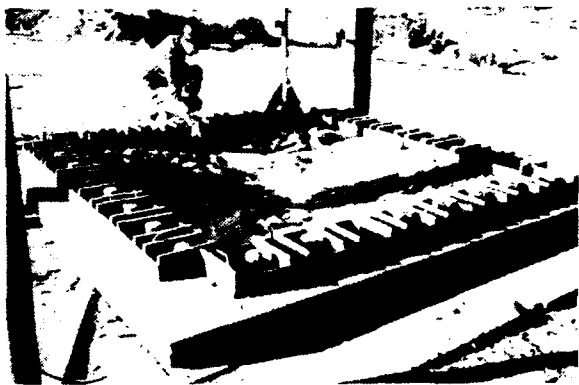


Figure 9. Finite element mesh.

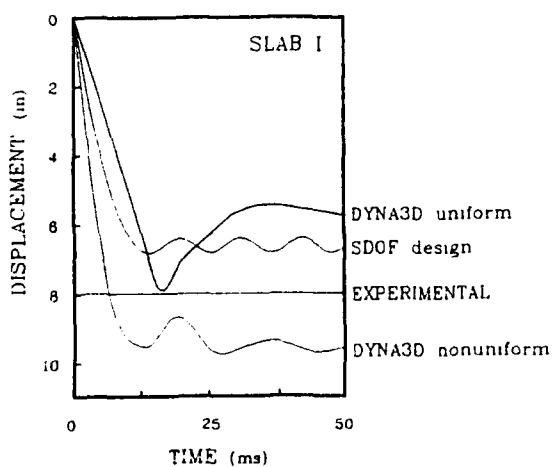


(a) Slab I

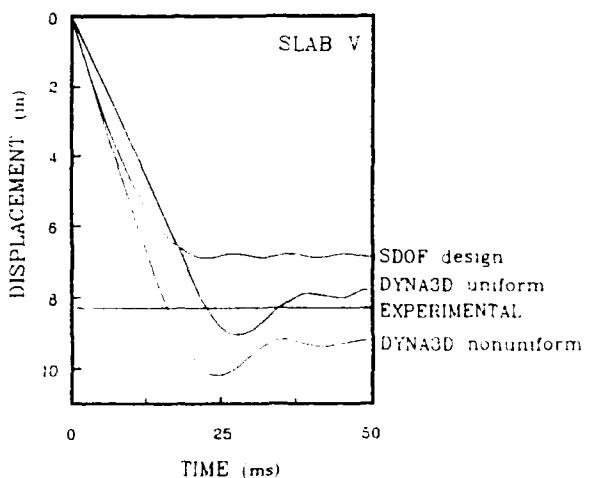


(b) Slab V

Figure 10. Top view of slabs after failure.



(a) Slab I



(b) Slab V

Figure 11. Dynamic response, center of slabs.

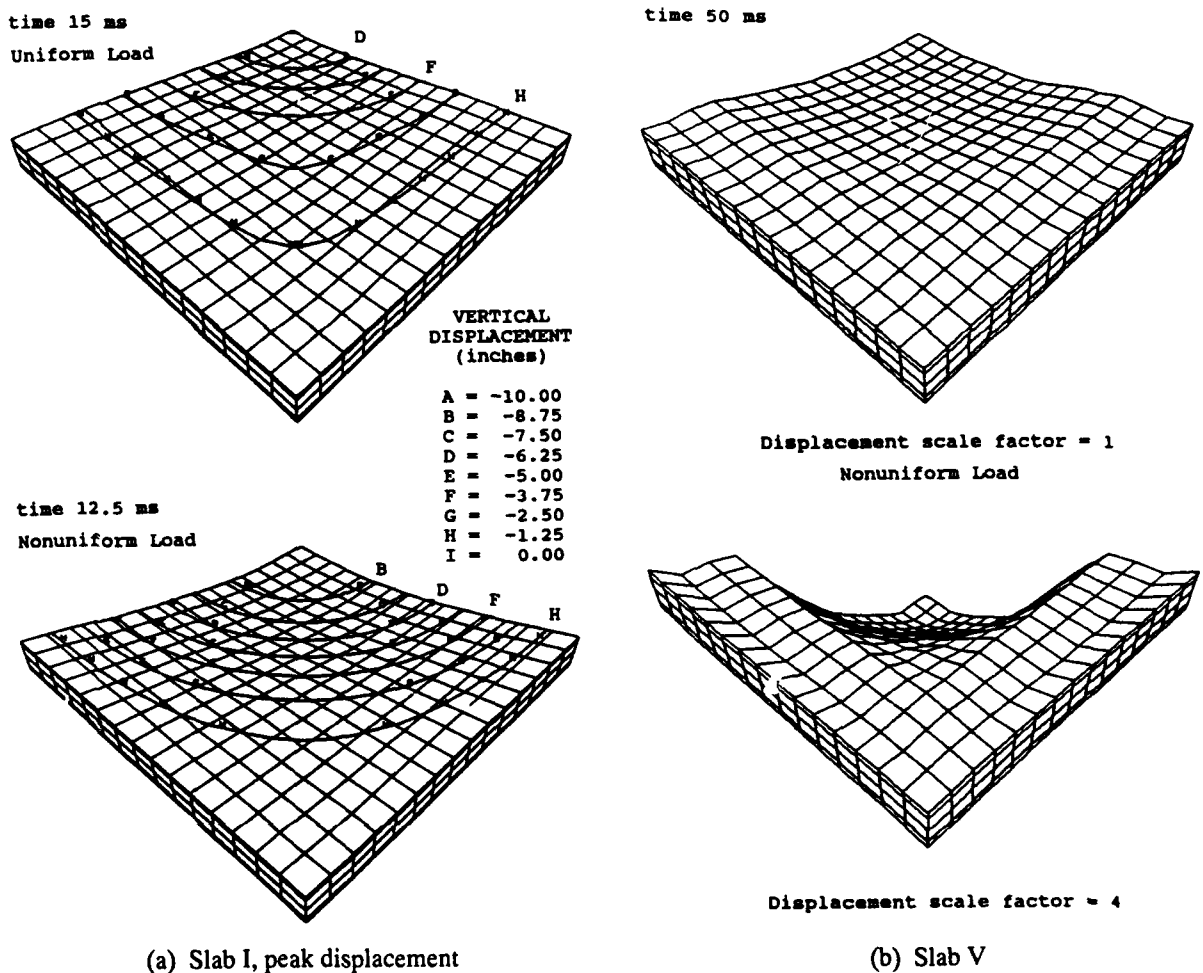


Figure 12. Deformed shapes.

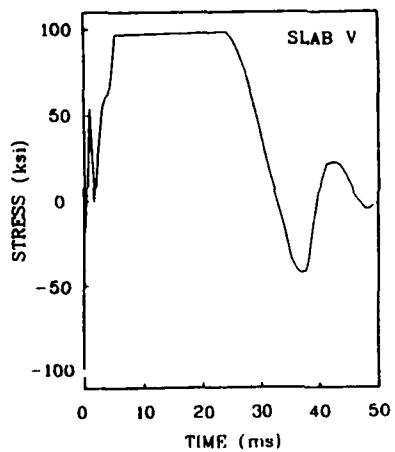


Figure 13. Rebar stress history;  
center, bottom bar  
non-uniform load.

## **Reinforced Concrete Roof**

The high performance magazine is designed to store a large amount of munitions in a small area, thus reducing the encumbered land around storage facilities required for safety. The preliminary design for the magazine is that of a large buried structure with munitions to be stored in cells, as shown in Figure 14.

The roof is a 2-foot thick reinforced concrete slab constructed of 4,000-psi concrete ( $150 \text{ lb}/\text{ft}^3$ ) with top and bottom reinforcement of Grade 60, #9 bars running in both directions at 10 inches on center. Shear reinforcement consisting of Grade 60, #4 bars connects each intersection of the longitudinal bars across the top and bottom of the slab.

The roof primarily functions as a one-way, simply supported plate carrying four feet of soil cover ( $110 \text{ lb}/\text{ft}^3$ ). The soil cover provides mass for enhancing kinetic energy dissipation of the blast energy. Since the soil cover is presumed to be unreinforced, no resistance is expected from its strength (only its inertia will contribute). The roof is supported by the outer walls and the middle wall in the long direction. It is lightly connected to these walls, and this connection is designed to offer no resistance to uplift due to an internal explosion.

The wall design of the cells is aimed at preventing sympathetic detonation, so that an explosion in one cell will not detonate munitions stored in another cell. The roof, however, will be subjected to the full force of the explosion and is designed to suffer considerable damage and absorb most of the energy released (through strain energy mechanisms involving nonlinear material behavior and large residual deflections). Due to the cell concept, the blast load will be off center and nonuniform, as shown in Figure 15a.

Blast loads were obtained using the program SHOCK, as described in the previous study. A charge of 10,000 lbs detonated in a central cell was simulated. Figure 15a shows the shock wave scaled impulse loading (units are  $\text{psi}\cdot\text{ms}/\text{lb}^{1/3}$ ). Pressure values are obtained from  $P = 2I/t$ , where  $I = \text{scaled impulse} \times 24.27$  (scaling factor,  $\text{lb}^{1/3}$ ) and  $t = 4.06 \text{ ms}$  is the load duration, which is assumed constant over the roof. The load time history at a point above the charge is shown in Figure 15b. It includes both the initial shock load and the residual gas pressure. The gas pressure load is relatively low but lasts for 20 seconds.

## **Finite Element Model of the Roof Slab**

The concrete slab was represented via eight-node three-dimensional solid elements. Two solid elements were used through the depth. To simplify the discretization, the concrete cover was not modeled but its mass was added to the concrete core. Element generation was carried out using the DYNA3D preprocessor program INGRID (Stillman and Hallquist, 1985), as well as a custom made preprocessor. A top view of the finite element mesh is shown in Figure 16. The single plane of symmetry for the problem is exploited.

To accurately capture the response of the reinforcement, a discrete reinforcement model of the steel in the roof was implemented. This method is generally more accurate than a smeared or an embedded reinforcement model, and well suited for reinforcement patterns which are regular. Although an embedded model would also be efficient, it is not available in DYNA3D.

Top and bottom steel meshes were modeled using discrete two-node truss elements located at 20 inches on center, i.e. each element representing the contribution of 2 bars. Similarly, the shear reinforcement was lumped at 20 inches on center, each truss modeling the cross sectional area of 4 bars lumped together. The way in which the steel bars are lumped together depends on the design of the three-dimensional discretization of the concrete slab.

### Material Models and Properties

An evaluation of the material models available in DYNA3D was performed to find suitable models for the reinforcing steel and the concrete. The evaluation consisted of compressive and tensile tests on single truss and solid elements in the expected stress and strain ranges. For steel, material model 3, an elastic-plastic model with isotropic/kinematic hardening, exhibited the expected elastic plastic behavior. For concrete, linear and nonlinear responses with materials models 17, 16, 5 and 25 were evaluated using an 8-node solid element. Material model 16, a concrete/geological material model, with no smeared reinforcement was determined most suitable for plain concrete. In tension, it accurately captured cracking of the concrete, whereas in confined compression it was able to reproduce the behavior of concrete under pressures in excess of the 24 ksi peak pressure. This peak pressure is four times higher than the compressive strength of concrete and could not be handled by the ABAQUS material model for concrete according to Resende (1989). The direct use of ABAQUS is precluded for this problem not only because it is an implicit code, but also because of acknowledged material model restrictions.

Concrete and reinforcement were modeled with the properties shown in Table 2. The program internally generates the remaining concrete properties. Yield stress and compressive strength were increased to account for strengthening due to high strain rates.

Table 2. Material Properties for the DYNA3D Roof Slab Model

Steel:	Young's modulus	$E = 29,000,000 \text{ ksi}$
	Poisson's ratio	$\mu = 0.3$
	Yield stress	$\sigma_0 = 82.5 \text{ ksi (DIF 1.25)}$
	Tangent modulus	$E_t = 447 \text{ ksi}$
	Hardening Parameter	$\beta = 1$
Concrete	Poisson's ratio	$\mu = 0.2$
	Compressive strength	$f_c' = 6000 \text{ psi (DIF 1.25)}$
	Cohesion	$a_0 = -1$

## Dynamic Response of Soil-Covered Roof Slab

The deformed shape of the roof slab (enhanced five times) is shown in Figure 17 at two different time steps in the dynamic response. It is observed that the displacement field is very localized. However, there is also a rigid body displacement component in the long-term computed dynamic response. For example, the entire roof rises uniformly about 8 inches in 30 ms.

Figure 18 shows the concrete stresses in the plane of the slab. Upon arrival of the shock wave the concrete goes temporarily into compression, then unloads, cracks in tension and loses all load-carrying capacity. The elements closest to the load are subjected to longer lasting and more severe compression, as should be expected due to local slab bending. After element cracking, the concrete mass is assumed to be still acting on the system. However, cracking of the top elements occurs at 2.5 milliseconds and it is expected that the concrete cover would then separate from the roof slab and generate debris.

Figure 19 shows the stresses in ten lower reinforcing bars along the plane of symmetry, five on each side of the point of maximum load. Some of the bars are seen to reach yield between 16 and 18 ms. At that point it is expected that additional debris will separate from the roof slab.

Figure 20 shows contours of the velocity field at 7 ms and at 27 ms. The velocity time history at the point just above the load yields the highest velocity, 2500 in/sec, which is reached at about 8.5 ms, as shown in Figure 21. Knowledge of the velocity field at various times facilitates computing the distance of debris fallout, which in turn will help characterize the effectiveness of the soil-covered roof slab concept.

Calculations for the dynamic response of the high performance magazine indicated that blast effects on the roof will be highly localized. The concrete directly above the blast should crush early, then carry pressure hydrodynamically during the shock load phase.

**Debris Prediction Data.** Calculations of the dynamic response also indicated that the rebar directly above the blast load will yield and snap early, thus reducing the concrete confinement and releasing parts of the roof slab as debris. The model did not allow for direct prediction of actual debris and release of broken bars, and the predicted dynamic response will therefore diverge from the actual one when the reinforcing bars reach their ultimate capacity. However, debris distance predictions can be facilitated with this data as follows:

- (1) knowledge of the complete concrete stress field and rebar stress response as a function of time allows the determination of the time and the amount of debris separation;
- (2) knowledge of the complete velocity field as a function of time allows the determination of initial debris velocities;

Similar calculations of debris velocity from slabs using DYNA3D have been reported (Terrier and Boisseau, 1989) where agreement is shown with debris velocity measurements.

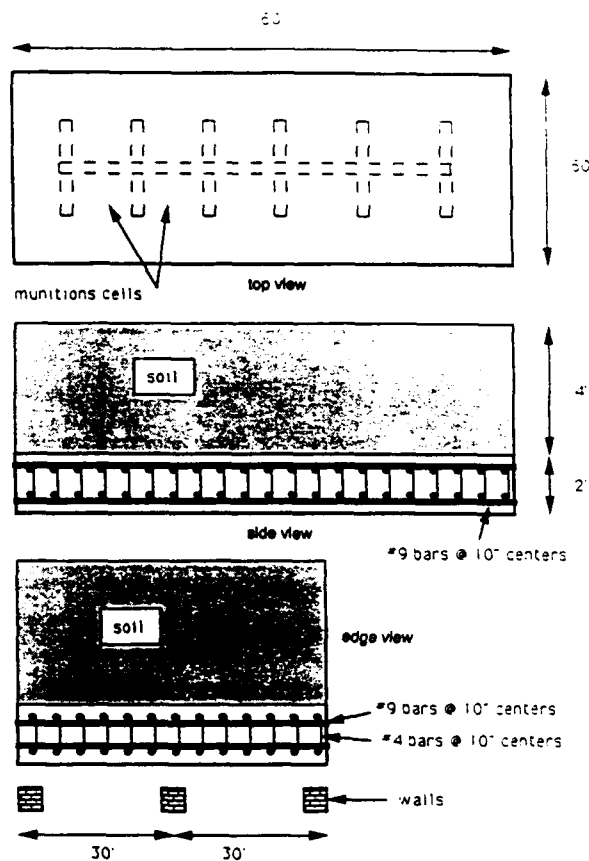
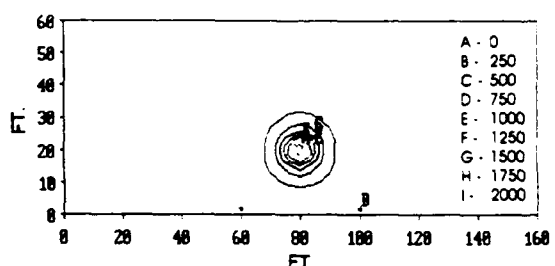
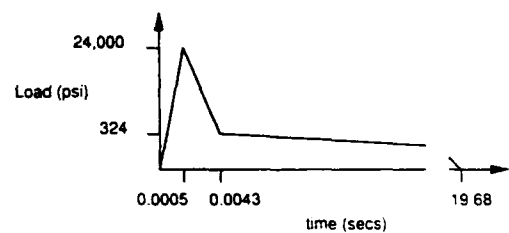


Figure 14. Preliminary high performance magazine roof design.



(a) Scaled shock impulse distribution



(b) Load time history (values at max. pt.)

Figure 15. Design roof slab load.

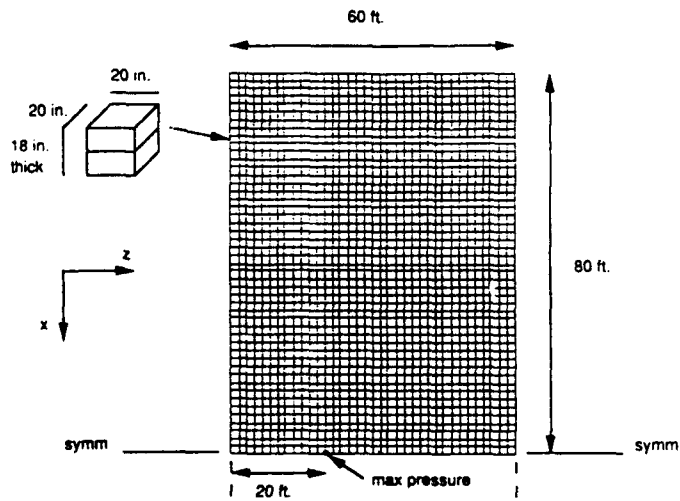
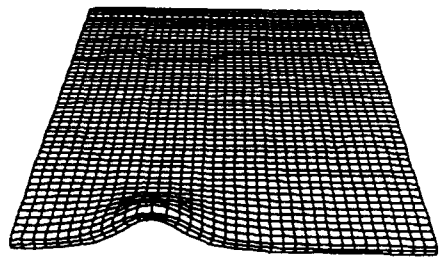
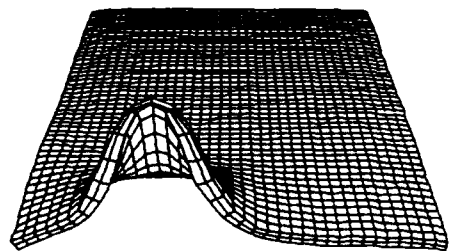


Figure 16. Finite element mesh.



(a) At 7 ms



(b) At 27 ms

Figure 17. Deformed shape (enhanced 5 times).

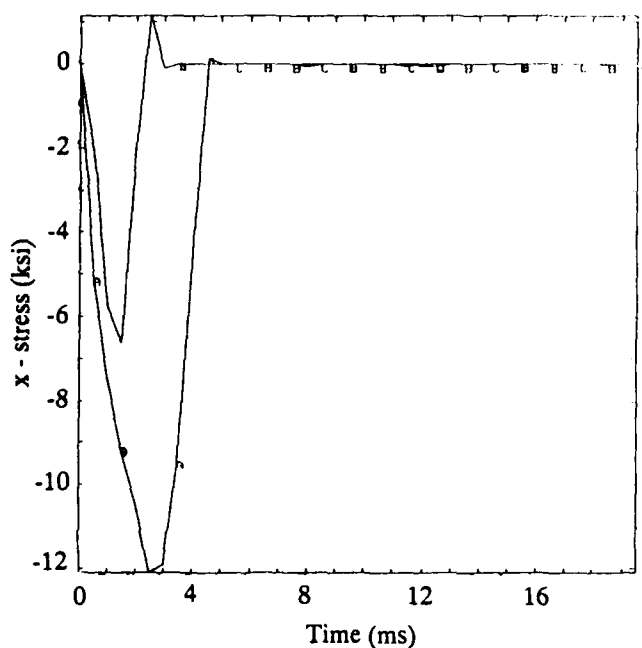


Figure 18. Horizontal stresses in concrete.

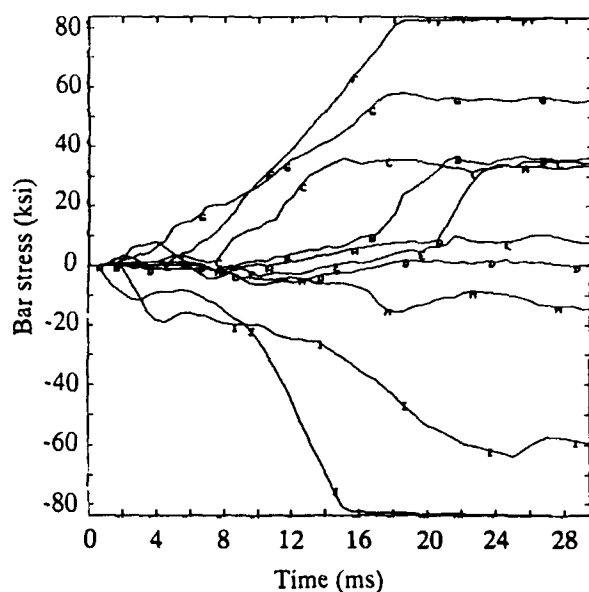
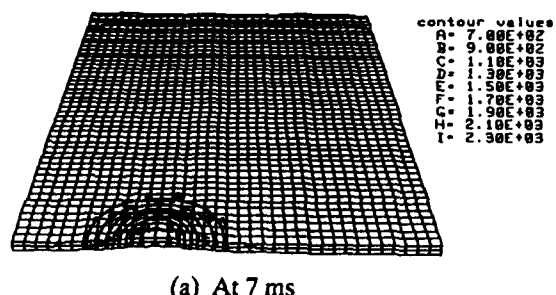
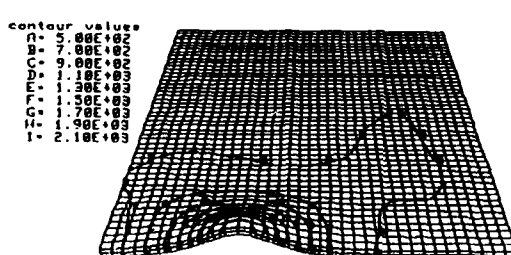


Figure 19. Reinforcing bar stresses.



(a) At 7 ms



(b) At 27 ms

20. Vertical velocity contours (in/sec).

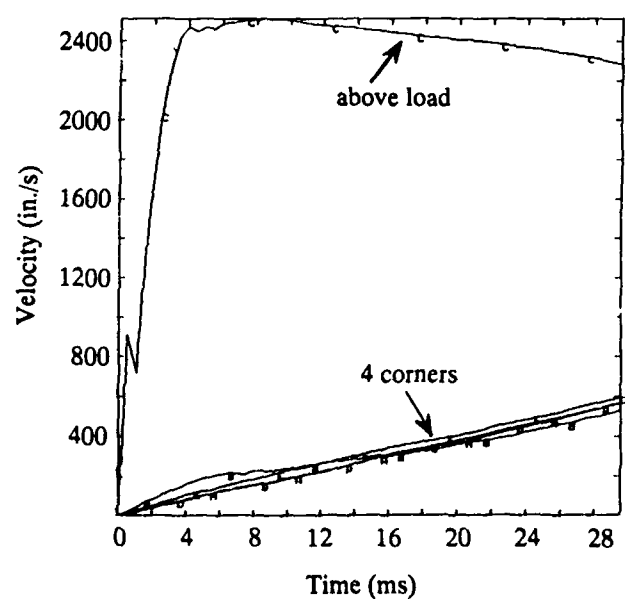


Figure 21. Vertical velocity histories.

Independent calculations using the program FRANG (Wager and Connet, 1989) determined the average velocity of debris from a 16- by 28-foot breached area directly above the cell. The program calculates pressure time histories resulting from an explosion in a room which has vents and frangible panels, i.e. panels designed to break loose and provide additional vent area. Displacement, velocity and acceleration histories of the frangible panels are also determined.

It was found that for the weight of a 4-foot soil cover, the average maximum velocity of the debris would be 2400 in/sec (Murtha, 1992). Those calculations assume that fragments have already separated from the roof, and their velocities were therefore expected to be somewhat higher than velocities calculated by DYNA3D. From Figures 20 and 21 it is observed that the velocity field above the cell at 8.5 ms (maximum values) varies between 700 and 2500 in/sec for an area of about 20 by 20 ft.

Recent NCEL field tests on a 1/10 scale model of a high performance magazine (Murtha, 1992) have qualitatively confirmed localization of the deformations and breaching of the roof above the cell which had been predicted by the results from the three-dimensional nonlinear dynamic finite element analysis.

**Summary of Soil-Covered Roof Slab.** The explicit finite element program DYNA3D was successfully used in modeling the soil-covered roof slab which was subjected to an unusually severe blast load. It was shown that concrete and reinforcing bar stress histories can be obtained, yielding information on cracking, concrete cover separation, bar yielding and rupture. Initial debris velocity fields can also be determined, which in turn facilitate the calculation of debris distances.

## CONCLUSIONS

Three-dimensional nonlinear dynamic finite element studies have been carried out for three classic problems in Navy explosive safety engineering; these include a specialized missile test cell design concept, reinforced concrete slabs with variable shear steel design, and a soil-covered roof design for a proposed high performance magazine. Two widely available general purpose computer programs were applied in these analyses, one based on implicit and the other based on explicit temporal integration of the equations of motion.

Application of these computer programs can provide a viable alternative to codified single-degree-of-freedom (SDOF) methods currently used in the design and analysis of explosive safety structures. This modern technology can be at least as accurate as historical SDOF methods for computing dynamic response, and can provide substantially more detail on structural behavior, particularly when special structural concepts are encountered.

Concrete material models which have been implemented in commercial implicit computer programs are sophisticated, but they can be unreliable and cause simulations to terminate prematurely. This difficulty is partially offset in programs that provide for users to supply their own specialized material model subroutines which may be more suited to specialized problems. Implicit programs were found to provide for excellent reinforcement modeling capability when

they supported embedded reinforcement modeling. This capability is important for explosive safety because many designs include heavily reinforced sections and complicated reinforcement patterns in both two- and three-dimensional configurations.

Explicit programs are more robust regarding large-scale numerical solutions of highly nonlinear equations of motion describing the dynamic response of explosive safety structures. However, their concrete material models are less mature than corresponding material models in implicit programs. Moreover, reinforcement modeling is not as well supported in explicit programs. Although they can model regular patterns of reinforcement, often found in slab designs for example, they cannot model more complex patterns efficiently without embedded modeling capability.

In summary, general purpose computer programs for three-dimensional nonlinear dynamic finite element analysis represent a powerful tool for specialized problems in explosive safety, as well as an attractive alternative for codified SDOF methods. Accurate models of specialized reinforced concrete missile test cells and magazines can be constructed more efficiently using available implicit programs, whereas, available explicit programs yield successful simulations with less difficulty.

## ACKNOWLEDGMENTS

The Computer Aided Design Division, Code 1082, NWTC, Point Mugu, supplied the Sun Workstation used in the MTC study; Doug Doi and Jim Thompson were instrumental in the MTC modeling work. At HKS (West), Inc., Nuno Rebelo and Tod Dalrymple provided valuable user support in the application of ABAQUS. Robert Whirley at Lawrence Livermore National Laboratory kindly supplied DYNA3D tapes and documentation to NCEL. At NCEL, Bob Murtha and Jim Tancreto provided useful discussions on aspects of explosive safety design and field test results.

## REFERENCES

- ABAQUS User's Manual, Version 4.8, Hibbit, Karlsson and Sorensen, Inc., 100 Medway St., Providence, RI 02906, 1989 (1080 Main St., Pawtucket, RI 02860).
- Army TM 5-1300 / Navy NAVFAC P-397 / Air Force AFR 88-22 (1991). Structures to Resist the Effects of Accidental Explosions. Washington, DC.
- Ayvazyan, H.E., M. Dede and N. Dobbs (1988). "Design of NAVFAC Type VB Missile Test Cell," Ammann & Whitney Consulting Engineers, New York, NY, Aug 1988.
- Biggs, J.M. (1964). Introduction to Structural Dynamics, McGraw-Hill Book Co., New York, NY, 1964.

Cervera, Hinton and Hassan (1987). "Nonlinear Analysis of Reinforced Concrete Plate and Shell Structures Using 20-Noded Isoparametric Brick Elements." *Computers and Structures*, Vol. 25, No. 6, pp 845-869, 1987.

Cox, J.V., and L.R. Herrmann (1992). "A Plasticity Model for the Bond Between Matrix and Reinforcement," 6th Japan-U.S. Conference on Composite Materials, Orlando, FL, 22-24 Jun 1992.

Elwi, A.F., and T.M. Hrudey (1989). "Finite Element Model for Curved Embedded Reinforcement," *ASCE J. of Engr. Mech.*, Vol. 115, No. 4, 1986. Discussion by P.C. Pandey, Vol 117, No. 3, pp 714-715, Mar 1991.

Hallquist, J.O., and R.G. Whirley (1989). DYNA3D User's Manual, UCID-19592, Rev. 5, Lawrence Livermore National Laboratory, P.O. Box 808, Livermore, CA 94550, May 1989.

Holland, T.J. (1989). SOLVER User's Guide, Version 2.2, Dynamic Response Analysis of SDOF Systems, CAE Structures Library UG-0020, Naval Civil Engineering Laboratory, Port Hueneme, CA 93043.

Murtha, R.N. and M. Dede (1988). Internal Working Memorandum: "Test Plan for Explosives Safety Certification of NAVFAC Standard Type V Missile Test Cell." Naval Civil Engineering Laboratory, Port Hueneme, CA 93043, Dec 1988.

Murtha, R. (1992). Small-scale High Performance Magazine Roof and Soil Cover Tests. Personal communication, Naval Civil Engineering Laboratory, Port Hueneme, CA 93043.

PATRAN Plus User Manual, Release 2.4, PDA Engineering, 2975 Redhill Ave., Costa Mesa, CA 92626, Sep 1989.

Resende, L. (1987). "A Damage Mechanics Constitutive Theory for the Inelastic Behavior of Concrete," *Computer Methods in Applied Mechanics and Engineering*, Vol. 60, pp 57-93, 1987.

Resende, L. (1989). Personal communication, ABAQUS Training Course, Providence, RI, Oct 1989.

Schnobrich, W.C. (1989). "Reinforced Concrete Shells: Some Problems," *Analytical and Computational Models of Shells*, Eds. Noor, Belytschko and Simo, CED-Vol. 3, ASME, 1989.

Shugar, T.A., T.J. Holland, and L.J. Malvar (1992). "Three-Dimensional Finite Element Analysis of Explosive Safety Facilities - A Technology Assessment," Naval Civil Engineering Laboratory, Port Hueneme, CA 93043 (in publication).

Stillman, D.W. and Hallquist, J.O. (1985). INGRID: A three-dimensional mesh generator for modeling nonlinear systems, Lawrence Livermore National Laboratory, CA.

Tancreto, J.E., and E.S. Helseth (1984). "Effect of Frangible Panels on Internal Gas Pressures," Minutes of the Twenty-First Explosives Safety Seminar, Department of Defense Explosives Safety Board, Aug 1984.

Tancreto, J.E. (1988). "Dynamic Tests of Reinforced Concrete Slabs," Proceedings, 23rd Department of Defense Explosives Safety Board Seminar, Atlanta, GA.

Terrier, J.M., and J.F.K. Boisseau (1989). "Numerical Simulation of Reinforced Structure Response Subjected to High Explosive Detonation," Proceedings of the Fourth International Symposium on the Interaction of Non-nuclear Munitions with Structures, Vol. 1, Panama City Beach, FL, Apr 17-21, 1989.

Wager, P. and Connet, J. (1989). FRANG Users's Manual, Naval Civil Engineering Laboratory, Port Hueneme, CA 93043.

# **Time Dependent Stress and Strain Distribution in a Blastloaded Steelplate**

Gerhard H. Guerke  
Fraunhofer-Institut fuer Kurzzeitdynamik  
Ernst-Mach Institut  
Freiburg / Germany

prepared for the 25. Explosives Safety Seminar, 1992

## **Abstract**

The stress and strain distribution in an impulsively blastloaded plate is far from equilibrium. Part of the plate will be elastically strained whilst other part will be strongly plastically deformed. A high explosive (HE) charge, detonating near to a flat steelplate produces an impulsive area-load. Stress and strain is time dependend and is different from element to element in the plate. The time-dependend displacement of nodes in the net of finite element calculation and the time dependend stress and strain in elements that correspond to the nodes will be discussed.

## **Contents**

1. Introduction
2. Test Arrangement, Experiments
3. Numerical Calculation
4. Phenomenology of Impulsive Blastloading
5. Stress and Strain in the Plate
6. References

### **1. Introduction**

The designer of blast resistant structures should be aware that in an impulsively blastloaded plate the distribution of stress and strain is far from equilibrium. Static design principles are based on equilibrium and must be used carefully.

A high explosive (HE) charge, detonating near to a plate produces an impulsive area-load. An impulse is imparted into the plate and any element of the plate is set into motion. Only a small fraction, in the order of 1% of the kinetic energy, can be transformed into elastic deformation. Most of the kinetic energy must be transformed into plastic deformation. Stress and strain is time dependend and is different from element to element in the plate. An extreme non-equilibrium loading situation was chosen in order to highlight the differences to static loading.

The time-dependend displacement of nodes in the net of finite element calculation and the time dependend stress and strain in elements that correspond to the nodes will be discussed.

## 2. Test Arrangement, Experiments

A spherical HE-charge (1 kg of PETN) detonates at some distance (HOB) above the center of a square steelplate ( $1 \times 1 \times 0.002 \text{ m}^3$ ). The plate was clamped along all edges to a rigid support. The test arrangement is shown in Figs.2.1 and 2.2 (Ref.1, 2).

A typical experimental result is shown in Figs.2.3 and 2.4. The final shape of the impulsively loaded plate is close to a pyramid, whilst a statically loaded plate results in a near spherical shape. If the final shape is different, there must be a different mechanism of deformation.

The maximum deflection of the plate's centerpoint as a function of the specific blastimpuls (impulse per unit area imparted to the plate) is shown in Fig.2.5. The results from 10 experiments with a plate  $1 \text{ m} \times 1 \text{ m}$  and 2 mm thick and HE-charges at different HOB and 8 results from numerical calculations obviously lie at one straight line. This diagram demonstrates that the DYNA 3D FE-code is suited to describe the large deformation of a steelplate under impulsive loading. More checks were done to confirm this result.

## 3. Numerical Calculation

The overall deformation of the steelplate, as well as stress and strain in different elements of the steelplate was calculated by means of the DYNA 3D code. Details, how to find the best net-discretisation, to minimize the machine time and to optimize the input- and output procedures can be found in the references 3, 4, 5, 6.

The numerical work with the FE-code can only be successful, if two sets of input parameters are correct:

- the load function in spacial and temporal distribution.

- the material properties.

The input load function was measured carefully with piezoelectric pressure gages at a nonresponding platform (Ref.1). At close-in detonation the spherical shockfront is not flat when it impinges the flat plate. It impinges first at the center of the plate (ground zero) and then spreads to the edges. Different pressure-time histories for up to 20 zones at the plate's surface were determined.

Additional numerical calculation was done for arrangements where no direct comparison with experimental results was planned. Identical input blast parameters had to be used for different arrangements. In that case blast parameters from the literature were taken (Ref.5; 6).

Most of the numerical calculation was done with standard values for the material properties of mild steel under "static" load:

Mass Density	7770	kg / m <sup>3</sup>
Modulus of Elasticity	207	GPa
Poisson's Ratio	0.3	
Yield Stress Tension	340	MPa
Yield Stress Shear	195	MPa (0.6 of tension)
Tangent Modulus	68.9	MPa / Strain (m/m)
Temperature	20	degree C

### Numerical calculation was done in the field of:

Different HoB for 1 kg HE charges (Ref.1, 4)  
Different spatial and temporal pressure distribution at the flat plate for spherical blast (Ref.3, 4)  
Centric and eccentric detonation (Ref.3)  
Square and rectangular plates (Ref.1; 3)  
Effect of tension yield stress (525 MPa instead of 340 MPa) (Ref.1)  
Effect of tangent modulus (3 GPa instead of 69.9 MPa) (Ref.1)  
Effect of stiffeners (Ref.4)  
Effect of a girder (Ref.5)  
Discretisation of the plate in 2 layers

Results from different reports will be discussed.

#### 4. Phenomenology of Impulsive Blastloading

A high explosive (HE) charge, detonating near a plate produces an impulsive aera-load. The time-scale of the process generally is milliseconds. The reflected blastpressure at the plates surface rises suddenly to its peak overpressure and decreases to zero in a time that is short relatively to the reaction-time of the plate.

An impulse is imparted into the plate and any element of the plate is set into motion. The plate's mass contains an amount of kinetic energy that must be transformed into deformation. Only a small fraction, in the order of 1% of the kinetic energy, can be transformed into elastic deformation. Most of the imparted energy must be transformed into plastic deformation. The reaction-time is over when all the kinetic energy is transformed and the plate is at rest.

The acceleration, velocity and displacement vs. time of a selected point (node) in the center of the square plate will be discussed. The shape of the plate at different moments of time will be shown as well as the final shape after the loading.

**Fig.4.1** The shape of the plates cross-section from the center (left) to the fixed edge in the middle of the span at 500 mm (right) is shown at 4 moments of time after the shock-front arrival (Ref.2). The plate was loaded from above and moves downwards. At 0.125 ms the movement starts with a flat plate. At 0.875 ms the flat bottom has reached a displacement of 30 mm. A "knee" moves along the plate from the fixed edge to the center and causes a rim at constant slope. The section of the plate that was passed by the knee is at rest. The flat bottom moves downwards at constant velocity. It gets smaller with time. At 2.2 ms the knee has reached the plate's center. The whole plate was plastically deformed and is at rest now. This is the end of the reaction time.

**Fig.4.2** The final cross-sectional shape of the deformed steelplate for different blastimpulses is shown. The plate was fixed at the left side. Different impulsive load was produced by different distances (HoB) of the HE-charge above the plate. The slope of the rim gets steeper with increasing impulse. The final shape was reached at the same time of 2.2 ms, independently of the load.

**Fig.4.3** The center of the square plate was accelerated during the positive pressure duration of 0.22 ms. Maximum acceleration is 58,000 g's. Acceleration is zero from 0.22 ms to 1.8 ms, when a force acts in the opposite direction. Maximum acceleration in the opposite direction is 36,000 g's at 2.2 ms.

**Fig.4.4** A certain amount of kinetic energy was imparted into the plate during the phase of acceleration. We are interested in the mechanism that reduces the kinetic energy. At 2.2 ms, at the end of the reaction time, there is no kinetic energy left, the plate is at rest.

**Fig.4.5** The velocity reaches a constant value of 75 m/s at the end of the acceleration phase. The plate's centerpoint moves at constant velocity from 0.22 ms to 1.8 ms and then is rapidly stopped. Zero velocity is reached at 2.2 ms.

**Fig.4.6** The centerpoint moves at nearly constant velocity for 2.2 ms where it reaches its maximum displacement of 150 mm. Some relatively small vibrations occur later than 2.2 ms.

**The discussion of the diagrams results in the following conception of the deformation mechanism:**

The deformation of steelplates at impulsive blastloading happens in the timeframe of milliseconds. An amount of kinetic energy is imparted into the plate and must be transformed into plastic deformation.

Any point of the plate is accelerated during the time of positive pressure duration. Extremely high values of acceleration occur (some 10,000 g's). At the end of the acceleration phase a constant velocity is reached (some 10 m/s). A plastic wave or knee starts in the moment of loading from all fixed edges and runs at constant velocity along the plate to the plate's center (225 m/s). Any point that is caught by the knee will be retarded roughly and comes to rest. Most of the kinetic energy must be transformed in the running plastic knee. The reaction-time is determined by the time that it takes for the plastic wave to run through the material from any fixed edge to the center of the plate.

The mechanism results in a rim at constant slope, that depends on the loading impulse, the mass and the strength of the material. The final shape of the deformed plate is pyramidal.

The mechanism of energy transformation and material deformation results in a spatial and temporal stress and strain distribution in the plate that will be discussed in the following section.

## 5. Stress and Strain in the Plate

The effect of a blastwave on a steelplate was computed by means of the explicit, 3-dimensional FE-code DYNA 3D (Ref.5, 6). Acceleration, velocity and displacement at different points (nodes) of the plate was calculated as well as the shear stress, the effective stress and the effective plastic strain in corresponding elements.

A spherical 150 kg TNT-charge detonates at a distance of 6 m from a steelplate. The plates dimensions are 7.2m \* 2.5m \* 0.004m. The blast data are 3.66 MPa reflected peak overpressure, 3 ms positive duration and 2564 Pa\*s specific reflected blastimpulse. The yield stress was 340 MPa. Large plastic deformation occurs.

The time-scale is 10 ms in all diagrams shown in this section.

**Fig.5.1** A pressure pulse of 3660 kPa peak overpressure and 3 ms positive duration impinges on the flat surface of the plate at time 0. It transfers impulse to the plate and induces the plate to movement. According to its mass and velocity the plate contains kinetic energy that has its maximum at 1.8 ms. The kinetic energy decreases continuously and is near 0 at 6 ms.

**Fig.5.2** The effective stress in 3 elements of the plate is shown as a function of time. The element B is situated near to the clamped edge and the element J at the midspan.

It takes 0.2 ms to reach the yield stress near the edge (B) and 1ms at the midspan (J). The stress rises very fast (sub-millisecond) in each element.

The sudden rise of stress starts at different time in the elements from "near zero" stress to yield stress. The "mechanism" that causes the stress to reach yield stress runs with longitudinal acoustic wave velocity (5800 m/s) from the clamped edge to the plate's center.

In all three elements the stress remains constant at a "yield stress plateau" for a period of time. The moment of time is marked by an arrow when the stress in an element exceeds the yield stress. This happens first at the clamped edge (B) and 2ms later at the midspan (J). **There must be a "mechanism" that causes the stress to exceed yield stress at different moment of time in different elements.**

When the Kinetic energy returns to zero ( $KE = 0$  at 6 ms) the effective stress in the elements decreases below yield stress.

**Fig.5.3** The time history of the shear stress in the elements is nearly identical to the effective stress. Shear yield stress was taken as 0.6 times the tension yield stress. **Shear stress is an important parameter in the deformation mechanism of the steelplate.**

**Fig.5.4 Effective plastic strain** arises in an element at the time when the stress exceeds yield stress in this element. The time to reach the maximum strain is different in the elements.

The strain rate in m/m/s can be calculated and is different in the elements.

When the Kinetic energy returns to zero ( $KE = 0$  at 6 ms) the plastic strain in the elements has reached its maximum and constant value.

**Fig.5.5 and 5.6** Stress and strain in 4 elements along the short fixed span are shown. The strain exceeds the yield stress at the same moment in all the elements. Highest stress arises in the middle of the span (A). In the corner (I) the stress exceeds yield stress marginally. The plastic strain is marginal in the corner (I, 0.25%) and maximum in the middle (A, 4.2%). Strain at the short span is smaller than at the long span (see Fig.5.4, Element B).

**Fig.5.7** The maximum strain in an element is directly proportional to the maximum stress in the element. The stress-time history does not have an effect on the final plastic strain.

## 6. References

1. Guerke, G. H. Buecking, P.W. et al. (1987), "Experimentelle Untersuchungen zum Versagen schiffstechnischer Bauteile unter Blastbelastung," (Experimental investigation of dynamic-plastic response of steel-plates to impulsive blast load), Report No. E 7/87, Jun. 1987 Ernst-Mach-Institut, Freiburg, Germany.
2. Guerke, G. H. (1987), "Dynamic-Plastic Response of Steelplates to Blastload", MABS 10.
3. Buecking, P. W. (1989), "Numerische Simulation der Druckstoßwirkung zentrischer und exzentrischer Nahbereichsexplosionen auf eingespannte quadratische und rechteckige Stahlplatten," (Numerical simulation of blasteffects from centric and non-centric HE-detonations to clamped square and rectangular steelplates), Report No. 10/89, Nov. 1989, Ernst-Mach-Institut, Freiburg, Germany.
4. Buecking, P. W. (1990), Numerische Simulation der Druckstosswirkung zentrischer Nahbereichsexplosionen auf eingespannte quadratische Stahlplatten", (Numerical Simulation of blasteffects from centric HoB detonation on clamped square steelplates), Report No. 6/90, Jun. 1990, Ernst-Mach-Institut, Freiburg, Germany.
5. Buecking, P. W. (1990), "Numerische Simulation der Druckstoßwirkung einer detonierenden Sprengstoffladung auf eine versteifte Schiffstruktur (Außendetonation)," (Numerical simulation of blasteffects from a detonating HE-charge to a stiffened ship structure, outside detonation), Report No. 7/90, Aug. 1990, Ernst-Mach-Institut, Freiburg, Germany.
6. Buecking, P. W. (1990), "Numerische Simulation einer detonierenden Sprengstoffladung auf eine versteifte Schiffstruktur mit verbesserter dynamischer Strukturstigkeit (Außendetonation), (Numerical simulation of blasteffects from a detonating HE-charge to a stiffened ship structure with improved dynamic resistance, outside detonation), Report No. 8/90, Aug. 1990, Ernst-Mach-Institut, Freiburg, Germany.
7. Baker, W. E. et al. (1983) "Explosion Hazards and Evaluation", Elsevier Scientific Publishing Company, Amsterdam-Oxford-New York.
8. "Structures to Resist the Effects of Accidental Explosions" (1990), TM 5-1300.
9. "Fundamentals of Protective Design for Conventional Weapons" (1989), TM5-855-11.



**Fig. 1 Test Arrangement:**  
Clamped Quadratic Steel Plate  
Parameters:  
Plate Side Length  $l$   
Plate Thickness  $h$   
Charge Height  $HoB$

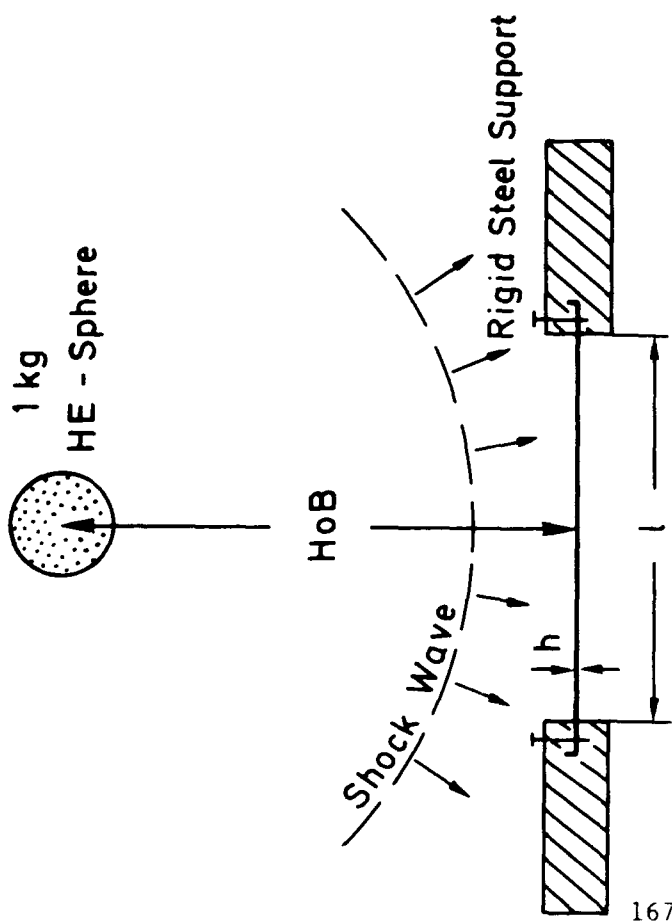


**Fig. 2 The test arrangement - a flat square steelplate  $1m \cdot 1m$  clamped and bolted to a rigid support. The 1 kg charge made of plastic explosive is wrapped into thin fabric and detonated at some height above the plate center.**

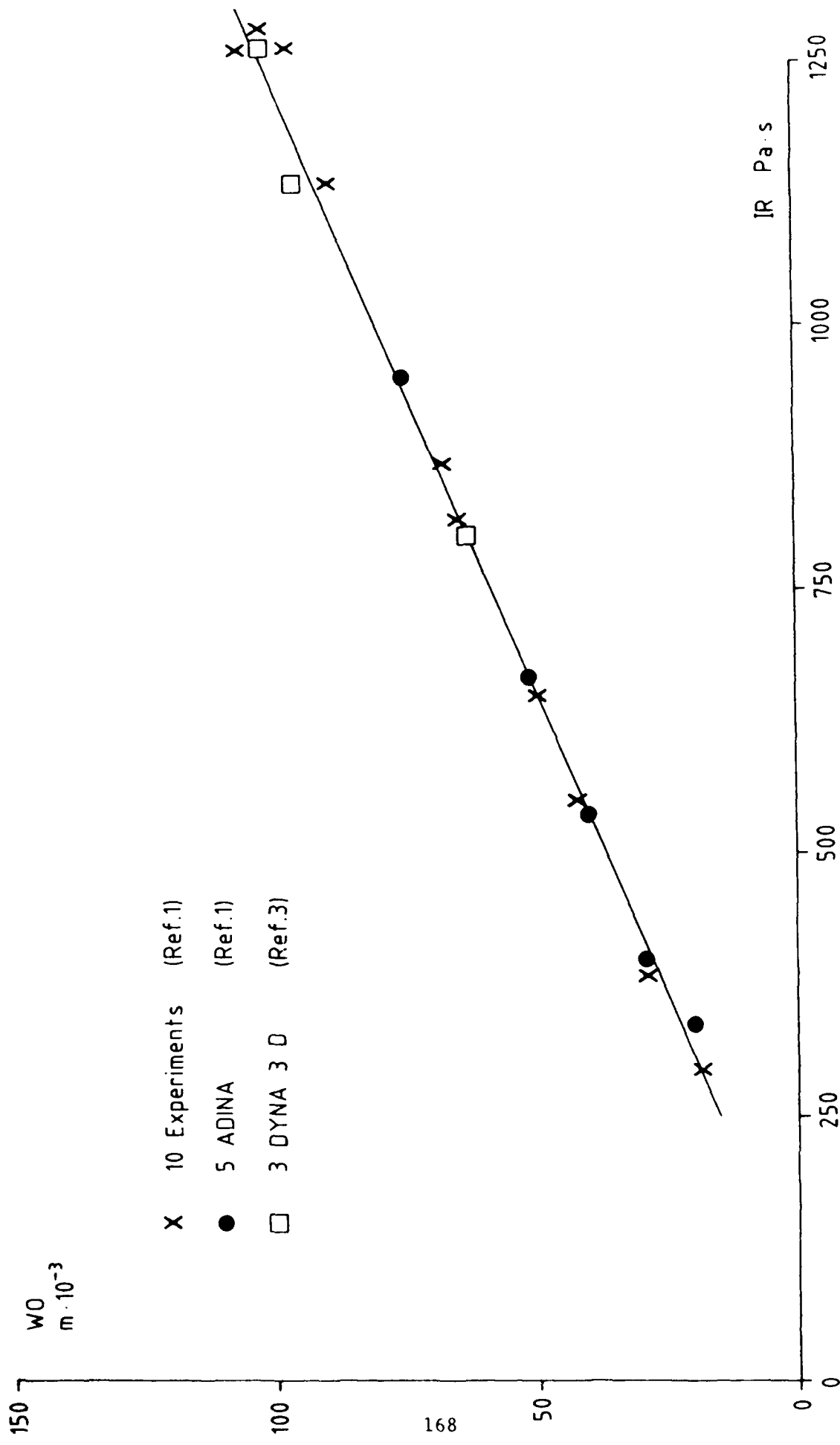


**Fig.2.5**  
Permanent Deformation vs Specific Blastimpulse  
Center of a square steelplate  $1 \times 1 \times 0.002$  under impulsive blastload

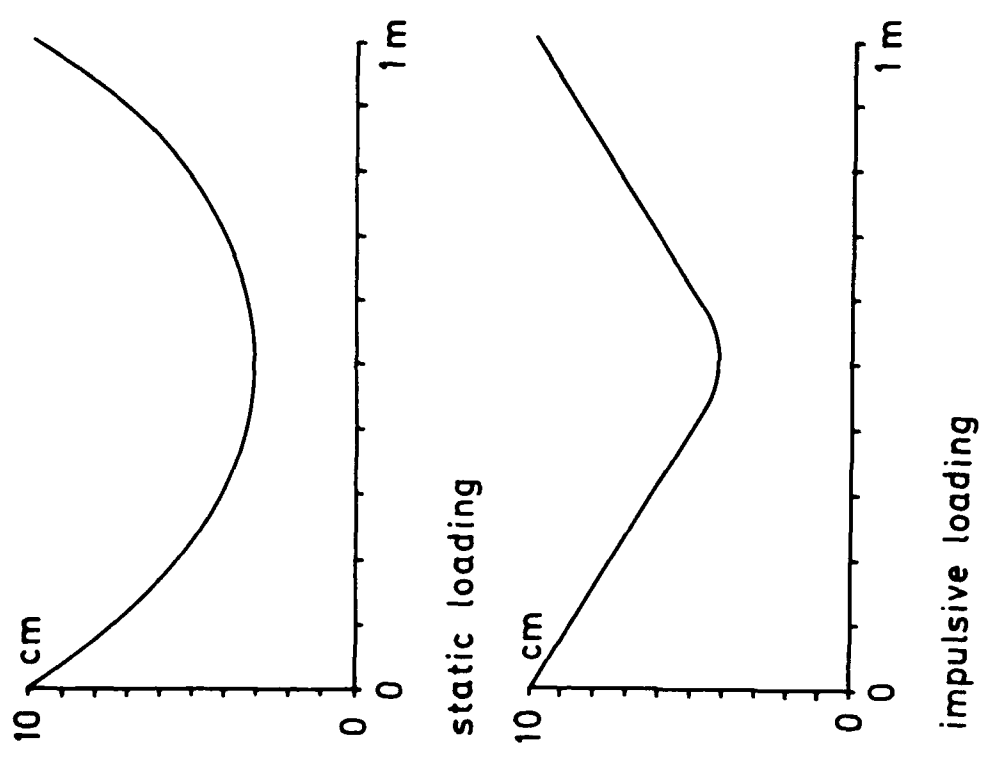


**Fig. 3 Typical Shape of Homogeneous Steel Plates at Static and Impulsive Loading**

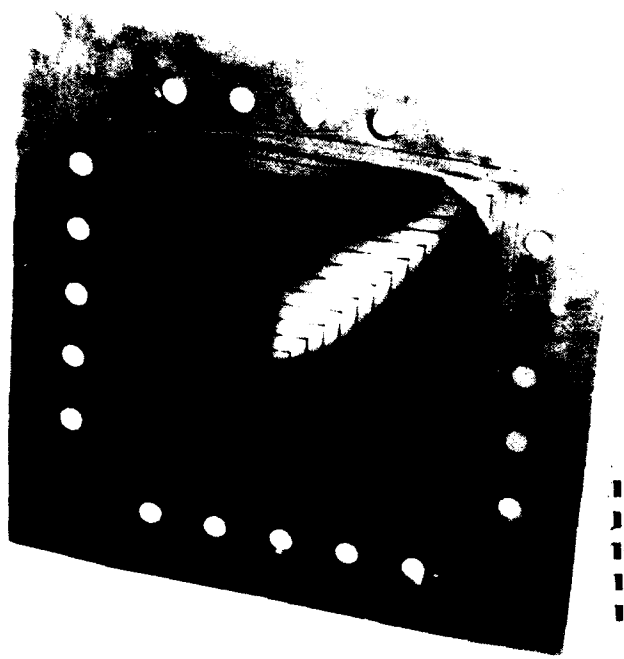
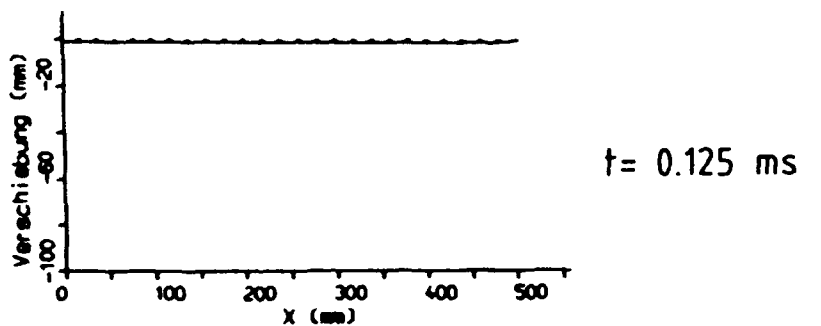
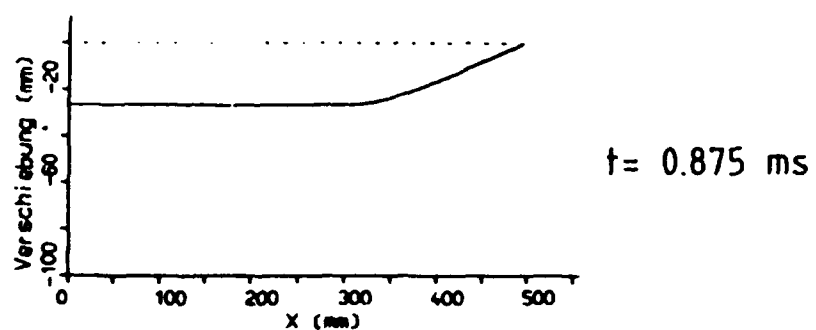


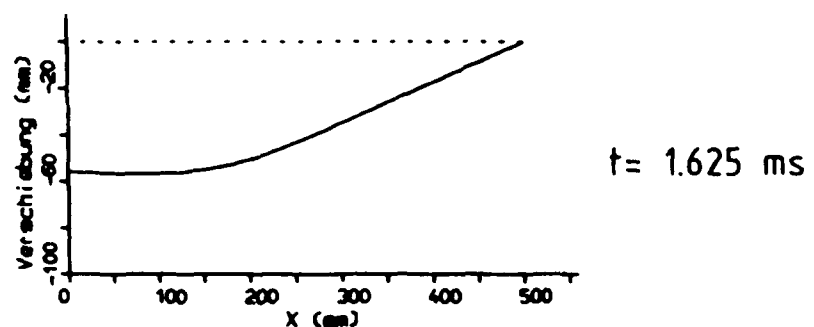
**Fig. 4 A clamped square steel plate deforms to a pyramid at high impulsive loading. The straight line pattern at the flat plate remains straight at the pyramid after deformation.**



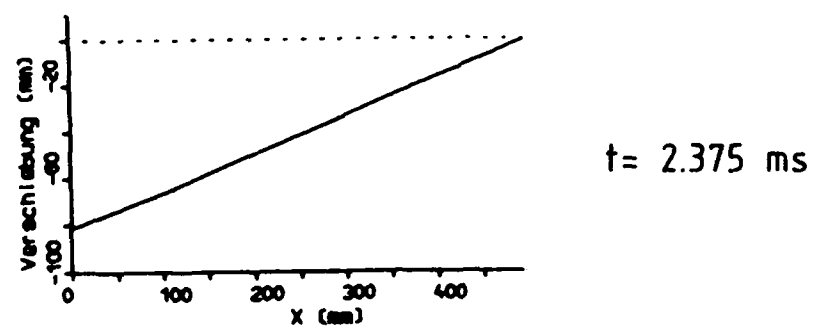
$t = 0.125 \text{ ms}$



$t = 0.875 \text{ ms}$



$t = 1.625 \text{ ms}$



$t = 2.375 \text{ ms}$

**Fig.4.1** The displacement of the plate's cross-section from the centerpoint to one clamped side at different instants of motion.

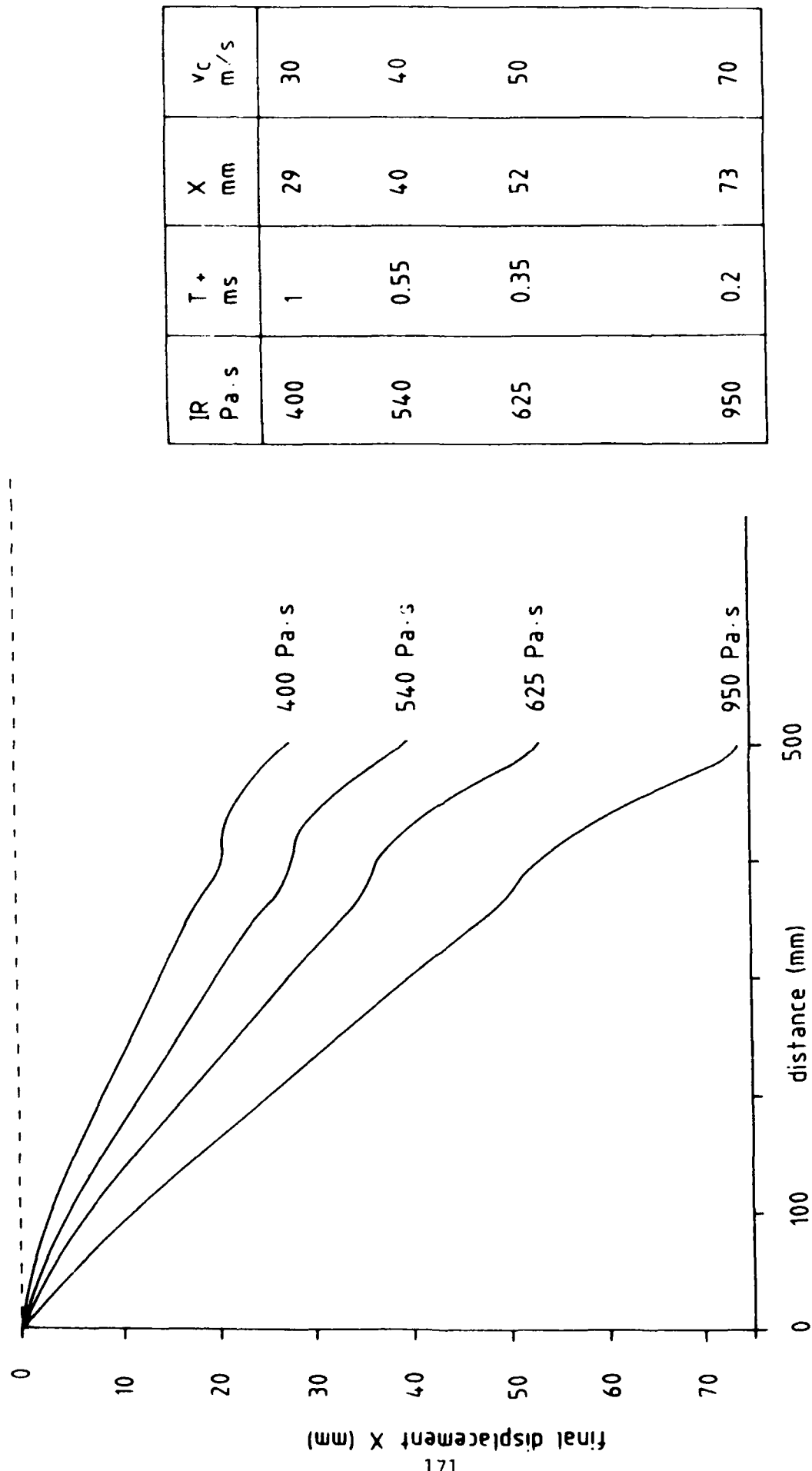


**Fig.4.2** Final Shape of the Deformed Steelplate at Different Blastload  
 Square Steelplate  $1 \times 1 \text{ m}^2$ ; 0.002 m thick  
 Final Position at 2.2 ms; Plastic Wave Velocity  $225 \text{ ms}^{-1}$

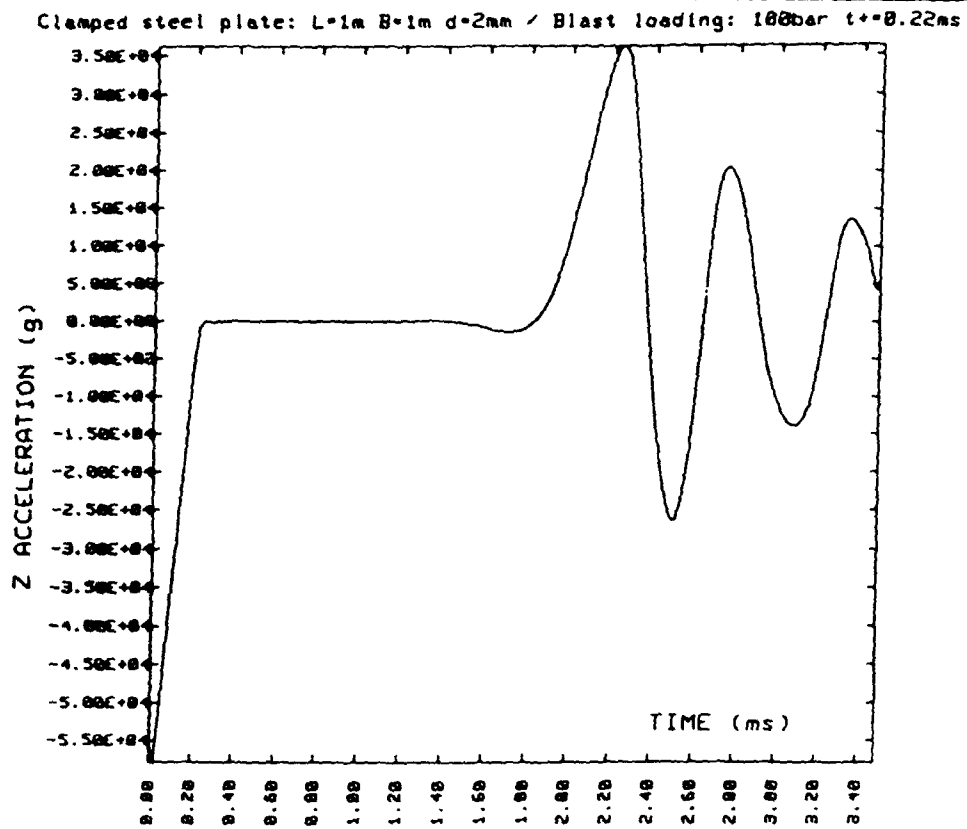


**Fig.4.3** Acceleration vs Time  
Centerpoint of a Blastloaded Square Steelplate

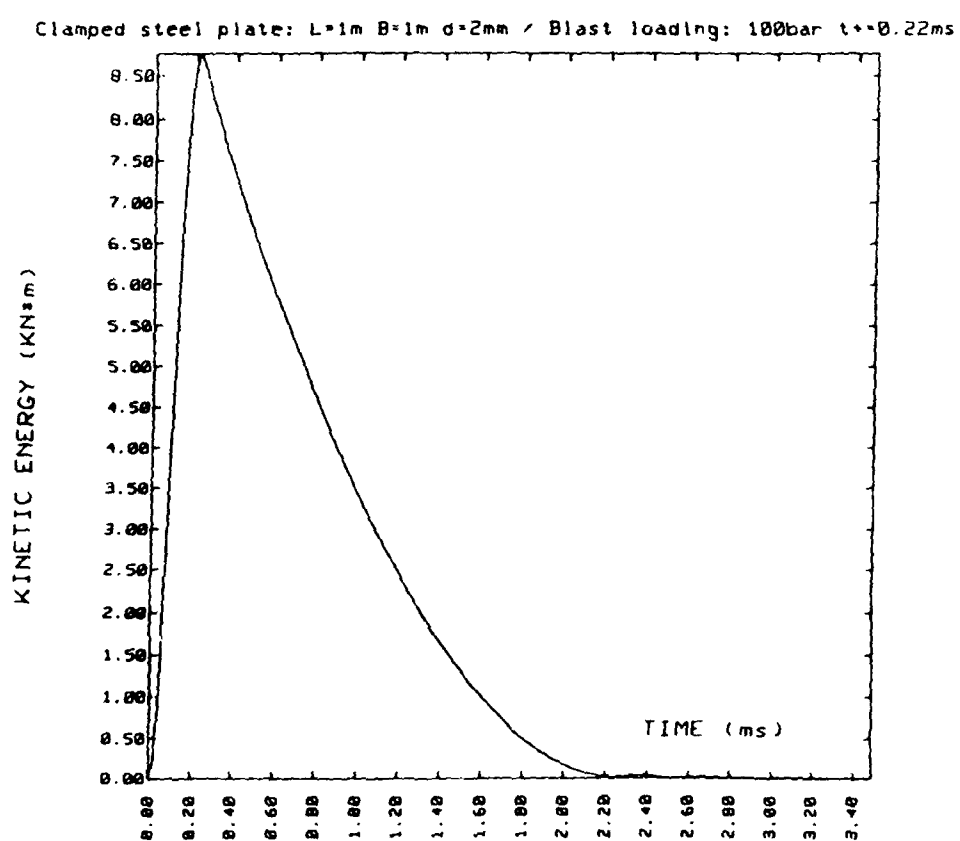


**Fig.4.4** Kinetic Energy vs Time  
Centerpoint of a Blastloaded Square Steelplate

Clamped steel plate: L=1m B=1m d=2mm / Blast loading: 100bar t+=0.22ms

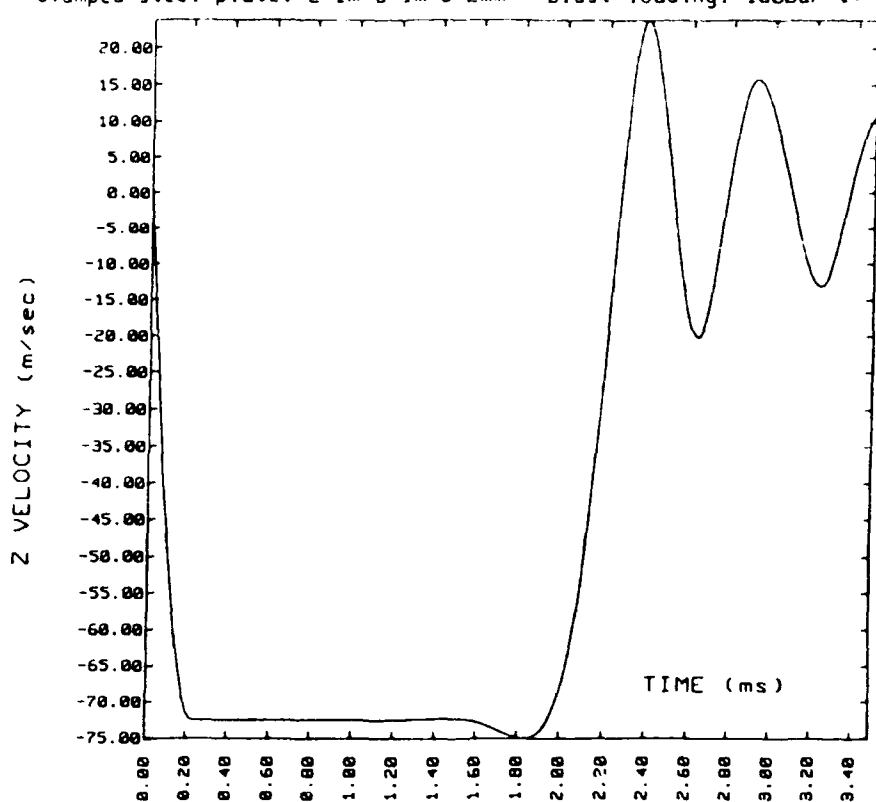


**Fig.4.5** Velocity vs Time  
Centerpoint of a Blastloaded Square Steelplate

Clamped steel plate: L=1m B=1m d=2mm / Blast loading: 100bar t+=0.22ms

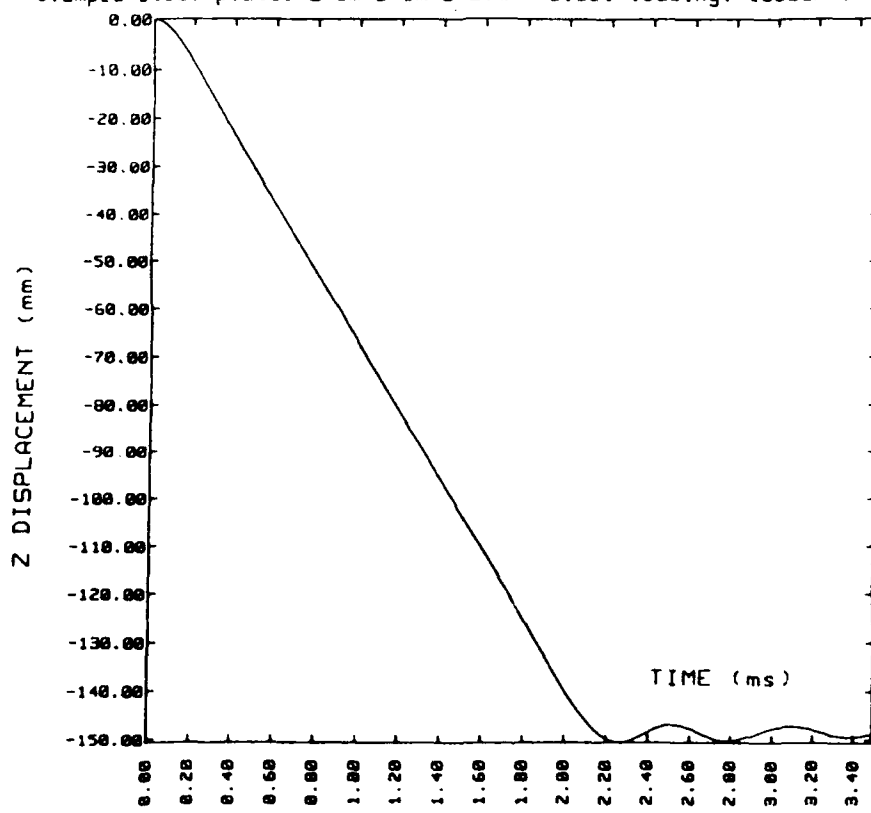


**Fig.4.6** Displacement vs Time  
Centerpoint of a Blastloaded Square Steelplate

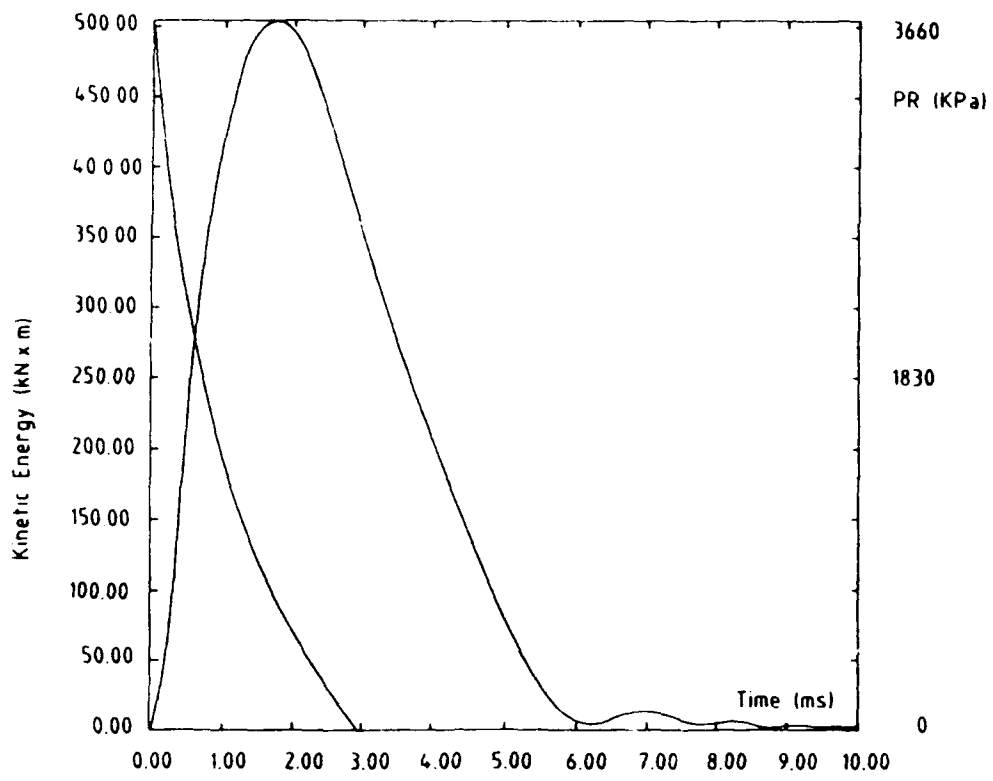


**Fig.5.1 Pressure Pulse and Time History of the Kinetic Energy in the Plate**

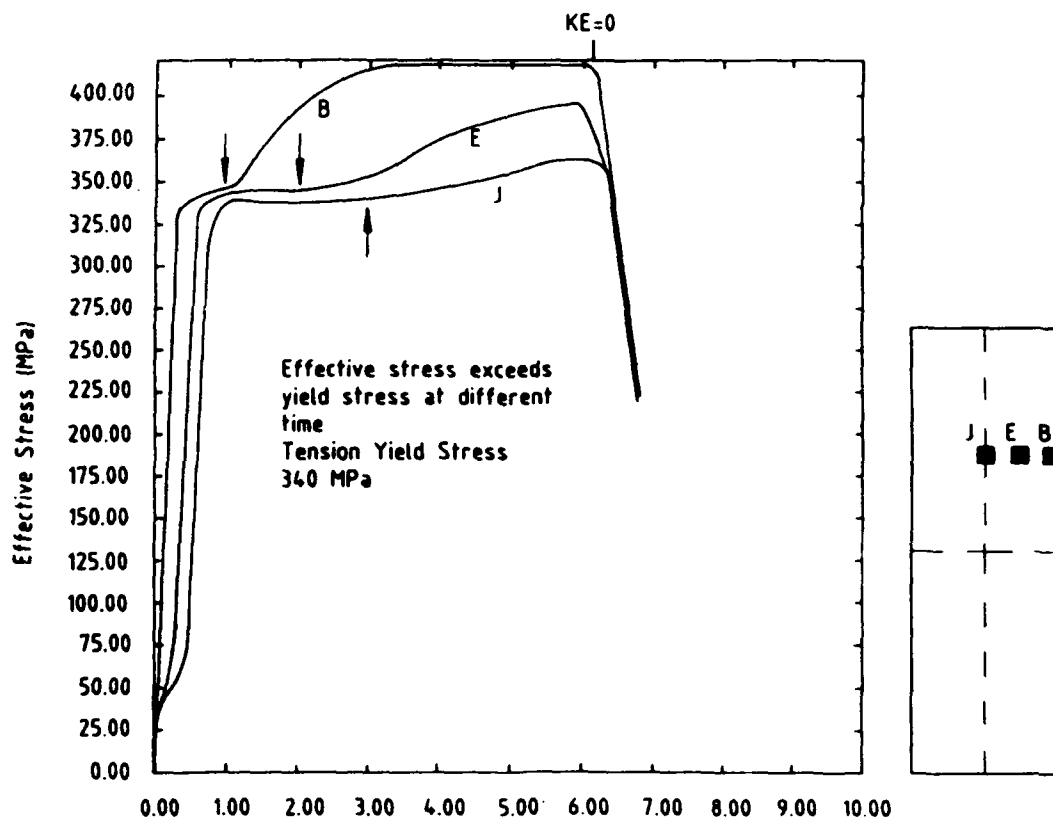


**Fig.5.2 Effective Stress in 3 Elements**  
**Element B - near the edge**  
**Element J - at midspan**

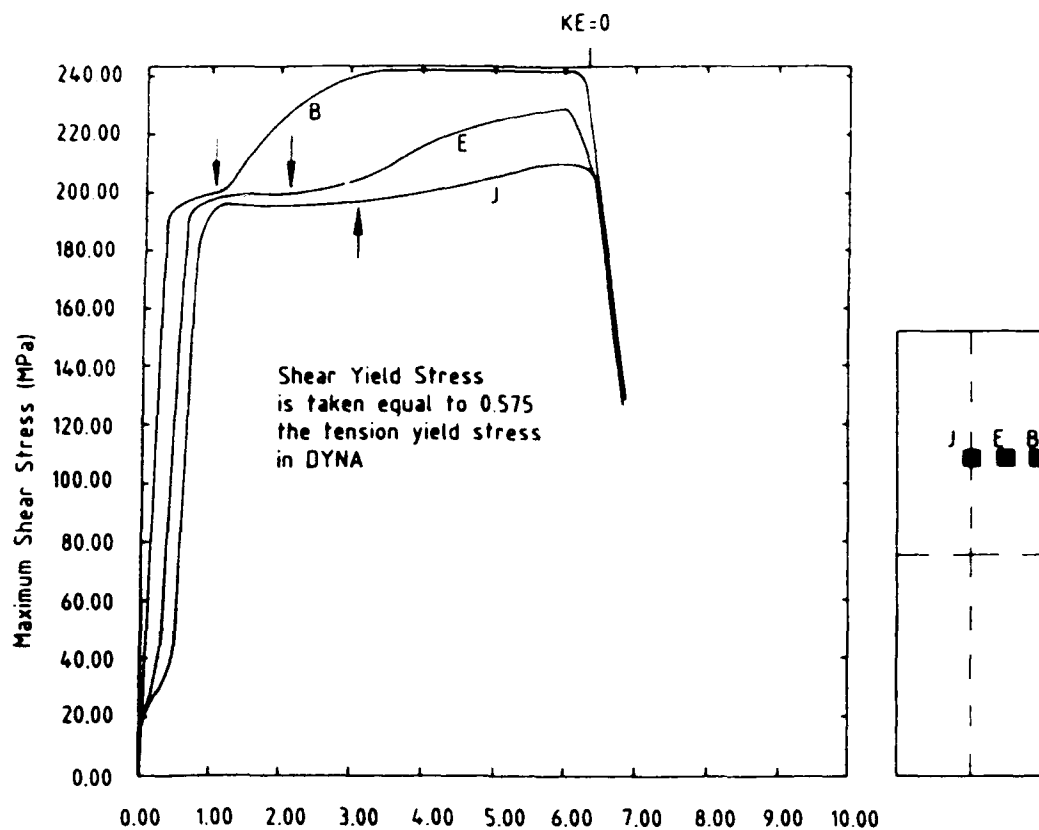


**Fig.5.3 Shear Stress in 3 Elements**

Element B - near the edge  
 Element J - at midspan

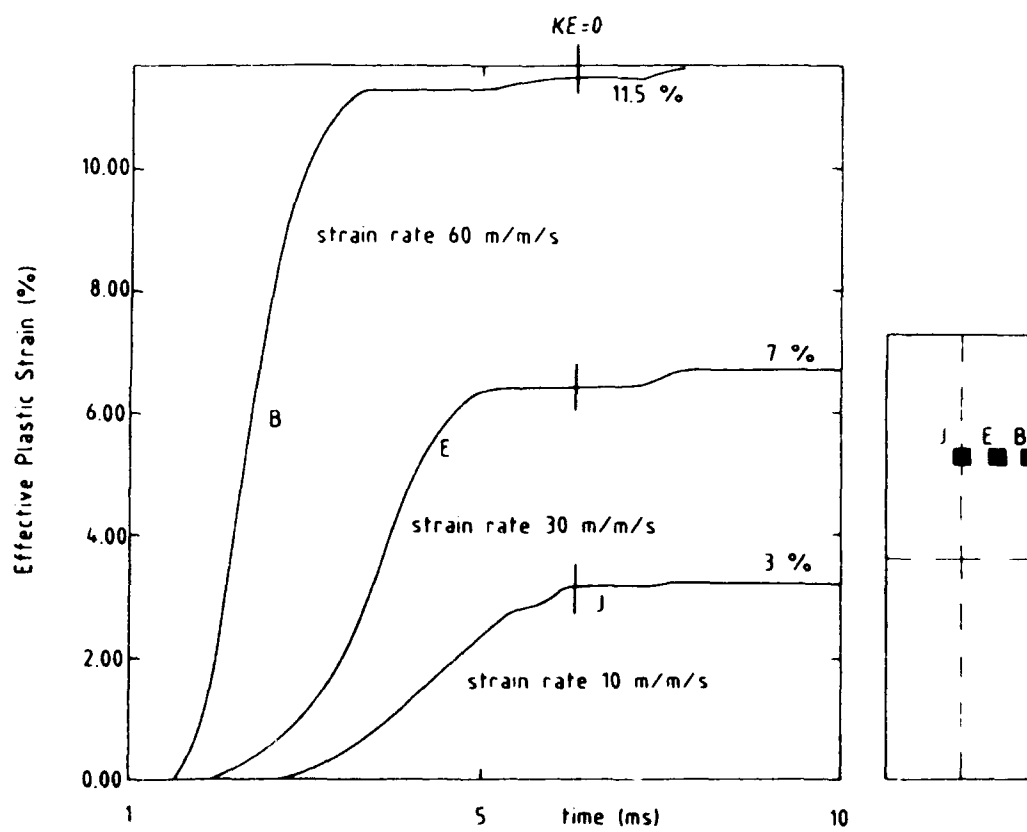


**Fig.5.4 Effective Plastic Strain (%) in 3 Elements**

Element B - near the edge  
 Element J - at midspan

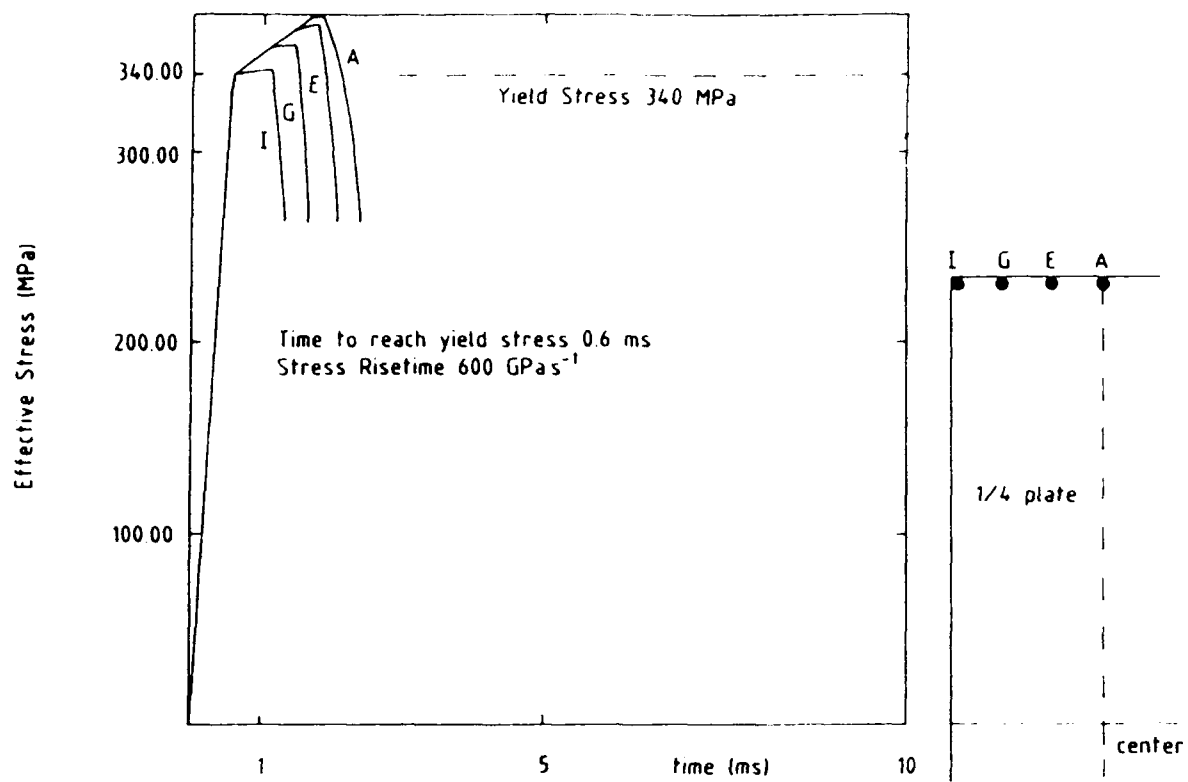


**Fig.5.5** Effective Stress vs Time  
Four Elements along the clamped edge

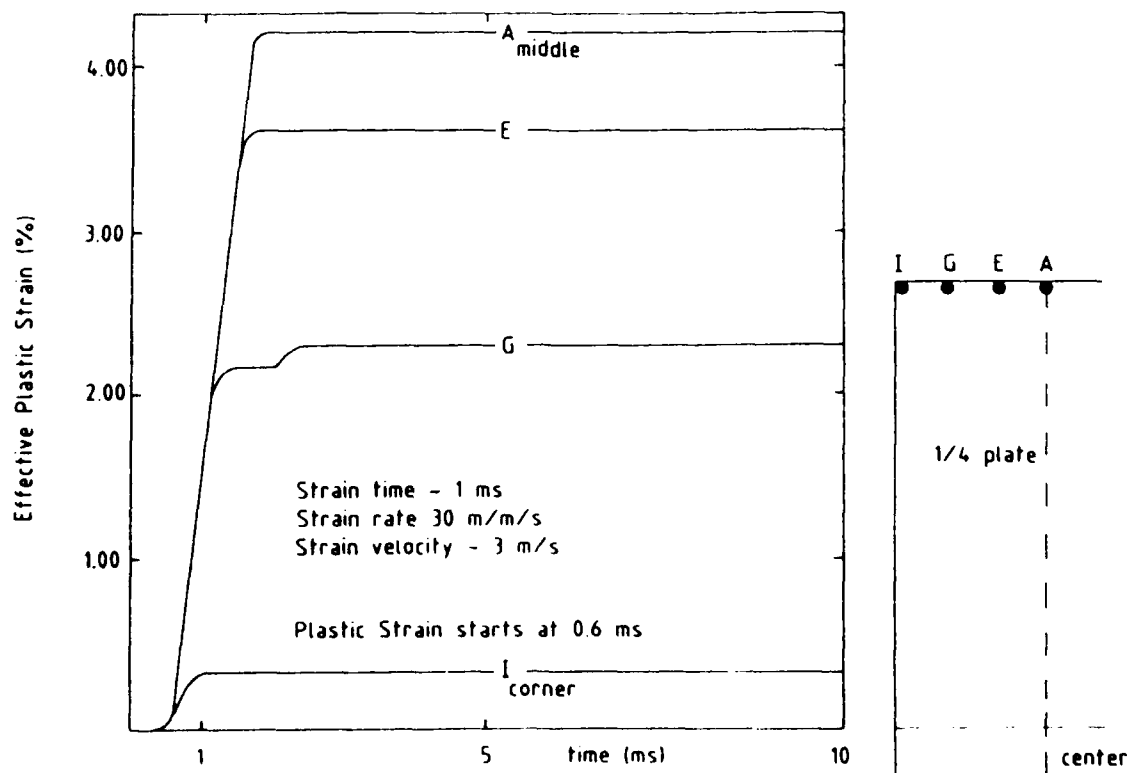


**Fig.5.6** Effective Plastic Strain (%) vs Time  
Four Elements along the clamped edge

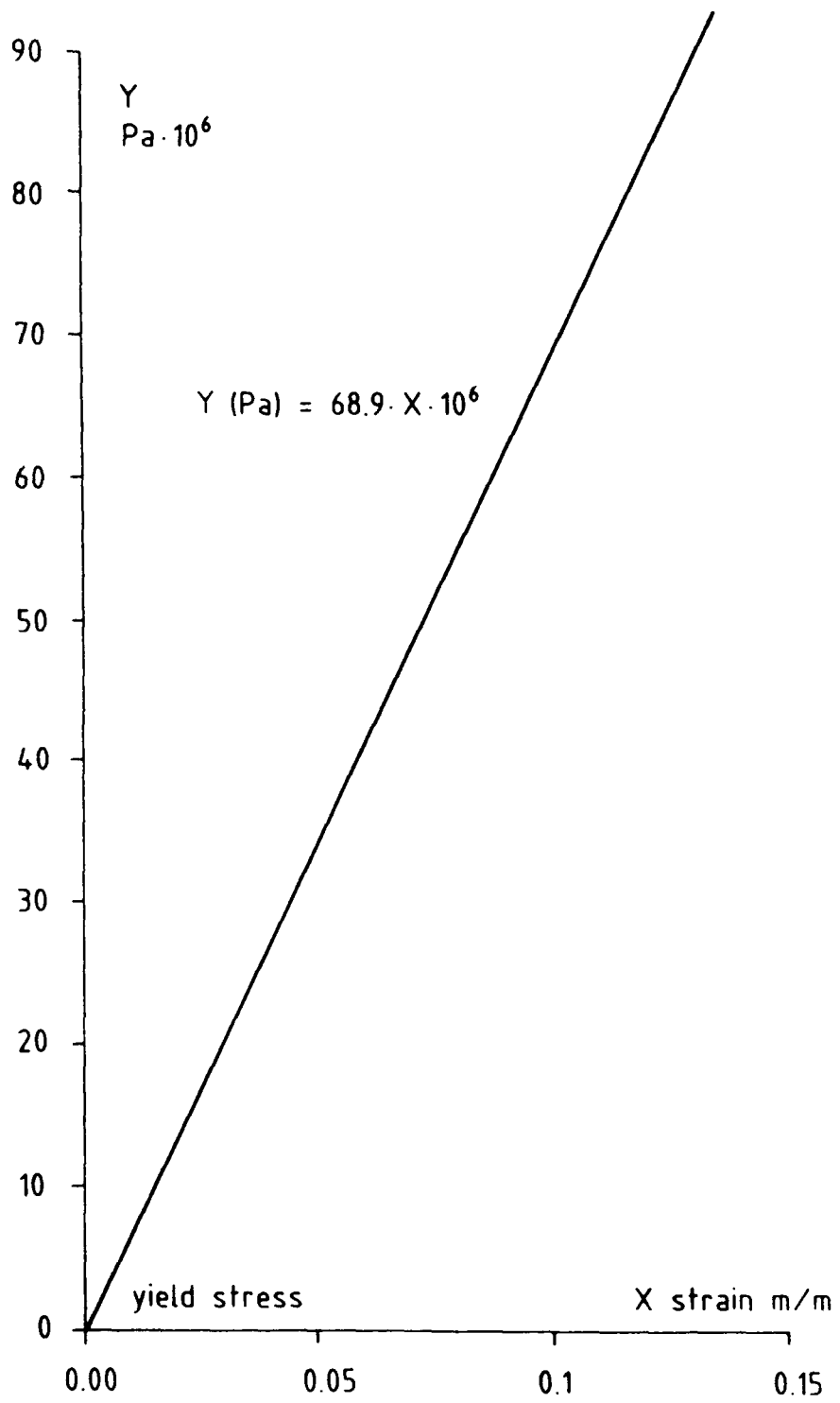


**Fig.5.7** stress exceeding yield  
stress vs permanent strain (DYNA)

**TWENTY-FIFTH DOD EXPLOSIVES SAFETY SEMINAR  
ANAHEIM HILTON HOTEL, ANAHEIM, CA  
18-20 AUGUST 1992**

**TRIALS TO DETERMINE THE CONSEQUENCES OF THE ACCIDENTAL  
IGNITION OF STACKS OF HAZARD DIVISION 1.2 AMMUNITION**

M.J. Gould,  
UK Ministry of Defence, Explosives Storage and Transport Committee

W.D. Houchins,  
Naval Surface Warfare Center, Dahlgren Division

**1. Introduction**

To date nearly all international effort in the field of accidental explosion consequence determination has been aimed at the quantification of the effects of a Hazard Division (HD) 1.1, mass detonation, event in an explosives storage facility. Trials such as those carried out in Australia, France and the United States (US) over recent years have assessed the effects of blast and fragment throw from accidental mass explosions in brick and concrete storehouses, igloos and tunnel magazines.

Little attention has been paid to quantifying the consequences of the accidental ignition of HD 1.2 ammunition. This class of ammunition is not expected to explode en masse. Individual rounds will explode when sufficiently stimulated (by, for example, fire) without causing others around them to explode. Such explosions will continue spasmodically over a period as further individual rounds receive sufficient stimulus. Current HD 1.2 quantity-distance (Q-D) guidance within NATO and UK is "based upon US trials". Unfortunately literature searches have, to date, failed to unearth any record of these trials. US guidance does not follow that of NATO and UK and their methodology is based on a determined maximum fragment throw distance for the munition under consideration. More detailed descriptions of the NATO, UK, and US methodologies are given below.

In 1989 NATO AC 258 (Group of Experts on the Safety Aspects of Transportation and Storage of Military Ammunition and Explosives), acknowledging the frailty of the basis for their HD 1.2 Q-D's, agreed that a program of trials should be carried out to investigate the consequences of an accidental HD 1.2 event with the aim of revising the current NATO quantity-distance relationships and placing them on a firmer footing. Exposed stack trials and trials within typical storehouse structures were proposed. This program would also offer the opportunity for the development of an approach common to and acceptable to NATO, UK and US for the calculation of HD 1.2 safety distances.

To enable the program of trials to proceed in a short timescale, the UK Explosives Storage and Transport Committee (ESTC) and US Department of Defense Explosives Safety Board (DDES) agreed to finance jointly an initial series of trials to examine the consequences of the accidental ignition of stacks of HD 1.2 ammunition in the open. This paper describes the current rules and underlying philosophies governing the storage of HD 1.2 ammunition in the US, UK and NATO. It then describes in detail the trials program, methodology and results obtained so far

and makes some initial suggestions for the revision of the quantity-distance relationships for HD 1.2 storage. In conclusion the future program of trials is described.

## 2. US Hazard Division 1.2 Quantity-Distances

US explosives quantity-distance standards are defined in DOD 6055.9-STD, the Department of Defense Ammunition and Explosives Safety Standards. For HD 1.2 items, safety distances are related to the maximum range of hazardous projections as determined by specified Hazard Classification Tests. Four Inhabited Building Distances (IBD) (400, 800, 1200 and 1800 feet) are specified within which "most projections for given items will fall". However, very recently a revised methodology has been introduced in which IBD's based on hazardous fragment range test results may be defined in 100 foot increments with a 200 foot minimum<sup>1</sup>. This method has only recently been approved by the US joint hazard classifiers and DDESB. The test method for assigning items to the four categories (400, 800, 1200 and 1800 ft) given in the US DOD Explosives Hazard Classification Procedures is still a valid method<sup>2</sup>.

The tests specified for definition of IBD in 100 ft increments for an item of ammunition are either a single or three "unconfined stack tests, bonfire tests or any combination thereof with 360 degree fragment recovery". To determine the IBD, if a single test is used, the maximum hazardous fragment throw distance is determined; it is rounded up to the next 100 ft and either 100 or 200 feet added dependent on the size of the item. If three tests are carried out, the maximum hazardous fragment throw distance is determined from all three trials and it is then rounded up to the next 100 feet. There is no additional increment added.

The remaining distances (public traffic route, intraline and above-ground magazine) are, with minor deviations, defined as percentages of IBD.

**Public Traffic Route Distance** takes account of the transient nature of the exposure and is calculated as 60% of IBD.

**Intraline or Explosives Workshop Distance** takes account of the extended period over which the event occurs and the consequent potential for evacuation. It is calculated as 50% of IBD. If the net explosive weight (NEW) at an operating line potential explosion site (PES) is limited to 5000 lb for items with IBD between 500 and 1200 ft then the Intraline Distance may be reduced to 200 ft.

**Above-ground Magazine Distance** "provides a high degree of protection against any propagation of explosion" excepting that "Items of this class/division with IBD requirements of 1200 ft or greater present a risk of propagation to adjacent above-ground magazines, particularly when packed in combustible containers. Storage in earth-covered magazines is therefore preferred". It is calculated as follows

For IBD less than 400 ft – 50% of IBD.

For IBD between 400 and 700 FT – 200 FT.

For IBD of 800 ft or greater – 300 ft.

The distances described above are independent of the NEW in the structure concerned. However, for items with IBD greater than 800 ft there is a storage limit of 500,000 lb NEW.

Recently a further "subset" of HD 1.2 has been defined – Unit Risk Class/Division 1.2. Ammunition. This type of ammunition is highly insensitive to accident stimuli and it is expected that only one round will react. IBD is calculated using the HD 1.1 areal number density criterion (one lethal fragment per 600 ft<sup>2</sup>) for a single round of the ammunition.

### **3. NATO and UK Hazard Division 1.2 Quantity Distances**

Current NATO and UK quantity-distance prescriptions are defined in Allied Ammunition Storage and Transport Publication 1 (AASTP-1) for NATO and ESTC Leaflet 5 Part 2 for UK. They differ in principle from those of the US in that they do not rely on the results of device-specific tests giving device-specific distances. There is a broad division, based loosely on calibre, into

- (i) those items which give small fragments of moderate range (HD 1.2\*).
- (ii) those items which give large fragments with considerable range (HD 1.2).

The generally accepted divide is 60mm calibre though it is emphasized that this is not absolute. Where explosion effects trials data exists for the item or it is considered necessary to produce it, this may be used to support the allocation of the appropriate classification.

The prolonged nature of the event is considered in terms of fire fighting response, time for evacuation of exposed sites both within and external to the explosives area and time for closure of traffic routes. The protection afforded to ammunition and personnel at exposed sites is also taken into account. As has been stated earlier, quantity-distances are based on US data which, to date, has not been traced.

Quantity-distances for HD 1.2 and 1.2\* ammunition are defined as follows:

**Inhabited Building Distance** is based on an acceptable risk from fragments and is defined

- (i) For HD 1.2\* as  $D1=53Q^{0.18}$  (D1 in meters, Q is NEW in kilograms) with a minimum of 180m and maximum of 410m. If the exposed buildings are isolated and can be evacuated promptly a fixed distance of 180m is allowed. Schools, hospitals, etc., must be at the D1 distance.
- (ii) For HD 1.2 as  $D2=68Q^{0.18}$  with a minimum of 270m and maximum of 560m. Under similar circumstances to the above a fixed distance of 270m is allowed. Schools, hospitals, etc., must be at the D2 distance.

It is believed that the IBD Q-D formulae may relate to a lethal fragment density (fragment energy > 80J) of one per 56m<sup>2</sup> though this is not certain.

**Public Traffic Route Distance** is based on "an acceptable risk from fragments and lobbed ammunition to be expected in the first half hour of an incident". It is defined such that if traffic can be stopped promptly, presumably within the half hour period, half the fixed IBD distances may be used. Failing this the full D1 and D2 distances are to be employed.

**Intraline or Explosives Workshop Distance** is a fixed distance of 25m for exposed sites with "virtually complete protection". Otherwise 90m or 135m are to be used for HD 1.2\* or HD 1.2 ammunition respectively.

**Inter-magazine distances** are fixed distances of 2m, 10m, 25m or 90m dependent on the degree of protection provided at the exposed site.

#### **4. Test Program**

The trials described herein are bonfire tests on palletized 105mm cartridges stored in the open. This initial series will consist of at least seven tests, five of which have already been completed. Each of the first three tests was conducted using a single pallet of cartridges (single pallet tests). The fourth and fifth tests were conducted using eight pallets each (8-pallet tests). The sixth test will be conducted using 27 pallets. The primary intent in using at least three different stack sizes is to determine which, if any, parameters scale as a function of stack size. The type and quantity of ammunition to be used in any test beyond the sixth is still to be decided.

The single pallet tests and the 8-pallet tests were conducted during the period May 1991 through April 1992. The 27-pallet test should be completed in the fall of 1992. The test site for the initial series of tests is the Naval Air Warfare Center, China Lake, California.

#### **5. Test Items**

The M1 105mm cartridge is a semi-fixed, high explosive artillery round. The general configuration of the assembled cartridge is illustrated in Figure 1. Several variants of the M1 cartridge have been produced with projectiles loaded with TNT explosive or Composition B explosive. This series of tests is being conducted using cartridges containing approximately 4.5 lbs of TNT explosive each. The projectile body is fabricated from forged steel and weighs approximately 25.8 lbs. An aluminum shipping plug is assembled into the nose of the projectile in lieu of a fuze. The propelling charge is comprised of approximately 3 lbs of M1 propellant contained in a spiral wrap steel case. Each propelling charge case weighs approximately 4.7 lbs.

The cartridges are packaged in wooden boxes for transport and storage. Each box contains two cartridges that are packaged individually in fiberboard sleeves as shown in Figure 2. The cartridges are oriented such that the projectile of one cartridge is adjacent to the propelling charge of the other cartridge (i.e., nose-to-tail arrangement). A complete pallet consists of 15 boxes. The boxes are secured on the pallet using steel banding.

#### **6. Test Method**

The first four tests (i.e., all three single pallet tests and the first 8-pallet test) were conducted generally in accordance with the methodology prescribed by the UN Recommendations on the Transport of Dangerous Goods (the UN Orange Book)<sup>3</sup>. The test items were stacked on a test stand that provided approximately 30 in clearance between the bottom of the stack and ground level. The stacking arrangements for the tests are illustrated in Figure 3. Dried lumber placed beneath the test stand and around the pallet(s) was used as kindling to provide fuel during the initial stages of the test. Four shallow troughs containing a small amount of gasoline were placed around

the base of the stack to provide an ignition source for the fire. The gasoline in the troughs was ignited using an electric squib. In order to eliminate ground cratering and burrowing of unexploded test items at the stack site (ground zero), the stack and bonfire were constructed over a steel deck that was supported by a concrete pad. A typical completed test setup is shown in Figure 4.

The fifth test (second 8-pallet test) was conducted in the same manner except that kindling was placed beneath the test stand only. This was done to simulate a more probable scenario in which the test item packaging and the energetic components are the primary fuel source for a fire. In the single pallet tests and the first 8-pallet test the amount of kindling lumber used was nominally the same (115 ft<sup>3</sup>). Each pallet of ammunition contained approximately 8.2 ft<sup>3</sup> of lumber. Thus, of the total lumber in the stacks (the wood of the ammunition boxes plus kindling), the ammunition box contribution was only 6.6% in the single pallet tests and 36% in the first 8-pallet test. In the second 8-pallet test the ammunition box contribution rose to 57%. Figure 5 is a photograph of the completed setup for the second 8-pallet test.

The debris recovery area, a flat, dried lake bed, encompasses a full 360° azimuthally about ground zero. It has been scraped clear of virtually all vegetation to a range of 1300 ft. In order to facilitate recovery of the test item debris, this cleared region has been marked with a 10° x 200 ft grid as illustrated in Figure 6. Recovery of the test item debris is accomplished manually through systematic visual searches of the area by test personnel. The debris that are recovered inside the 200-ft range are not retained for analyses due to their large numbers. These debris are segregated according to type (i.e., projectile case piece, cartridge case piece, or miscellaneous) and the total weight of all pieces of each type is determined. The pieces of debris that are recovered between the 200-ft and 1300-ft ranges are identified according to the grid sector in which they are found. The pieces of debris that are recovered beyond 1300 ft are identified individually by the appropriate azimuthal zone and range. The post-test searches conducted to date have been limited to a range of approximately 2000-ft. Recovery beyond this range was not considered cost effective because the numbers of fragments landing beyond 2000-ft were thought to be too small to justify the time and manpower required to search such a vast area. Additionally, the likelihood of finding any of the few fragments that might lie in this region was considered low due to the presence of vegetation.

The test events are recorded using closed circuit video systems. Typically one or two video cameras are positioned approximately 500 ft from the test stack to record the events that occur within the immediate confines of the fire. Another two or three video cameras are positioned on hillsides overlooking the test area to record the general location of larger debris as it impacts the ground. The video signals are recorded on standard 1/2 in VHS videocassette tapes.

An attempt was made during each of the first four tests to determine the terminal flight characteristics (e.g., velocity, angle of fall, etc.) of fragments impacting within a selected sector by capturing their terminal stages of flight on video. However, a fragment impacted within the selected sector in only one test and in that instance the image size of the fragment was below the resolution of the video record.

Blast overpressures are measured to provide a means of analyzing each explosion (in particular, "simultaneous" multiple explosions) and to provide a time record of the whole event. Eight piezoelectric pressure transducers are located along the 0° and 90° radials at ranges of 50, 70, 100, and 200 ft. The elevation of each transducer is approximately 20 in above ground level. The response of each pressure transducer is recorded using analog FM tape recorders providing 20 kHz frequency response. Due to constraints on the instrumentation cable lengths that can be used with this type of transducer, the recorders and ancillary signal conditioning equipment are housed in a

shelter that is located approximately 500 ft from the test site. Because personnel cannot be adequately protected at this range, the recording equipment is controlled and monitored from a remote site located approximately 4000 ft from the recording equipment. The recording systems are controlled by a master remote control station that sends commands and receives status reports through Dual Tone Multi-Frequency (DTMF) encoded radio transmissions. Each recorder, when operated at the required frequency response, provides approximately 50 minutes of usable recording time. Extended continuous recording for these relatively prolonged tests is obtained by operating multiple recorders sequentially so that their recording times overlap slightly.

## 7. Results

In general each of the tests produced events that were on the order of 1 hour duration. After ignition, the fire developed rapidly, enveloping the entire stack within three to five minutes. Typically the first reactions were observed about 15 to 20 minutes after ignition of the fire. These initial reactions were seen as localized areas of intense burning and were occasionally accompanied by a small flash and/or a low level audible report (pop). It is believed that these initial reactions were mild deflagrations of propelling charges and subsequent burning of the spilled propellant. Significantly more violent reactions, believed to be explosions of projectiles, would begin to occur several minutes later. These reactions were characterized by abrupt instantaneous expansion of the fire, a loud audible report, and localized scattering of burning wood and other debris about the test site. Additionally, large pieces of test item debris could often be seen impacting in the recovery area following one of the larger reactions (explosions).

Typically the fire would continue to burn at full intensity only until the first few explosions had occurred. It would then begin to die out slowly due to scattering of the stack by each successive explosion. Both the smaller, burning type reactions and the explosions continued to occur intermittently throughout the duration of the fire. Additionally, in each test, several explosions were observed after the fire was reduced to broadly scattered pieces of smoldering debris. It has appeared in all instances that the explosion reactions have occurred in the immediate vicinity (i.e., within 50 ft) of the fire. Neither on-site observations nor video records from the tests have provided any indications of test items being thrown significant distances prior to reacting. However, in each test some unreacted projectiles have been recovered several hundred feet from ground zero. The following sections summarize briefly specific observations for each of the tests. The event times are given in the form "minutes:seconds", e.g. 20:35.

Single Pallet Test No. 1. The first indications of test item reactions were observed 15:32 after ignition of the fire. The first major reaction, believed to be a projectile explosion, occurred 18:24 after ignition of the fire. The fire was reduced to broadly scattered smoldering debris after approximately 25 minutes. A total of 13 explosions were observed during and after the fire. Following the test, 17 projectile bodies were recovered intact. A total of 78 pieces of debris were recovered beyond the 200 ft range including 44 projectile case (and rotating band) pieces with a total mass of 139.5 lb<sub>m</sub> and 19 cartridge case pieces with a total mass of 5.1 lb<sub>m</sub>. The projectile case pieces and cartridge case pieces that were recovered inside the 200-ft range had total masses of 118.5 lb<sub>m</sub> and 130 lb<sub>m</sub>, respectively. The total mass of all recovered projectile case pieces accounts for approximately 77% of the estimated mass of the projectile bodies that were not recovered intact (i.e., estimated percentage of recovery based on mass). Similarly, the total mass of all recovered cartridge case pieces accounts for approximately 96% of the mass of the cartridge cases that were in the pallet.

Single Pallet Test No. 2. The first indications of mild deflagration reactions and burning reactions were observed 20:22 after ignition of the fire. The first explosion occurred 24:14 after ignition of the fire. The fire was reduced to broadly scattered smoldering debris after approximately 35 minutes. A total of 9 explosions were observed during and after the fire. Following the test, 21 projectile bodies were recovered intact. A total of 37 pieces of debris were recovered beyond the 200 ft range including 31 projectile case pieces with a total mass of 153.5 lb<sub>m</sub> and one cartridge case piece with a mass of 2.5 lb<sub>m</sub>. The projectile case pieces and cartridge case pieces that were recovered inside the 200-ft range had total masses of 66.0 lb<sub>m</sub> and 136.3 lb<sub>m</sub>, respectively. The corresponding estimated percentages of recovery based on mass are 95% for projectile case pieces and 99% for cartridge case pieces.

Single Pallet Test No. 3. The first indications of test item reactions were observed 20:05 after ignition of the fire. However, the first explosion was not observed until 36:48 after ignition of the fire. The fire was reduced to broadly scattered smoldering debris after approximately 60 minutes. A total of 11 explosions were observed during and shortly after the fire. Following the test, 18 projectile bodies were recovered intact. Additionally, a 19th projectile body was recovered nearly intact (moderate splintering in nose region). A total of 49 pieces of debris were recovered beyond the 200 ft range including 42 projectile case pieces with a total mass of 140.5 lb<sub>m</sub> and three cartridge case pieces with a total mass of 4.1 lb<sub>m</sub>. The projectile case pieces and cartridge case pieces that were recovered inside the 200-ft range had total masses of 85.6 lb<sub>m</sub> and 134.5 lb<sub>m</sub>, respectively. The corresponding estimated percentages of recovery based on mass are 73% for projectile case pieces and 98% for cartridge case pieces.

8-Pallet Test No. 1. The first indications of test item reactions were observed 18:13 after ignition of the fire. The first explosion occurred 20:48 after ignition of the fire. A total of 66 explosions were observed during and shortly after the fire. Following the test, 174 projectile bodies were recovered intact. A total of 808 pieces of debris were recovered beyond the 200 ft range including 263 projectile case pieces with a total mass of 593.4 lb<sub>m</sub> and 320 cartridge case pieces with a total mass of 88.4 lb<sub>m</sub>. The projectile case pieces and cartridge case pieces that were recovered inside the 200-ft range had total masses of 754 lb<sub>m</sub> and 874 lb<sub>m</sub>, respectively. The corresponding estimated percentages of recovery based on mass are 79% for projectile case pieces and 85% for cartridge case pieces.

8-Pallet Test No. 2. The first indications of test item reactions were observed approximately 14:15 after ignition of the fire. The first explosion occurred approximately 18:37 after ignition of the fire. A total of 65 major reactions were observed during and shortly after the fire. Following the test, 174 projectile bodies were recovered intact. Fragment recovery data for this test are not yet available.

The event times for the explosions that were observed during the single pallet tests are provided in Table 1. The event times for the explosions that were observed during the 8-pallet tests are provided in Table 2. The azimuthal and radial distributions of fragments recovered outside the 200-ft range (far-field fragments) after the single pallet tests and the first 8-pallet test are illustrated in Figures 7 through 10. Photographs of typical fragments are provided in Figures 11 and 12.

Table 1. Elapsed Times Until Explosions During Single Pallet Tests

<u>Explosion No.</u>	Elapsed Time (min:sec)		
	<u>Test No. 1</u>	<u>Test No. 2</u>	<u>Test No. 3</u>
1	18: 24	24: 14	36: 48
2	18: 51	27: 01	47: 05
3	19: 58	30: 57	49: 02
4	20: 43	33: 25	51: 10
5	20: 55	33: 33	54: 50
6	27: 40	38: 24	56: 29
7	27: 44	39: 09	57: 09
8	28: 50	41: 03	61: 29
9	29: 34	42: 36	63: 13
10	29: 51		67: 35
11	33: 48		78: 40
12	35: 21		
13	48: 53		

Table 2. Elapsed Times Until Explosions During 8-Pallet Tests

<u>Test No. 1</u>				<u>Test No. 2</u>			
<u>No.</u>	<u>Time</u>	<u>No.</u>	<u>Time</u>	<u>No.</u>	<u>Time</u>	<u>No.</u>	<u>Time</u>
1	20:48	26	33:49	51	41:18	1	18:37
2	23:47	27	34:07	52	42:00	2	18:56
3	23:57	28	34:10	53	42:16	3	18:53
4	25:51	29	34:12	54	42:19	4	21:18
5	26:32	30	34:44	55	42:23	5	21:25
6	26:37	31	34:49	56	42:50	6	21:35
7	27:13	32	35:04	57	43:13	7	21:43
8	27:36	33	35:27	58	43:44	8	21:51
9	27:44	34	35:28	59	44:13	9	21:53
10	27:58	35	35:47	60	44:39	10	22:07
11	28:22	36	36:11	61	46:25	11	22:12
12	28:29	37	36:30	62	47:05	12	22:17
13	29:23	38	36:42	63	47:46	13	22:57
14	29:23	39	37:05	64	51:41	14	23:11
15	29:58	40	37:15	65	52:58	15	23:34
16	30:59	41	37:47	66	61:08	16	23:37
17	31:04	42	38:38			17	23:40
18	31:16	43	40:01			18	23:42
19	31:22	44	40:07			19	23:56
20	31:48	45	40:15			20	24:07
21	31:54	46	40:22			21	24:09
22	32:17	47	40:24			22	24:40
23	32:24	48	40:24			23	24:44
24	33:12	49	40:29			24	24:54
25	33:16	50	41:18			25	24:55

The blast data from these tests are too voluminous for inclusion in this paper. To date the blast data from each test have been used primarily to confirm, based merely on the presence of air shock, the number of explosions that occurred. However, analyses of the blast data are continuing in an attempt to estimate the locations of the test items when they reacted and to determine their yield.

## 8. Analyses

The recovery data for these tests have not been subjected to rigorous statistical tests. However inspection of Figures 7 through 10 suggests that the distribution of far-field fragments with respect to azimuthal angle about the stack is fairly random. Therefore, the following analyses are oriented primarily towards description of fragment hazards in terms of range, independent of azimuthal angle.

The recovery data were used to calculate areal densities of lethal fragments analogous to those used to establish hazard ranges for HD 1.1 items. In the absence of any means of determining fragment energies, all recovered fragments were assumed to be lethal, including some of the cartridge case pieces and miscellaneous debris recovered within the 200-ft to 400-ft range interval which had masses as low as 0.01 lb<sub>m</sub>. Additionally, it was assumed that the distribution of fragments with respect to azimuthal angle is indeed random. Thus the areal density for each range interval was calculated as the total fragment count for the range interval divided by the area of the corresponding annulus. Pseudo trajectory-normal methods were used to determine the fragment count for each range interval inside the 1200-ft range<sup>4</sup>. For example, the fragment count for the 200-ft to 400-ft range interval was the number of fragments recovered between 200-ft and 1200-ft, for the 400-ft to 600-ft range interval it was the number of fragments recovered between 400-ft and 1200-ft, etc. The areal density for each range interval beyond 1200-ft was calculated based solely on the number of fragments recovered in that interval. The underlying assumption for this approach is that each fragment recovered inside the 1200-ft range followed a relatively low, flat trajectory and thus would pose a hazard to personnel and small structures located at ground level along its entire flight path. Conversely, each fragment landing beyond 1200-ft is assumed to have followed a relatively high trajectory with an extremely steep angle of fall in its terminal phase of flight. Under these circumstances, the fragment would not pose a hazard to personnel or small structures located at ground level except in the immediate vicinity of the point of ground impact.

The fragment densities determined in the preceding manner are shown graphically in Figure 13. In this figure the value of fragment density for each range interval is plotted at the midpoint of the interval. Additionally, densities are expressed in units of fragments per 600 square feet so that the results may be compared easily with the current HD 1.1 areal number density criterion. It can be seen immediately upon inspection of Figure 13 that the fragment densities for each of the single pallet tests were well below this criterion for all ranges beyond 200 ft. It can also be seen that the fragment densities for the first 8-pallet test were below the HD 1.1 areal number density criterion for all range intervals beyond 400 ft.

The fragment densities depicted in Figure 13 are based on the numbers of fragments actually recovered following each test. However, as indicated previously, these recoveries were incomplete. This is particularly true for projectile case fragments, which are the only type of debris thrown more than a few hundred feet. Thus the densities depicted in Figure 13 are probably optimistic; that is, they probably tend to underestimate the actual fragment hazard at most ranges, especially the further ranges. In order to derive more conservative estimates of fragment densities, the fragment recovery data were adjusted as follows to compensate for the apparent shortfalls.

a. The total mass of all far-field projectile fragments ( $m_f$ ) was estimated as

$$m_f = N m_p - m_0$$

where:  $N$  is the number of projectile bodies not recovered intact

$m_p$  is the mass of each projectile body (25.8 lb)

$m_0$  is the total mass of all projectile pieces recovered inside 200-ft

b. The number of far-field projectile case fragments that were not recovered after each test ("missing" fragments) was estimated as

$$n_m = n_r [(m_f/m_r) - 1]$$

where:  $n_m$  is the number of "missing" far-field projectile fragments

$n_r$  is the number of far-field projectile fragments recovered

$m_f$  is the estimated mass of all far-field projectile fragments

$m_r$  is the total mass of all recovered far-field projectile fragments

c. The "missing" fragments were assumed to be located between the ranges of 1200-ft and 2600-ft. It is thought that this is the region where fragments are most likely to have landed but not been recovered for several reasons:

- (1) The presence of vegetation may have shielded some fragments from the view of test personnel during post-test searches.
- (2) Most of the fragments falling in this region would probably impact the ground at a relatively steep angle of fall thereby increasing the likelihood that they would penetrate the surface and remain buried.
- (3) The region beyond the 2000-ft range was not searched thoroughly.

The specific distribution of the "missing" fragments was assumed to be such that an equal number were present in each 200-ft wide range interval between the 1200-ft and 2600-ft ranges. This assumption is considered conservative in that the fragment counts for the outer-most range intervals are probably much greater than would be expected for a more realistic scenario in which the number of fragments decreases with increasing range.

The preceding adjustment was applied for projectile case pieces only. The recovery data indicate that nearly all of the cartridge case pieces were recovered after each test and thus no further adjustment appears warranted.

The fragment densities obtained using the adjusted fragment counts are shown graphically in Figure 14. It can be seen that the fragment densities for each of the single pallet tests are still much less than one fragment per 600 ft<sup>2</sup> for all ranges beyond 200 ft and that the densities for the first 8-pallet test are still below this level for all range intervals beyond 400 ft. However, the indicated densities are considerably higher at the greater ranges than those obtained using the unadjusted fragment counts.

These same data are shown again in Figure 15 except that in this case the densities have been normalized on a per pallet basis. Inspection of this figure shows that the normalized fragment densities for the first 8-pallet test are roughly the same as those for the single pallet tests. This suggests that, at least for smaller stack sizes, fragment densities scale roughly linearly with respect

to the number of items in the stack. If it is assumed that fragment densities scale linearly as a function of the number of rounds for a broad range of stack sizes, then the results of the tests conducted thus far may be used to estimate the fragment densities that would be expected for events involving considerably larger stacks. The results of each of the single pallet tests and the first 8-pallet test were scaled up to obtain density-range estimates for various stack sizes up to 50000 rounds. The density-range estimates for each selected stack size were then fitted using a cubic spline fit to determine the range at which the fragment density would exceed one fragment per 600 ft<sup>2</sup>. These estimated ranges are shown graphically in Figure 16. A comparison between these estimated ranges and the corresponding IBD's prescribed by current NATO/UK and US quantity-distance requirements for HD 1.2 items is provided in Figure 17.

All of the preceding description of fragment hazards has been based on final fragment densities resulting from the cumulative buildup of far-field fragments throughout each test. One of the distinguishing features of a HD 1.2 event relative to a HD 1.1 event is the prolonged period of time over which reactions occur. As can be seen in Tables 1 and 2, the time intervals over which explosions have been observed in the tests completed thus far range from approximately 19 minutes to approximately 42 minutes. The cumulative frequency distribution of the explosions that occurred in each test are shown in Figure 18 and Table 3 gives the times at which 20%, 50%, and 100% of the explosions have occurred for each test.

Table 3. Times After First Explosion at Which 20%, 50%, and 100% of Explosions Have Occurred

	Time in Minutes		
	T <sub>20%</sub>	T <sub>50%</sub>	T <sub>100%</sub>
Test 1	<5	10	31
Test 2	<5	9	19
Test 3	12	18	42
Test 4	9	14	41
Test 5	<5	8	24

## 9. Discussion

The current program of trials addresses the consequences of an accidental fire in exposed stacks of HD 1.2 ammunition. No work has yet been done to quantify the consequences of similar events inside structures (e.g., storehouses). Although the trials program is, as yet, incomplete, some patterns and trends are beginning to emerge from the results.

Times to first propellant reaction and to first explosion have all been in excess of 15 minutes and have not occurred until the stack is fully engulfed by fire with the wooden ammunition boxes contributing significantly to the fire. This is perhaps the worst case in the sense that the wooden ammunition cases formed a considerable proportion of the total fuel available (36% and 57% in the case of the two 8 pallet tests). The time to first event will vary with many factors (e.g., the amount of fuel available, packaging materials, calibre of rounds (thermal mass)), and the thermal sensitivity of the explosives used.

Following the first explosion the frequency of explosions builds up rapidly with time and then reduces at a lower rate towards the end of the event. Approximately one third of the rounds in the stack explode during the event.

No evidence of full detonation or of sympathetic reaction has yet been found. Pressure records indicate pressures less than those from a complete detonation and post-test examination of debris indicates that the aluminum closure plugs are forced out, presumably by expansion of the fill, and molten TNT then drains from the shell. Burning of the TNT has also been observed prior to explosions. Each round that explodes fragments the case in a "banana skin" fashion (Figures 11 and 12). Thus only a small number of heavy fragments per round are generated. If it is conjectured that HD 1.2 events in general will be low order explosions and cases fragment in similar fashion, the Q-D's may be related in part to number of rounds and not to NEW. A broad division by calibre similar to that used in the NATO definitions may then be used to define hazard distance bands (similar to those used in the US) as the range of fragment scatter will depend on the fragment dimensions and weights.

It is important to note that, although complete rounds are projected as far as 1100 ft from ground zero, there has been no occasion on which a round has exploded on or after impact other than those thrown a few feet and remaining within the zone of the fire. Thus, in calculating quantity distances, it will not be necessary to include any additional fragmentation effect attributed to far-field explosions.

As may be expected in an event in which the orientation of the rounds in the stack is destroyed after the first one or two explosions, there is no noticeable directional trend in the far-field fragmentation. The addition of the "missing" fragments into the overall fragment array assumes the same azimuthal randomness. The radial distribution of "missing" fragments (equal numbers per 200-ft annulus) implies a degree of conservatism as there is no decrease in numbers with range. There is of course a decrease in fragment density with range as the area of each annulus increases with its range. More realistic distribution of the "missing" fragments is still being investigated. The assumption that the trajectory normal analysis should only apply to fragments within 1200 ft of ground zero is based on the premise that, beyond that range, fragments must have been launched at high trajectory and thus would not contribute to lethality in the nearer field. Given the weight distribution of the far-field fragments all have been considered as lethal.

As Figure 15 shows, between the one and eight pallet tests, the fragment densities scale reasonably. Although the trials data gathered to date gives a good indicator of far-field fragment densities for small NEW's, extrapolation to larger quantities relies almost entirely on the "missing" fragments and the way they were introduced into the analysis. The estimated range to exceed one lethal fragment per 600 ft<sup>2</sup> asymptote (Figure 17) is an artifact of the "missing" fragment distribution used and illustrates

1. In the short term, the need to refine the distribution used for these "missing" fragments.
2. In the longer term, the need to examine the fragment pick-up philosophy and technique to reduce the number of "missing" fragments and get a realistic picture of the very far-field fragmentation.

Given a more realistic distribution, it is suggested that the curves should go asymptotic to the "No. of Rounds" axis at a range representing the maximum possible projection range for the fragments.

Figure 17 illustrates that, at small NEW's (where the gathered data applies), some savings over the existing criteria can be gained. However above 10000 rounds there is a sharp increase above the criteria. It must be re-emphasized that this is due to the conservatism built into the treatment of the "missing" fragments. As might be expected, all results fall below the IBD curve for HD 1.1.

Figure 18 and Table 3 clearly illustrate that there is considerable variation in the rate of explosions once they have started. It is therefore considered inadvisable to consider any period following the first explosion during which reduced lethal radii might be inferred. Thus any consideration of a time for evacuation should be limited to the minimum 15 minutes before the first explosion. The alarm must be raised when the fire starts. Thus automatic fire detection and alarm systems are an important requirement for optimum evacuation time availability. For similar reasons the use of automatic drench systems may be the only effective and safe means of fire fighting.

It is important to note that all the above discussion refers to the effects from exposed stacks of ammunition. Further reductions in the range of explosion effects will almost certainly be gained when the stacks are contained within storehouses.

## 10. Conclusions

A fire in an exposed stack of M1 105mm Cartridges will result in the progressive explosion of about one third of the projectiles over a period of one hour.

Full detonation of the rounds is not observed and the lower order explosions result in small quantities of large fragments. Due to their size, these are considered lethal over the whole projection range.

Fragments are dispersed randomly in azimuthal angle and the fragment density decreases rapidly with range from ground zero.

There is a minimum period of 15 minutes before any explosion occurs. After the first explosion the rate of explosions and consequent fragment projection increases unpredictably and rapidly. Time for fire fighting and evacuation may be limited to the initial 15 minutes.

Comparison of the results of these tests with existing Q-D definitions indicates that some lowering of Q-D's may be possible with small stacks (10,000 rounds) but further analysis of the existing data and development of the fragment recovery techniques is needed before reliable extrapolation to larger stack sizes can be made.

Further development of the post-trials fragment collection techniques must be made to improve the very far-field collection efficiency.

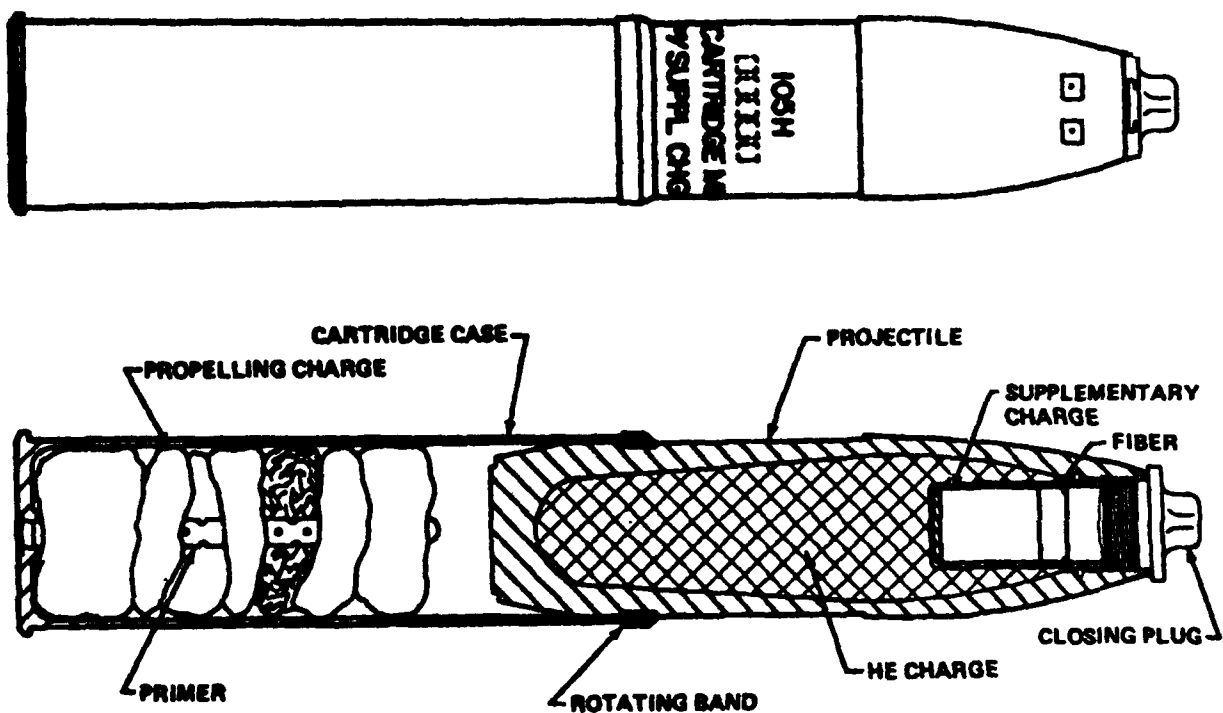
## 11. Future Work

At least two more firings are planned in the exposed stack program. A 27 pallet test is planned for October 1992 followed by a further 8 pallet test in 1993, possibly with a different calibre munition.

A program of tests to evaluate the consequences of accidental explosions in structures has been proposed. Current US and UK opinion is that the Q-D's predicted in this paper can be significantly reduced when surrounded by a reasonably strong building. Currently, efforts are aimed at determining the scope and depth of international interest in the program.

## 12. References

1. DDESB-KT memorandum dated 9 April 1991, Subj: New Class/Division 1.2 Hazard Classification Test Result Interpretations, Alternate Test Procedures, and New Quantity-Distance Considerations
2. Department of Defense Explosives Hazard Classification Procedures, NAVSEAINST 8020.8A (Army TB 700-2, Air Force TO 11A-1-47 Defense Logistics Agency DLAR 8220.1), December 1989.
3. United Nations Recommendations on the Transport of Dangerous Goods, ST/SG/AC.10/1 Current Revision
4. Swisdak, M.M., Jr., "Procedures for the Analysis of the Debris Produced by Explosion Events", Minutes of the Twenty-Fourth Explosives Safety Seminar, Adams Mark Hotel, St. Louis, MO, 28-30 August 1990, pp.2159 - 2175.



#### Nominal Characteristics

Projectile Body:	Forged Steel
Projectile Body Weight :	25.8 lb
Explosive Fill:	TNT
Explosive Weight:	4.5 lb
Propelling Charge Case:	Spiral Wrap Steel
Propelling Charge Case Weight:	4.7 lb
Propellant:	M1 propellant
Propellant Weight:	2.8 lb

Figure 1. M1 105mm Cartridge

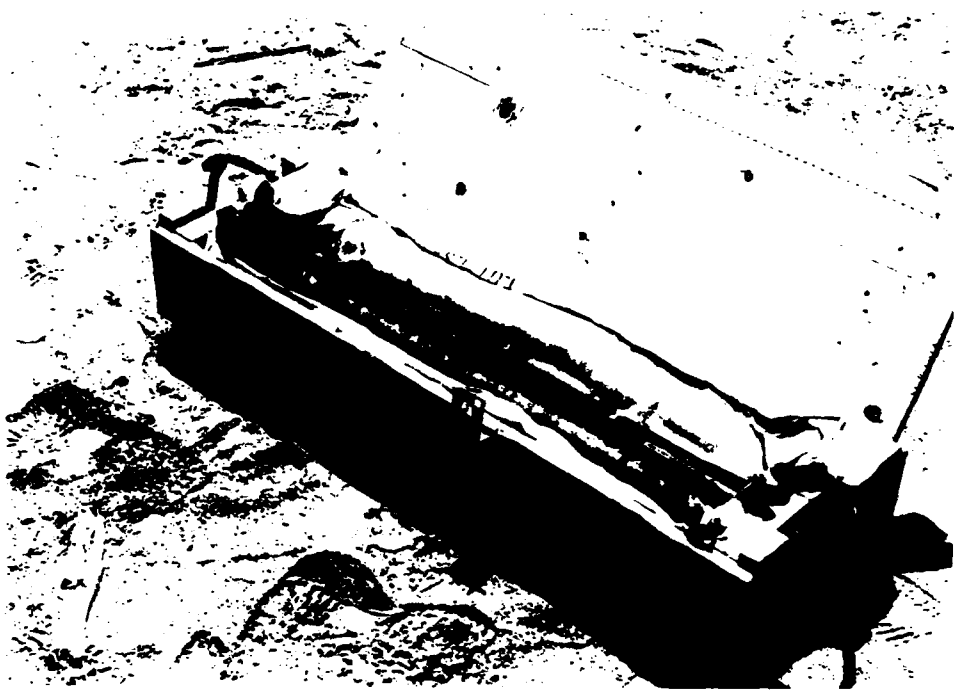
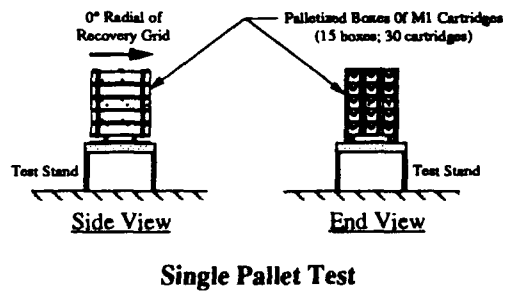
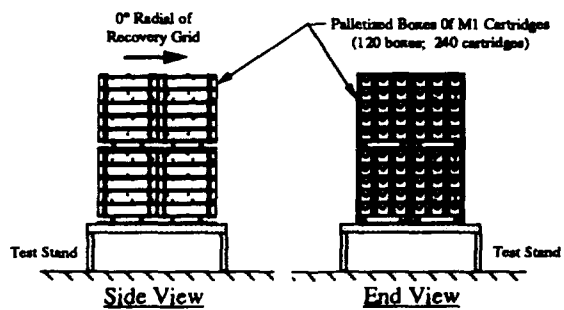


Figure 2. Packaging of M1 105mm Cartridges



#### Single Pallet Test



#### 8-Pallet Test

Figure 3. Stacking Arrangement for Single Pallet and 8-Pallet Tests



Figure 4. Typical Completed Test Setup for the Single Pallet Tests and the First 8-Pallet Test

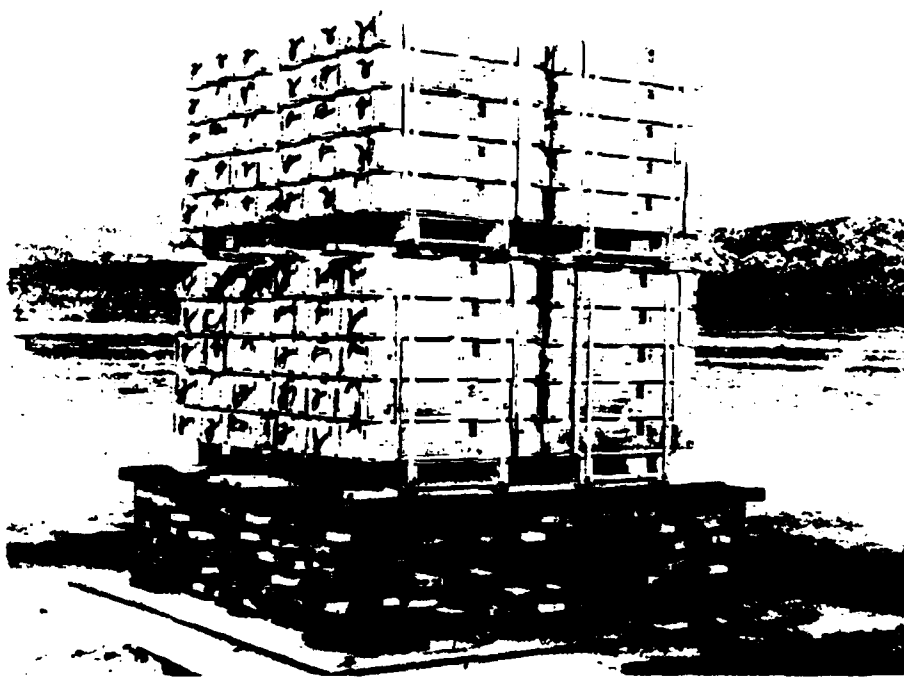


Figure 5. Completed Test Setup for Second 8-Pallet Test

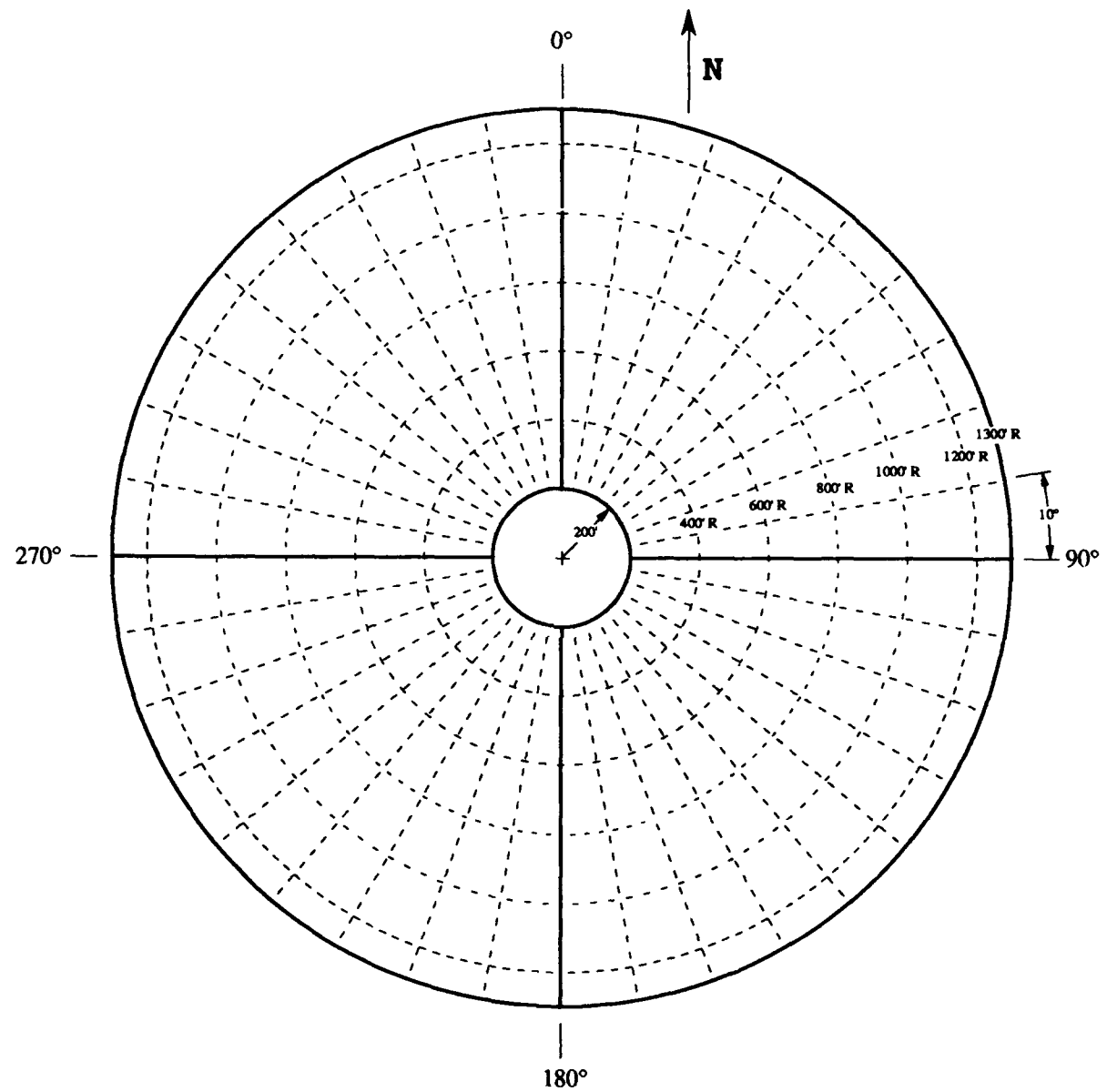


Figure 6. Recovery Grid for HD 1.2 Ammunition Hazards Tests

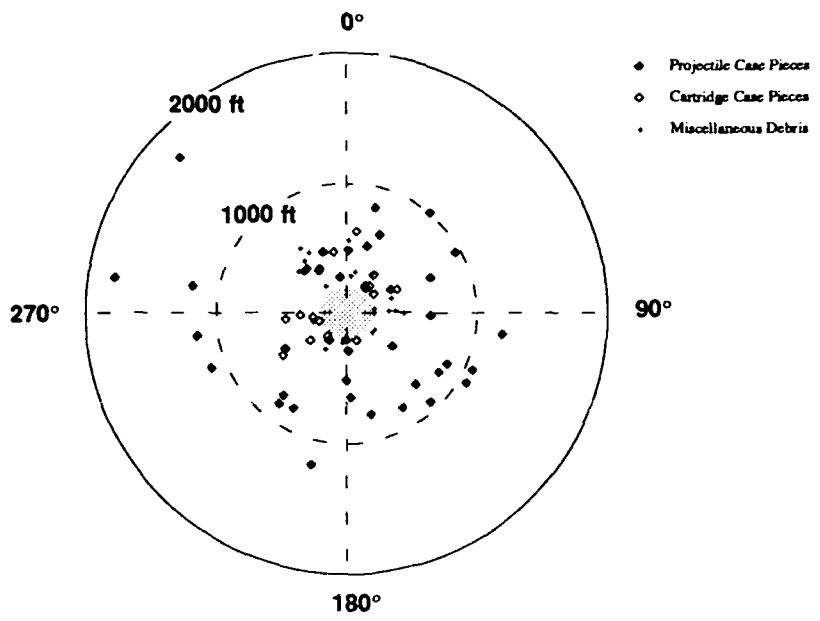


Figure 7. Approximate Distribution of Far-Field Fragments After First Single Pallet Test

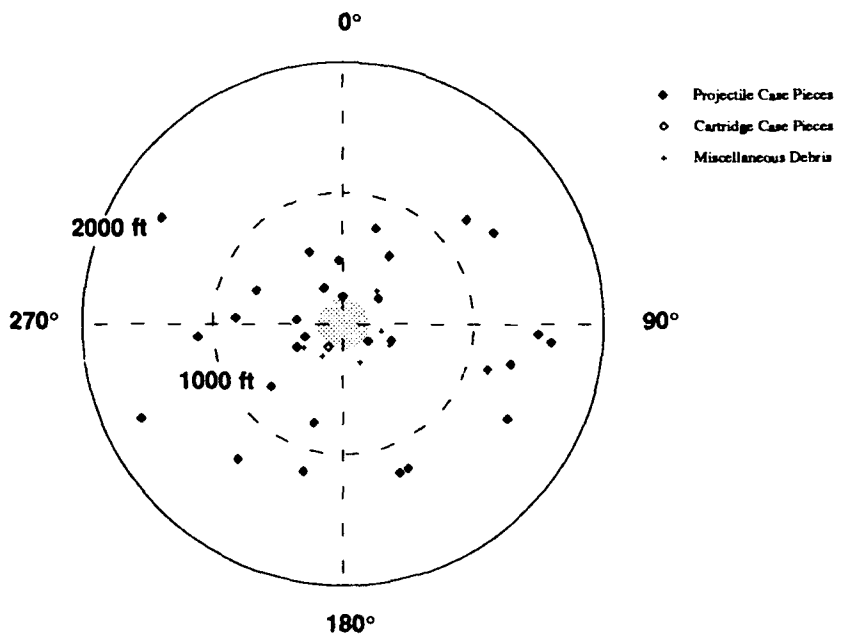


Figure 8. Approximate Distribution of Far-Field Fragments After Second Single Pallet Test

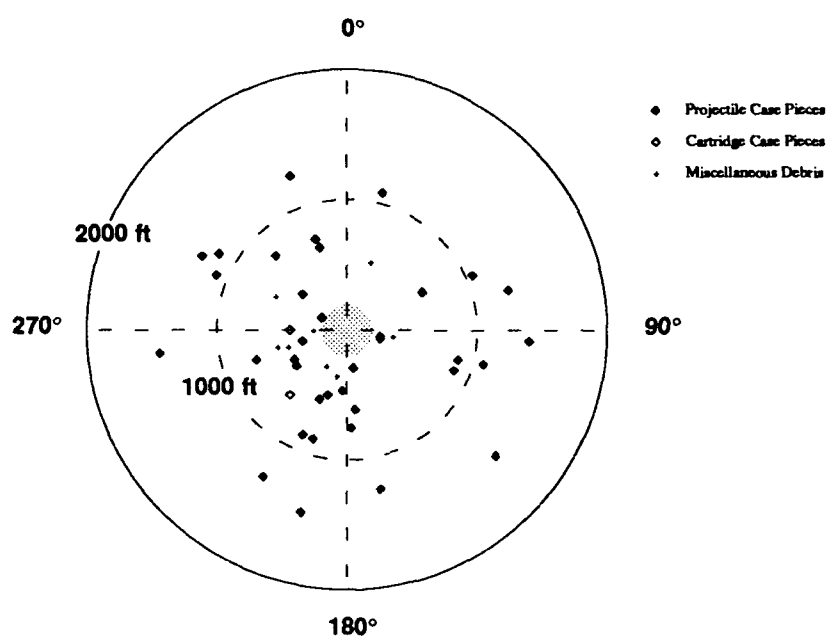


Figure 9. Approximate Distribution of Far-Field Fragments After Third Single Pallet Test

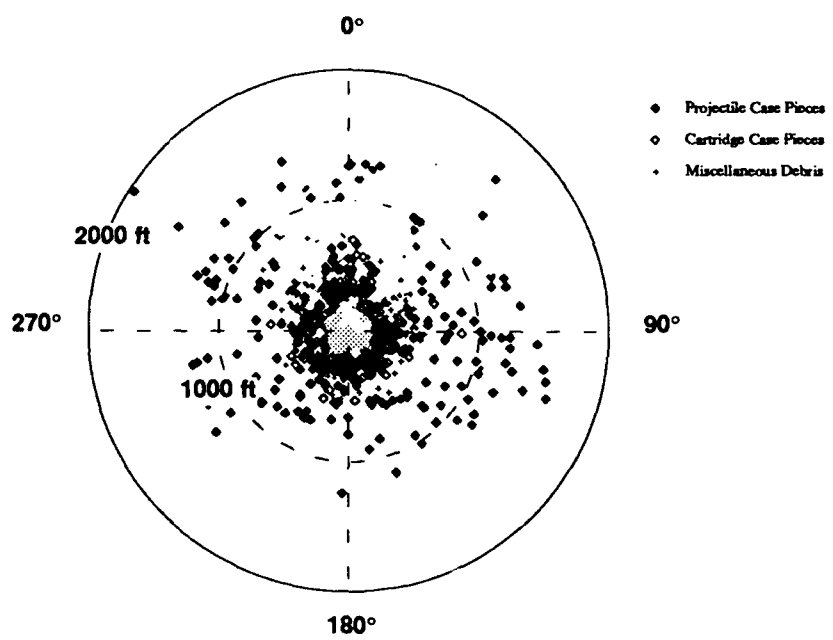


Figure 10. Approximate Distribution of Far-Field Fragments After First 8-Pallet Test



Figure 11. Typical Projectile Case Fragments from Single Pallet Tests



Figure 12. Typical Projectile Case Fragments from First 8-Pallet Test

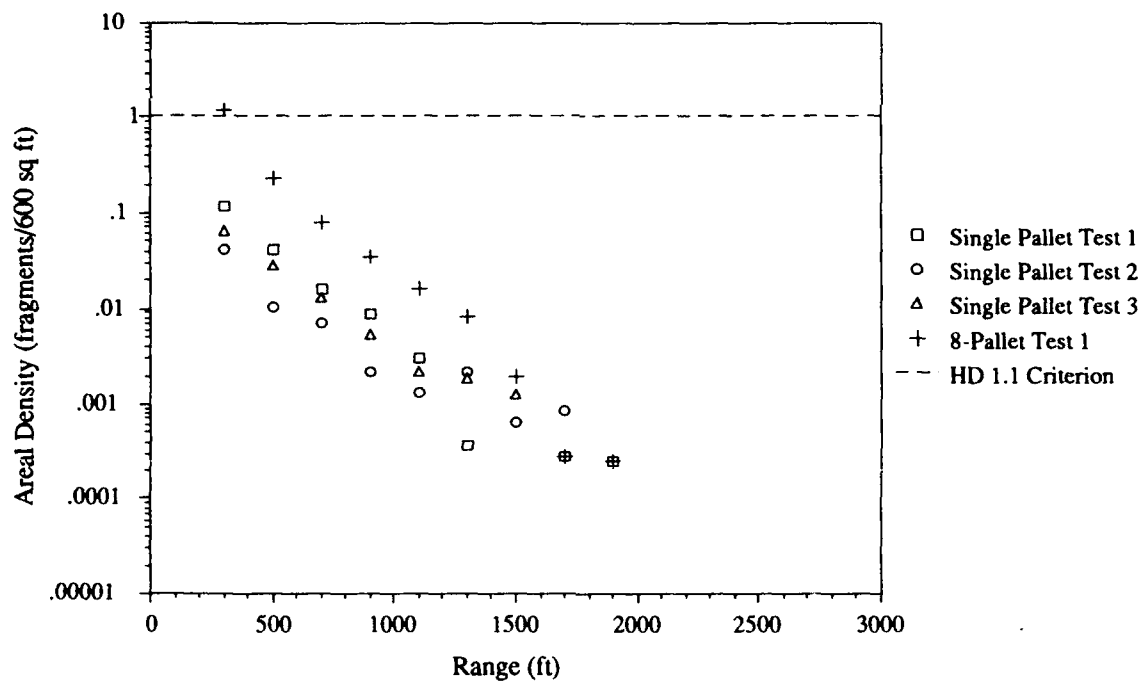


Figure 13. Indicated Fragment Densities Based on Numbers of Fragments Actually Recovered

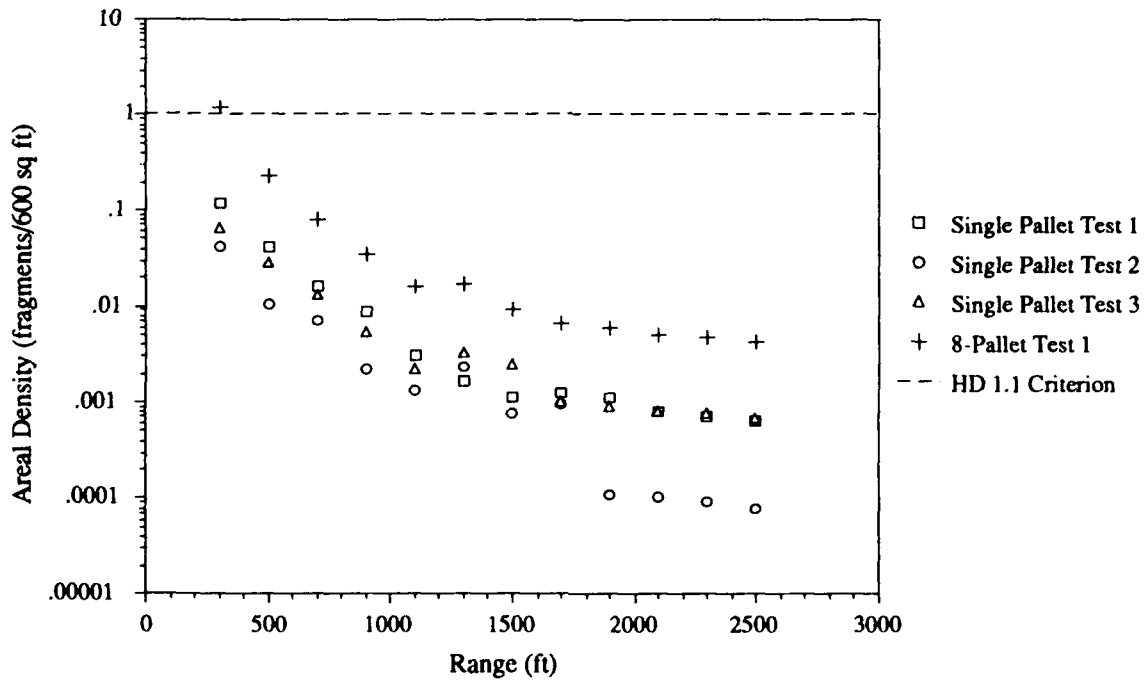


Figure 14. Fragment Densities Obtained Using Adjusted Fragment Counts

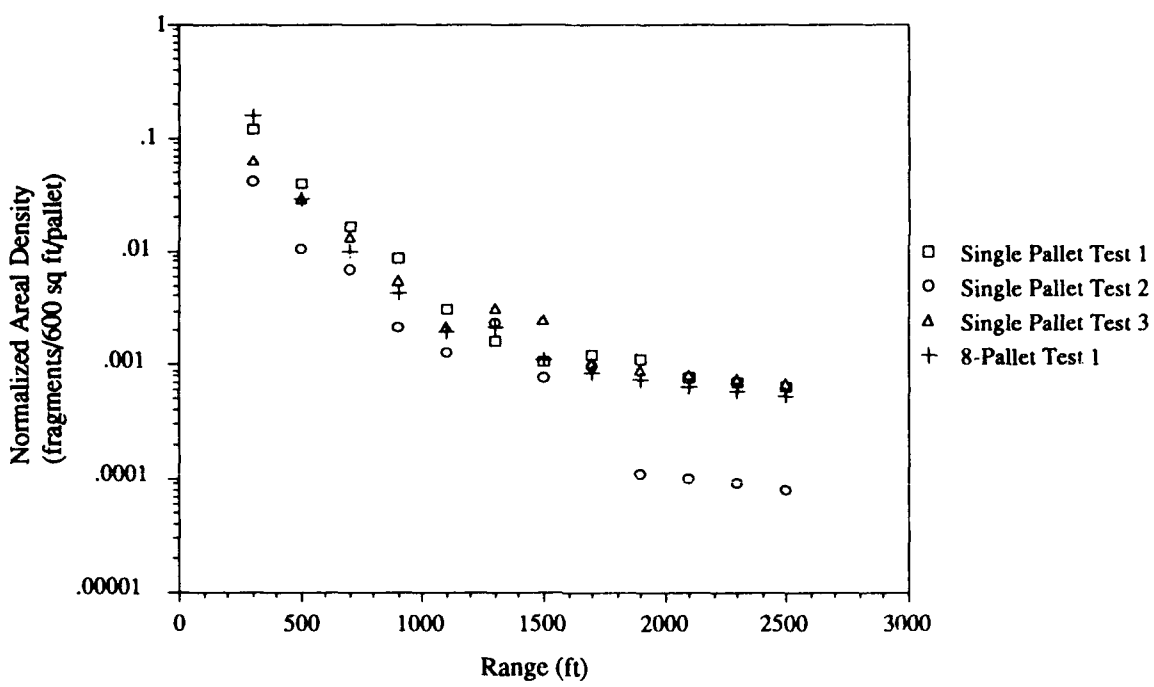


Figure 15. Normalized Fragment Densities

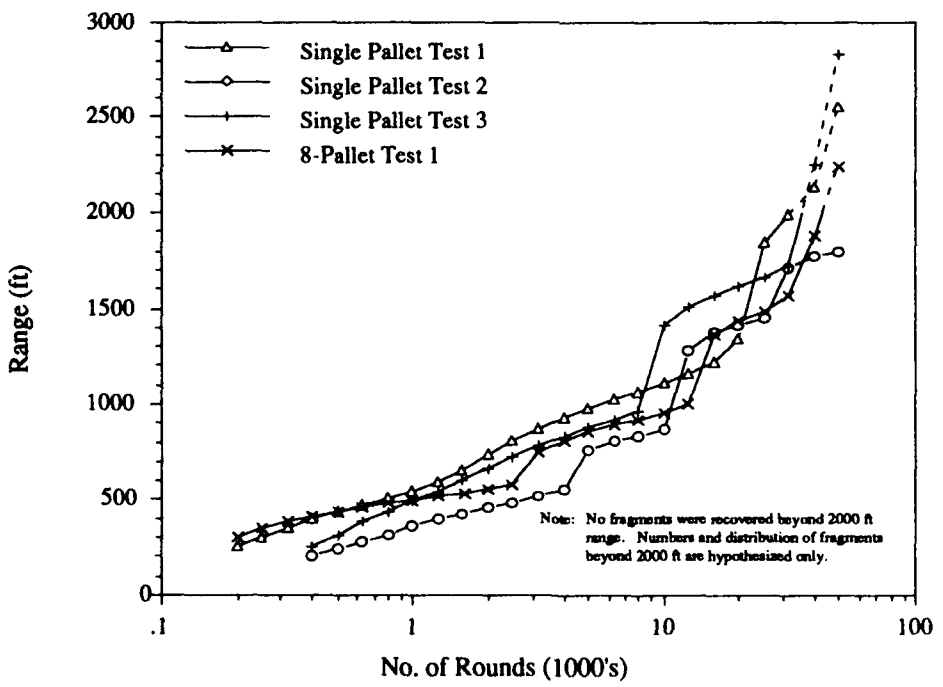


Figure 16. Estimated Ranges to Exceed 1 Lethal Fragment Per 600 sq ft  
Based on Scaled Single Pallet and 8-Pallet Test Results

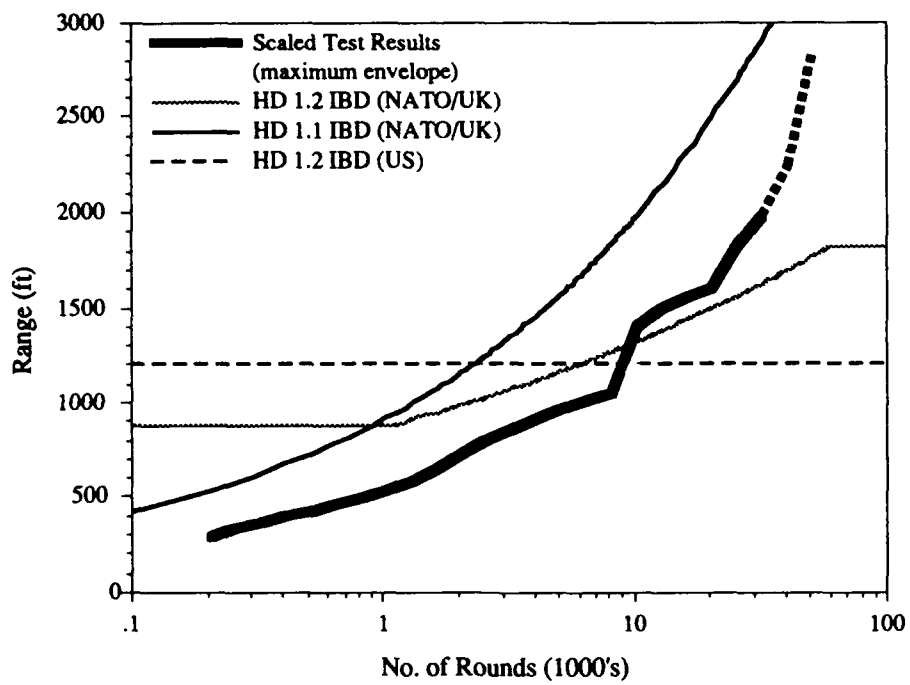


Figure 17. Comparison of Estimated Ranges to Exceed 1 Lethal Fragment per 600 sq ft With Current Quantity-Distance Requirements

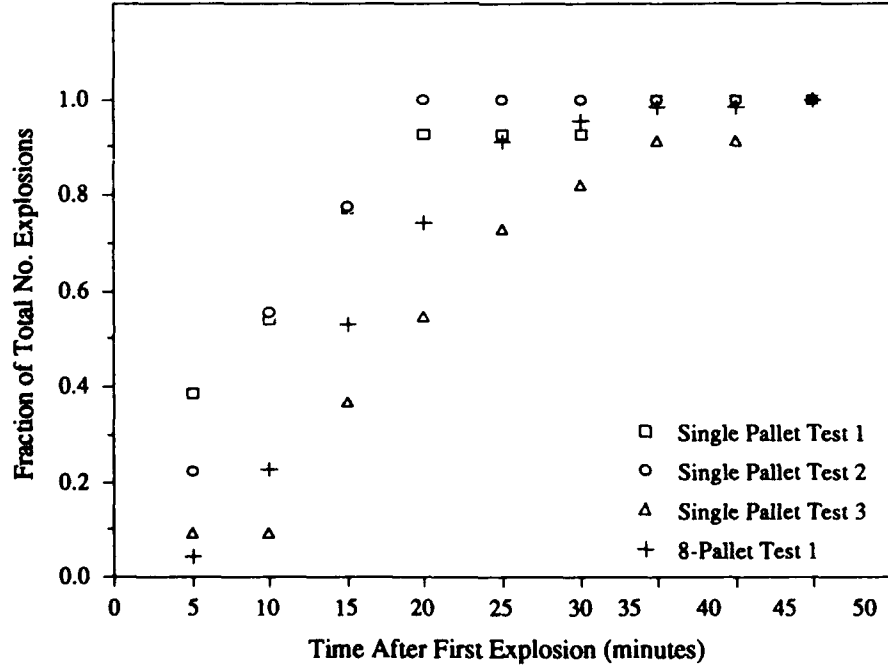


Figure 18. Cumulative Frequency Distributions of Explosions

## **DEFLAGRATING MUNITIONS AND THE MASS DETONATION HAZARD**

**M. Chick, T.J. Bussell, D. McQueen and L. McVay**

**DSTO  
Materials Research Laboratory,  
Melbourne, Australia**

**TWENTY FIFTH DOD EXPLOSIVES SAFETY SEMINAR  
ANAHEIM, CALIFORNIA, USA  
18-20 AUGUST 1992**

### **Abstract**

We have previously reported that collisions, impacts and fragment strikes resulting from violently deflagrating 105 mm shell did not produce detonation of neighbouring rounds and thus were unlikely to be the cause of a mass detonation hazard. This paper reports an extension of that work using 81 mm mortar as a representative thin skinned munition, further tests with 105 mm shell and the determination of parameters that define the behaviour of the violently deflagrating donor. Some tests were conducted with a mixture of the two types of munitions using a 105 mm shell as the deflagrating donor and the 81 mm mortar as acceptors; this was to investigate the effect of larger, thicker fragment strikes on cased ordnance. The investigation relates to the conditions that may be encountered during the storage, transportation and deployment of munitions. All rounds were filled with Composition B.

The investigation did not isolate any process that was likely to be the direct cause of escalating a deflagrating reaction to a mass detonation hazard in a stack of similar munitions. However results from the mixed munition array tests suggests further work to investigate the effect of large, thick fragment impacts on thin cased, damaged fillings. There is some evidence that nose end plugs produce a confinement effect on the deflagration reaction.

## **1.0 INTRODUCTION**

There is convincing evidence [1,2] that mass detonations can result from reactions other than the shocks generated by detonating rounds. In this context Frey and Trimble [3] have demonstrated that non-detonative reactions can propagate through Composition B fillings at up to 2.5 km/s in experimental, tubular assemblies. These reactions are subsonic but close to the shock velocity threshold (bulk sound speed ~2.6 to 2.7 km/s) and thus may be considered to produce the most hazardous effects (fragmentation, overpressure/adjacent shell projection) next to those from a detonating round. We have developed and reported [4] a technique that can produce a predetermined deflagration rate in an explosive filled munition that covers the velocity range from 2.0 km/s up to the bulk sound velocity without a transition to detonation occurring. The development of this technique has enabled a study of the processes that may be considered as candidates in escalating a non-detonative reaction into a mass detonation.

We have previously reported [5] on the first part of the study which used 105 mm shell as representative thick cased munitions. This showed that violently deflagrating 105 mm donor shell did not produce detonation of neighbouring rounds by direct fragment strike, inter-round collisions and single and multiple impacts of projected receptors onto hard surfaces.

This paper reports another stage of the investigation which covered the use of 81 mm mortars as representative thin skinned munitions, further tests with 105 mm shell and the determination of parameters that define the behaviour of the violently deflagrating donor round. All rounds were filled with Composition B. The tests with munition arrays relate to the conditions that may be encountered during the storage, transportation and deployment of munitions.

## **2.0 CONTROLLED DEFLAGRATION FOR MASS DETONATION HAZARD ASSESSMENT**

### **2.1 Technique for Producing Controlled Deflagration of Munitions**

The technique for producing violently deflagrating munitions is described in detail in references [4] and [6] and is summarised as follows. A shaped charge jet is fired along the axis of the munition with a velocity below the threshold to produce detonation of the filling. In this way the reaction produced in and behind the bow wave set-up in front of the penetrating jet sweeps through the length of the filling leaving no bulk explosive for a deflagration to detonation transition. Detonation does not result directly from the bow wave since the pressure-time profile is subcritical [7].

The application of the technique to a Composition B filled 105 mm HE M1 donor shell is shown in Figure 1. The baffle was incorporated in the set-ups that used high speed photography to record the characteristics of the deflagrating munition. The baffle prevented reaction products from the shaped charge device from obscuring the image of the shell. A witness block acted as a check for the type of reaction of the shell filling; a deflagration produced only superficial marks on the surface while a detonation produced a well formed dent with sharp edges. The MRL 38 mm diameter shaped charge was used in the tests since there is a considerable data base on its effect on munition fillings [7,8]. The selected subcritical jet velocity was produced by firing the jet at 2 charge diameters standoff through a steel barrier of appropriate thickness placed in contact with the base of the shell. The jet penetration velocity through the filling can be varied by adjusting the thickness of added steel; this is calculated using the method detailed elsewhere [4,6]. The preselected thickness is based on the requirement to erode a sufficient portion of the front of the jet so that the velocity of the tip that enters the filling is at the required value. In the majority of these experiments the total steel thickness (barrier, baffle, shell base) was calculated to be 93.5 mm to give the selected jet penetration velocity in the filling of 2.5 km/s. Since the jet penetration bow wave is coupled to the jet and reactions occurs within the bow wave, it is assumed that the deflagration velocity has a similar value.

## 2.2 Characterisation of Deflagrating Munitions

The characteristics of the deflagrating munitions were recorded with a rotating high speed camera by the method described in detail in reference 6. The framing rate of 35,000 to 40,000 frame/s gave an exposure time per frame and an interframe time of about 2.7  $\mu$ s and 25  $\mu$ s respectively.

Parameters selected to characterise the deflagrating munitions were; case expansion rate, initial fragment velocity, time to case burst, time to reaction from the nose end and the deflagration rate of the filling, see Figure 2. Values for these parameters for the 105 mm shell are given in Table 1. Results from the 81 mm mortar are not included since early case breakup limited the data extracted from the high speed camera records. The listed times were taken from the detonator firing pulse. The times from jet entry into the Composition B filling are 55  $\mu$ s less than these values; this is the estimated time for the functioning of the shaped charge device and for the jet to travel across the standoff distance and penetrate through the steel into the filling. Deflagration commencement was assumed to coincide with jet entry into the explosive. The fragment velocities are taken as half the final case expansion velocities. The first sign of products escaping from the case was taken as the onset of case burst. Products escaping from the fracturing case eventually obscured the photographic image and this was the limiting factor in the measurements, in some tests this precluded an estimate of some data. The limit on the accuracy of the time is the interframe time of about 25  $\mu$ s.

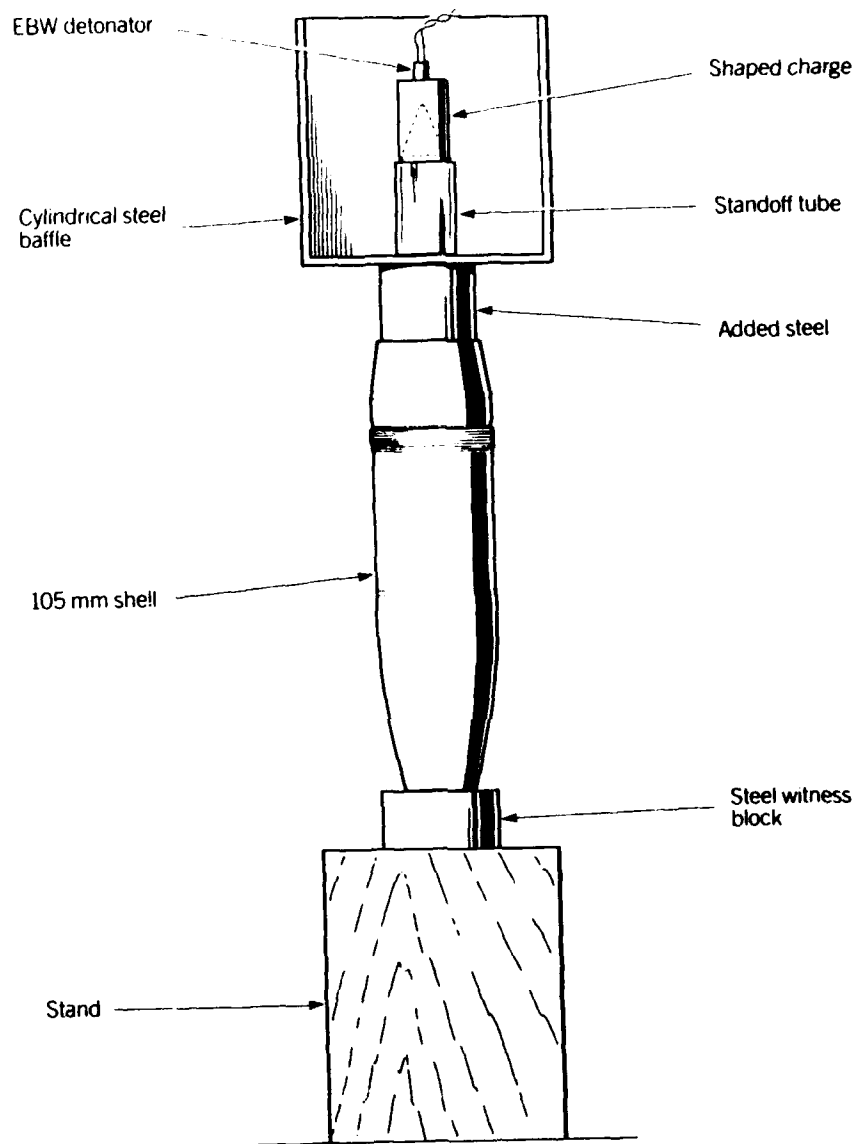


FIGURE 1

Experimental set-up for the controlled deflagration of a 105 mm shell

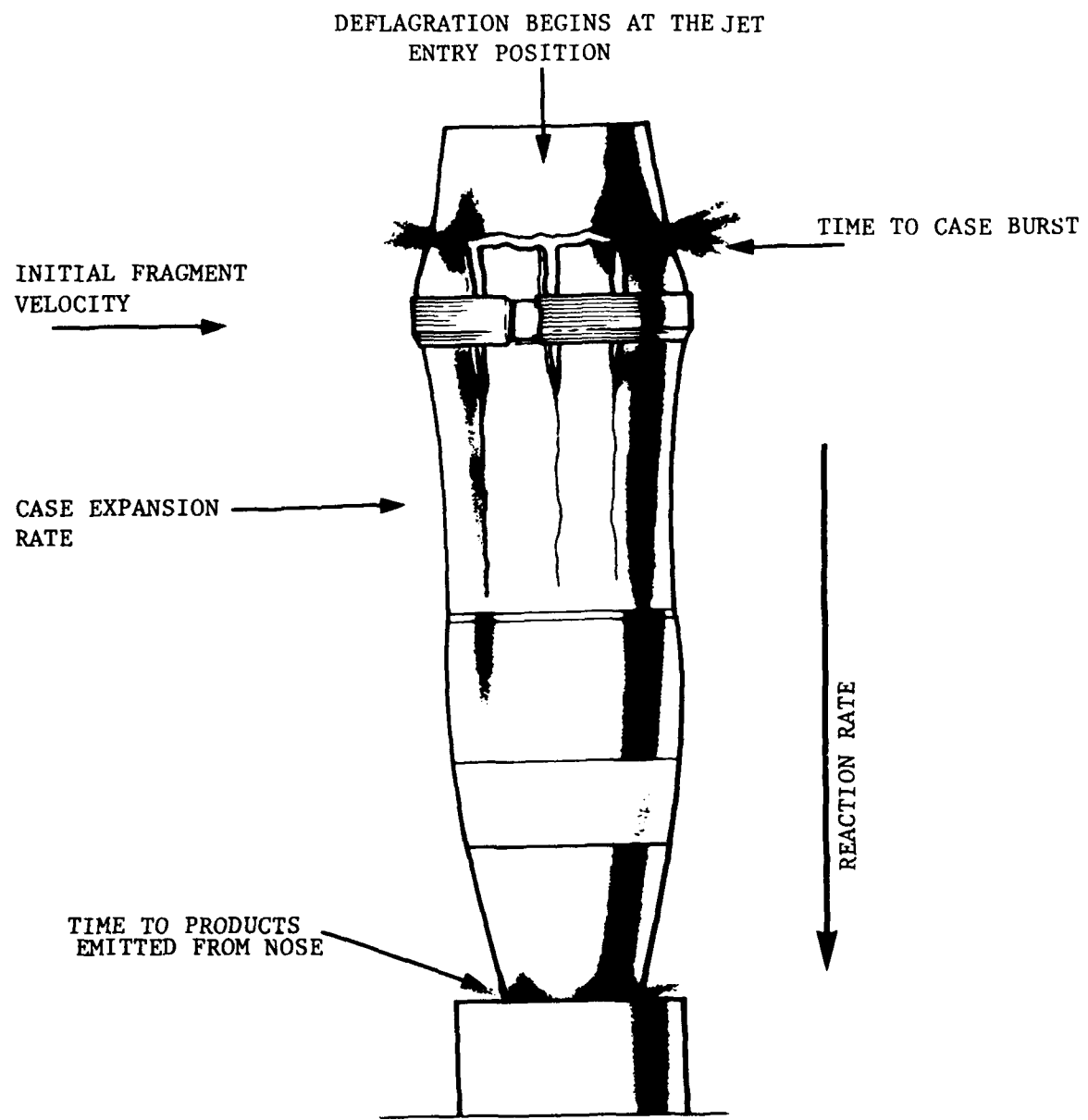


FIGURE 2

Parameters selected to characterise  
a deflagrating munition

Time to signs of reaction from the nose end and the time to case burst were used to assess the effects of the confinement provided by plugs that represented fuzes (PRF) and transit plugs. The use of a PRF rather than a fuze avoided complications from the effects of the jet and/or reaction on the booster and explosive components in the fuze. Case expansion rate and initial fragment velocity were used to assess the effects of impacts from the deflagrating donor shell case on neighbouring rounds. The deflagrating rate was estimated from the measurement of the time to the onset of case expansion at several positions along the length of the munition. Reference to Table 1 shows that the measured values are in reasonable agreement to the preset calculated values.

Figure 3 shows a representative high speed camera film sequence of a deflagrating unplugged 105 mm shell that corresponds to shot 1 in Table 1. The jet deflagration device was fired from the top of the picture. The baffle around the shaped charge device prevents the detonation products from the shaped charge device from obscuring the view of the shell. Three frames from the start of the sequence in Figure 3, reaction products can be observed escaping from the nose end of the shell; this is followed five frames later by products escaping from the fracturing case in the region of the driving band. Graphical representation of case expansion data for the 105 mm unplugged shell is given in Figure 4. The three curves correspond to three positions on the shell case; the first point was 120 mm from the base just below the driving band, the second was 180 mm from the base near the mid length position and the third was 240 mm from the base near the booster cavity. Shell expansion prior to breakup was about 30% of the initial diameter (ie 15 mm increase in the shell radius).

### **3.0 HAZARD ASSESSMENT OF DEFLAGRATING DONORS IN MUNITION ARRAYS**

#### **3.1 105 MM HE Shell**

We have previously reported [5] on candidate processes by which a deflagrating donor Composition B filled 105 mm HE shell may produce a mass detonation hazard. The 105 mm shell was taken as a representative thick cased munition. The study showed that deflagrating donors did not produce detonation of neighbouring rounds by direct fragment strike, inter-round collisions, single and repeated impacts of projected shell onto hard surfaces and transient interactions in a shell filling induced by near simultaneous collisions.

The data in Table 1 indicates that initial case fracture of the 105 mm shell occurred earlier for the plugged than for the unplugged rounds. This suggests that product pressure build-up may have influenced the process. However Table 1 data also suggests that any confining effect by the plug may not have been translated into higher case expansion and fragment velocities although the fragment velocity data is limited. In order to assess the role of plugged donor rounds and to investigate

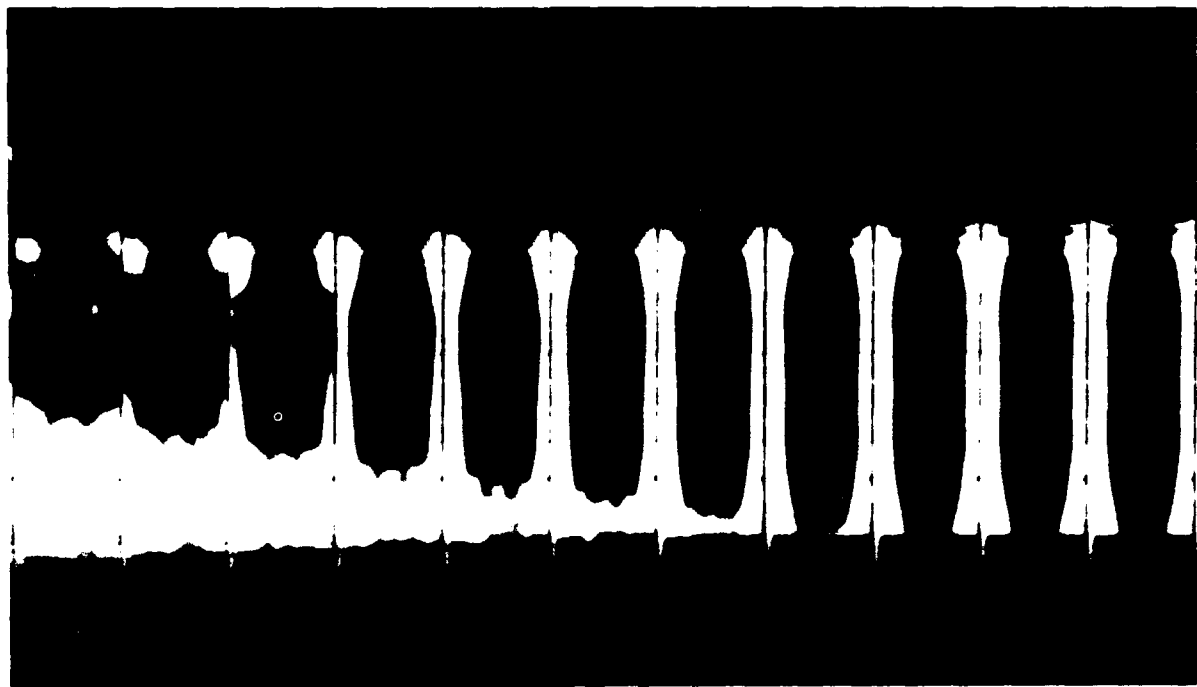


FIGURE 3

Section of high speed camera record showing the deflagration of an unplugged 105 mm HE shell

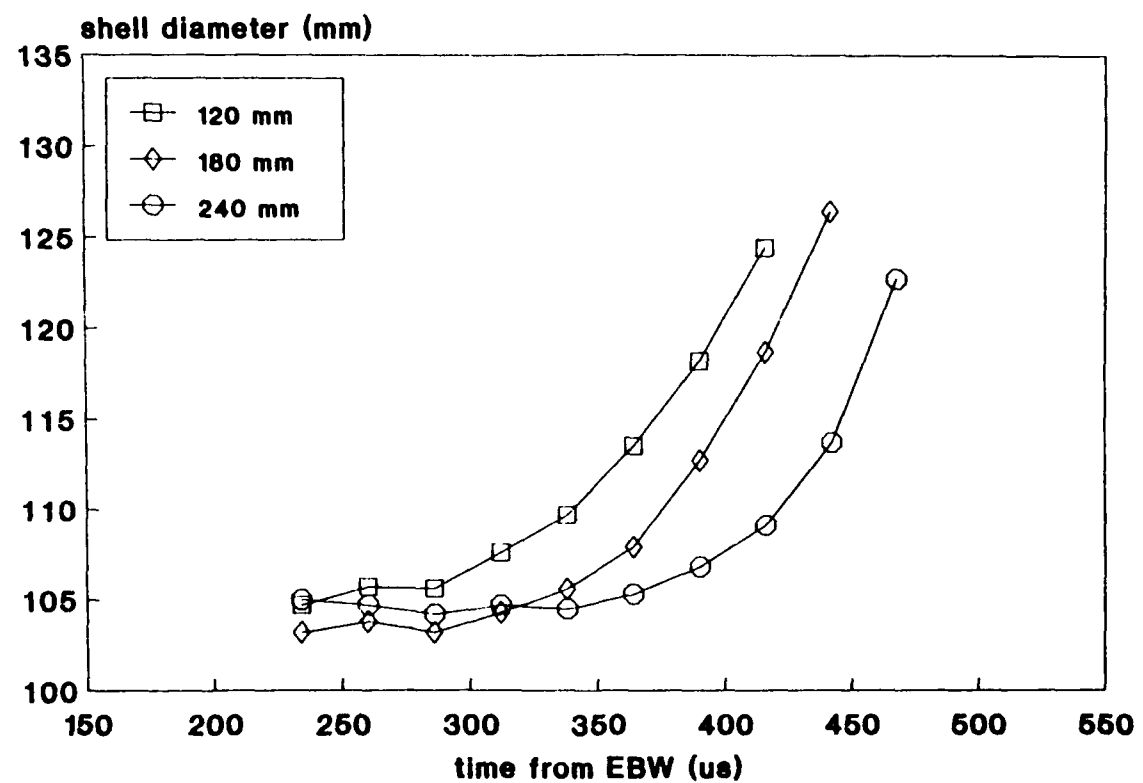


FIGURE 4

Plots of the expansion of a deflagrating 105 mm shell case

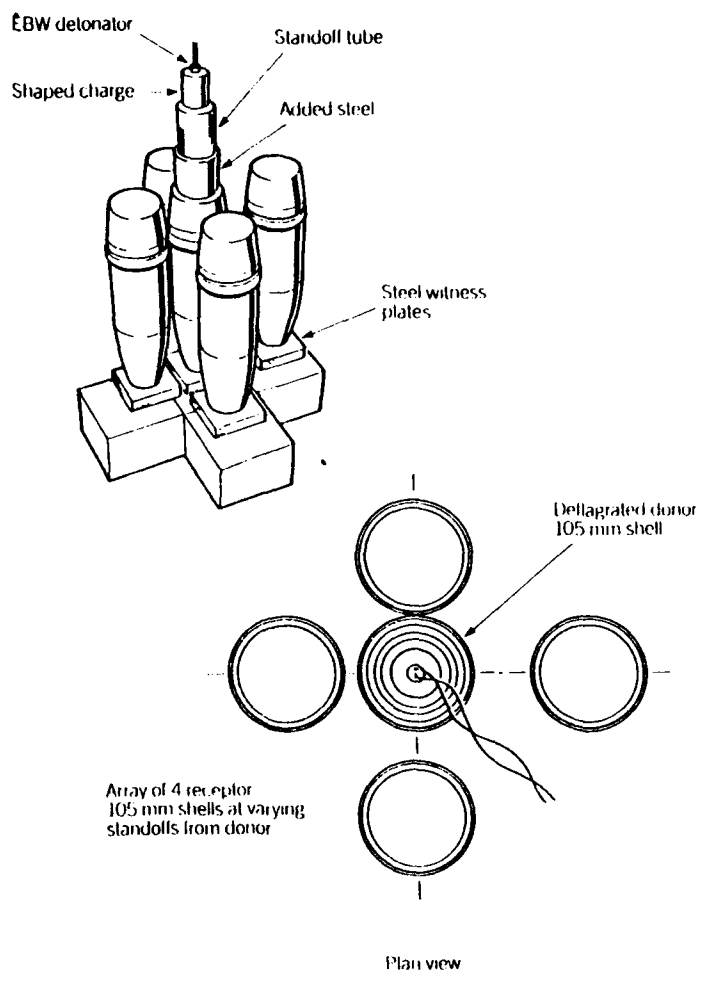


FIGURE 5  
Set-up for deflagration donor - multiple receptor tests

TABLE I  
Characteristics of the controlled deflagration of  
Composition B filled 105 mm shell  
(Pt represents points as defined in the text, Section 2.2)

Shell Configuration	Time from the Detonator Pulse to Event			Deflagration Propagation Velocity		Maximum Expansion Velocity km/s	Estimated Initial Fragment Velocity km/s
	Initial Case Fracture $\mu$ s	Products from Nose $\mu$ s	Image Obscured $\mu$ s	From Case Expansion Data km/s	Calculated km/s		
Unplugged SHOT 1	440	310	490	2.3	2.5	*Pt 1, 0.24 Pt 2, 0.30 Pt 3, 0.35	Pt 1, 0.12 Pt 2, 0.15 Pt 3, 0.17
Unplugged SHOT 2	460	460	530	2.5	2.5	Pt 1, 0.22 Pt 2, 0.36 Pt 3, 0.22	Pt 1, 0.12 Pt 2, 0.18 Pt 3, 0.11
Plugged SHOT 3	340	470	440	-	2.5	Pt 1, 0.12 Pt 2, 0.08	Obsured by Products
						Pt 3, 0.20	0.1
Plugged SHOT 4	320	450	370	-	2.5	Obsured by products	

fragment strikes on the central region of receptor shell where the case is at its thinnest (10 mm), further donor-receptor standoff tests were conducted using 105 mm shell. The experimental assembly is shown in Figure 5. Two experiments were undertaken with donors plugged with a PRF. Donor heights were adjusted to maximise fragment impacts on the central region of the receptor cases. In one test the 3 receptor rounds were placed at 1 charge diameter (105 mm) standoff from the donor and in the other the standoff distances were  $\frac{1}{2}$ , 1 and 2 charge diameters. Soft recovery of projected shell was provided by sand bag walls 1 m from ground zero.

In both tests the receptors were recovered intact but with flattened faces. Some exhibited imprints of fragment strikes along the central region of the case; the largest imprint being about 160 mm by 20mm by 1 mm deep. Two repeat shots were undertaken using the recovered receptors with the flattened faces away from the donor. In one test the 3 receptors were placed at  $\frac{1}{2}$  charge diameter standoff and in the other they were placed at 1 charge diameter standoff. The receptors were again recovered intact but exhibiting two flattened faces and further imprints from fragment strikes.

Reference to Table 1 shows that both plugged and unplugged 105 mm shell produced fragment velocities in the range 100 to 180 m/s, although the limited data for the plugged rounds should be treated with caution. These velocities are considerably lower than the critical impact velocity for the detonation threshold of several hundred meters per second for Composition B receptors with a 10 mm steel cover [9]. Also the fragment velocities for detonating Composition B loaded 105 mm shell are about 1.1 km/s [10] and these have produced receptor detonations in other tests in our study using the set-up shown in Figure 5. However it should be noted that in many of our tests the shell filling was damaged and exhibited increased sensitivity compared to a normal round [5]. A further feature of these tests is that the shell/target impacts represent fragment sizes beyond those reported in Reference 9.

The effect of heavy side confinement produced by a munition stack surrounding a single deflagrating 105 mm shell was investigated. This was undertaken by placing a shell as a push fit into a 15 mm thick, steel walled tube that covered the length of the munitions. The assembly was designed to prevent the deflagration process from producing an early break in confinement by restricting the initial stages of case expansion. We consider this test represents an extreme example of side confinement. The round was deflagrated in the normal manner. The steel tube was split open and recovered within 1 m of the firing position. Shell case fragments were recovered inside and around the steel tube and they were typical of a deflagrating munition. Therefore we conclude that a deflagration to detonation transition did not occur.

Thus neither the experiments investigated in this study or those previously reported with Composition B loaded 105 mm HE shell produced results to support a process by which a violently deflagrating donor may produce a mass detonation. This was despite some evidence that nose plugs may produce a confinement effect that influences case expansion.

### **3.2 81 mm Mortar**

The 81 mm mortar was selected to investigate the propensity for deflagrating thin cased munitions to produce mass detonation in neighbouring rounds. The mortar is filled with Composition B and the thickness of the case around the central region is 5 mm.

One series of tests was conducted using a set-up similar to that shown in Figure 5 except that the deflagrating central donor and the receptors were 81 mm mortar. Experiments were conducted with the receptors at 0,  $\frac{1}{2}$ ,  $\frac{3}{4}$  and 1 charge diameter standoff. Like the 105 mm shell firings, tests were undertaken without booster and fuzes, with pressed TNT flake boosters and PRF's and with recovered damaged rounds. In two tests the donor height was adjusted in order to allow fragment strikes at the central region of the receptors. All donors deflagrated as planned. Recovered receptors had flattened faces and damaged fillings but the cases were intact; some had markings from fragment strikes. Recovered receptors from repeated firings had 2 flat faces.

In another series of tests the deflagrating donor was used to project an adjacent round to impact a concrete wall or steel plate. Firings were conducted with mortars without boosters and fuzes, with boosters and PRF's and recovered damaged rounds. The projection velocity of the receptor was determined using high speed photography to be 30 m/s. In these tests the explosive filling will have been damaged (sensitised) prior to impact on the hard surface by the projection process.

All donors deflagrated as planned and the recovered projected rounds had flattened faces, damaged fillings but the cases were intact.

These experiments suggest that for simple arrays a violently deflagrating 81 mm mortar is unlikely to be the direct cause of a mass detonation by the effects of fragmentation/blast on near neighbours or by the projection and impact on adjacent rounds.

### **3.3 105 mm Shell and 81 mm Mortar Mixed Arrays**

Experiments with mixed munition arrays with 105 mm shell as the deflagrating donor and 81 mm mortar as the receptors were undertaken to assess the effects of large, thick fragments on thin cased damaged fillings. In this context the 105 mm shell has a significantly larger explosive mass than the 81 mm mortar (3.5 kg compared to 1.0 kg) and the central region case thicknesses are 10 mm and 5 mm

respectively. The test array set-up was similar to that shown in Figure 5. The damaged mortar rounds were recovered from other tests; therefore their fillings would be more sensitive than unused rounds and thus have a lower detonation threshold to fragment impact.

In two tests undertaken with a plugged 105 mm shell as donor, the 81 mm mortar receptors detonated and witness block marks indicated the donor deflagrated as planned. For the third experiment which had an unplugged 105 mm shell as donor, the 81 mm receptors did not detonate but were split open with the filling dispersed. It is not possible to draw any firm conclusions from these few tests but the results suggest further study with the conditions that may be expected to maximise the mass detonation hazard from deflagrating rounds.

#### **4.0 CONCLUSIONS**

The characteristics of Composition B loaded 105 mm shell and 81 mm mortar deflagrating at a rate of about 2.5 km/s have been determined. Some of these characteristics are important in assessing the role of violently deflagrating rounds in mass detonation. There is some evidence to suggest that nose plugs may confine the deflagration process and affect the onset of case breakup. Violently deflagrating 105 mm shell and 81 mm mortar did not cause detonation of neighbouring munitions in tests with multiple acceptors and projected acceptors impacting on hard surfaces. These tests used receptors with and without boosters and nose plugs; repeat shots used recovered damaged receptors.

Preliminary results using deflagrating, plugged 105 mm shell donors that detonated damaged 81 mm mortars suggest further study into the conditions that may be expected to maximise the mass detonation hazard from violently deflagrating munitions.

#### **5.0 ACKNOWLEDGMENTS**

We express our gratitude to the Officer Commanding and support personnel of the Army Proof and Experimental Establishment, Graytown, Victoria for assistance with the field firings and ensuring the ready availability of support resources.

#### **6.0 REFERENCES**

1. Frey R.B., Watson J., Gibbons G., Boyle V. and Lyman D. Proceedings of the Joint Government Industry Symposium on Insensitive Munitions Technology, NSWC, White Oak, Maryland, US, March 1990.
2. Stosz M. TTCP WAG-11 Workshop, Quebec, Canada, 1987.

3. Frey R.B. and Trimble J.J. Proceedings Seventh International Symposium on Detonation, NSWC, MP82-334, 1981.
4. Chick M. and Bussell T.J. Paper in course of publication.
5. Chick M., Bussell T.J. and McVay L. Proceedings of 24th DOD Explosives Safety Seminar, St. Louis, Missouris, USA, August 1990.
6. Kinsey T.J., Bussell T.J. and Chick M. MRL Technical Report MRL-TR-91-42, 1992.
7. Chick M., Bussell T.J., Frey R.B. and Bines A. Proceedings of Ninth Symposium (International) on Detonation, Portland, Oregon, USA, 1989.
8. Chick M. and Hatt D.J. Proceedings of the Seventh Symposium (International) on Detonation, NSWC MP82-334, 1981.
9. Howe P., Watson J.L. and Frey R.B. Proceedings of Seventh Symposium (International) on Detonation, NSWC, MP82-334, 1981.
10. Jenks G.J., Lynch B.J., Masinskas J.J. and Oliver D.J. DSL Report 489, 1972, Confidential.

# **FRAGMENTATION CHARACTERISTICS OF HORIZONTALLY STACKED BOMBS**

by  
**Frank McCleskey**  
**Booz•Allen & Hamilton**

**For Information Contact:**

**Frank McCleskey  
Route 3, Box 105  
King George, Virginia 22485  
703-775-7210**

**25th DOD Explosives Safety Seminar  
18-20 August 1992  
Anaheim, California**

## INTRODUCTION

The FRAGHAZ Computer Program<sup>1</sup> was developed by the Naval Surface Warfare Center (NSWC/Dahlgren) for the Department of Defense Explosives Safety Board (DDESB). The primary purpose of the program was to provide a means for estimating the fragment hazards to personnel from the inadvertent detonation of stacks of stored munitions.

The Computer Program is primarily a Monte-Carlo type incorporating the capability of statistically handling a number of uncertain variables. The model relies on small-scale fragmentation arena tests to provide the fragment data for full-scale ammo stack investigations. Each fragment recovered from the test, greater than a specified minimum weight, forms the basis for a trajectory which is calculated in its entirety using a fourth order Runge-Kutta routine.

The intersection of the fragment trajectory with a hazard volume (a pie-shaped volume with an angular width, usually 10 degrees or less, and a height equal to the target height) provides the means for calculating the fragment hazard to the target in terms of density and probability of hit. Since we calculate the entire trajectory, we know both the static and dynamic characteristics of the fragment at all ranges where the trajectory intersects the hazard volume. The target is assumed to be randomly located within the hazard volume and the hazard volume ranges are normally divided into 100 feet increments.

A number of fragments is associated with each trajectory to represent the number expected from a full-scale stack. The results for the intersection of each trajectory with the hazard volume are recorded and accumulated. After all fragments trajectories are run, the procedure is repeated (replicated) about 60 times with different values for the uncertain variables. This is normal for a Monte-Carlo procedure. Statistical data are then obtained from the results of the 60 replications as a function of range (usually in 100 foot increments).

The FRAGHAZ program includes the effects of ground ricochet, altitude (air density and Mach number), complete drag curves, wind, target impact angle, and varying fragment velocity.

Correspondence of the predictive number of fragments versus range and actual pickup tests in the desert has been checked for two stacked munition cases. The comparison was good and is contained in the FRAGHAZ Computer Program report.<sup>2</sup>

### MK 82 (500 LB) BOMB HORIZONTALLY STACKED MUNITIONS

For projectiles and bombs, there are basically two types of storage: (1) vertical storage (155mm projectiles) and (2) horizontal storage (MK 82 bombs). These two types of storage are depicted in Figure 1 - horizontal storage on the top left and vertical storage on the top right. For both types of storage, a hazard elevation sector is shown. The sides of the elevation sector form a

---

<sup>1</sup>Quantity-Distance Fragment Hazard Computer Program (FRAGHAZ), NSWC TR 87-59, Frank M<sup>c</sup>Cleskey, Feb 1988, Unclassified.

<sup>2</sup>Ibid

dihedral angle; the intersection of the dihedral planes form a vertical line on the face of the stack. All fragments are assumed to begin their trajectories along this vertical line which is acceptable so long as the width of the stack is no more than 200 feet or so. All fragment trajectories contained within the dihedral angle will ultimately intersect the hazard volume whose angular width is equal to the dihedral angle.

The most hazardous fragmentation is contained within the hazard elevation sector. Between adjacent projectiles or bombs, interaction areas (jets) are formed which have higher velocities, higher fragment densities, and higher fragment weights than those produced by a single projectile or bomb detonation. In order to obtain the approximate fragment characteristics of the hazard elevation sector, the projectiles or bombs are rotated 90 degrees and tested in a horizontal fragmentation test arena as shown in the left bottom and right bottom of Figure 1. The hazard elevation sectors are shown as dotted lines in the bottom views of Figure 1. Note the relation of elevation angles (EL) and polar angles (PA) in the Figure.

The fragmentation characteristics from the vertically stored munitions are fundamentally different from the horizontally stored munitions. On the right top of Figure 1, the top of the vertically stored stack does not appear to produce any significant down range fragmentation. Conversely, the horizontally stored munitions have both top and side interaction areas (jets) when the stack is detonated simultaneously or nearly so. Depending on the initiation point, the top interaction areas will produce downrange fragmentation. Fragmentation from the top interaction areas will normally go to shorter ranges than the fragmentation from the side of the stack. Since the hazard elevation sector (Figure 1) is like an orange slice coming to a point at Elevation Angle = 90 degrees (Polar Angle = 0 degrees), a smaller portion of the fragmentation from the top interaction areas will be used in the FRAGHAZ Program.

Fragmentation from vertically stored munitions will consist of only one zone while fragmentation from horizontally stored munitions will consist of four zones as shown in Figure 2. Here the bottom-middle bomb is assumed to be the initiation point and the remainder of the bombs are initiated by sympathetic detonation. Lines drawn from the center of the initiator bomb can be drawn to show approximately the four zones of downrange fragmentation from a single pallet (6 bombs) of MK 82 bombs. The fragmentation in zones 1 and 3 comes from 180 degrees of the bomb cases. This is only approximate since the dynamics of the interaction areas (jets) are not clearly understood. Zones 2 and 4 are taken to be normal fragmentation areas as you would experience with a single bomb.

Looking at fragment numbers or fragment weight does not clearly outline the four zones. Looking at initial velocity versus polar angle, Figure 3, does show the zone separations. The actual velocities from a single test, shown in Figure 3, still leave some questions, but the existence of zones appears to be clearly defined. Note that the initial velocities of fragments in the interaction areas (zones 1 and 3) are approximately 40 percent higher than the initial velocities of a single round beam spray. The initial velocities in the normal areas (zones 2 and 4) are somewhat lower than the velocities obtained from a single bomb. This is not clearly understood.

It is interesting to note the effect on a fragment's range produced by changes in its initial velocity, average presented area to mass ratio, or drag coefficient. Range is dependent on initial kinetic energy, a function of  $V^2$ , but the retarding effects of air drag are also a function of  $V^2$ . The two tend to offset one another with the initial kinetic energy dominant, but not as much as one might suspect. As shown in Table 1, increasing initial velocity threefold, with other variables held constant at any values, produces only a 30 percent increase in range. For example, if the range at an elevation angle of 20 degrees was 1000 feet for an initial velocity of 2000 ft/sec, it would only

increase to 1300 feet when the initial velocity was increased to 6000 ft/sec. On the other hand, if the drag coefficient or  $\bar{A}/m$  was decreased by a factor of 3, the range would increase by 120 and 150 percent, respectively. The range increases are 4 and 5 times greater than those obtained with a similar factor of 3 increase in initial velocity. For the MK 82 bomb, where we have only a 40 percent increase in initial velocity for an interaction area (jet) over a single bomb, we would see only a 5 percent increase in range. Apparently it is fragment density rather than initial velocity which controls hazard range. Hazard range depends not only on fragment range but on the hazard density being greater than one fragment per 600 square feet (hazard probability of hit being greater than .01 with a constant presented area of the personnel target equal to 6 square feet). The density of fragments in the interaction area (jet) for the MK 82 bomb is at least twice that for the beam spray of a single bomb.

In all mass detonation tests to date the projectiles or bombs have been in contact with one another. Separation (maybe by only inches) of the projectiles and bombs in the stack would ultimately prevent the formation of interaction areas (jets) and thus significantly reduce hazard range due primarily to reduced fragment density. Future tests are worth considering since hazard ranges in some cases might be reduced by as much as 500 or 1000 feet.

FIGURE 1

## FRAZHAZ STORAGE AND TEST ATTITUDES

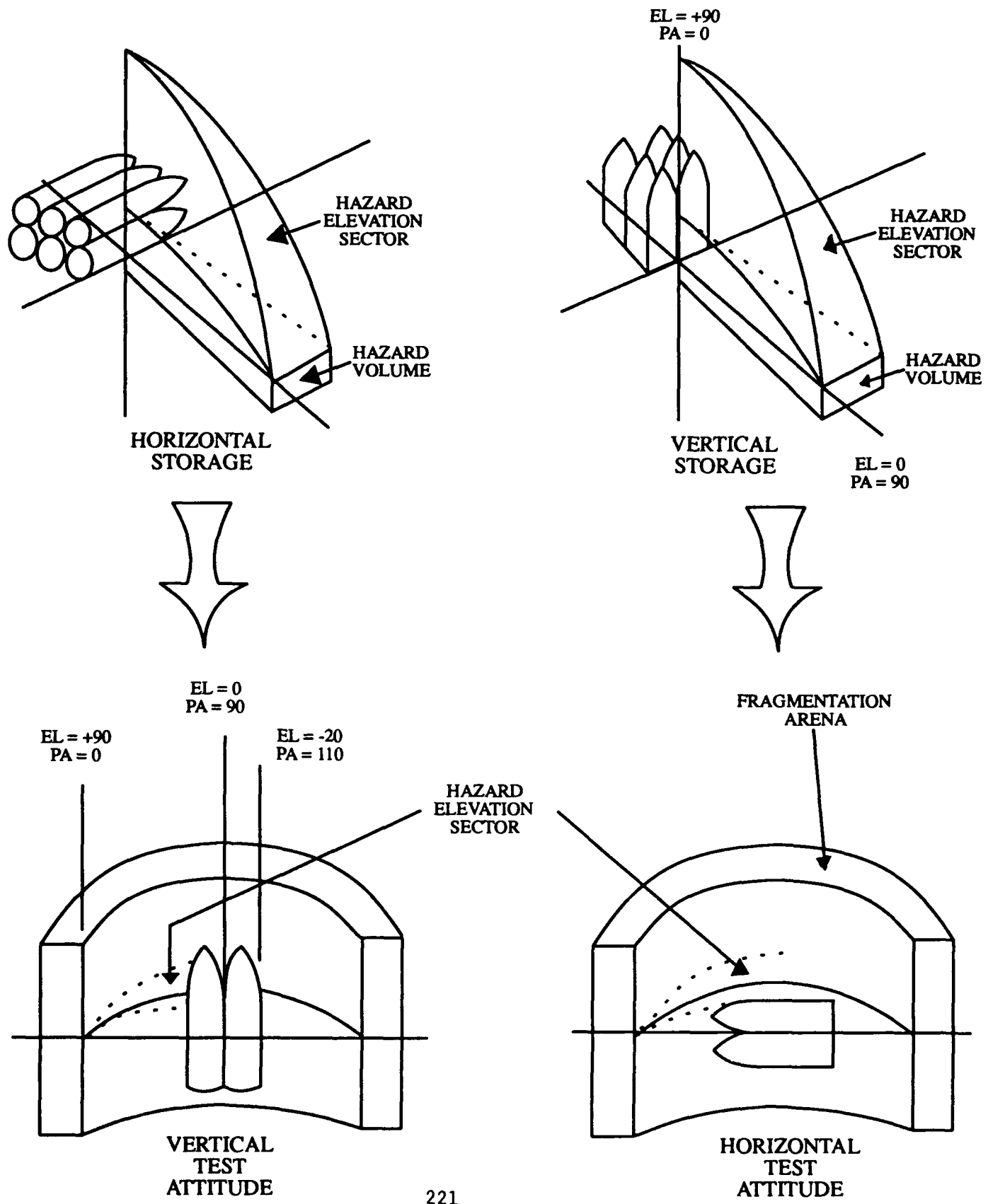
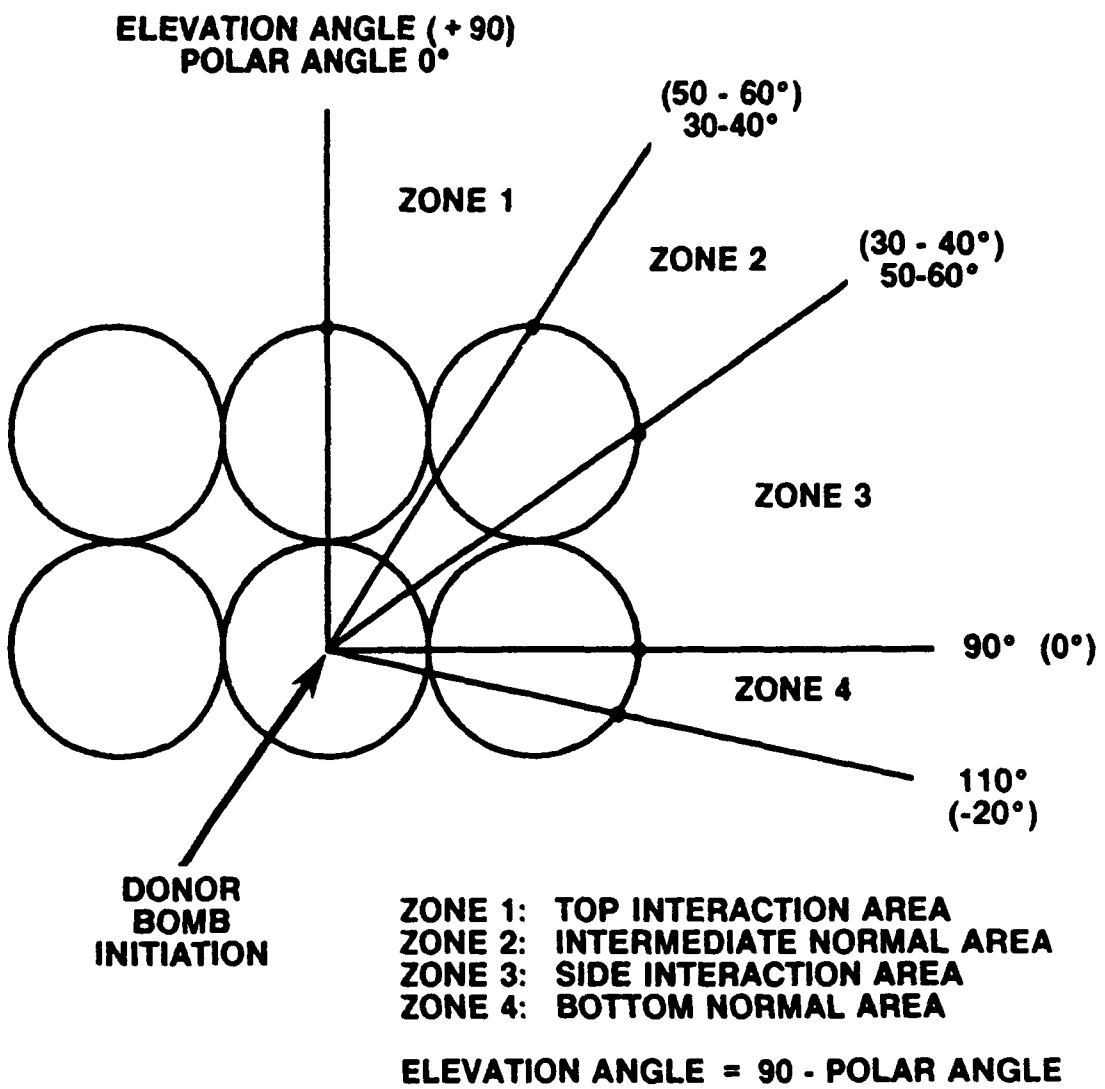


FIGURE 2

## MK 82 BOMB PALLET FRAGMENTATION MASS DETONATING



**FIGURE 3**  
**MK 82 (500 lb) BOMBS**  
**INITIAL VELOCITIES - MASS DETONATING**

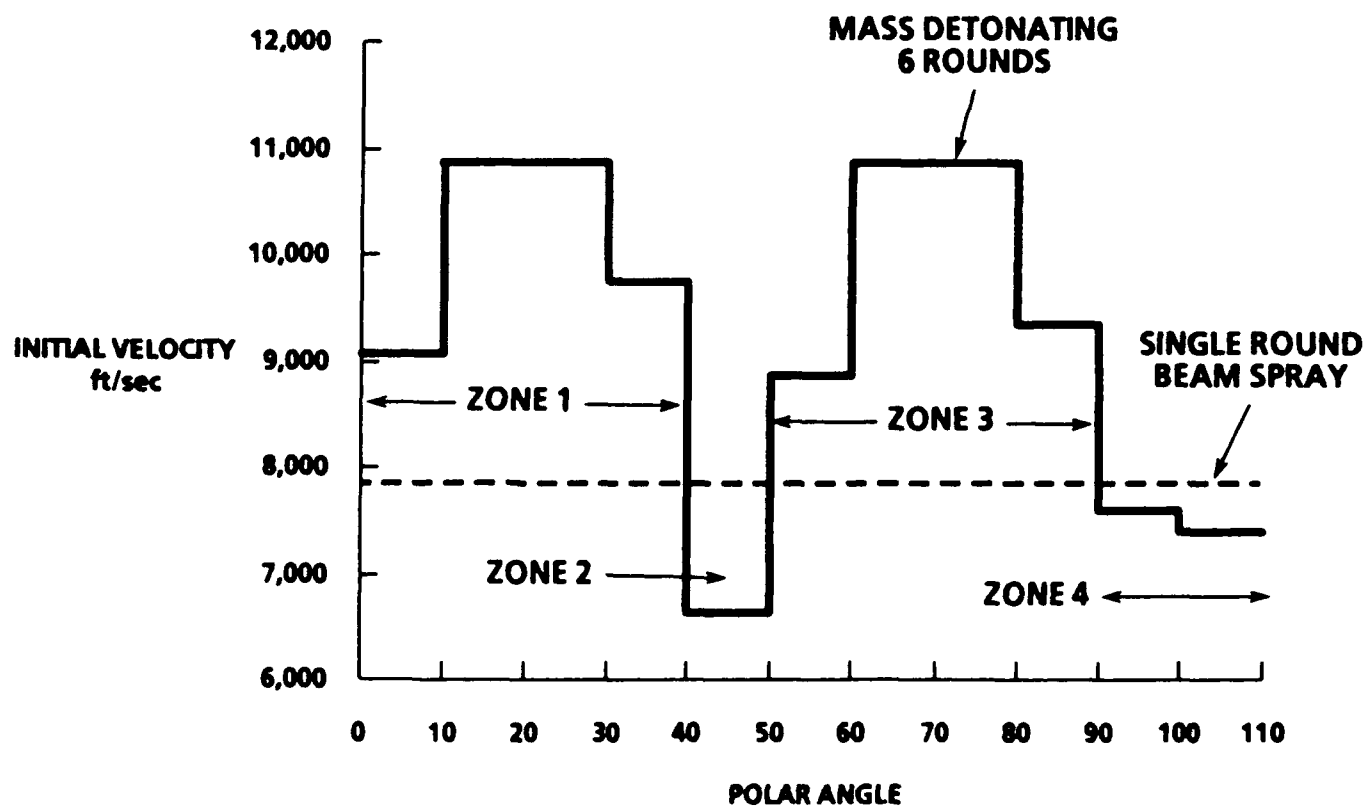
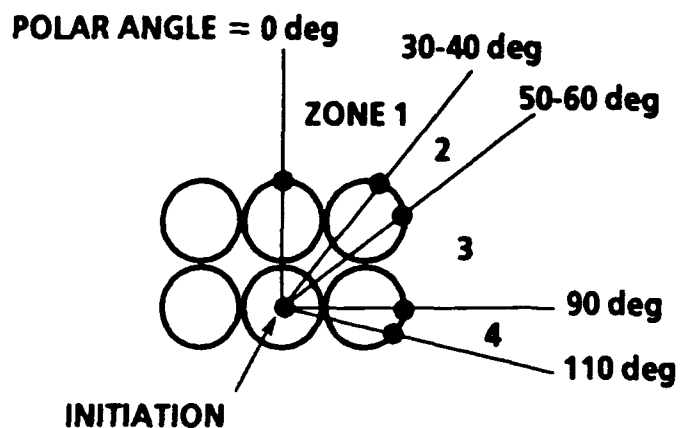


TABLE 1

## PARAMETER SENSITIVITY

SEA LEVEL NO WIND ELEVATION = 20 deg

PARAMETER	VALUE CHANGE	APPROXIMATE RANGE INCREASE (PERCENT)
$V_0$	3500 to 10500	30
$C_D(M \approx .1)$	1.8 to 0.6	120
$\bar{A}/M$	18 to 6	150

 $V_0$  = INITIAL VELOCITY (ft/sec) $C_D(M \approx .1)$  = DRAG COEFFICIENT AT MACH NO.  $\approx .1$  $\bar{A}/M$  = AVERAGE PRESENTED AREA TO MASS RATIO (in.<sup>2</sup>/lb)

$$a = \frac{\rho C_D \bar{A} V^2}{2 M}$$

NEGATIVE DRAG ACCELERATION

## LARGE CLASS 1.3 ROCKET MOTOR DETONATION CHARACTER

CLAUDE MERRILL, OL-AC PHILLIPS LABORATORY, EDWARDS AFB, CA

### ABSTRACT

Large explosive class 1.3 solid propellant rocket motors utilizing polybutadiene binder, aluminum fuel, and ammonium perchlorate oxidizer are typically considered explosively "safe". That is, the required stimulus is so large that motor detonation is extremely unlikely, even when donorized by a sizeable high explosive charge. Two large ground cratering events have occurred during recent years in motor destruct operations. Recently, a 10,000 kilogram grain containing 90 percent combined aluminum and ammonium perchlorate solids was subjected to a 25 kilogram C4 donor. Discussion of the nature of these events and the large test and how observed results affect our outlook on large motor hazards will be presented.

### INTRODUCTION

Hydrocarbon binder/aluminum (Al)/ammonium perchlorate (AP) solid propellants having burn rates near one centimeter per second have been usually considered to have almost negligible explosive character. This had come in part by analogy with the 84% total solids (68% AP and 16% Al) Minute Man (MM) I carboxy terminated polybutadiene-acrylonitrile (PBAN) propellant that was shown to have a critical diameter between 1.676 and 1.829 meters (66 and 72 inches) (1). However, with the French publication in 1988 (2) where a slow burning hydroxy terminated polybutadiene (HTPB) propellant containing 90% total solids (70% AP and 20% Al) was reported as having a critical diameter near 85 mm (3.35 inches), our concept of detonability of our "safe" propellants having total solids loadings above 84% may have to be changed considerably.

A cratering event was observed during destruction with C4 explosive charges of a SRAM (short range attack missile) propulsion unit at Hill AFB in 1989. This was considered somewhat unusual but didn't raise any great concerns since the propellant has its burn rate catalyzed by a mixture of n-butylferrocene and di-n-butylferrocene. Due to this burn rate catalyst system SRAM propellant has been known to produce fires by friction and impact events encountered with the SRAM propellant since its introduction into use.

During C4 donorized destruction of a MM II, stage 3 motor in 1990 at Hill AFB a large cratering event occurred. This was the first apparently full energetic yield explosion ever observed with the MM II, stage 3 motor. This motor contains

about 7300 pounds of an 88% total solids (73% AP and 15% Al) carboxy terminated polybutadiene (CTPB)/aluminum/AP uncatalyzed solid propellant. Since the motor is 1.32 meters (52 inches) in outer diameter, the propellant critical diameter must be substantially smaller than for the 84% solids PBAN propellant tested during the 1960s.

During the 1960s, several launch failures with explosive class 1.3 boosters exploded violently when impacting the earth or ocean according to Lou Ullian of the Patrick AFB safety group (3). Thus, explosive class 1.3 propellants producing a lack of detonation at zero cards in the large card gap test have exhibited significant explosive character in large rocket motors. The lack of atmospheric overpressure gauges has not allowed estimation of explosive yield in the observed US explosive events by class 1.3 propellants. Craters produced by the SRAM and MM motor violent explosions were large enough to cause belief that complete energetic yields had been obtained.

Presently, the USAF has a lack of quantitative knowledge as to the relative explosive and fire initiatability of our safer propellants that are used in larger booster motors. Although it is generally believed that large motors are more vulnerable at lower impact velocities than for small motors, the change in explosive character with increasing motor size has not been experimentally determined. Poorly quantified events with large critical diameter explosives such as, safer solid propellants, has indicated that their explosive characteristics might be quite different from high explosives. Later, a short discussion will cover the rather strange (to me) behavior of a 90% total solids propellant during an explosive process. Explosive potentials of large solid boosters that weigh about 250,000 kilograms or more (Titan and Space Shuttle) have been a growing concern of range safety officers during launches. Study of large motor explosive traits and how to increase their explosive resistance has been suggested by several people.

Figure 1 exhibits two plots involving critical diameter of solid propellants. The first plot involves my concept of propellant critical diameters versus large card gap test results. The range of critical diameters, 0.25 to 2500 millimeters (roughly, 0.01 to 100 inches), includes critical diameters for all rocket propellants used by the US military services and NASA. Seventy cards in the card gap test divides the explosive class 1.1 and 1.3 solid propellants. Since many propellants have critical diameters in steel pipe above the 37 mm (1.44 inches) inside diameter employed in the large card gap test, our generally recognized as "explosively safe" solid

propellants provide only negative results at zero cards. Thus, the card gap test doesn't provide a relative measure of explosive sensitivity for zero card propellants. Without quantitative evidence in hand it is relatively easy for us to imagine, incorrectly, that all of these propellants are of about equal explosive insensitivity.

In the second plot of Figure 1 the safe propellant critical diameters are expanded versus solid propellant solids loadings for hydrocarbon binder/aluminum/AP propellants. Only two data points come from experimental data. The first data point is the roughly 1700 to 1800 mm (about 70 inches) critical diameter at 84% total solids for the stage 1, Minute Man I missile propellant. The second data point was obtained from French workers referred to in the footnote. They determined an 83 mm (3.27 inches) critical diameter for a 90% total solids HTPB propellant. By interpolating between the two experimental points, critical diameters can be roughly estimated for 86 and 88 weight percent solids loaded solid propellants of the HTPB, CTPB, PBAN, etc. types. Considerable variation in critical diameters at a particular solids loading for propellants would be expected as the AP particle sizes, AP content, burn catalyst contents, and other formulation parameters were varied. Critical diameters cover a considerable range for the "safe" solid propellants. We are just beginning to recognize that explosive characteristics associated with very large rocket motors might be a substantial range safety concern. A large portion of the concern is due to the fact that relatively low impact velocities may be capable of stimulating detonations of the largest rocket motors in launch failure fallbacks near the launch pad.

Figure 2 exhibits an artistic attempt at illustrating how threshold fire and violent explosion stimulating impacts might decrease as the quantity of propellant increases. Some very limited data has been generated for explosive class 1.1 propellant samples of less than 10 kilogram weight that indicates a roughly linear logarithmic impact velocity-propellant weight relationship. However, no systematic study of large critical diameter propellant explosive vulnerability as a function of sample size has been conducted. Several serious fire incidents have been experienced with HTPB propellants indicating that a relationship between fire threshold impact velocities and sample size could also be useful. At the present time no data is available to show how fire initiation impact velocities vary with impacting sample weight.

#### EXPERIMENTAL

As a means of getting limited information on relative

explosive nature for a high solids HTPB propellant, a simple experiment was planned at the Edwards AFB section of the Phillips Laboratory early this year. See Figure 3. The sample was a 10,000 kilogram (22,622 lbs) grain that is normally used in our Super HIPPO nozzle survivability test motor. Our cylindrical propellant grain was 2.13 meters (7.0 feet) in outer diameter, 2.24 meters (7.3 feet) in length, and contained a 0.61 meter (2 feet) center perforation. This resulted in a web thickness of 0.76 meter (2.5 feet). Propellant making up the Super HIPPO grain was a 90% total solids HTPB formulation containing 21% aluminum and 69% AP that had an uncatalyzed, relatively slow burn rate of about 1.0 centimeters (0.40 inches) per second at 6.9 megapascals (one thousand psi). A right circular cone of C4 donor explosive was placed sitting at mid-web on one side of the vertically oriented grain sitting on a dry soil surface. The cone had a 0.30 meter (one foot) maximum outer diameter by 0.60 meter (2 feet) in height. Total C4 explosive donor weight was near 24.5 kilograms (54 pounds). Instrumentation was a few Bikini overpressure gauges (variable size paper disk gauges) and a pair of 30 frame per second color video cameras.

The Super HIPPO grain explosive test was based on a few simple concepts: (1) The propellant was quite similar to that used by the French that yielded an 83 mm critical diameter, 69% AP and 21% Al versus 70% AP and 20% Al. Thus, a similar critical diameter might be expected. (2) A 0.30 meter diameter C4 explosive donor was used so that lack of violent explosion would be reassuring that the propellant was roughly as explosively safe as initially thought or that we would consider further study if the propellant produced a violent explosion. (3) If the donor exceeded the propellant critical diameter, all of the propellant should detonate. (4) If critical diameter was not exceeded, air shock pressures would be relatively weak. (5) At less than critical diameter a violent explosive event initiated by the donor should die before the bottom end of the grain. (6) With a dying supersonic shock event in the propellant unconsumed solid propellant should be lying on the earth directly below the C4 donor.

When the C4 donor was set off by an exploding bridgewire initiator, an explosion considerably stronger than could be produced by the donor charge alone was observed. Large amounts of the propellant was not consumed in the process and an enormous number of burning and nonburning propellant fragments were thrown out of the reaction zone. Unconsumed propellant was not located in the crater although a very large number of unconsumed propellant pieces in sizes sometimes exceeding 10 kilograms (20 pounds) were observed on the ground out to distances beyond 0.75 kilometer (2500 feet) from the

event. A large, clean, somewhat assymetric crater was produced in the soil about 1.2 meters (4 feet) in depth and 5 meters (16 feet) in diameter. An illustration of the approximate cross section of the crater is provided in Figure 4. By past experience on the same ground with large explosive charges the crater size seemed to indicate an explosive charge equivalent to roughly 700 kilograms (1500 pounds) of TNT. Observation of the sizes of torn paper circles in the Bikini overpressure gauges indicated a TNT equivalence somewhere between 450 and 2300 kilograms (1000 and 5000 lbs).

#### DISCUSSION/CONCLUSIONS

From the evidence produced by the C4 donor 90% solids HTPB propellant in the large grain several factors seemed to stand-out.

(1) The size of the overpressures and the substantial crater produced indicated that partial detonation or a partial full yield explosive event had occurred. (2) Further support for this view came from the crater that had no evidence of free propellant within it. If a detonative process had died before exiting the propellant grain bottom, some evidence of solid propellant being in the crater after the event should have been observed. If propellant had burned in the crater following the event aluminum oxide stains would have been present, and some amount of green glass formed by heating of our low temperature melting soil should have also been seen. No propellant fragments, burn stains, or green glass were present in the crater produced by the experimental event. From this it appeared that a detonation proceeded from the donor out the bottom of the Super HIPPO grain. (3) If a detonative type of process transited 2.13 meters (7 feet) through the propellant grain, the critical diameter had been exceeded. This indicated that the French report for the relatively small critical diameter of 90% solids HTPB solid propellant was correct. (4) Why wasn't the propellant completely consumed in a detonative process? After some thought, a plausible explanation seems to be that the directed supersonic shock transmitted by the C4 donor into the solid propellant could not turn fast enough or build up fast enough in lateral directions to involve greater amounts of energetic material. In Figure 5 is indicated the way such a shock might pass through the propellant. That is, a gradually widening conical section of material that would produce full energetic explosive yield while the remainder of the propellant would be thrown out in fragments. For me this was a new concept. That is, that large critical diameter explosives have a great reluctance for bending detonation waves once a directional shock process has been initiated.

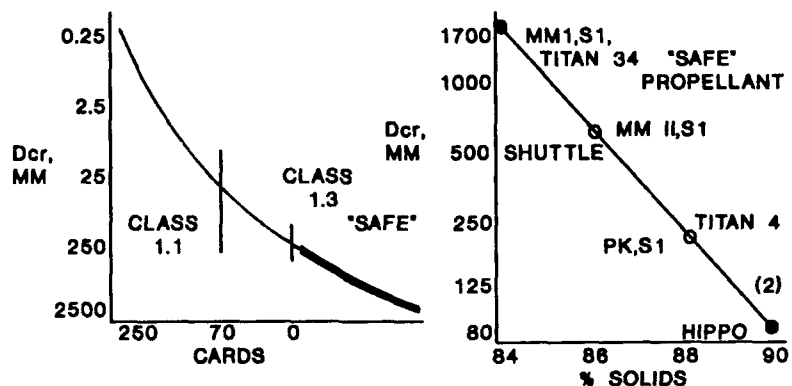
I believe that further study of the explosive

characteristics of "explosively safe" solid rocket propellants should be further studied. Funding to support study of the Super HIPPO propellant has not yet been obtained. However, limited support is being made available to conduct experimentation with 88% solids HTPB propellant. Such studies are sure to provide interesting information about reactive traits of large critical diameter explosives and to provide some new and needed qualitative and quantitative observations on the relative safety of workhorse solid propellants.

#### REFERENCES

1. Restricted source.
2. "Detonation Critical Diameter of Advanced Solid Propellants", J. Brunet - B. Salvetat, Joint International Symposium on Compatibility of Plastics, Pyrotechnics and Processing of Explosives, Propellants and Ingredients, New Orleans, 1988.
3. Lou Ullian, private communication.

#### FIGURES



(2) 'DETONATION CRITICAL DIAMETER OF ADVANCED SOLID PROPELLANTS', J BRUNET - B SALVETAT, JOINT INTERN. SYMP. ON COMPATIBILITY OF PLASTICS, PYROTECHNICS AND PROCESSING OF EXPLOSIVES, PROPELLANT AND INGREDIENTS; NEW ORLEANS, 1988

Figure 1. Propellant Critical Diameter Versus Gap Sensitivity and Solids Loading

**FIGURES (CONTINUED)**

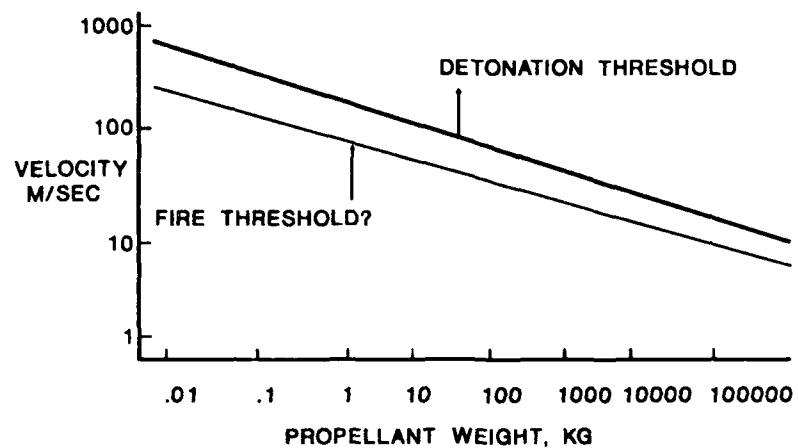


Figure 2. Explosive Threshold Velocities Versus Propellant Weight (Ignition Thresholds?)

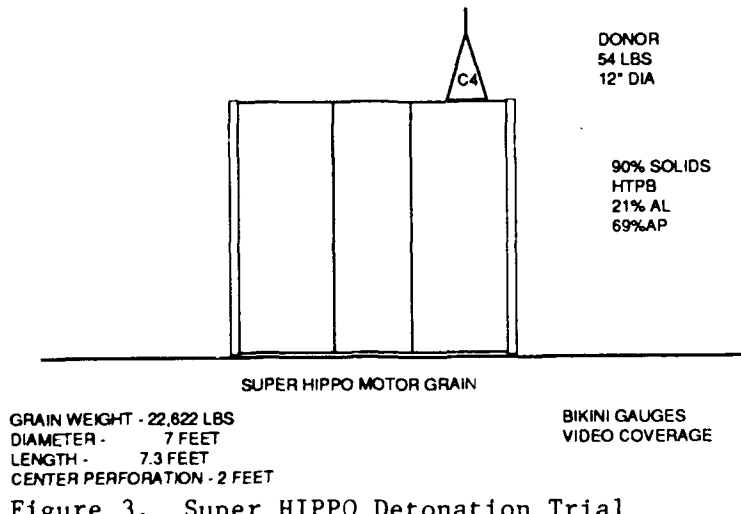


Figure 3. Super HIPPO Detonation Trial Configuration

## FIGURES (CONTINUED)

- LARGE, CLEAN CRATER - 4 FT DEEP, 18 FT DIAMETER
- 20 LB + PROPELLANT CHUNKS TO 2500 FT
- CRATER SIZE INDICATED 1500 LB TNT EQUIVALENT
- BIKINI GAUGES INDICATED TNT EQUIVALENCE BETWEEN 1000 AND 5000 LBS

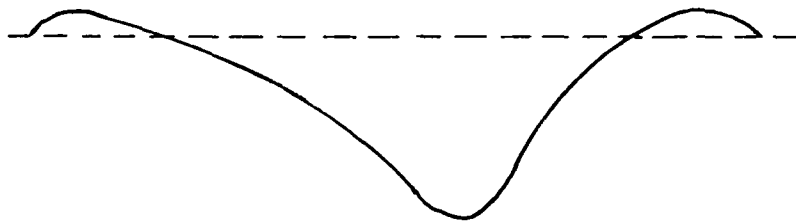


Figure 4. Super HIPPO Detonation Trial Results

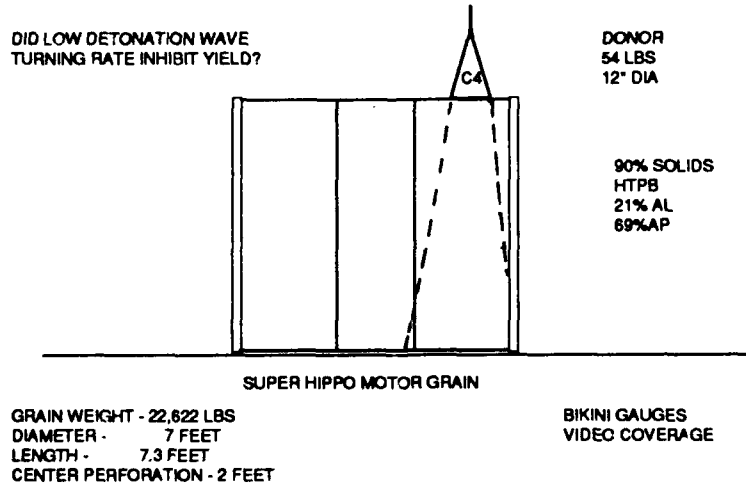


Figure 5. Super HIPPO Detonation Trial;  
Probable Shock Path Through Grain

## SCALING STUDIES OF THERMAL RADIATION FLUX FROM BURNING PROPELLANTS

J. Edmund Hay and R. W. Watson

### ABSTRACT

The radiant thermal flux from various masses and configurations of burning bulk gun propellants was measured at distances of 2.4 to 20 meters from the source. The propellants used consisted of small-arms propellants and large-caliber artillery propellants. The masses burned ranged from 45.4 kg. to 400 kg; the configurations included open-top fiber drums of various diameters and the original shipping containers (closed). Both internal ignition and exposure to external bonfire were included.

In the burns in the open-top drums with top ignition it was confirmed that the propagation rate through the bulk material controls the overall burning rate. Additionally this rate is essentially independent of the mass, so that the burning rate is virtually proportional to the area of the burning surface, thus validating (for masses of similar shape) the two-thirds-power-of-mass law. The data also indicate that the thermal flux can be estimated from the burning time. The inverse-square-of-distance law is found to be substantially in error at close distances. This is associated with the fact that the flame is a column rather than a "fireball". Immediate propagation of burning between containers was not observed; some forms of packaging were found to give significantly greater delay-to-ignition in an external fire than others. Approximately 20 percent of the thermochemical energy appeared as radiant heat.

### INTRODUCTION

The Department of Defense Explosives Safety Board (DODESB) asked the Bureau of Mines to conduct research to establish the scaling relationships involved in the radiant heat flux from quantities of burning propellants. The results of this work are to be used to determine the appropriateness of the radiation criteria used for the classifications of materials under the U.N. scheme. Since it is not practical to actually test the burning behavior of large shipments of propellant, the determination of the hazard involved in the exposure of large masses to accidental ignition relies on the ability to extrapolate results from smaller scale tests. One of the most important hazards in the combustion of an energetic material is the radiant thermal energy emitted. It is therefore important to establish the dependence of the radiant thermal flux on the mass of propellant and the distance from the fire to personnel and property which could be injured/damaged thereby.

Six gun propellants of different physical characteristics were chosen, three of which were selected to be burned in three different quantities, in the 50 to 500 kg range, in the normal shipping package(s) including single packages and small groups of packages and in a "bulk", i.e., lightly confined, configuration up to the maximum mass, measuring the radiant heat fluxes at various distances from the propellant. This was supplemented by a few tests

on three fine-grain propellants to determine whether there were any gross differences in behavior.

#### MATERIALS & EQUIPMENT

The propellants chosen in the first phase of the work were IMR 5010 powder (a small arms powder packaged in fiberboard drums), M-1 single-perforated (SP) propellant for 8" howitzer (packaged in rectangular copper cans with wooden overpacking), and M-1 multi-perforated (MP) propellant for 8" howitzer (packaged in rectangular galvanized steel cans). Approximately 1500 kg of each of these were received from Rock Island Army Ammunition Plant. For the second phase of the work it was decided to investigate the burning behavior of more fine-grained propellant powders. The propellants chosen were WC844 for 5.56 mm M-196 ball, WC846 for 7.62 mm tracer, and WC blank for .30 cal. Approximately 700 kg of each were received from Rock Island AAP.

The basic instrumentation consisted of radiometers (Thermogage model 2000-8) with sensitivities ranging from 1.5 to 25 cal/sq cm/sec/volt, a Honeywell model 1858 Visicorder with model 1883A-MPD preamplifier modules, and an NEC model APC-IV Powermate field-portable computer with a Data Translation model 2821 analog/digital converter board. Six channels of instrumentation were used. The radiometers were recalibrated by the manufacturer just prior to being used in these tests.

The quantity of IMR 5010 in the as-received packages was 45.4 kg (100 lbs). For the M-1 8" SP powder this was 49.9 kg (110 lbs) and for the M-1 8" MP propellant this was 47.7 kg (105 lbs). These quantities were used as standard increments in mass for the respective propellants. The WC844 and WC846 were received in 45.4 kg (100 lb) (net wt) fiber drums and the WC Blank propellant was received in 27.2 kg (60 lb) (net wt) cans with wood overpacking. For the last three propellants the bulk burns were conducted with a standard quantity of 100 kg (220.4 lbs).

The "bulk" configuration was an open-top fiberboard drum. The original plans were to use drums of a height-to-diameter ratio reasonably close to 1:1. For this purpose commercial fiberboard drums of 45 and 60 cm dia were obtained and cut to the appropriate height depending on the quantity and bulk density of the propellant to be burned. It was found early in the program that the burning rate and thus the heat flux is controlled by the cross-sectional surface area of the propellant, so in order to have a consistent basis for comparing different burns, most of the burns were actually done at a fixed diameter of 60 cm.

The radiometers were laid out at the burning ground at the Bureau's Lake Lynn Laboratory as shown in figure 1. The (logarithmic) increments in distance between successive radiometer stations were chosen to be ratios of approximately the cube root of 2. (A maximum of six radiometers was used in any one test.) This scheme of deployment of the radiometers represents an attempt to simultaneously view the test from widely different angles, and

obtain data at widely different distances, while staying within the physical constraints imposed by the topography of the burning ground. The radiometers were deployed with those of successively higher sensitivity at successively greater distances from the burning propellant. The distances which correspond to the radiometer locations in figure 1 are listed in table 1.

All burns were initiated with an Atlas electric match assembly in a small 0.0013 cm thick polyethylene bag containing 10 grams of FFFg black powder. All tests were video-taped. A brief summary of the 49 tests performed is shown in table 2.

#### DESCRIPTION OF TESTS

The initial tests (Nos. 1-6) were run using one container each of the various propellants, both in open-top fiberboard drums and in the original (closed) shipping containers. (For the closed containers two small holes just sufficient for the electric match leads were drilled in the lid of the container.)

In the first test with 45.4 kg of IMR 5010 in an open-top drum the ignitor was placed in the center of the drum. The result was that both burning and unburned propellant were violently ejected from the drum so that neither the quantity actually burned nor the location of the center of the "fireball" could be accurately determined. Thus in all subsequent tests the ignitor was just buried (approximately 2 cm deep) in the center of the top surface of the propellant.

In the initial tests with the closed shipping containers (Nos. 4-6), the result was similar to that with the central ignitor, i.e., the container burst, throwing a mixture of burning and unburned propellant (in one case more than 20 meters from the original location). Thus the attempt to burn any propellant in closed containers was abandoned, except for the UN 6(b) tests (Nos. 44 - 46) and the bonfire burns (Nos. 31 to 36 and 47 to 49) and one test (No. 14) in which a closed container was ignited next to another closed container with no ignitor, to determine whether the explosion of one container was sufficiently violent to rupture and ignite the second container (the result of this test was negative).

The early tests (Nos. 1 - 15) were run with the radiometers closely spaced, i.e., from 2.5 to 8.0 meters, in order to maximize the signal-to-noise ratio. However it was noticed in these tests that the reproducibility from one test to another was poorer than expected and that the radiant heat flux was falling off less rapidly with increasing distance than an inverse-square law would dictate. Visual observation showed that: (1) there is a tendency to throw showers of burning (and unburned) propellant from the containers, which upsets the symmetry of the experiment, and (2) the fire was not a fireball but a fire column, i.e., it approximates a line source more than a point source at close distances, and for a line source the flux should vary inversely with the first power rather than the second power of the radius. This effect is discussed

further below. Thus the remaining tests were run at larger radiometer distances of 6.4 to 20.0 meters. As will be seen, this resulted in closer conformity to the inverse-square relation.

For the bonfire burns and all the burns using the fine-grain propellants, a fixed radiometer distance of 15.0 meters was used. For the multi-package tests, the containers were tightly wired together with 12 wraps of No. 16 gauge steel wire.

The results of all the tests are shown in tables 3 to 8 for the IMR 5010, M1-8"-SP, M1-8"-MP, WC844, WC846, and WC Blank propellants, respectively. The tables show, for each mass of propellant, and each of six radiometer positions (in some cases fewer than six positions are given, either by design or through failure of the instrumentation), the instantaneous peak radiant heat flux, the maximum value of the radiant heat flux observed over any 5 second interval, and the average radiant heat flux over the duration of the burn. For each test it also shows the burn time, the total radiant heat flux that would be emitted if the average radiant heat flux seen by the radiometers (weighted by the square of their distances from the source) were emitted uniformly in every direction, and the last two quantities divided by the propellant mass. The burn times in most cases are taken from visual observation of the video tapes. In a few cases this was not practical (in one case the video camera stopped prematurely, in a few others the burning tapered off too slowly and sporadically to judge the end point). Therefore, the burn time was picked from the recorded data using the criterion that the end point was the point at which the radiant flux dropped below one-half its average value for the duration of the burn. In the initial test with the fine-grain propellants (No. 40) the very slow burning rate and low radiant flux were not anticipated so the instrumentation stopped recording before the burn was completed. The results of this test are included anyway in Table 6 for completeness. Also shown, where appropriate, are the exponents derived by a least-squares fit to the radiant heat flux vs distance.

## DISCUSSION

Although the main emphasis of the work was determination of scaling relationships for the radiant thermal flux from propellants burned in the bulk mode, some other observations are worth noting. One of these is that the coarse-grain propellants burned much faster than the fine-grain ones. Another is that, in no case in the multiple package tests where one package was internally ignited did burning propagate from one package to another.

The propellant burning rate seems to be controlled by the burning rate through the bulk of the powder, the burning rate across a free surface being much faster. The burning times plotted as a function of propellant mass, for those propellants which were burned in the bulk configuration at more than one mass, are shown in figure 2. The data used to plot this figure excluded those data for which complicating factors such as internal ignition, package burns, and bonfire burns would affect the burning rate. From this figure it can be seen

that the burning time or rate is essentially linear with the mass of propellant, apart from a small offset of ca 3 sec, which presumably is the time required for the burning to become established at a constant rate. Since the cross-sectional area normal to the direction of propagation of burning is constant, the dimension in the direction of propagation is proportional to the propellant volume or mass, so that these data show that the linear propagation rate is constant, which is what would be expected.

The data in tables 3-8 can also be used to extract the total radiant thermal energy per unit mass for each propellant type. In doing this, the data taken at small distances were excluded; these data show a systematic bias toward smaller values of thermal energy. This is probably connected with the fact that, as previously pointed out, the fire is actually a tall column, so the source of much of the radiant energy is considerably above ground level, making the effective distance from the source to the radiometers larger than the distance from the propellant to the radiometers. This is discussed further below. The calculations of total radiant energy were made assuming spherical symmetry; no attempt was made to correct for the height of the fire plume since this would introduce a factor which could not be measured accurately and thereby introduce inconsistency into the results. The data extracted are given in table 9.

The heats of combustion for IMR and M1 propellants are 2.402 and 2.727 Kcal/g, respectively. When this is compared with the values obtained above, it is seen that the total radiant heat energy derived from these measurements is 18 to 21 percent of the total available thermal energy. This is on the low end of the range normally found for the fraction of total energy converted to thermal radiation (1). The most likely explanation for this is that, as pointed out above, much of the radiant energy is radiated from portions of the fire plume which are considerably above ground level and which therefore are at a greater distance from the radiometers than the burning propellant itself. Therefore, the thermal flux measured at ground level for tall plumes will thus be less than that which would be measured for a compact fireball at ground level. This is particularly true if one considers that part of the thermal energy released is due to secondary oxidation of the products in the surrounding air, a process which requires mixing of the products with the air and which is probably not complete until the products reach the top of the plume. The heat released at the base of the plume is probably that released in the monopropellant mode of burning, i.e. the heat of explosion, which for these propellants is 0.896 Kcal/g (IMR) and 0.751 Kcal/g (M1).

It is also of interest to examine the hypothesis that the thermal flux is proportional to the mass of propellant burned and inversely proportional to the burning time, as suggested by Watson (1). These data are presented in figures 3 through 5. For each test the values of the "5 - second average peak" flux were converted to an equivalent value at 15 meters using the distance scaling exponent appropriate to the data in that test. These values were then averaged over all of the radiometers used in that test. The results are the ordinates in figures 3-5. The abscissae are the mass of propellant

divided by the burning time. The data in figures 3-5, unlike figure 2, include all the tests, including the close-range data, package, and bonfire burns except for test no. 14, in which the container exploded so violently that the results are meaningless. The figures show a reasonably good fit. It is of interest to note that in figure 3 the point which lies farthest above the line is for test No. 1 (internal ignition).

The implications of this, together with the observation above, that the linear propagation velocity of the burning through the mass of propellant is constant, are that, for quantities of propellant having a given shape and bulk density but different masses, the thermal flux will be proportional to the propellant mass to the two-thirds power. The linear dimension of the body of propellant will be proportional to the cube root of the volume (and hence of the mass). Thus, the burning time will also be proportional to the cube root of the mass, and the radiant flux will be proportional to the mass divided by the burn time and thus proportional to the mass to the two-thirds power. Another way of looking at this is that the flame spreads much more rapidly across a free surface than it does through the bulk of the propellant, so that the burning rate is effectively controlled by the surface area, which for a given shape and bulk density will be proportional to the two-thirds power of the mass. Thus the results are consistent with the two-thirds power law for scaling thermal flux with burning mass provided that the shape of the burning mass considered is the same as that of the reference mass.

The inverse square law for scaling thermal flux with distance is substantially in error at close distances because the flame is in reality a column rather than a sphere. Conformity with the inverse square law improves as the distance becomes comparable to the height of the column. This is taken into account by the so-called "view factor" (2), which is a function of the height-to-diameter ratio ( $H/D$ ) of the fire plume and the ratio  $R/D$  of the distance to the plume diameter. The  $H/D$  for these tests varied widely, not only from test to test, but with time in any given test. The variation ranged from a value of approximately 1 to approximately 6 in a seemingly random way. A general average value for all tests was approximately 4. The view factor varies approximately as the inverse square of  $R/D$  for values of  $H/D$  which are much less than  $R/D$ , but approximately as the inverse of  $R/D$  for values of  $H/D$  which are much greater than  $R/D$ . This is shown by the values of the "Distance scaling exponent" in tables 3 to 5, which show a systematic trend from smaller values for the close-range measurements to larger values for the longer-range measurements. At the larger ranges these results are essentially consistent with the inverse-square "law" and with similar measurements by Harmanny (3). As pointed out above, however, these results differ from Harmanny's in that they are consistent with a two-thirds-power dependence on the mass rather than the 0.82 power reported by Harmanny.

In comparison to these results, Allain(4) has measured the radiant thermal flux from large quantities of propellant in igloos. The propellant used [French LB.7T.72 (0.8)] "is similar to US M1". The quantity burned was approximately 2220 kg. In spite of the larger quantity of propellant used,

the apparent burning times recorded by Allain were relatively short and sharply peaked (15 sec total, with the flux exceeding half its maximum value for only about 6 sec). There are probably 2 reasons for this: (1) the propellant was stacked in cylindrical bags which provides many channels for the flame to spread between the bags, greatly increasing the burning area; (2) the igloo partially contains the hot gases until it ruptures, releasing them suddenly. In one of the 3 trials the igloo exploded and the thermal flux was significantly less than in the other two. If this trial is ignored, the average flux for the remaining two trials was 12.7 w/sq cm (= 3.0 cal/sq cm/sec) at a total distance of 19.2 m, and 5.8 w/sq cm (= 1.4 cal/sq cm/sec) at a total distance of 27.7 m. This is consistent with a distance-scaling exponent of 2.1. The total integrated thermal flux (at 27.7m) is approximately 1.74 billion calories. The heat of combustion of this propellant is not given, only its heat of explosion (720 cal/g). If one assumes that it is similar to that of US M1, viz 2727 cal/g, then the fraction of energy released as radiant heat is approximately 29 percent of the total available thermal energy.

The two-thirds power scaling law is used for the classification of propellants and other flammable substances according to the United Nations Recommendations. One of the aims of this project was to determine the impact of these recommendations on the classifications of substances important to the military. The criteria for Test 6(c) place limits on blast, fragmentation, and thermal effects, and in the absence of explosion, the only criterion of concern is the thermal flux produced by the bonfire. The present criterion outlined in paragraph 44.4.4 (c) of ST/SG/AC 10/11 (5) reads: if . . . "the irradiance of the burning product exceeds that of the fire by more than 4 kW/m<sup>2</sup> at a distance of 15 m from the edge of the stack" . . . then the product, as packaged is assigned to UN Division 1.3. For substances, the value is corrected to correspond to a mass of 100 kg net content. For bonfire tests involving net weights larger or smaller than 100 kg or for flux measurements made at distances other than 15 m, a (mass)<sup>2/3</sup>/(distance)<sup>2</sup> scaling law is used to normalize the data. However, thermal flux values can be estimated from a knowledge of observed burning time using the equation outlined in reference (1):

$$I = \frac{C \cdot E}{4\pi R^2 t} \quad \text{where,}$$

I = Irradiance in kw/m<sup>2</sup>,

C = Constant,

E = Total energy content in joules,

R = Distance from fire to gauge position,

t = Observed burn time in seconds.

A more important factor is the effect of packaging on reducing the rate of fire spread in a full cargo load of material. This factor is not realistically handled in the prescription for the UN bonfire test where the

packaged test substance is completely engulfed in flames at the outset. This is an important point that bears further discussion.

Some idea of the effect of packaging on delaying the ignition of individual packages in a massive fire event can be gained from an examination of shots 34, 35, and 36, the 3-package bonfire trials. Times to ignition of the individual packages are shown in table 10. These times were estimated from TV tapes of the burns and are measured from the ignition of the fuel-oil bonfires. In tests 34 and 35 only two times are given since the third package was ejected from the bonfire and did not burn. In shot 34 the first package ignited in 125 sec followed by the ignition of the second package 12 sec later at  $t = 137$  sec. Similar behavior was observed in shot 36 with the first ignition at  $t = 104$  sec, the second, 15 sec later at  $t = 119$  sec, and the third, 10 sec later at 129 sec. This indicates little difference between the level of protection provided by the fiberboard drum used for the IMR 5010 and the steel can used for the M-1 8" MP. However, in the case of the M-1 8" SP packaged in copper cans with a wood overlay (Shot 35), ignition of the first package did not occur until 331 sec after the ignition of the bonfire. The second package ignited 60 sec later at  $t = 391$  sec. The same behavior is shown in shot 49 in which the delay to ignition for a metal can with wood overpacking was 395 sec as opposed to shots 47 and 48 (fiber drum packages) in which the delays to ignition were 60 and 110 seconds respectively. Thus the copper-wood packaging is superior to the other types in delaying ignition. From these results it is reasonable to assume that packaging would have a significant influence on the total burning time of a full cargo of similar packages and the attendant thermal radiation from the fire. The UN bonfire test 6(c) does not account for this effect and probably overestimates the thermal flux from a cargo fire. To give a concrete example, it is worthwhile to apply the criterion for UN Test 6(c) to shot 34 of this series of tests. Table 3 shows that the 5 second average peak flux from the second ignition, the most intense event, was about 7.0 at 15 m for a net mass of 45.4 kg. Using the  $M^{2/3}$  scaling rule this flux level scales to 12  $\text{kW}/\text{m}^2$  for 100 kg which is well above the limiting criterion of 4  $\text{kW}/\text{m}^2$ . So far there is no problem. However, if we scale this value to 10,000 kg (a typical cargo load) we obtain a flux level of 258  $\text{kW}/\text{m}^2$  at 15 m, enough to spontaneously ignite wood at 41.6 m (33.5  $\text{kW}/\text{m}^2$ ). In applying the  $M^{2/3}$  scaling rule we assume that the 10,000 kg cargo behaves like a single big package, rather than numerous individual packages producing a random series of 7.1  $\text{kW}/\text{m}^2$  events, or small multiples of this value when several packages ignite spontaneously. In this case the thermal flux could be significantly lower than that predicted by the  $M^{2/3}$  scaling rule used to scale results from test 6(c). Additional research is required to resolve this problem.

## CONCLUSIONS

The results reported herein for burning of gun propellants in bulk are consistent with a two-thirds power dependence of the radiant thermal flux on

the propellant mass, and with an inverse-square dependence of the flux on the distance from the fire.

In multiple-package burns there is no evidence that ignition of a package directly causes ignition of an immediately adjacent package.

Propellant packages consisting of a metal can with wood overpacking provided significantly more protection (in terms of delay to ignition) against exposure to external fire.

#### REFERENCES

1. An Alternative to Thermal Flux Measurements in UN Test 6(c), Watson, R. W., Proceedings of the 24th Department of Defense Safety Seminar, St. Louis, MO, 8/28-30/90.
2. Fire Protection Handbook, National Fire Protection Association, Cote, A.E., ed., 16 th Edition (1986) p.21-40.
3. Thermal Radiation Flux of Fireworks, Harmanny, A., Prins Maurits Laboratorium, TNO, OECD-IGUS Report (1984).
4. Allain, L., Combustion of Gun Propellant in Igloo Thermal Flux measurements. SNPE NT No. 153/91/CRB-S/TS/NP, 12/30/91 pp 12/63-22/63.
5. United Nations Recommendations on the Transport of Dangerous Goods, Tests and Criteria, United Nations ST/SG/AC 10/11/Rev 1, Second edition 1990.

Table 1 Radiometer Distances

Radiometer Position (see Fig. #1)	Distance from Propellant (meters)
1	2.5
2	3.2
3	4.0
4	5.0
5	6.4
5A	6.4
6	8.0
7	10.0
7A	10.0
8	12.8
9	16.0
10	20.0
2A	15.0
3A	15.0
5B	15.0

Table 2. Summary of Tests

Test. No.	Propellant	Mass (kg)	Package /bulk	No. of pkgs	Radiometer dist.(m)	Comments
1	IMR	45.4	B	-	2.5 - 8.0	Central ign
2	M1-8"SP	49.9	B	-	2.5 - 8.0	
3	M1-8"MP	47.7	B	-	2.5 - 8.0	
4	IMR	47.7	P	1	2.5 - 8.0	
5	M1-8"SP	49.9	P	1	2.5 - 8.0	
6	M1-8"MP	47.7	P	1	2.5 - 8.0	
7	IMR	45.4	B	-	2.5 - 8.0	
8	M1-8"SP	49.9	B	-	2.5 - 8.0	
9	M1-8"MP	47.7	B	-	2.5 - 8.0	
10	IMR	45.4	B	-	2.5 - 8.0	
11	M1-8"SP	49.9	B	-	2.5 - 8.0	
12	M1-8"MP	47.7	B	-	2.5 - 8.0	
13	IMR	90.7	B	-	2.5 - 8.0	
14	M1-8"SP	99.8	P	2	2.5 - 8.0	
15	M1-8"SP	49.9	B	-	2.5 - 8.0	
16	M1-8"MP	47.7	B	-	6.4 - 20.0	
17	M1-8"MP	47.7	B	-	6.4 - 20.0	
18	IMR	45.4	B	-	6.4 - 20.0	
19	IMR	45.4	B	-	6.4 - 20.0	
20	M1-8"SP	49.9	B	-	6.4 - 20.0	
21	M1-8"SP	49.9	B	-	6.4 - 20.0	
22	IMR	90.7	B	-	6.4 - 20.0	
23	IMR	90.7	B	-	6.4 - 20.0	
24	M1-8"MP	95.3	B	-	6.4 - 20.0	
25	M1-8"MP	95.3	B	-	6.4 - 20.0	
26	M1-8"SP	99.8	B	-	6.4 - 20.0	
27	M1-8"SP	99.8	B	-	6.4 - 20.0	
28	IMR	181.5	B	-	15.0	
29	M1-8"SP	199.6	B	-	15.0	
30	M1-8"MP	190.6	B	-	15.0	
31	IMR	45.4	P	1	15.0	Bonfire
32	M1-8"SP	49.9	P	1	15.0	Bonfire
33	M1-8"MP	47.7	P	1	15.0	Bonfire
34	IMR	136.1	P	3	15.0	Bonfire
35	M1-8"SP	149.7	P	3	15.0	Bonfire
36	M1-8"MP	142.9	P	3	15.0	Bonfire
37	IMR	362.9	B	-	10.0 - 20.0	
38	M1-8"SP	399.2	B	-	10.0 - 20.0	
39	M1-8"MP	381.0	B	-	10.0 - 20.0	
40	WC-844	100.0	B	-	15.0	
41	WC-846	100.0	B	-	15.0	
42	WC-844	100.0	B	-	15.0	
43	WC Blank	100.0	B	-	15.0	
44	WC-844	226.8	P	5	15.0	
45	WC-846	226.8	P	5	15.0	
46	WC Blank	136.1	P	5	15.0	
47	WC-844	136.1	P	3	15.0	Bonfire
48	WC-846	136.1	P	3	15.0	Bonfire
49	WC Blank	81.6	P	3	15.0	Bonfire

Table 3  
Summary of data for IMR5010

Test no 1	Mass 45.4 Kg	Centr.Ign.	
Distance (Meters)	Radiant heat flux(cal/sq cm/sec)		
	Peak	5 Sec avg peak	Average
3.2	1.750	1.070	0.482
4.0	1.050	0.700	0.329
5.0	1.068	0.703	0.289
6.4	0.576	0.382	0.161
8.0	0.468	0.301	0.127

Burn time: 35.0 sec

Total radiant heat: 13.8 Megacalories

Total radiant heat/unit mass: 0.303 Kilocalories/gram

Total burn time/unit mass(sec/kg): 0.772

Distance scaling exponent=-1.47

Test no 4	Mass 45.4 Kg	Packaged	
Distance (Meters)	Radiant heat flux(cal/sq cm/sec)		
	Peak	5 Sec avg peak	Average
3.2	1.400	0.767	0.348
4.0	0.900	0.450	0.154
5.0	0.780	0.432	0.191
6.4	0.372	0.184	0.075
8.0	0.234	0.118	0.049

Burn time: 42.0 sec

Total radiant heat: 19.7 Megacalories

Total radiant heat/unit mass: 0.433 Kilocalories/gram

Total burn time/unit mass(sec/kg): 0.926

Distance scaling exponent=-2.03

Test no 7	Mass 45.4 Kg		
Distance (Meters)	Radiant heat flux(cal/sq cm/sec)		
	Peak	5 Sec avg peak	Average
2.5	0.700	0.640	0.448
3.2	0.450	0.440	0.283
4.0	0.350	0.320	0.191
5.0	0.288	0.278	0.170
6.4	0.192	0.180	0.106
8.0	0.138	0.130	0.081

Burn time: 23.0 sec

Total radiant heat: 12.7 Megacalories

Total radiant heat/unit mass: 0.281 Kilocalories/gram

Total burn time/unit mass(sec/kg): 0.507

Distance scaling exponent=-1.43

Table 3 (continued)

Test no	10	Mass	45.4 Kg	
Distance (Meters)		Radiant heat flux(cal/sq cm/sec)		
		Peak	5 Sec avg	peak Average
	2.5	0.600	0.600	0.435
	3.2	0.550	0.530	0.339
	4.0	0.450	0.430	0.287
	5.0	0.336	0.319	0.218
	6.4	0.240	0.230	0.146
	8.0	0.168	0.154	0.099

Burn time: 17.0 sec

Total radiant heat: 13.7 Megacalories

Total radiant heat/unit mass: 0.303 Kilocalories/gram

Total burn time/unit mass(sec/kg): 0.375

Distance scaling exponent=-1.26

Test no	13	Mass	90.7 Kg	
Distance (Meters)		Radiant heat flux(cal/sq cm/sec)		
		Peak	5 Sec avg	peak Average
	2.5	1.600	1.467	1.032
	3.2	1.400	1.350	0.918
	4.0	0.650	0.633	0.437
	5.0	0.780	0.768	0.501
	6.4	0.228	0.216	0.154

Burn time: 31.2 sec

Total radiant heat: 39.8 Megacalories

Total radiant heat/unit mass: 0.439 Kilocalories/gram

Total burn time/unit mass(sec/kg): 0.344

Distance scaling exponent=-1.90

Test no	18	Mass	45.4 Kg	
Distance (Meters)		Radiant heat flux(cal/sq cm/sec)		
		Peak	5 Sec avg	peak Average
	8.0	0.150	0.142	0.085
	10.0	0.113	0.113	0.070
	12.8	0.060	0.057	0.032
	16.0	0.039	0.039	0.023
	20.0	0.027	0.026	0.015

Burn time: 25.0 sec

Total radiant heat: 22.1 Megacalories

Total radiant heat/unit mass: 0.488 Kilocalories/gram

Total burn time/unit mass(sec/kg): 0.551

Distance scaling exponent=-2.02

Table 3 (continued)

Test no	19	Mass	45.4 Kg	
Distance (Meters)		Radiant heat flux(cal/sq cm/sec)		
		Peak	5 Sec avg	peak Average
6.4		0.275	0.242	0.141
8.0		0.213	0.183	0.108
10.0		0.150	0.133	0.080
12.8		0.081	0.070	0.041
16.0		0.057	0.050	0.029
20.0		0.038	0.032	0.018

Burn time: 19.0 sec

Total radiant heat: 19.4 Megacalories

Total radiant heat/unit mass: 0.427 Kilocalories/gram

Total burn time/unit mass(sec/kg): 0.419

Distance scaling exponent=-1.85

Test no	22	Mass	90.7 Kg	
Distance (Meters)		Radiant heat flux(cal/sq cm/sec)		
		Peak	5 Sec avg	peak Average
6.4		0.250	0.250	0.178
8.0		0.188	0.188	0.122
10.0		0.150	0.146	0.101
12.8		0.075	0.073	0.049
16.0		0.051	0.049	0.032
20.0		0.033	0.032	0.021

Burn time: 35.0 sec

Total radiant heat: 39.6 Megacalories

Total radiant heat/unit mass: 0.437 Kilocalories/gram

Total burn time/unit mass(sec/kg): 0.386

Distance scaling exponent=-1.92

Test no	23	Mass	90.7 Kg	
Distance (Meters)		Radiant heat flux(cal/sq cm/sec)		
		Peak	5 Sec avg	peak Average
6.4		0.275	0.242	0.157
8.0		0.188	0.188	0.122
10.0		0.138	0.137	0.088
12.8		0.078	0.073	0.044
16.0		0.051	0.049	0.032
20.0		0.035	0.034	0.021

Burn time: 30.0 sec

Total radiant heat: 37.4 Megacalories

Total radiant heat/unit mass: 0.412 Kilocalories/gram

Total burn time/unit mass(sec/kg): 0.331

Distance scaling exponent=-1.83

Table 3 (continued)

Test no	28	Mass	181.4 Kg	Pkg/bonfire
Distance (Meters)		Radiant heat flux(cal/sq cm/sec)		
		Peak	5 Sec avg	peak Average
	15.0	0.051	0.051	0.037
	15.0	0.051	0.051	0.040

Burn time: 72.0 sec

Total radiant heat: 82.6 Megacalories

Total radiant heat/unit mass: 0.455 Kilocalories/gram

Total burn time/unit mass(sec/kg): 0.397

Test no	31	Mass	45.4 Kg	Pkg/bonfire
Distance (Meters)		Radiant heat flux(cal/sq cm/sec)		
		Peak	5 Sec avg	peak Average
	15.0	0.240	0.133	0.052
	15.0	0.126	0.082	0.036
	15.0	0.126	0.084	0.035

Burn time: 12.0 sec

Total radiant heat: 19.6 Megacalories

Total radiant heat/unit mass: 0.431 Kilocalories/gram

Total burn time/unit mass(sec/kg): 0.265

Test no	34	Mass	136.1 Kg	Pkg/bonfire
Distance (Meters)		Radiant heat flux(cal/sq cm/sec)		
		Peak	5 Sec avg	peak Average
	15.0	0.288	0.166	0.072
	15.0	0.294	0.162	0.081
	15.0	0.324	0.174	0.086

Burn time: 16.0 sec

Total radiant heat: 67.5 Megacalories

Total radiant heat/unit mass: 0.496 Kilocalories/gram

Total burn time/unit mass(sec/kg): 0.118

Table 3 (continued)

Test no	37	Mass	362.9 Kg
Distance (Meters)		Radiant heat flux(cal/sq cm/sec)	
		Peak	5 Sec avg peak
10.0		0.114	0.114
15.0		0.060	0.060
20.0		0.033	0.033

Burn time:140.0 sec

Total radiant heat:156.9 Megacalories

Total radiant heat/unit mass: 0.432 Kilocalories/gram

Total burn time/unit mass(sec/kg): 0.386

Distance scaling exponent=-1.88

Table 4  
Summary of data for M1-8-SP

Test no 2	Mass 49.9 Kg	Radiant heat flux(cal/sq cm/sec)		
Distance (Meters)	Peak	5 Sec avg	peak	Average
3.2	0.650	0.650		0.365
4.0	0.450	0.417		0.241
5.0	0.432	0.408		0.221
6.4	0.240	0.236		0.150
8.0	0.186	0.180		0.107

Burn time: 29.0 sec

Total radiant heat: 22.3 Megacalories

Total radiant heat/unit mass: 0.447 Kilocalories/gram

Total burn time/unit mass(sec/kg): 0.581

Distance scaling exponent=-1.27

Test no 5	Mass 49.9 Kg	Packaged		
Distance (Meters)	Radiant heat flux(cal/sq cm/sec)			
	Peak	5 Sec avg	peak	Average
2.5	1.300	1.140		0.665
3.2	1.350	1.070		0.659
4.0	0.700	0.570		0.352
5.0	0.972	0.710		0.381
6.4	0.384	0.329		0.170
8.0	0.312	0.268		0.145

Burn time: 23.0 sec

Total radiant heat: 20.4 Megacalories

Total radiant heat/unit mass: 0.408 Kilocalories/gram

Total burn time/unit mass(sec/kg): 0.461

Distance scaling exponent=-1.43

Test no 8	Mass 49.9 Kg	Radiant heat flux(cal/sq cm/sec)		
Distance (Meters)	Peak	5 Sec avg	peak	Average
2.5	0.600	0.560		0.359
3.2	0.450	0.430		0.285
4.0	0.350	0.310		0.185
5.0	0.396	0.326		0.191
6.4	0.288	0.240		0.143

Burn time: 27.0 sec

Total radiant heat: 8.0 Megacalories

Total radiant heat/unit mass: 0.161 Kilocalories/gram

Total burn time/unit mass(sec/kg): 0.541

Distance scaling exponent=-0.96

Table 4 (continued)

Test no	11	Mass	49.9 Kg	Radiant heat flux(cal/sq cm/sec)		
Distance (Meters)		Peak	5 Sec avg	peak	Average	
2.5		2.000		1.900		1.226
3.2		2.250		1.950		1.242
4.0		1.100		0.940		0.584
5.0		1.716		1.428		0.875
6.4		0.528		0.420		0.261
8.0		0.420		0.331		0.197

Burn time: 15.0 sec

Total radiant heat: 29.8 Megacalories

Total radiant heat/unit mass: 0.597 Kilocalories/gram

Total burn time/unit mass(sec/kg): 0.301

Distance scaling exponent=-1.66

Test no	14	Mass	99.8 Kg	Packaged		
Distance (Meters)		Peak	5 Sec avg	peak	Average	
2.5		5.800		3.640		1.393
3.2		4.000		2.300		0.950
4.0		1.600		1.060		0.483
5.0		2.136		1.426		0.617
6.4		0.648		0.403		0.183
8.0		0.444		0.302		0.145

Burn time: 8.0 sec

Total radiant heat: 18.3 Megacalories

Total radiant heat/unit mass: 0.184 Kilocalories/gram

Total burn time/unit mass(sec/kg): 0.080

Distance scaling exponent=-1.98

Test no	15	Mass	49.9 Kg	Radiant heat flux(cal/sq cm/sec)		
Distance (Meters)		Peak	5 Sec avg	peak	Average	
2.5		1.500		1.200		0.900
3.2		1.250		0.940		0.635
4.0		0.800		0.660		0.474
5.0		0.984		0.667		0.425
6.4		0.648		0.492		0.316
8.0		0.498		0.371		0.236

Burn time: 15.0 sec

Total radiant heat: 20.8 Megacalories

Total radiant heat/unit mass: 0.417 Kilocalories/gram

Total burn time/unit mass(sec/kg): 0.301

Distance scaling exponent=-1.10

Table 4 (continued)

Test no	20	Mass	49.9 Kg	
Distance (Meters)		Radiant heat flux(cal/sq cm/sec)		
		Peak	5 Sec avg	Average
6.4		0.375	0.342	0.206
8.0		0.263	0.250	0.160
10.0		0.300	0.271	0.154
12.8		0.159	0.149	0.089
16.0		0.117	0.105	0.063
20.0		0.083	0.075	0.044

Burn time: 15.0 sec

Total radiant heat: 31.0 Megacalories

Total radiant heat/unit mass: 0.622 Kilocalories/gram

Total burn time/unit mass(sec/kg): 0.301

Distance scaling exponent=-1.38

Test no	21	Mass	49.9 Kg	
Distance (Meters)		Radiant heat flux(cal/sq cm/sec)		
		Peak	5 Sec avg	Average
6.4		0.400	0.375	0.247
8.0		0.313	0.300	0.188
10.0		0.300	0.275	0.165
12.8		0.153	0.146	0.087
16.0		0.114	0.107	0.062
20.0		0.080	0.074	0.043

Burn time: 15.0 sec

Total radiant heat: 32.4 Megacalories

Total radiant heat/unit mass: 0.649 Kilocalories/gram

Total burn time/unit mass(sec/kg): 0.301

Distance scaling exponent=-1.59

Test no	26	Mass	99.8 Kg	
Distance (Meters)		Radiant heat flux(cal/sq cm/sec)		
		Peak	5 Sec avg	Average
6.4		0.875	0.742	0.418
8.0		0.350	0.350	0.179
10.0		0.625	0.533	0.287
12.8		0.171	0.153	0.081
16.0		0.111	0.100	0.051
20.0		0.072	0.063	0.031

Burn time: 28.0 sec

Total radiant heat: 68.4 Megacalories

Total radiant heat/unit mass: 0.685 Kilocalories/gram

Total burn time/unit mass(sec/kg): 0.281

Distance scaling exponent=-2.25

Table 4 (continued)

Test no	27	Mass	99.8 Kg	
Distance (Meters)		Radiant heat flux(cal/sq cm/sec)		
		Peak	5 Sec avg	Average
	6.4	0.750	0.717	0.426
	8.0	0.375	0.350	0.194
	10.0	0.700	0.629	0.330
	12.8	0.174	0.160	0.079
	16.0	0.108	0.106	0.051
	20.0	0.063	0.062	0.030

Burn time: 28.0 sec

Total radiant heat: 71.8 Megacalories

Total radiant heat/unit mass: 0.719 Kilocalories/gram

Total burn time/unit mass(sec/kg): 0.281

Distance scaling exponent=-2.34

Test no	29	Mass	199.6 Kg	
Distance (Meters)		Radiant heat flux(cal/sq cm/sec)		
		Peak	5 Sec avg	Average
	15.0	0.111	0.111	0.063
	15.0	0.111	0.111	0.068

Burn time: 52.0 sec

Total radiant heat: 111.6 Megacalories

Total radiant heat/unit mass: 0.559 Kilocalories/gram

Total burn time/unit mass(sec/kg): 0.261

Test no	32	Mass	49.9 Kg	Pkg/bonfire
Distance (Meters)		Radiant heat flux(cal/sq cm/sec)		
		Peak	5 Sec avg	Average
	15.0	0.480	0.292	0.140
	15.0	0.285	0.142	0.068
	15.0	0.288	0.143	0.068

Burn time: 10.0 sec

Total radiant heat: 28.6 Megacalories

Total radiant heat/unit mass: 0.573 Kilocalories/gram

Total burn time/unit mass(sec/kg): 0.200

Table 4 (continued)

Test no	35	Mass 149.7 Kg	Pkg/bonfire	
Distance (Meters)		Radiant heat flux(cal/sq cm/sec)		
		Peak	5 Sec avg peak	Average
	15.0	0.654	0.294	0.151
	15.0	0.588	0.293	0.132
	15.0	0.570	0.296	0.132

Burn time: 23.0 sec

Total radiant heat: 121.4 Megacalories

Total radiant heat/unit mass: 0.811 Kilocalories/gram

Total burn time/unit mass(sec/kg): 0.154

Test no	38	Mass 399.2 Kg		
Distance (Meters)		Radiant heat flux(cal/sq cm/sec)		
		Peak	5 Sec avg peak	Average
	10.0	0.345	0.345	0.138
	15.0	0.318	0.318	0.090
	20.0	0.111	0.111	0.045

Burn time: 95.0 sec

Total radiant heat: 229.2 Megacalories

Total radiant heat/unit mass: 0.574 Kilocalories/gram

Total burn time/unit mass(sec/kg): 0.238

Distance scaling exponent=-1.57

Table 5  
Summary of data for M1-8-MP

Test no	3	Mass	47.6 Kg	Radiant heat flux(cal/sq cm/sec)		
Distance	(Meters)	Peak	5 Sec avg	peak	Average	
	3.2	1.600		1.433		0.733
	4.0	1.000		0.833		0.467
	5.0	1.032		0.936		0.464
	6.4	0.504		0.404		0.212
	8.0	0.420		0.336		0.166

Burn time: 15.0 sec

Total radiant heat: 20.8 Megacalories

Total radiant heat/unit mass: 0.436 Kilocalories/gram

Total burn time/unit mass(sec/kg): 0.315

Distance scaling exponent=-1.64

Test no	6	Mass	47.6 Kg	Packaged		
Distance	(Meters)	Peak	5 Sec avg	peak	Average	
	2.5	1.800		1.560		0.900
	3.2	1.600		1.500		0.888
	4.0	0.800		0.720		0.432
	6.4	0.552		0.480		0.257
	8.0	0.600		0.539		0.274

Burn time: 20.0 sec

Total radiant heat: 21.2 Megacalories

Total radiant heat/unit mass: 0.446 Kilocalories/gram

Total burn time/unit mass(sec/kg): 0.420

Distance scaling exponent=-1.20

Test no	9	Mass	47.6 Kg	Radiant heat flux(cal/sq cm/sec)		
Distance	(Meters)	Peak	5 Sec avg	peak	Average	
	3.2	1.400		1.300		0.710
	4.0	1.200		1.070		0.580
	5.0	1.008		0.905		0.481
	6.4	0.660		0.600		0.316

Burn time: 12.0 sec

Total radiant heat: 19.6 Megacalories

Total radiant heat/unit mass: 0.411 Kilocalories/gram

Total burn time/unit mass(sec/kg): 0.252

Distance scaling exponent=-1.14

Table 5 (continued)

Test no	12	Mass	47.6 Kg	Radiant heat flux(cal/sq cm/sec)	
Distance (Meters)		Peak	5 Sec avg	peak	Average
2.5		2.400		1.900	0.954
3.2		1.800		1.500	0.746
4.0		1.400		1.190	0.581
5.0		1.308		1.150	0.569
6.4		0.732		0.617	0.290
8.0		0.510		0.424	0.203

Burn time: 9.0 sec

Total radiant heat: 16.9 Megacalories

Total radiant heat/unit mass: 0.354 Kilocalories/gram

Total burn time/unit mass(sec/kg): 0.189

Distance scaling exponent=-1.31

Test no	16	Mass	47.6 Kg	Radiant heat flux(cal/sq cm/sec)	
Distance (Meters)		Peak	5 Sec avg	peak	Average
6.4		0.500		0.455	0.287
8.0		0.475		0.430	0.265
10.0		0.325		0.303	0.186
16.0		0.156		0.137	0.080

Burn time: 13.0 sec

Total radiant heat: 27.6 Megacalories

Total radiant heat/unit mass: 0.580 Kilocalories/gram

Total burn time/unit mass(sec/kg): 0.273

Distance scaling exponent=-1.47

Test no	17	Mass	47.6 Kg	Radiant heat flux(cal/sq cm/sec)	
Distance (Meters)		Peak	5 Sec avg	peak	Average
6.4		0.500		0.435	0.265
8.0		0.463		0.330	0.196
10.0		0.288		0.247	0.148
12.8		0.192		0.163	0.096
16.0		0.132		0.112	0.065
20.0		0.099		0.085	0.048

Burn time: 12.0 sec

Total radiant heat: 24.4 Megacalories

Total radiant heat/unit mass: 0.513 Kilocalories/gram

Total burn time/unit mass(sec/kg): 0.252

Distance scaling exponent=-1.53

Table 5 (continued)

Test no	24	Mass	95.3 Kg	Radiant heat flux(cal/sq cm/sec)	
Distance (Meters)		Peak	5 Sec avg	peak	Average
8.0		0.738		0.663	0.352
10.0		1.275		1.103	0.551
12.8		0.348		0.328	0.169
16.0		0.240		0.215	0.110
20.0		0.155		0.136	0.070

Burn time: 15.0 sec

Total radiant heat: 69.1 Megacalories

Total radiant heat/unit mass: 0.725 Kilocalories/gram

Total burn time/unit mass(sec/kg): 0.157

Distance scaling exponent=-2.11

Test no	25	Mass	95.3 Kg	Radiant heat flux(cal/sq cm/sec)	
Distance (Meters)		Peak	5 Sec avg	peak	Average
6.4		1.425		1.210	0.665
8.0		0.713		0.647	0.346
10.0		1.150		0.950	0.494
12.8		0.360		0.326	0.170
16.0		0.249		0.228	0.117
20.0		0.161		0.149	0.076

Burn time: 15.0 sec

Total radiant heat: 66.6 Megacalories

Total radiant heat/unit mass: 0.699 Kilocalories/gram

Total burn time/unit mass(sec/kg): 0.157

Distance scaling exponent=-1.90

Test no	30	Mass	190.5 Kg	Radiant heat flux(cal/sq cm/sec)	
Distance (Meters)		Peak	5 Sec avg	peak	Average
15.0		0.246		0.232	0.127
15.0		0.210		0.194	0.108

Burn time: 25.0 sec

Total radiant heat: 99.7 Megacalories

Total radiant heat/unit mass: 0.523 Kilocalories/gram

Total burn time/unit mass(sec/kg): 0.131

Table 5 (continued)

Test no	33	Mass	47.6 Kg	Pkg/bonfire
Distance (Meters)		Radiant heat flux(cal/sq cm/sec)		
		Peak	5 Sec avg	peak Average
15.0		0.210	0.162	0.083
15.0		0.162	0.133	0.072
15.0		0.168	0.134	0.073

Burn time: 12.0 sec

Total radiant heat: 27.9 Megacalories

Total radiant heat/unit mass: 0.585 Kilocalories/gram

Total burn time/unit mass(sec/kg): 0.252

Test no	36	Mass	142.9 Kg	Pkg/bonfire
Distance (Meters)		Radiant heat flux(cal/sq cm/sec)		
		Peak	5 Sec avg	peak Average
15.0		0.576	0.386	0.155
15.0		0.432	0.250	0.094
15.0		0.360	0.211	0.083

Burn time: 19.5 sec

Total radiant heat: 109.2 Megacalories

Total radiant heat/unit mass: 0.764 Kilocalories/gram

Total burn time/unit mass(sec/kg): 0.136

Test no	39	Mass	381.0 Kg	Pkg/bonfire
Distance (Meters)		Radiant heat flux(cal/sq cm/sec)		
		Peak	5 Sec avg	peak Average
10.0		0.420	0.414	0.252
15.0		0.366	0.348	0.201
20.0		0.135	0.132	0.090

Burn time: 45.0 sec

Total radiant heat: 211.6 Megacalories

Total radiant heat/unit mass: 0.555 Kilocalories/gram

Total burn time/unit mass(sec/kg): 0.118

Distance scaling exponent=-1.43

Table 6  
Summary of data for WC844

Test no. 40 Mass 100.0 Kg

Distance (Meters)	Radiant heat flux (cal/sq.cm/sec)		
	Peak	5 Sec avg	Average
15.0	0.062	0.026	0.014
15.0	0.052	0.021	0.009

Burn time: 62.6 sec  
 Total radiant heat: 20.190 Megacalories  
 Total radiant heat/unit mass: 0.202 kilocalories/gram  
 Total burn time/unit mass (sec/kg): 0.626

Test no. 42 Mass 100.0 Kg

Distance (Meters)	Radiant heat flux (cal/sq.cm/sec)		
	Peak	5 Sec avg	Average
15.0	0.052	0.034	0.013
15.0	0.043	0.027	0.010

Burn time: 161.7 sec  
 Total radiant heat: 54.208 Megacalories  
 Total radiant heat/unit mass: 0.542 kilocalories/gram  
 Total burn time/unit mass (sec/kg): 1.617

Test no. 44 Mass 226.8 Kg Pkg

Distance (Meters)	Radiant heat flux (cal/sq.cm/sec)		
	Peak	5 Sec avg	Average
15.0	0.090	0.048	0.013
15.0	0.090	0.059	0.021

Burn time: 165.3 sec  
 Total radiant heat: 80.912 Megacalories  
 Total radiant heat/unit mass: 0.357 kilocalories/gram  
 Total burn time/unit mass (sec/kg): 0.729

Table 6 (continued)

Test no. 47 Mass 136.1 Kg Pkg/bonfire

Distance (Meters)	Radiant heat flux (cal/sq.cm/sec)			Average
	Peak	5 Sec avg	peak	
15.0	0.268		0.123	0.065
15.0	0.267		0.140	0.083
15.0	0.253		0.123	0.074

Burn time: 65.3 sec

Total radiant heat: 136.728 Megacalories

Total radiant heat/unit mass: 1.005 kilocalories/gram

Total burn time/unit mass (sec/kg): 0.480

Table 7  
Summary of data for WC846

Test no. 41 Mass 100.0 Kg

Distance (Meters)	Radiant heat flux (cal/sq.cm/sec)		
	Peak	5 Sec avg	Average
15.0	0.029	0.018	0.011
15.0	0.073	0.039	0.025

Burn time: 215.0 sec  
 Total radiant heat: 106.975 Megacalories  
 Total radiant heat/unit mass: 1.070 kilocalories/gram  
 Total burn time/unit mass (sec/kg): 2.150

Test no. 45 Mass 226.8 Kg Pkg

Distance (Meters)	Radiant heat flux (cal/sq.cm/sec)		
	Peak	5 Sec avg	Average
15.0	0.246	0.188	0.097
15.0	0.130	0.100	0.090

Burn time: 44.2 sec  
 Total radiant heat: 185.711 Megacalories  
 Total radiant heat/unit mass: 0.819 kilocalories/gram  
 Total burn time/unit mass (sec/kg): 0.195

Test no. 48 Mass 136.1 Kg Pkg/bonfire

Distance (Meters)	Radiant heat flux (cal/sq.cm/sec)		
	Peak	5 Sec avg	Average
15.0	0.637	0.189	0.076
15.0	0.612	0.209	0.094
15.0	0.654	0.191	0.087

Burn time: 46.8 sec  
 Total radiant heat: 113.684 Megacalories  
 Total radiant heat/unit mass: 0.835 kilocalories/gram  
 Total burn time/unit mass (sec/kg): 0.344

Table 8				
Summary of data for WC Blank				
Test no. 43 Mass 100.0 Kg				
Distance (Meters)	Peak	Radiant heat flux (cal/sq.cm/sec) 5 Sec avg peak	Average	
15.0	0.233	0.062	0.060	
15.0	0.220	0.052	0.050	
Burn time:	65.0 sec			
Total radiant heat:	108.855 Megacalories			
Total radiant heat/unit mass:	1.089 kilocalories/gram			
Total burn time/unit mass (sec/kg):	0.650			
Test no. 46 Mass 136.1 Kg Pkg				
Distance (Meters)	Peak	Radiant heat flux (cal/sq.cm/sec) 5 Sec avg peak	Average	
15.0	0.364	0.091	0.032	
15.0	0.351	0.081	0.042	
15.0	0.437	0.097	0.032	
Burn time:	21.9 sec			
Total radiant heat:	21.867 Megacalories			
Total radiant heat/unit mass:	0.161 kilocalories/gram			
Total burn time/unit mass (sec/kg):	0.161			
Test no. 49 Mass 54.4 Kg Pkg/bonfire				
Distance (Meters)	Peak	Radiant heat flux (cal/sq.cm/sec) 5 Sec avg peak	Average	
15.0	0.553	0.136	0.093	
15.0	0.604	0.131	0.091	
15.0	0.490	0.119	0.076	
Burn time:	13.8 sec			
Total radiant heat:	33.876 Megacalories			
Total radiant heat/unit mass:	0.623 kilocalories/gram			
Total burn time/unit mass (sec/kg):	0.254			

Table 9 - Linear burn rates and total radiant thermal energy per unit mass.

Propellant	Linear burn rate (cm/sec)	Radiant energy/mass (Kcal/g)
IMR 5010	1.12	0.433
M1-8"-SP	2.54	0.574
M1-8"-MP	4.88	0.555

Table 10 - Effect of packaging in delaying ignition

Shot No	Propellant type	Package type	Time to ignition (s)		
			$t_1$	$t_2$	$t_3$
34	IMR 5010	Fiberboard drum	125	137	ejected
35	M-1 8" SP	Copper can with wood overlay	331	391	ejected
36	M-1 8" MP	Steel can	104	119	129

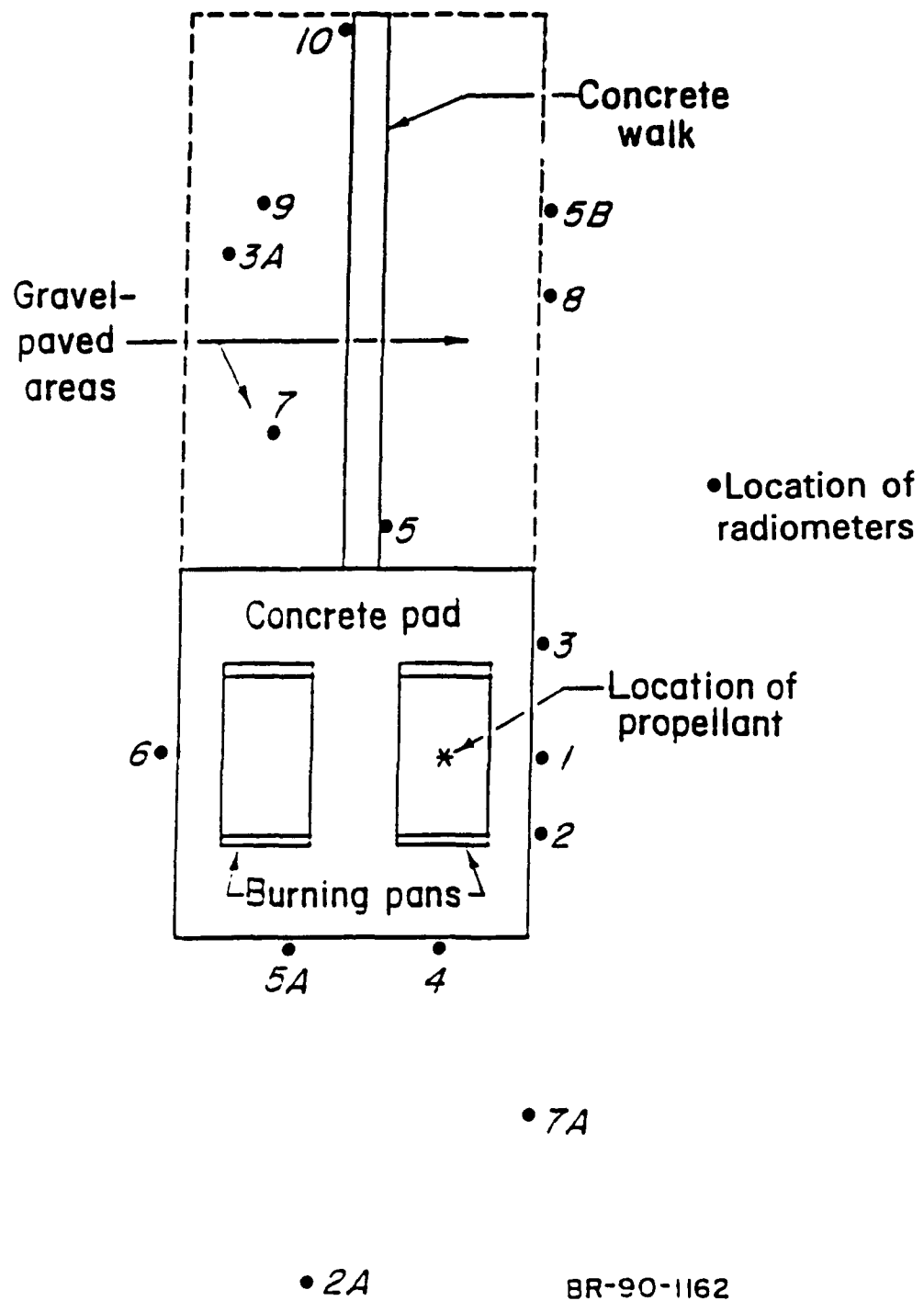


Figure 1. Layout of Radiometers at Lake Lynn Laboratory Burning Ground

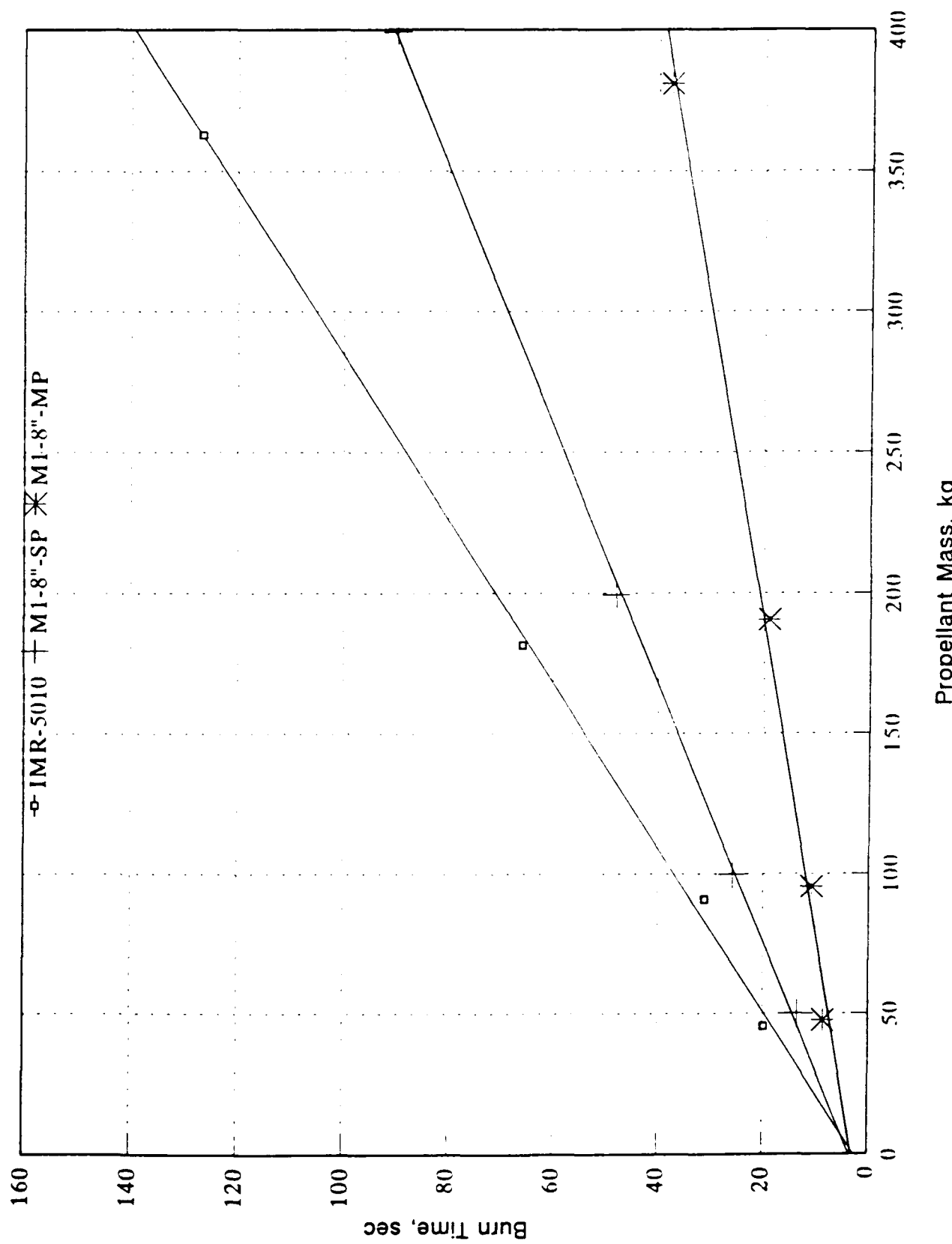


Figure 2. Burn Time vs. Propellant Mass

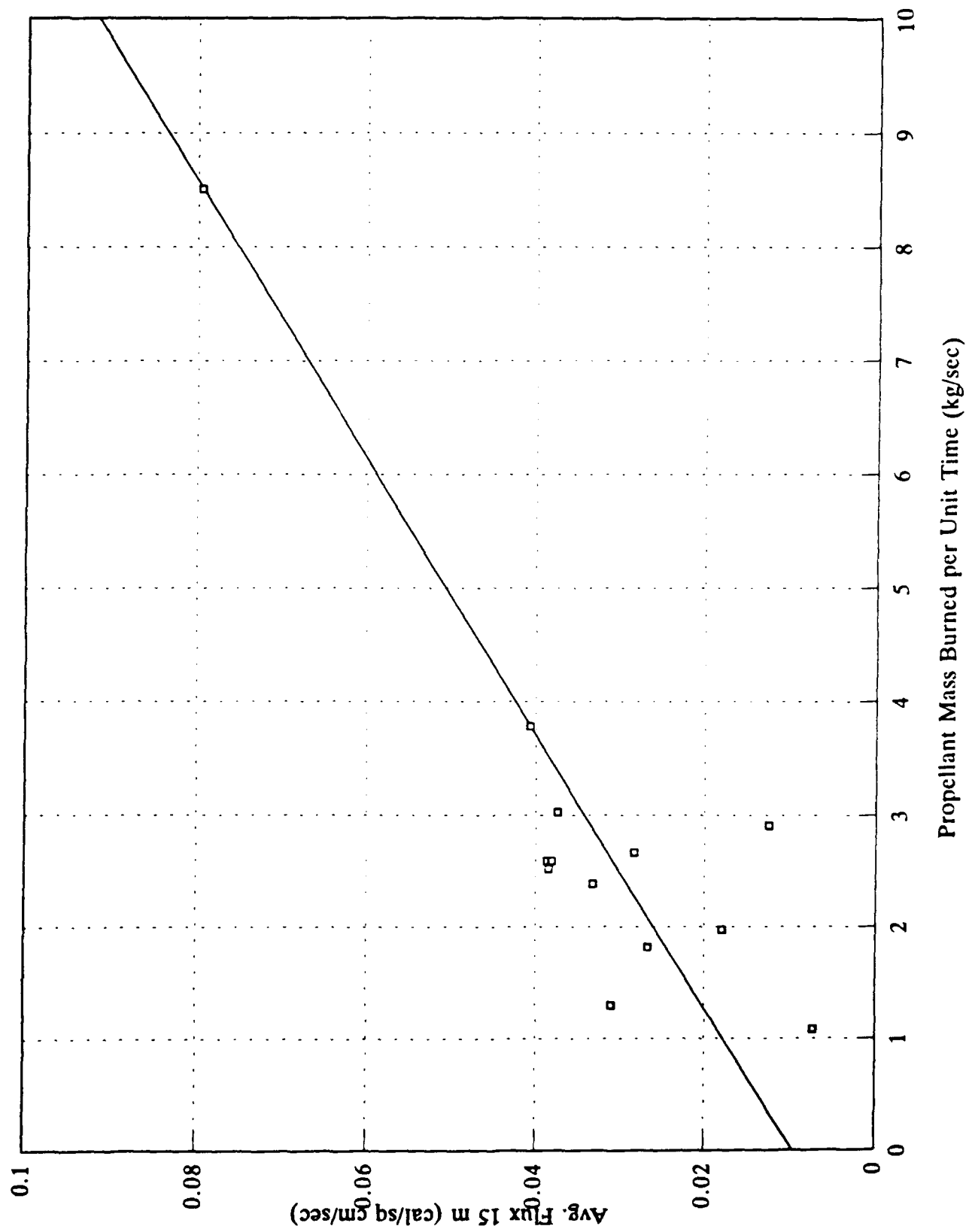


Figure 3. Average flux at 15 m vs. propellant mass burned per unit time for IMR5010 propellant

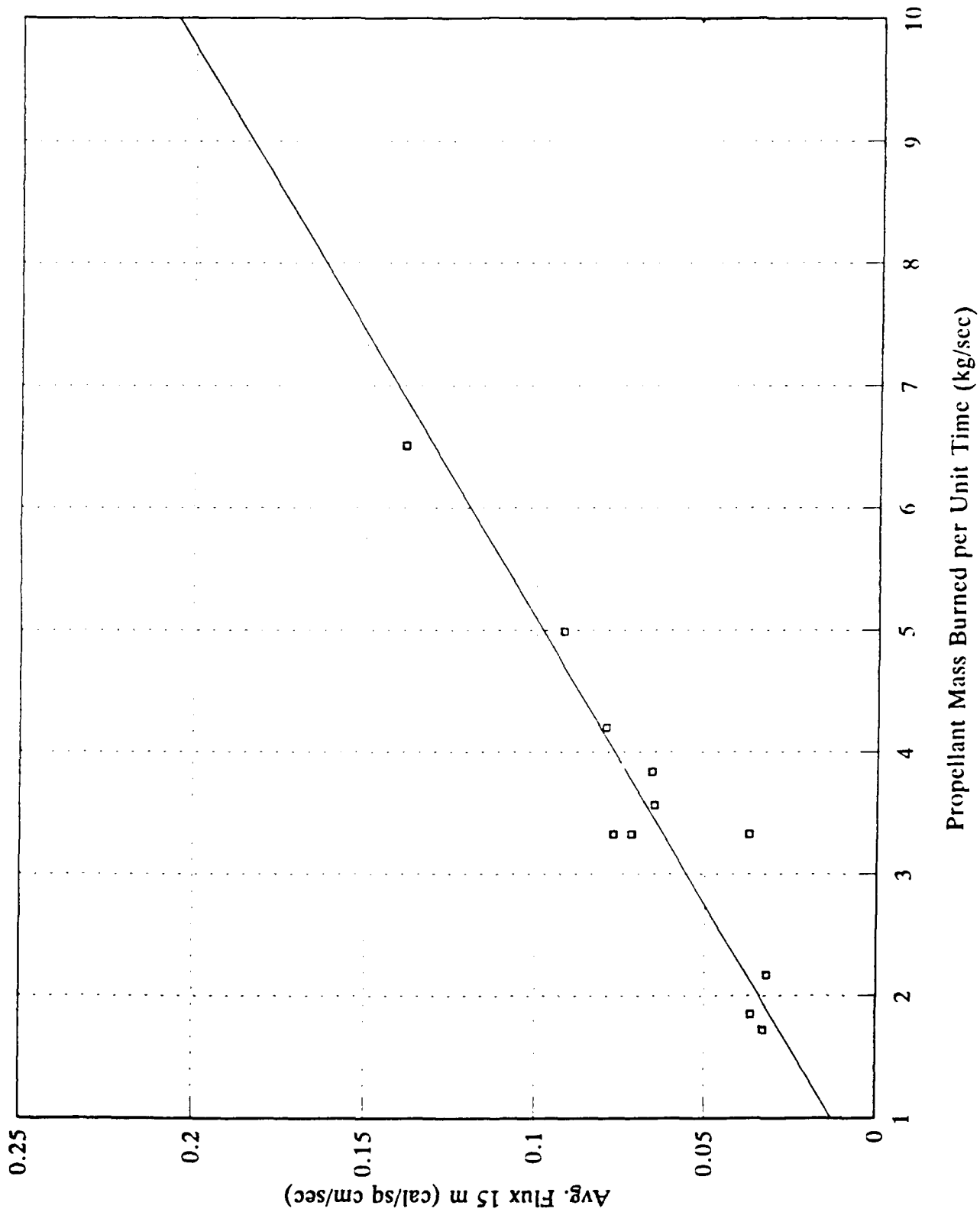


Figure 4. Average flux at 15 m vs. propellant mass burned per unit time for M1 8"SP propellant.

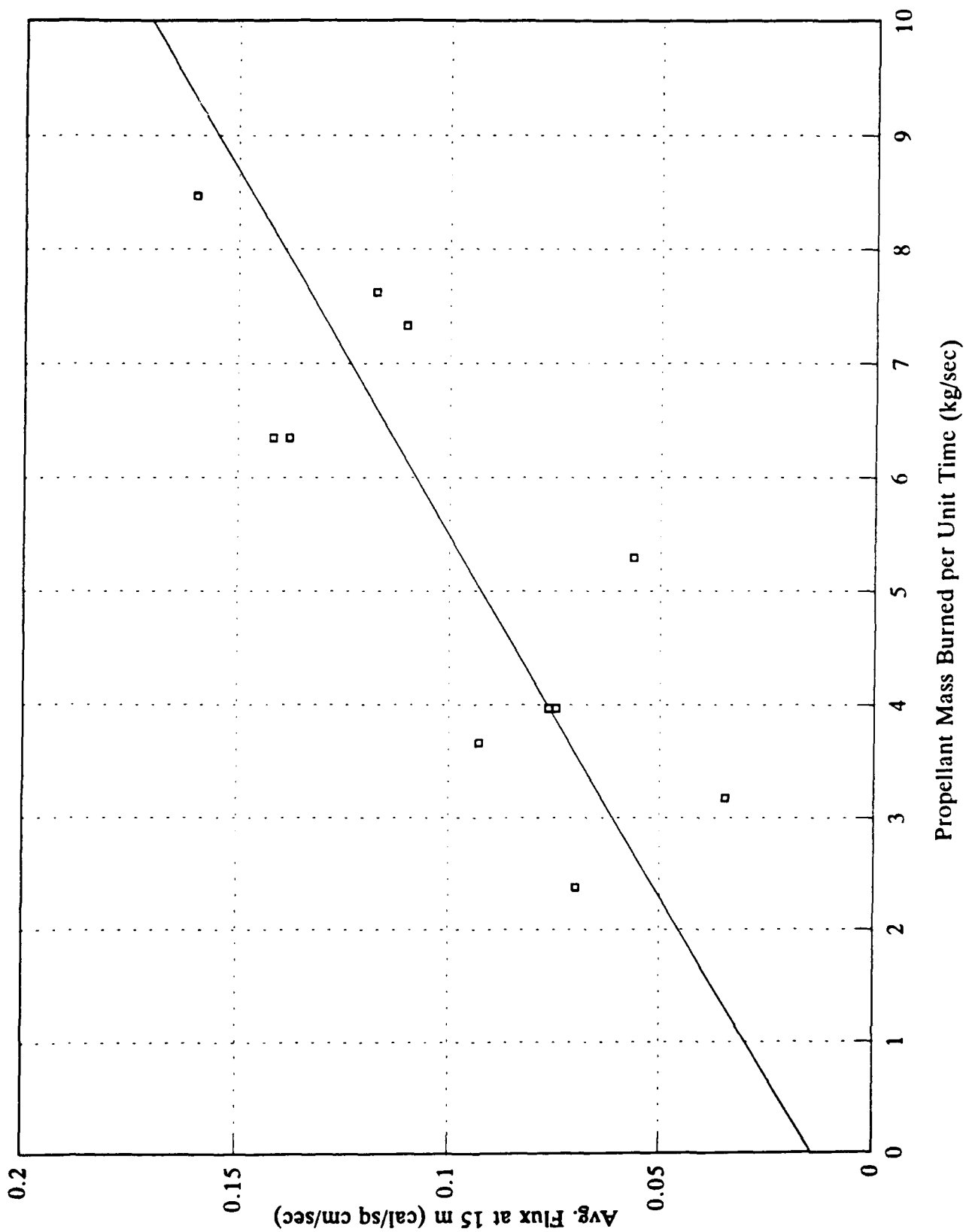


Figure 5. Average flux at 15 m vs. propellant mass burned per unit time for M1 8"MP propellant

## HAZARDS OF ALTITUDE TESTING AT AEDC

Paul K. Salzman  
TRW  
San Bernardino, CA

**ABSTRACT** The detonability (explosion) hazards associated with testing large solid rocket motors in low pressure altitude chambers are largely unknown. Because of the potential damage to these unique facilities, quantification of the hazards involved in such testing is needed.

TRW performed an extensive analytical study to determine the probabilities of generating various explosive yields inside the J-4 vertical test cell at Arnold Engineering Development Center (AEDC) assuming that a failure occurred during an altitude test of a large solid propellant rocket motor (approximately 55,000 lbs of Class 1.3 propellant).

Three failure modes of significance were identified. Two involved axial ejection of the propellant grain downward toward the bottom of the test cell while the third involved radial ejection of the grain toward the test cell wall due to the internal gas pressure.

This paper describes the approach used to evaluate the key elements of the study: (a) identification of failure modes and the associated probability chain, (b) determination of the specific rocket motor initial (failure) conditions and parameters, (c) utilization of detonation theory and test results to develop a required impact velocity for detonation, correlation, (d) calculation of the fragment weight distribution and impact velocities and (e) development of statistical methods to determine the probability for each failure mode.

The results show that radial ejection contributes very little to the overall probability because of the large number of small fragments generated in this failure mode and that the axial failure mode probabilities decrease very rapidly with explosive yield. The overall result indicates that the probability of significant damage to other than the test cell itself is very low.

**INTRODUCTION** In the design and development of the upper stages of large solid rocket motors, test conditions close to actual flight can only be achieved at the unique altitude facilities currently available at Arnold Engineering Development Center (AEDC) in Tullahoma, Tennessee. These test cells, denoted J-4, J-5 and J-6, are large, expensive to build and repair and are a national resource because they do not exist anywhere else in the U.S. They provide the only means available for full stage static testing at altitude, other than actual flight testing.

A 1982 accident in J-4 with a large diameter, class 1.3 rocket motor and another in J-5 with a class 1.1 motor in 1985, which resulted in an explosion, caused AEDC to be concerned with damage to nearby facilities and culminated in the fall of 1990 with the cessation of altitude testing of these motors at AEDC.

Because of the potential damage to the test cells and the surrounding, unique AEDC facilities, quantification of the detonability (explosion) hazards involved in low pressure altitude testing of solid rocket motors was needed. Therefore, an extensive analytical study was undertaken to determine the probabilities of generating various explosive yields inside the J-4 test cell assuming that a failure occurred during simulated altitude testing of a large rocket motor containing approximately 55,000 lbs of Class 1.3 propellant. The objective was to determine if it was safe to resume large diameter rocket motor altitude testing in test cell J-4.

**J-4 TEST CELL** The low pressure test cell consists of an above ground steel capsule which sets over the test stand and below which is a long diffuser tube through which the exhaust gases flow to the main underground chamber where the gases are deflected sideways by a conical steel plate called the "witches' hat". A layout of the cell is shown in Figure 1. The upper capsule is maintained at a low pressure (approximately 1.6 psi) while the lower chamber usually is at a higher pressure (5 - 7 psi) because of the exhaust gases and added cooling water.

For a motor case failure it is possible that propellant would be ejected radially outward to the capsule wall or ejected downward through the diffuser tube ultimately impacting the witch's hat. These are the events that actually took place in the 1985 and 1982 incidents, respectively. A detonation (or explosion; the words are used interchangeably) at the capsule wall might destroy it and allow blast waves to propagate to surrounding facilities causing significant damage. Likewise, detonation at the witches' hat will cause a blast wave to propagate up the diffuser tube, into the capsule, causing it to be removed or destroyed, and then to propagate to other facilities. In either case, the probability of such events needs to be determined.

**APPROACH** The objective of this study was to perform a hazards analysis to determine the risk associated with a detonation event in J-4. The specific goal is to determine the probability of exceeding a given explosive yield in J-4 (inside the capsule).

The approach involved the following key elements: (a) identify failure modes and the associated probability chain; (b) determine the specific rocket motor initial (failure) conditions and parameters; (c) utilize detonation theory and test results to develop a required impact velocity for detonation; (d) calculate the fragment weight distribution and impact velocities; (e) develop statistical methods to determine probability for each failure mode and compute the overall results.

**FAILURE MODES AND PROBABILITY CHAIN** Three failure modes were considered; Axial Full Grain Ejection, Axial Partial Grain Ejection and Radial Ejection. In the first mode, the cylindrical portion of the case unravels and the internal pressure in the space between the top of the grain and the case ejects the entire mass downward; acceleration is due both to gravity and the internal pressure above the grain. It is also possible that lower sections of the grain will break-up and fall away by their own weight, such that the remaining weight ejected downward is less than the full grain weight. In this axial partial grain ejection mode the same driving pressure will accelerate a lesser weight and thus yield a higher velocity than in the full grain case. In either case detonation at the witch's hat will cause a blast wave to propagate up the diffuser tube into the capsule, possibly causing it to be removed or destroyed and then to propagate to other facilities.

Radial ejection assumes that the failure causes the case to unravel and the cylindrical section of the case to "disappear" leaving an unsupported circular core cylinder of propellant having little strength to contain the internal core pressure. This failure leads to fragmentation of the propellant, acceleration of the fragments and multiple impacts at the capsule wall. Detonation at the capsule wall might destroy it and allow blast waves to propagate to surrounding facilities causing significant damage.

The weight ejected for all failure modes depends on the random variable time of failure and also, in the case of axial partial ejection, the fraction of the grain ejected.

The probability of these individual events must be properly combined to determine the overall probability of the explosive yield in J-4. This is given by the probability "chain" equation for the probability of a given weight or greater, detonating, which depends on the probability of a failure of any kind during a test (historically set at 0.02), the probability of an ejection of any kind given a failure (conservatively set equal to 1) and product probability terms representing the types of ejection discussed above. The first term of each product is the probability of the failure mode; the second is the probability of detonation of the given weight, or greater, in the capsule, given the failure mode.

The only unknown terms are the probability of detonation for each failure mode, and they are to be determined.

As described above, axial ejection results in impact at the witch's hat and these failure modes do not directly yield the (desired) weight detonating in the capsule. This was solved by correlating weight detonating at the bottom with (equivalent) weight detonating at the top and is discussed below.

**INITIAL CONDITIONS** The driving force for any ejection is the energy of the hot gas in the bore at the time of the failure. As the motor burns the internal volume increases, the weight of propellant and the web thickness decrease and the internal gas

(chamber) pressure and other thermodynamic properties vary in their characteristic fashion. Nominal burning conditions are assumed up until the time of the failure; then the chamber pressure is assumed to jump to an "upper limit" instantaneous pressure of 2835 psi at 0 sec (as recorded in the 1982 test which failed nearly at 0 sec) decreasing linearly to the  $+3\sigma$  value at 15 sec. For times  $\geq 15$  sec the upper limit follows the  $+3\sigma$  curve. The pressure along these upper limit lines determines the acceleration of the propellant axially or radially.

**DETINATION THEORY** Each failure mode results in an impact event or events leading to the possibility of detonation of some or all of the propellant ejected. The velocity of the impact events is to be compared to that required for initiation of detonation of all or part of the propellant mass. For the axial cases a single large mass impacts the witch's hat while in the radial case a distribution of fragments impacts the inner capsule wall.

For large propellant masses critical geometry theory predicts the critical dimensions above which an initiated detonation will be sustained. Application to the propellant being considered indicates the grain is above critical and will sustain detonation. For initiation of detonation the required shock pressure for SDT (Shock-to-Detonation-Transition) generally ranges from about 25 kbar at critical dimensions to about 8 kbar at very large dimensions; for the particular motor being considered the value is about 12 kbar.

Initiation can also take place by XDT (Unknown-to-Detonation-Transition) under conditions less severe than for SDT. This might occur when a large propellant mass impacts a surface; the velocity required for initiation is less for XDT than for SDT. In this study it is assumed that XDT is SDT in unconsolidated (damaged) propellant caused by the impact. The damage to the propellant dynamically introduces porosity which is well known to significantly reduce the critical diameter and shock pressure requirement compared to consolidated propellant. The criterion is modified for XDT by defining a family of curves below the SDT criterion, for various values of porosity. This defines a more sensitive initiation criterion for XDT of approximately 3 kbar.

**DETINATION REQUIREMENTS AND DISTRIBUTION FUNCTION** Ullian<sup>1</sup> reported the "TNT Equivalent" of a series of aborted flights at the Eastern Space and Missile Center where various missile stages (Minuteman, Polaris, Poseidon) containing Class 1.3 propellant impacted various surfaces at various velocities. Results ranged from 1% to 100% TNT Equivalent. The XDT initiation proposed above is consistent with these data and when converted to an equivalent impact on steel (for convenience; the witches' hat and capsule are made of steel), the data provide a correlation of TNT equivalent versus impact velocity. Although this applies to a single large mass impacting in the axial ejection cases, the radial failure mode involves many, much smaller, fragments than the data reported by Ullian and a more general approach is required.

To do this, a large data base covering 6 orders of magnitude of propellant weight were compiled including those from Wierick<sup>2</sup> (Sandia), Lee et al<sup>3</sup> (LLNL), Merrill<sup>4</sup> (AFRPL) using a Titan III C rocket motor weighing 82000 lbs and the Ullian data. These results, all converted to steel impact, are shown in Figure 2 which correlates impact velocity vs. propellant weight with TNT equivalent as a parameter and represents a general steel impact requirement for Class 1.3 propellant.

Figure 2 is the desired detonation requirement correlation; the curves are taken to represent a 50% probability of detonation for a given equivalent. The variability around this midpoint is determined from a log-normal distribution, developed by Hercules for Class 1.1 propellants, from which the standard deviation is determined<sup>5</sup>. Thus the probability of various TNT equivalents resulting from any propellant fragment, at any impact velocity, can be computed.

**AXIAL EJECTION - IMPACT VELOCITIES** Based on a detailed examination of the 1982 event it was concluded that due to propellant gas flow restriction near the igniter, the upper (forward dome) bond line failed leading to overpressurization of the entire Kevlar wound case. The motor case disintegrated and the gas pressure, which was able to penetrate between the grain and the liner at the forward end, "unzipped" the grain and ejected it downward toward the witch's hat. The measured pressure was applied to the grain cross-section and decayed to atmospheric in an estimated 4 - 6 msec. From the drop height to the witch's hat using energy conservation and Newton's laws, the velocity at impact was computed. Because the detonation requirement in Figure 2 implies normal impact and the witches' hat is conical, the calculated impact velocity was adjusted by the sine of one-half the cone interior angle.

Detonating weights at the top (in the capsule) and bottom (at the witches' hat) of the cell were correlated to account for the fact that axial ejection leads to detonation at bottom not at the top as discussed above. This was done using a well-known hydrocode called CSQ<sup>6</sup>. Representative values of weights at the bottom were chosen and using J-4 cell geometry the total blast wave impulse on the capsule dome was determined for full detonation at the witches' hat. Again using CSQ, values of weights at the top were chosen and a "centered" detonation at the original location of the motor was allowed to occur (simulating the geometry of an equivalent blast coming from the witches' hat), and the total impulse on the capsule dome was again determined. These results were used to correlate weight at the bottom with weight at the top by eliminating impulse between them.

**RADIAL EJECTION - IMPACT VELOCITIES - FRAGMENT SIZE DISTRIBUTION** It was assumed that when the motor case fails, the internal pressure breaks that portion of the grain not in the upper dome and accelerates the resulting fragments; it was also assumed that acceleration is rapid and therefore that all fragments have the

same velocity. Impact on the steel wall of the capsule causes initiation of detonation of some of the fragments but each fragment impact can be shown to be an independent event that would not sympathetically detonate other fragments.

Because of the complete lack of data, five different approaches to an acceleration model were used to determine impact velocity. A careful review of these methods led to a range of "realistic" velocities; we chose the uppermost values to be conservative.

There are limited data on the size of the fragments produced in a radial failure. In field testing they are gathered only when an operating motor is destroyed deliberately by a FTOS (Flight Termination Ordnance System) or randomly by an unplanned failure of the type being investigated here. In either case, the propellant is burning at the time of the event and it is very difficult to collect propellant fragments after the test. Nevertheless the data collected after three such tests (Peacekeeper Stage III<sup>7</sup>, Trident C-4<sup>7</sup> and Small ICBM Stage I<sup>8</sup>) were used in this study.

A fragment size distribution model was developed based on a set of theoretical distributions from various models of crushing and fracture of solids. It was concluded that only the very simplest concept was justified; the exponential distribution. This states that the number of fragments greater than a given size is exponentially related to that size. The existing data above are consistent with this distribution at the higher values of fragment size but there are missing data at lower values. This is understandable since the data collection process was very rough and we may assume that many small-sized fragments are either lost on the ground or are burned-up in the fireball. The distributions were developed by "treating" the data to estimate the "missing" fragments, using the above model and extrapolating "backwards" to zero size. This was used to reconstitute the data and the parameter that fully describes the fragment size distribution for each test (average fragment size), was determined. This quantity was shown to correlate well with web thickness for the three data sets above and the resulting expression was applied to the current rocket motor.

The fragment size distribution was converted to a fragment weight distribution by mathematically relating average size to average weight. Thus the fragment size/weight distribution is fully described at any time.

Calculations show that radial failure leads mainly to many small fragments. This is qualitatively consistent with the available post-test data and available films of two of the tests.

**PROBABILITY CALCULATIONS - AXIAL EJECTION** At any time, the propellant weight impacting the witches' hat is known for the full and partial axial cases respectively. The velocity of impact is to be compared to the velocity requirement specified in Figure 2. The procedure is as follows. Weights of TNT outside the cell that

approximately yield a range of blast pressures at range are chosen. These weights are converted to weights at the top of the cell using the inherently conservative assumption of a "paper" capsule. That is, it is assumed that the capsule dome is removed in such a way that it does not extract any energy from the blast inside the cell. Using the weight at the top versus weight at the bottom correlation, the TNT equivalent is defined for each value of weight at the bottom.

The velocity required for 50% probability of detonation is read from Figure 2. From this and the log-normal distribution, the probability that this amount of propellant will detonate is determined. This calculation conservatively determines the probability of detonating this amount or more and is the appropriate calculation. Integration over the burn time gives the desired probability.

The same reasoning applies to axial partial grain ejection except that for each value of weight at the bottom the time integration has to be performed for each value of the fraction of the grain ejected which is itself a random variable. Thus for partial axial ejection a double integration is required.

**PROBABILITY CALCULATIONS - RADIAL EJECTION** This failure mode is qualitatively different from the axial ejection case in that a distribution of fragment sizes is produced (as opposed to a "single" fragment) and that each fragment must be evaluated as a separate impact event. This is treated as follows.

For a given time of failure the web thickness and weight ejected are defined. The fragment weight distribution is given by the cumulative exponential distribution function. For a chosen fragment weight band the mean fragment weight is computed and the number of fragments in the band is determined using the exponential distribution function. The radial impact velocity is compared to that required for 50% probability of detonation from Figure 2 which depends on the fragment weight and the TNT equivalent that is assumed to prevail. From the log-normal distribution the probability can be calculated. A complication occurs because the TNT equivalent is not known. This was resolved by adopting an approach which finds the TNT equivalent that gives the maximum value of the product of the TNT equivalent and the probability. This gives the most weight detonating, a conservative assumption. Once known the mean amount detonating for the fragment is known.

Because there are several fragments in each band, the number of fragments detonating is binomially distributed which is assumed to be approximated by a normal distribution with the same mean and variance. This describes the statistical properties of the weight detonating for the given weight band. To generalize to all fragments at any time, this is repeated for all other weight bands of interest each of which has its own mean and variance for the amount detonating. Because these distributions are approximated by normal distributions, and the sum of normal distributions is a

normal distribution with a mean equal to the sum of the means and a variance equal to the sum of the variances, the distribution of detonating weight for all bands is defined. These distributions are expressed as the cumulative normal distribution of the probability of a given weight, or greater, detonating vs. the weight detonating.

This procedure is generalized for several values of time over the burn time. These are used to plot the probability of detonating a chosen set of weights, or greater, vs. time. Integration of this curve for each of the chosen weights, gives the desired result.

**OVERALL PROBABILITY ASSESSMENT** Expressions for the three additive terms in the probability chain equation were developed and applied to a series of chosen values for weight detonating at the top of the cell. These are combined to yield the value of the probability of a given weight, or greater, detonating. The results show that; (1) radial ejection contributes very little to the overall probability because of the large number of small fragments generated in this failure mode and (2) the axial failure mode probabilities decrease very rapidly. The overall probability thereby also decreases sharply.

The calculated probabilities for selected values of weight at the top are plotted on Figure 3 which is a standard probability assessment chart used by AEDC. When compared to the estimated containment value for J-4 (hatched area in Figure 3) it is seen that the probability of exceeding the cell containment limit is less than one in a million! Thus damage other than to J-4 itself is considered highly improbable (seen as category E in Figure 3).

These results show that the probability of exceeding a significant explosive yield in J-4, and thus in doing much damage to nearby facilities, is very low. It is concluded that it is safe to resume testing in J-4 with these rocket motors.

**ACKNOWLEDGEMENT** This study was the result of the combined efforts of a team of collaborators. The author was just one of the team and wishes to recognize the substantial contributions of Dr. Hoyt Andersen (detonability issues), Stanton Fink (CSQ calculations), Dr. Richard Hoar (structural issues), Clint Jaco (fragment velocity calculations), Graham Morgan (pioneering fragment velocity analysis) and Gus Soux (probability and statistics) to this effort. It would truly not have been possible without them.

#### **REFERENCES**

1. Louis J. Ullian, "Detonability of Large Solid Rocket Motors," ESMC/SEM Report #84-1, Patrick Air Force Base, Florida, 10 August 1984.

2. L. J. Weirick and D. W. Dugan. "Characterization of Morton-Thiokol Booster-Rocket Propellant TP-H1207C and its Simulant H-19," SAND88-0930, Sandia National Laboratories/Albuquerque, New Mexico, May 1989.
3. LeRoy Green, Edward James and Edward Lee, "The Detonability of Composite Propellants," UCRL-94174 Preprint, Lawrence Livermore National Laboratory, February 24, 1986, (presented at the JANNAF Propulsion Systems Hazards Meeting, Monterey CA, March 3-7, 1986).
4. (Quoted by Dr. Claude Merrill) Robert F. Vorwerk and Frederick H. Weal, "624A Solid-Propellant Motor Impact Test", Technical Progress Report 381, NOTS TP 3674, U. S. Naval Ordnance Test Station, China Lake, California, October 1964.
5. D.E. Richardson to K. J. Dickerson, "Critical Impact Velocity for Peacekeeper Stage III (T&H and Rail Garrison Applications)," Interoffice Memo SS-1192-88-9617P, Hercules Incorporated, Bacchus Works, Magna, Utah, 06 May 1988.
6. S. L. Thompson, "CSQII - An Eulerian Finite Difference Program for Two-Dimensional Material Response - Part 1, Material Sections," SAND77-1339, Sandia National Laboratories, June 1984.
7. J. M. Anderson to S. C. Browning, "Report on Trip to Witness MX DT-01 Destruct Test at AFRPL," Interoffice Memo 0012/6/20-0746, Hercules Incorporated, Bacchus Works, Magna Utah, 23 March 1982.
8. R. W. Darr, "Final Test Report for SICBM Stage I Command Destruct Test," TWR-90596, Morton Thiokol, Inc., Wasatch Operations, Brigham City, Utah, 12 December 1987.

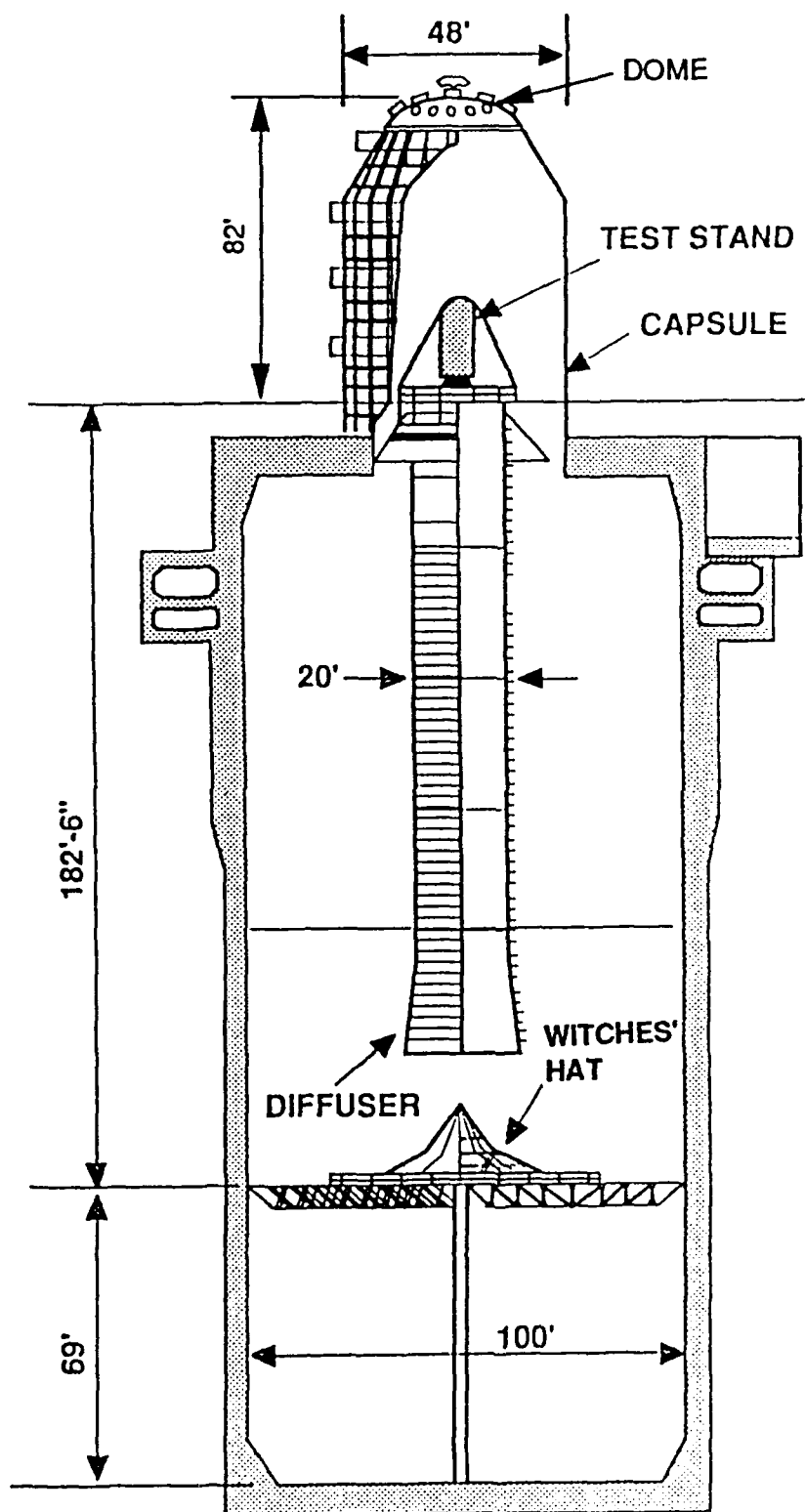


**Figure 1 - J-4 Test Cell**

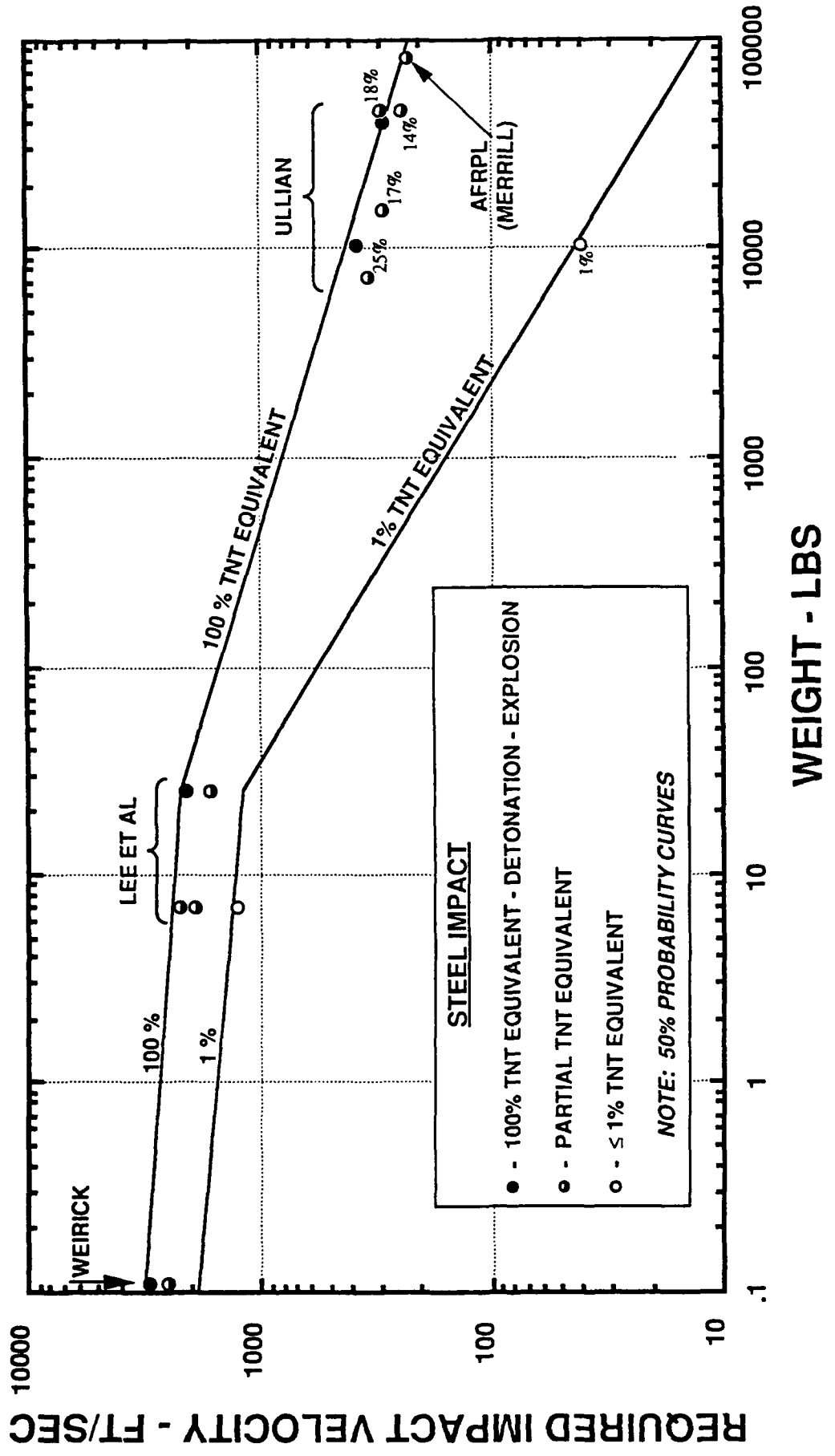


**Figure 2 - Detonation Probability Correlation**

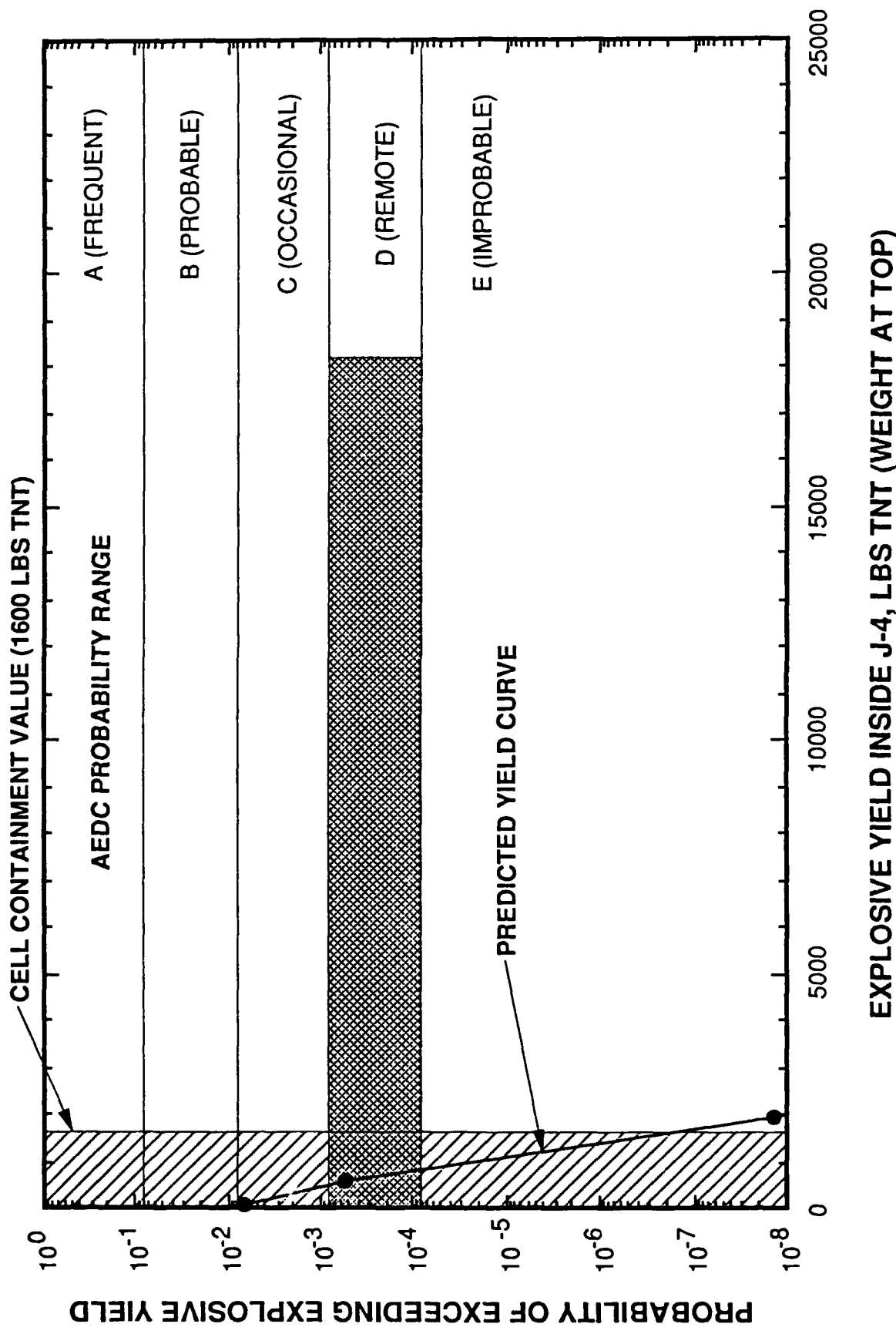


**Figure 3 - Probability Assessment**

SUMMARY OF CHANGES AND AVAILABILITY OF THE REVISED TM5-1300  
NAVFAC P-397, AFM 88-22 "DESIGN OF STRUCTURES  
TO RESIST THE EFFECTS OF ACCIDENTAL EXPLOSIONS"

Paul M. LaHoud, P.E.  
Huntsville Division, Corps of Engineers  
106 Wynn Drive, Huntsville Alabama 35807

ABSTRACT

Design of hardened structures to resist the effects of accidental explosions must comply with specific criteria defined in Department of Defense explosive safety regulations, DoD 6055.9.Std. The implementation these criteria in structural design were first formalized in 1969 in the Tri-Service Design Manual, "Structures to Resist the Effects of Accidental Explosions" (TM 5-1300, NAVFAC P-397, AFM 88-22). This manual has been under revision for several years and the status of that revision effort has been reported at previous DDESB Seminars. The Manual is now officially released and available for government and public use. This paper summarize and highlights significant changes from the original manual and discusses the availability of both the hardcopy and microcomputer software version.

INTRODUCTION

Design of structures to resist blast effects produced by accidental detonation of explosives and propellants represents a specialized field of structural engineering. Methods for determination of loading functions, material properties and acceptable deformation are not defined by structural engineering building codes. In 1969 formal criteria was officially defined for explosive safety design applications through the release of the technical manual "Design of Structures to Resist the Effects of Accidental Explosions" (Reference 1). The release of this manual was significant in that it provided for the first time, Department of Defense Explosive Safety Board (DDESB) approved analysis procedures and criteria which could be used to design structures to provide protection for personnel, equipment and facilities. Explosive safety protection requirements in processing, manufacturing, transporting and storing explosives are more stringent than in for military combat applications. Figure 1 highlights the area of application of TM5-1300 in the overall arena of hardened structures within the Army. Figure 2 shows the specific Army and Air Force safety regulations requiring application of the manual.

The 1969 version of the manual received world wide distribution and application for over twenty-five years and is still widely used. Even though its primary application was for reinforced concrete structures, it provided the first consistent standardized guidance for determination of loads,

# TM5-1300 DESIGN APPLICATIONS

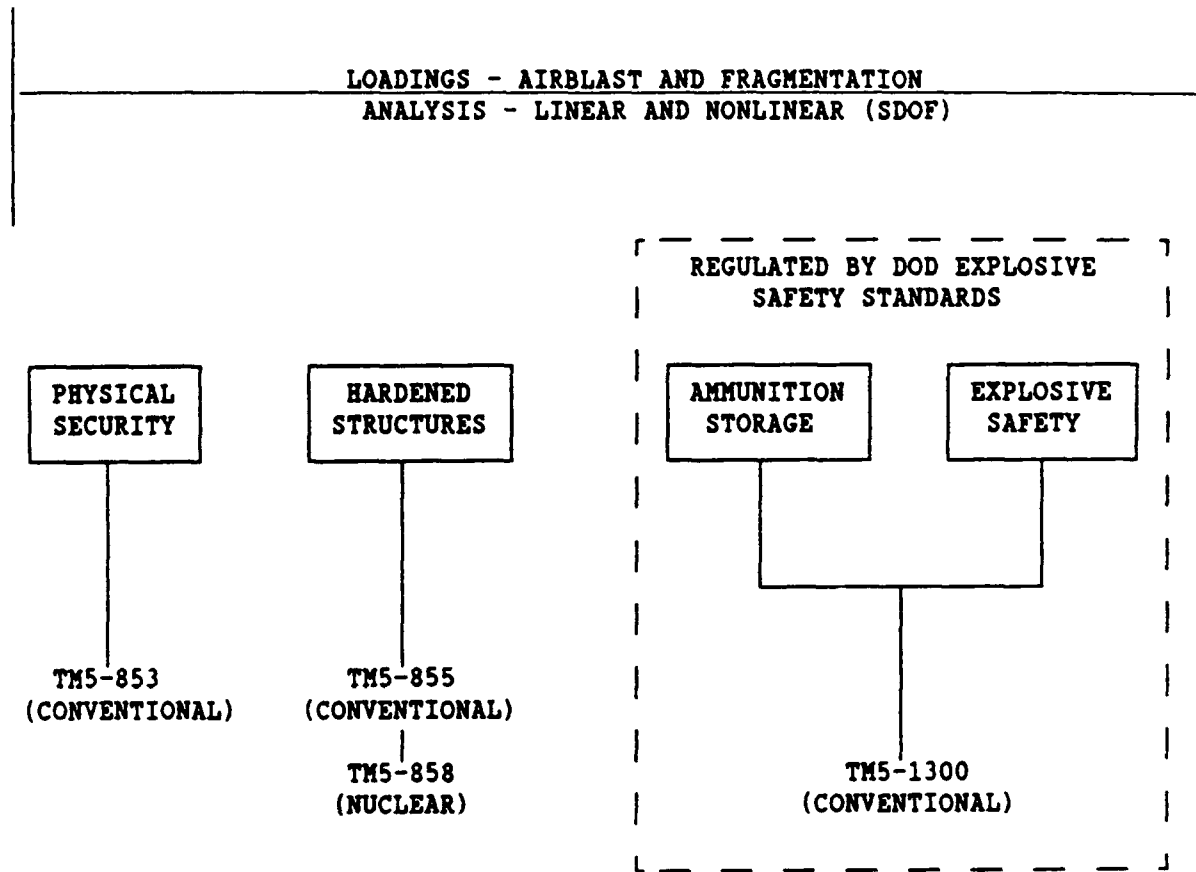
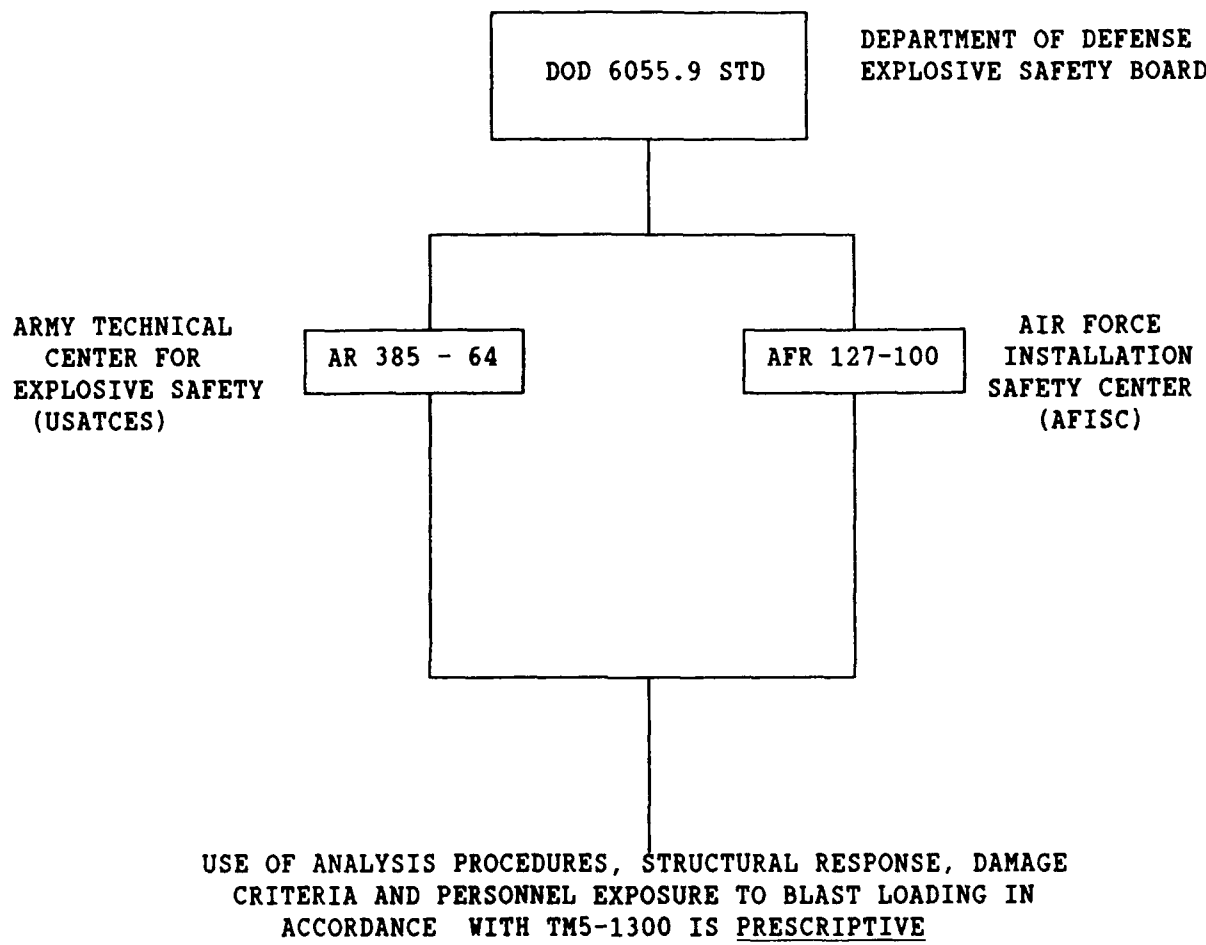


FIGURE 1

## GOVERNING EXPLOSIVE SAFETY STANDARDS



MANDATORY

FIGURE 2

material properties and acceptable deformation criteria for structures exposed to blast loads. As a consequence it has been used as guidance for all types of structures. In 1981 a revision was initiated to capture a large accumulation of research and experimental work that had occurred since the original publication. This revision effort was extensive and has been discussed in previous DDESB Seminars.

The revision effort to the manual was initially guided by a steering committee with subcommittees for blast technology and design applications. In 1987 with most of the research completed and the draft manual released for technical review, the management structure was streamlined to a combined management/technical steering group. Figure 3 shows the historical evolution of the committee. The current steering group, will continue to manage the manual and provide periodic revisions.

The revision to "Structures to Resist the Effects of Accidental Explosions" presents an enormous amount of improved technical data in loading prediction, material properties, deformation criteria, and analytical procedures. This is reflected in the physical size of the new hardcopy of the manual as depicted in Figure 4. One of the most popular features of the original manual was the detailed example design problems. The new manual provides the same type of examples throughout, demonstrating both original and new material. This paper will briefly highlight the changes in content of the new manual.

## CHAPTER 1 - Introduction

The material contained in Chapter I consists of an expanded discussion of the topics contained in Chapters 1, 2, and 3 of the original manual. Significant additional data and discussion are provided on the topics of human tolerance to blast overpressures, ground shock and fragments. New discussion is provided on tolerances of explosives to blast effects. New data is also provided on equipment response to blast forces. Figure 5 shows an example of information on human tolerance to overpressure. Extensive information on safe separation distance for numerous types of munitions is also included. The contents expands from 7 pages in the original manual to 42 pages in the new manual. The number of source material technical references provided increases from 8 to 17.

## CHAPTER 2 - Blast, Fragment, and Shock Loads

This Chapter replaces Chapter 4 of the original manual and reflects the abundance of new data incorporated in the revision. Technical discussion provided on blast, fragment and shock loading increases from 65 pages in Chapter 4 of the original manual to over 500 pages in this chapter. Source technical references increase from 25 to 138. A significant new topic discussed is the effect of explosive source geometry on blast pressure and impulse. This is an important concern in estimating the energetic output of explosive processing and manufacturing operations. Figure 6 shows examples of source geometries. Figure 7 is one example of 32 pages of new data on this topic obtained from various references.

## MANUAL STEERING COMMITTEE

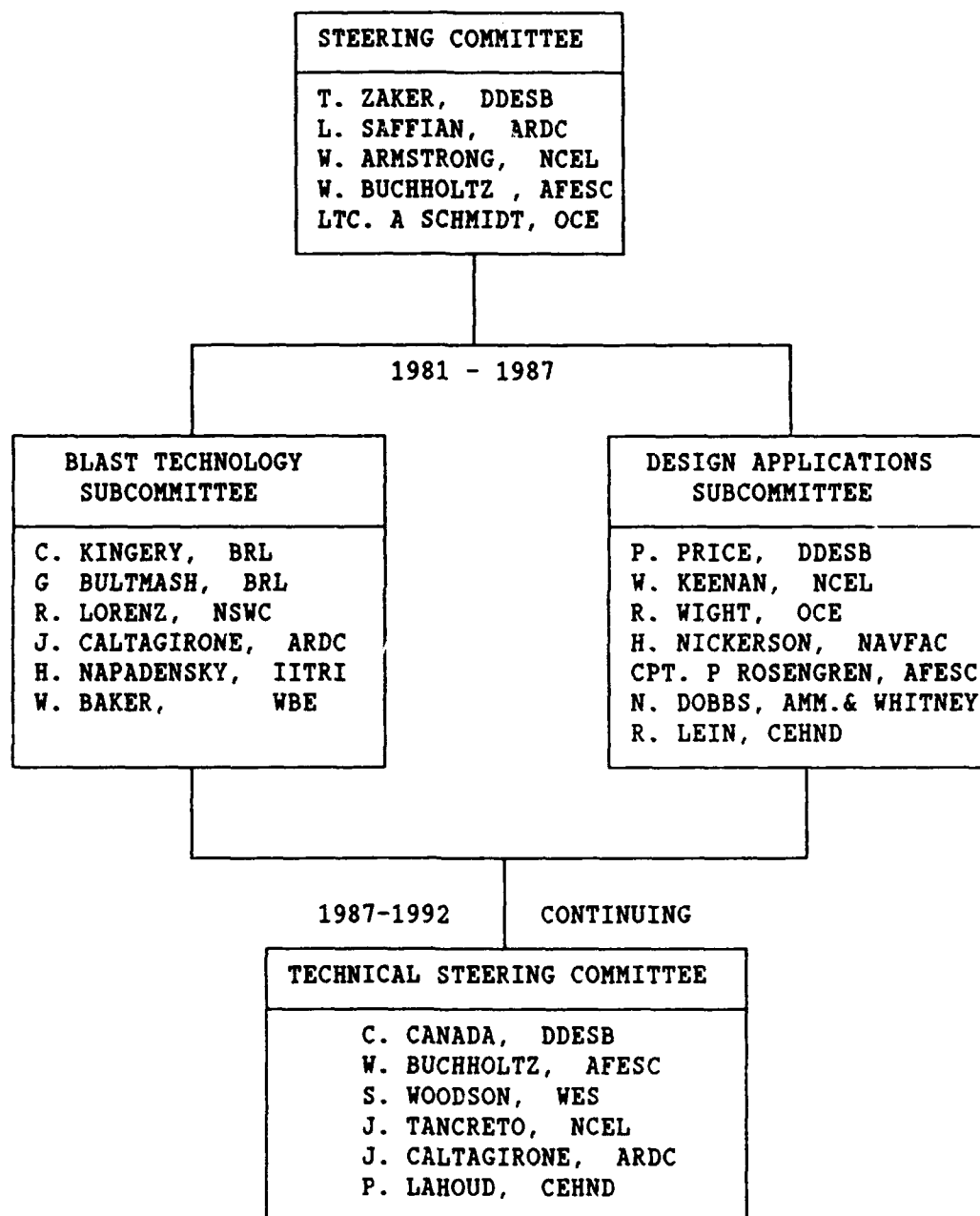
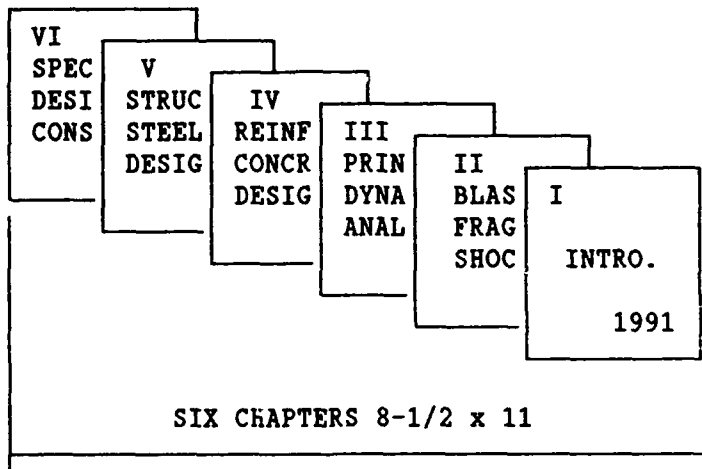


FIGURE 3

## THE OLD

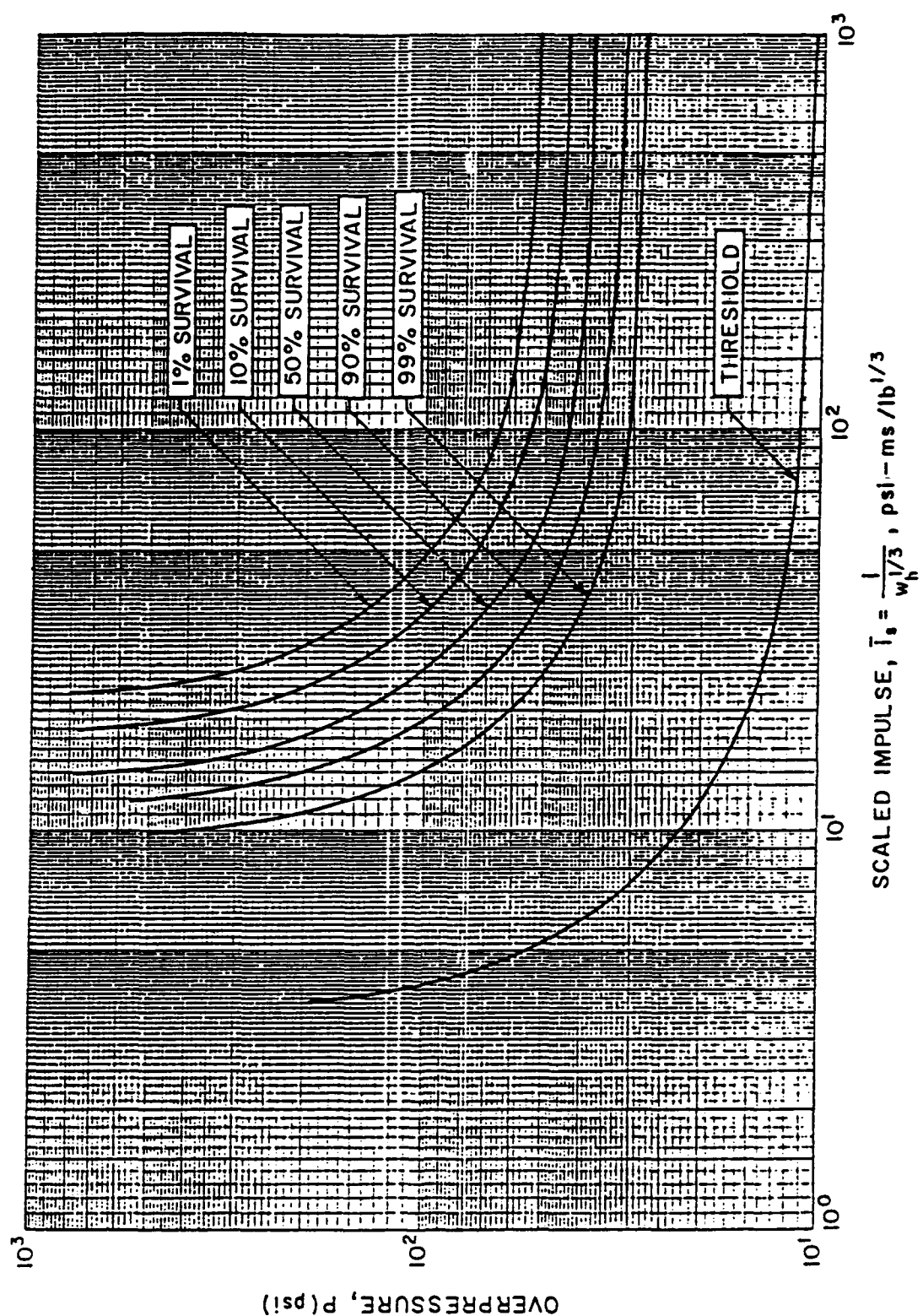
TM 5 - 1300  
SINGLE VOLUME 11 X 17  
188 PAGES 1969

## THE NEW



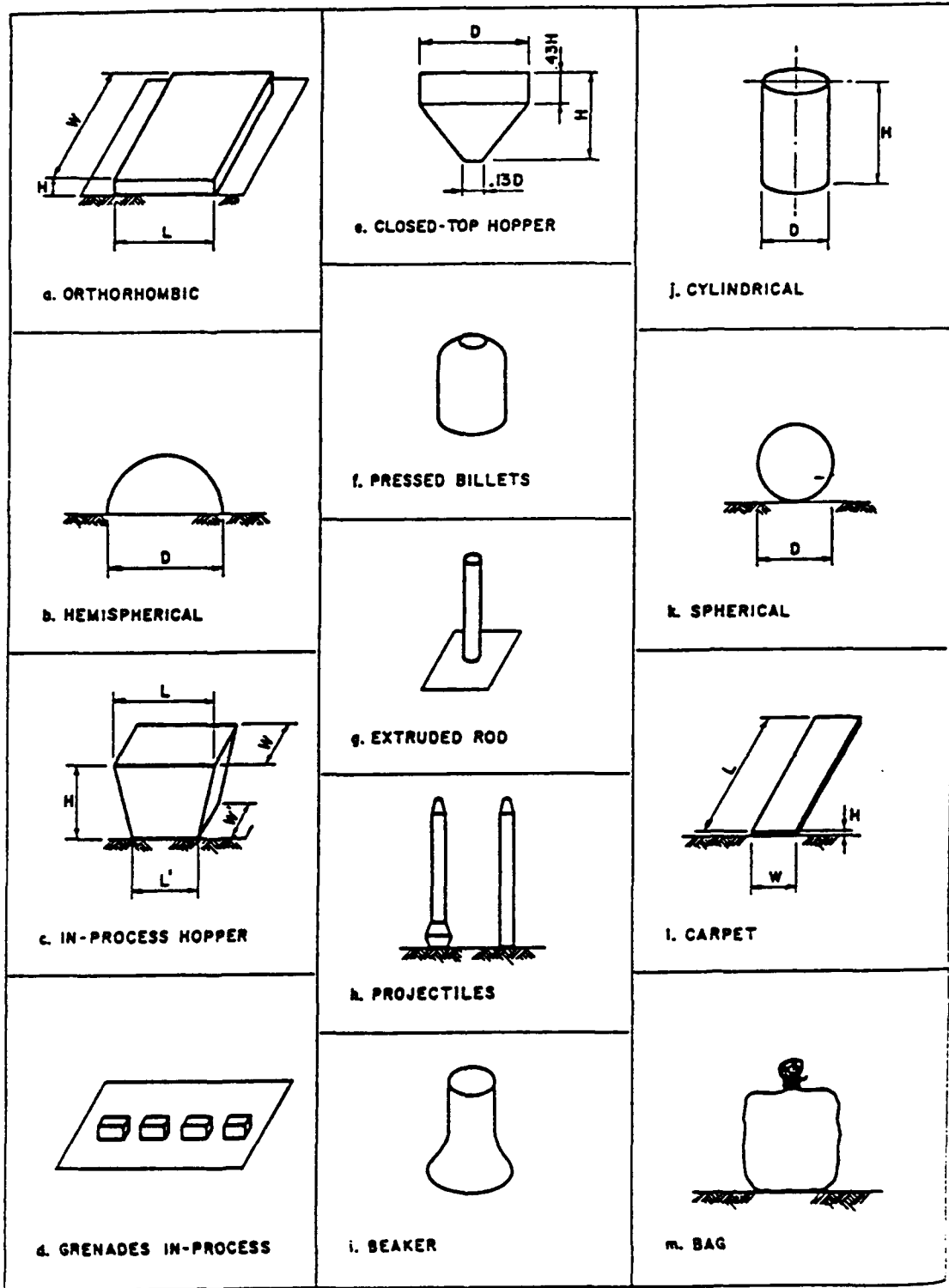
- |         |   |   |
|---------|---|---|
| CHAPTER | 1 | INTRODUCTION  |
| CHAPTER | 2 | BLAST, FRAGMENTATION AND SHOCK LOADS                |
| VOLUME  | 3 | PRINCIPLES OF DYNAMIC ANALYSIS                      |
| VOLUME  | 4 | REINFORCED CONCRETE DESIGN                          |
| VOLUME  | 5 | STRUCTURAL STEEL DESIGN                             |
| VOLUME  | 6 | SPECIAL CONSIDERATIONS IN EXPLOSIVE FACILITY DESIGN |

FIGURE 4



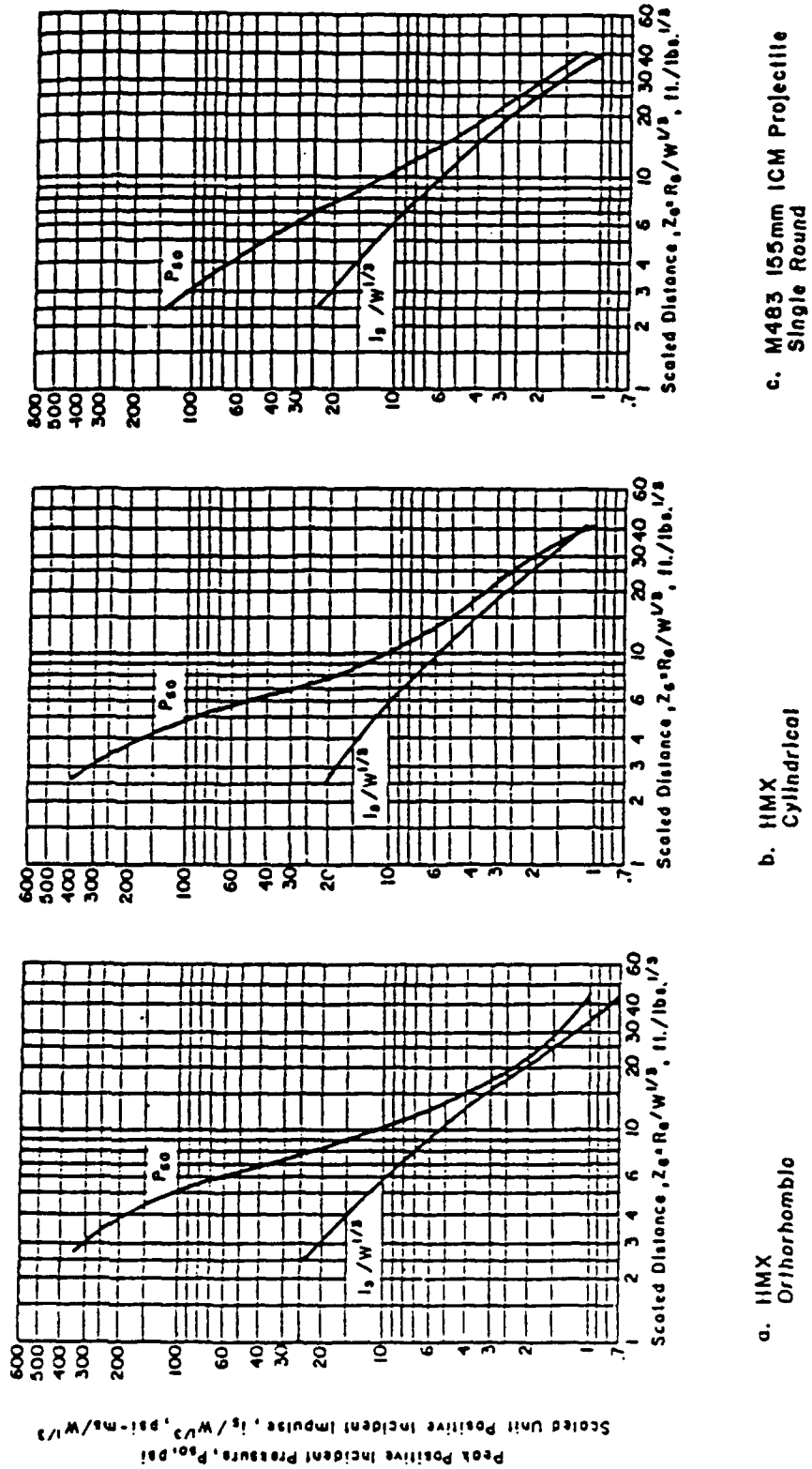
SURVIVAL CURVES FOR LUNG DAMAGE

FIGURE 5



### EXPLOSIVE SHAPES

FIGURE 6



PEAK POSITIVE INCIDENT PRESSURE AND SCALED IMPULSE  
FOR AN EXPLOSION ON THE SURFACE AT SEA LEVEL

FIGURE 7

Another topic which has benefitted from extensive new research is the calculation of blast loads on cubicles wall. The original manual provide charts to analyze only for impulse loads on cubicle walls with various boundary conditions. Subsequent research and experiment has shown that in many cases a pressure-time solution may be required rather than an impulse solution. Therefore in addition to the original impulse charts, 38 new charts are provided which allow the calculation of the average reflected pressure on the same cubicle walls.

Extensive Naval Civil Engineering Laboratory (NCEL) research on blast load environments in and adjacent to fully and partially vented cubicles has been incorporated in the new manual. Thirty-two additional new charts are provided which allow the estimation of gas pressures in, and shock pressures adjacent to, various configurations of cubicles.

Fragmentation prediction procedures in the original manual were limited, addressing only primary fragment effects from conventional explosive filled munitions. More detailed analytical models for primary fragmentation have been developed and incorporated in this chapter. These expanded procedures allow the estimation of primary fragment mass and velocity for many Non-cylindrical geometries. Additional experimental and analytical material on primary fragmentation from liquid filled munitions developed from the chemical weapons demilitarization program (Reference 2) have also been included. This chapter also incorporates extensive additional analytical procedures developed by the Department of Energy (Reference 3) on prediction of secondary debris from equipment and building elements.

Chapter 2 also incorporates procedures for the estimation of groundshock from accidental explosions. This data was extracted from Reference 4. Methods are presented for determining the structure motion caused by ground shock and air blast effects as well as their interaction. Other procedures are presented for determining shock spectra which may be used for evaluation of structure motion as well as the design of shock isolation systems.

Another topic which has received considerable additional treatment is the calculation of gas pressures as a contributor to total loading from internal explosions in buildings. Research and experimentation has shown that even with frangible walls or vents, gas pressure is a major contributor to total loading. This phenomena was not clearly recognized in the original manual.

Expanded methods and examples are provided for the calculation of exterior loads on structures as well as interior loads on structures due to leakage of exterior blast pressures through openings. This is very valuable in the design of shelter type structures where personnel protection from overpressure is required.

### Chapter 3 - Principles of Dynamic Analysis

In the original manual basic principles of dynamic analysis were provided as sub-paragraphs of chapters 5 and 6. The new manual has reorganized this material into a single chapter and extensively supplemented and expanded the methods presented to cover a more complete range of possible structural

response situations. Material provided has increased from approximately 50 pages in the original manual to over 375 pages in this chapter. Data for determining resistance-deflection functions and yield line locations have been significantly increased in this chapter. This new material includes the determination of elastic and elasto-plastic moment and deflection coefficients for numerous support and loading conditions, including both one and two-way elements, and flat slabs.

As in the original manual, and most other widely used hardened structures design references, the new manual utilizes single-degree-of-freedom (SDOF) methods to estimate the maximum response of structures subjected to blast loads. Only two design charts were provided in the original manual for determining structure response to blast overpressures. One chart pertained to structure response to direct loading while the second was used to determine rebound forces. The number of design charts furnished in this chapter have been increased to 216 and covers maximum elastic response to triangular loads, rectangular loads, gradually applied loads, triangular pulse loads, and sinusoidal loadings. The new charts also cover maximum response to elasto-plastic systems for triangular loads, rectangular loads, gradually applied loads, triangular pulse loads, and bilinear-triangular loads as well as rebound forces.

Other beneficial new additions to Chapter 3 are procedures for performing numerical integration analyses. These include both the average-acceleration-method and the acceleration-impulse-extrapolation-method. Procedures are presented for including damping in a system as well as for analyzing two-degree-of-freedom systems. These procedures are attractive with the availability of microcomputer spreadsheets with graphics, such as LOTUS 123, and they provide a very flexible analysis tool.

#### Chapter 4 - Reinforced Concrete Design

The technical data from chapters 5 through 9 of the original manual have been combined in this chapter. The original manual was concerned primarily with the design of laced reinforced concrete walls to resist the effects of close-in detonations. A considerable amount of new data has been added to address other types of concrete elements. Less than 90 pages of material in the original manual has been increased to over 250 pages in this chapter. Source references cited have increased from 38 to 77. This additional data will facilitate the design of a wider range of reinforced concrete structures.

The new manual provides much better guidance for the estimation of the dynamic capacity of both concrete and reinforcing steel. Based on recent research and testing, the dynamic increase factors for both concrete and reinforcing steel are presented as a function of the actual response of the structural elements as well as the values needed for design. In addition, the static yield strength of the reinforcement is increased 10 percent beyond the minimum specified by the ASTM to account for the actual steel that is furnished by steel producers. Finally, the procedures for the determination of shear capacity have been significantly revised (Reference 5)

New material has been provided for small deflections (less than 2 degrees support rotation) design of slabs reinforced with single-leg stirrups rather than lacing. This type of shear reinforcement will greatly simplify construction and result in considerable cost savings.

This volume also provides greatly expanded design procedures for conventionally reinforced slabs and walls of various support conditions, as well as design procedures and deflection criteria for beams and both interior and exterior columns. The design of slabs includes, not only one and two-way slabs of various support conditions, but also flat slabs. When support conditions permit, tension membrane action of the slabs is incorporated in the design. The recognition of membrane action permits the slab to attain relatively large deflections at reduced strength, thereby achieving greater economy in design.

Data on spalling of concrete has been increased to more realistically predict the need for costly structural steel spall plates. In addition, material on structural response to primary and secondary fragment impact is expanded.

The last part of this chapter greatly expands the number of typical design details provided. These details include information acquired from numerous blast resistant construction projects. Detailing procedures are provided for laced concrete elements, conventionally reinforced concrete, flat slabs, beams columns, and foundations. Figures 8 and 9 are typical of details provided.

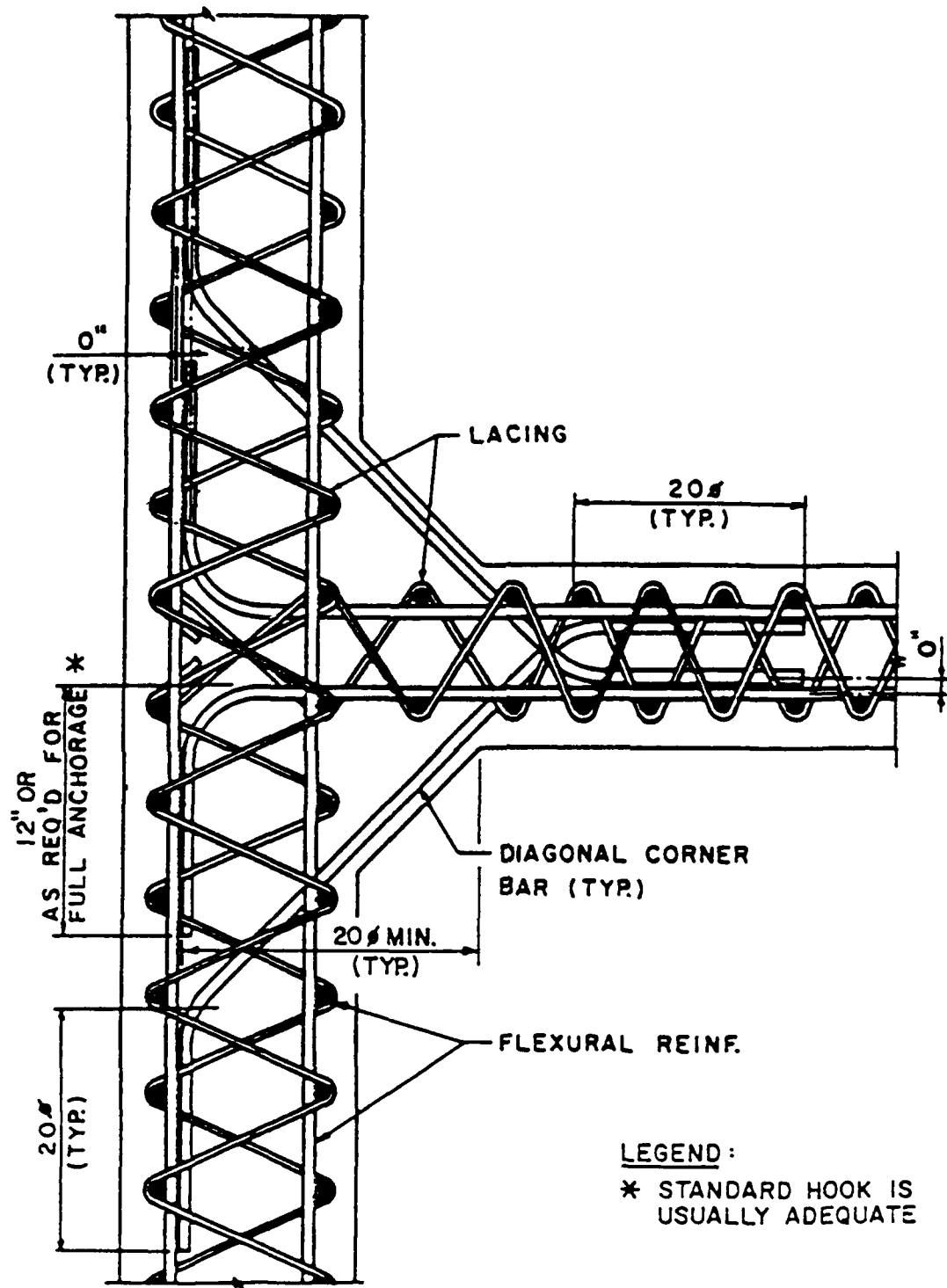
#### Chapter 5 - Structural Steel Design

The material provided in this chapter is entirely new since the original manual did not address structural steel at all. References 6 and others provided are the sources of the procedures in this volume. The design procedures for response of steel structures follow from the SDOF analysis procedures provided in Chapter 3. Material properties of structural steel elements are presented, along with recommended dynamic design stresses, acceptable maximum displacement, and plastic deformations within the broad range of steels available. The structural steels for plastic design covered by the AISC Specifications are discussed with regard to their uses in protective structures subjected to blast loads.

A method for performing preliminary blast load plastic design of structural steel frames is presented. The analytical procedures can consider both single and multi-bay arrangements for both rigid and braced frames. Based on the results of the preliminary analysis, a final frame analysis can be performed. This chapter also provides recommended methods of detailing connections for structural steel.

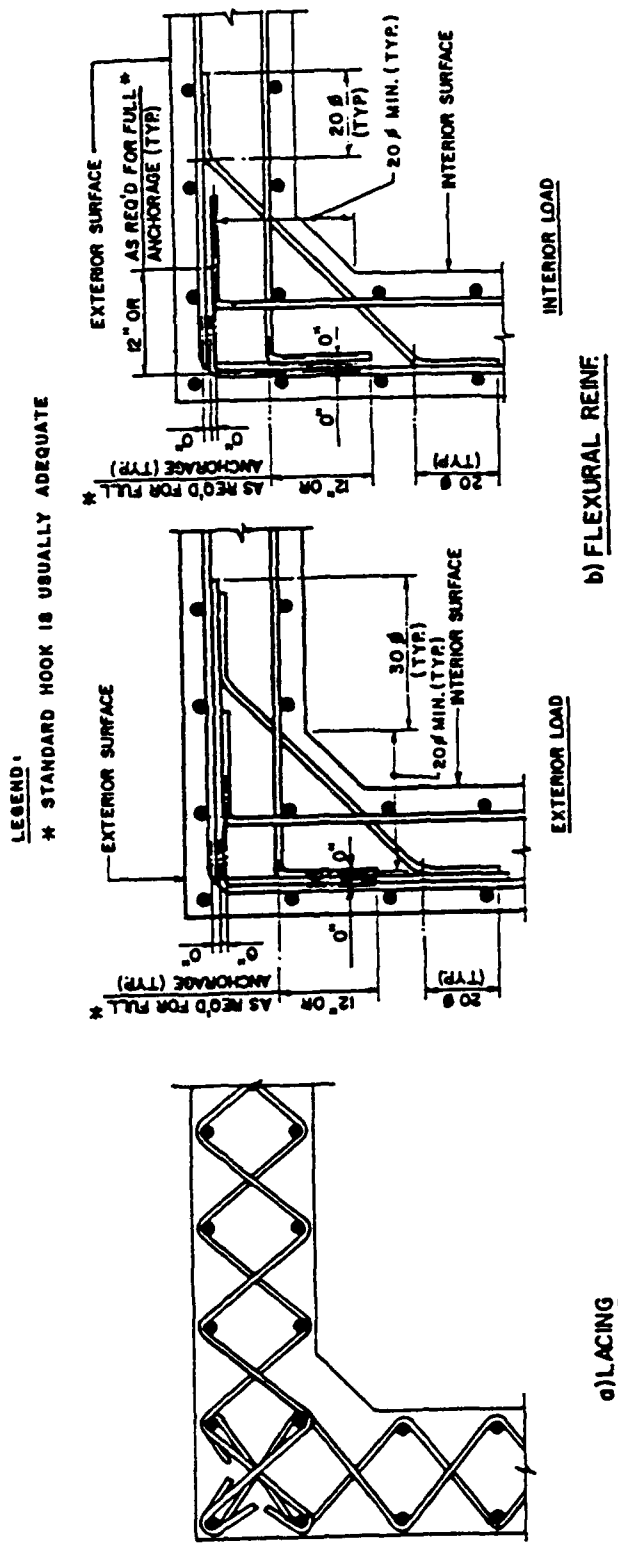
#### Chapter 6 - Special Considerations in Explosive Facility Design

Chapter 10 of the original manual discussed several miscellaneous topics related to explosive safety protective construction. This chapter includes that data and other new data on a wide list of topics including: (1) masonry design; (2) precast concrete design; (3) pre-engineered buildings;



INTERSECTION OF CONTINUOUS AND DISCONTINUOUS  
LACED WALLS WITHOUT EXTENSIONS

FIGURE 8



CORNER DETAILS FOR LACED WALLS WITHOUT WALL EXTENSIONS

FIGURE 9

(4) suppressive shielding; (5) blast resistant windows; (6) design loads for underground structures; (7) earth-covered arch-type magazines; (8) blast valves; and (9) shock isolation systems.

Masonry Design - This section provides procedures for design of masonry walls subjected to blast overpressures. Included in the design procedures are methods for calculating the ultimate strength of masonry walls as well as resistant-deflection functions. Criteria is presented for allowable deflections.

Precast Concrete Design - Described in this section are the procedures used for design of precast elements subjected to blast overpressures. Methods are included for design of precast concrete slabs, beams and columns. The procedures include methods for calculating ultimate resistance and resistance-deflection functions as well as deflection criteria.

Special Provisions for Pre-Engineered Buildings - Standard pre-engineered buildings are usually provided by a performance specification and designed by the supplier for conventional loads (live, snow, wind loads, etc.). These buildings are very vulnerable to blast overpressures. Blast resistant pre-engineered buildings are designed in the same manner as standard structures. However, the performance specification must require considerably higher conventional loads to provide the equivalent blast resistance. This section presents the magnitude of these larger conventional loads as well as present details of both the main frame members and foundations which must be incorporated into the building design. To assist the design a template specification for hardened pre-engineered buildings is provided.

Suppressive Shielding - Presented is a summary of design and construction procedures which are outlined in the design Manual, titled "Suppressive Shields - Structural Design and Analysis Handbook" HNDM 1110-1-2, (Reference 7). This section describes the application of suppressive shielding as well as design criteria and procedures. Methods of designing equipment penetrations through walls, as well as blast doors to be used with suppressive shielding, are discussed.

Blast Resistant Windows - Historically, explosion effects have produced airborne glass fragments from failed windows which are a risk to life and property. Guidelines are presented for the design, evaluation, and certification of windows to safely survive a prescribed blast environment. Design criteria is presented for both glazing and window frames. The design procedures include a series of design charts for both the glazing and frames.

Design Loads for Underground Structures - This section is a summary of the data presented in the design Manual, "Fundamentals of Protective Design for Conventional Weapons" (TM 5-855-1). The data contained in this Manual pertains primarily to effects produced by explosions on or below the ground surface and the blast pressures they produce on below ground structures. Procedures are presented for evaluating blast loads acting on the structure surface as well as structure motions caused by explosions.

**Earth Covered Arch-Type Magazines** - This provides information on typical earth-covered magazines which are used for storage of explosives. Included are requirements for both metal arch and reinforced concrete arch magazines, including semicircular and oval types. Discussed are the investigations performed in connection with magazines, general design procedures, construction, and standard designs. Additional information is available from Reference 8.

**Shock Isolation Systems** - Data presented for shock isolation systems has been greatly expanded from that given in the present Manual. The data given in the original manual was basically qualitative rather than quantitative. Although a full discussion of the subject is beyond the scope of this chapter an introduction to isolation system design is presented. Included are various methods of achieving shock isolation for both equipment and personnel. Typical designs for equipment supports are presented.

**Blast Valves** - This section discusses several types of blast valves that are available commercially including sand filters, hardened louvers, and poppet valves. Also presented are the advantages and disadvantages of blast-actuated vs remote-actuated blast valves, the effect of plenum chambers, and a typical specification for the design, testing, and installation of a poppet valve.

#### COMPUTER ANALYSIS PROCEDURES

TM5-1300 is recognized and applied worldwide. One of the main objectives of the steering committee was to assure that the new manual provided complete methods suitable for hand calculations. This resulted in the large number of new charts and graphs for direct design. However many valuable Micro-computer codes have been developed to solve segments of the analysis procedures in the manual. Computer codes which are currently approved by the DDESB as equivalent to methods in this manual are described briefly.

**TM5-1300 PC VERSION** - This is an impressive piece of software written by David Hyde of the Corp of Engineers Waterways Experiment Station (CEWES). The entire text of the manual as well as all figures and tables have been committed to a microcomputer program. The text can be called up, reviewed, printed, and key word or phrase searches conducted. All graphs and tabular data are accessible for viewing, and a "cross-hair" function allows the user to accurately pick graphical data points. Many numerical calculation procedures in the manual have also been automated.

**CBARCS/PCBARCS** - This is a structural analysis code which performs nonlinear analysis of rectangular reinforced concrete slabs. It was developed by the Naval Civil Engineering Laboratory (NCEL). The program can compute blast shock and gas pressures based on the type of explosive. It calculates structural properties, slab resistance using yield line theory and then determines the dynamic response of the slab. It is primarily applicable to pressure-time loadings.

**SHOCK** - This is a program that calculates shock pressures and impulses on arbitrary rectangular surfaces. It was also developed by NCEL.

**FRANGE** - This program calculates the gas pressure-time history inside a room resulting from an explosion. The program also computes the time required for a frangible panel to blow away from a wall and allow full venting. Program also written by NCEL.

**SOLVER** - This program calculates the dynamic response of a user defined single-degree-of-freedom system and loading. It predicts nonlinear response based on user defined resistance deflection function. It was also written by NCEL.

**TRAJECT** - This program calculates fragment and debris trajectories based on user defined velocity, launch angles, drag and mass characteristics. This Code was written by Naval Surface Warfare Center.

Each of the three services will maintain repositories which contain the computer programs described above:

(1) Department of the Army, Commander, U.S. Army Waterways Experiment Station, P.O. Box 631 Vicksburgh Miss, 39180-0631 Attn: WESKA

(2) Department of the Navy, Commanding Officer, Naval Civil Engineering Laboratory, Port Hueneme, California 93043 Attn: Code L51

(3) Department of the Air Force, Aerospace Structures, Information Analysis Center, Wright Patterson AFB, Ohio 45433 Attn: AFFDL/FBR

The TM5-1300 steering committee will continue to evaluate new codes and requirements for revisions to existing codes. These programs will be periodically updated or revised as required.

#### SUMMARY

The new version of TM5-1300 is now available for general use. The manual is greatly respected worldwide and many nations use it as a basis for their own explosive safety guidance. Within the United States numerous other government agencies direct its application including DOE and NASA. The manual is available from both The Defense Technical Information Center (DTIC) and the National Technical Information Center (NTIC). The Hard copy version can be ordered as AD A243272. The PC version is AD M000097.

## REFERENCES

1. Structures to Resist the Effects of Accidental Explosions; Department of the Army Technical Manual, TM 5-1300; Department of the Navy Publication, P-397; and Department of the Air Force Manual, AFM 88-22, June 1969.
2. A Manual to Predict Blast and Fragment Loadings from accidental Explosions of Chemical Munitions Inside an Explosive Containment Structure, Prepared by Southwest Research Institute under contract DACA87-81-C-0099, to the Huntsville Division for the Program Managers Office for the Chemical Weapons Stockpile Disposal Program, April 1983.
3. Prediction of Blast and Fragmentation Loading on Structures, DOE/TIC 11268, prepared by Southwest Research Institute, San Antonio Texas, under contract DACA87-79-0091, to the Huntsville Division for the Department of Energy, Amarillo Area Office, September 1980.
4. Fundamentals of Protective Design for Conventional Weapons, TM 5-855-1, prepared by U.S. Army Engineer Waterways Experiment Station, Vicksburg, MS, for Office, Chief of Engineers, U.S. Army, Washington, D.C.
5. Changes to TM5-1300 Governing Shear Reinforcing Requirements for Blast Resistant Reinforced Concrete Structures, Ross, B., Zehrt W., Huntsville Division, presented at the 24th DDESB Safety Seminar August 1990.
6. Design of Steel Structures to Resist the Effects of HE explosions, TR 4837, prepared by Ammann & Whitney, New York, NY; for Picatinny Arsenal, Dover New Jersey, August 1975.
7. Suppressive Shields - Structural Design and Analysis Handbook, HNDM 1110-1-2, U.S. Army Corps of Engineers, Huntsville Division, Huntsville, AL, 18 November 1977.
8. Explosive Safety Siting of Corps of Engineers Standard Igloo Designs, Williams, E., Farsoun, A., Watanabe, W., Huntsville Division, presented at the 24th DDESB Safety Seminar, August 1990.

## **"CONSTRUCTIBILITY PROBLEMS IN BLAST RESISTANT, REINFORCED CONCRETE STRUCTURES"**

by

**Darrell D. Barker and Mark G. Whitney  
Wilfred Baker Engineering, Inc.  
San Antonio, Texas, USA 78209-1128**

### **ABSTRACT**

Design of reinforced concrete containment buildings and shelters to resist blast loads is a complex process which involves a great deal of coordination between the engineer and contractor. The high density of reinforcing normally present in these types of structures necessitates close scrutiny by the designer to anticipate fabrication and construction problems. Solutions to these problems are much less expensive to incorporate in the design office than in the field. The problem many designers face is a lack of firsthand information regarding construction techniques for these types of buildings. It is almost impossible to fully appreciate the extent of these problems without observing the actual construction. This paper attempts to point out some the most common problem areas to assist the engineers in evaluating their designs.

Discussion is provided regarding rebar congestion, lacing placement, honeycombing, concrete placement, blast door anchorage, and other problems which frequently occur in construction of blast resistant, reinforced concrete containment bays and shelters. Causes of the problems and suggested solutions are addressed. These discussions will facilitate evaluation of designs by designers, independent reviewers, and sponsoring agencies. This paper reflects the experience of many design professionals involved in blast resistant design and construction obtained through informal surveys.

### **INTRODUCTION**

For many engineers, the primary challenge of designing a blast resistant, reinforced concrete structure is to develop sections capable of resisting the design loads within the allowable response range. Achieving this design at the lowest practical construction cost is also high on the list of priorities. As computational methods become increasingly sophisticated and automated, the ability to determine response with great theoretical accuracy produces a tendency to refine the calculations to an unwarranted degree to achieve the "lowest cost." This approach can produce shallow sections with a high reinforcing ratio which are difficult to construct. Ironically, these are not truly the lowest cost sections in many cases because the cost is measured in terms of material quantities rather than complexity of construction. In practice, a design should be evaluated as much on feasibility of construction as it is on structural performance. Problems with constructibility of the design will always evidence themselves during construction. By contrast, structural response problems may never be discovered since most of these structures are designed for accidental explosions and are never subjected to the design loads. It is prudent, therefore, to examine the potential for construction problems during design and eliminate them prior to bidding the job.

The design of a facility to resist significant blast loads typically produces construction requirements that often do not even resemble those required for conventional loads. This situation is easily understood when the magnitude of the loads involved is considered. Blast pressures as low as a few psi for a long duration are much more demanding of the structure than the most severe natural phenomena loads likely to be encountered by the design engineer.

These unique requirements necessitate a greater attention to constructibility issues during the design phase than would normally be required in conventional construction. The design engineer should also remember that more information concerning fabrication and installation techniques will need to be conveyed to the contractor for blast resistant facilities than for conventional design. The contractor, in many cases, is dealing with a totally new type of construction than he has experienced before. The engineer cannot simply specify a bar size and spacing for each concrete element and leave it to the rebar detailer to iron out the details. If this is done, the chances are good that bar conflicts will require design of new sizes and spacings at construction time when the engineer and contractor can least afford it. Redesign at this stage can also affect adjacent structural elements since most blast resistant facilities involve a system of structural elements rather than individual elements.

This paper describes many of the problems experienced by the authors and several design professionals and construction managers around the country. The problems described are certainly not all encompassing, but they are ones which are encountered frequently. The paper is intended to give the designer with limited experience in this type of construction an indication of what may be encountered and the additional considerations necessary in blast design. The experienced designer will be able to relate to the problems described from personal experience.

## **IDENTIFICATION OF PROBLEMS**

Construction problems associated with this type of facility can be attributed to both design and construction methods. Parties on both sides can be faulted when problems arise, so it is prudent to address factors which are important to both, although this paper is focused on solutions during design. Potential problem areas can be segregated into two broad categories: procedural and technical. Procedural problems involve the way in which design and construction projects are accomplished and include such topics as drawing review and contractual relationships. Technical problems are much narrower in scope and include specific reinforcement and concrete placement issues which can be addressed by designers and contractors.

### **Procedural Problems**

Problems in this category involve procedures, methodologies, and contractual relationships which the design engineer and possibly the contractor have little control over. Consequently, overcoming problems in these areas may be more difficult to solve. The parties involved, however, do have an obligation to influence decisions by owners which can enhance the quality of the completed job.

Constructability review is a procedural item that is frequently forgotten during design. This review should be an integral part of the design process much like safety and quality assurance reviews have become. Designs should be reviewed not only by the design engineer but also by construction inspection personnel or others with practical construction experience. These reviews should focus on insuring that a reasonable method of construction exists for the specified design. Alternative designs which become apparent at this stage should be considered for adoption if the

original design is not feasible. It is not acceptable, as is the practice of some, to simply let the contractor solve the problem. Since this review may impact the design significantly, it should be performed during preliminary design as well as the final stages. An important consideration to remember is that a design is only as good as the constructed product, never better.

The practice of many Architect-Engineers (A-E) is to limit the amount of information on the drawing to reduce their liability should problems arise during construction with a faulty detail or specification. In practice, however, they will still be held responsible if the contractor proves that the design is not constructible. There have been cases where the design was constructible, even though difficult to construct, and blame was still placed on the designer. The moral of the story is make sure you know how to build it and put the necessary information in the construction documents.

It is time consuming, and thus costly, for the A-E to develop detailed reinforcement drawings for particularly congested areas, such as intersecting walls, embedment areas, and blast door frames. In many cases these costs are not bid into the proposal and there is a tendency to cut this work short when budgets are tight. An important point to remember if this route is taken is that these details must be developed by the contractor and will require review by the A-E. Without guidance from the contract documents, the details may undergo several review cycles before they are correct and thus will cost the A-E just as much as if they had been detailed in the first place. The owner bears some responsibility here also with regard to allowances for additional hours in the A-E's proposal for detailed design of these areas.

Review of shop drawings by the design engineer is another important requirement for this type of work. All of the required reinforcing obviously cannot be "scheduled out" in the contract documents, so the fabricator's detailer must use considerable judgement when preparing the shop drawings. Review of these drawings can be a very tedious job, but its importance should not be forgotten. The design engineer must insure that the intent of the design is incorporated into the shop drawings. The only other chance to review the accuracy of the detailer's work is during a site inspection of the construction. At this point, discovery of errors becomes expensive and unpleasant. The owner has a responsibility in this area also. Review of shop drawings costs money, and tight budgets cause everyone to look for savings. Elimination of reviews, however, can be very costly. Project funding should include provisions for involving the A-E in the construction phase of the project to cover these situations.

On the construction side of the project, a great many problems arise from the inexperience of contractors in this type of work. The contractor must have an experienced superintendent and foreman to plan and oversee reinforcing and concrete placement. Knowledge of proper construction sequence and potential problems is an important asset for the contractor's supervisor to have. An inexperienced supervisor can quickly dissolve the profit margin in this type of facility if reinforcing must be removed and reinstalled because of improper installation.

Government funded projects present a particular problem in this area because of the procurement regulations regarding competitive bidding. It is difficult to exclude contractors with minimal experience from bidding for work even with explicit experience requirements. These requirements are difficult to enforce when protests are filed because they are deemed to be too restrictive. This doesn't mean, however, that there aren't alternatives for getting a good quality facility. One such option is a thorough discussion of the complexity of the job during a prebid conference. This will alert bidders that special attention should be paid to fabrication and labor efforts when preparing their bids. Another important option is the use of an on-site representative of the design team during construction. This representative can help to avoid many of the major

problems which occur because of familiarity with the design and the ability to make a quick assessment of the situation. Because he/she has a rather direct line of communication with the other designers, a solution can normally be prepared before the A-E is notified through official channels. This expedites resolution of the problem and saves considerable downtime for the contractor. Since the A-E's representative is normally not the contracting officer, care must be taken to avoid attempting to direct the contractor during resolution of these problems.

Contractor Q-C programs specified by many government contracts warrant special consideration for these projects for two reasons. The first is the availability of personnel with experience in this type of construction. The contract must have specific requirements regarding the qualifications of Q-C personnel. The second is the philosophy of the program itself. To realize the goal of improved quality in the constructed project, the contractor's Q-C personnel must be accountable to the project manager and not controlled by the superintendent or foreman. When reinforcement or concrete placement problems arise in this type of construction, as they frequently do, it is vitally important that they are identified and resolved rather than ignored and forgotten. The consequences associated with this situation should be emphasized to all parties involved.

### Technical Problems

Problems in this category involve physical situations which are encountered during construction and thus are more easily recognized than procedural problems. Unfortunately, while these are evident during construction, they are more difficult to recognize during design, and thus may not be resolved before they become expensive. This section will describe some of the more common problem areas and options for minimizing their impact.

#### **Reinforcing**

Construction of reinforced concrete elements can be quite complex for blast resistant structures. This is due primarily to the quantity of reinforcing steel in the sections, but is also due to volume of concrete required in confined areas. This congestion stems from requirements placed on the structural elements by the magnitude of the blast loads and space requirements. The presence of lacing, diagonal, and tension bars presents a much greater construction challenge than conventional reinforcing. The size of the flexural steel compared with conventional designs also adds to the congestion. A typical blast resistant structural section is shown in Figure 1.

In many reinforced concrete structures, problems result from an attempt to minimize element thickness by increasing bar sizes and decreasing spacing. This is normally done because it is perceived that the thinnest section is the most economical. While this may be true for conventionally loaded elements, it is not true for most blast designs because of the high cost of rebar placement in congested sections. Increasing element thickness will not increase forming costs, so the only increase is additional concrete and placement cost, and some additional real estate. If space availability is not a problem, use of earth separation between explosives bays to eliminate common walls can result in significant savings in wall construction. These options should be investigated during preliminary design.

As mentioned above, placement of reinforcing steel in sections is the most prominent construction problem in blast resistant structures designed for high pressure loads. The basic types of reinforcing include lacing, stirrups, diagonals, tension, and flexure bars.

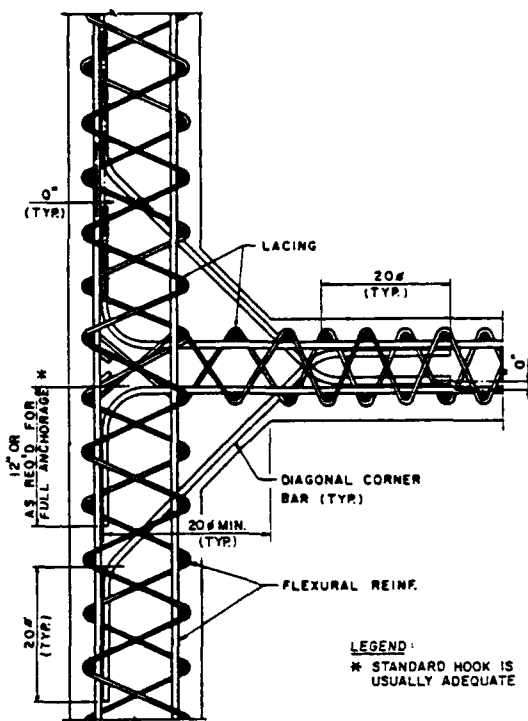


**Figure 1. Typical Blast Resistant Structural Section  
(From TM 5-1300, Ref. 1)**

### *Lacing*

Facilities designed for close-in charges require lacing to resist high shear stresses. For sections where lacing is required, it is to be continued through the entire element, not just the region affected by the high shear stresses. This requirement generally necessitates a splice in the lacing at the floor or wall, depending on the height or width. These splices are required to be lapped over three bends (Figure 2), which can make the section very congested, especially where diagonal bars are present. Unfortunately, there isn't a lot of relief from this situation. The best remedies are increasing the bar spacing, using mechanical splices, and lap splicing away from the diagonals. A downside to mechanical splices, however, is the space needed to make the splice, which can be considerable depending on the method selected.

Vertical lacing along the vertical edges of an element makes installation of horizontal diagonal bars extremely difficult. Diagonal bars must be threaded through the lacing, which is physically impossible in some situations. The best solution for this problem is to use horizontal lacing at the vertical edges. These bars can then be placed in layers in conjunction with the diagonal bars.

Normal construction practice for lacing is installation of full height vertical lacing bars along with the vertical flexure bars. Horizontal flexure bars are then added by threading through the bend of the lacing. This becomes a problem when 90° tails are used on the flexure bars. Tails on flexural bars should be eliminated and separate hook bars added after installation to provide anchorage.

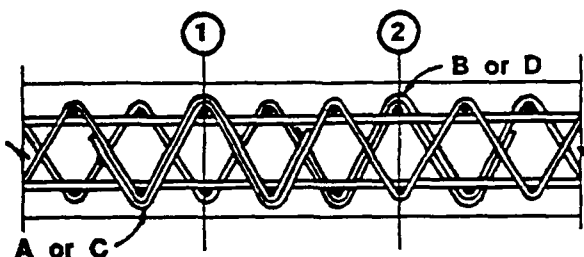


**Figure 2. Typical Details for Splicing of Lacing Bars  
(From TM 5-1300, Ref. 1)**

Given the difficulties presented by lacing reinforcement, the best advice is to avoid its use wherever possible. This may include such measures as limiting rotation below  $4^\circ$  to allow use of stirrups, creating appropriate barriers to increase the standoff beyond a scaled distance of 1.0, and increasing section thickness to reduce shear stresses.

#### *Stirrups*

Stirrups in conventional construction are fairly common and normally do not present many installation problems. A few additional requirements for blast design purposes, however, make their use more complicated. Where stirrups are required in a section, they must be designed for the critical section and continued through the length of the slab regardless of the actual shear stress in sections away from the support. This requirement is intended to prevent buckling of compression flexure bars. Since stresses above the concrete capacity may exist only for short distances from the support, this requirement adds a significant amount of reinforcing. Another requirement is the use of  $135^\circ$  bends on all hooks, as shown in Figure 3. This makes placement of stirrups after flexural steel very difficult if the reinforcing is very stiff and won't bend enough to loop the stirrup hooks over the bar. In most cases the stirrups must be laid out through the slab and flexural bars threaded through. This is not necessarily difficult, but it can require a significant increase in manpower to install the reinforcing. Another option is to specify a  $135^\circ$  bend on one end and a  $90^\circ$  bend on the other. The  $90^\circ$  bend can then be bent in the field after the stirrup is in place. This option may not be viable, however, if the stirrups are very large.

#### *Diagonals*

Diagonal bars are required for slabs in which the actual direct shear exceeds the concrete capacity, support rotations are greater than  $2^\circ$ , or the section is in net tension. In practice, the concrete capacity is usually sufficient, and thus diagonals are normally only necessitated by the latter two requirements. Since internal explosions will produce net tension in most structural elements, diagonals will be quite common in the slabs.

There will always be interference between diagonal bars where orthogonal walls meet because the bars extend into a common element such as a floor or roof slab. There are several remedies for this situation; however, none of these completely eliminates the problem. One approach is to take advantage of the assumed distribution of shear stress on the elements and distribute diagonal steel area based on the  $2/3$  Vu at the corners as described in Figure 4. This effectively reduces the number of bars at the corners, but doesn't completely eliminate the problem. Another remedy is to adjust the height of the bars in adjacent elements in the field to solve this interference. It

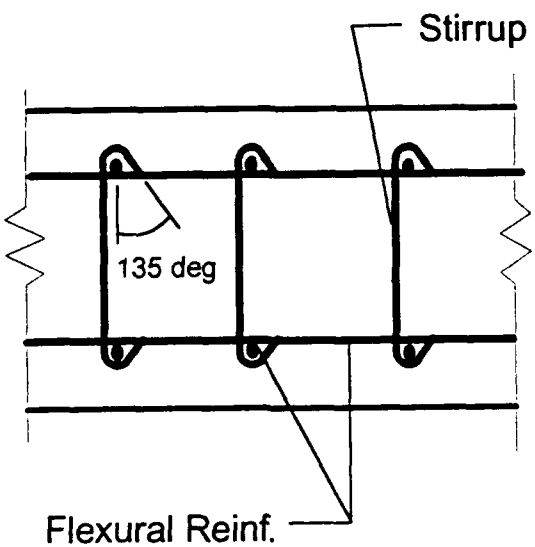


**Figure 3. Stirrups for Blast Resistant Sections**

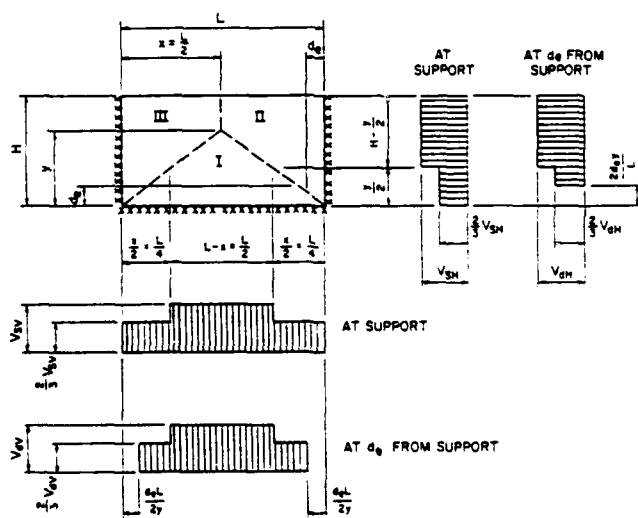


**Figure 4. Determination of Ultimate Shears  
(From TM 5-1300, Ref. 1)**

is advisable to address these solutions in the construction drawings. This indicates to the contractor that an interference may occur, and it allows the detailer a chance to design the reinforcing dimensions to facilitate field placement.

The use of haunches in the slab where diagonals are required greatly facilitates the placement of these bars and should be used wherever possible. If it is not possible, the bars will have to be dropped farther into the slab and may interfere with flexure bars.

#### *Tension Bars*

These bars are placed in the center of a section to provide a reaction to the shear forces from adjacent elements when the section is in net tension. Because the bars must be anchored at each end of the slab, a hook is normally used. If this hook is integral to the bar, placement of orthogonal lacing becomes very difficult. Use of separate hook bars placed after installation of the tension bars and lacing is suggested. Another solution is to use wall extensions to develop anchorage and eliminate hooks. The spacing of diagonal bars is normally the same as tension steel and many times is detailed to be in the same plane. This interference can be eliminated by staggering the starting point for the tension bars.

#### *Flexure*

The most common problem with installation of flexural bars is congestion with the nominal spacing. On paper, a chosen bar spacing can appear to be adequate for installation; however, when actual bar dimensions and fabrication tolerances are considered, the actual free space can be quite small using the out-to-out rebar dimensions. The most obvious solution is use of larger bar spacings. A minimum spacing of 12 in. is suggested to accommodate the various types of reinforcing. A typical section is shown in Figure 5, indicating the various planes of bars required. Calculations of actual free space should be made at the most congested areas. Provision for bending tolerances, even by ACI specifications, can be quite large and must be addressed in the design.

An obvious, yet many times forgotten consideration, is the free space left where adjacent elements intersect. While some bars can remain in the same plane in both elements, many cannot, and thus the nominal spacing must accommodate additional bars. Lap splicing of all the reinforcing, which doubles the number of bars for a particular type, is also a very important consideration for calculation of free space. Use of wall extensions to develop the strength of bars is also an option to minimize the congestion of lap splices at element intersections. A typical section with extensions is shown in Figure 6. The out-to-out dimensions of the reinforcing should be used in the calculations. Although the height of the deformations is relatively small, the total additional space for all the bars can be important.

Interference of flexural bars with other types of reinforcing can be minimized by specifying an offset in the spacing patterns for bars which conflict. This offset should be carefully planned for in the design and should be plainly detailed in the construction documents. It is important that reinforcing be installed as accurately as possible to avoid interference with adjacent slabs. One suggestion to help achieve this is use of temporary structural steel sections in a framework to which the reinforcing is attached. This method has produced excellent results for very heavy reinforcing.

A final suggestion regarding elimination of reinforcing conflicts is the use of three-dimensional graphical or physical models to plan the construction sequence. This step can be very beneficial to the project by facilitating recognition of problems before construction. Problems encountered during construction are almost always much more expensive to remedy than those found during

design. The major difficulty here is convincing the owner to pay for this additional work. The necessity of these methods is not readily seen by those unfamiliar with these types of structures, and there may be a reluctance to fund additional design work.

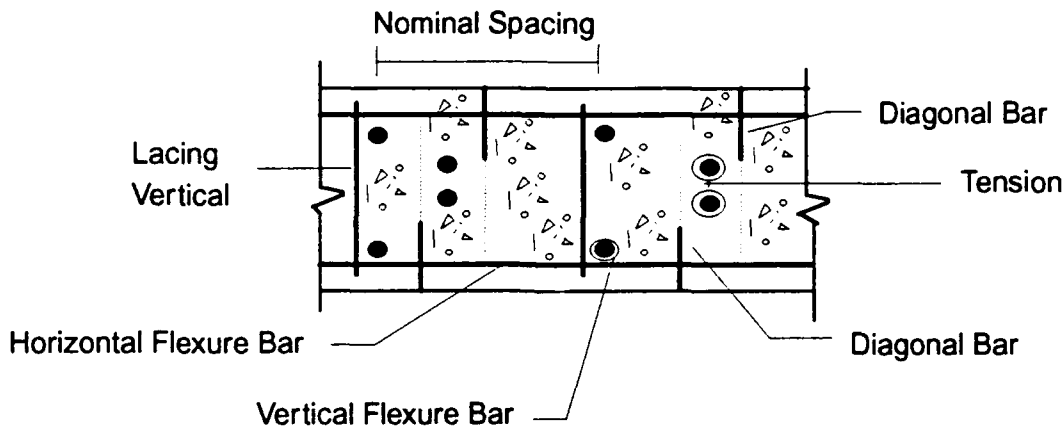


**Figure 5. Typical Spacing Pattern**  
(From TM 5-1300, Ref. 1)

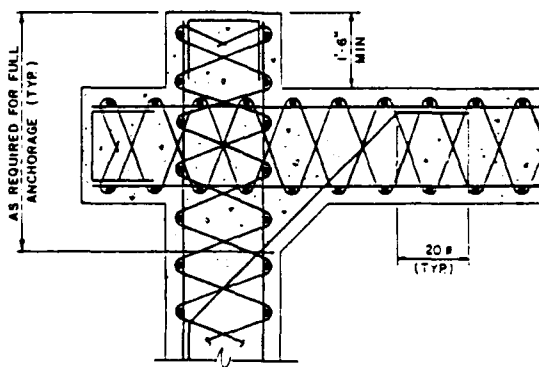


**Figure 6. Typical Detail at Corner of Laced Walls**  
(From TM 5-1300, Ref. 1)

### **Concrete**

The most significant problem with concrete material encountered during construction is proper consolidation. Because of the congestion produced by the reinforcing, flow of the concrete is impeded and voids are left in the section. This result is called honeycombing.

#### *Admixtures*

There are several methods of eliminating this problem which are best used together. The first is the use of a high-range water reducer (superplasticizer). This is an additive to the concrete mix which essentially lubricates the cement grains and greatly enhances the flowability of the mix. As the concrete begins to cure, the protective coating around the grains breaks down and the adhesion process begins. Use of these additives can make a low water-cement ratio concrete flow as a liquid without adverse effects on the final cured strength. This is especially beneficial when pumped delivery is used because the concrete loses an inch or two of slump as it travels through hose. Since the concrete behaves more like a liquid when initially poured, the lateral pressures on formwork is greatly increased and must be accounted for in design of the forms.

#### *Placement*

Vibration of the concrete is a vital step in assuring a sound cross-section, and strict adherence to proper vibration techniques will eliminate most of the honeycombing problems. Contractors must devote special efforts in teaching these techniques to the operators. With heavy reinforcing congestion, insertion points for the vibrators must be spaced closer together than for conventional sections. The contractor should also be prepared for entanglement of the vibrator head in the reinforcing and provide backup equipment. Use of small diameter heads will help to avoid this problem.

Honeycombing can also be caused by segregation of the coarse aggregate from the cement matrix. This occurs when the concrete mix travels a significant distance through a maze of reinforcing. This can be minimized by use of windows in the formwork. Concrete is placed directly into the wall through the side of the forms with the aid of a concrete pump hose or chute and is deposited closer to its final position without traveling through the rebar. Use of preset steel tremies in the reinforcing is another alternative which works well.

#### *Cover*

Generous specifications for concrete cover at the forms and use of smaller coarse aggregate can eliminate many problems associated with honeycombing at the exterior surfaces. Reinforcing which doesn't fit well in the formwork will prevent flow of concrete around the bars and present a void upon removal of the forms. Because much of this reinforcing is relatively large bars, it isn't easy to move the steel away from the forms, and use of a larger cover is well worth the additional cost.

## **CONCLUSION**

Construction of reinforced concrete containment structures and shelters can present some very formidable challenges. The congestion of reinforcing in typical sections requires special considerations by the contractor, but also by the design engineer. Many facilities have been constructed with minimal problems, while others have been plagued with problems which threaten the performance of the structure during a design basis accident.

The design engineer must be aware of these potential problems and adjust the section designs accordingly. It is imperative that sufficient information is included in the drawings to allow the contractor to fabricate and install the reinforcing properly. Attempts to place the burden of resolving all of the constructibility problems on the contractor will ultimately cost the client additional time and money. As most design professionals know, success of the design will be based on the completed structure rather than the contract drawings.

#### **ACKNOWLEDGMENTS**

The authors would like to thank the respondents to the constructibility survey for their valuable input during preparation of this paper: in particular, individuals at Booker and Associates, Southwest Research Institute, and Black & Veatch, Engineers-Architects.

#### **REFERENCES**

1. "Structures to Resist the Effects of Accidental Explosions" (Revision 1), Army TM 5-1300, Navy NAVFAC P-397, Air Force AFR 88-22, Department of Defense Explosives Safety Board, Alexandria, Virginia, November 1990.

**MITIGATION OF CONFINED EXPLOSION EFFECTS  
BY PLACING WATER IN PROXIMITY OF EXPLOSIVES**

By

W.A. Keenan and P.C. Wager  
Structures Division, Code L51  
Naval Civil Engineering Laboratory  
Port Hueneme, CA 93043-4328

25th DoD Explosives Safety Seminar  
Anaheim Hilton Hotel, Anaheim, California  
18-20 August 1992

**ABSTRACT**

Water, placed in the near proximity of a confined explosion, can mitigate the gas pressure loading developed inside a structure confining an explosion. This phenomenon can be exploited in the design and operation of new and existing facilities exposed to a potential internal explosion. This water concept offers the potential for major savings in the cost for explosives safety of ordnance facilities from accidental explosions, for survivability of combat facilities from enemy weapons, and for physical security of sensitive facilities from terrorist bombings.

This paper describes the mechanism by which water absorbs energy from a confined explosion and how this phenomenon reduces the gas pressure loading from a confined explosion; presents test data demonstrating that water can indeed mitigate the gas pressure loading from a confined explosion; describes how water could be exploited in the design of facilities impacted by confined explosions, and estimates the benefits derived from water, in terms of the reduction in land area encumbered by hazardous debris from unhardened ordnance facilities, reduction in the cost of structures designed to fully or partially contain the effects from an internal explosion, and the increase in the safe explosive limit for existing ordnance facilities.

**1.0 INTRODUCTION**

**1.1 Purpose**

This paper describes how water, placed in the near proximity of a confined explosion, can mitigate the gas pressure loading developed inside the structure confining the explosion, and how this phenomenon can be exploited in the design and operation of new and existing

facilities exposed to a potential internal explosion. This water concept offers the potential for major savings in the cost for explosives safety of ordnance facilities from accidental explosions, for survivability of combat facilities from enemy weapons, and for physical security of sensitive facilities from terrorist bombings.

## 1.2 Background

In early 1991, the Carderock Division, Naval Surface Warfare Center (NSWC), Code 1740.2, conducted high explosive tests for the Naval Civil Engineering Laboratory (NCEL). These tests support NCEL development of the High Performance (HP) Magazine.

The HP Magazine is a multi-cell, earth-covered, R/concrete, box-shaped structure with a tunnel entrance. Ordnance is stored in the cells. The cells are designed to prevent an inadvertent detonation in any storage cell from causing sympathetic detonation of ordnance stored in any other cell. Consequently, the maximum credible explosion (MCE) for the HP Magazine is the net explosive weight (NEW) capacity of a single cell.

The NSWC tests were designed to measure the benefit of constructing HP cells using water-filled walls in order to reduce the peak gas pressure and total gas impulse generated by the MCE in the confined space of an HP Magazine. The test results demonstrated that water, placed in the near proximity of a potential explosion, can reduce the peak gas pressure and total gas impulse from a confined explosion by as much as 90 percent, at least for the range of test parameters investigated!

In late 1991, the Naval Weapons Station, Concord, California, contracted NCEL to determine the safe explosive limit for the Radiography Building 35, Pittsburg, California. The normal explosive limit for Building 35 was 5,000 lb NEW but the AMHAZ Review Board reduced the limit to 50 lb NEW until a study could show a higher limit is safe. Building 35 faced shut-down due to inefficient operations unless the limit could be increased to at least 1,680 lb NEW. The NCEL study concluded that the safe explosive limit for Building 35 is less than 10 pounds NEW for protection of people and property at the nearby government property line from hazardous roof debris caused by an inadvertent explosion inside the building (Ref 1). However, NCEL proposed a risk mitigation strategy that increases the safe explosive limit to at least 2,240 pounds NEW by replacing the roof system and requiring a water blanket to be draped over each pallet of ordnance when the pallet is anywhere inside Building 35 (Ref 2). The cost-benefit of this risk mitigation strategy is very high and expected to prevent shut-down of Building 35.

The dramatic benefits derived to date suggest that water, deployed in very specific ways, may prove to be one of the best strategies for mitigating the effects from confined explosions since the discovery of high explosives! Hence, publication of this paper which attempts to capture the potential applications and benefits of water in the design and operation of new and existing facilities exposed to a potential internal explosion.

### **1.3 Scope**

This paper provides the following information:

- Describes the mechanism by which water absorbs energy from a confined explosion.
- Presents test data demonstrating that water can indeed mitigate the effects from a confined explosion, at least within the range of current test data.
- Identifies the types of Naval facilities that are designed to control confined explosions and describes how the benefits of water could be exploited.
- Presents a gross description of concepts for deploying water in various types of facilities to optimize its effectiveness in mitigating effects from confined explosions.
- Estimates the benefits derived from water, in terms of the reduction in land area encumbered by hazardous debris from unhardened ordnance facilities, the reduction in the cost of structures designed to fully or partially contain the effects from an internal explosion, the increase in the safe explosive limit for existing ordnance facilities and bomb disposal devices, and the increased survivability of Command and Control Centers against enemy weapons.
- Identifies the design criteria and research and development needed to exploit the benefits of water in mitigating effects from confined explosions.

## **2.0 PROBLEM**

### **2.1 Confined Explosion**

An explosion in a confined space causes the accumulation of high-temperature gases from the by-products of the explosion. These high-temperature gases, if expanding in a space with restricted venting, cause the buildup of gas pressures inside the structure. The magnitude of the peak gas pressure depends primarily on the weight of explosive relative to the volume of the structure. The duration and total impulse of the gas pressure depend primarily on the degree of venting available for these gases to escape from the structure. The degree of venting, in turn, depends on the area of openings and volume of space in the building envelope, the mass and strength of the building envelope, and the magnitude and location of the explosion inside the structure. The degree of confinement and venting in most facilities is sufficient to produce significant gas pressure loads inside the structure.

## 2.2 Debris Hazard

Most Navy ordnance facilities used for the production, maintenance, assembly and repair of weapons are conventional (unhardened), above-ground buildings containing less than 30,000 lbs NEW. These ordnance buildings must be sited a large distance from nearby inhabited facilities in order to limit the risk of injuries and damage from hazardous debris produced by the maximum credible explosion (MCE) in the ordnance facility.

The minimum safe separation distance from an ordnance facility encumbers a large area of land. For example, the safe separation distance to inhabited facilities is 1,250 feet minimum for an MCE  $\leq$  30,000 pounds NEW. Thus, an ordnance facility containing less than 30,000 pounds NEW, a common situation, encumbers at least 112 acres of land (the area of a circle with a 1,250 feet radius). The safe separation distance and encumbered land area are dictated by the strike range of hazardous fragments and debris. At today's real estate prices, especially near the Navy waterfront, the value of encumbered land often exceeds the acquisition cost of the ordnance facility!

The safe separation distance from building debris is dictated, in part, by the gas impulse developed when the explosion is confined by the building envelope. This gas impulse contributes significantly to the launch velocity of building debris and the resulting maximum strike range of hazardous debris. Thus, any scheme that reduces the magnitude of this gas impulse would significantly reduce the maximum strike range of hazardous debris and the corresponding encumbered land area needed for the safety of people and property.

## 2.3 Containment Structures

Containment structures are hardened structures designed to control the escape of blast pressures, weapon fragments, and facility debris from the MCE inside the structure. Containment structures are designed to either fully or partially contain effects from the MCE.

The TRIDENT Reentry Body Complex, Kings Bay, Georgia, is an example of a full containment structure (Ref 3). Several rooms in this facility were designed to fully contain MCE effects within the room in order to satisfy explosives and contamination safety objectives. The MCE for several relatively large rooms was only 30 lb NEW. The rooms ranged in size from  $26,411 \text{ ft}^3$  for explosive storage rooms to  $98,172 \text{ ft}^3$  for warhead maintenance rooms. Thus, the high-temperature gases were generated by a relatively small MCE and were allowed to expand in a relatively large space, i.e., the maximum explosive weight ( $W$ ) to room volume ( $V$ ) was quite small ( $3 \times 10^{-4} \leq W/V \leq 11 \times 10^{-4} \text{ lb}/\text{ft}^3$ ). Yet, the gas pressure loading, not just the shock pressure loading, dictated the design of the R/concrete walls, ceiling, and doors needed to fully contain effects from the MCE. Any scheme that would have reduced the magnitude of the gas impulse from the MCE would have significantly reduced the structural cost to fully contain MCE effects within the room. Alternatively, any scheme that would reduce the magnitude of the

gas impulse could be deployed today in the existing Reentry Body Complex, thereby increasing the safe explosive limit for the rooms!

The NAVFAC standard design for a missile test cell (MTC) is an example of a partial containment structure (Ref 4). The MTC is used to test all-up-round missiles which could detonate accidentally during the test. The test is conducted remotely from an adjoining Missile Maintenance Facility. The MTC partially contains effects from the MCE, and vents effects in a safe direction away from the adjoining Missile Maintenance Facility. The MTC design is a massive R/concrete, box-shaped structure. Three walls, the floor, the roof, and the access door are hardened designs that prevent the escape of blast pressures, weapon fragments, and facility debris. The fourth wall is a frangible surface designed to fail and blow away under the force from the MCE, thereby venting MCE effects in a safe direction away from the adjoining Missile Maintenance Facility. The frangible wall area and mass, structure volume, and MCE magnitude are in a range that constitutes a partially confined explosion, in which significant gas impulse develops inside the MTC. This gas impulse, in combination with the shock impulse, dictates the structural design of surfaces that are hardened to prevent these surfaces from venting effects from the MCE. Thus, any scheme that would reduce the magnitude of the gas impulse from the MCE would significantly reduce the structural cost to harden the MTC. Alternatively, any scheme that would reduce the magnitude of the gas impulse could be deployed today in many existing MTCs, thereby increasing significantly their safe explosive limit!

#### **2.4 Combat Survivability**

Special combat facilities, such as Navy Command and Control Centers, are designed to protect operations from enemy weapons. This performance objective is very difficult to achieve, given the extreme accuracy and penetrating power of today's weapons. Even massive amounts of reinforced concrete, steel, soil cover, and rock rubble can fail to prevent today's weapons from perforating an interior space. Once inside the structure, detonation of the warhead constitutes a fully confined explosion, developing a gas impulse that destroys all spaces in the facility. Consequently, combat facilities are often subdivided by hardened partitions designed to limit the spread of damage to the room where the weapon perforated the structure. However, this strategy is often very expensive because the gas impulse generated by the explosion is large when the high-temperature gases are confined to a single room. Consequently, survivable structures against today's threats are very expensive, if not impractical! Any scheme that would reduce the magnitude of the gas impulse from the MCE would significantly reduce the structural cost of survivable combat facilities. Alternatively, any scheme that would reduce the magnitude of the gas impulse could be deployed today in existing combat facilities, thereby increasing the survivability of these facilities against enemy weapons!

## **2.5 Terrorist Bombings**

Given a choice, terrorists will typically detonate bombs in a confined space, such as a lobby, to achieve maximum damage to a building. The damage enhancement results from the gas impulse associated with a confined explosion. Any scheme that would reduce the magnitude of the gas impulse would significantly reduce the structural cost of hardening confined spaces to protect sensitive facilities from terrorist bombings. Alternatively, any scheme that would reduce the magnitude of the gas impulse could be deployed today in confined spaces of sensitive facilities, thereby increasing the physical security of these facilities against terrorist bombings!

## **3.0 SOLUTION**

### **3.1 Water Concept**

The water concept requires water to be deployed in the near proximity, but not necessarily in contact, with the explosive material. The water must be in the near proximity of the explosive at all times when an inadvertent explosion is a credible event.

One possible concept for deploying the water is a water blanket, as illustrated in Figure 1. For the case of palletized ordnance, the water blanket would be draped over the top of each pallet of ordnance. The blanket(s) dedicated to a pallet of ordnance would contain a minimum amount of water, the amount depending on the type and NEW of high explosive stored on the pallet. In theory, TNT explosive would require about 1.8 lb of water for each pound of TNT while H-6 explosive would require about 3.8 lb of water for each pound of H-6. The blanket would be some commercial off-the-shelf design. The blanket material would be puncture resistant, yet not retard aerosolization of the water by the shock wave from an explosion. The blanket width would be fixed at about 38 inches, slightly less than the minimum width of any pallet of ordnance. The length and number of blankets dedicated to each pallet will vary, depending on the NEW and type of explosive stored on the pallet.

### **3.2 Phenomenon**

Detonation of a high explosive produces high pressure shock waves which travel outward in all directions from the explosion at extremely high velocity. These high speed shock waves strike and aerosolize the water located in the near proximity of the explosion. The aerosolized water prevents combustion of detonation products by preventing access to oxygen and by cooling gases below the temperature required to sustain combustion. For this to occur, the aerosolized water must absorb the detonation energy of the explosive. Typical heats of detonation for high explosives range from 980 calories/gram for TNT explosive to 2030 calories/gram for H-6 explosive. Vaporization of water absorbs 539

calories/gram plus one calorie/gram/degree to heat the water to 100 degrees Celsius. Thus, the aerosolized water can absorb all of the detonation energy of the explosive if the weight ratio of water to explosive is  $980/539 = 1.8$  for TNT explosive and  $2030/539 = 3.8$  for H-6 explosive. These ratios assume the aerosolized water is 100% efficient in eliminating the heat detonation, thereby eliminating the heat of combustion and associated burning of explosive by-products in the air. In practice, the weight ratio of water to explosive should probably be slightly greater than the above values to account for less than 100% efficiency in eliminating the heat of detonation. In any case, the net effect of the water absorbing the detonation energy of the explosive is a major reduction in the peak gas pressure and total gas impulse from the confined explosion.

Ideally, the shock waves need to aerosolize the water very quickly (in a matter of milliseconds) into a fine mist of water droplets suspended in the atmosphere of the containment structure. Hence, the need for the sheet, layer, pillow or blanket of water to be located in the near proximity of, but not necessarily in contact with, the explosive producing the explosion. The water mist presents a huge surface area of water, an ideal condition for efficiently converting the water from a liquid state to a vapor state. The later-time buildup of high-temperature gases from the by-products of the explosion, expanding in a fully or partially confined space with restricted venting, cause huge amounts of energy released by the explosion to be quickly dissipated by changing the water mist from a liquid state to a vapor state. The consequence of this phenomenon is a peak gas pressure and total gas impulse much less (as much as 90% less based on test data) than the peak gas pressure and total gas impulse would have been in the absence of water.

The utility of the water concept is expected to diminish with an increasing ratio of net explosive weight to structure volume (W/V). Although there are no test data to prove this to be the case, certain negative factors are obvious at high values of W/V. For example, at some very high W/V, there is insufficient space to accommodate the volume of explosive (and the attached inert components) and water. Because of the volume of inert components, the critical W/V for bombs (high explosive density) would be higher than for containerized missiles (low explosive density). At some lower W/V, the available space can accommodate the volume of water and explosive items but there is insufficient air space inside the structure to allow the shock waves from the explosion to aerosolize the water. In this case, the total surface area of water-in-air is too low relative to its total weight, thereby preventing the gas temperatures from converting much water from the liquid state to the vapor state, and, hence, no significant absorption of the detonation energy by the water. A third constraint is the capacity of the structure to confine, at least partially, the explosion at the high shock plus gas pressures associated with a high W/V. Unless the structure can confine the high temperature gases for some minimum time, then the water cannot absorb much detonation energy from the explosive. Thus, there is some upper bound value of W/V that defines the limit for

application of the water concept. This critical value of  $W/V$  will vary of course, depending on several parameters, such as type of explosive, type of ordnance, logistics constraints, and the architectural and structural design of the containment structure.

The utility of the water concept is also limited by the capability of logistics systems to cope with the weight and volume of water needed to absorb the detonation energy of the explosive. However, it is anticipated that the water concept is a very practical, useful, cost effective concept for a very broad range of scenarios faced every day in the "explosives world," as illustrated by the broad range of applications described in Section 4.0 of this paper.

### 3.3 Demonstration Tests

Results from high explosive tests conducted by NSWC demonstrate that water can reduce the peak gas pressure and total gas impulse generated by fully and partially confined explosions. The NSWC tests were 1/12th scale model tests of storage cells in HP Magazines (Ref 5). The cells were 3-wall cubicles with water-filled walls, as shown in Figure 2a. The tests involved detonating a cylinder-shaped TNT charge (right cylinder with  $L/D = 1.0$ ) at the geometric center of a 3-wall cell with water-filled walls. The water-wall cell rested on a table located inside a hardened, unvented, steel chamber that fully contained effects from the test explosion. In all tests, the weight of explosive,  $W$ , was 4.67 lb TNT, the test chamber volume,  $V$ , was 1,150 ft<sup>3</sup>, and the vent area of the chamber,  $A_V$ , was 0 ft<sup>2</sup>.

Typical plots of the gas pressure versus time measured inside the test chamber are shown in Figure 2b. The scope of these tests and the peak gas pressure measured inside the test chamber are summarized in the table below. Note that providing 2.89 pounds of water for each pound of TNT explosive ( $W_W/W = 2.89$ ) reduced the peak gas pressure from 54.1 psi (average of tests 1 and 10) to 5.85 psi (average of tests 7 and 8) for a total reduction of nearly 90%!

Test No.	Test Configuration	TNT Weight W (1b)	Water Weight W <sub>W</sub> (1b)	W <sub>W</sub> /W	W/V (1b/ft <sup>3</sup> ) <sup>a</sup>	Peak Gas Pressure P <sub>g</sub> (psi) <sup>b</sup>
1	Hung bare charge	4.67	0	0	0.00406	55.4
2	Bare charge on table	4.67	0	0	0.00406	51.3
3	Charge immersed in cube of water	4.67	9.0	1.93	0.00406	5.1
4	Charge immersed in cube of water	4.67	13.5	2.89	0.00406	4.4
5	3-Wall cubicle with 2" thick water walls	4.67	9.0	1.93	0.00406	8.3
6	3-Wall cubicle with 2" thick water walls	4.67	9.0	1.93	0.00406	7.5
7	3-Wall cubicle with 3" thick water walls	4.67	13.5	2.89	0.00406	5.9
8	3-Wall cubicle with 3" thick water walls	4.67	13.5	2.89	0.00406	5.8
9	Charge immersed in cube of ethylene glycol (50/50)	4.67	9.0	1.93	0.00406	6.0
10	Hung bare charge	4.67	0	0	0.00406	52.7

<sup>a</sup>Test chamber volume, V = 1,150 ft<sup>3</sup>; scaled vent area of test chamber, A<sub>V</sub>/V<sup>2/3</sup>=0.0.

<sup>b</sup>Average value from 11 pressure transducers located inside test chamber.

## **4.0 APPLICATION**

### **4.1 Explosives Safety**

Ordnance facilities house ordnance operations supporting the Naval Ammunition Logistics System (NALIS). The designs for these ordnance facilities are heavily influenced by Navy explosives safety regulations intended to limit the risk of injuries and damage from an accidental explosion inside the facility. The ordnance facility is either a hardened design, resulting in a high construction cost to either fully or partially contain effects from an accidental explosion inside the structure, or an unhardened design, resulting in a high encumbered land cost to accommodate Explosives Safety Quantity Distance (ESQD) arcs. The following sections illustrate the potential applications and benefits of deploying water in ordnance facilities to significantly reduce the cost of facilities and land supporting the NALIS.

**4.1.1 X-ray Facilities.** X-ray facilities are used to X-ray ordnance items and explosive components, such as warheads, projectiles, fuzes, and rocket motors, to evaluate their state of readiness. Radiography Building 35, Pittsburg, California, is a typical X-ray facility.

The USN AMHAZ Review Board recently reduced the NEW limit for Building 35 from 5,000 lb NEW to 50 lb NEW because of their concern about hazardous pressures, fragments, and debris at the government property line from the MCE in Building 35. The reduced NEW limit severely degrades the efficiency of X-ray operations. Consequently, Naval Weapons Station, Concord, California, contracted NCEL to evaluate the hazards and develop a risk mitigation strategy that would increase the safe NEW limit for Building 35 to at least 1,680 lb NEW.

Radiography Building 35 is a large, rectangular-shaped structure with very massive reinforced concrete walls and equipment door; a sloped, frangible, corrugated metal roof; and a small attached structure of conventional construction. The main structure has one large room, called the X-ray Exposure Room, where explosives are x-rayed. The floor plan, elevation view, and roof details are shown in Figure 3.

NCEL analyzed the hazards from Building 35 and concluded that the safe explosive limit is less than 10 lb NEW because damage to the frangible roof produces hazardous blast pressures and hazardous roof debris at the property line for an MCE  $\geq$  10 lb NEW (Ref 1). NCEL developed a risk mitigation strategy that increases the safe NEW limit from less than 10 lb NEW to at least 2,240 lb NEW. The strategy requires the following renovations to Building 35:

a. Require a water blanket to be part of each pallet of ordnance while the pallet is anywhere inside Building 35. The design and deployment concepts for the water blanket are shown in Figure 1.

b. Replace the existing corrugated metal roof with a precast, R/concrete roof, consisting of precast, R/concrete T-beams positioned side-by-side; a cast-in-place R/concrete topping slab; and a chimney

vent, as shown in Figures 4a and 4b. The average thickness of the R/concrete roof,  $T_c$ , is 18 inches. The chimney vent, located an equal distance from the property lines, restricts the venting of shock waves from the MCE in Building 35. This restriction limits the peak incident pressure at the property line to 1.2 psi maximum, the limit allowed by NAVSEA OP-5 safety regulations for the safety of people and property at government property lines. The cast-in-place, R/concrete topping slab provides a critical roof mass that controls the maximum strike range of roof debris, stops weapon fragments, slopes the roof for water runoff, and holds the T-beams together when the roof moves upward from effects of the MCE.

c. Add four ready-service magazines inside the building, each magazine separated by a nonpropagation wall, as shown in Figure 4c. The magazines are ventilated, skid-mounted, and relocatable. Designs are commercially available that meet all federal specs for safety and security of explosives storage. The magazines are sized to accommodate the water blanket draped over the top and down two sides of each pallet load. The nonpropagation walls prevent sympathetic detonation between any two magazines, thereby limiting the MCE to 560 lb NEW, the safe storage capacity of each magazine.

d. Conduct all ordnance receipt/shipment operations inside the building by parking the flatbed trailer (trailer containing the ordnance) inside the building with the entry door closed before any ordnance is transferred to or from the trailer. This arrangement mitigates the hazards associated with ordnance transfer operations, as shown in Figure 3a.

The water blanket is a major element of the risk mitigation strategy for Building 35. The shock wave from the MCE will aerosolize the water in the blanket, thereby allowing the water to absorb huge amounts of energy (that would normally create gas pressure) by changing the water mist from a liquid state to a vapor state. Consequently, the water blanket reduces the peak gas pressure and total gas impulse generated by the MCE. This reduction, in turn, reduces the maximum strike range of roof debris from about 124 ft (without water blanket) to about 12.6 ft (with water blanket), as shown in Figure 4d for  $T_c = 18$  inch. Thus, the water blanket reduces the strike range of debris by 90%! To gain the same result without a water blanket would require a 12-ft deep soil layer covering the entire 3,200 ft<sup>2</sup> area of the roof! This soil mass would weigh 2,112 tons! Thus, the water blanket eliminates the need to place 2,112 tons of soil on the roof which would be very expensive and surely impractical. Without the water blanket, NCEL found no practical strategy for increasing the safe explosive limit for Building 35 to the minimum limit needed for efficient ordnance operations.

**4.1.2 Missile Maintenance Facilities.** A Missile Maintenance Facility (MMF) is an intermediate-level maintenance activity for the assembly, repair, and testing of Navy missiles. A typical MMF is a very large, unhardened structure with R/concrete walls and a metal or R/concrete roof. The safe explosive limit for an MMF is usually less than 30,000 lb NEW, in which case the ESQD distance to nearby inhabited facilities is 1,250 ft. This ESQD arc encumbers at least 112 acres of land!

Missiles are delivered to the MMF in their container. Once inside the MMF, the missile is removed from its container and placed on a Missile Assembly and Maintenance (MAM) stand. The missile remains on the MAM stand during the entire maintenance cycle.

A water-filled cradle mattress could be a permanent part of the MAM stand, as illustrated in Figure 5a. By so doing, the proper amount of water would be deployed in the ideal locations of the MMF, i.e., in the near proximity of each explosive component in the MMF, regardless of when or where the missile was moved inside the MMF. Given an inadvertent explosion as illustrated in Figure 5b, the distribution of water throughout the MMF would be the ideal distribution at all times!

The MAM stand could easily accommodate the water mattress, without the mattress interfering with maintenance operations on the missile. If necessary, the water mattress could be located below the main beam assembly (Figure 5a) of the MAM stand.

The characteristics of the water mattress depend on the characteristics of the missile. The net explosive weight is less than about 300 lb NEW for most surface-launched missiles and less than about 100 lb NEW for most air-launched missiles. Based on a weight ratio of water-to-explosive equal to 2.0, the approximate characteristics of the water mattress would be as follows:

Missile Type	Maximum Explosive W (lb NEW)	Weight Ratio $\frac{W_w}{W}$	Water Quantity $\frac{V_w}{W}$ (ft <sup>3</sup> )	Mattress Size L x W x H
Surface Launched	300	2.0	600	10'x 2'x 0'-6"
Air Launched	100	2.0	200	6'x1'-6"x0'-4"

The mattress material would be puncture resistant, yet not retard aerosolization of the water by the shock waves from inadvertent detonation of the missile on the MAM stand.

The debris prediction model shown in Figure 6a was used to estimate the benefits of deploying water mattresses in a Missile Maintenance Facility and other similar types of unhardened, aboveground, ordnance facilities. The model is crude in terms of simulating the actual breakup pattern of the building envelope. However, the model correctly accounts for all critical parameters, including the following:

- The mass of the building envelope.
- The shock pressure loading applied to each individual building surface, as a function of time, based on the computer program SHOCK.
- The vent area created for gases to escape around the perimeter of each building surface, as a function of time, when these building surfaces are displaced outward by the internal gas and shock pressure loadings, based on computer program FRANG 2.0 which simultaneously tracks the displacement-time history of five building surfaces.
- The internal gas pressure, as a function of time, as the building vent area increases with time and allows gas pressures to vent from the building, based on computer program FRANG 2.0.
- The critical launch angle of debris from each building surface, based on the rotation capacity of the building envelope at its supports.
- The flight trajectory and strike range of building debris, based on computer program TRAJ.
- The reduction (assumed to be 89%) in the initial peak gas pressure due to the water, and the internal gas pressures at all subsequent times based on FRANG 2.0, using a pseudo explosive weight that would produce the initial peak gas pressure inside the building.

It was assumed that a typical building is  $L = 100'$  long,  $w = 50'$  wide, and  $H = 15'$  high. The MCE is assumed to be located at the center of the building, 4'-0" above the floor. The building envelope has no initial vent area, i.e., the building has no windows and no open doors. The mass of the building envelope,  $\gamma$ , is 25 psf minimum and 200 psf maximum. Breakup of the building envelope requires no work to be done, i.e., the strain energy absorbing capacity of the building envelope is zero. The critical mass of launched debris is 1.0 lb.

The benefits of the water mattress are described by the curves presented in Figures 6b, 6c, and 6d. The predicted reduction in the total gas plus shock impulse due to water,  $R_i$  (%), is presented in Figure 6b as a function of the net explosive weight,  $W$ , of the MCE and the unit mass,  $\gamma$ , of the building envelope. The predicted reduction in the debris distance due to water,  $R_d$  (%), is presented in Figure 6c as a function of  $W$  and  $\gamma$ . The predicted reduction due to water in the land area (including the area of the building footprint) encumbered by wall debris,  $R_A$  (%), accounting for differences in the debris distance from sidewalls and endwalls, is presented in Figure 6d, as a function of  $W$  and  $\gamma$ . Note in these figures that  $R_i$ ,  $R_d$ , and  $R_A$  decrease with increasing  $W$  and decreasing  $\gamma$ , as one would expect. Most important, these figures forecast that major reductions in the land area encumbered by building debris can be achieved by deploying water mattresses on MAM stands in Missile Maintenance Facilities! The reduction in encumbered land area,

$R_A$ , ranges from 75 to 90% for  $W < 1000$  lb NEW, from 20 to 75% for  $W = 1000$  lb NEW, and from 15 to 50% for  $W = 30,000$  lb NEW! These reductions represent huge savings in valuable waterfront real estate needed to protect people and property from accidental explosions in ordnance buildings! NCEL could not identify an alternative strategy that even approaches the cost-benefit of the water concept.

**4.1.3 Missile Test Cells.** The standard design for a NAVFAC Type I Missile Test Cell (MTC) is shown in Figure 7a. The MTC is used to test the reliability of all-up-round (AUR) missiles before delivery to the Fleet.

A mishap during the test could lead to inadvertent detonation of the missile. Consequently, the AUR test is conducted remotely from a control room located in the adjoining Missile Maintenance Facility.

The MTC is a massive reinforce concrete, box-shaped structure, as shown in Figure 7a. The interior of the box is 40'-0" long, 25' wide, and 15' high. The floor, roof and 3 walls are blast hardened to prevent the escape of blast pressures, weapon fragments, and debris. The fourth wall is a frangible wall, as shown in Figure 7a. This frangible wall is designed to fail and vent explosion effects in a safe direction away from the adjoining Missile Maintenance Facility.

The test missile is restrained on a test restraint fixture about 3'-6" above the MTC floor, as shown in Figure 7a. The MTC houses various test support equipment and an overhead bridge crane which travels the length of the MTC. The bridge crane is used to position the test missile on the test restraint fixture.

A water pillow could be deployed in the MTC, as illustrated in Figure 7b. Given a mishap during the AUR test, the shock waves from the MCE would aerosolize the water, thereby reducing the total gas impulse generated inside the MTC. The water pillow would be moved into position, directly over the test missile, with the bridge crane just before the MTC is evacuated to begin the AUR test. The water pillow would be suspended from the bridge crane, maybe 3 or 4 feet above the test missile, for the duration of the AUR test.

The chart in Figure 7c illustrates the potential benefit derived from the water pillow. The two curves in Figure 7c describe the total shock plus gas impulse,  $i_s + i_g$ , applied by the maximum credible explosion,  $W$ , to the ceiling of the MTC, with and without the water pillow. These curves were generated using computer programs SHOCK and FRANG, based on a frangible wall mass,  $\gamma = 30$  psf; a design explosive weight equal to  $1.2 W$ ; and the MCE located at midlength of the box, 3'-6" above the floor.

The water pillow could significantly increase the safe explosive limit for an existing MTC. From Figure 7c, the water pillow reduces the total gas plus shock impulse by about 78% for  $W = 100$  lb NEW, by about 37% for  $W = 300$  lb NEW, and by about 27% for  $W = 1000$  lb NEW!

The NAVFAC Type I MTC was designed for a safe explosive limit of  $W = 300$  lb NEW which according to Figure 7c will apply  $i_s + i_g = 16,000$  psi-msec to the ceiling of the MTC. Therefore, if the total impulse

capacity of the ceiling is 16,000 psi-msec then it follows from Figure 7c that the water pillow could increase the safe explosive limit to about  $W = 780$  lb NEW or 160%. Actually, the explosive limit is more likely to increase about 100% or to  $W = 600$  lb NEW, because the duration of the gas impulse exceeds the time required for the ceiling slab to reach its maximum deflection. In any case, deployment of the water pillow concept could significantly increase the safe explosive limit of existing missile test cells!

The water concept would require the pillow to hold about 600 lb NEW  $\times 2.0 = 1200$  lb or  $1200 / 62.4 = 19$  ft<sup>3</sup> of water for  $W = 600$  lb NEW. The weight ratio 2.0 accounts for propellant in missiles. Assuming an average missile is about 12' long, the pillow would be about 12' long, 2' wide, and 0'-9" thick. The bridge crane in existing MTCs could easily support this pillow load and there is ample space above the test restraint fixture to position the water pillow directly above the test missile.

**4.1.4 Ready Service Magazines.** Ready Service (RS) magazines are small, earth-covered, box-shaped, reinforced concrete structures designed to store small quantities of high explosives. Typical RS magazines have a storage capacity of about 100 lb NEW and their ESQD arcs encumber as much as 112 acres of land to protect people and property from an accidental explosion. Deployment of water blankets in RS magazines would significantly reduce the land area encumbered by ESQD arcs, especially if the water concept was combined with the use of non-propagating walls designed to reduce the MCE in RS magazines. Further, the water concept may allow RS magazines to be sited closer to the operating buildings they are intended to support.

**4.1.5 Missile Storage Magazines.** Missile Storage (MS) magazines are large, earth-covered, box-shaped, reinforce concrete structures used to store containerized, all-up-round missiles. A typical MS magazine is the NAVFAC Type C magazine. The magazine interior is 94'-8" wide, 50' deep, and 15' high which contains about 71,000 ft<sup>3</sup> of air space. To facilitate the storage and retrieval of containers, the magazine is used to store no more than about 120 large missile containers or about 14,000 ft<sup>3</sup> of cargo. This number of containers represents no more than about 60,000 lb NEW. Thus, only about 20 percent of the magazine space is used to store missiles. This storage plan provides an explosive density for the magazine equal to  $60,000 \text{ lb NEW} / 71,000 \text{ ft}^3 \text{ of space} = 0.85 \text{ lb NEW}/\text{ft}^3$  which is relatively high compared to the range of existing test data ( $4 \times 10^{-3}$  lb NEW/ft<sup>3</sup> of space). Preliminary calculations indicate that water blankets deployed over missile containers may not reduce the ESQD arcs and associated encumbered land area by very much. However, test data need to be collected in this W/V range to determine if the benefits of deploying water blankets in MS magazines are significant enough to be used in this application.

## 4.2 SURVIVABILITY

Structural survivability of today's combat facilities is difficult to achieve, given the extreme accuracy and penetrating power of today's weapons. Even massive amounts of reinforced concrete, steel, soil cover, and rock rubble can fail to prevent today's weapons from perforating an interior space. Once inside the structure, detonation of the warhead constitutes a fully confined explosion, developing a gas impulse that destroys all spaces in the facility. Dispersion of resources is often the only practical strategy to achieve reasonable levels of survivability, but this strategy is very expensive. The following section illustrates a potential application and the benefits of deploying water in combat facilities to reduce the construction cost and increase the survivability of the structure.

**4.2.1 Command and Control Centers.** A Navy Command and Control Center is shown in Figure 8. The structure is a deeply buried, R/concrete structure subdivided into rooms by partitions designed to confine explosion effects to the room where the enemy weapon happens to perforate the structure.

Water blankets could be deployed in a Command and Control Center, as illustrated in Figure 8. The water blankets could be suspended from the ceiling or hung as drapes near the walls of each room. Given that an enemy weapon perforates the structure, the shock waves from the explosion would aerosolize the water, thereby reducing the peak gas pressure and the total gas impulse generated inside the room where the explosion occurs.

The water blankets would significantly reduce the structural cost of new Command and Control Centers, and significantly increase the survivability of existing Command and Control Centers! For most deep penetration weapons, the ratio of warhead explosive weight,  $W$ , to room volume,  $V$ , is probably no greater than the  $W/V$  ratio of existing test data ( $W/V = 0.004 \text{ lb}/\text{ft}^3$ ). Consequently, the water blankets could be expected to reduce the peak gas pressure and total gas impulse by nearly 90%, based on test results presented in Section 3.3.

If the design threat was a 100 lb NEW warhead, then the water blanket must contain about  $100 \times 2.5 = 250 \text{ lb}$  of water or  $250/62.4 = 4 \text{ ft}^3$  of water. This quantity of water could be conveniently supplied by one blanket per room, measuring about 6' long x 4' wide x 0'-2" thick. The blanket could be either suspended 2 or 3 ft below the ceiling or hung as a drape at some minimum standoff distance from the nearest wall.

The water blanket concept offers significant increases in survivability and reductions in construction cost. In existing facilities, a 90% reduction in the peak gas pressure,  $P_g$ , translates into about a 90% reduction in the maximum dynamic deflection of the partitions, resulting in major reductions in damage to existing facilities. In new facilities, a 90% reduction in  $P_g$  reduces the required thickness of partitions by at least about 50%, resulting in major reductions in the construction cost of blast resistant partitions and doors. These potential benefits need to be quantified in more detail.

### **4.3 Physical Security**

The water concept offers a cost effective strategy for quickly upgrading the physical security of sensitive facilities against terrorist bomb threats.

**4.3.1 Terrorist Bombings.** Physical security of sensitive facilities is difficult to achieve against the threat of terrorist bombings. Detonated in any fully or partially confined space, the confined explosion will develop a significant gas pressure impulse that can cause major damage to a facility. Water blankets or water drapes could be concealed in confined spaces of the facility, thereby reducing the gas impulse and associated level of damage to the facility.

### **4.4 Explosive Ordnance Disposal**

The water concept could enhance the safety and capability of Explosive Ordnance Disposal (EOD) teams when transporting explosive devices to disposal sites.

**4.4.1 Bomb Carts.** A bomb cart is a mobile containment vessel used to transport explosive devices. The vessel is designed to fully contain explosion effects if the explosive device(s) were to detonate inside the vessel. A typical bomb cart is shown in Figure 9. Located inside the vessel is a basket formed from wire screen. The bomb is carried in the basket which holds the bomb a minimum standoff distance from the walls of the containment vessel.

Water-filled hotdogs could be hung at several points along the outer perimeter of the bomb basket, as shown in Figure 9. Given an accidental explosion, the shock waves from the explosion would aerosolize the water, thereby reducing the peak gas pressure generated inside the containment vessel. Depending on the bomb's explosive weight and the containment vessel volume, the aerosolized water could absorb the detonation energy of the explosive, thereby reducing the peak gas pressure by as much as 90 percent. Thus, the water hotdogs could significantly increase the explosive weight capacity of existing bomb carts and significantly reduce the fabrication cost of new bomb carts.

## **5.0 BENEFITS**

Major benefits can be realized by deploying the water concept to mitigate the gas pressures from confined explosions. The major benefits include:

- Major reductions in the structural cost of containment structures designed to either fully or partially contain effects from an internal explosion.

- Major reductions in the land area encumbered by ESQD arcs designed to protect people and property from explosions in ordnance facilities.
- Major increases in the explosive limit of existing facilities that fully or partially confine an internal explosion.
- Major reductions in the extent of damage to existing facilities from an internal explosion.

## **6.0 RECOMMENDATIONS**

- Begin research on water concepts in FY93. The magnitude of the potential benefits to the Department of Defense justify initiating the project immediately.
- A major research project should be initiated to develop the design criteria needed to safely deploy water that mitigates effects from confined explosions in new and existing facilities.

## **7.0 REFERENCES**

1. Naval Civil Engineering Laboratory. Memorandum to files on the analysis of blast and debris hazards for safe explosives limit of ordnance operations in Radiography Building 35, Pittsburg, California, by P.C. Wager and W.A. Keenan, Port Hueneme, CA, Nov 1991.
2. Naval Civil Engineering Laboratory. Memorandum to files on the NCEL proposal for development of design criteria to mitigate blast, fragment, and debris hazards at property line from ordnance operations in Radiography Building 35, Pittsburg, California, by W.A. Keenan and P.C. Wager, Port Hueneme, CA, Jun 1992.
3. Naval Civil Engineering Laboratory. Technical Note N-1706: Basis of Design Document for Explosives and Contamination Safety of MCON Project P-312M, Reentry Body Complex, SWFLANT, Kings Bay, Georgia, by W.A. Keenan, et al., Port Hueneme, CA, Sep 1984.
4. Naval Civil Engineering Laboratory. Technical Note N-1752R: Basis of Design for NAVFAC Type I Missile Test Cell, by W.A. Keenan, R.N. Murtha, et al., Port Hueneme, CA, Apr 1990.
5. Wilson, David T. "Explosion Suppression by Water Surrounds," Paper presented at the Eighth IEP ABCA-7 Quadripartite Conference, 11-15 May 1992, Halifax, Nova Scotia, Canada. CONFIDENTIAL.

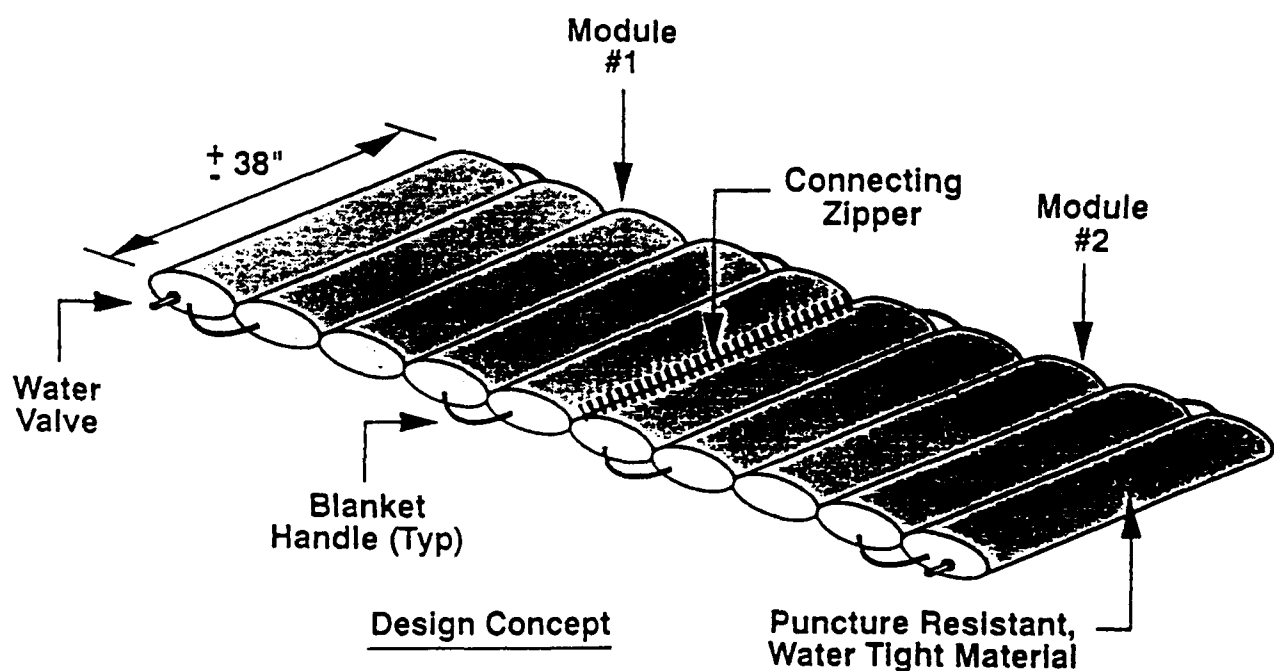
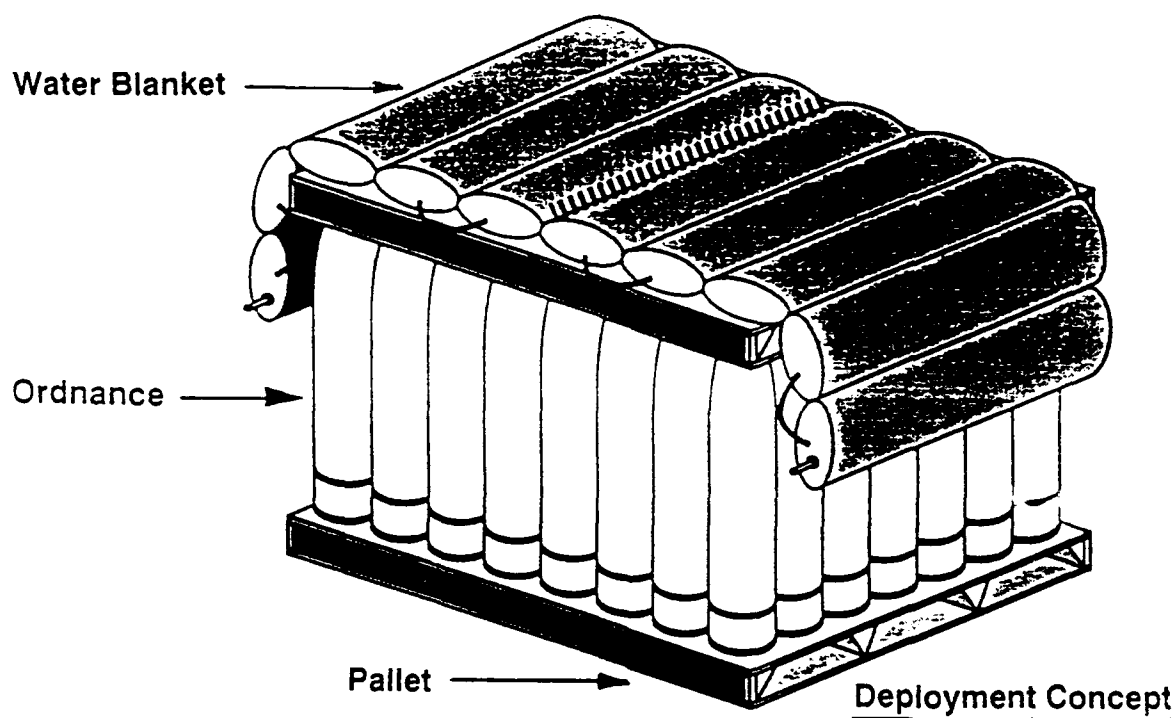


Figure 1. Conceptual design and deployment of water blanket.

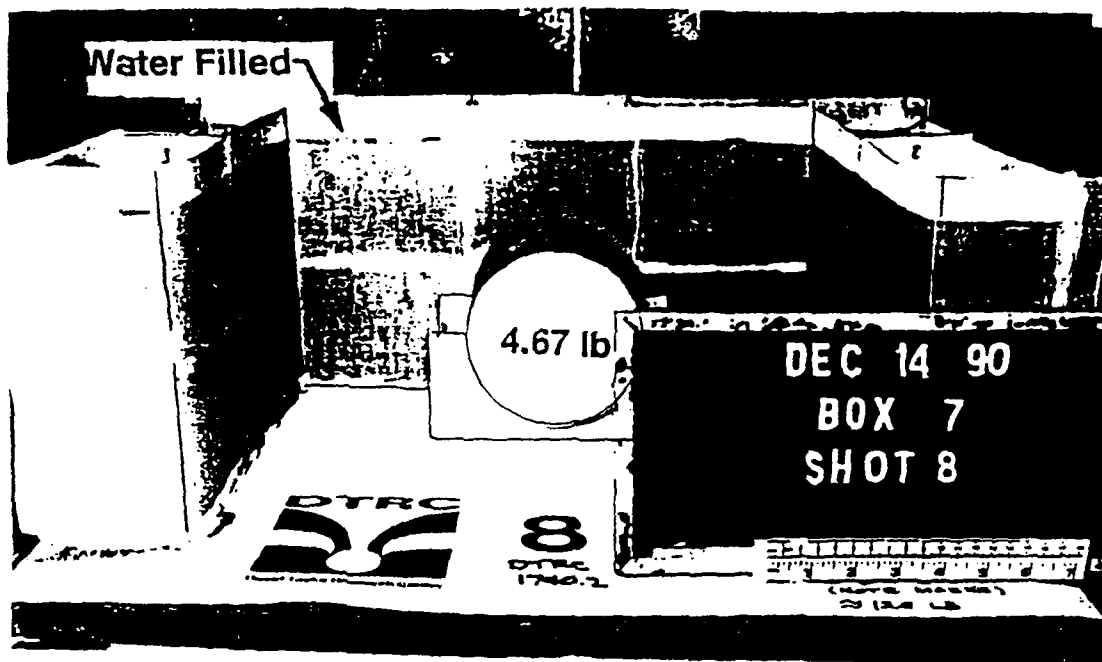


Figure 2a. Typical setup for NSWC tests showing water filled cell located on a table inside an unvented test chamber with test explosive located at geometric center of the 3-wall cell.

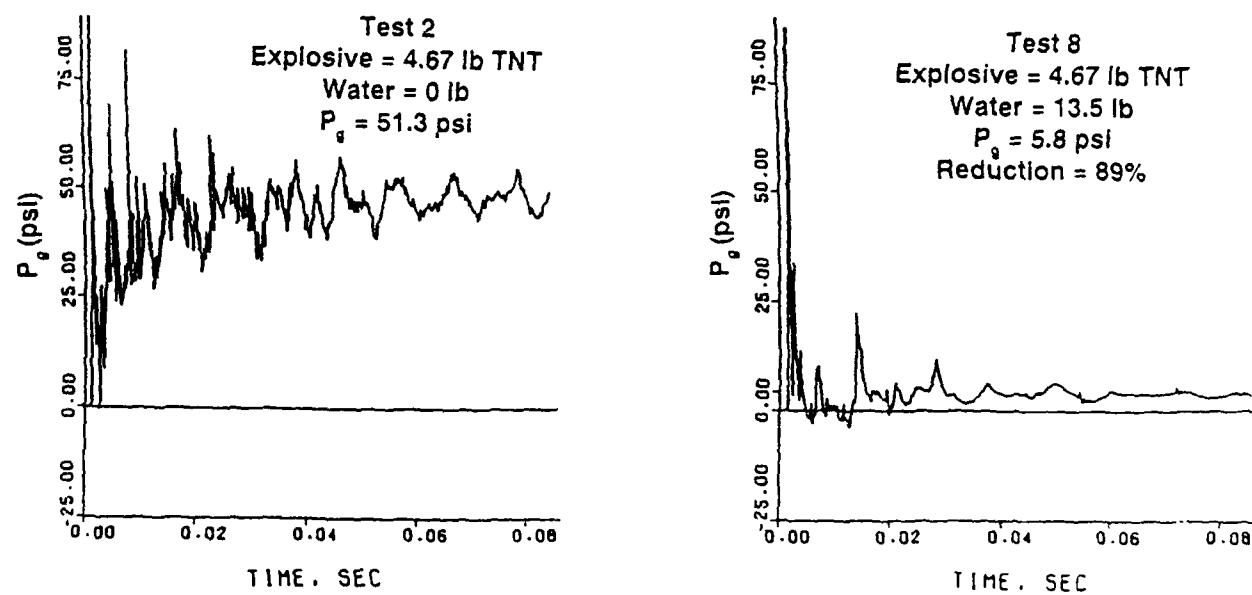


Figure 2b. Gas pressure versus time measured inside unvented test chamber from detonation of test explosive without water-filled walls (Test 2) and with water-filled walls (Test 8).

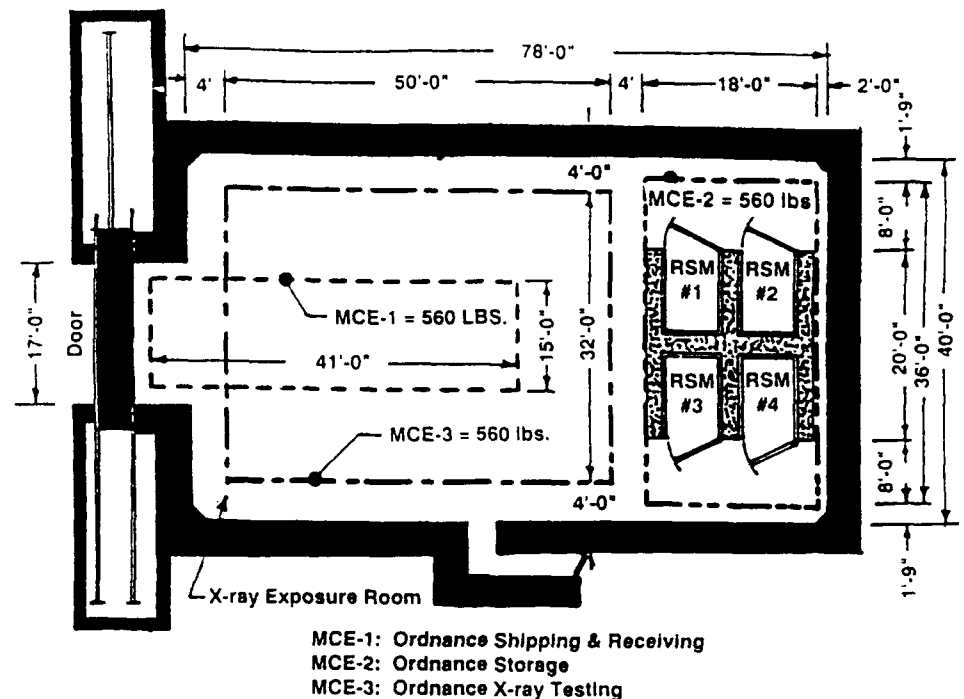


Figure 3a. Floor plan and MCE envelopes - Radiography Building 35, Pittsburgh, CA.

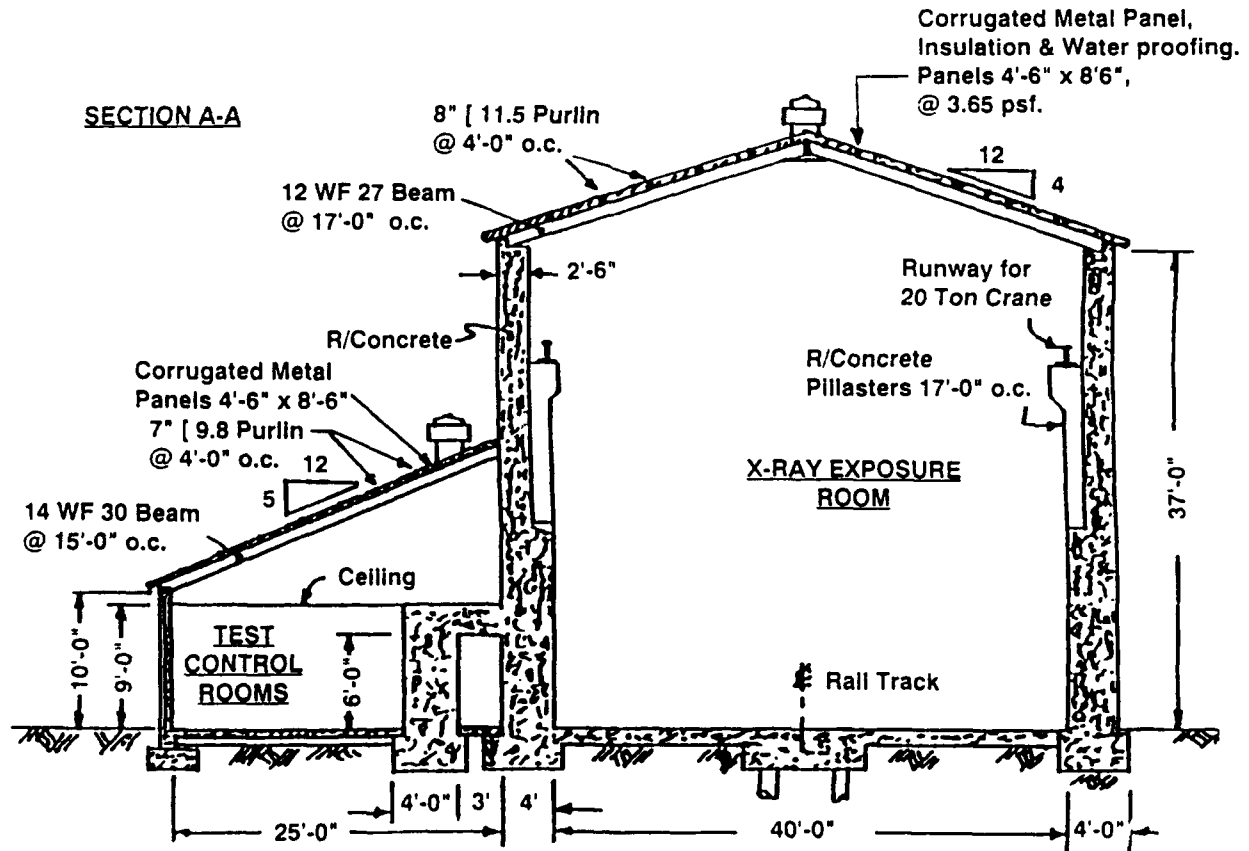
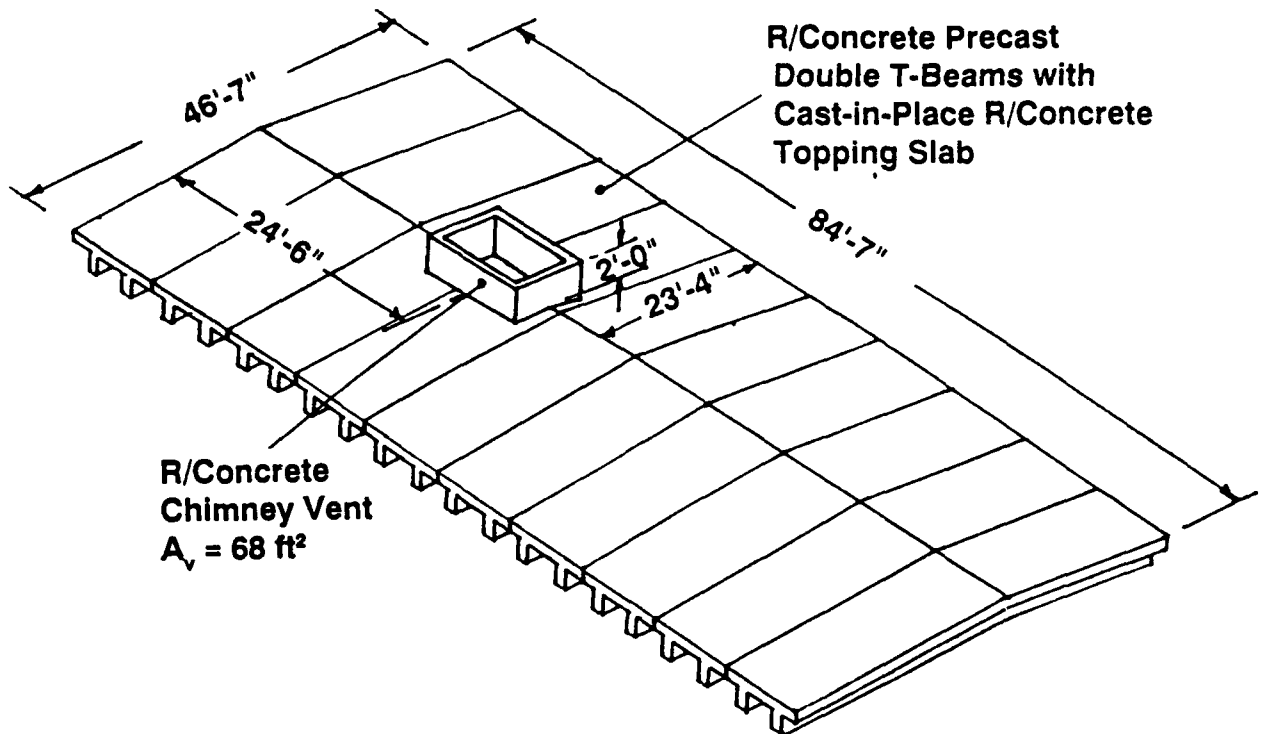
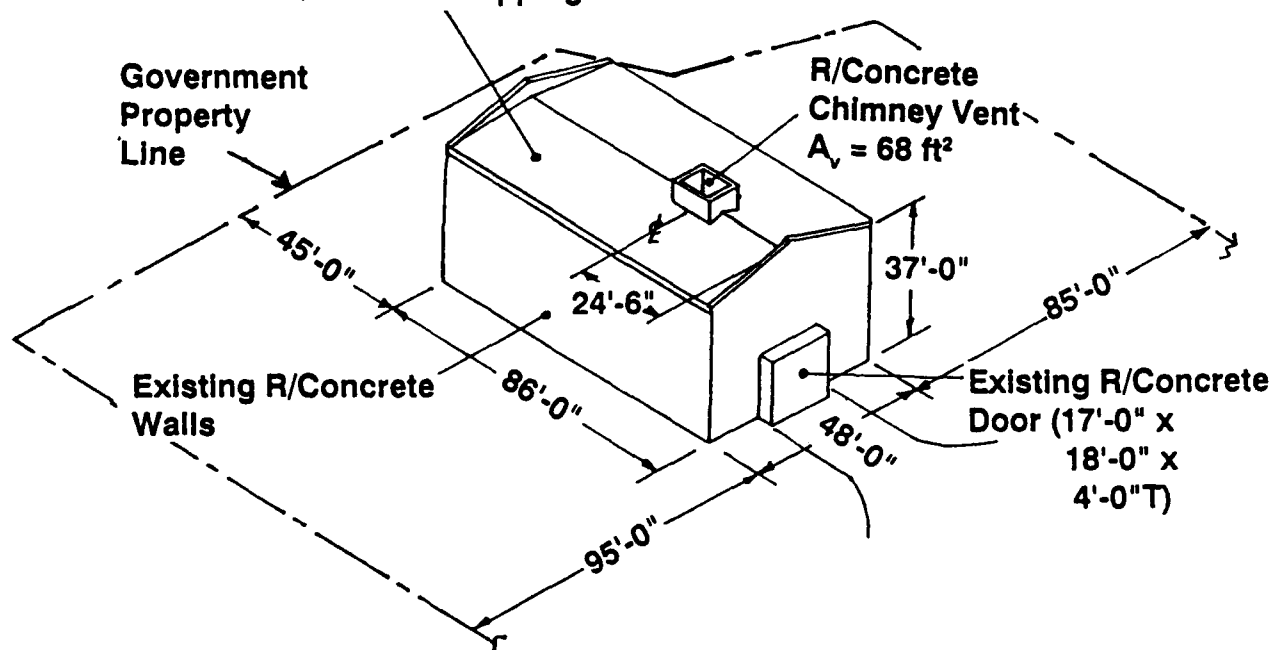


Figure 3b. Elevation view - Radiography Building 35, Pittsburgh, CA.



**Figure 4a.** Conceptual design of new roof and chimney for Building 35 - precast R/concrete T-beams with cast-in-place topping slab.

**Remove & Discard Existing Corrugated Metal Roof, Steel Purlins, & Steel Beams. Add PreCast R/Concrete Double T-Beams with Cast-In-Place R/Concrete Topping Slab.**



**Figure 4b.** Conceptual design of new roof and chimney vent to mitigate hazardous blast pressures, weapon fragments, and facility debris at government property line.

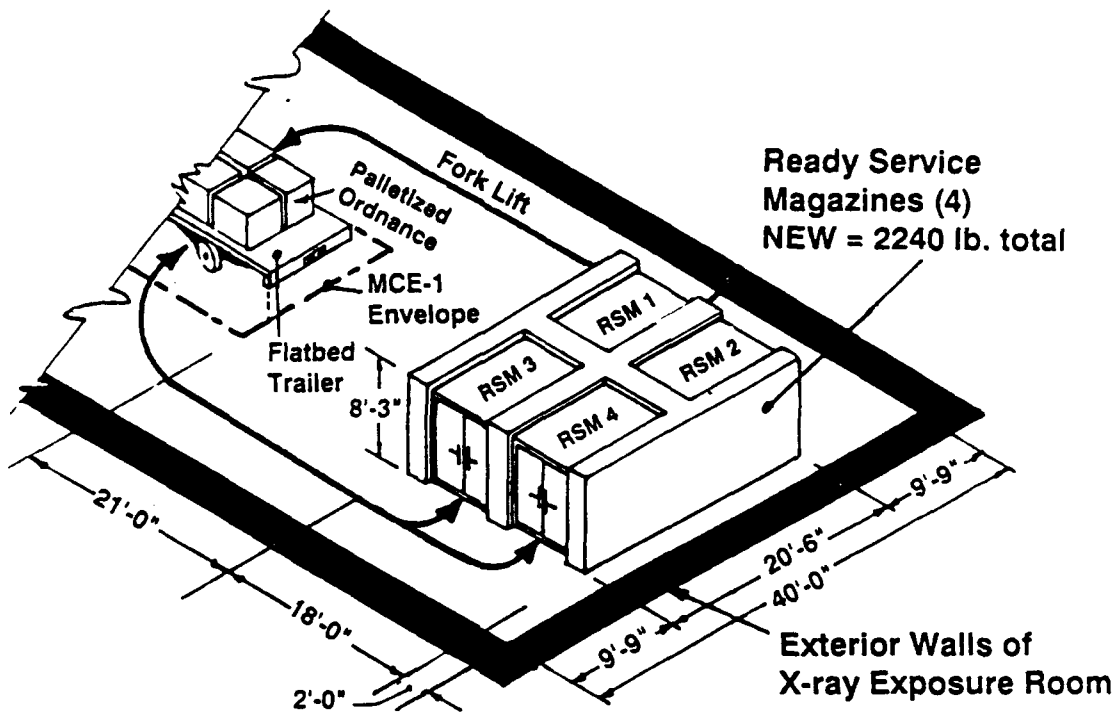


**Figure 4c.** Conceptual design and arrangement of four ready-service magazines to safely store 2,240 lb NEW and limit MCE to 560 lb NEW.

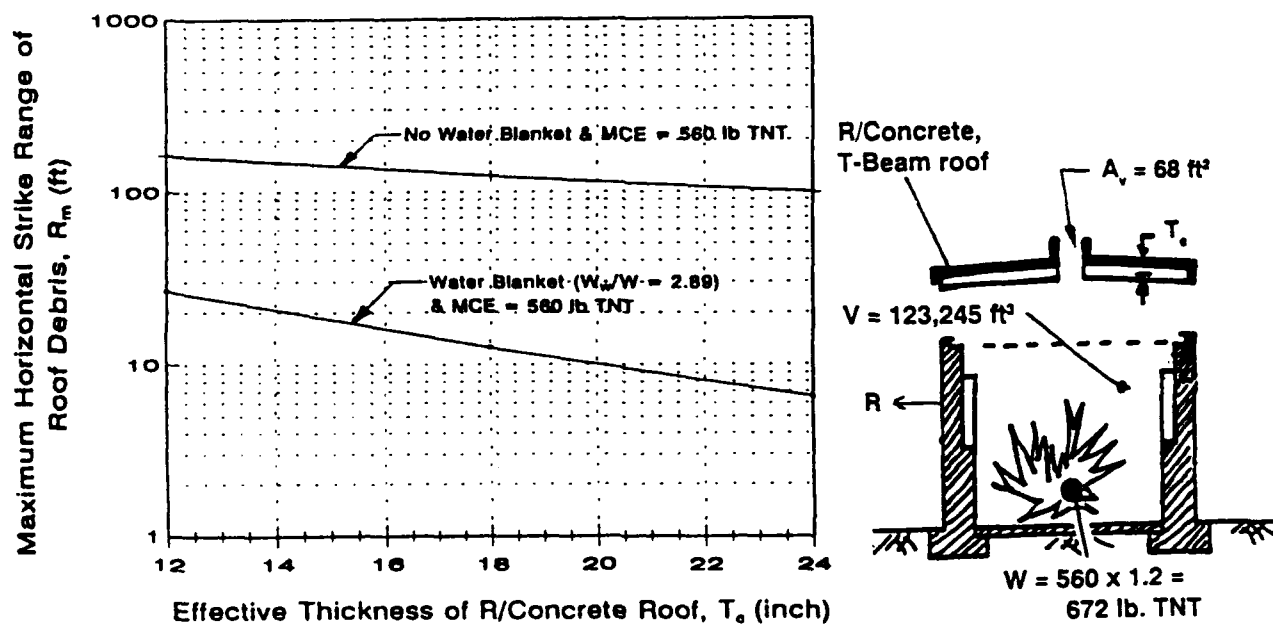


**Figure 4d.** Effect of water blanket on maximum strike range of R/concrete roof debris for MCE = 560 lb NEW.

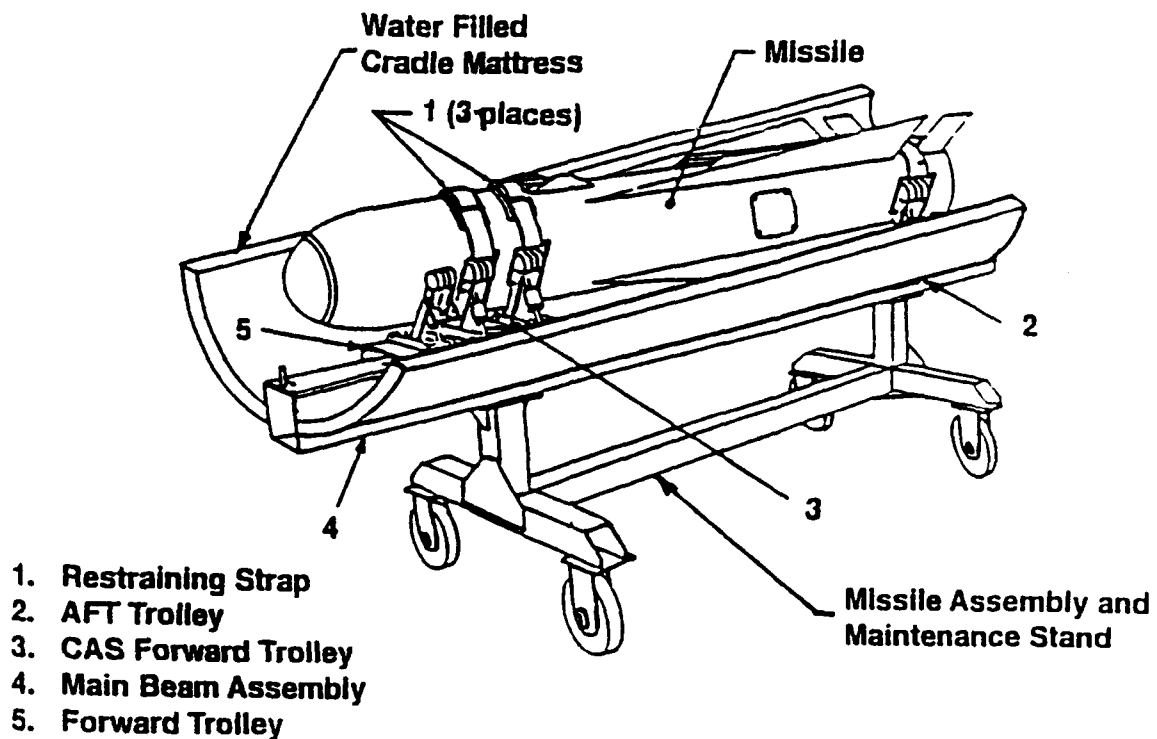


**Figure 5a.** Conceptual design of water mattress deployed on a Missile Assembly and Maintenance Stand.

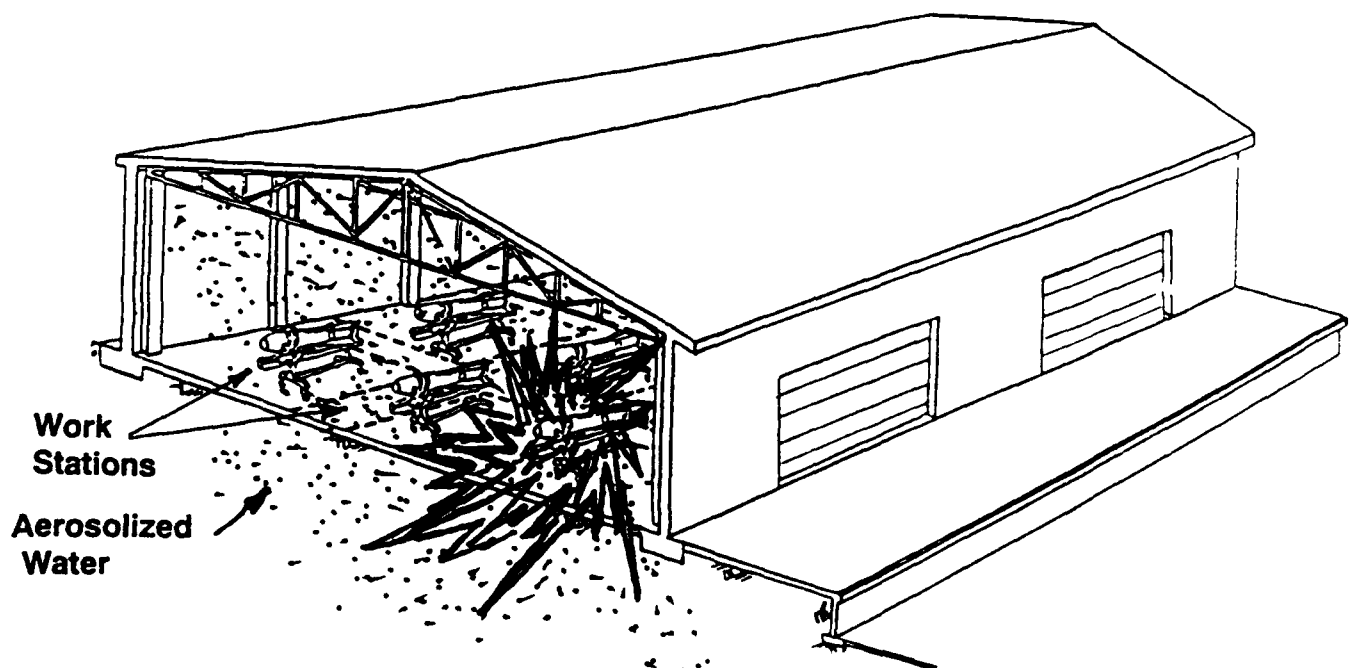


**Figure 5b.** Missile Maintenance Facility - missiles at their work stations with water deployed on Missile Assembly Stands when explosion occurs.

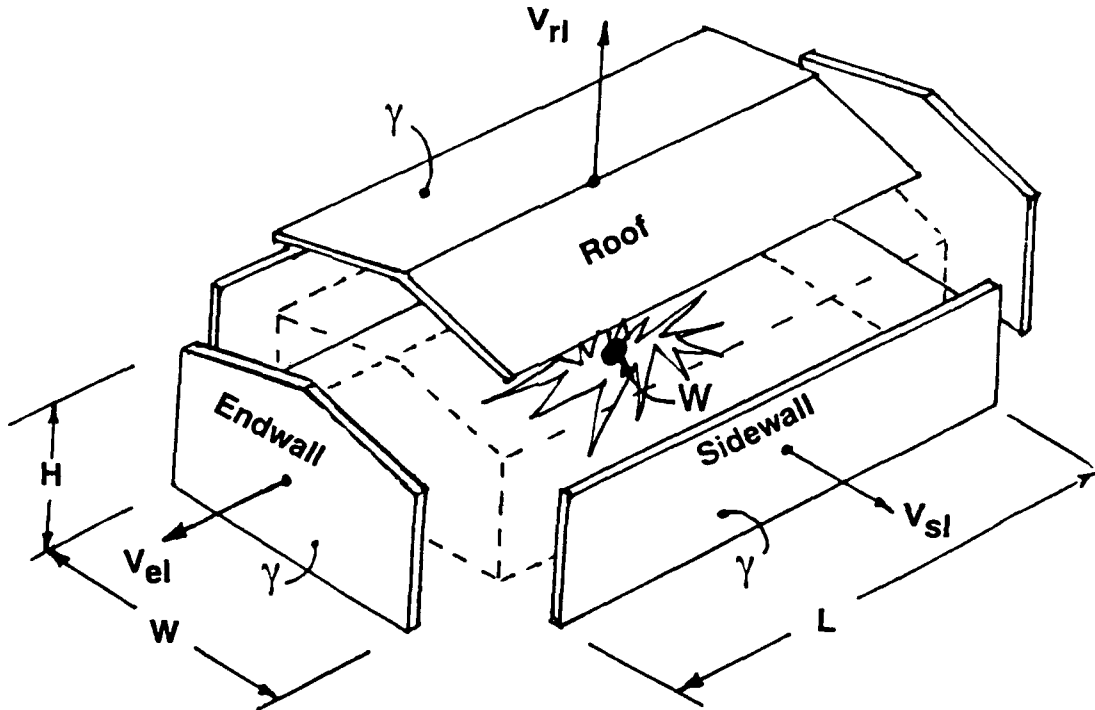


**Figure 6a.** Debris prediction model - assumed breakup pattern for a building.

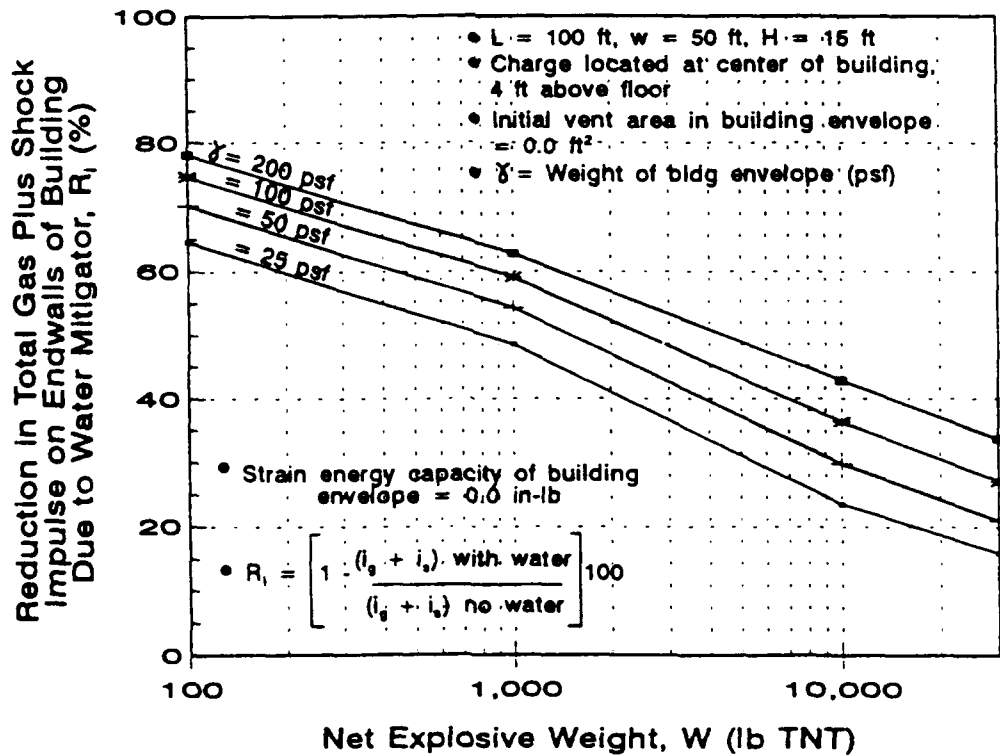


**Figure 6b.** Reduction in total gas plus shock impulse ( $i_g + i_s$ ) acting on endwalls of building from water mitigator, as a function of net explosive weight ( $W$ ) and weight of building envelope ( $\gamma$ ).

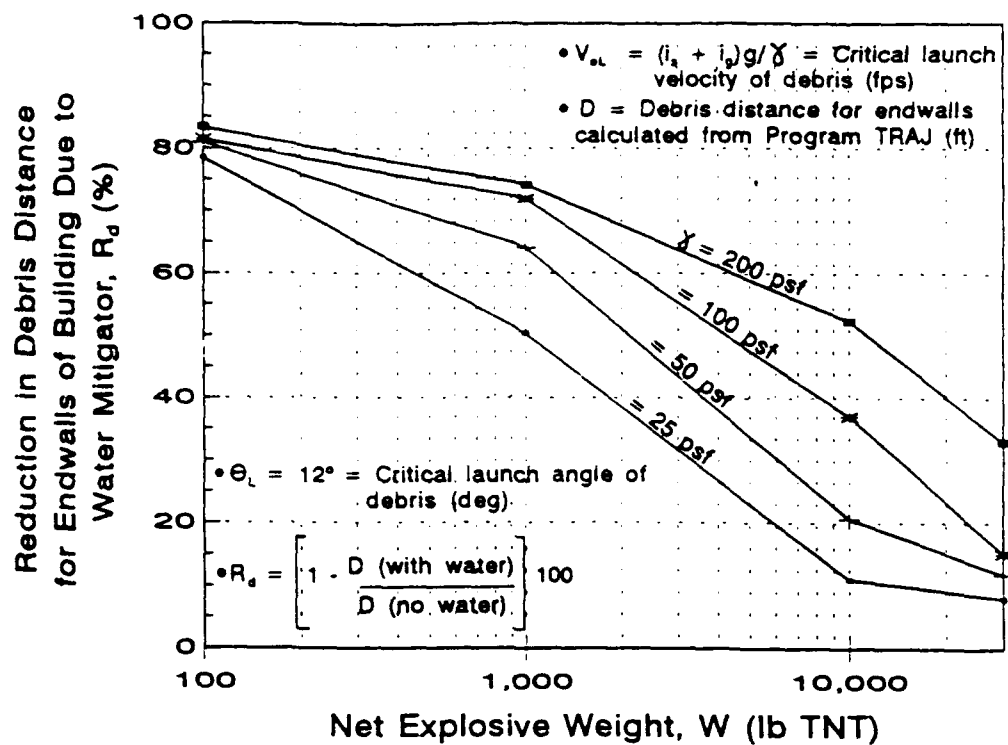


Figure 6c. Reduction in debris distance ( $R_d$ ) from water mitigator as a function of net explosive weight ( $W$ ) and weight of building envelope ( $\gamma$ ).

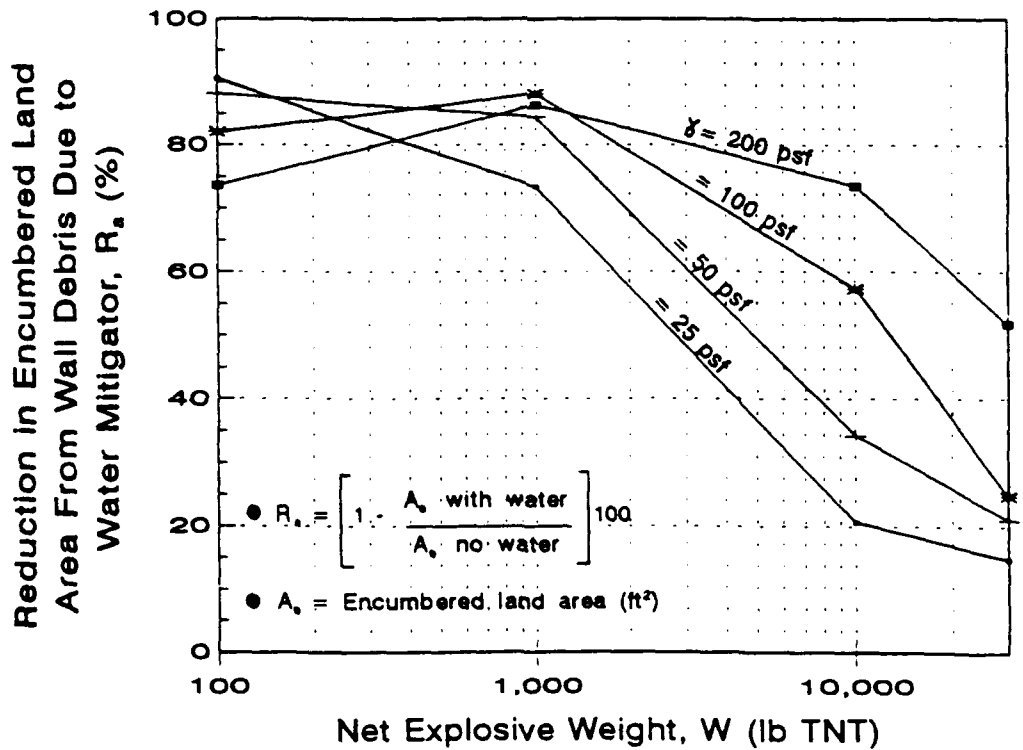
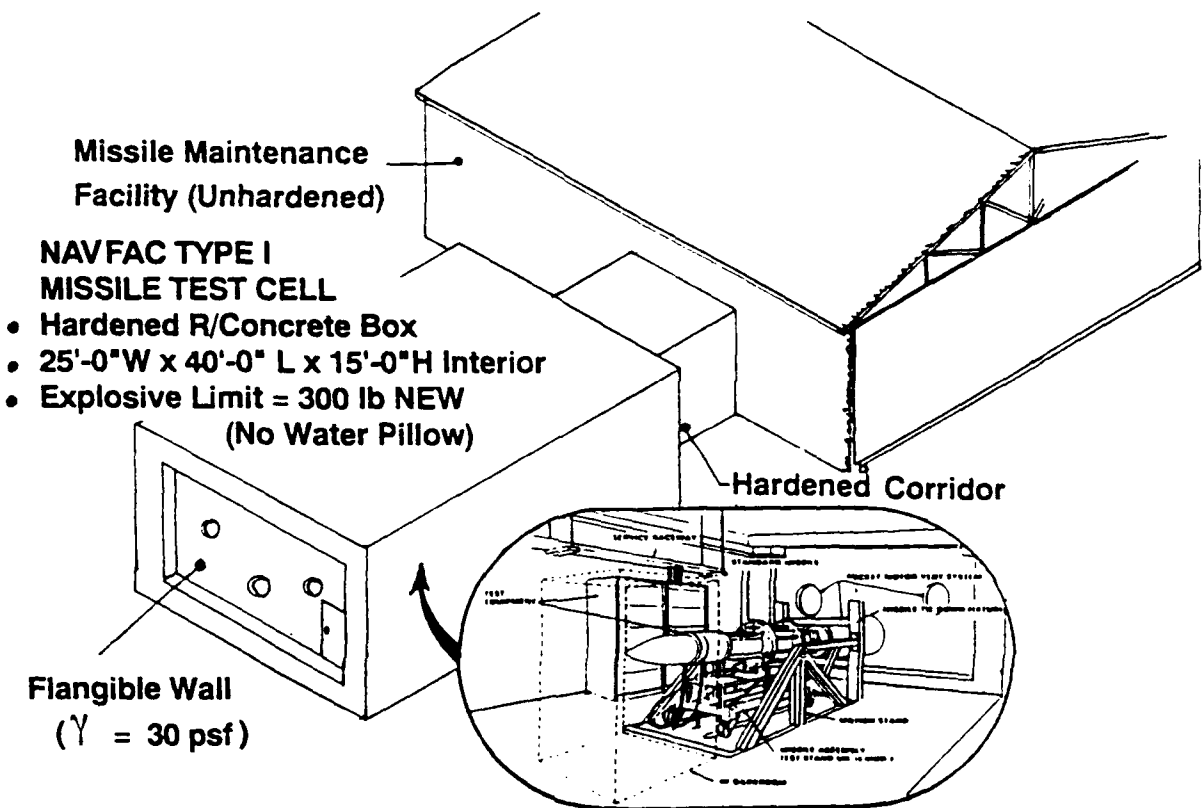
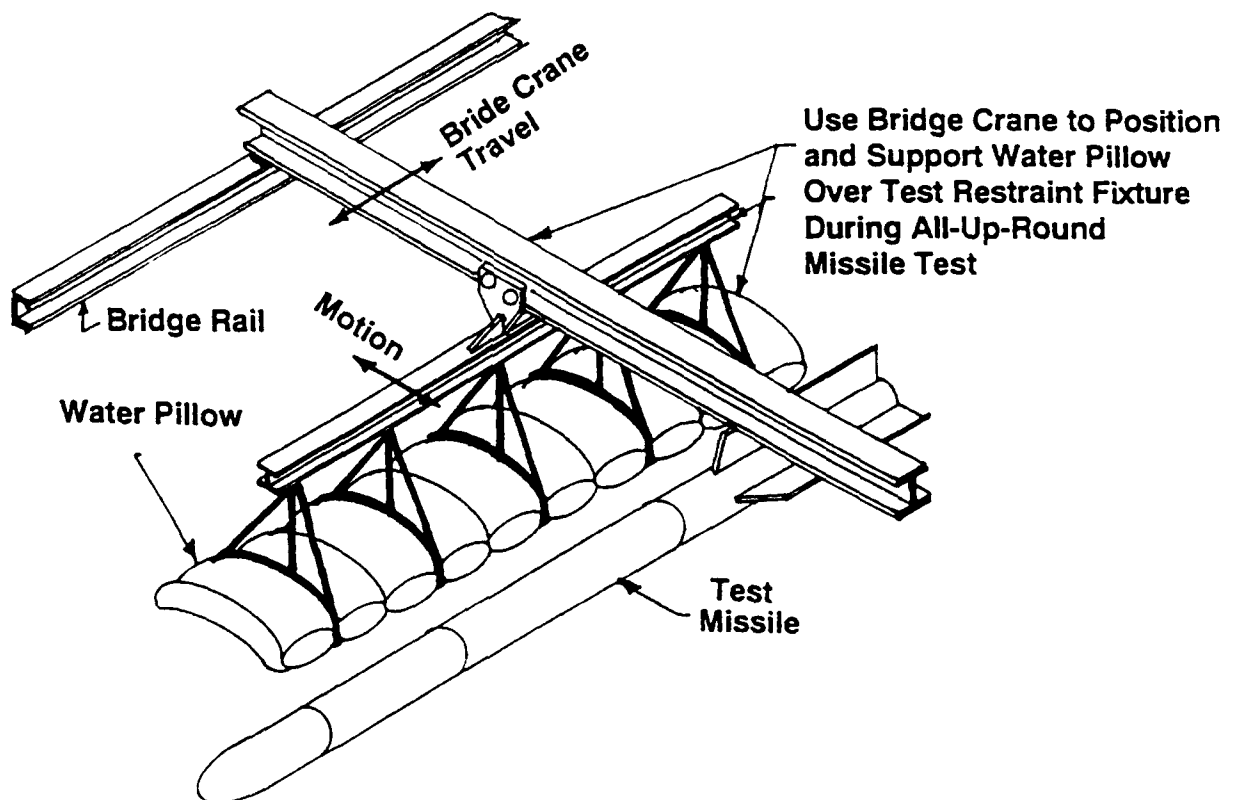


Figure 6d. Reduction in encumbered land area ( $R_a$ ) from water as a function of net explosive weight ( $W$ ) and weight of building envelope ( $\gamma$ ).



**Figure 7a.** NAVFAC Type I missile test cell adjacent to Missile Maintenance Facility for all-up-round testing of missiles.



**Figure 7b.** Conceptual design of water pillow deployed above all-up-round missile in missile test cell.

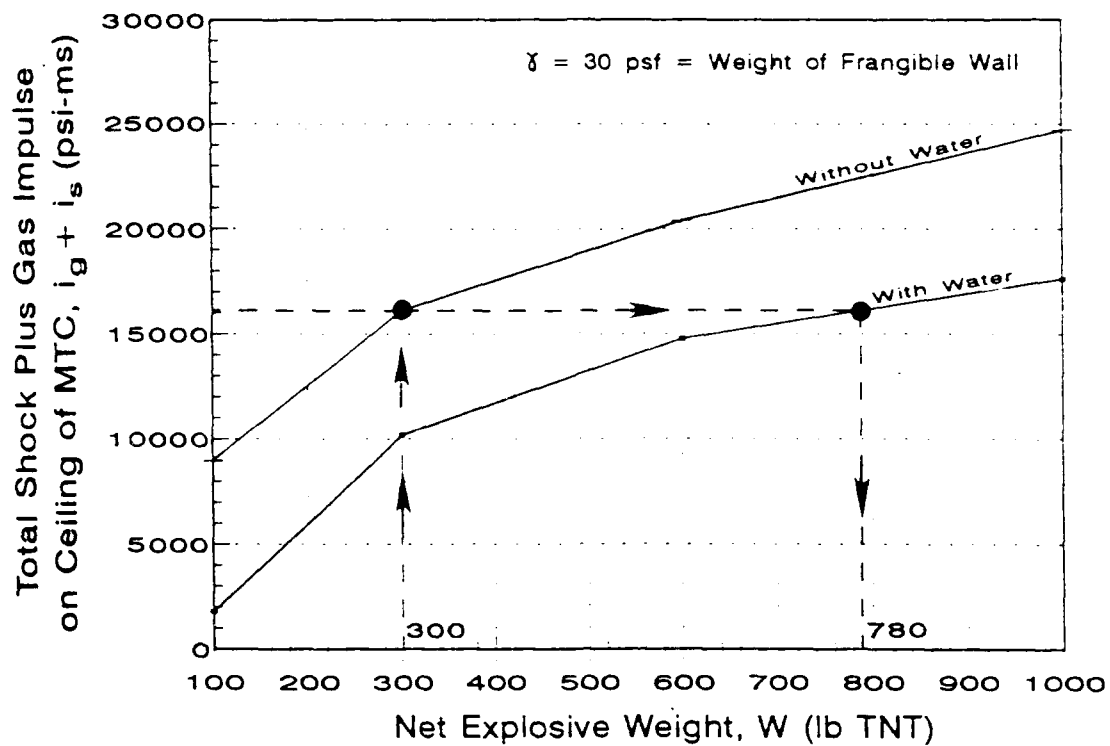


Figure 7c. Increase in explosive weight capacity of NAVFAC Type I missile test cell by deploying water pillow.

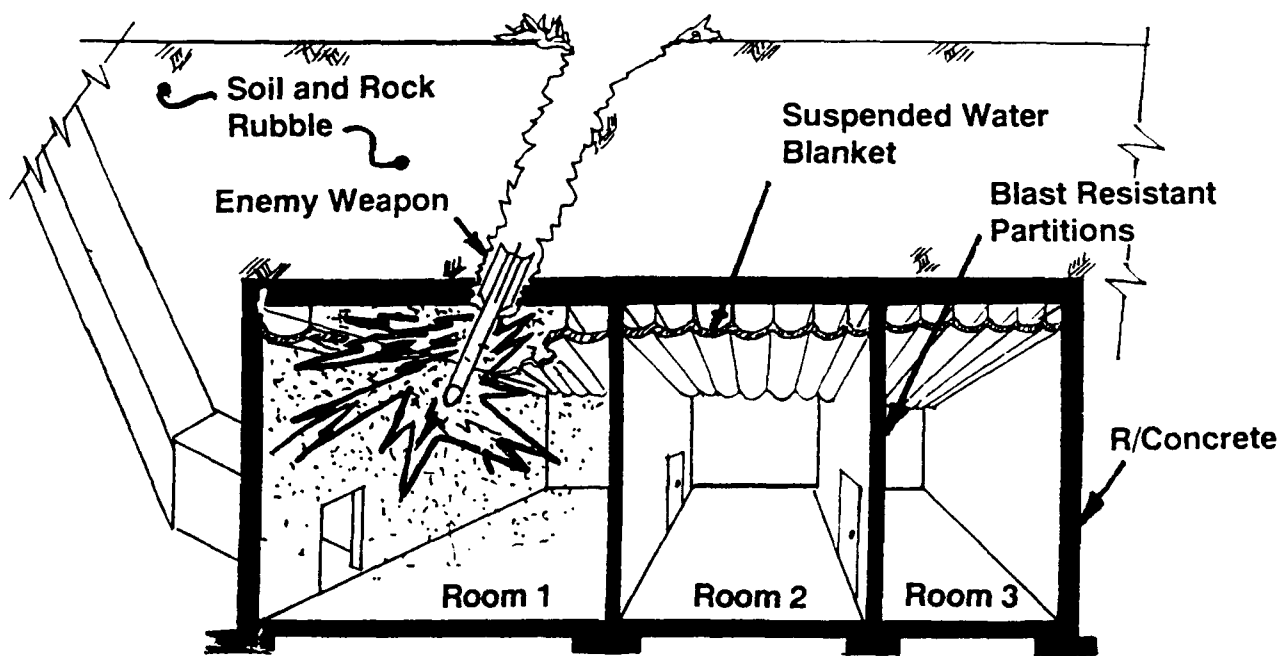
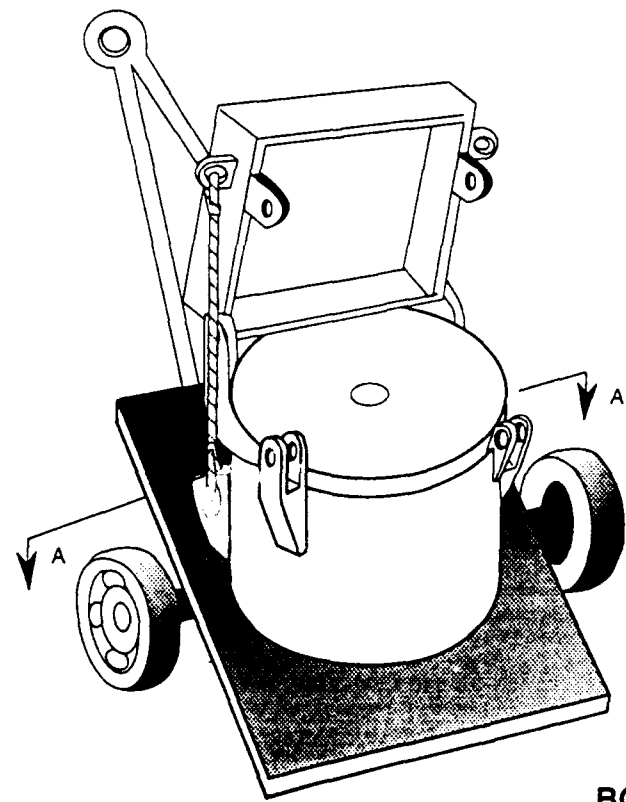
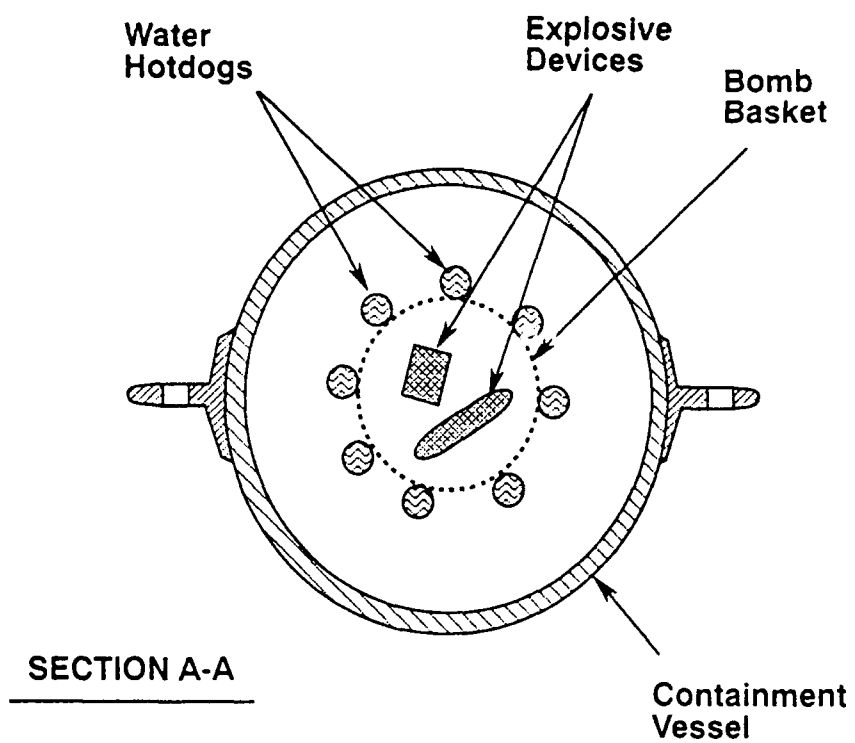


Figure 8. Navy Command & Control Center - water blanket suspended from ceiling to enhance survivability against penetrating weapons.



**Figure 9. Conceptual design of a bomb cart with water hotdogs suspended from outer rim of bomb basket.**

**Safety First: Environmental Compliance and Approvals  
for  
Large-Scale Explosive Safety Tests**

by  
**Carl C. Halsey**  
Head, Ordnance Evaluation Branch  
Naval Air Warfare Center Weapons Division  
China Lake, California

**William T. Eckhardt**  
Staff Archaeologist/Historic Preservation Officer  
Naval Air Weapons Station  
China Lake, California

and  
**Robin M. Hoffman**  
Project Coordinator  
Naval Air Warfare Center Weapons Division  
China Lake, California

The Maritime Pre-positioning Ships test performed at China Lake presents a number of valuable, real-world problems surrounding the planning and development of large-scale explosive tests. This paper examines the scope, level of effort, and complexities involved in achieving environmental compliance while meeting the sponsor's time frames, budgets, and objectives. Lessons learned in this recent example are presented with a view toward their utility for future safety testing.

### **Introduction**

Environmental compliance for large-scale explosive testing is, in many ways, an issue of *safety first*. In these times of rigorous regulatory oversight and growing agency accountability for consideration of environmental issues, much can be gained when test plans and objectives are subjected to a proactive approach to environmental compliance and approval.

The Maritime Pre-positioning Ships Explosive Safety Quantity Distance Test was performed 7 September 1990 at the Naval Air Weapons Station (NAWS), China Lake,

California. This controlled detonation test presents a number of valuable lessons surrounding environmental compliance and the planning and development of large-scale explosive tests. This paper examines the scope, level of effort, and complexities involved in achieving environmental compliance while meeting the sponsor's time frames, budgets, and objectives.

## Background

Currently, the U.S. Marine Corps operates a number of Maritime Pre-positioning ships (MPSs) in support of the Department of Defense Forward Deployment strategy. As part of the maintenance cycle for the equipment and ordnance located on board these vessels, the vessels are returned every two years to Blount Island on the St. Johns River at Jacksonville, Florida. Equipment is off-loaded, and ordnance is shipped elsewhere for inspection and refurbishing. The ordnance is then shipped back to Blount Island and reloaded aboard the ships. The explosive safety arc for this operation is based on a net explosive weight of 1,500,000 pounds—the projected maximum amount aboard any of the MPSs (Halsey et al. 1991:3).

In August 1990, the Marines were scheduled to begin operating under a new lease at a new location on Blount Island. At the "eleventh hour" in 1989, it was discovered that the explosive safety quantity distance arc for the new facility encompassed several privately owned dwellings across the river channel from Blount Island. With a certain air of immediacy, a study was performed and a test plan prepared to determine if prudent stowage methods existed that could reduce the explosive safety arc. Although this study indicated that stowage arrangements could be used to reduce the maximum credible event, historically these methods have been deemed unacceptable, and gaining approval from the Department of Defense Explosives Safety Board (DDESB) would require a large number of test replications for verification.

Further discussions with DDESB indicated a willingness to accept another approach, using predictions and a large-scale test to determine the "trinitrotoluene (TNT) equivalence" of the net explosive weight aboard the ship. The test would have to be large, approximately one-third of the total shipboard load, and would have to be configured to represent two levels of one hold of the ship. Moreover, the mix of the live and inert munitions used in the test would have to be based on the actual amounts and types of materials found on the ship. This, then, constituted the test plan that was

prepared to conduct an MPS Explosives Safety Quantity Distance test at NAWS China Lake.

## Scope

The scope of this MPS test plan was—in anyone's parlance—enormous. The undertaking called for a test site permitting a controlled detonation study to allow examination of explosive factors such as actual blast force, destructive extent, and distribution patterns of explosive munitions contained and stored under conditions that model those presently employed by MPS. For the purpose of this test, the load out for the MPS *PFC Dwayne T. Williams* was studied in detail and used as a guide for planning the program. Consisting of approximately one-third of the appropriate material located aboard the *Williams*, the test called for a total ordnance weight of 2,265,770 pounds with 523,790 pounds of net explosive weight.

Site plan development required construction of a dirt-bermed, multitiered, two-level detonation platform half-buried below present ground surface to simulate the confinement provided by water surrounding the ship. This arrangement simulated two levels within one hold of the ship, with the lower level (Level 1) resting below the water line. Level 2 represented a level just above the water line.

When the blast force and distribution patterns of the explosive munitions were factored in, the MPS Explosives Safety Quantity Distance Test required an area of roughly 1.8 square miles. From a center point represented by the location of the detonation platform, instrumentation was extended along three vectors for distances of 4,000 feet. This distance represented the computed maximum extent of the debris field projected for this controlled detonation study.

## Environmental Issues

Environmental awareness and compliance with applicable environmental laws and regulations are central to all project planning at NAWS China Lake. The MPS Explosives Safety Quantity Distance Test was no exception. For this test plan to go forward on time and on schedule, it was necessary to initiate an environmental review process (almost) from the moment NAWS China Lake was selected as the location for the test. NAWS China Lake possesses an Environmental Project Office staffed for

precisely this sort of endeavor; its specialists are "mission oriented" and acutely aware of what is necessary to satisfy environmental compliance requirements.

The Environmental Project Office at NAWS China Lake is involved in every facet of environmental compliance, working closely with federal, state, county, and local agencies. These agencies include the U.S. Environmental Protection Agency, Advisory Council on Historic Preservation, and Fish and Wildlife Agency, as well as the California State Historic Preservation Office, Department of Fish and Game, Air Resources Board, and Department of Health Services. Without this expertise onboard at China Lake, accomplishment of the MPS test plan might never have been realized on time.

Nonetheless, safety remained an overriding consideration among the selection factors used in siting the MPS test plan. The most obvious factors included concerns for the safety of personnel and existing range facilities. Less obvious—but no less necessary—were concerns for the safety of wildlife, historic properties, and other land-based resources present at NAWS China Lake. The potential for harm to these resources as a result of the proposed controlled detonation test led directly to the requirements for careful selection in siting the test plan and performance of environmental assessments for each candidate site location.

Over several months (April through June 1990), selecting the actual test site was a seemingly unending process. Five possible locations were selected. Each was evaluated for safety and compatibility with existing range operations and then subjected to preliminary environmental assessment. This process proved to be an excruciatingly time-consuming and labor-intensive exercise, but, in the end, the most suitable location was identified for siting the MPS test plan. By 30 June 1990, the MPS test site was fixed at Airport Dry Lake, a long-established impact range on the Northern Test Complex at NAWS China Lake.

The Airport Dry Lake Impact Range has a 45-year history of use as an aerial target range. Despite Airport Dry Lake's land-use history and general condition, environmental compliance and approval would require ancillary study of natural and cultural resource concerns and the development of a Preliminary Environmental Assessment.

Considering the Sponsor's original time frame (August 1990), precious little time remained to complete the environmental documentation and conduct the MPS test plan on schedule.

## **Environmental Compliance**

Following selection of the actual test range location for the MPS test plan, what remained was to conduct the necessary environmental studies to support the development of formal documentation (e.g., Preliminary Environmental Assessment) and, through consultation with appropriate regulatory agencies, seek authority and approval to proceed with the MPS test.

Translating the scope and description of this large-scale explosive safety test into the language of environmental compliance was one of the easier tasks associated with obtaining the compliance and approval documentation necessary for the proposed test. For instance, the scope of the project needed simply to be restated in a land-based perspective; the proposed test plan was translated into a nontechnical project description and the test site requirements described in terms of affected acreage. Borrowing from one of the ancillary reports supporting the environmental documentation for this test (Eckhardt and McDonald 1990), such translation reads like this:

This undertaking provides a test site for a controlled detonation study in support of the U.S. Marine Corps Maritime Pre-positioning Ships program. The test will examine actual blast force, destructive extent and distribution patterns associated with a controlled detonation of some 500,000 pounds of explosive material....(T)he Area of Potential Effect (APE) must allow for a radius of some 4,000 feet (1,153.9 acres total area). Within this region, the proposed undertaking consists of the development of an explosive detonation platform (ground zero) that will be excavated to a depth of up to 15 feet, and measure roughly 110 by 170 feet in size. Surrounding ground zero is an operations area measuring some 1200 feet in diameter (25.96 acres, inclusive), and three gauge lines bordered by debris lines radiating from ground zero for distances of roughly 3500 feet each (36.88 acres).

Literature searches, reviews of cultural resource site records, and reviews of existing records and habitat maps covering the region of the Airport Dry Lake Impact Range commenced immediately following this (hopefully) final site selection for the MPS test plan. These processes—and the actual field review and ground surveys of the proposed project—are the grist for development of environmental documentation when the primary issues remaining are those concerned with land-based resource concerns.

Field review of Airport Dry Lake Impact Range and ground surveys for natural resource concerns were initiated on Tuesday, 3 July 1990. Typically this level of field

effort focuses on inventorying all manner of biological information for a given area: plant communities and their composition; precise characterization of habitat zones; and the nature, relative number, and composition of animal life present within the proposed project area. In this case, requirements focused on confirming the nature of previous disruption to the natural environment and making doubly sure that no native species (floral or faunal) of extraordinary value resided within the project's sphere of influence.

Owing to their known distribution and the presence of marginally suitable habitat in the region, the possible presence of two species—Mojave Ground Squirrel and Desert Tortoise—were the primary natural resource concerns for Airport Dry Lake Impact Range. These two species are recognized on state and federal threatened and endangered species lists (respectively), and their presence in the project area, if confirmed, would require lengthy consultation with state and federal regulatory agencies before approval and authority to proceed with the MPS test plan could be obtained.

Within two days sufficient analysis and groundwork had been conducted to ensure that implementing the test plan in this region would have no adverse impact to sensitive natural resources, and the absence of threatened and endangered species within the project area precluded any potential for inadvertent "taking" of a listed species.

Cultural resource assessment for the MPS test plan at Airport Dry Lake Impact Range was initiated on Monday, 2 July 1990. The National Register of Historic Places was consulted, and no listed or nominated sites were identified within the project's sphere of influence. Archaeological site records and an index of cultural resource surveys maintained by the Resources Management Branch for NAWS China Lake were consulted, resulting in a determination that a portion of the project area had been previously examined, but that no cultural resources were encountered. One previously recorded site (CA-Iny-2532), located just outside a one-mile radius from the project area, was noted in the archaeological records search. Records described this as a small petroglyph (rock art) site recorded in 1966. The potential for discovery of significant cultural resources within the project area was considered to be low, judging by the general terrain, the large areas of disturbed surface, and the results of the previous survey.

Vertebrate fossil remains had been excavated in the 1930s and 1970s from locations near Airport Dry Lake, including Pleistocene Lake China (Davis et al. 1978), the western

escarpment of the Coso Range (Schultz 1937; Van Huene 1971), and directly south of Airport Lake in the White Hills (Van Huene 1971; Fortsch 1972). There remained a high probability of uncovering fossil remains during construction of the dirt-bermed pit in which the explosives would be detonated, although the placement of the detonation platform away from the Airport Lake shoreline and the badlands area of the White Hills lowered that probability somewhat.

Cultural resource surveys were initiated on 9 July 1992. A two-person team intensively surveyed the proposed MPS test plan project area. Field methods consisted of walking transects at 30-meter intervals (northwest/southeast) across the entire project area. No vertebrate fossil remains and no prehistoric or historic archaeological sites were located during this surface inventory effort. The inventory resulted only in the discovery of two isolated finds: a single obsidian flake in a braided streambed channel bottom, and two bifacial thinning flakes of obsidian in a zone of previously debrushed alluvium. All three obsidian flakes were extremely weathered and exhibited edgeware indicative of tumbling and alluvial transport.

In addition to the survey of the proposed project area, the cultural resource inventory included a detailed examination of site CA-Iny-2532, the previously recorded rock art site located to the west and outside the project area. This examination revealed that the site was much larger than originally recorded, possessing numerous other cultural elements in addition to the petroglyphs; however, it was found to be contained entirely outside of the proposed project area. Certainly these new findings would warrant more thorough examination and re-recordation of site CA-Iny-2532 in preparation for a reconsideration of the site's National Register eligibility sometime in the foreseeable future.

The results of the cultural resource inventory were assessed, and the surface of the proposed project area had earned a clean bill of health: no significant cultural resources and no vertebrate fossil remains had been discovered. However, some concern remained over potential buried deposits of either vertebrate fossil remains or prehistoric (e.g., Pleistocene) human occupations that might be uncovered during construction of the detonation platform. And, of course, the reconsideration of site CA-Iny-2532 warranted continued concern for the safety and welfare of this resource.

By close of business on Wednesday, 11 July 1990, the literature reviews and field inventories were completed. A process that might typically take a month or more had been completed in under twelve calendar days, and all efforts were now focused on

completing the documentation and agency consultations necessary to achieve authority and approval to proceed with the MPS test plan.

Within an additional 12 calendar days, environmental documentation and agency consultations were completed. For natural resources, the baseline information, results of the field survey, and documentation of the entire process brought closure to any continuing concerns for the protection of sensitive natural resources. Cultural resources presented a slightly more complex process. Because of the continuing concerns for potential buried deposits and the nearby rock art site, China Lake entered into consultations with the State Historic Preservation Office (SHPO) with recommendations that both during construction of the test platform and after the MPS test plan event, test activities be monitored daily to ensure that no significant cultural resources would be damaged. Working on a "fast track" with SHPO staff, correspondence was forwarded to the SHPO on Thursday, 12 July 1990, and review comments (and authority to proceed) were received back at China Lake the following Monday. The completed environmental documentation, a Preliminary Environmental Assessment, was issued on 24 July 1990. The MPS Explosives Quantity Safety Distance test proceeded on time and on schedule.

## **Lessons Learned**

In truth, one really shouldn't try to conduct a test of this magnitude in this fashion without the dedicated expertise and labor support that was available at NAWS China Lake. Far too much reliance—in terms of resources, finances, and coordinated effort—was placed on China Lake's ability to accomplish the tasks and goals necessary to accommodate the MPS test plan. This particular gamble paid off, but such a gamble can't always be counted on to do so.

No. What is needed in instances such as this is extremely far-sighted preparation and long-lead development of range resources for exactly this sort of test endeavor.

A reorienting of our priorities warrants serious consideration. Typically, once a test plan is conceived and programmed, the priorities are set on funding, procurement, development, and implementation. Where is the concern for environmental compliance? Well, if it's considered at all, it's nominally considered somewhere between development and implementation. In today's milieu, this is entirely unsatisfactory. Even elevating environmental compliance to a second-tier priority, as in the case of this MPS test plan, proved to be too little and—almost—too late. Better to

"take the bull by the horns" and bring environmental compliance right to the top along with conceptual development and programming. In this way, our endeavors in large-scale explosives safety testing can be assured a successful and brilliant future even in times of rigorous regulatory oversight and growing agency accountability.

### References Cited

- Davis, E. L., D. E. Fortsch, P. J. Mehringer Jr., C. Panlaqui, and G. I. Smith. 1978. *The Ancient Californians: Rancho LaBrea Hunters of the Mojave Lakes Country*. Natural History Museum of Los Angeles County, Science Series 29, Los Angeles, Calif.
- Eckhardt, W. T. and A. M. McDonald. 1990. *Cultural Resource Inventory and Evaluation of Shipboard Container Test Site, Naval Weapons Center, China Lake*. Resources Management Branch (Code 2662), Naval Weapons Center, China Lake, Calif..
- Fortsch, D. E. 1972. *A Late Pleistocene Vertebrate Fauna from the Northern Mojave Desert of California*. MS thesis, University of Southern California.
- Halsey, C. C., S. L. Berry, M. J. Windsor, and P. E. Greene. 1991. *Maritime Pre-Positioning Ships Explosives Safety Quantity Distance Test Data Report*. NWC Technical Publication 7172. Naval Weapons Center, China Lake, Calif.
- Schultz, J. R. 1937. "A Late Cenozoic Vertebrate Fauna from the Coso Mountains, Inyo County, California." *Contributions to Paleontology*, Illinois.
- Van Huene, R. 1971. *Fossil Mammals of the Indian Wells Valley Region and How to Collect Them*. Maturango Museum Publication 5, Ridgecrest, Calif.

## **ESQD ARCS FOR MARITIME PREPOSITIONING SHIPS**

by

Michael M. Swisdak, Jr.

### **ABSTRACT**

The United States Marine Corps operates 13 Maritime Prepositioning Ships (MPS). Each of these ships can contain up to 1.3 million pounds (Net Explosive Weight (NEW)) of all types of Marine Corps munitions. These ships are periodically returned to Blount Island in the St. Johns River, Jacksonville, Florida, for refurbishment of their equipment. At an NEW of 1.3 million pounds, the standard value of the inhabited building distance encroaches upon several private dwellings.

In order to address this problem, the U.S. Navy has conducted a large scale test (NEW of over 500,000 pounds) and series of analyses to determine a more realistic estimate of the inhabited building distance. This report presents the background and history of the the problem, describes the set-up and conduct of the event, and summarize the data collected and its interpretation. One outcome of this program was the reduction of both the inhabited building distance and the public traffic route distances by approximately 18%. These ranges were driven by airblast and not by fragmentation.

### **INTRODUCTION**

The United States Marine Corps (USMC) currently operates thirteen (13) maritime pre-positioning ships (MPS). The concept of these ships is that each squadron contains all the stores, ammunition, and equipment needed by a Marine Expeditionary Brigade for 30 days of combat operations. Because of the ammunition carried aboard these ships, an explosive safety quantity-distance (ESQD) arcs must be in place whenever these ships come into port.

The thirteen ships are drawn from three separate ship classes; however, the Net Explosive Weight (NEW) associated with each ship is quite similar, ranging from 1.0 to 1.3 million pounds. All three classes of ships are breakbulk, container ships (note: The containers utilized are International Standards Organization (ISO) vans). In the Maersk class, the energetic materials are stored in Holds 2, 3, and 4. Hold 4 is separated from Hold 3 by approximately 50 feet of general cargo. In the Waterman class, the energetic material is stored in Holds 1, 2, and 3, while in the Amsea class it is stored in Holds 1 and 2.

All of the energetic material is stored in either standard ISO containers whose external dimensions are 19.875' L x 8.0' W x 8.0' H or half-height containers whose external dimensions are 19.875' L x 8.0' W x 4.17' H. The standard ISO container has walls and roof whose minimum thickness is 4 mm of mild steel. The half-height container has walls of 4 mm steel, but a canvas top.

Every two years, under normal conditions, these ships are returned to Blount Island (in the St. Johns River at Jacksonville, Florida) as part of the maintenance cycle for the ordnance and equipment located on board. Here the equipment is off-loaded and the ordnance is shipped by rail to the Naval Weapons Station, Charleston, South Carolina, for inspection and refurbishing (as needed). The material is then shipped back to Blount Island and reloaded aboard the ships. The current explosive safety arc for this operation is based on a NEW of 1,300,000 pounds--the projected maximum amount aboard any of the MPS ships.

### STATEMENT OF THE PROBLEM

The applicable ESQD arcs are defined in Navy publication OP-5, Volume 1.<sup>1</sup> The arcs for two conditions are of interest--Inhabited Building Distance (IBD) and Public Traffic Route (PTR). Table 1 gives the standard values for three NEW's. After examination of maps of the area, it was determined that the problem area was the IBD for the 1,300,000 pound NEW--an ESQD range of 5,460 feet. A hazard arc of this size would encroach on several private dwellings located across the St. Johns River.

### POTENTIAL SOLUTIONS

Five potential solutions to the encroachment problem at Blount Island were discussed. These were: (1) Purchase the civilian properties involved, (2) Apply to the Chief of Naval Operations for a waiver of the rules, (3) Reduce the NEW aboard each ship, (4) Reduce the Maximum Credible Event (MCE) for an accident aboard ship, and (5) Conduct one (or more) large scale tests to measure the TNT equivalence of the ship and make a direct estimate of the ESQD ranges. Each of these will be discussed in more detail in the following sections.

Purchase Land Involved. This option was felt to be too expensive and could set an unwanted precedent.

Apply for Waiver. It was felt that if this option were pursued, then the owners of the encroached land could bring a law suit for reduction of their property values. Further, a temporary restraining order causing the cessation of all explosive operations at Blount Island would probably be issued until the case could be adjudicated.

Reduce NEW. This option was deemed operationally unacceptable. However, based upon lessons learned from the war in Southwest Asia, ammunition requirements have been reconfigured. The required 30-day fighting capability still exists as advertised, but at an NEW of 1.3 million pounds..

Reduce MCE. Less sensitive ordnance/ammunition items already carried aboard the ships would be used as buffer materials between stacks of more sensitive items. This effort has been pursued/implemented by the USMC and will be discussed below. However, because of the number of tests and analyses that would be required by the Department of Defense Explosives Safety Board (DDESB) to prove an MCE reduction, formal recognition of its use was not pursued.

Conduct Large Scale Test(s). After discussions with the DDESB Secretariat, a single large-scale test was devised--a test involving at least 500,000 pounds NEW of ordnance. The results of this test form the basis for the proposed and accepted reductions of the ESQD arcs for the thirteen MPS ships.

#### **MAXIMUM CREDIBLE EVENT REDUCTION**

There are ongoing programs in both the Army and the Air Force on the use of less sensitive energetic items as buffers or shields between stacks or containers of munitions. Two of these programs are called "Quickload" in the Army and "Buffered Storage" in the Air Force.

Quickload. The one aspect of the Quickload program which is of use here is the concept of using propellant charges as shielding material. The Army has conducted extensive tests using 5-inch and 8-inch propellant charges between stacks of 5 and 8 inch projectiles filled with Composition B, TNT, and with sub-munitions. They have had success with the TNT-loaded and the 5" Composition B loaded projectiles. However, even with 19 rows of propellant charges intervening, the 8-inch Composition B rounds and the ICM (Improved Conventional Munition) rounds still sympathetically detonate.

It should be noted that these results were obtained from tests which were conducted with, essentially, no confinement--i.e., either in the open or the minimum confinement provided by the individual stacks of munitions.

Buffered Storage. The Air Force Buffered Storage concept utilizes less sensitive (or inert) items as buffer material between stacks of MK 80 series bombs. Through a combination of separation distance and buffer density, the concept has been demonstrated by preventing sympathetic detonation between 60,000 pound stacks of tritonal-loaded bombs. From the standpoint of application to this problem, one of the most interesting aspects of the Air Force tests is the successful use of cluster bombs (both MK 20 and MK 58) as buffer material. In operational use, however, the Air Force has decided not to use any Class 1.1 material as a buffer. This does not mean that it doesn't work--merely that they have the option of having other suitable materials available to use as buffers. Also, the concept of using Class 1 ammunition between stacks of Class 1 ammunition would require extensive test and analysis by the DDESB Secretariat.

The concept, as proposed for the MPS ships, is not to totally eliminate sympathetic detonation; rather, it is to use prudent stowage techniques, utilizing certain containers as buffer material, to isolate one hold from another and thus delay the times of reaction of the additional holds and reduce the total event.

The suitable barrier or provision of adequate separation required can be supplied by double rows of containers--one along the aft wall of the forward hold and another along the forward wall of the next adjacent hold. These buffer containers must be placed on every deck of both holds. The containers would be filled with materials which are normally stored aboard the ship and which have been demonstrated to act as a shield or buffer to prevent

detonation.

Buffer Materials. If the concept is to be implemented with a double row of buffers (one on each side of the wall separating the two holds) approximately 120 containers will be required--60 along each side of the wall (note: this number will vary somewhat between the various classes of ships).

Let us make the following definitions of material which may be used either separately or in combination as buffer material:

- (1) Class B propellant charges
- (2) Cluster bombs
- (3) Illuminating projectiles or smoke producing warheads
- (4) Non-mass-detonating munitions
- (5) Special fireworks and/or small arms ammunition
- (6) Time fuze/detonating cord.

The selection for the first two of these has been discussed above and is based on the Army and Air Force test results. The remaining categories were chosen because they would be the least likely to propagate a detonation to subsequent containers.

If the hazardous cargo manifest of a typical MPS ship is examined, it can be shown that there are sufficient containers to act as buffer material. Any arrangement of containers, selected from the types of material presented in the list above, which achieves the goal of a double buffer layer would be acceptable.

## DISCUSSION

The containers and the material which are located therein will act as fragment suppressors, greatly reducing the number and velocity of fragments reaching the potential acceptor munitions.

Previous tests<sup>2,3</sup> conducted during the 1970's addressed the propagation of detonation between stacks of containers. These tests, in some cases, added the extreme confinement which would be present during shipboard storage below the water line. In the final test of the series described in Reference 5, 33 MILVANS were loaded side-by-side, stacked three high in a 21-foot deep hole. The donor was 2 MILVANS containing 144 MK 82 bombs. The acceptor was 16 MILVANS containing 1,152 MK 82 bombs. The buffer consisted of 15 MILVANS of palletized 90 mm cartridges (a total of 7200). The buffer material was described as Shell, fixed, HE, M71 (DODIC C267). The donor had a NEW of 27,468 pounds; the acceptor 221,184. The buffer contained 15,480 pounds of explosive and 52,635 pounds of propellant. The result was a high order detonation. One MK 82 bomb and five 90 mm projectiles were recovered.

All of the smaller tests leading up to this proof of concept test had indicated success. The major differences between the previous tests and the final test were twofold: (1) the size of the test (scale-up of smaller results), and (2) the effects of confinement.

The previous test results should have a bearing on the current effort, but the negative

results should not cause disheartenment. The situations are not the same. The buffer material has been tested and proven to work up to the 60,000 pound NEW donor size. The 90 mm cartridges used previously will not be used--only propellant charges or charges without warheads (the cluster bombs proposed have been verified by tests with heavy confinement).

These concepts were discussed on an informal basis with the DDESB Secretariat. They (the DDESB Secretariat) indicated that their current philosophy is to require testing for all new or drastically-revised stowage concepts. As was discussed above, all of the concepts upon which these recommendations are based have been tested separately; however, the combination (or system of concepts) have not. As the MILVAN tests indicated, there may be synergistic effects which we have not addressed or recognized. The DDESB also has very strong concerns about Class/Division (C/D) 1.1 materials as potential buffers between other C/D 1.1 materials.

Because of this and the number of tests and analyses which would be required before the DDESB Secretariat would approve the process, it was decided not to seek formal approval or recognition for the utilization of this concept. However, the USMC would, on their own, implement as much as possible of this loading concept on all future ship loadouts.

### **MPS TEST CONCEPT AND ARRANGEMENT**

After many discussions with the DDESB, a single large-scale test was agreed upon. This test was to have the following attributes:

- (a) Must include approximately 1/3 of all ordnance carried aboard ship.  
Nominal NEW of test should be 500,000 pounds.
- (b) All material should be stored in ISO containers as it would be aboard ship.
- (c) Material should be arranged in a similar manner as aboard ship. It should be configured to represent two levels of one vertical hold.
- (d) Numbers and types of items to be included should be determined from manifest of typical MPS ship.
- (e) Test should include confinement effects produced by material stored below water-line of ship.
- (f) C/D 1.3 materials should be placed in positions of greatest confinement
- (g) Test must provide multiple detonation sources.

Since only one test was to be performed, the test must be configured to represent a truly "worst case"; i.e, the test would not, necessarily, represent a viable hazard or threat scenario. Rather, everything should be done to maximize the output of the event.

### **TEST OBJECTIVES**

As planned, the test would have several objectives. These would include:

- (1) For a realistic arrangement of ordnance stored in ISO vans, determine the airblast propagation characteristics (pressure-distance and impulse-distance).
- (2) At selected locations, determine the dynamic pressure produced by the detonation.
- (3) From the measured blast characteristics, determine a TNT equivalence for the event.
- (4) Determine the debris density as a function of range from the center of the charge.
- (5) From the measured airblast and debris characteristics, determine the ESQD arcs which should be applied to a full scale ship.
- (6) Determine the number and NEW of unexploded ordnance produced by the event.
- (7) Compare pre-test airblast predictions with the measured results.

## TEST PARTICIPANTS

At the start of this effort, several potential test sites were examined. As the size and complexity of the test became clear, it was decided that the test would be conducted at the Naval Weapons Center (NWC) (currently, the Naval Air Warfare Center (NAWC), China Lake, CA). They (NWC) would have the responsibility for final site selection, site preparation, loading and stacking of containers, charge detonation, high speed photography, and preliminary report preparation.

Airblast would be measured by the U.S. Army Waterways Experiment Station, Vicksburg, MS. The airblast measurements would include side-on overpressure at all gauge locations and dynamic pressure at selected locations.

## CHARGE ARRANGEMENT

The charge arrangement was patterned after the loadout of the MPS ship PFC DEWAYNE T. WILLIAMS. The loadout for this ship was examined in detail. The contents of every third container of ordnance material were selected for inclusion on this test. These contents were compared with material which was available from the DEMIL (Demilitarization) inventory. Where material was not available, substitutions were made. The basic rules for substitution were that materials of the same hazard class/division should be used. Further these should have the same approximate sensitivity as the items being replaced. For safety reasons, cluster bombs would not be included on the test. Instead, the cluster bombs would be replaced by 155 mm projectiles. It was felt that the projectiles would be more likely to mass detonate than the cluster bombs. Moreover, if detonation did occur, the blast and fragmentation from the projectiles would be more likely to propagate a sympathetic detonation.

The confinement produced by the fact that portions of the holds are below the waterline would be simulated by placing the lower portion of the ordnance below the ground level. As finally configured, the test would consist of 96 ISO vans of ordnance and 38 vans of inert material-- configured to represent two levels of one hold.

Figure 1, provided by NAWC shows a front view drawing of the test configuration. Figure 2 (also provided by NAWC) shows a plan view of each level. A total of 134 ISO vans were used in the test. The total ordnance weight was 2,265,770 pounds with a net explosive weight of 523,790 pounds. The simulated deck plates shown in these figures were made from 1/4-inch steel plates (10' x 40'). The south side of the stack (with a sloping side rather than dirt confinement) represented the lessened confinement present toward the bow of the ship.

The ordnance and containers were pre-staged at the Cactus Flats Ordnance Field Test Site. When the containers were loaded and their contents documented, they were transported to the actual test site. The test site was located at Airport Lake on the Naval Weapons Center North Range. Marine Corps personnel assisted in transporting the loaded containers from Cactus Flats to Airport Lake.

Fourteen containers were selected as donors. These fourteen containers were scattered throughout the charge stack. All of the donor containers were primed and simultaneously detonated. The total NEW of the donor was 103,555 pounds.

The test was detonated on 7 September 1990. The remainder of this report discusses the results of that detonation.

## DATA COLLECTION

Data were collected along three five-degree radials extending outward from the ground zero area. Figure 3 is a schematic of the area showing the locations and types of measurements undertaken.

Airblast. Side-on overpressure was measured at five locations along three radial lines. Piezoresistive transducers mounted flush with the ground surface were used to make these measurements. The data were recorded on transient data recorders with analog FM (Frequency Modulation) tape recorders as back up. Reflected pressure was measured on two ISO vans placed at ranges of interest. Near the same location as the vans, side-on overpressure gauges were also located. Dynamic pressure would be inferred from the combination of reflected and side-on pressure.

Debris. The three 5°-sectors shown in Figure 3 were sub-divided into hundred-foot increments for purposes of debris recovery and analysis. The debris survey was accomplished by USMC EOD (Explosive Ordnance Disposal) personnel under the direction of the Naval Surface Warfare Center.

Within each 5° radial, the debris survey was started at a range greater than 4000 feet from ground zero, with the survey proceeding inward toward ground zero. Everything located beyond 4000 feet was consolidated into a single reading. Each 100-foot sector was surveyed independently. The criteria for consideration was that the material had to be larger than 1/2" x 1/2" x 1/2". Calculations had shown that material smaller than this would not be hazardous (i.e., have an impact energy greater than 58 ft-lbs).

## TEST RESULTS

### AIRBLAST

The airblast results, which are provided by the Waterways Experiment Station, are presented in Table 2.

Least Square Curve Fits. In order to best utilize all of the airblast data, the method of least squares was used to fit curves to the data. These are shown in Figures 4 for peak pressure and Figure 5 for positive impulse. Shown on each graph are the forms of the curve fits. The pressure-distance data was best fit by a quadratic to the logarithms of the data. The impulse-distance data was best fit by a simple power law.

Dynamic Pressure Estimates. As stated above, reflected pressure measurements were made at two locations. The gauges were placed in the center of the side-wall of ISO vans and the gauge/van placed perpendicular to the direction of blastwave propagation. The results are given at the bottom of Table 2.

The purpose of the reflected pressure measurements was to determine if there were unexpected dynamic pressure effects produced either by the size of the charge, its contents, or its configuration. Using the Rankine-Hugoniot relationships and the procedures described in Reference 4, the reflected pressure was estimated from the measured side-on overpressure. This estimate assumes that the blast wave producing the shockwave meets the requirements for a classical blast wave; i.e., that there is no additional component to the dynamic pressure. This comparison between the measured and predicted is shown in Table 3. It is obvious from the small differences in the measured and predicted reflected pressures that the dynamic pressure effects are those predicted for a classical shockwave produced by the detonation of the given NEW.

Kingery Hemispherical Standard. The scaled distances to which airblast quantity-distance criteria refer are directly related to peak overpressure. The relationship is based on the Kingery compilation of surface burst hemispherical TNT data,<sup>5,6</sup> referred to hereafter as the Kingery TNT standard. Figures 6 and 7 show the comparison between the MPS results and the Kingery standard for both peak pressure and positive impulse. Clearly, the data fall well below the Kingery curves for the NEW of the test.

### DEBRIS

As indicated in the previous section, debris data were collected along three radial directions. Tables 4, 5, and 6 present the debris data collected during this test. On the South radial, no debris recovery was attempted inside a radius of 1600 feet. The debris density in this area was so high that recovery was not feasible. Along the North radial and a portion of the West Radial (between 1000 and 1600 feet), the ground was extremely soft and sandy. It was felt that some of the fragments may have become buried in this area and would not have been counted. The on-site personnel felt that to be conservative the number of fragments recovered in these areas should be increased by 25%. This would alleviate any problems of undercounting. The data in Tables 4 and 5 were increased by this

amount before the data were plotted or debris densities computed.

Recently accepted standardized procedures<sup>7</sup> for the analysis of debris have been used in this study. These involve the computation of a pseudo-trajectory normal debris density as a function of range. Figure 7 presents the debris density data produced by this test.

#### UNEXPLODED ORDNANCE

After the debris survey in the five degree sectors was completed, the USMC EOD team swept the entire test area to render it safe. During that sweep, the amount of unreacted ordnance was determined. This is shown in Table 7. By far, the largest amounts, both in quantity and NEW were the 155 mm projectiles. A total of 49,551 pounds of ordnance was recovered. This means that about 9.5% of the total NEW did not react.

#### DATA ANALYSIS AND INTERPRETATION

TNT Equivalence. One of the objectives of this program was to determine the TNT equivalence (relative to the Kingery Hemispherical TNT Standard) of the event. TNT equivalence can be based on any of the measured airblast parameters. In this effort, TNT equivalences based on peak overpressure and positive impulse will be reported. Graphs of TNT equivalence are shown in Figure 8. As can be seen, the TNT equivalence varies greatly with the pressure level (range). A single value for the equivalence could be extremely misleading.

Prior to the conduct of the test, nominal TNT equivalences were assigned to each item included on the test. The result was an estimated average TNT equivalence for the energetic material of 0.80. The actual average TNT equivalence (compared to the hemispherical standard), as determined from the information in Figure 8, was 0.55 based on peak pressure and 0.57 based on positive impulse. The difference between the 0.80 and the 0.55-0.56 values represent the effects of the casing material, the confinement provided by the structure and the configuration, and differences between hemispherical and nearly cubical charge geometries.

Airblast Hazard Range. The two airblast hazard ranges of interest are the inhabited building distance (IBD) and the public traffic route distance (PTR). Reference 1 states that for charge weights greater than 250,000 pounds, IBD occurs at a pressure level of 0.9 psi. Likewise, PTR occurs at a range of 1.7 psi. The least squares curve given in Figure 4 best represents all of the pressure-distance data. It will be used to determine these ranges. They are 3250 feet for IBD and 1910 for PTR. These ranges, however, only represent the test conditions. They still have to be scaled up to the full scale event. This is accomplished by using Hopkinson or cube root scaling. The full scale numbers would be obtained by multiplying the ranges shown above by the factor (FULL SCALE NEW/523,790)<sup>1/3</sup>. These results are given in Table 8 for a range of full scale NEW's.

Debris Hazard Range. The debris hazard range is defined at that range at which the density of hazardous fragments (those having an impact energy of 58 ft-lbs or greater) reaches 1 per 600 ft<sup>2</sup>. These ranges can be obtained from the debris density-distance curves given in Figure 9. Once the debris ranges for the test are obtained, the problem still

remains how to scale them up to the full scale event.

Debris range does not Hopkinson scale. The author has not found an approved debris scaling methodology. He has examined two approaches, both of which seem conservative, and has decided to use the approach which gave the greater ranges. These two approaches are:

- (a) The number of debris pieces is directly proportional to the charge weight ratio. This means that the number of debris would be multiplied by 3 ( $1,500,000/500,000$ ) in a full scale event. The 1 per 600 ft<sup>2</sup> range would then be determined from this new, increased distribution.
- (b) The number of debris pieces is proportional to the cube of the charge weight ratio. This means that the number of debris would be multiplied by 27 ( $1,500,000/500,000$ )<sup>3</sup> in a full scale event. The 1 per 600 ft<sup>2</sup> range would then be determined from this new, increased distribution.

The major portion of the ship's structure was not modeled in this test. This structure would contribute to the debris, increasing the range. The author feels that by choosing the method giving the greatest range, the effects of this added debris are, essentially, included.

The debris ranges are presented in Table 9. Included are the "as built ranges" determined from Figure 9, as well as the results obtained by increasing the number of debris by both a factor of 3 and a factor of 27. The greatest debris range is less than 4000 feet--less than the airblast ranges given above. It should be pointed out, however, that this does not mean that there will be no debris beyond this range; rather, that the debris density falls below the accepted criteria.

#### RECOMMENDED ESQD RANGES

The ESQD range is the larger of the two ranges determined by airblast and debris. For the MPS ships, the airblast produced drives the ESQD ranges. This program and its experimental results were presented at the 304th formal meeting of the Department of Defense Explosives Safety Board held on November 27-28 1990. At that time, the NEW of the test was thought to be 503,516 pounds, rather than the current figure of 523,790 pounds. For this reason, the ranges recommended to and accepted by the DDESB are slightly different than those given in the preceding section. The following are the recommended ESQD ranges adopted by the DDESB:

- (a) Debris Range of 4400 feet
- (b) Airblast range of  $40.85W^{1/3}$  for IBD and  $24.81W^{1/3}$  for PTR, where W is the total NEW in pounds.

These relationships were used to generate Table 10, which currently will apply only to the original thirteen USMC MPS. These newly accepted ranges will greatly alleviate the encroachment problem described above.

## ADDITIONAL DISCUSSIONS

Before the proposed ranges were accepted, there were many detailed discussions with the DDESB Secretariat as to the proper interpretation of the airblast results. As a result of the least squares curve fitting process, approximately 50% of the data points will lie above the fitted curve. Because safety decisions will be based on the airblast pressure-distance data and because there is only a limited test data base, the DDESB Secretariat has recommended that some type of safety factor be applied to the data to make it more safety conservative. This is discussed further in Reference 8.

The MPS program did not have to meet this requirement since it was ongoing when this guidance was developed.

## REFERENCES

1. NAVSEA OP 5 VOLUME 1, Ammunition and Explosives Ashore, Safety Regulations for Handling, Storing, Production, Renovation, and Shipping, Fifth Revision, 1 August 1990.
2. Parkinson, A. J. and Smith, K. T., "MILVAN Container Stowage Tests," Army Equipment Office Report T-205, 20 November 1973.
3. Dienes, R., "Safe Transport of Munitions (STROM)," MTMC Report MTT 81-1, June 1981.
4. Swisdak, M. M., "Explosion Effects and Properties: Part I--Explosion Effects in Air," NSWC/WOL/TR 75-116, 6 October 1975.
5. Kingery, C. N. and Bulmash, G., "Airblast Parameters From TNT Spherical Air Burst and Hemispherical Surface Burst," ARBRL-TR-02555, April 1984.
6. Kingery, C. N., "Air Blast Parameters Versus Distance for Hemispherical TNT Surface Bursts," BRL Report 1344, Sep 1966.
7. Swisdak, M. M., "Procedures For the Analysis of the Debris Produced By Explosion Events," Minutes of the Twenty-Fourth Explosives Safety Seminar, August 1990.
8. Swisdak, M. M., "Hazards Produced By Explosions Inside Earth Covered Igloos," Minutes of the Twenty-Fifth Explosives Safety Seminar, August 1992.

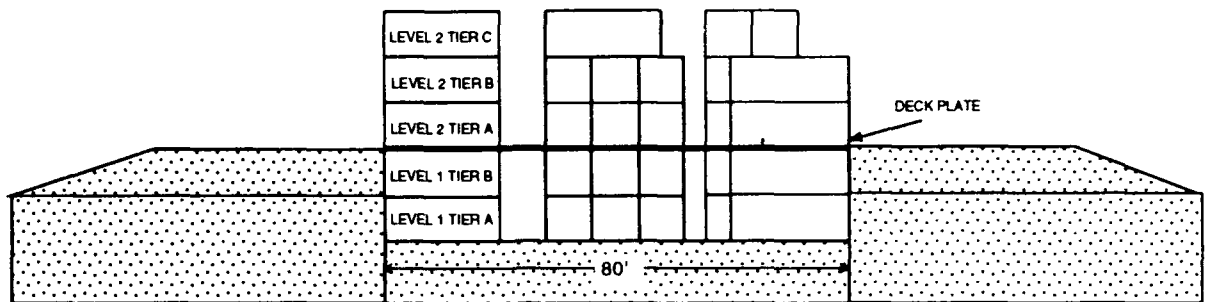


**FIGURE 1. FRONT VIEW DRAWING OF THE TEST CONFIGURATION**

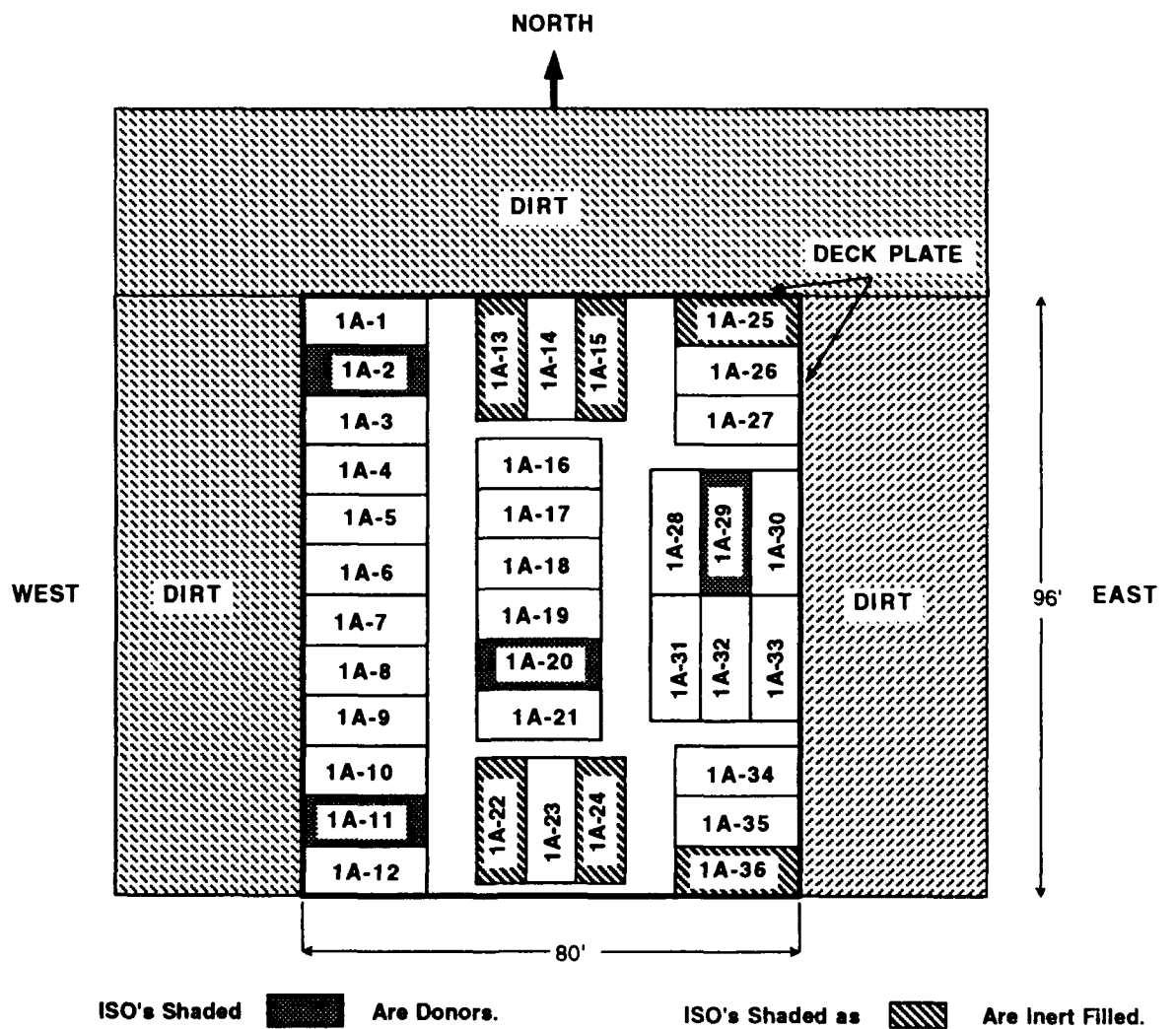


**FIGURE 2A. PLAN VIEW OF LEVEL 1, TIER A OF THE TEST CONFIGURATION**

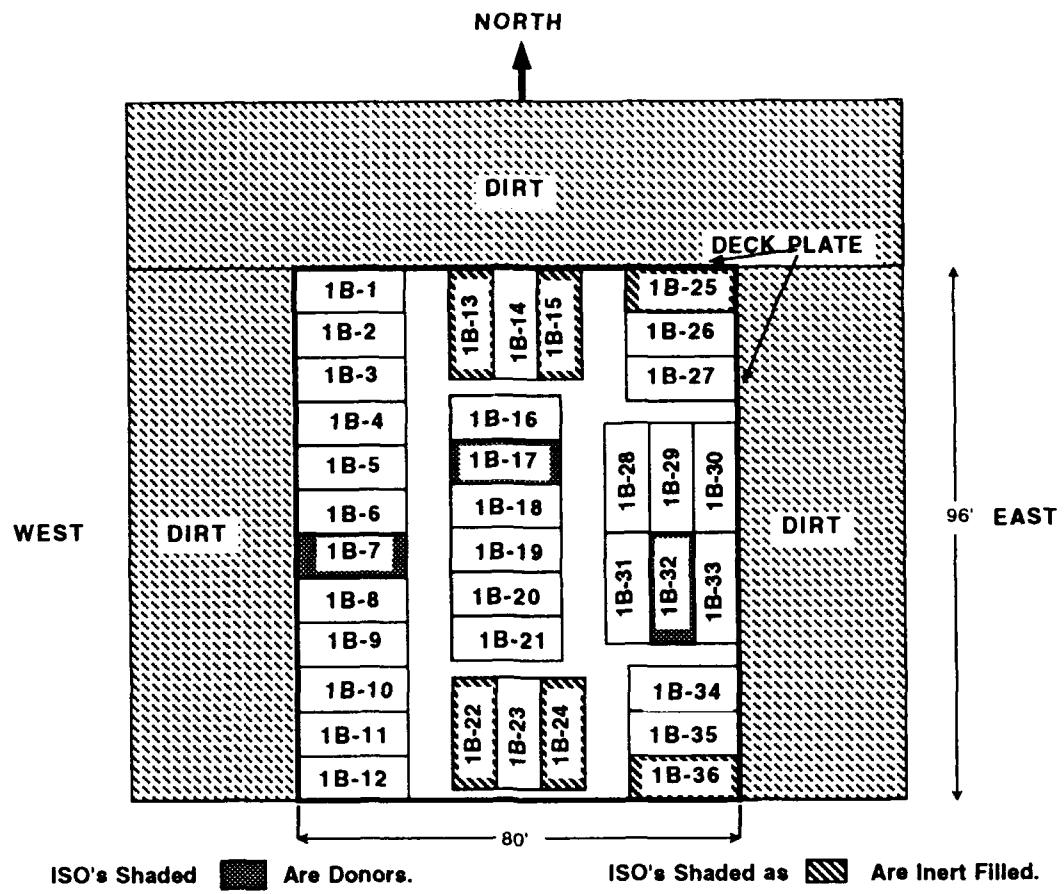


FIGURE 2B. PLAN VIEW OF LEVEL 1, TIER B OF THE TEST CONFIGURATION

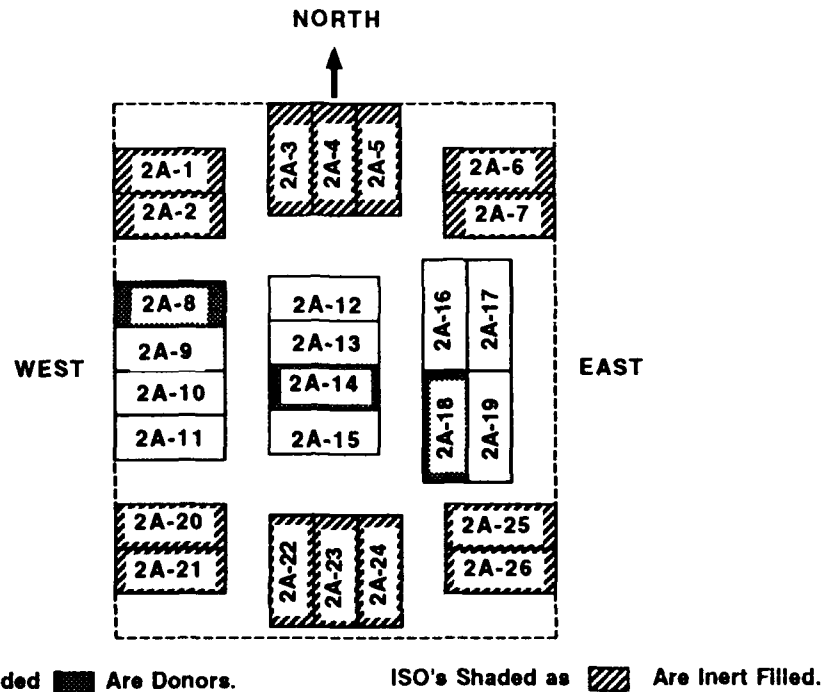
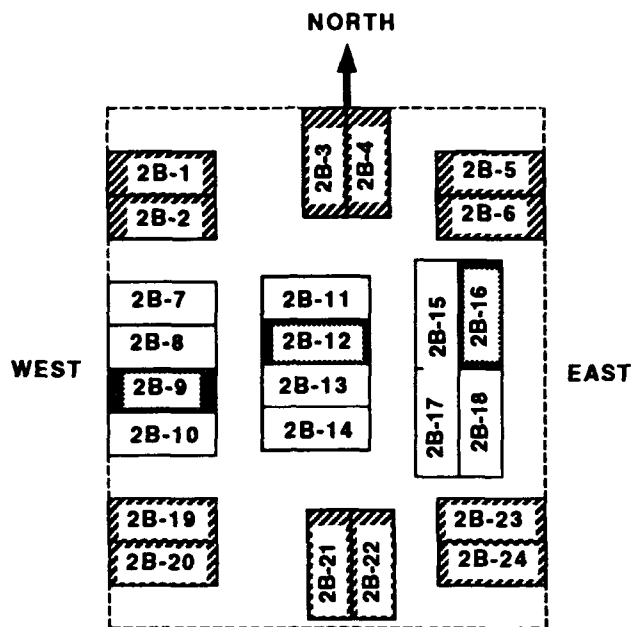


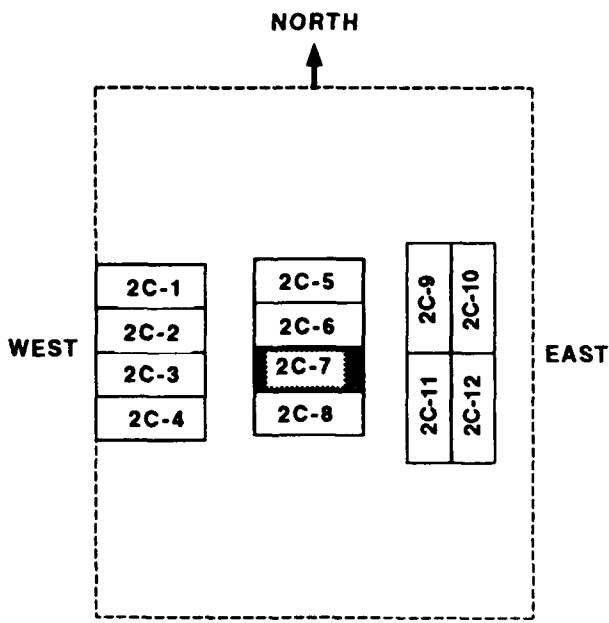
FIGURE 2C. PLAN VIEW OF LEVEL 2, TIER A OF THE TEST CONFIGURATION



ISO's Shaded ■ Are Donors.

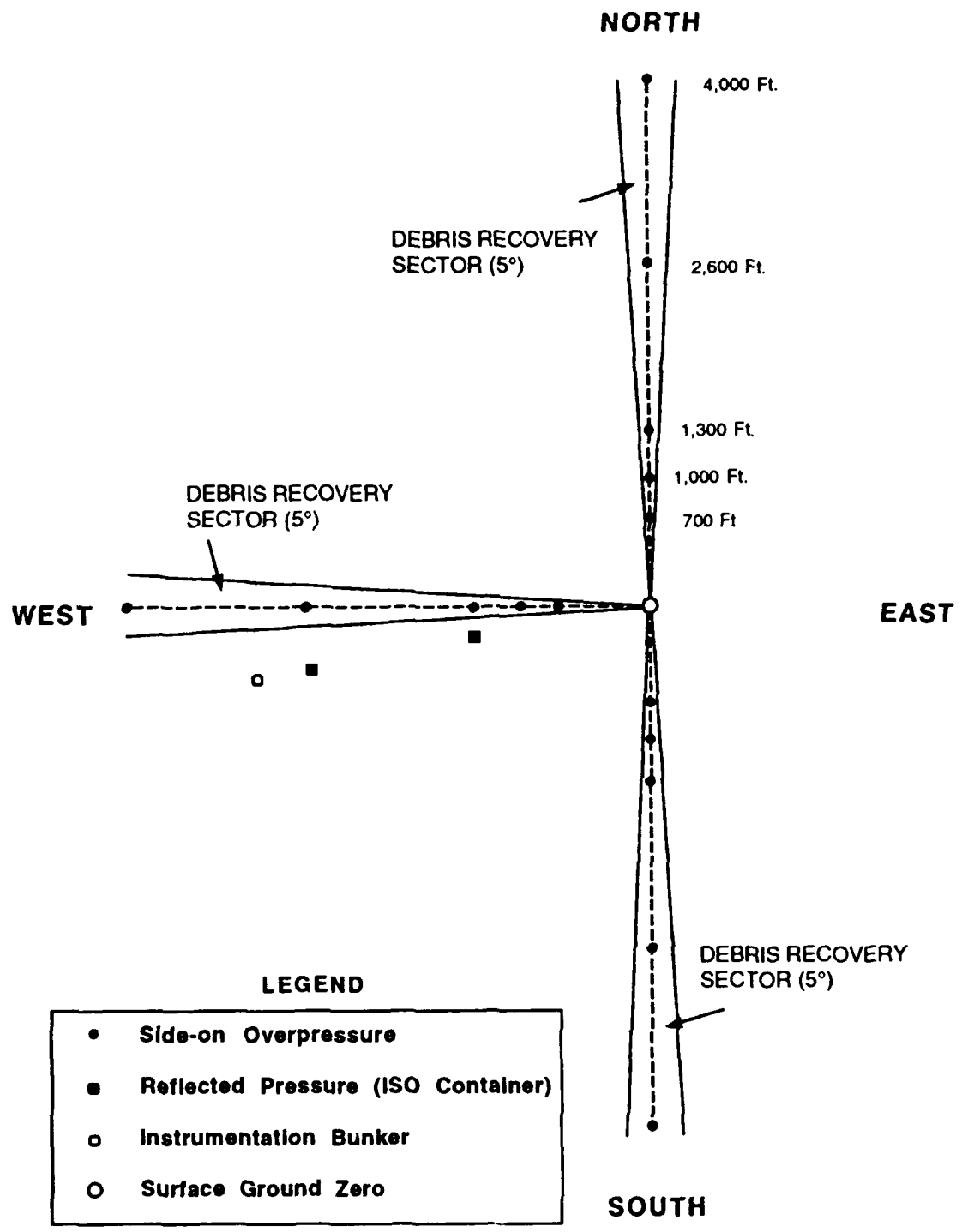
ISO's Shaded as ▨ Are Inert Filled.

FIGURE 2D. PLAN VIEW OF LEVEL 2, TIER B OF THE TEST CONFIGURATION



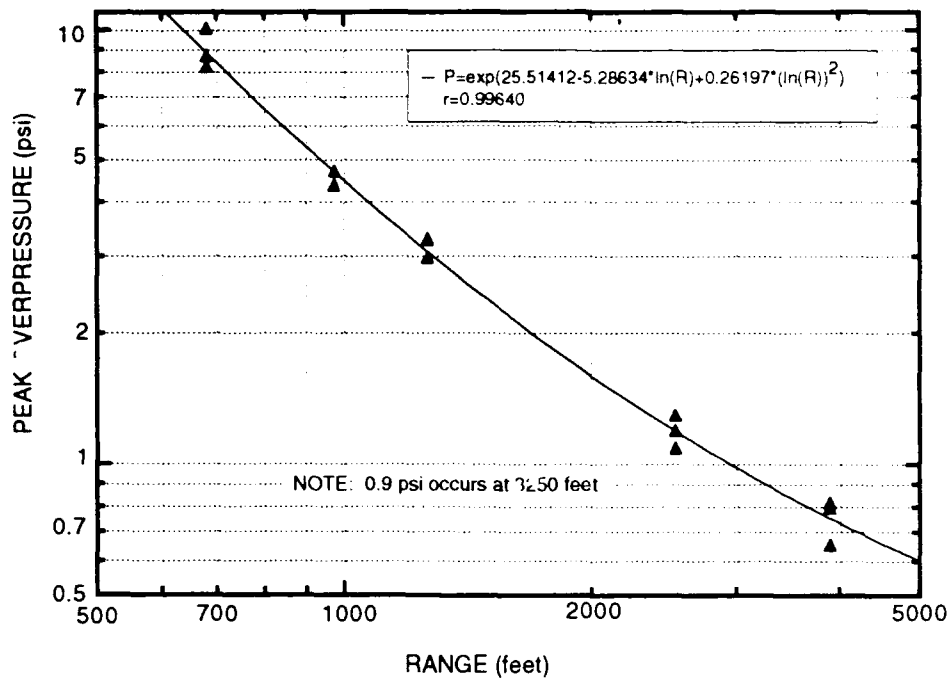
ISO Shaded ■ Is Donor.

FIGURE 2E. PLAN VIEW OF LEVEL 2, TIER C OF THE TEST CONFIGURATION



**FIGURE 3. MPS ESQD DEBRIS SECTORS AND INSTRUMENTATION LAYOUT**

**FIGURE 4. MPS AIRBLAST OVERPRESSURE DATA:  
LEAST SQUARES FIT**



**FIGURE 5. MPS POSITIVE IMPULSE DATA:  
LEAST SQUARES FIT**

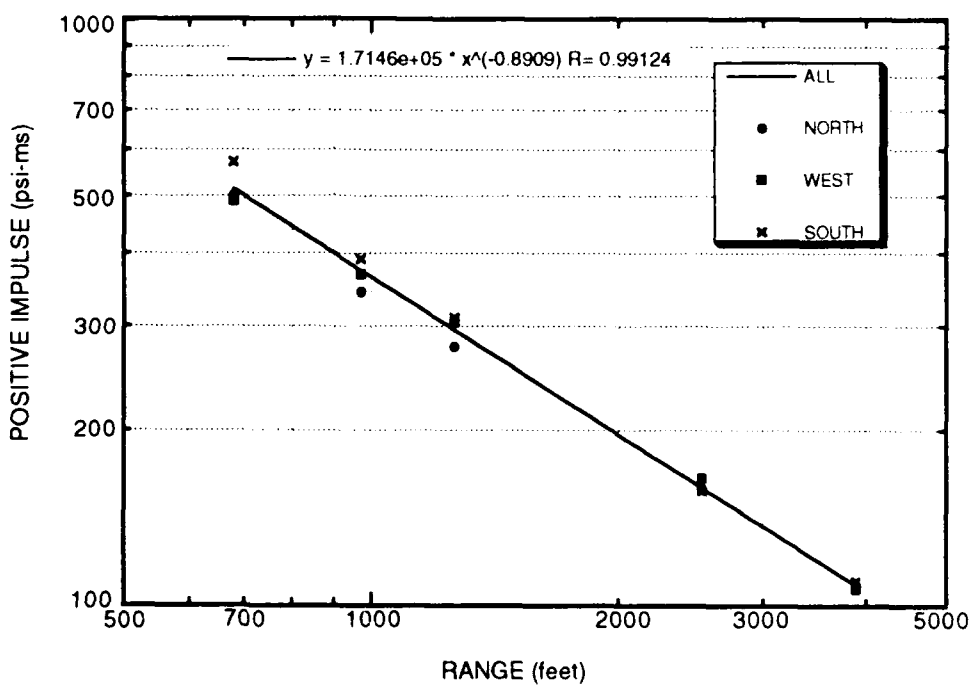


**FIGURE 6. COMPARISON OF MPS PRESSURE-DISTANCE DATA WITH KINGERY TNT STANDARD**

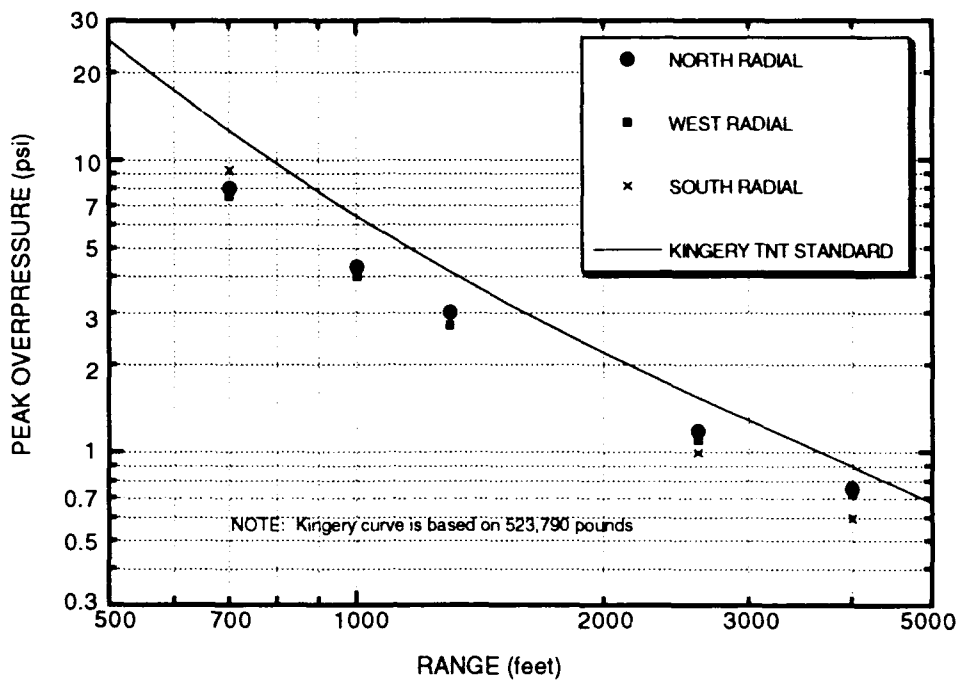


**FIGURE 7. MPS IMPULSE-DISTANCE DATA COMPARISON WITH KINGERY TNT STANDARD**

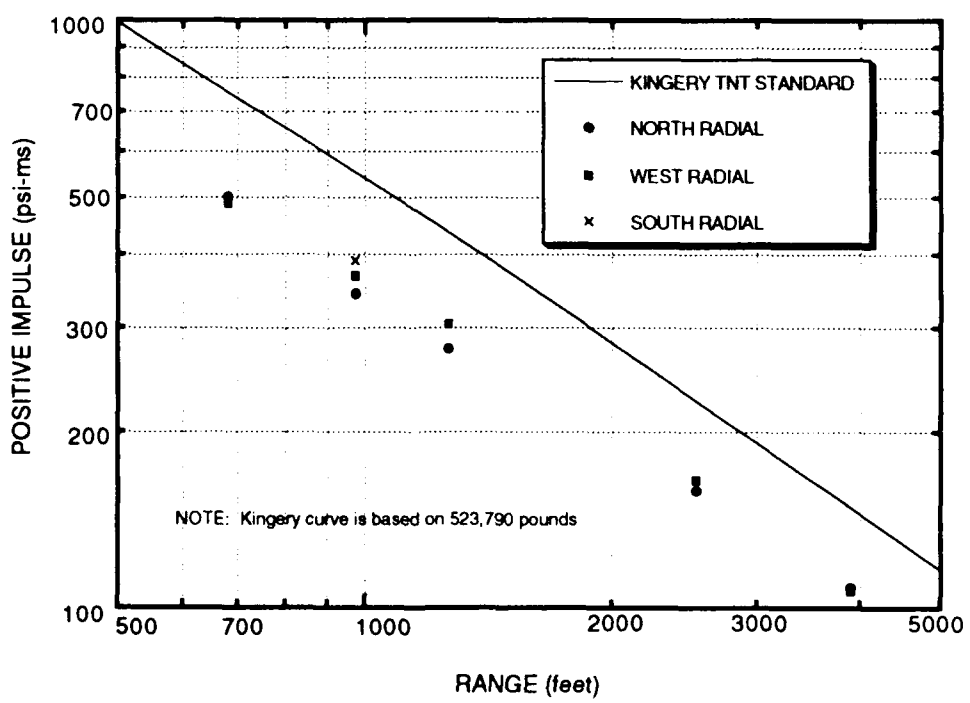


**FIGURE 8. MPS EQUIVALENT WEIGHT**

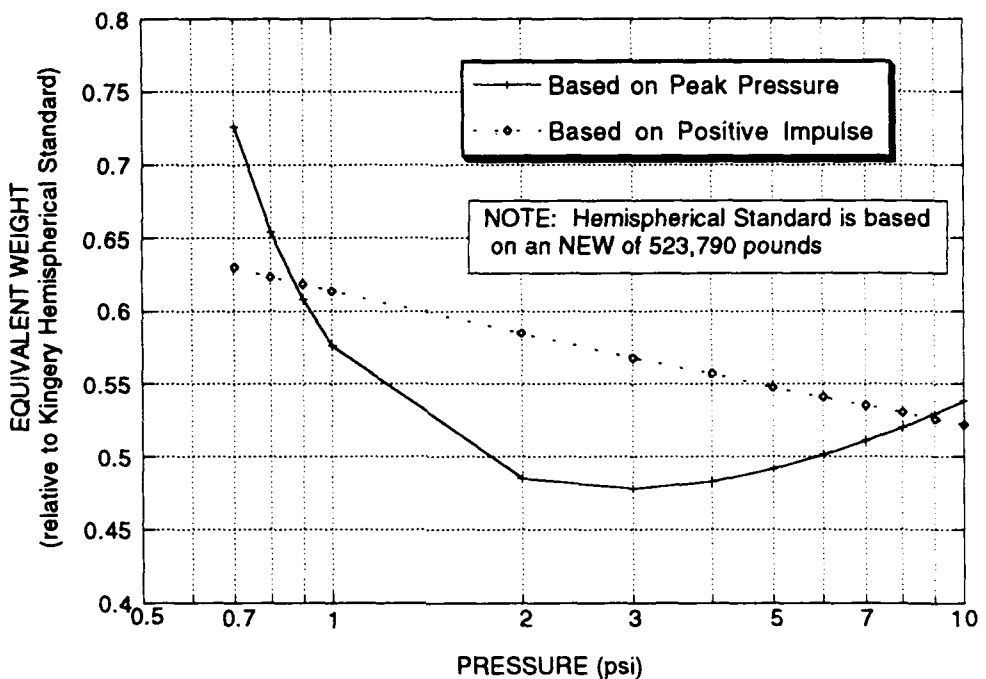


**FIGURE 9. MPS DEBRIS RECOVERY**

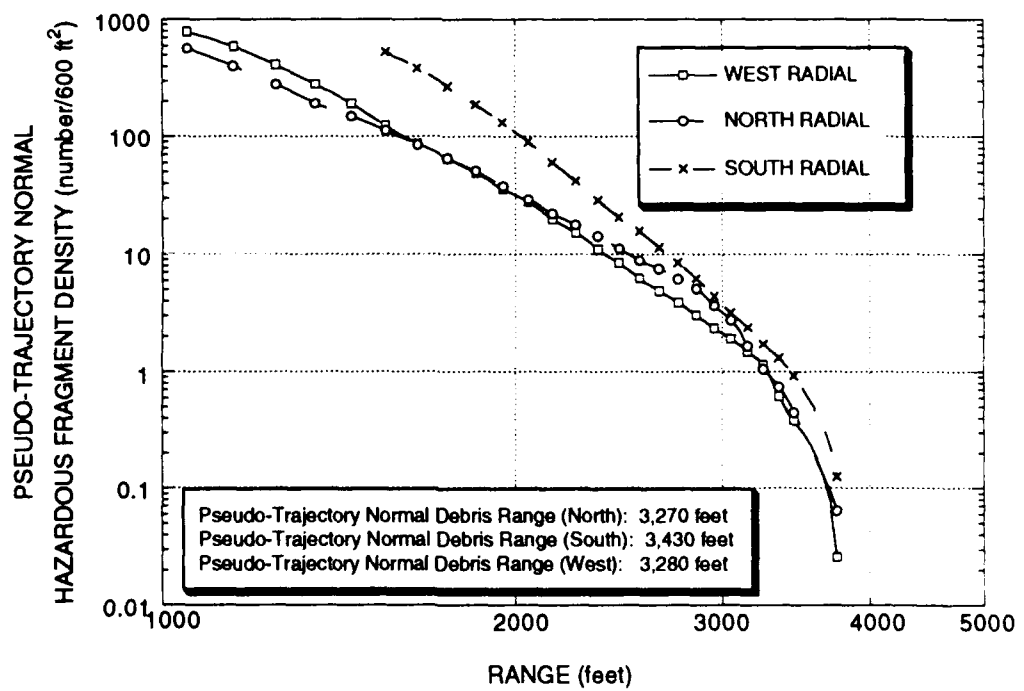


TABLE 1. ESQD RANGES

NEW (pounds)	INHABITED BUILDING DISTANCE (feet)	PUBLIC TRAFFIC ROUTE (feet)
1,000,000	5,000	3,000
1,150,000	5,240	3,145
1,300,000	5,460	3,280

SOURCE: OP-5 (Reference 1)

TABLE 2. RESULTS OF AIRBLAST MEASUREMENTS

RADIAL	HORIZONTAL DISTANCE (feet)	PEAK PRESSURE (psi)	POSITIVE IMPULSE (psi-ms)
North	700.2	8.02	449.62
North	1000.0	4.32	307.48
North	1299.9	3.02	248.01
North	2600.2	1.18	142.14
North	4000.2	0.75	97.18
West	700.2	7.54	438.01
West	1000.0	4.02	329.24
West	1299.9	2.73	272.67
West	2600.2	1.10	147.94
West	4000.2	0.73	95.73
South	700.2	9.24	510.53
South	1000.0	4.00	349.54
South	1299.9	3.00	277.02
South	2600.2	1.00	140.69
South	4000.2	0.60	98.63
West-reflected	1299.9	5.70	Cable Cut
West-reflected	2600.2	2.36	142.14

TABLE 3. DYNAMIC PRESSURE EFFECTS

RANGE (ft)	MEASURED SIDE-ON OVERPRESSURE (psi)	MEASURED REFLECTED OVERPRESSURE (psi)	PREDICTED REFLECTED OVERPRESSURE*	PERCENT DIFFERENCE
1300	2.73	5.70	5.90	-3.4%
2600	1.10	2.36	2.31	2.2%

\*prediction based on measured side-on overpressure using Rankine-Hugoniot relationships to predict reflected pressure

NOTE: Reflected impulse also measured-however, finite size of reflecting surface allowed pressure to relieve before total reflected impulse could develop

TABLE 4. DEBRIS RECOVERY DATA—NORTH RADIAL

LOWER (feet)	HIGHER (feet)	AREA (sq. feet)	155 mm	106 mm	105 mm	4.2"	FUZES	50 CAL	FRAGMENTS	TOTAL
1000	1100	9,163	1	1			3		1	1,554
1100	1200	10,036					1		1,277	1,280
1200	1300	10,908	1				6		1,055	1,062
1300	1400	11,781					5	3	498	506
1400	1500	12,654	2				9	2	476	489
1500	1600	13,526	2				4	4	373	383
1600	1700	14,399					5	1	303	309
1700	1800	15,272	1				1	3	234	239
1800	1900	16,144		1			4	4	222	231
1900	2000	17,017	1				2	1	159	163
2000	2100	17,890					4	2	135	141
2100	2200	18,762					2	2	86	90
2200	2300	19,635					1		75	76
2300	2400	20,508					1		70	71
2400	2500	21,380	2				1		54	57
2500	2600	22,253	1				1		28	30
2600	2700	23,126	1						33	34
2700	2800	23,998					2		27	29
2800	2900	24,871	2				1		41	44
2900	3000	25,744	1				4		22	27
3000	3100	26,616	1				1		35	37
3100	3200	27,489	2						19	21
3200	3300	28,362	1	1					9	11
3300	3400	29,234		1					9	11
3400	3500	30,107	1						3	4
3500	4000	163,625	1	2	1				13	14
	>4000						0	58	23	6,819
										6,929

**TABLE 5. DEBRIS RECOVERY DATA--WEST RADIAL**

FLOWER (feet)	RUPPER (feet)	AREA (sq. feet)	155 mm	106 mm	105 mm	4.2"	fuzes	50 cal	fragments	total
1000	1100	9,163				2			1,756	1,758
1100	1200	10,036				3			1,834	1,834
1200	1300	10,908	1			5			1,576	1,580
1300	1400	11,781				2			1,164	1,169
1400	1500	12,654				2			1,002	1,004
1500	1600	13,526	1			2			535	538
1600	1700	14,399				3			439	442
1700	1800	15,272				1			337	333
1800	1900	16,144				1			297	298
1900	2000	17,017				2			188	190
2000	2100	17,890				2			202	204
2100	2200	18,762							124	124
2200	2300	19,635							122	122
2300	2400	20,508							76	76
2400	2500	21,380				2			68	70
2500	2600	22,253							43	43
2600	2700	23,126							33	33
2700	2800	23,998							29	29
2800	2900	24,871	1						24	25
2900	3000	25,744							16	16
3000	3100	26,616							16	16
3100	3200	27,489							12	14
3200	3300	28,362		1					22	24
3300	3400	29,234							10	11
3400	3500	30,107							11	12
3500	4000	163,625		1					7	7
	>4000								3	4
			<b>Total</b>	<b>3</b>	<b>2</b>	<b>0</b>	<b>0</b>	<b>30</b>	<b>0</b>	<b>9,946</b>
										<b>9,981</b>

TABLE 6. DEBRIS RECOVERY DATA--SOUTH RADIAL

FLOWER (feet)	RUPPER (feet)	AREA (sq. feet)	155 mm	106 mm	105 mm	4.2"	fuzes	50 cal	fragments	total
1000	1100	9,163								*
1100	1200	10,036								*
1200	1300	10,908								*
1300	1400	11,781								*
1400	1500	12,654								*
1500	1600	13,526								*
1600	1700	14,399	2							*
1700	1800	15,272		3						*
1800	1900	16,144			4					*
1900	2000	17,017								*
2000	2100	17,890	1							*
2100	2200	18,762		3						*
2200	2300	19,635			2					*
2300	2400	20,508								*
2400	2500	21,380								*
2500	2600	22,253								*
2600	2700	23,126								*
2700	2800	23,998		3						*
2800	2900	24,871			1					*
2900	3000	25,744								*
3000	3100	26,616	1							*
3100	3200	27,489								*
3200	3300	28,362								*
3300	3400	29,234								*
3400	3500	30,107	1							*
3500	4000	163,625	3	2	3					*
>4000			2	2	25		1			*
TOTAL		38	12	44	32	75	0	11,867	0	11,868

\*No recovery in this area

**TABLE 7. UNEXPLODED ORDNANCE**

TYPE OF ORDNANCE	QUANTITY	NEW (pounds)
155 mm H.E.	2148	33,508
105 mm H.E.	277	1,662
4.2" mortar	791	6,328
106 mm	521	6,773
MK 81 bombs	6	600
Sparrow warhead	38	680
<b>TOTAL</b>		<b>49,551</b>

**TABLE 8. AIRBLAST ESQD RANGES**

NET EXPLOSIVE WEIGHT (pounds)	INHABITED BUILDING DISTANCE (feet)	PUBLIC TRAFFIC ROUTE (feet)
1,000,000	4,032	2,400
1,100,000	4,162	2,480
1,200,000	4,284	2,550
1,300,000	4,400	2,620
1,400,000	4,510	2,690
1,500,000	4,615	2,750

NOTE: TABLE IS BASED ON SCALING RANGES OBTAINED ON MPS TEST FOR 0.9 AND 1.7 PSI.  
THESE RANGES WERE 3250 FEET (0.9 PSI) AND 1910 FEET (1.7 PSI)

**TABLE 9. DEBRIS HAZARD RANGES**

FRAGMENT MULTIPLIER	NOTE	DIRECTION		
		NORTH	SOUTH	WEST
1		3270	3430	3280
3	1	3500	3650	3480
27	2	3780	3820	3740

- Notes: 1. The number of fragments is proportional to the charge weight ratio  
     multiplier =  $1,500,000/500,000=3$   
 2. The number of fragments is proportional to the cube of the charge weight ratio  
     multiplier =  $(1,500,000/500,000)^3=27$

**TABLE 10. MPS ESQD RANGES ADOPTED BY DDESB**

NEW (pounds)	INHABITED BUILDING DISTANCE (feet)	PUBLIC TRAFFIC ROUTE DISTANCE (feet)
1,000,000	4,085	2,480
1,100,000	4,220	2,560
1,200,000	4,345	2,640
1,300,000	4,460	2,710
1,400,000	4,570	2,780
1,500,000	4,680	2,840

NOTE: These ranges apply only to the thirteen USMC MPS ships

EVALUATION OF TRENCH STORAGE  
OF AMMUNITION TRUCKS

Twenty-Fifth DOD Explosives Safety Seminar  
Anaheim, CA  
18-20 August 1992

by  
L. K. DAVIS

Explosion Effects Division  
Structures Laboratory  
U.S. Army Engineer Waterways Experiment Station  
Corps of Engineers  
3909 Halls Ferry Road  
Vicksburg, MS 3980-0631

# EVALUATION OF TRENCH STORAGE OF AMMUNITION TRUCKS

BY

L. K. DAVIS

U.S. ARMY ENGINEER WATERWAYS EXPERIMENT STATION  
3909 HALLS FERRY ROAD, VICKSBURG, MS 39180

## BACKGROUND

Combat troops are often involved in operations which require temporary storage of fully-loaded ammunition supply trucks at field locations. In peacetime, such temporary storage may be required as a part of training exercises. In wartime, temporary storage sites may be established as a source point for rapid distribution of ammunition to forward-based armor or artillery units.

U.S. safety standards<sup>1</sup> specify separation distances between individual storage units, and between the storage area and troop locations, to minimize the risk of sympathetic explosions and personnel casualties in the event of an accidental explosion of a storage unit. Although the separation distances are less restrictive for temporary storage in "theaters of operations" than for permanent storage sites, they still pose a problem for commanders who want to concentrate a group of ammunition trucks for tactical reasons.

As a possible solution to this problem, the U.S. Army Project Manager for Ammunition and Logistics (PM/AMMOLOG) developed the concept of using trenches for temporary storage of ammo trucks at field sites. Such trenches could be constructed quickly and cheaply, and would, as a minimum, reduce the risk of sympathetic detonations of closely-spaced ammo trucks, in the event that one would accidentally explode. The U.S. Army Engineer Waterways Experiment Station (WES) was tasked to evaluate the feasibility and effectiveness of trench storage.

---

<sup>1</sup>U.S. Dept. of Defense; "Ammunition and Explosives Safety Standards;" DOD 6055.9-STD, July 1984; Office of the Asst. Secretary of Defense (Manpower, Installations, and Logistics).

## **RESEARCH APPROACH**

### **a. Model Tests.**

The evaluation of the trench storage concept was performed in two phases. The first phase was a series of 1:6-scale model tests of four different trench designs to determine their relative effectiveness (see Figure 1). Small explosive charges were detonated in each model trench, simulating explosions of a portion or all of the ammunition in a truckload; i.e., a Unit Basic Load of 1,488 kg (net explosive weight) of artillery ammunition. For each test, two lines of airblast gages were used to record side-on overpressures as a function of distance from the detonation; one line along an extended axis of the trench (0-degree line), and one line extending from the charge in a direction normal to the trench axis (90-degree line). To evaluate the relative debris hazards, small solid metal cylinders were packed around each explosive charge to simulate unexploded projectiles (in model scale). The distribution of the cylinders (and other debris) was surveyed after each test.

An analysis of the model test results clearly showed that the most effective trench design was the timber-framed, earth-covered trench shown in Figure 1(f).

### **b. Full-scale Experiment.**

After selection of the covered trench as the most effective design, a series of three full-scale experiments were conducted to quantify and demonstrate the hazard suppression capabilities of trench storage. The experiments were conducted by WES at the U.S. Army's Dugway Proving Ground, Utah.

The first experiment, called the "Control Data Test," involved the detonation of a full ammo load on an unprotected (i.e., not in a trench) truck to provide a baseline set of airblast and debris data, against which the trench test results could be compared. The ammunition load consisted of 160 TNT-loaded 155 mm projectiles, and 80 propellant canisters, each containing 5 kg of M3A1 propellant. The net explosive weight was 1,488 kg. The load was placed on a surplus M814 cargo truck, with the propellant separated into five groups of canisters, with four groups of projectiles placed in-between (Figure 2). The load was detonated by initiating one projectile at the end of each projectile group. As in the model tests, side-on overpressure measurements were made along two lines extending from the truck; one line extending along the truck axis, and the other normal to the axis. After the detonation, debris was collected and weighed from sampling areas established along four mutually perpendicular radials, at distances of 70 to 550 m from the truck.

For the second experiment, called the Trench Storage Validation Test, a trench 3.7 m wide was excavated to a depth of 1.5 m. The central portion of the trench was 12.8 m long, with ramped excavations extending from each end of the central portion up to the ground surface, at a slope of about five percent. Timber posts, measuring 20 by 20 cm in cross-section, were used to frame the sides and roof of the cover structure in the central portion of the trench. Wooden planks measuring 5 by 20 cm in cross-section were installed against the sides and on the top of the timber frame. The soil excavated from the trench was then placed against the sidewalls and to a depth of 75 cm over the top of the cover structure.

For the Trench Storage Validation Test, a single truck was loaded with projectiles and propellant, as in the Control Data Test, and parked inside the trench cover (see Figure 3). Airblast and debris measurements were made for the Trench Validation Test in the same manner as in the Control Data Test, except that debris samples were taken along only the two radial lines of the airblast gages; i.e., a 0-degree line (along the trench axis), and a 90-degree line (normal to the axis).

The third and final experiment was called the Two-Truck Trench Test, and was designed to see if two trucks could be parked end-to-end in the same trench, without one being sympathetically detonated by an accidental explosion of the other. For this experiment, the covered portion of the trench was about 27 m long. At the center of the trench, a floor-to-ceiling barrier wall was constructed to separate the trucks. The barrier was made of two plywood panels, separated 1.2 m apart at the top and 2.4 m at the base, with sand filled in between them.

As shown in Figure 4, three lines of airblast gages were used for the Two-Truck Trench Test; one normal to the trench axis and one parallel to the axis, both extending from the center of the detonated (donor) truck, and one parallel to the trench axis but extending in the opposite direction, from the undetonated (acceptor) truck. Figure 5 shows the layout of the debris sample areas for the Two-Truck Trench Test.

To provide further information on the detonation process (for the donor ammo load) and the blast environment (for the acceptor ammo truck), two additional sets of measurements were made. Time-of-arrival gages were attached to projectiles around the perimeter of the donor load in an attempt to measure the velocity with which the detonation propagated through the ammo stack. Self-recording gage packages were also used to measure the blast overpressures experienced by the acceptor ammo load.

## TEST RESULTS

### a. Airblast Effects.

Figure 6 shows the peak airblast pressures, as a function of distance, recorded for the Trench Validation Test. These results are compared with the averaged values (i.e., average for the two radial lines) from the Control Data Test. It is clear that the trench cover suppressed the close-in blast pressures normal to the trench axis. However, the reduction in pressure decreased from a maximum reduction of over 90 percent just outside the trench cover slope, to only about a 30 percent reduction at a distance of 100 m, compared to the pressures measured without a trench.

Figure 7 shows the range of airblast peak pressures recorded on the Two-Truck Trench Test, compared to both the Control Data Test and the Trench Validation Test. For the Two-Truck Trench Test, the peak pressures extending out from the donor truck along the trench axis (0 degrees) were almost identical to those measured along the same axis in the previous tests. In the opposite direction for the Two-Truck Test, however, the pressures along the axis extending from the acceptor truck (180 degrees) were much lower than any previous measurements. At the close-in distances (less than 100 m), the pressures normal to the trench axis (90 degrees) for the Two-Truck Trench Test were also somewhat lower than similar measurements for the Trench Validation Test.

### b. Debris Effects.

The fragment and debris sample data from the three full-scale experiments showed a considerable degree of scatter, as can be seen in Figure 8 for the Two-Truck Trench Test. By drawing a curve through the mean of the data, however, the effect of the trench structures on the average debris densities at different ranges could be seen. Figure 9 compares the average debris densities, as a function of distance, for the Two-Truck Trench Test and the Control Data Test. While the trenches produced a greater density of debris impacts at the close-in ranges (less than 100 m), there was a clear reduction at greater ranges. Using the criterion of one hazardous impact per  $56\text{ m}^2$ , the debris hazard distance for the Two-Truck Trench Test was about 270 m, compared to 450 m for the Control Data Test. This represented a Q-D reduction of about 40 percent.

### **c. Acceptor Truck Damage**

In the Two-Truck Trench Test, peak airblast pressures of about 200 kPa (30 psi) were recorded at the rear of the acceptor ammo truck, just behind the sand wall separating the acceptor truck from the donor truck. A peak pressure of 30 kPa (4.5 psi) was measured on top of the acceptor ammo stack. The force of the blast was sufficient to push the acceptor truck about 10 m forward, and to throw most of the munitions off the truck. Except for a few dents in the propellant canisters, however, there was little damage to the acceptor munitions.

## **CONCLUSIONS**

The study indicated that covered trenches are relatively simple to design and easy to construct as an expedient storage method for ammo trucks at field sites. The technique appears to be ideally suited for dry, desert environments, but construction and use may be more difficult in temperate zones, where the soil may be wet.

The explosion hazard measurements indicate that the safe separation distances presently required for open storage of ammo trucks (to prevent sympathetic detonations) can be reduced by 55 to 90 percent using trench storage. There is also a 30 to 40 percent reduction in the Q-D for personnel safety. Table 1 summarizes the Q-D reductions provided by trench storage, compared to the present standards for unbarricaded and barricaded storage.

In addition to suppression of explosion hazards, trench storage offers several other benefits in combat areas. In deserts or other regions of long-range visibility, the ammo trucks are extremely difficult to detect by enemy observation. The trench cover also provides excellent protection against direct hits by enemy artillery or mortar fire, and against near-miss detonations of air-delivered weapons.

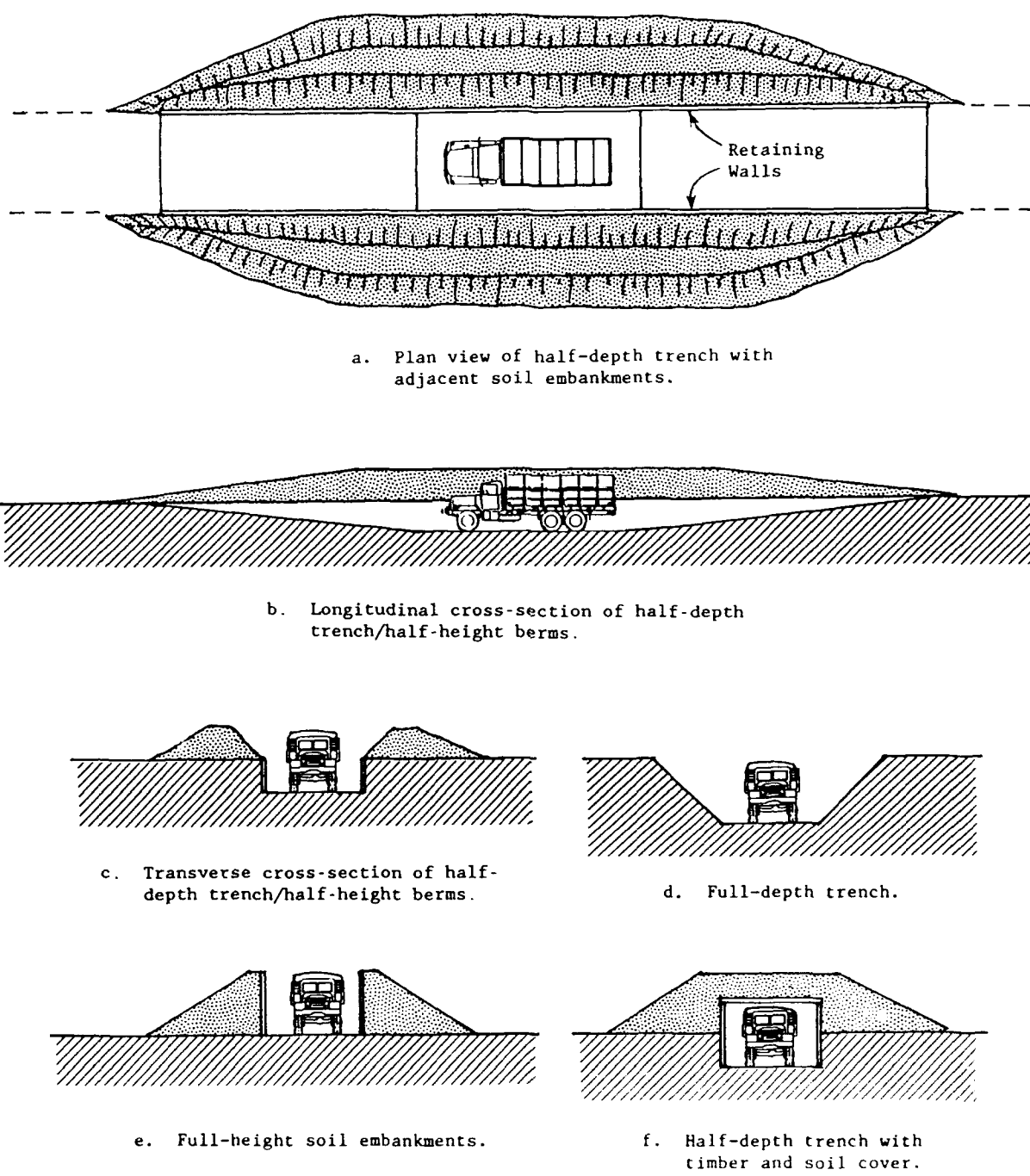


**Figure 1.** Trench design variations identified for evaluation for field storage of ammunition trucks.

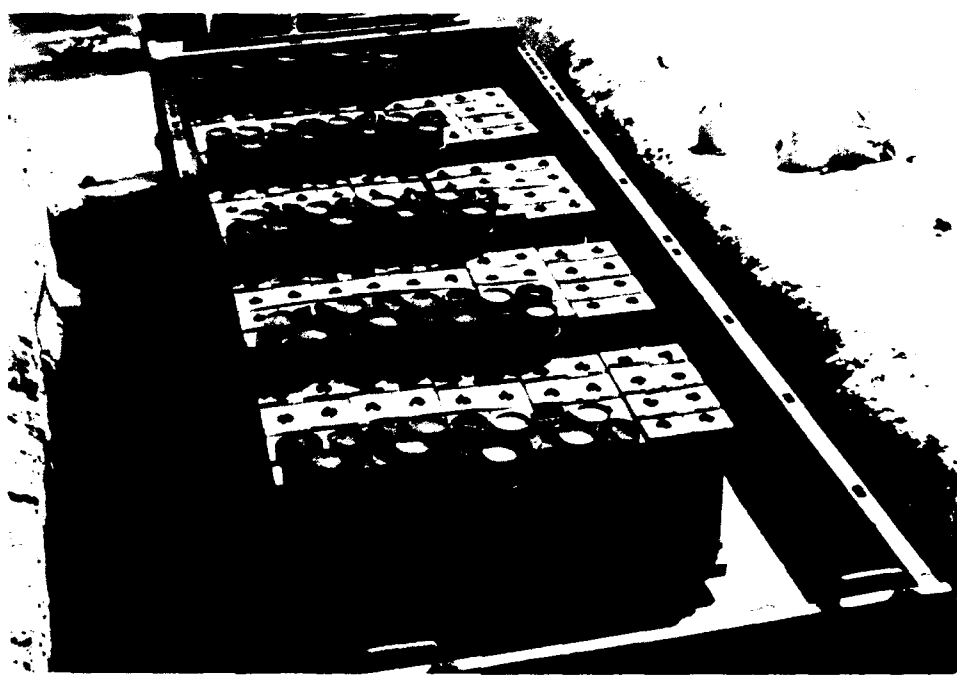


Figure 2. Placement of Unit Basic Load of 155-mm projectile pallets and propellant canisters on truckload for trench storage tests.



Figure 3. Ammo truck being backed into covered trench structure.

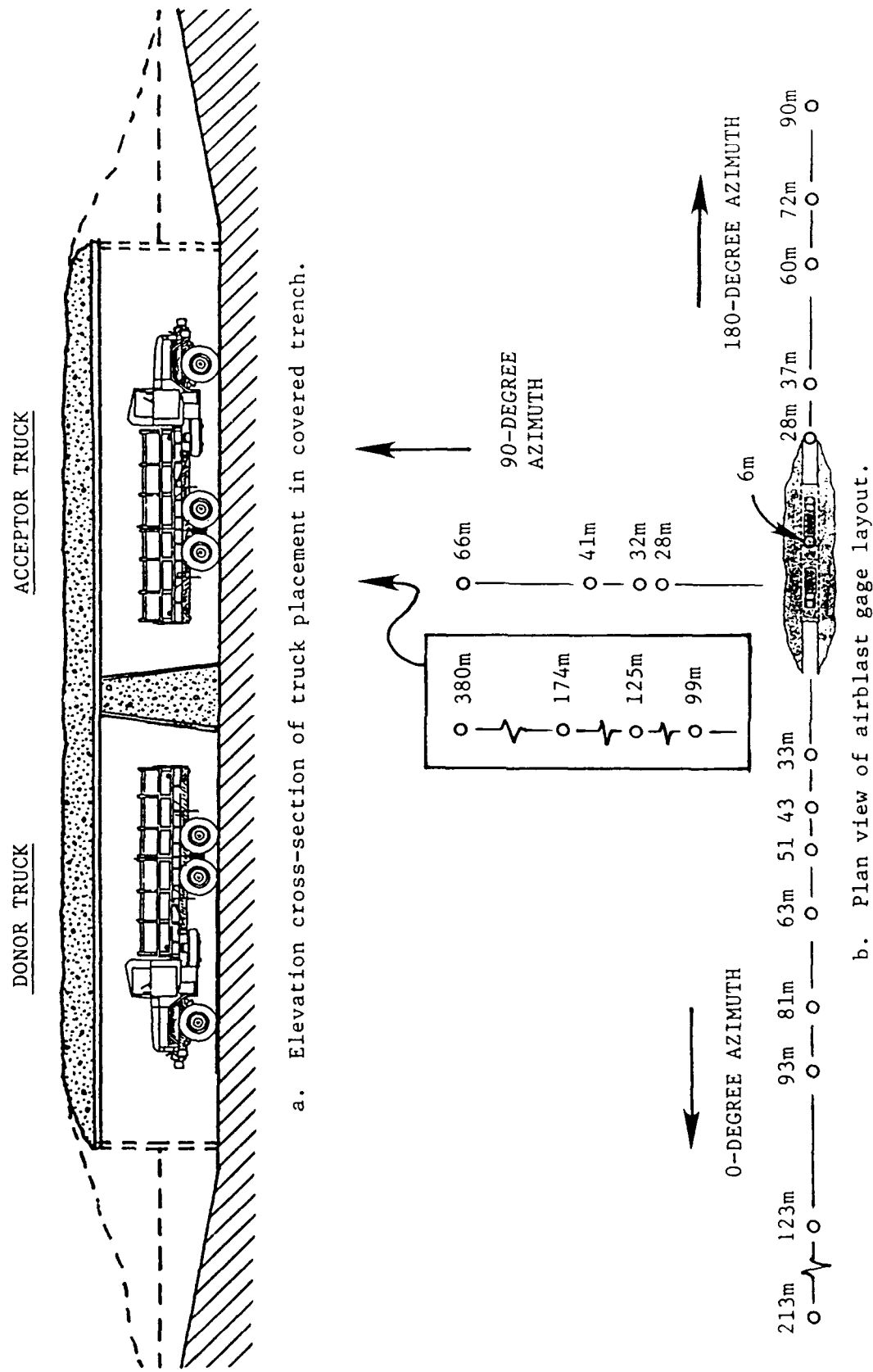


Figure 4. Design of Two-Truck Trench Test and airblast gage locations.

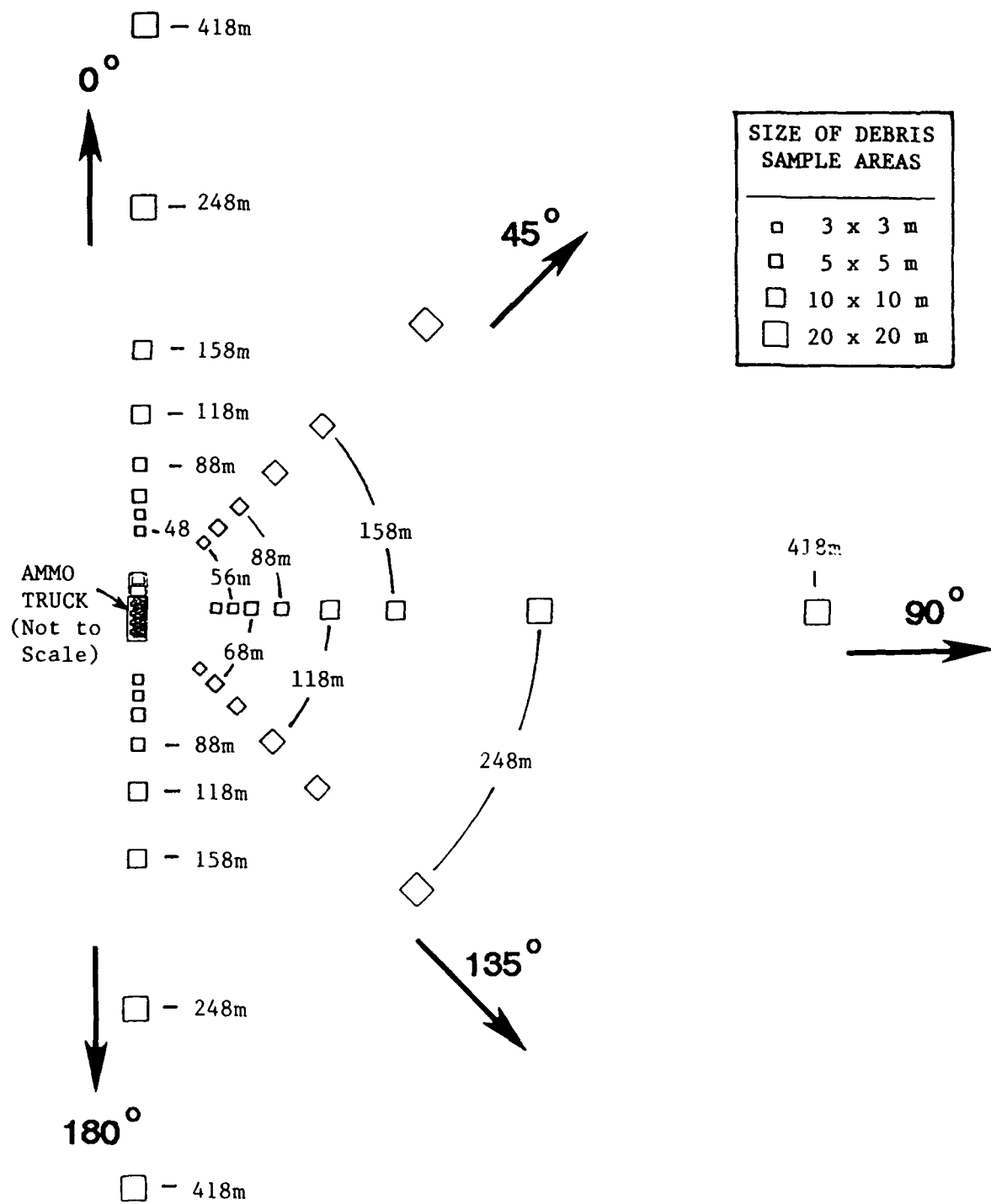


Figure 5. Layout of pre-established fragment/debris sampling areas for the Two-Truck Trench Test.

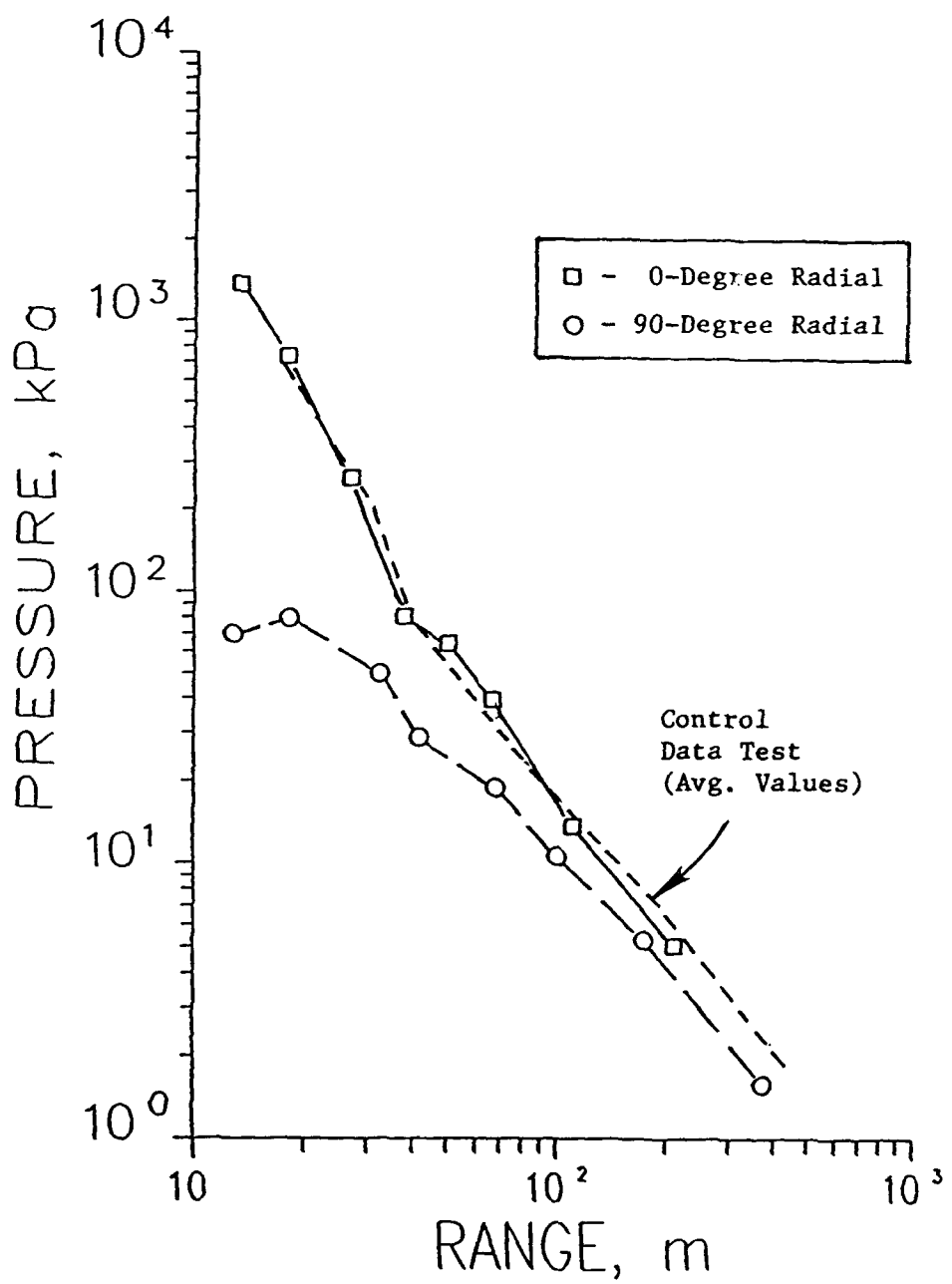


Figure 6. Attenuation of airblast peak pressures with range along the 0-degree (parallel to trench axis) and 90-degree (normal to trench axis) radials for the Trench Validation Test.

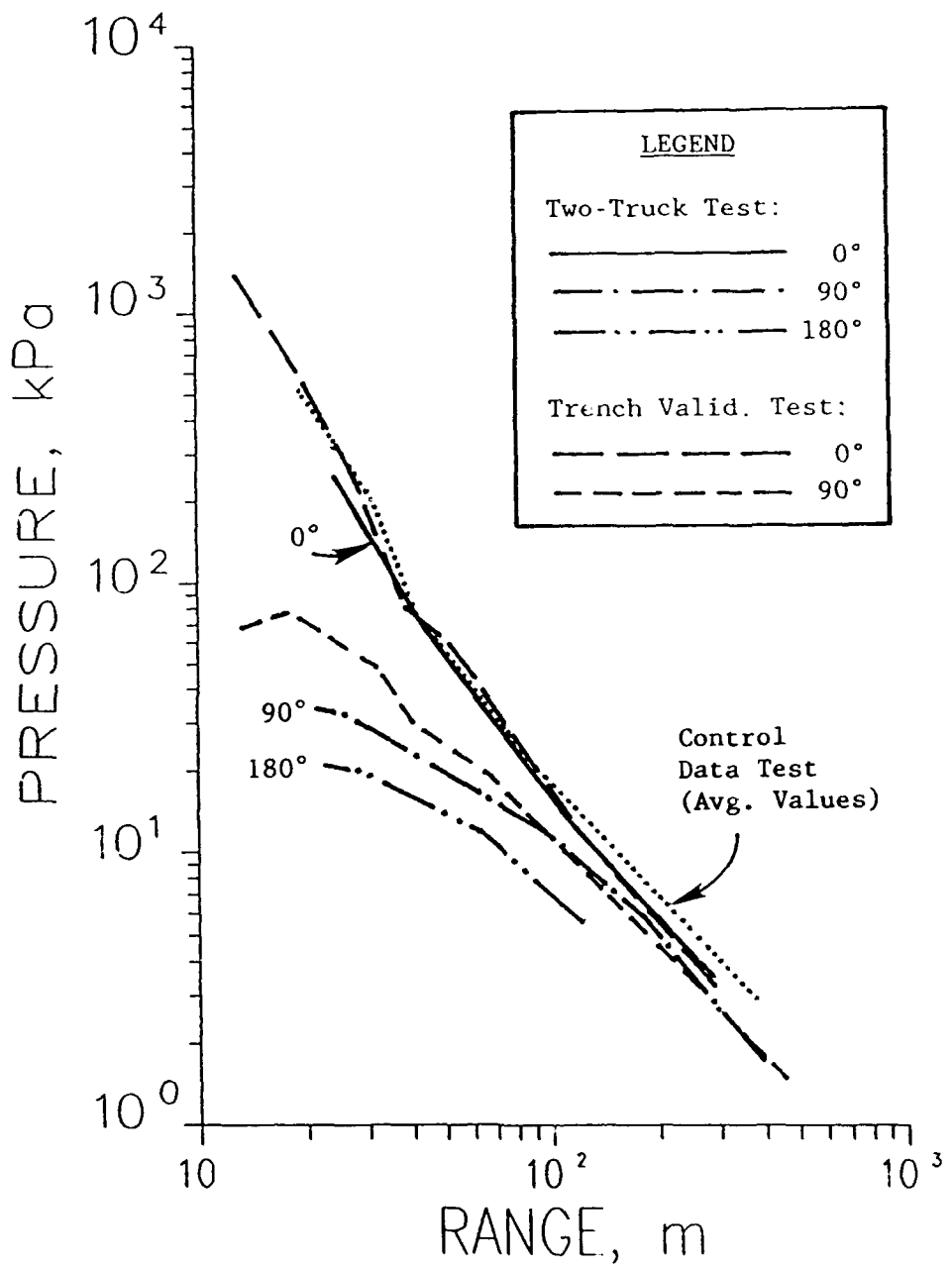


Figure 7. Peak airblast pressures from the Two-Truck Trench Test compared to those from the Trench Validation Test (single-truck trench) and Control Data Test (no trench).

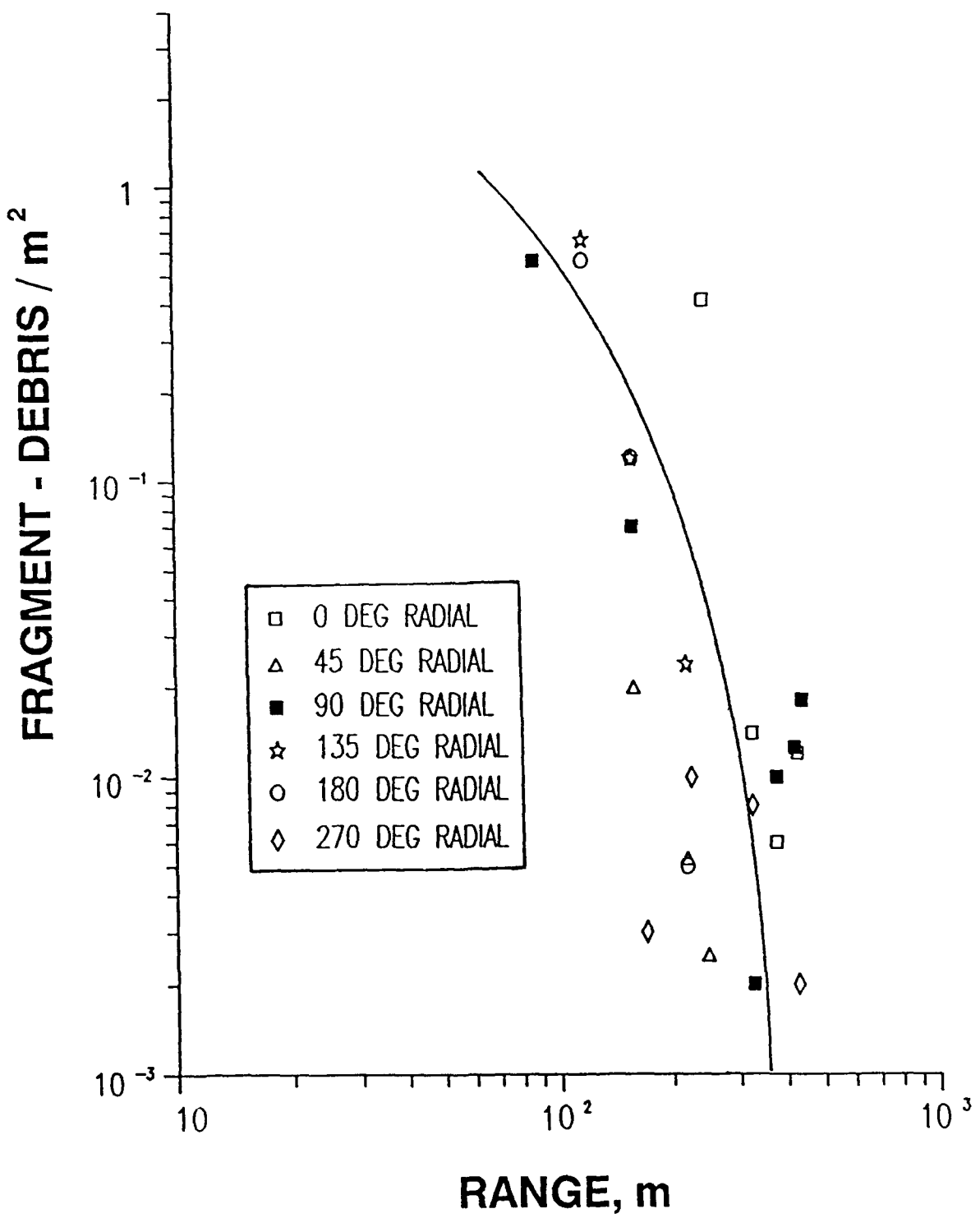


Figure 8. Areal Density (impacts per square metre) of fragments and debris as a function of range for the Two-Truck Trench Test. The curve is drawn through the mean spread of the data points.

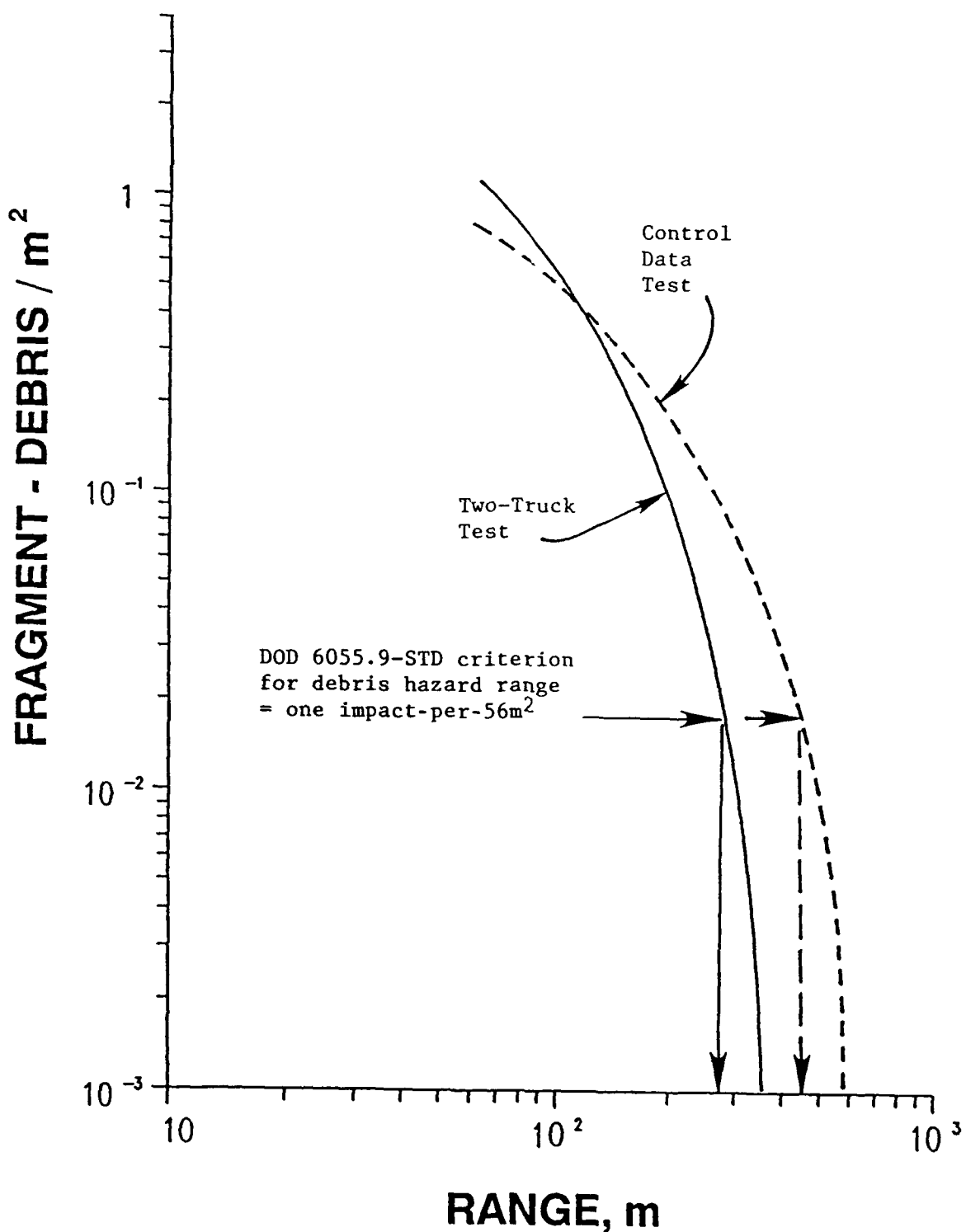


Figure 9. Average debris density versus range for Two-Truck Test compared to Control Data Test. Arrows indicate hazard ranges as defined by current safety standards.

**TABLE 1**  
**QUANTITY-DISTANCE REDUCTIONS**  
**FOR FIELD STORAGE OF UNIT BASIC LOADS**  
**ACHIEVED BY TRENCH STORAGE**

**QUANTITY-DISTANCES:**

	<u>Unbarricaded Storage</u>	<u>Barricaded Storage</u>	<u>Trench Storage<sup>a</sup></u>
<b><u>Safe Separation Distance:</u></b>	187 ft	33 ft	15 ft
Reduction -	92%	55%	
<b><u>Exposed Personnel - Airblast:</u></b>	268 ft	268 ft	170 ft <sup>b</sup>
Reduction -	40%	40%	
<b><u>Exposed Personnel - Fragments:</u></b>	1,480 ft <sup>a</sup>	1,480 <sup>a</sup>	900 ft
Reduction -	40%	40%	
<b><u>Inhabited Building Distance:</u></b>	885 ft	885 ft	625 ft
Reduction -	30%	30%	

<sup>a</sup> Measured on Trench Storage Tests. All other distances are taken from Chap. 10, DOD 6055.9 - STD.

<sup>b</sup> Normal to trench axis.

# **HAZARDS FROM UNDERWATER EXPLOSIONS**

by

Michael M. Swisdak, Jr.  
and  
Paul E. Montanaro

## **ABSTRACT**

The airblast and fragmentation produced in air by underwater explosions has been reexamined and reanalyzed. The data were examined with the following questions in mind: (1) At what range does the Inhabited Building Distance (1.2 psi) and the Public Withdrawal Distance (0.07 psi) occur? (2) What are the fragmentation characteristics (velocity, launch angle, dispersion, mass) produced by underwater explosions? Both goals were met. A series of equations relating overpressure to scaled depth and scaled distance are derived and presented. Similarly, equations relating fragmentation characteristics to scaled depth are derived.

## **INTRODUCTION**

Recently, there has been an increased interest in using both water-filled quarries and man-made ponds for underwater explosion testing. This has led to questions which must be answered for any new facility: (1) What is the Inhabited Building Distance? (2) What is the Public Withdrawal Distance? and (3) What are the fragmentation characteristics produced by the tests?

To answer these questions, the Department of Defense Explosives Safety Board asked the Naval Surface Warfare Center to review the available data and then to propose empirically-based prediction methodologies. This paper describes the result of that effort.

## **AIRBLAST**

The airblast produced by underwater explosions is a complicated phenomenon. In general a multi-pulse wave train is produced. Depending upon the scaled depth of burst (depth divided by the cube root of an effective charge weight), the scaled range (range divided by the cube root of an effective charge weight), and the type of explosive either the first, second, and sometimes later pulses may have the largest amplitude. At some depths the maximum pulse is produced by the underwater

explosion shockwave. At other depths, the maximum-amplitude pulse is produced by the oscillating explosion-products bubble. In a rigorous treatment, the amplitude and location of the pulses is also determined by the height above the surface at which the measurement is taken; i.e., at the same scaled range, gauges at two different heights may experience significantly different pulse forms.

For the purposes of this study, the only parameter of interest is the maximum pressure as a function of scaled depth and range. The range is the slant range between the point on the water surface above the detonation and the measurement point. Figure 1 is a sketch defining these parameters.

The original data were collected over a span of about 15 years by several agencies; most of the data, however, was collected by the Naval Ordnance Laboratory (now part of the Naval Surface Warfare Center). The data were collected in the following manner: An explosive charge of known weight and composition was detonated at a given depth. Airblast was measured at various heights and ranges above the water surface. Figure 2 is a sample for one depth of burst. As was indicated above, only the maximum pressure as a function of range is of interest. Figure 3 shows this sub-set of the Figure 2 data. For each scaled charge depth, a separate graph of maximum pressure versus scaled range was generated. For each such graph, a power law of the form:

$$P = A \cdot Z^b \quad (1)$$

was fitted to the data using the method of least squares.

Here

P = maximum pressure (psi)

Z = scaled range ( $\text{ft}/\text{lb}^{1/3}$ ) (range divided by the cube root of an effective charge weight)

A, b = fitting constants (A=Coefficient, b=Slope)

A sample of this type of curve fit is also shown in Figure 3. The results of these curve fits (values of A, b) and a measure of the goodness of fit generated by the least squares fitting process are shown in Table 1.

An examination of the value for the slope of the fit ("b" in the equation shown above) indicates that it approaches a value of 1 as the scaled depth of burst increases. This indicates that as the explosion source is moved deeper, the airblast decay approaches that of an acoustic wave with an amplitude proportional to  $1/Z$ .

In the original data, the low pressure measurements were made at extremely long ranges (on the order of miles) because of the charge weights involved.

Propagation over long ranges always introduces weather-induced variations. To provide additional data in this regime which would not be as greatly affected by weather, a series of measurements was undertaken on a recent underwater test series. Here, the charge weights, depths, and ranges were such that the pressure levels of interest occurred at ranges of under 500 feet. Propagation over these shorter distances minimizes the effects of weather. In these tests, the scaled depth was greater than  $10 \text{ ft/lb}^{1/3}$ . Based on the information in Table 1, at this depth, the wave should exhibit acoustic decay ( $1/Z$ ). This was assumed in the analysis. The raw data are presented in Table 2. The average coefficients determined from these data were added to those given in Table 1. This complete data set is presented in Table 3 and forms the basis for the development of the prediction equations. Table 3 is based upon data taken from several different types of explosives. These differences must be taken into account in any analysis. Table 4 presents a Weight Factor for each explosive. This Weight Factor is related to the underwater explosion bubble energy. When the actual explosive weight is multiplied by this Weight Factor, an effective charge weight is produced. This effective charge weight is then used in all subsequent calculations.

An examination of Table 3 indicates that both the Coefficient and Slope vary with scaled charge depth. Curve fits were made to both parameters as a function of scaled charge depth. These are shown in Figures 4 and 5. These curve fits were then used to generate Table 5. Either Table 5 or the curve fits shown in Figures 4 and 5 can be used to generate the airblast as function of depth and range.

For each scaled depth of interest, determine (from Table 5 or Figures 4 and 5) a coefficient and slope. These are then used in an equation of the form:

$$P = \text{Coefficient} * \text{Scaled Range}^{(\text{slope})}, \quad (2)$$

where P is maximum pressure in psi and scaled range is in  $\text{ft/lb}^{1/3}$ .

These equations are valid over the following range:

$$0.3 \text{ ft/lb}^{1/3} \leq \text{scaled depth} \leq 20 \text{ ft/lb}^{1/3}$$

$$4.0 \text{ ft/lb}^{1/3} \leq \text{scaled range} \leq 100 \text{ ft/lb}^{1/3}.$$

As an example, determine the airblast at a range of 200 feet from the detonation of 1000 pounds of HBX-1 at a depth of 10 feet. For this same depth of burst and charge weight, determine the inhabited building range (1.2 psi) and the public withdrawal distance (0.07 psi). From Table 4, the Weight Factor is 1, so the effective weight is 1000 pounds. The scaled depth is  $1.0 (10/(1000))^{1/3} \text{ ft/lb}^{1/3}$  and the scaled range is  $20 (200/(1000))^{1/3} \text{ ft/lb}^{1/3}$ . Entering Table 5, we find that the coefficient and slope are 11.63 and -1.02. Thus our prediction equation becomes:

$$P = 11.63 \cdot Z^{-1.01}.$$

At a scaled range (Z) of 20 ft/lb<sup>1/3</sup>, the predicted maximum pressure is 0.56 psi. This same prediction equation can be used to determine the ranges to 1.2 and 0.07 psi. The Inhabited Building Distance (range to 1.2 psi) would occur at a scaled range (Z) of 9.48 ft/lb<sup>1/3</sup>; this corresponds to an actual range of 94.8 feet. The Public Withdrawal Distance (range to 0.07 psi) occurs at a scaled range of 157.9 ft/lb<sup>1/3</sup>, corresponding to an actual range of 1579 feet. It must be pointed out however, that this prediction for public withdrawal distance is outside the validity range of the prediction equations and, therefore, must be used cautiously. It should be further noted that the prediction equation is designed to give the maximum pressure. Actual measurements at the specified location may be lower.

## FRAGMENTATION

Previously, the throw of case fragments into the air from underwater detonations has, generally, been ignored. Statements such as "fragmentation was not considered" or "our experience is that we don't have a problem" have often been the rule.

Although considerable effort has gone into the study of fragmentation by weapons designed to explode in the air or the ground, very little information is available concerning fragmentation produced by underwater detonations. The only available data were generated during the investigation of the fragmentation produced by shallow explosions of MK 82 general purpose bombs. This extremely limited data set forms the basis for the prediction equations developed below.

In general, as the explosion source is moved deeper, the fragmentation problems are lessened--the launch velocities decrease (the fragments must travel through more water) and the fragment ejection angle becomes smaller. In order to describe the fragmentation, the following information is needed: vertical fragment velocity as a function of scaled depth of burst, the variation of the fragment velocity with launch azimuth, the maximum launch azimuth as a function of scaled depth of burst, and a description of the fragments (shape and mass). Descriptors for each of these will be developed in the following paragraphs. Figure 6 is a sketch defining the variables involved. It is based on the MK 82 tests from which most of the data are derived.

Figure 7 presents the variation in the vertical fragment velocity with scaled depth of burst. The two end points were not part of the original data set. At a zero depth of burst, the charge is half in the air and half in the water. Thus, the fragment velocity is simply the measured fragmentation velocity in air--approximately 8200 ft/s for a MK 82 bomb. The point at a scaled depth of 4 corresponds to evidence that for

scaled depths greater than about  $4 \text{ ft/lb}^{1/3}$ , there is no appreciable fragmentation. Also shown on the figure is a least squares curve fit to the data; this will be used for prediction purposes.

Figure 8 gives the variation of the fragment velocity as a function of launch azimuth. The data have been normalized to 1 for an azimuth of  $0^\circ$  (N.B.:  $0^\circ$  azimuth is vertical). As the scaled depth increases, the maximum azimuth angle decreases. This variation is shown in Figure 9. The two end points have been added to the data set. At the surface (scaled depth of zero), the fragments can come out in all  $90^\circ$  of azimuth. At a scaled depth of 4, other data indicate that, very few fragments escape. At the intermediate azimuths, Figure 9 gives the maximum azimuth at which the fragments can escape the water.

It must be pointed out, however, that the prediction equations generated in Figures 7-9 are for MK 82 bombs loaded with H-6 explosive. When the explosive is changed, the maximum velocity will also change. A velocity factor, derived from the Gurney Constant for each explosive composition is given in Table 4.

The fragments produced by underwater detonations are much larger than those produced by corresponding detonations on the surface. In the MK 82 underwater detonations, the fragments were long "spear-like" fragments rather than the usual chunky fragments. The worst-case fragments had length-to-width ratios of approximately 14, with a length approximately equal to the length of the cylindrical section of the bomb. Analysis indicated that these fragments, although spear-like, were best described with a Fragment Shape Factor of 0.25, indicating that, while spear-like, they are also tumbling.

There is now sufficient information to predict the fragmentation. For a given type explosive weight and charge depth, calculate the scaled depth of burst (actual depth of burst (measured to the center of gravity of the charge) divided by the cube root of the explosive weight). Using Figure 7, calculate the vertical fragment velocity. Next multiply this velocity by the velocity factor chosen from Table 4. This new velocity and Figure 8 gives the azimuthal velocity variation. Figure 9 is then used to determine the maximum azimuth angle. Determine the length of an equivalent cylindrical section of the explosive charge. A worst-case fragment has a length-to-width ratio of 14, so a width can be calculated. The fragment thickness should be taken as the thickness of the case. Knowing the case material, the weight of the fragment can then be calculated. The weight, velocities, and azimuths are then used as inputs to a trajectory program such as TRAJ<sup>1</sup>, to predict maximum fragment range.

Let us consider two examples. During the MK 82 bomb underwater tests (described above), the locations of fragments recovered outside the water were mapped. One such fragment, weighing 800 grams, was found at a range of 1952 feet. This was the maximum range of all the fragments recovered on that test. The

explosive weight was 192 pounds of H-6; the center of gravity of the weapon was 2.25 feet below the water surface. This depth corresponds to a scaled depth of 0.39 ft/lb<sup>1/3</sup> ( $2.25/(192)^{1/3}$ ). Using Figures 7-9, Table 6 can be generated as input for a trajectory program (TRAJ). The case material is steel and the fragment weight is 800 grams. The fragment shape factor is 0.25. The ranges determined by the trajectory program are also shown in Table 6. The maximum range is 1956 feet--matching almost exactly the measured range.

As a second example, let us consider the worst-case fragments produced by the detonation of a 1-to-1 cylinder of HBX-1 with an explosive weight of 10,000 pounds. The case thickness is 0.375" and the case material is steel. The depth of burst is 16 feet (measured to the center of the charge). A 1-to-1 cylinder containing 10,000 pounds of HBX-1 has a diameter of approximately 4.9 feet and a height of 4.9 feet. The scaled depth of burst is  $16/(10,000)^{1/3}$  or 0.74 ft/lb<sup>1/3</sup>. Since the charge is cylindrical, the length of the cylindrical section is simply the height--4.9 feet. If we assume that a worst-case fragment has a length-to width ratio of 14, then the width is  $4.9/14$  or 0.35 feet. The fragment thickness is the case thickness, 0.375 inches. Thus the fragment weighs 26 pounds. The input conditions derived from Figures 7-9 and Table 4 are shown in Table 7. Also shown on this table are the results of the trajectory calculations. The maximum fragment range is 2888 feet.

It must be remembered that the ranges determined using this method are the maximum ranges--not the ranges at which the hazardous fragment density reaches a value of 1 per 600 ft<sup>2</sup>.

#### REFERENCES

1. Montanaro, P. E., "TRAJ--A Two Dimensional Trajectory Program For Personal Computers," Minutes of the Twenty-Fourth DoD Explosives Safety Seminar, August 1990.

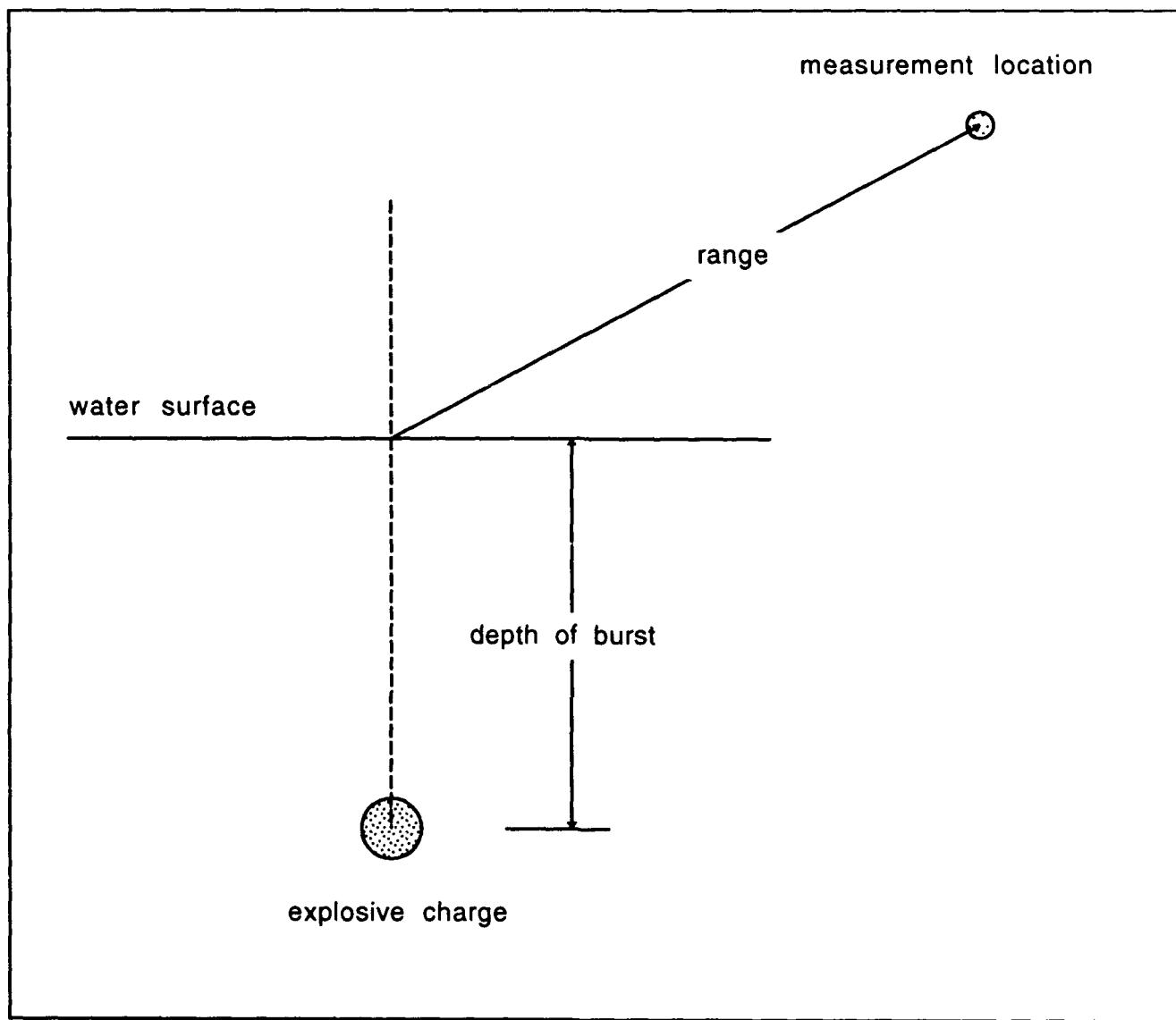
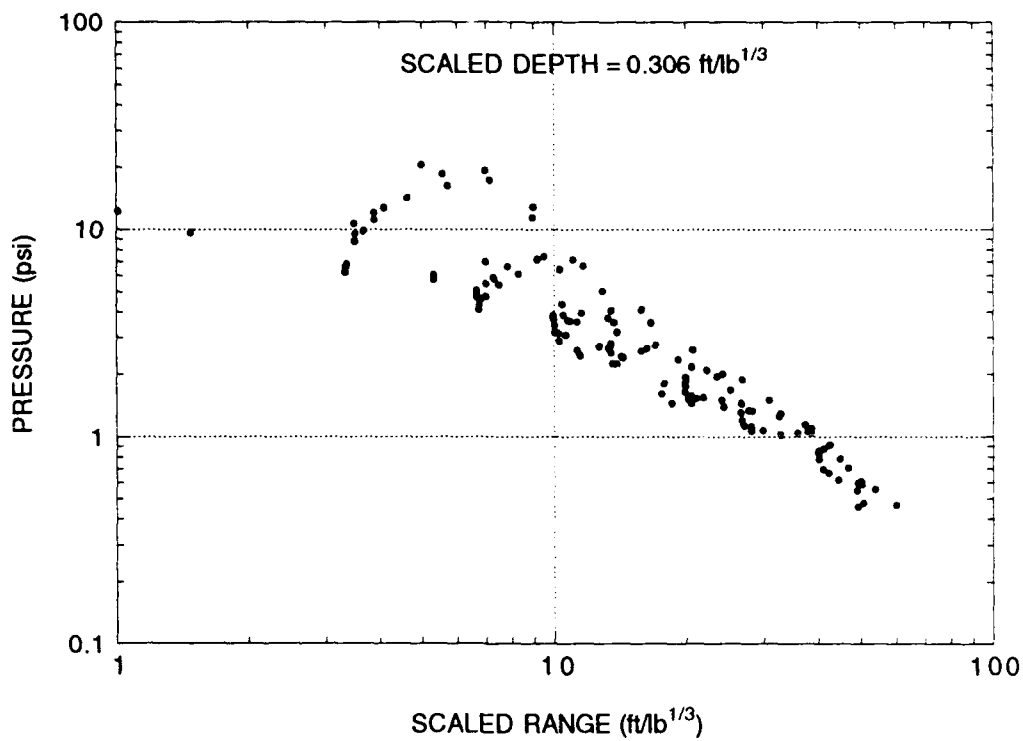
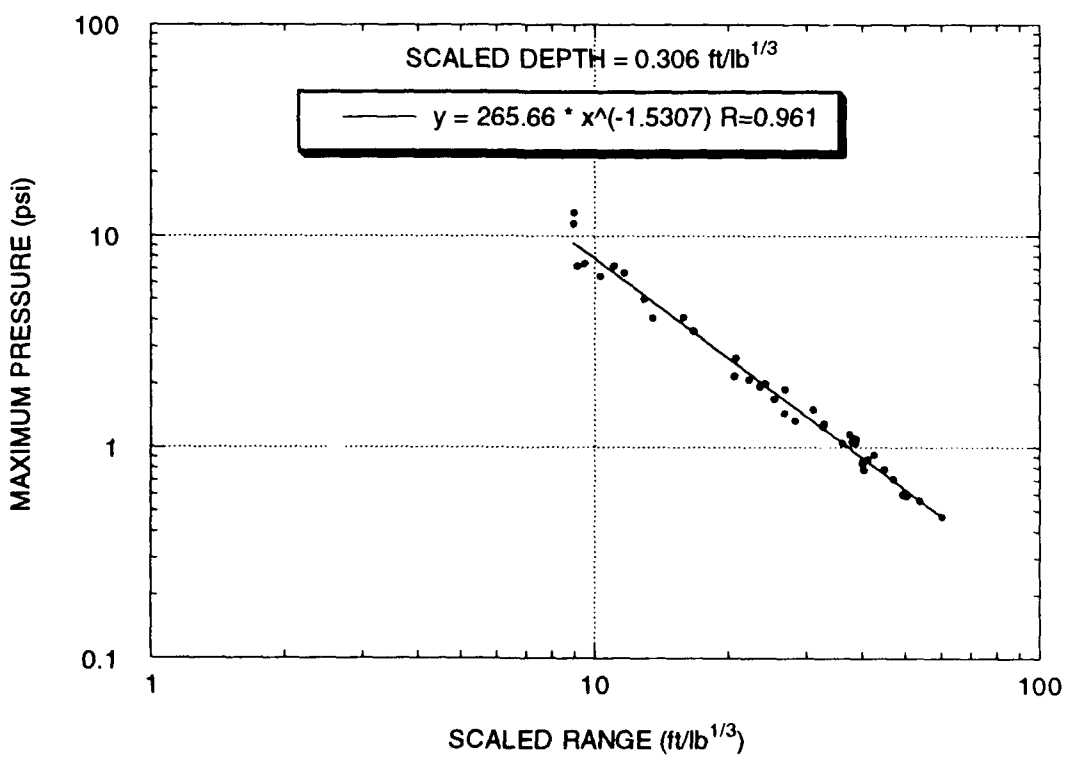


FIGURE 1 SCHEMATIC OF TEST ARRANGEMENTS

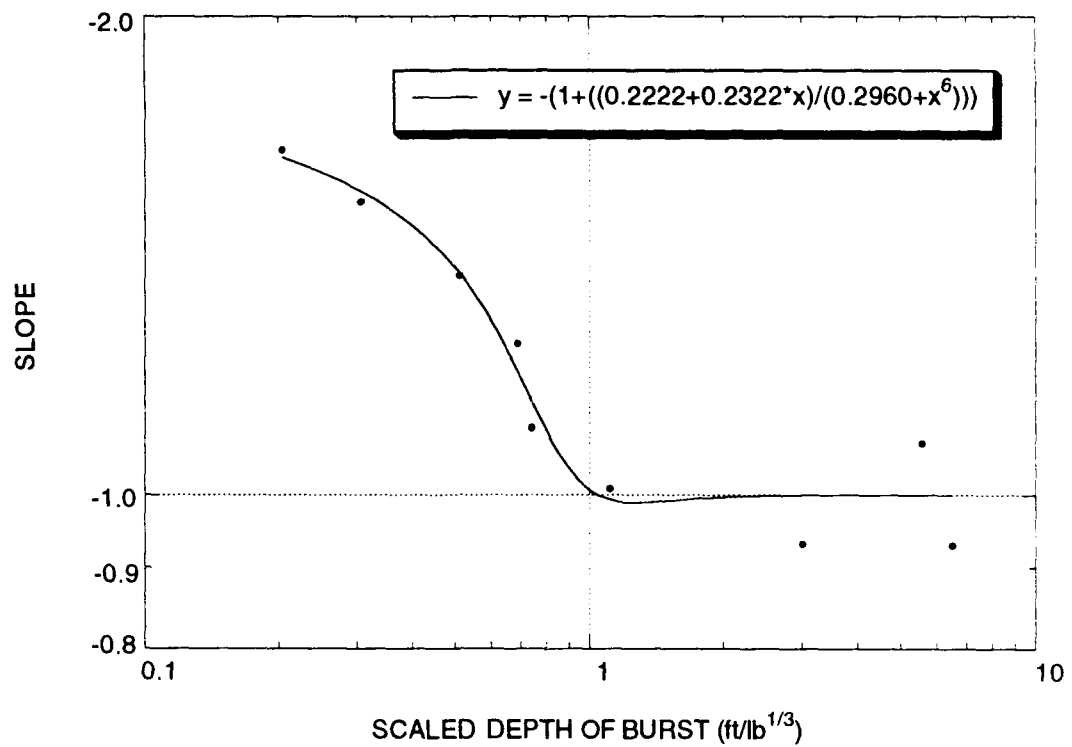
**FIGURE 2. PRESSURE VERSUS SCALED RANGE**



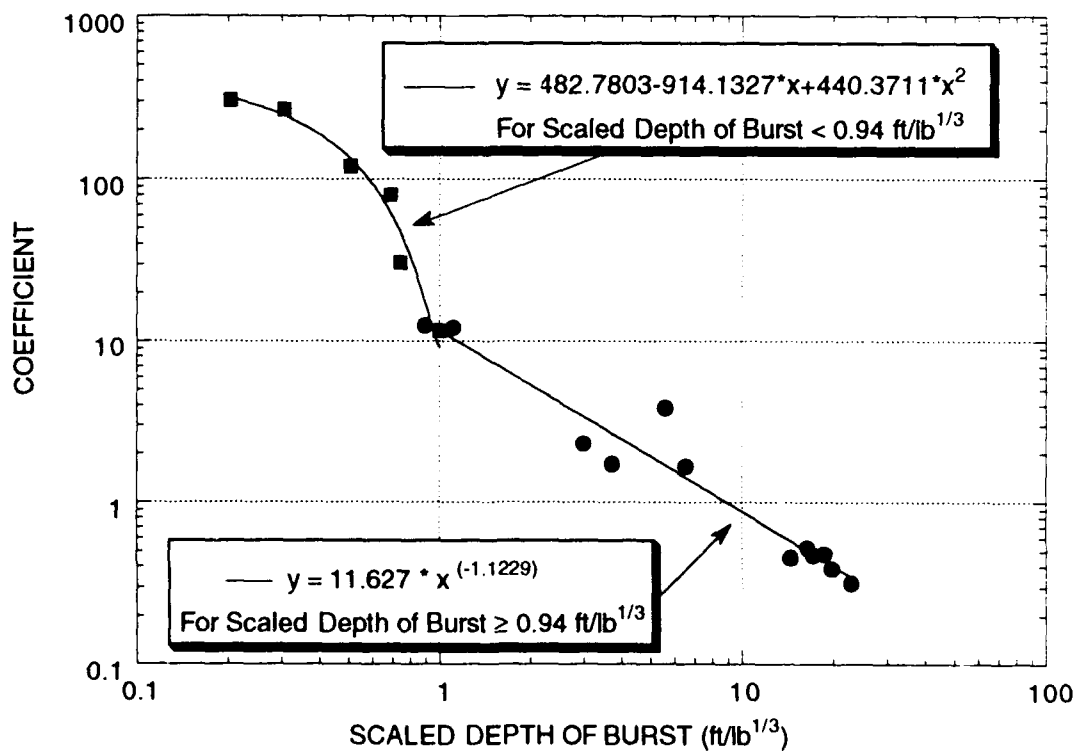
**FIGURE 3. MAXIMUM PRESSURE VERSUS SCALED RANGE**



**FIGURE 4. SLOPE VERSUS SCALED DEPTH OF BURST**



**FIGURE 5. COEFFICIENT VERSUS SCALED DEPTH**



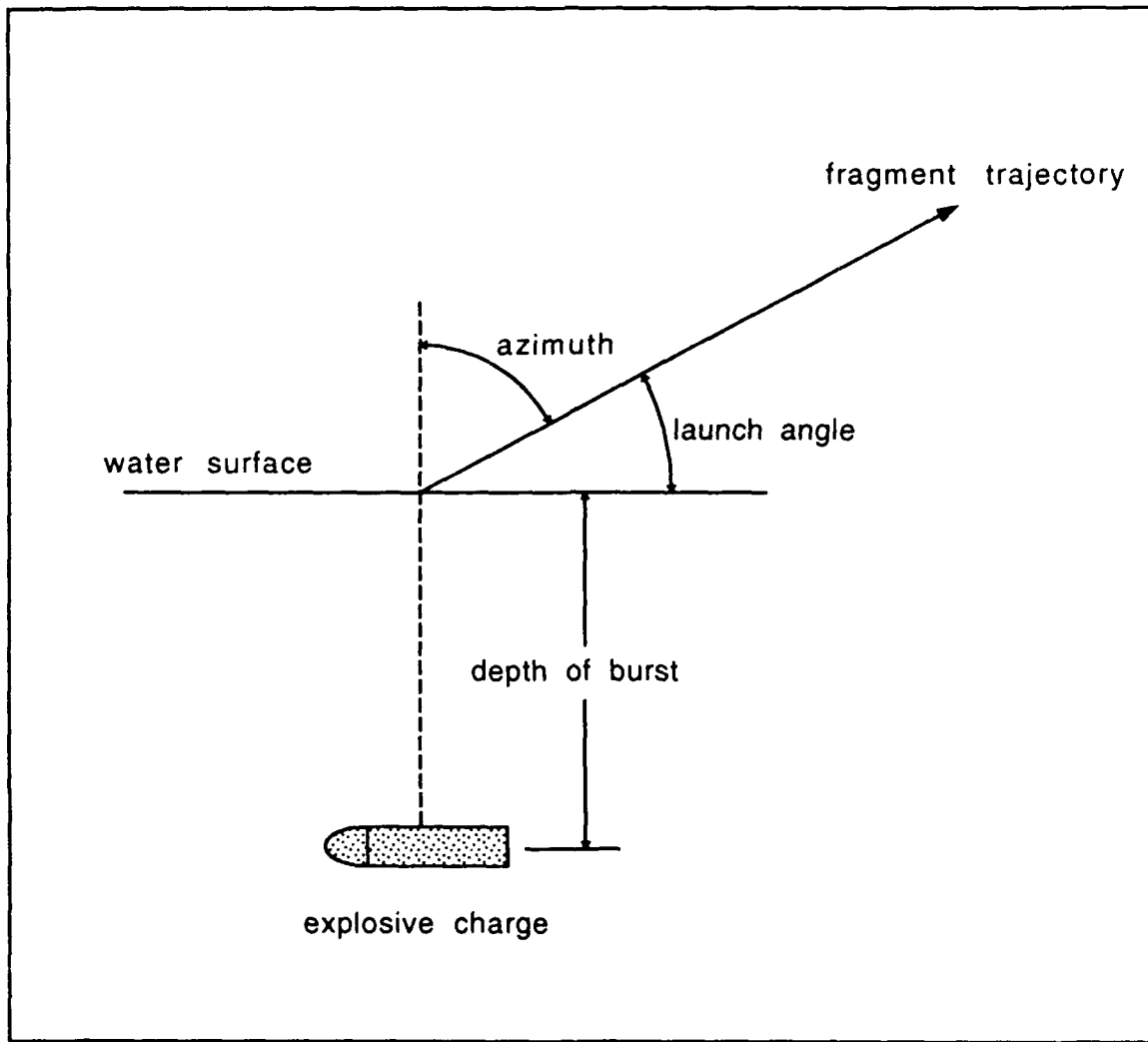
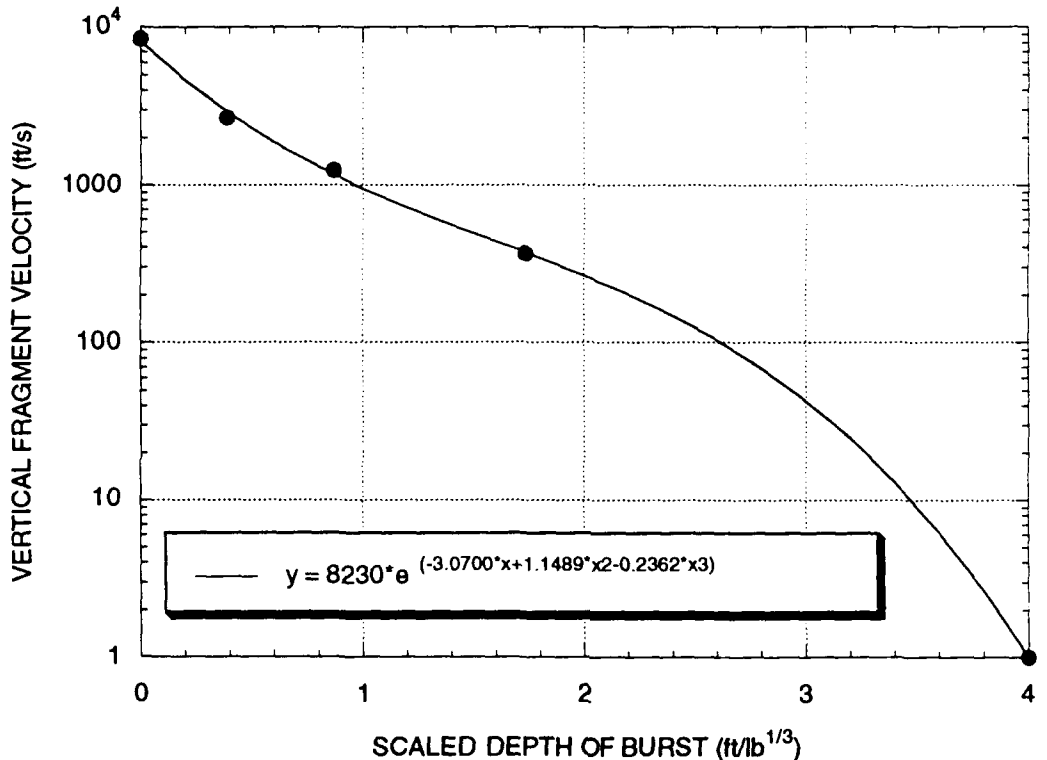
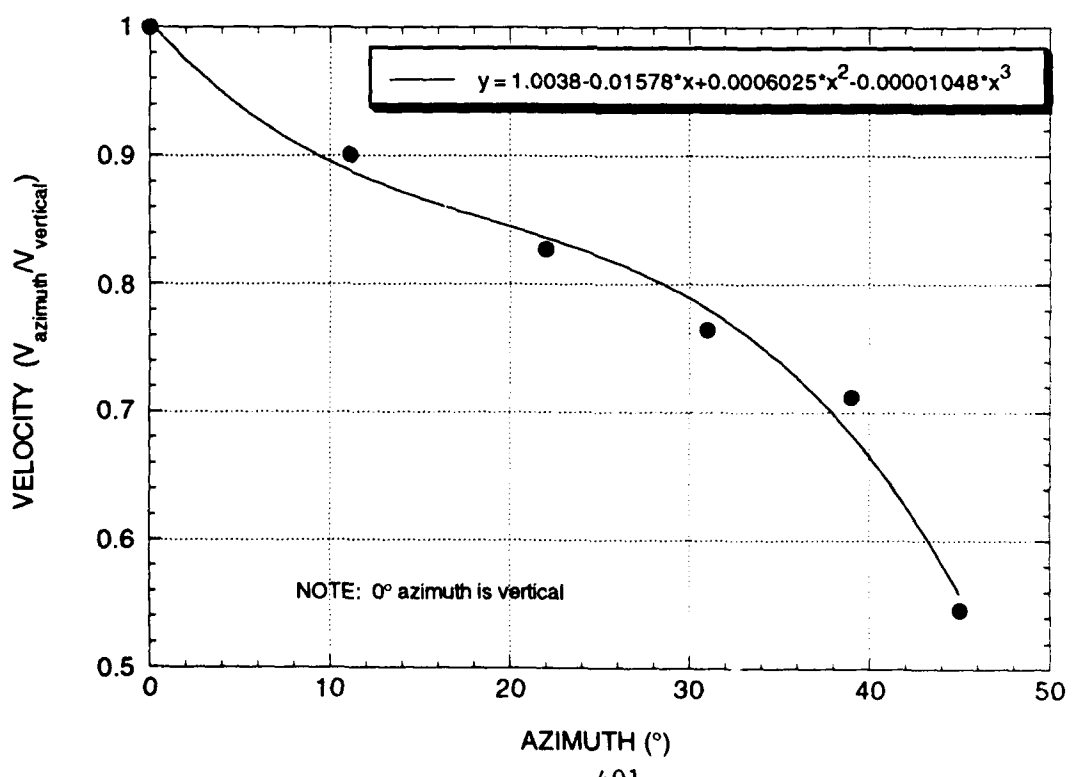


FIGURE 6. FRAGMENTATION FROM UNDERWATER EXPLOSIONS

**FIGURE 7. FRAGMENT VELOCITY VERSUS SCALED DEPTH OF BURST**



**FIGURE 8. FRAGMENT VELOCITY VERSUS AZIMUTH**



**FIGURE 9. MAXIMUM AZIMUTH ANGLE VERSUS SCALED DEPTH OF BURST**

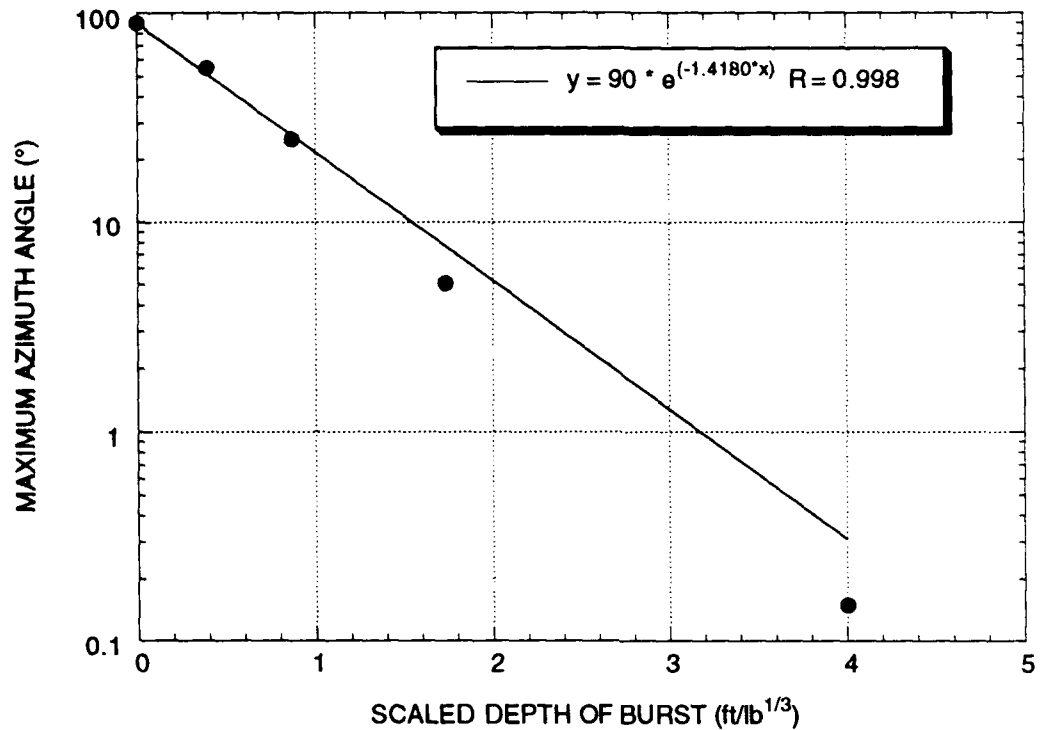


TABLE 1. CURVE FIT COEFFICIENTS

SCALED DEPTH OF BURST (ft/lb <sup>1/3</sup> )	COEFFICIENT	SLOPE	GOODNESS OF FIT
0.306	265.660	-1.531	0.961
0.509	119.370	-1.374	0.989
0.688	79.583	-1.246	0.974
0.740	30.647	-1.103	0.989
0.893	12.535	-1.020	0.997
1.110	12.149	-1.009	0.998
3.000	2.301	-0.931	0.898
3.713	1.717	-0.819	1*
5.570	3.846	-1.078	1*
6.498	1.657	-0.930	1*

\*limited data

NOTE: For each depth, P=coefficient\*scaled range ^ (slope)

TABLE 2. QUARRY AIRBLAST

Charge Weight (lb)	Booster Type	Booster Weight (lb)	Charge Depth (ft)	Maximum Pressure (psi)	Weight Factor	Eff. Charge Weight (lbs)	Scaled Depth (ft/lb <sup>1/3</sup> )	Scaled Range (ft/lb <sup>1/3</sup> )	Coefficient	Average Coefficient
27.28	Pentolite	2.901	50	0.00606	1.53	44.56	14.1	60.5	0.367	
27.11	Pentolite	2.865	50	0.00725	1.53	44.26	14.1	60.6	0.440	
26.36	Pentolite	2.822	50	0.00633	1.50	42.36	14.3	61.5	0.390	
26.09	Pentolite	2.831	50	0.00604	1.49	41.79	14.4	61.8	0.373	
25.80	Pentolite	2.820	50	0.00751	1.50	41.52	14.4	61.9	0.466	
25.58	Pentolite	2.854	50	0.00747	1.50	40.34	14.6	62.5	0.468	
24.93	Pentolite	2.803	50	0.00763	1.54	40.34	14.6	62.5	0.477	0.457
24.78	Pentolite	2.810	50	0.00682	1.54	40.11	14.6	62.7	0.428	
53.91	Pentolite	7.853	75	0.01120	1.70	96.85	16.3	46.7	0.523	
53.36	Pentolite	7.327	75	0.01123	1.70	95.55	16.4	46.9	0.527	
48.95	Pentolite	7.200	75	0.00943	1.65	85.67	17.0	48.7	0.459	
48.07	Pentolite	7.455	75	0.01024	1.65	84.39	17.1	48.9	0.501	
52.37	Pentolite	7.583	75	0.00935	1.50	83.79	17.1	49.0	0.458	
39.36	Pentolite	7.534	75	0.00944	1.66	70.62	18.1	51.9	0.490	
39.03	Pentolite	7.490	75	0.00949	1.66	70.04	18.2	52.0	0.494	
38.15	Pentolite	7.563	75	0.00829	1.48	61.67	19.0	54.3	0.450	
37.15	Pentolite	7.519	75	0.00875	1.48	60.16	19.1	54.7	0.479	
23.80	None	50	0.00489	0.69	16.42	19.7	84.4	0.412	0.389	
10.64	Pentolite	0.154	50	0.00429	1.50	16.07	19.8	85.0	0.365	
8.03	Pentolite	0.153	50	0.00336	1.50	12.15	21.7	93.3	0.314	
7.05	Pentolite	0.155	50	0.00287	1.50	10.68	22.7	97.4	0.280	
7.00	Pentolite	0.154	50	0.00285	1.50	10.61	22.8	97.6	0.278	
45.00	None		75	0.00586	0.69	31.05	23.9	68.2	0.400	

NOTE: COEFFICIENT = MAXIMUM PRESSURE \* SCALED RANGE

**TABLE 3. CURVE FIT COEFFICIENTS--DATA BASE**

SCALED DEPTH OF BURST (ft/lb <sup>1/3</sup> )	COEFFICIENT	SLOPE	GOODNESS OF FIT
0.306	265.660	-1.531	0.961
0.509	119.370	-1.374	0.989
0.688	79.583	-1.246	0.974
0.740	30.647	-1.103	0.989
0.893	12.535	-1.020	0.997
1.110	12.149	-1.009	0.998
3.000	2.301	-0.931	0.898
3.713	1.717	-0.819	1*
5.570	3.846	-1.078	1*
6.498	1.657	-0.930	1*
14.400	0.457	assumed to be -1	
16.400	0.525	assumed to be -1	
17.100	0.437	assumed to be -1	
18.600	0.478	assumed to be -1	
19.700	0.389	assumed to be -1	
22.800	0.318	assumed to be -1	

\*limited data

NOTE: For each depth, P=coefficient\*scaled range ^ (slope)

**TABLE 4. WEIGHT AND VELOCITY FACTORS**

EXPLOSIVE	WEIGHT FACTOR	VELOCITY FACTOR
TNT	0.69	0.87
PENTOLITE	0.69	0.98
HBX-1	1.00	0.94
HBX-3	1.30	0.84
H-6	1.14	1.00
PBXN-103	1.52	1.00
COMPOSITION C4	0.71	1.02
Other Plastic Bonded Underwater Explosives	1.5-1.72	0.8-1.2

**TABLE 5. AIRBLAST CURVE FIT CONSTANTS FOR VARYING SCALED DEPTHS OF BURST**

SCALED DEPTH	SLOPE	COEFFICIENT	SCALED DEPTH	SLOPE	COEFFICIENT
0.30	-1.56	248.17	3.00	-1.00	3.39
0.35	-1.52	216.78	3.20	-1.00	3.15
0.40	-1.48	187.59	3.40	-1.00	2.94
0.45	-1.43	160.60	3.60	-1.00	2.76
0.50	-1.39	135.81	3.80	-1.00	2.60
0.55	-1.34	113.22	4.00	-1.00	2.45
0.60	-1.29	92.83	4.20	-1.00	2.32
0.65	-1.24	74.65	4.40	-1.00	2.20
0.70	-1.19	58.67	4.60	-1.00	2.10
0.75	-1.14	44.89	4.80	-1.00	2.00
0.80	-1.10	33.31	5.00	-1.00	1.91
0.85	-1.06	23.93	5.50	-1.00	1.71
0.90	-1.04	16.76	6.00	-1.00	1.56
0.95	-1.02	12.32	6.50	-1.00	1.42
1.00	-1.01	11.63	7.00	-1.00	1.31
1.10	-0.99	10.45	7.50	-1.00	1.21
1.20	-0.99	9.48	8.00	-1.00	1.13
1.30	-0.99	8.66	8.50	-1.00	1.05
1.40	-0.99	7.97	9.00	-1.00	0.99
1.50	-0.99	7.38	9.50	-1.00	0.93
1.60	-0.99	6.86	10.00	-1.00	0.88
1.70	-0.99	6.41	11.00	-1.00	0.79
1.80	-1.00	6.01	12.00	-1.00	0.71
1.90	-1.00	5.66	13.00	-1.00	0.65
2.00	-1.00	5.34	14.00	-1.00	0.60
2.10	-1.00	5.06	15.00	-1.00	0.56
2.20	-1.00	4.80	16.00	-1.00	0.52
2.30	-1.00	4.56	17.00	-1.00	0.48
2.40	-1.00	4.35	18.00	-1.00	0.45
2.50	-1.00	4.16	19.00	-1.00	0.43
2.60	-1.00	3.98	20.00	-1.00	0.40
2.70	-1.00	3.81			
2.80	-1.00	3.66			
2.90	-1.00	3.52			

P=coefficient\*scaled range^(slope)

**TABLE 6. EXAMPLE 1--FRAGMENT RANGE**

DEPTH (ft)	CHARGE WEIGHT (lbs)	SCALED DEPTH (ft/lb <sup>1/3</sup> )	MAXIMUM AZIMUTH (°)	VERTICAL VELOCITY (ft/s)
2.25	192	0.39	52	2919
VELOCITY FACTOR = 1.0				
AZIMUTH (°)	AZIMUTH FACTOR	VELOCITY (ft/s)	LAUNCH ANGLE (°)	RANGE (ft)
0	1.00	2919	90	
5	0.94	2740	85	314
10	0.90	2615	80	621
15	0.87	2531	75	903
20	0.85	2467	70	1181
25	0.82	2400	65	1432
30	0.79	2305	60	1652
35	0.74	2161	55	1826
40	0.67	1944	50	1932
45	0.56	1631	45	1956
46	0.53	1555	44	1947
47	0.50	1474	43	1933
48	0.48	1388	42	1913
49	0.44	1297	41	1886
50	0.41	1200	40	1894
51	0.38	1097	39	1899
52	0.34	989	38	1897

**TABLE 7. EXAMPLE 2--FRAGMENT RANGE**

DEPTH (ft)	CHARGE WEIGHT (lbs)	SCALED DEPTH (ft/lb <sup>1/3</sup> )	MAXIMUM AZIMUTH (°)	VERTICAL VELOCITY (ft/s)
16	10000	0.74	31	1354
VELOCITY FACTOR = 0.94				
AZIMUTH (°)	AZIMUTH FACTOR	VELOCITY (ft/s)	LAUNCH ANGLE (°)	RANGE (ft)
0	1.00	1354	90	
5	0.94	1271	85	528
10	0.90	1213	80	1058
15	0.87	1174	75	1541
20	0.85	1144	70	2018
25	0.82	1113	65	2451
26	0.82	1105	64	2528
27	0.81	1097	63	2603
28	0.80	1089	62	2677
29	0.80	1079	61	2749
30	0.79	1069	60	2818
31	0.78	1058	59	2888

## EXTREMELY INSENSITIVE DETONATING SUBSTANCE TESTS

Kenneth J. Graham  
Atlantic Research Corporation  
5945 Wellington Road  
Gainesville, VA 22065

### ABSTRACT

The United Nations (UN) Committee of Experts on Transportation of Dangerous Goods approved a new test protocol (UN Test Series 7) and a new hazard class/division (C/D 1.6) in 1988. C/D 1.6 was developed to classify extremely insensitive explosive articles that contain only extremely insensitive detonating substances (EIDS) as determined by passing the criteria of UN Test Series 7. The United States Air Force has played a major role in advancing the development of EIDS. This paper describes in particular, the current substance tests of Test Series 7, some of their shortcomings, and recommendations for improvements in these tests. Formulation effects for bomb and warhead fills are described elsewhere. [1,2].

### INTRODUCTION

Over the past twenty years, there has been demonstrated a need for less-sensitive explosive fills for munitions that maintain or exceed current explosive performance. The benefits to be gained include greater materiel and personnel safety in all logistics phases in the munitions' life-cycle, and the potential for increased munitions density in land-limited storage areas that are adversely affected by encroachment of civilian populations. In the United States, the military services and the national laboratories have provided the driving forces for the development of less-sensitive explosives, through the promulgation of needs documents, numerous advisory committees, and the ultimate publication of military standards on how to determine whether a substance or an article is indeed insensitive [3,4,5,6]. In Europe, the North Atlantic Treaty Organization (NATO) has been the focal point for a similar effort, culminating in guidelines to be used for the testing, storage, and transportation of extremely insensitive explosive articles (now called "EIDS Ammunition") [7]. The history of the development of these tests and standards has been summarized by Ward [3] and Swisdak [4]. Currently, the United States is undergoing major revisions to DOD 6055.9-STD [5,8] to implement the UN hazard classification tests and criteria for C/D 1.6 [8].

### UN TEST SERIES 7

UN Test Series 7 requires passing all of the tests at the substance level before testing is performed on articles, generally in their transportation configuration. These tests are summarized briefly in Table I. Part A describes the tests to be performed on substances. Passing all of the substance tests allows the material to be categorized as an Extremely Insensitive Detonating Substance (EIDS), and permits article tests to be performed. Part B of Table I describes the tests to be performed on actual articles filled with EIDS. If the articles pass all of these tests, they can be assigned UN hazard class/division 1.6, allowing increased storage density over that for other hazard categories.

### EIDS TESTS, PROBLEMS AND SOLUTIONS

In the United States, six types of EIDS test are performed at the substance level. These include a #8 blasting cap test, an extended card gap test (at one fixed gap), external fire, slow cookoff, bullet, and SUSAN impact tests. In Europe, the friability test may be substituted for the bullet impact and the SUSAN impact tests. Testing apparatus and methods are documented in UN Test Series 7 [7].

**EIDS Cap Test** - The EIDS cap test is straightforward, testing for the detonability of the explosive material in response to initiation of a #8 blasting cap. It is performed in triplicate. Figure 1 shows a typical passing test result.

**EIDS Gap Test** - The EIDS gap test is a variant of the Expanded Large-scale Gap Test (ELSGT) developed at the Naval Surface Warfare Center, White Oak. [10]. The test is performed in triplicate. The hardware is well-specified in the UN Test Series 7 documentation, providing wall thicknesses and specifications for materials of construction for both the explosive-filled tube and the witness plate. The difference between the Navy test and the UN test, is that the UN test is only run at one fixed gap (70 mm). This gap will attenuate the donor shock to about 53 kbar at the end of the gap. Unfortunately, it provides no information on the real shock sensitivity of the explosive fill. For example, in the sympathetic detonation of MK-82 bombs, the diagonal acceptor experiences in excess of 70 kbar, and may detonate even though it is classified as an EIDS. Also, while the scale of the test is more realistic than the NOL Large Scale Gap Test (1/2 the scale of the ELSGT), the test item may still be too small for many of today's insensitive high explosives having a large critical diameter. There is no provision for measuring explosive critical diameter in UN Test series 7. Three examples of passing reactions are shown in Figure 2.

---

This work was performed under Contract Number F08635-90-C-0197 with Eglin AFB, FL.

Approved for public release - Distribution unlimited.

**TABLE 1. UN TEST SERIES 7  
FOR CLASS/DIVISION 1.6 ARTICLES**  
**A. EXTREMELY INSENSITIVE DETONATING SUBSTANCE TESTS**

TEST NUMBER	TEST NAME	NUMBER OF TRIALS	TEST VEHICLE	FAILURE CRITERIA
7(a)	EIDS Cap Test	3	No. 8 blasting cap in explosive contained in 80 mm x 160 mm cardboard tube and resting on a 1 mm thick steel plate.	Detonation as evidenced by hole punched in witness plate.
7(b)	EIDS Gap Test	3	73 mm x 280 mm Steel Pipe with 70 mm long Plexiglas gap between Pentolite donors and explosive fill, and resting on a 20 mm-thick witness plate	Detonation as evidenced by hole punched in witness plate.
7(c)(i)	SUSAN Test	5	51 mm x 102 mm explosive billet in aluminum cup as nose of massive steel projectile. Launched from 81.3 mm gun @ 333 m/s into steel wall.	$\geq 27$ kPa overpressure at 3.05 m.
7(c)(ii)	Friability Test (Alternate for SUSAN test)	3	Explosive billet 18 mm diameter launched at 150 m/s into standard wall. Impacted material burned in closed bomb.	$> 15$ MPa/ms pressure rise rate in closed bomb.
7(d)(i)	EIDS Bullet Impact Test	6	Single 50-caliber AP bullet impact into explosive-filled 45 mm id x 200 mm steel pipes with torqued end caps.	Explosion or detonation.
7(d)(ii)	Friability Test (Alternate for EIDS Bullet Impact Test)	3	Explosive billet 18 mm diameter launched at 150 m/s into standard wall. Impacted material burned in closed bomb.	$> 15$ MPa/ms pressure rise rate in closed bomb.
7(e)	EIDS External Fire Test	3	Explosive-filled 45 mm id x 200 mm steel pipes with torqued end caps tested in kerosene-soaked wood fire. Five items per trial or fifteen in one trial.	Detonation or $> 15$ m fragment throw.
7(f)	EIDS Slow Cookoff Test	3	Explosive-filled 45 mm id x 200 mm steel pipes with torqued end caps tested to destruction at $3.3^{\circ}\text{C}/\text{hr}$ rise in temperature.	Detonation or $> 3$ fragments.

**B. ARTICLE TESTS**

TEST NUMBER	TEST NAME	NUMBER OF TRIALS	TEST VEHICLE	FAILURE CRITERIA
7(g)	1.6 Article External Fire Test	1	Ammunition in shipping configuration containing EIDS in kerosene-soaked wood fire. Three items, minimum.	C/D 1.1, 1.2, or 1.3 response
7(h)	1.6 Article Slow Cookoff Test	2	Ammunition containing EIDS heated to destruction at $3.3^{\circ}\text{C}/\text{hr}$ rise in temperature.	$>$ Burning
7(i)	1.6 Article Bullet Impact Test	3	Ammunition containing EIDS subjected to triple 50-caliber AP bullet impact.	Detonation
7(k)	1.6 Article Stack Test	3	Ammunition containing EIDS in both unconfined and confined shipping configuration stacks.	Propagation

EIDS SUSAN Test - This test gives a measure of the formulation's sensitivity to crushing impact. Standard procedures have been developed by Lawrence Livermore National Laboratory for this test. Presently there is only one facility that is capable of performing the test in the United States (New Mexico Institute of Mining and Technology, TERA facility, Socorro, New Mexico). While the procedure allows casting 51 mm x 102 mm explosive billets and then placing them in the "SUSAN cup" (the nose of the projectile), most explosives are simply cast in place. If the explosive is placed in the cup after cure, care should be taken to bond the explosive to the cup. Otherwise, variable test results can be obtained. Five tests are performed. Figure 3 shows the SUSAN projectile and its aluminum SUSAN "cup" nose filled with explosive.

EIDS Bullet Impact Test - Six steel pipes are filled with explosive, sealed with torqued end caps, and tested in triplicate in each of two orientations. (See discussion of pipes, following). Each pipe is impacted by a single 0.50-caliber armor-piercing bullet. Three are impacted on the side of the pipe, and three are impacted through the endcap along the long axis of the container. Reaction violence is recorded. Typical passing reactions are shown in Figure 4.

EIDS External Fire Test - 15 steel pipes (see discussion of pipes, below) are loaded with explosive and sealed with torqued end caps. Triplicate tests of 5 pipes each may be performed or one test with all 15 pipes can be performed. These are subjected to a fuel-soaked wood bonfire of specified geometry and materials. Figure 5 shows a typical set up in progress. Witness panels of thin aluminum are placed 4 m away on three sides of the fire to help gauge reaction. The test layout, while well-described in the UN document, leaves much to the experience of the test engineer. Attachment of the pipes to a grate and the design of the grate are unspecified. At best, this kind of fire is variable, and ambient weather conditions influence the test significantly. The use of kiln-dried wood stacked 100 mm apart, and at right angles every other layer, provides the best fire. There are a number of problems and suggestions for improving this test. First, good video coverage is required over a wide field of view to help spot the location of pipes after reaction. The video coverage should also provide audio coverage, so that the number of reacted pipes can be counted as they react. Many times, a number of the pipes exposed to the fire do not react, but lofted out of the fire by ones that do react. These pipes may contain partially reacted explosive. Therefore, a standard waiting period of at least eight hours after the test is completed should be required. After mapping the debris, the unreacted units need to be disposed of. This disposal can be quite hazardous if done improperly. A disposal procedure should be in place before attempting to perform this test. Figure 6 shows typical passing test results and a number of unexploded pipes requiring disposal.

EIDS Slow Cookoff Test - Three steel pipes (see below) loaded with the explosive of interest are individually subjected to a slow, specified temperature rise in an oven. Each is tested to destruction, while the air and item temperatures are monitored with thermocouples. We have found that commercially available "toaster ovens" with a top and bottom heating element can be economically modified to perform this test. Thermostats are removed, and the heating elements are directly connected to the proportional controller. A 3-inch-diameter pancake fan (available from Radio Shack) is inserted on the same wire rack as the test item to circulate the air. We have found that the orientation of this fan is critical to getting reproducible test results. It should be placed horizontally on the rack to circulate the air from bottom to top of the oven. If it is placed vertically to circulate air side to side, large temperature gradients are observed. A typical test set up is shown in Figure 7. There are a number of items to remember when performing this test. First, the test takes a long time -- typically 12 - 30 hours. This can impede the performance of other tests at the facility. Second, it needs to be performed in an area large enough to accomodate the launching of the heavy pipe endcaps without hazard to other operations. Finally, continuous video coverage is desireable to record reaction violence, but since the end time of the test is indeterminant, provision must be made to change videotapes remotely every eight hours. Third, since the test is of long duration, night lighting for the video coverage is imperative. ARC uses an expendable halogen outdoor light. Figure 8 shows a typical passing reaction in which the bomb body has not fragmented at all.

Pipes - Of all the test geometries and containers, perhaps the one type with the biggest potential for variability in results is the "pipe bombs". The same 45-mm-id x 200-mm long (in the US, 1-1/2 x 8-inch schedule 40 seamless steel pipe) container with 4-mm wall thickness is used for bullet impact (6), slow cookoff (3) and fast cookoff (15) tests. These pipes are first loaded with the explosive of interest. In the case of cure cast systems, one end of the clean, grit-blasted pipe is blanked off, while it is filled from the other end in a vacuum casting bell. Regardless of how good your casting technique is, some explosive always gets into the pipe threads, and must be removed prior to installing the end caps. The open end is then covered and the filled pipes are placed in the cure oven.

After curing, the protective coverings are removed, and the threads scrupulously cleaned. This is a tedious and time-consuming job. Once the threads are certified as free of explosive, the endcaps are ready to be installed. This requires a special remote operation fixture, in which the loaded pipe body is held in a sturdy vise, and the first endcap is placed in the tightening fixture. This consists of a long steel rod with set screws to hold the pipe cap (at one end), and proceeding through the steel protective barrier to a fitting that mates with a large torque wrench on the other end. The pipe cap is threaded onto the pipe until resistance is encountered, then the requisite 204 N-m (150 ft-lb) torque is applied to that endcap. Note that this is a significant torque setting, requiring a skilled, strong person to get reproducible results. Once the first endcap is installed, the pipe is unfixed, turned 180 degrees, and the whole remote procedure repeated for the other end. With practice, the average turnaround time per bomb is somewhat under 10 minutes. Thus, for one EIDS test series of 24 pipes, 240 minutes (4 hours) will be used just to tighten end caps, and an equal or greater time will be used just to clean and certify the threads as free of explosive.

There are problems that can be encountered, both with the pipes and with the end caps. The pipe is supposed to be seamless steel pipe, but no specification is given in the UN document. There are at least two ASTM specification numbers and at least 5 grades of seamless carbon steel pipes [10]. The chemical compositions of these carbon steels are identical, but those meeting ASTM Specification A106 have been tested more thoroughly. Both ASTM A53 and A106 are made in Grades A and B. A106 is also made in Grade C. Tensile strength increases with Grade letter, while ductility decreases. Tensile strength at room temperature is 48,000 psi for Grade A; 60,000 psi for Grade B; and 70,000 psi for Grade C. There also exist various welded pipes including butt welded, lap welded and electric fusion welded. While these have tensile strengths on the order of Grade A seamless pipe (ca. 40-45,000 psi), their useful service temperature is significantly lowered. We have on occasion received pipe certified as seamless that was obviously welded along a straight seam and, upon reaction, failed along the seam line. This

is shown graphically in Figure 9. Pipe end caps are only specified as steel or cast iron. We have found that the material of construction, its finish, and its form of fabrication can influence the test results. We have tested with end caps of cast iron and of steel, as well as galvanized steel. Ungalvanized steel is the best choice. Galvanized steel can catalyze early reactions with the explosive in the cookoff scenarios and is to be avoided. Pipe caps meeting general plumbing standards vary significantly. We have used steel endcaps from a number of US manufacturers, as well as ones from Mexico and from Thailand. Those of foreign manufacture were significantly worse in the EIDS tests than those from domestic sources. Within the end caps produced in the United States, there was significant variation in the cap geometry. Apparently, pipe cap geometry is something of an art form in the plumbing world. Caps range from unlabeled to inscribed to those with raised lettering. This lettering may be anywhere on the cap. Lettering may act as a stress riser. There are those with flat ends of uniform wall thickness and those that are dome-shaped with variable wall thickness. Those that are flat tend reproducibly to punch out a disc of the pipe inner diameter, and at relatively low pressures, thereby venting the system early and minimizing any pipe sidewall reactions. Those that are domed generally stay attached to the bomb until pressure rupture occurs, almost always failing at the first exposed thread beyond the attached endcap. Note that these endcaps can become hazardous fragments because of their large mass and velocity.

#### EXTREMELY INSENSITIVE PLASTIC-BONDED EXPLOSIVES TEST RESULTS

In our explosives development work ARC has formulated a number of insensitive explosives that have been subjected to the EIDS small-scale test series, and several that have been carried on to the article level. These formulations have all incorporated fine nitramines to reduce shock sensitivity, aluminum and ammonium perchlorate as blast impulse enhancers, and varying amounts of nitroguanidine as a coolant and burning rate modifier. The test results to date are shown in Table 2.

TABLE 2. UN TEST SERIES 7 RESULTS FOR INSENSITIVE EXPLOSIVES DEVELOPED BY ATLANTIC RESEARCH CORPORATION

TEST TYPE	Formulation A RDX/AI/NQ	Formulation B RDX/AI/AP	Formulation C RDX/AI/AP/NQ	Formulation D RDX/AI/AP/NQ	Formulation E RDX/AI/AP/NQ
EIDS Cap	PASS	PASS	PASS	PASS	PASS
EIDS Gap	PASS	PASS	PASS	PASS	PASS
EIDS SUSAN	PASS	PASS	PASS	PASS	PASS
EIDS Bullet Impact	PASS	PASS	PASS	PASS	PASS
EIDS External Fire	PASS	PASS	PASS	PASS	PASS
EIDS Slow Cookoff	PASS	PASS	PASS	PASS	PASS
ARTICLE External Fire	NT	Propulsive burning in MK-82	Propulsive burning in MK-82	PASS - in MK-82	1 PASS/1 Mildly propulsive burning in MK-82
ARTICLE Slow Cookoff	NT	PASS - in MK-82	NT	NT	1 PASS/1 Pressure burst in MK-82
ARTICLE Bullet Impact	NT	PASS - in MK-82	NT	NT	1 PASS in MK-82
ARTICLE Stack	NT	PASS - ADJACENT in MK-82 Stack of 6 FAIL - DIAGONAL in MK-82 Stack of 6	PASS - ADJACENT in MK-82 Stack of 6 FAIL - DIAGONAL in MK-82 Stack of 6	PASS - ADJACENT in MK-82 Stack of 6 PASS - DIAGONAL in MK-82 Stack of 6	PASS - ADJACENT in MK-82 Stack of 6 PASS - DIAGONAL in MK-82 Stack of 6
EIDS Substance?	YES	YES	YES	YES	YES
EIDS Ammunition?	NT	NO	NO	NT	YES

\* TBD = To be determined    \* NT = Not tested

While all of these explosives are extremely insensitive detonating substances, most have not passed all of the subsequent article tests. There seems to be little connection between the EIDS external fire test results and the article results. Also, there is a problem relating the EIDS gap test to sympathetic detonation response in the article stack tests. However, through careful formulation to maintain performance while decreasing sensitivity, formulation E is both an EIDS, and MK-82 bombs loaded with formulation E are EIDS ammunition.

#### RECOMMENDATIONS AND CONCLUSIONS

In this paper, some lessons learned have been presented that relate to the testing of insensitive high explosives. It must be remembered that UN Test Series 7 is used to classify articles for storage and transportation purposes, and that the tests are not meant to be used to obtain quantitative explosive and article sensitivity data. This is unfortunate since threshold sensitivity data could be obtained in some of the tests. For example, performing the EIDS gap test at different gaps after starting at the 70-mm gap would be useful for better predicting sympathetic detonation response. Additionally, a point of clarification needs to be added to the UN Test Series 7 EIDS pass/fail criteria. While it is implied, it is not at all clear that the side wall of the pipe bombs is all that should be taken into account. Endcaps should not be included in the evaluation, since the real criterion for these tests is distinguishing between detonation and no detonation by the fragmentation of the side wall.

To obtain more consistent data between test facilities, much tighter specifications are required for the 45-mm x 200-mm pipes and their endcaps. ARC recommends the use of ASTM A53 Grade A seamless steel pipe and A53 Grade A steel endcaps that have a radius of curvature on the end and either cast, raised lettering or no lettering on the end cap. These materials are widely available in the United States. For the external fire test, a suggested improvement that would minimize early fire conditions would be to insert the grate with the attached rounds into a fully developed fire (e.g., via a gantry arrangement) instead of starting the fire with the rounds already in place. This would provide a more uniform basis for comparison of tests performed at different facilities.

Atlantic Research Corporation has developed a significant EIDS testing database while formulating insensitive explosives for the US Air Force. A number of EIDS formulations have been developed. Although these formulations are extremely insensitive to hazards stimuli, they have been shown to also have good performance characteristics.

#### LIST OF REFERENCES

1. Lynch, R.D., K.J. Graham, and E.M. Williams, "Characterization of Plastic-Bonded Explosive Formulations for Bomb Applications", in *Proceedings of the 1992 JANNAF Propulsion Meeting*, Indianapolis, Indiana, February 1992.
2. Williams, E.M., K.J. Graham, and R.D. Lynch, "Plastic-Bonded Explosive Formulations for Warhead Applications", in *Proceedings of the 1992 JANNAF Propulsion Meeting*, Indianapolis, Indiana, February 1992.
3. Ward, Dr. Jerry M., "Hazard Class/Division 1.6 Test Protocol", in *Minutes of the Twenty-Fourth Department of Defense Explosives Safety Seminar*, Department of Defense Explosives Safety Board, St. Louis, Missouri, 28-30 August 1990.
4. Swisdak, Michael M., Jr., *Hazard Class/Division 1.6: Articles Containing Extremely Insensitive Detonating Substances (EIDS)*, NSWC TR 89-356, Naval Surface Warfare Center, Silver Spring, Maryland, 1 December 1989.
5. *Department of Defense Ammunition and Explosives Safety Standards*, DOD 6055.9-STD, Department of Defense, Washington, D.C., July 1984, with revisions 1 (June 1986) and 2 (October 1988).
6. *Hazard Assessment Tests for Non-Nuclear Munitions*, MIL-STD-2105A (NAVY), Department of Defense, Washington, D.C., 8 March 1991.
7. *Recommendations on the Transport of Dangerous Goods; Tests and Criteria*, Second Edition, United Nations Publication, ST/SG/AC.10/11, New York, 1990.
8. Ward, Dr. Jerry M., "DRAFT Secretariat Proposed Changes to DoD 6055.9-STD for Implementation of UN Class/Division (C/D) 1.6 Test Protocol and Concurrent Changes for Unit Risk C/D 1.2 Ammunition," private communication, 7 August 1991.
9. Baumeister, Theodore, *Marks' Standard Handbook for Mechanical Engineers*, Eighth Edition, chapter 8, McGraw Hill Book Company, New York, NY.
10. Liddiard, T.P. and D. Price. *The Expanded Large Scale Gap Test*, NSWC-TR-86-32, Naval Surface Warfare Center, Silver Spring, MD. March 1987.

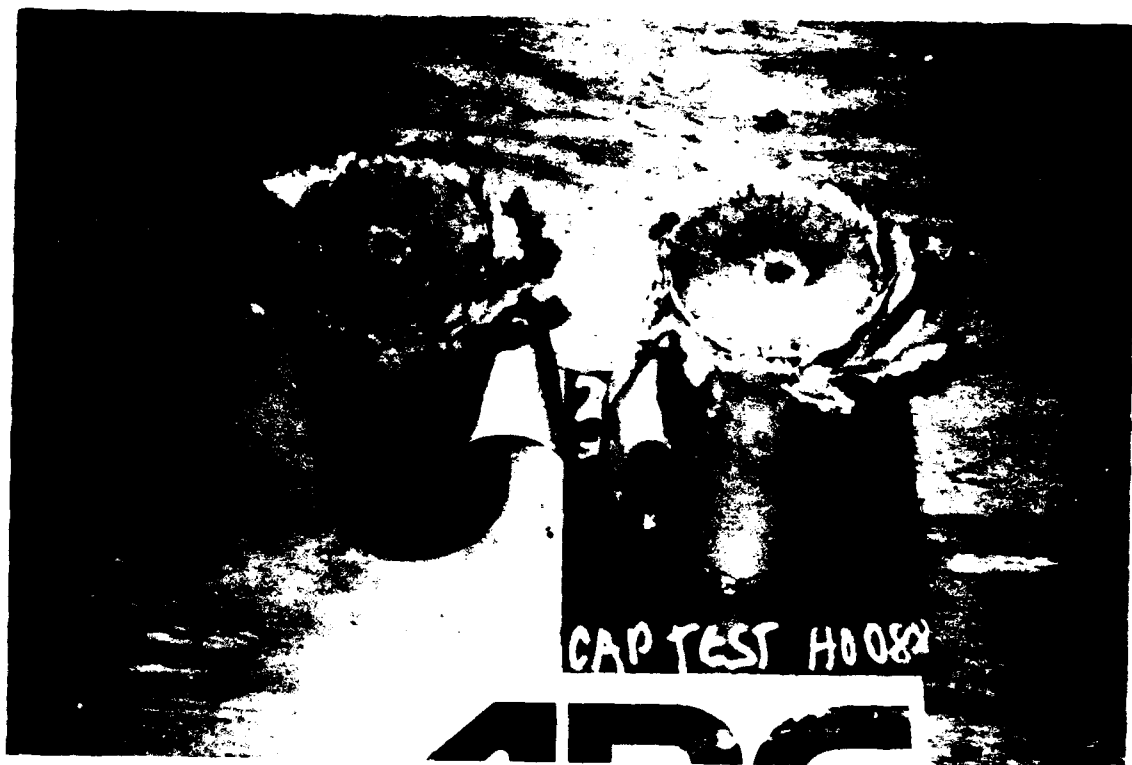


Figure 1. EIDS cap test.



Figure 2. EIDS gap test.

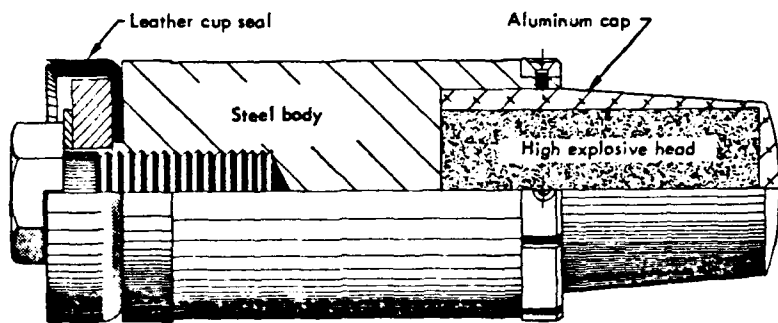


Figure 3. EIDS SUSAN test.



Figure 4. EIDS bullet impact test.



Figure 5. EIDS external fire test setup.

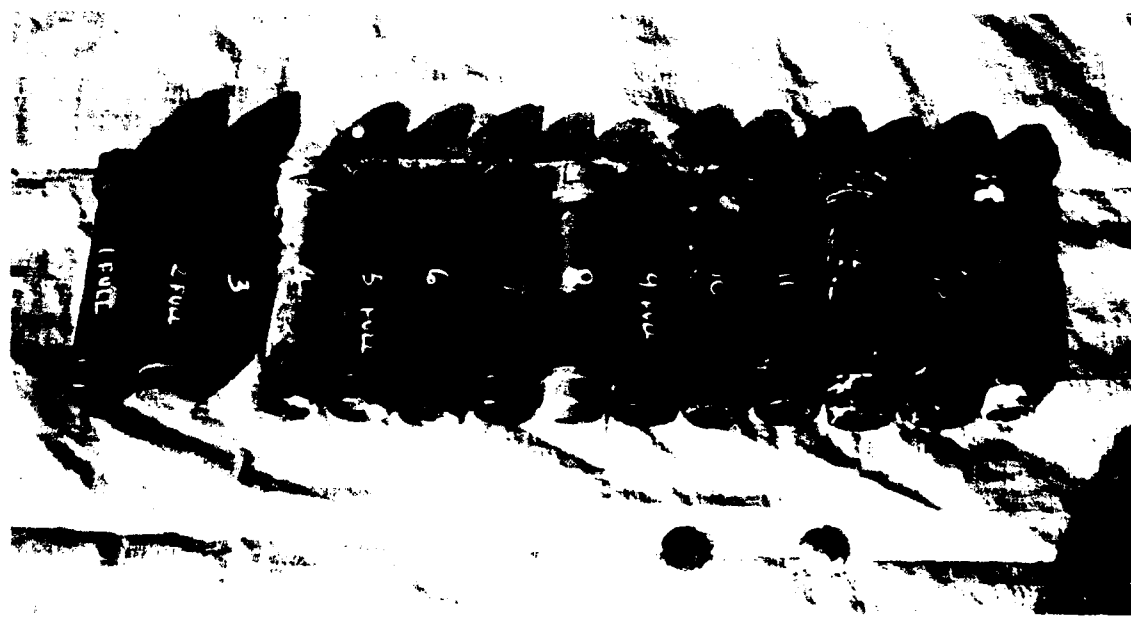


Figure 6. EIDS external fire results.

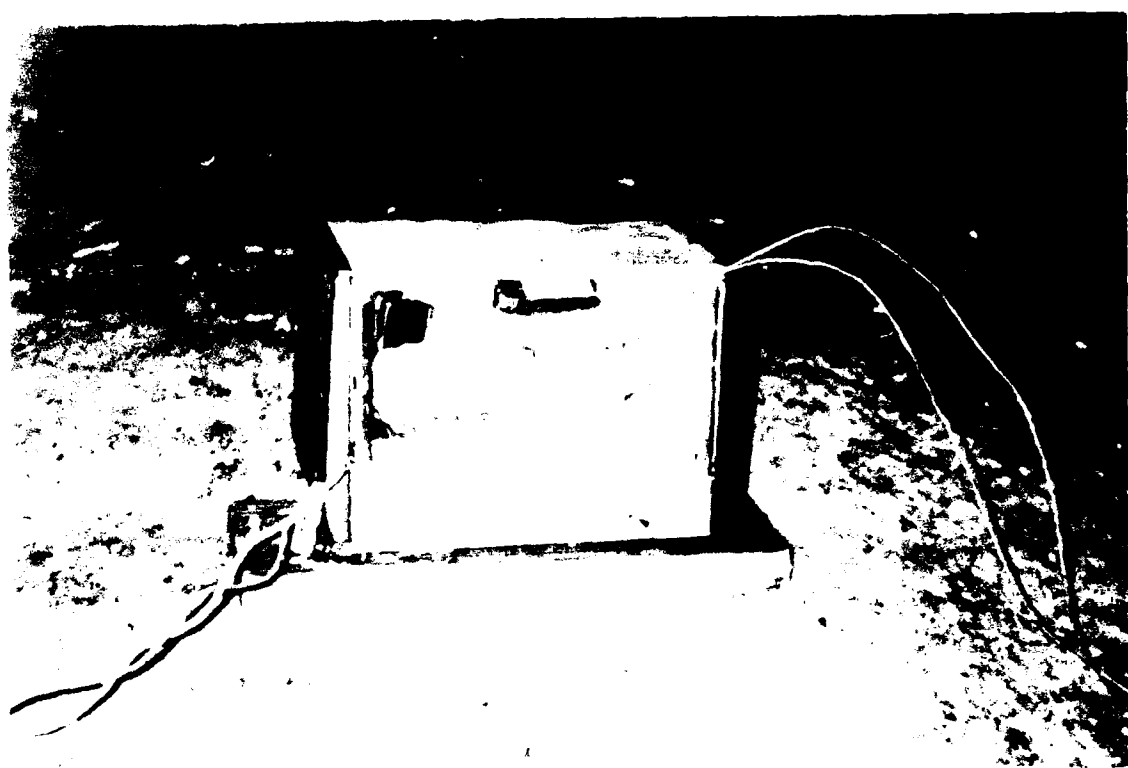


Figure 7. EIDS slow cookoff test setup.

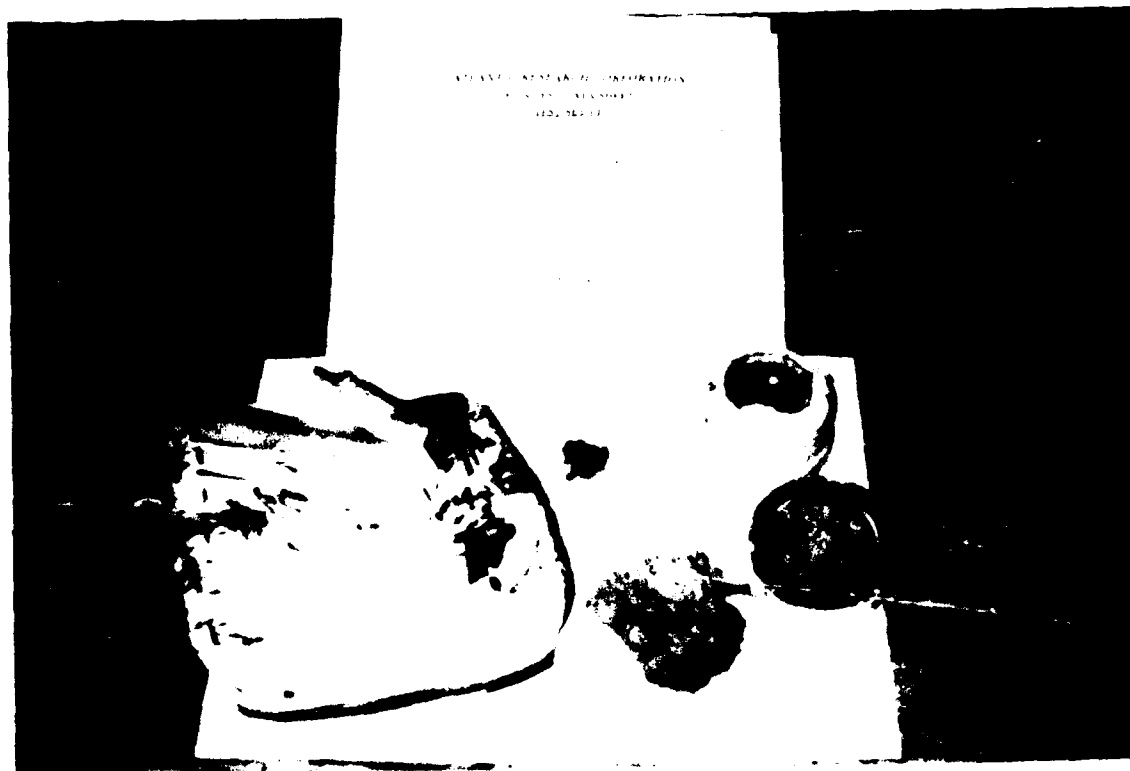


Figure 8. EIDS slow cookoff test results.



Figure 9. Effect of using welded seamed pipe instead of seamless.

**CLASSIFICATION TESTS FOR ASSIGNMENT  
TO HAZARD CLASS/DIVISION 1.6 :  
SNPE TWO YEARS EXPERIENCE**

**J. ISLER**

**S.N.P.E.**

**DIVISION DEFENSE ESPACE**

**DIRECTION DE LA TECHNOLOGIE ET DE LA RECHERCHE**

**CENTRE DE RECHERCHES DU BOUCHET**

**91710 - VERT LE PETIT - FRANCE**

**Tél : (33) 1.64.99.12.34**

**ABSTRACT :**

The UN Test series 7 can be considered as the most complete, and severe, list of requirements for insensitive munitions. So, it has been extensively used at SNPE, as a screening method for the new high explosives formulations studies. This two years experience provided us valuable information to analyse the pertinence of the substances tests [7(a) to 7(f)], from different points of view :

- at first, the equivalence of distinct ways permitted for a same test has been looked (high explosive donor for Gap Test, Susan Test/Friability Test comparison)
- secondly, some experimental procedures may be discussed, at the light of results and observations during tests. (External Fire Test, Slow Cook-off Test, Bullet Impact Test)
- finally, the knowledge of EIDS behavior in large scale models or in warheads, allows to confirm the substances tests interest, while also indicating some of their limitations.

This three points are discussed in the paper, with the support of results and observations provided by assessments of EIDS candidates, as well as expected advantages with C/D 1.6.

## **1) INTRODUCTION**

The new hazard class/division (C/D) 1.6, for articles, explosives, extremely insensitive, has been first created by the transportation community, under the impulse of the United Nations Comitee of Experts on the Transport of Dangerous Goods.

This Comitee approved a new test protocol (Test Series 7), which is described in ref [1]. The tests and pass/fail criteria required by the test series 7 are briefly summarized in appendix 1 :

- Tests 7a) to 7f) for substances, to "qualify" a new material as an "Extremely Insensitive Detonating Substance" (EIDS), or "Matière Détonante Extrêmement Peu Sensible" (MDEPS) in French.
- Tests 7g) to 7k), for articles, to assign a classification in C/D 1.6 to a new ammunition, containing only EIDS as high explosives.

Since that time, the C/D 1.6 has been adopted in other regulations or classification procedures :

- by the US DOT, in its new document 49 CFR, vol. 55, n° 246
- by the US DOD, in DOD 6055-9-STD, change n° 3, which adopted the EIDS and C/D 1.6 appellations, but not yet the UN tests.
- by the NATO AC/258, in a draft AASTP3 (Allied Ammunition Storage and Transport Publication n° 3)

Then this new C/D is progressively on the way to become a standard for hazard classification of insensitive munitions, concerning both storage and transportation.

So SNPE has been interested, for more than two years now, in using this protocol to assess its new insensitive high explosives.

This experience has been used, and analysed, to improve the knowledge about the new EIDS materials, concerning mainly the following topics :

- the significance of the tests and criteria for EIDS, which have already been widely described in former presentations [2,3].
- the differences between the allowed alternatives methods,
- the consequences and limitations of the pass/fail criteria,
- the expected advantages for C/D 1.6 ammunition.

## 2) SUBSTANCES TESTS :

### 2.1. EIDS Cap Test - 7a) :

This test is used to assess the sensitivity of an EIDS candidate to a standardized detonator, the sample being an unconfined cylinder (80mm diameter, 160mm length). Results obtained with this procedure are presented in table n° 1.

In this table, and in all others coming, (-) means the acceptance criterion is met, while (+) means it is not.

Some details about the test substances in this tables are also given in appendix 2.

Test substance	Result	Data reference	Remarks : unconfined critical diameter (mm)
TNT	(-)	SNPE	40
Compo. B	(+)	US [4]	4.3
PBX 9502	(-)	US [4]	8-10
CPX 305	(-)	UK/DRA [5]	42-47
AFX 644	(-)	US/EGLIN [6]	
ORA 86	(-)	SNPE	4
B2214	(-)	SNPE	65
B2211	(-)	SNPE	65
B3017	(-)	SNPE	10-15
B3021	(+)	SNPE	< 10

Table n° 1 : Cap Test results ((-) means no detonation)

In a first approximation, this test selects the materials mainly according to their critical diameter :

- a critical diameter larger than 10mm will surely lead to pass the test.
- but some negative results may also be obtained with cast PBX having smaller critical diameter than 10mm.

## 2.2. EIDS Gap Test - 7b) :

This test is used to assess the shock sensitivity of an EIDS candidate (73mm diameter, 280mm length, 11mm steel confinement) which is subjected to a shock pulse, delivered by a donor charge through a PMMA barrier.

The UN protocol allows to use :

- either a Pentolite 50/50 donor,
- or a RDX/Wax 95/5 donor.

Pressure measurements have been done at SNPE with the RDX/Wax donor. They are compared with NSWC data on the figure in appendix 3, which shows that the two donors give roughly the same peak pressure, especially near the 70mm criterion, and then can be considered as equivalent for comparisons between Gap Test data.

Results obtained at SNPE are gathered in table n° 2, as well as some other data.

Test substances	Result	Critical PMMA thickness (mm)	Critical equivalent pressure(GPa)	Data reference
TNT	(+)	110	1.8	SNPE
TNT-Al 85/15	(+)	95	2.7	"
HBX3	(+)	110	2.0	"
Compo. B	(+)	155	0.7	"
Octol 75/25	(+)	195	0.2	"
ORA 86	(+)	90	3.5	"
B2214	(-)	35	9.5	"
B2211	(-)	50	8.0	"
B3017	(-)	35	10.0	"
B3021	(-)	< 70	> 4.0	"
PBX 9502	(-)	52	7.0	US/NSWC [4]
CPX 305	(+)	76		UK/DRA [5]
AFM 644	(-)	52		US/EGLIN AFB [6]

Table n° 2 : Gap Test results ((-) means no detonation with 70mm PMMA)

According to the calibration curves in appendix 3, the candidates meeting the pass/fail criterion at 70mm PMMA, have a shock sensitivity higher than about 4.0 GPa, measured in the 73mm diameter. We will see later in the paper how this selection is pertinent when talking about sympathetic detonation.

### **2.3. EIDS Impact sensitivity - 7c) and 7d) :**

The assessment of impact sensitivity is the only point of the protocol where two alternative methods are offered :

- the US proposal has been to perform the Susan Test 7c)i) and a Bullet Impact test 7d)i),
- the French proposal has been to perform only the Friability test 7c)ii) and 7d)ii).

At this time both of these procedures are used respectively in US and in France. Then some additional work have been undertaken in US (DDESB and NSWC) and in France (STPE and SNPE), in order :

- to have a recognition of the French alternative method in US,
- to study the possibility of reducing the number of test for assessing the impact sensitivity.

So answers have been searched for the two questions asked by this alternativity :

- Is the Friability test equivalent to Bullet Impact Test ?
- Is the Friability test equivalent to Susan Test ?

To the first question, the answer is definitely yes. This can be easily demonstrated by all the works made by SNPE concerning the DDT hazard due to bullet impact on confined warhead [7,8,9]. The table in appendix 4 summarizes these works, by comparing for sixteen high explosives :

- their behavior at 0.5 caliber bullet impact in a 20mm steel confinement generic unit, with inside diameter 125 mm, and length 90 mm,
- their Friability level.

It is clear from these results that a detonation hazard to 0.5 bullet impact may not be expected any more with cast PBX having a Friability level lower than 15 MPa/ms.

Concerning the second question, results obtained by both Friability test and Susan Test are gathered in table n° 3.

Test substances	Friability test			Susan Test		
	MPa/ms at 150 m/s	Result	Data ref.	ΔP or TNT equiv. at 333m/s	Result	Data ref.
TNT	7.8	(-)	SNPE	17.7KPa	(-)	UK/DRA[1]
TNT-AI 85/15	6.5	(-)	"	190g (80/20)	(+)	DOBRATZ[11]
HBX3	3.0	(-)	"	/	/	
Compo. B	51	(+)	"	32KPa	(+)	US/NSWC[4]
Octol 75/25	> 33	(+)	"	> 250g	(+)	DOBRATZ[11]
ORA 86	8.0	(-)	"	25KPa	(-)	US/NSWC[4]
B3103	3.9	(-)	"	46KPa	(+)	US/NSWC[4]
B3003	> 26.5	(+)	"	43KPa	(+)	US/NSWC[4]
B2214	0.2	(-)	"	4.9KPa	(-)	UK/DRA[11]
B2211	4.5	(-)	"	/	/	/
B3017	1.3	(-)	"	/	/	/
B3021	7.5	(-)	"	/	/	/
PBX9502	/	/	/	6.7KPa	(-)	US/NSWC[4]
CPX 305	0.2	(-)	"	11.1KPa	(-)	UK/DRA[6]
AFX 644	0.3	(-)	"	17.1KPa	(-)	US/EGLIN[7]
AFX 930	/	/	/	12.0KPa	(-)	US/NSWC
AFX 931	/	/	/	25.0KPa	(-)	US/NSWC

Table n° 3 : Results to Friability test and Susan Test ((-) means less than 15 MPa/ms at Friability test, or less than 27KPa or 45 g TNT at Susan Test).

These comparisons show some discrepancy between the two methods in only two cases : TNT-AI and B 3103. In each of these two cases the substance passes the Friability criterion and fails the Susan Test criterion. Our explanation to these differences is that in the Friability test, the substance is first impacted, being only damaged but not burning, and is secondly burned in a closed vessel.

On the contrary, the Susan Test may be considered as well as a shock sensitivity test and as an impact test, since the substance is reacting at impact.

That's why we suggest that, in the mind of the Test Series 7 for substances, those results would no be considered separately but rather all together, especially by taking into account the Gap Test result.

By doing so it can be demonstrated that both the two alternative methods lead to the same global verdict, as shown by the next table.

Test substances	Friability result	Susan result	Gap Test result	Friability + Gap Test global result	Susan + Gap Test global result
TNT	(-)	(-)	(+)	(+)	(+)
Compo. B	(+)	(+)	(+)	(+)	(+)
TNT-AI 85/15	(-)	(+)	(+)	(+)	(+)
AFX 644	(-)	(-)	(-)	(-)	(-)
PBX 9502	(-)	(-)	(-)	(-)	(-)
CPX 305	(-)	(-)	(+)	(+)	(+)
HX 76	(-)	(-)	(+)	(+)	(+)
B2214	(-)	(-)	(-)	(-)	(-)
ORA 86	(-)	(-)	(+)	(+)	(+)
B3103	(-)	(+)	(+)	(+)	(+)
B3003	(+)	(+)	(+)	(+)	(+)

Table n° 4 :Global comparison between Friability - Susan - Gap Test

The reason for that is : since the Susan Test may be considered also as a shock sensitivity test, then the Gap Test will filter more severely the candidates in that way, as shown by the figure in appendix 5 where :

- 3/12 substances fail to both Susan and Gap Tests
- 5/12 substances pass both Susan and Gap Tests
- 4/12 substances pass the Susan Test but fail at Gap Test.
- No substance passes the Gap Test while failing the Susan Test.

#### 2.4. EIDS External Fire Test - 7e)

This test has the objective of indicating the reaction level at fast cookoff of a substance contained in a 4mm thickness steel pipe (40mm ID, 200mm length) ended by two steel caps.

The test 7e) consists in putting five of these pipes in a fuel fire.

In France the test is performed differently at this time :

- either with only one pipe, for the substances having a small critical diameter
- or with a 3 liters confined generic unit, for substances with larger critical diameter. The sample has then a 123mm diameter.

Some results obtained at SNPE and GERBAM\* by these two methods are presented in the next table.

Test substances	40mm pipe		3 liters generic unit	
	Reaction level	Result	Reaction level	Result
TNT	Detonation	(+)	Violent Reaction	(+)
TNT-A185/15	Pressure burst	(-)	Pressure burst	(-)
Compo. B	Detonation	(+)	Partial deto.	(+)
Octol	Detonation	(+)	Partial deto.	(+)
HBX3	Pressure burst	(-)	Pressure burst	(-)
ORA 86	Pressure burst	(-)	Pressure burst	(-)
B2214	/		Pressure burst	(-)
B2211	/		Pressure burst	(-)
B3017	/		Pressure burst	(-)

Tableau n° 5 : External fire results ((-) means no detonation and no violent reaction)

Similar responses are obtained in both those two containers in fuel fire. On another hand, we observed that when performing the test with five pipes, as recommended by the UN procedure, only one pipe reacts, the others being expelled out of the fire. Then now, only one pipe is tested.

\* Groupe d'Etudes et de Recherches en Balistique des Armes et Munitions - DCN Lorient

### 2.5. EIDS Slow Cookoff Test - 7f) :

This test is used to determine the reaction of an EIDS candidate when heated in an oven at 6 F/hr (3,3°C/hr), in the same pipe as for test 7e).

The next table presents some results obtained at SNPE with the UN procedure, and at GERBAM in the 3 liters generic unit.

Test substances	40mm pipe		3 liters generic unit	
	Reaction level	Result	Reaction level	Result
TNT	Violent reaction	(+)	Violent Reaction	(+)
Compo. B	/		Detonation	(+)
TNT-Al85/15	/		Pressure burst	(-)
ORA 86	Pressure burst	(-)	Pressure burst	(-)
B2214	Pressure burst	(-)	Pressure burst	(-)
B2211	Pressure burst	(-)	Pressure burst	(-)
B3017	Violent reaction	(+)	Pressure burst	(-)
B3021	Detonation	(+)	/	

**Table 6 : Slow Cookoff results ((-) means no detonation and no violent reaction)**

These results show some discrepancy between the two methods, which can be explained by the interpretation of the pipe fragmentation given in the UN protocol. A reaction is considered as violent as soon as the pipe fragments in more than three pieces, without making any difference between :

- a complete fragmentation of the pipe, due to a violent reaction,
- a fragmentation of only one part of the pipe, generally near one of the two caps, which may be the result of a pressure burst.

### 3 - ARTICLES TESTS :

Having much less experience with articles tests than with substances tests we can only, in that part of the paper, analyse the validity of pass/fail criteria, and their consequences, for predicting the behavior of a munition. In fact, what we consider as important is the interest of the substances tests in preventing the use, in C/D 1.6 articles, of high explosives with intrinsical properties not sufficient to guarantee an intrinsical safety of the munition.

### **3.1. External Fire :**

The expected behavior for passing the criterion is a reaction no more severe than a burning, which, as shown by the hazard analysis protocol we have established for fuel fire response (see appendix 6), can be reached by several ways:

- ① by a temperature deconfinement of the case,
- ② by a pressure deconfinement of the case before ignition, due to pyrolysis gases,
- ③ or, in case of ignition, by having a high explosive which will burn slowly enough to only mildly break the case.

The EIDS External Fire Test 7e) will provide information for points ② and ③, but only in a medium confinement system (4mm steel).

Then it can be considered as a good screening test for high explosives candidates for C/D 1.6 articles with medium or high confinements, since it reproduces well the physical behavior allowing a smooth response of such an ammunition. But on the contrary, this filter may be severe for low confinement munitions, and for temperature degradable structures.

### **3.2. Slow Cookoff :**

The mechanisms playing a role for the munition response to such a stimulus are more complex than for the fuel fire.

The works performed at SNPE for some years allowed us to establish a draft of hazard analysis protocol, based on the fuel fire protocol (see appendix 7).

A reaction no more severe than a burning may also be expected by several ways :

- ① by a temperature deconfinement of the case, which is very unlikely by heating at only 6F/hr
- ② by a pressure deconfinement of the case before ignition, due to pyrolysis gases
- ③ or, in case of ignition, by having a high explosive which will burn slowly enough to only mildly break the case, but this after a "cooking" of more than 25 hours.

The EIDS Slow Cookoff Test 7f) will provide informations for points ② and ③, but also only in a medium confinement system (4mm steel).

Then once again this test can be considered as a good screening test for high explosives candidates for C/D 1.6 articles, with the same observations than for fuel fire, regarding the confinement.

### **3.3. Bullet Impact :**

According to the protocol in appendix 8, and as shown by all the works performed at SNPE for more than ten years about this topic [9, 12], two of the EIDS tests are representative of the most important parameters regarding to the hazard of detonation or violent reaction to bullet impact, which is dependent on :

- 1) the ignitability of the high explosive, which isn't taken into account by any of the EIDS tests. But the absence of reaction is not a requirement for C/D 1.6.
- 2) the mechanical behavior to high rate sollicitation and the quickness of the damaged material, which are both covered by the Friability Test. Both of these properties are very important in the process of transition from burning to deflagration, and to detonation.
- 3) the ability of the high explosive to burn layer by layer, even at pressures as high as some Kbar. We generally are used to assess this behavior by burning in high pressure closed vessel [8]. But the EIDS External Fire test has also be found able to assess that property, since a mild reaction at this test is only possible with high explosives remaining compact during burning under confinement.

Then among the EIDS tests, the Friability and External Fire tests are together good filters to screen high explosives candidates for C/D 1.6 articles, with no violent reaction to bullet impact.

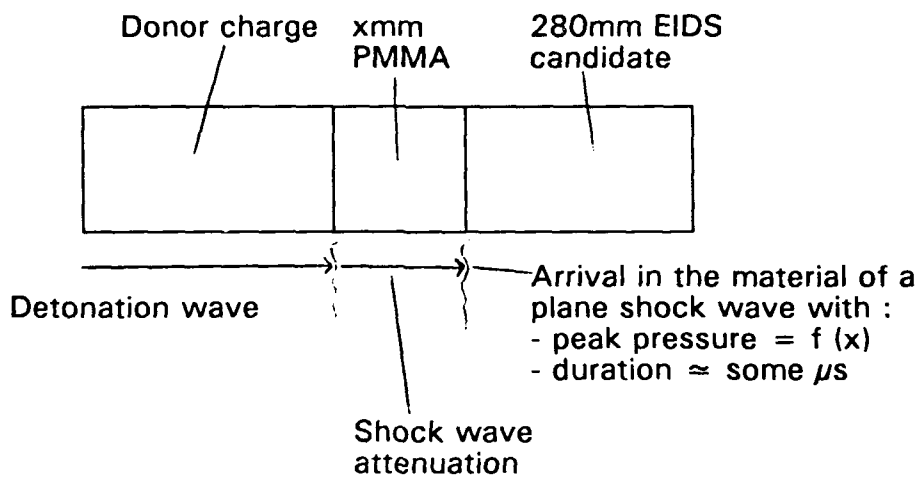
For example, in the case of a heavily confined warhead :

- $5 < \text{Friability} < 20 \text{ MPa/ms}$  ---> good chance of pneumatic burst
- $\text{Friability} < 5 \text{ MPa/ms}$  ---> good chance of burning only

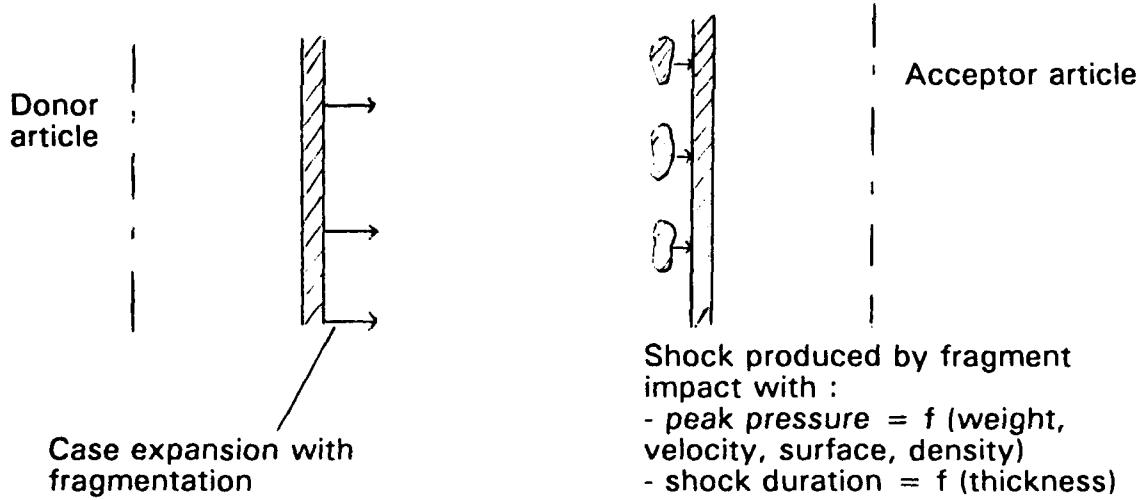
### **3.4. Detonation Propagation :**

The Gap Test is the only EIDS test acting as a filter regarding to the hazard of detonation propagation.

But if we look at the description of that test, we can see that the EIDS candidate is only assessed regarding to its initiation in detonation by a plane shock wave generated through an inert material :



The situation is different when talking about sympathetic detonation :



The sympathetic detonation process is then not only dependent on the high explosive shock sensitivity, but also on the energy put into the fragments by the donor charge.

These figures only summarise the difficulty in simply correlating the Gap Test data to the sympathetic detonation process. But some results available now allow nevertheless to better precise the limitation of such an interpretation.

For example, in the case of articles with 12.5mm thickness steel structure, the figure in appendix 9 shows which kind of information can be expected from the EIDS Gap Test.

So, in such a configuration (1 donor/1 acceptor, 12.5mm steel confinement naturally fragmentated), an EIDS candidate which just passes the 70mm PMMA criterion could no sympathetically detonate in articles with only diameters less than 110mm.

But this interpretation must be taken with care since it doesn't take into account many important aspects of the problem :

- the stack effects due to higher confinement,
- the notions of run distance and critical diameter,
- the presence of a booster,
- shock waves reflections which can occur in a munition.

So, the EIDS Gap Test occurs as a filter not too severe with the 70mm PMMA criterion ( $\approx 4.0$  GPa), and as less severe as the confinement will be heavy and the article diameter will be large.

#### **4 - CONCLUSIONS**

The number of data obtained by performing the test series 7 from the UN protocol for C/D 1.6 has now reach a level sufficient to better know what means exactly that protocol :

1° The EIDS tests have been demonstrated to well exhibit the hazardous behaviors of known unsafe high explosives : mainly compo.B and Octol, and at a lower degree TNT, Tritonal and HBX3.

2° On another hand, regarding to the impact sensitivity assessment, the two alternative methods lead globally to the same verdict, when taken together with the Gap Test.

3° As a consequence we can now figure more precisely what looks like a true EIDS, with the key point being to pass the Gap Test criterion :

- not sensitive to the standard detonator ( $D_c > 10$ mm)
- no go at Gap Test behind 70mm PMMA ( $P_i > 4.0$  GPa)
- Friability less than 5 MPa/ms at 150m/s, or  
Susan result less than 10KPa at 333m/s and no more than burning at 0.5 caliber bullet impact.
- no more than pneumatic burst at fast cookoff in confined pipe (then burning layer by layer under high pressure)
- no more than pneumatic burst at slow cookoff in confined pipe (burning layer by layer under high pressure after "cooking").

SNPE can propose at this time two true EIDS :

- B 2211 for underwater and air blast applications,
- B 2214 for naturally fragmented warheads. Some others candidates are on the way to pass all the criteria, with higher performances.

4º Among the five EIDS tests, four have been found very pertinent as screening tests before performing the article tests :

- the EIDS tests for fuel fire, slow cookoff and bullet impact are well fitting with hazard analysis protocols established by SNPE
- the EIDS Gap Test has to be interpreted carefully, because of the limitations about its meaning as a function of the important parameters playing a role in the sympathetic detonation process.
- the Cap Test has not been found relevant of any accidental situation.

As a conclusion :

- the use of EIDS is probably the best way of offering loadings with intrinsical properties which can guarantee an intrinsical safety of a munition. In some cases this guarantee could probably seem at a higher level than what could be required for the munition (munitions with very low confinement). But on another hand, those munitions would be severely damaged in a disaster, and then require more intrinsically safe substances.
- the four article tests are well in accordance with most of the other IM requirements, although some adaptations could be interesting in order to be fully similar (with STANAG for example). Even if those requirements are narrowly specified (0.5 caliber bullet at 850 m/s for example), the use of EIDS allows to expect good behaviors in a larger range of stimulus (for instance with tumbling bullets).

## REFERENCES

- [1] Recommendations on the Transport of Dangerous Goods : Test and Criteria Manual, ST/SG/AC 10/11/Rev.1, 1990
- [2] WARD, J.M., "Hazard Class/Division 1.6 Test Protocol," presented at the 1990 JANNAF Propulsion Systems Hazards Subcommittee Meeting, April 1990.
- [3] SWISDAK, M.M., "Hazard Class/Division 1.6 Articles Containing Extremely Insensitive Detonating Substances" 24th Explosives Safety Seminar, p. 1025-1041, 1990
- [4] SWISDAK, M.M., "Hazard Class/Division 1.6 Articles Containing Extremely Insensitive Detonating Substances" (EIDS), "NSWC TR 89-356, 1 Decembre 1989 review
- [5] CUMMING, A.S. et al., "Insensitive High Explosives and Propellants - The United Kingdom Approach", ADPA Insensitive Munitions Technology Symposium, Williamsburg, 1992
- [6] CORLEY, J.D. et al. "Fuzed Insensitive General Purpose Bomb Containing AFX 644", ADPA Insensitive Munitions Technology Symposium, Williamsburg, 1992
- [7] R. KENT and J.M. PINCHOT, "Study of the Explosive Behavior of Highly Confined Cast PBXs Submitted to Bullet Impact", Propellants, Explosives, Pyrotechnics 16, 221-226, 1991
- [8] J. ISLER, "Combustion Mechanisms of High Explosives and their Relation with the DDT Process", Propellants, Explosives, Pyrotechnics 16, 151-155, 1991
- [9] J. ISLER, M. QUIDOT, "Evaluation du risque de transition en détonation des chargements explosifs", 22nd International Annual Conference ICT, Karlsruhe, 1991
- [10] Air Senior National Representative (ASNR) Long Term Technology Project (LTTP) with a MOU between US, UK, Germany and France : Insensitive High Explosives
- [11] DOBRATZ B.M., CRAWFORD P.C., "LLNL Explosives Handbook," UCRL - 52997 change 2, 1985
- [12] J. ISLER, P. GIMENEZ, S. HAMAIDE, "Experimental Assessing of Energetic Materials for IM Applications", ADPA Meeting on Compatibility of Plastics and other Materials with Explosives", San DIEGO, 1991.

Appendix 1 : C/D 1.6 Test Series (from [3])

TEST NUMBER	NAME OF TEST	COUNTRY OF ORIGIN	FAILURE CRITERIA
<b>TESTS ON SUBSTANCES</b>			
7(a)	EIDS CAP TEST	Germany/US	Detonation of any sample
7(b)	EIDS GAP TEST	US	Detonation at gap of 70 mm
7(c) (i)	SUSAN TEST	US	P>27kPa @ v=333 m/s
7 (c)(ii)	FRIABILITY TEST	France	dp/dt >15 MPa/ms for v=150 m/s
7(d) (i)	EIDS BULLET IMPACT TEST	US	Explosion/Detonation
7(d)(ii)	FRIABILITY TEST	France	dp/dt >15 MPa/ms for v=150 m/s
7(e)	EIDS EXTERNAL FIRE TEST	UN	Detonation, fragment throw > 15 m
7(f)	EIDS SLOW COOK-OFF TEST	US	Detonation, > 3 fragments
<b>TESTS ON ARTICLES</b>			
7(g)	1.6 ARTICLE EXTERNAL FIRE TEST	UN	C/D 1.1, 1.2, or 1.3 response
7(h)	1.6 ARTICLE SLOW COOK-OFF TEST	US	Reaction > burning
7(j)	1.6 ARTICLE BULLET IMPACT TEST	US	Detonation
7(k)	1.6 ARTICLE STACK TEST	UN	Propagation

Appendix 2 : Details on SNPE test substances

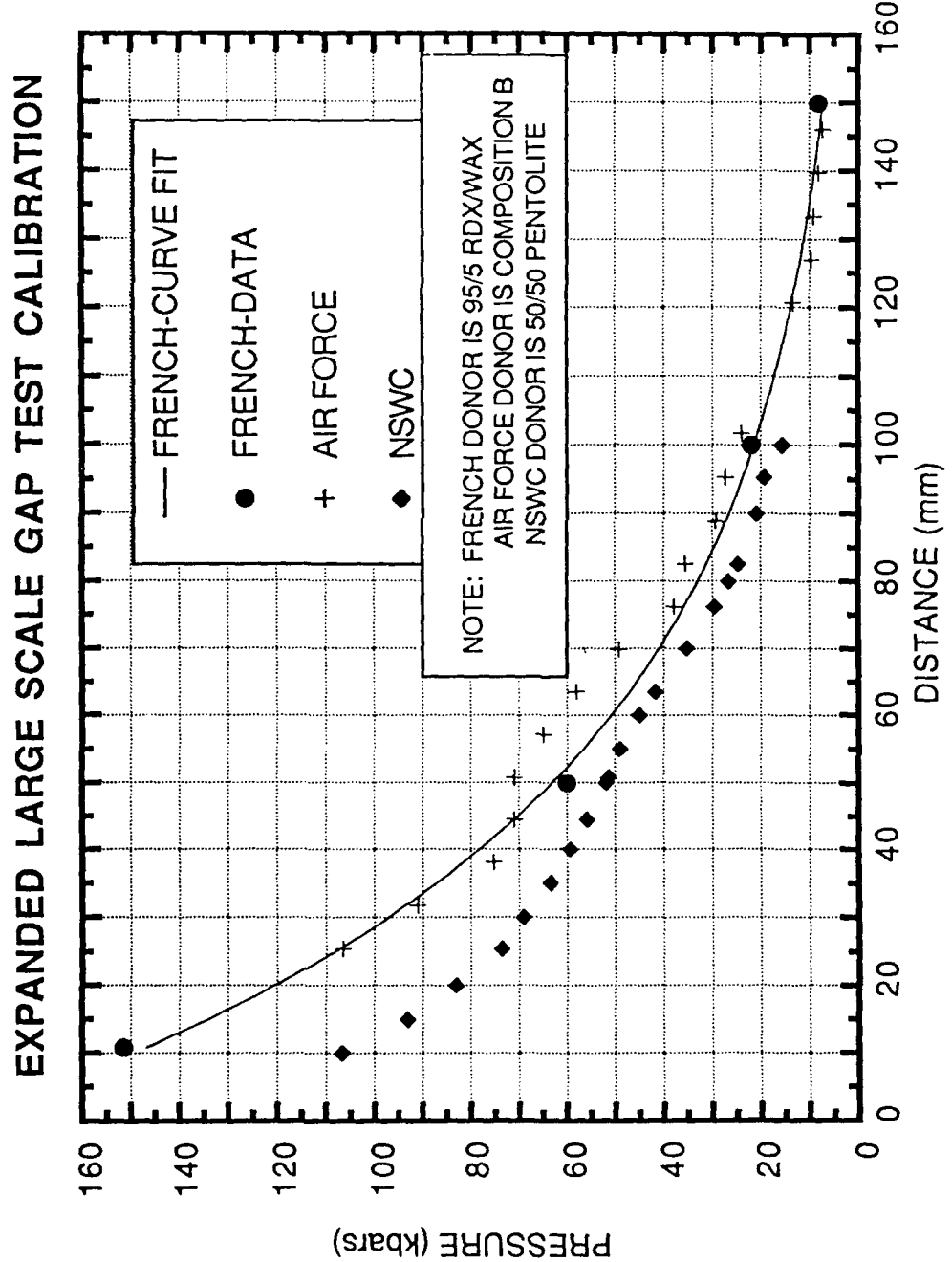
- Inert binder PBXs :

ORA 86 : HMX  
 B2214 : HMX - NTO  
 B2211 : RDX - AP - AI

- Energetic binder PBXs :

B3003 : HMX  
 B3103 : HMX - AI  
 B3017 : NTO  
 B3021 : HMX - NTO

Appendix 3 : EIDS Gap Test calibration



**Appendix 4 : Friability and Bullet Impact data**

REFERENCE	COMPOSITION	BULLET IMPACT (m/s)				FRIABILITY D <sub>max</sub> (MPa/ms) at V = 150 m/s
		740	810	930	1140	
HEXOLITE 65/35	- TNT - RDX	D	D	D	D	114
E1	- PU - HMX	E	E	E	D	51
E2	- PU - HMX	E	E	E	D	42
E3 (B 3003)	- G - HMX	D	D	D	D	26,5 at V = 87 m/s
E4	- PU - HMX	A	E	E	D	24
E5	- PU - HMX	E	E	E	D	21,6
E6	- PB - RDX			DEF	DEF	17
E7	- PB - HMX		DEF	DEF	DEF	15,4
E8 (ORA 86A)	- PU - HMX	A	DEF	DEF	DEF	8,0
E9	- PB - HMX		DEF	DEF	DEF	6,7
E10	- PB - RDX - Alu	DEF	DEF	DEF	C	5,5
E11 (B 3103)	- G - HMX - Al	DEF	DEF	DEF	DEF	3,9
E12	- PU - HMX	DEF	DEF	DEF	DEF	3,3
E13	- PU - TATB - HMX			A	A	0,5
E14	- PU - HMX - NTO	-	-	A	C	0,5
E15 (B 2214)	- NTO - HMX - PB	-	-	C	C	0,2

G = energetic binder

PU = polyurethane binder

PB = IITPB binder

D = detonation

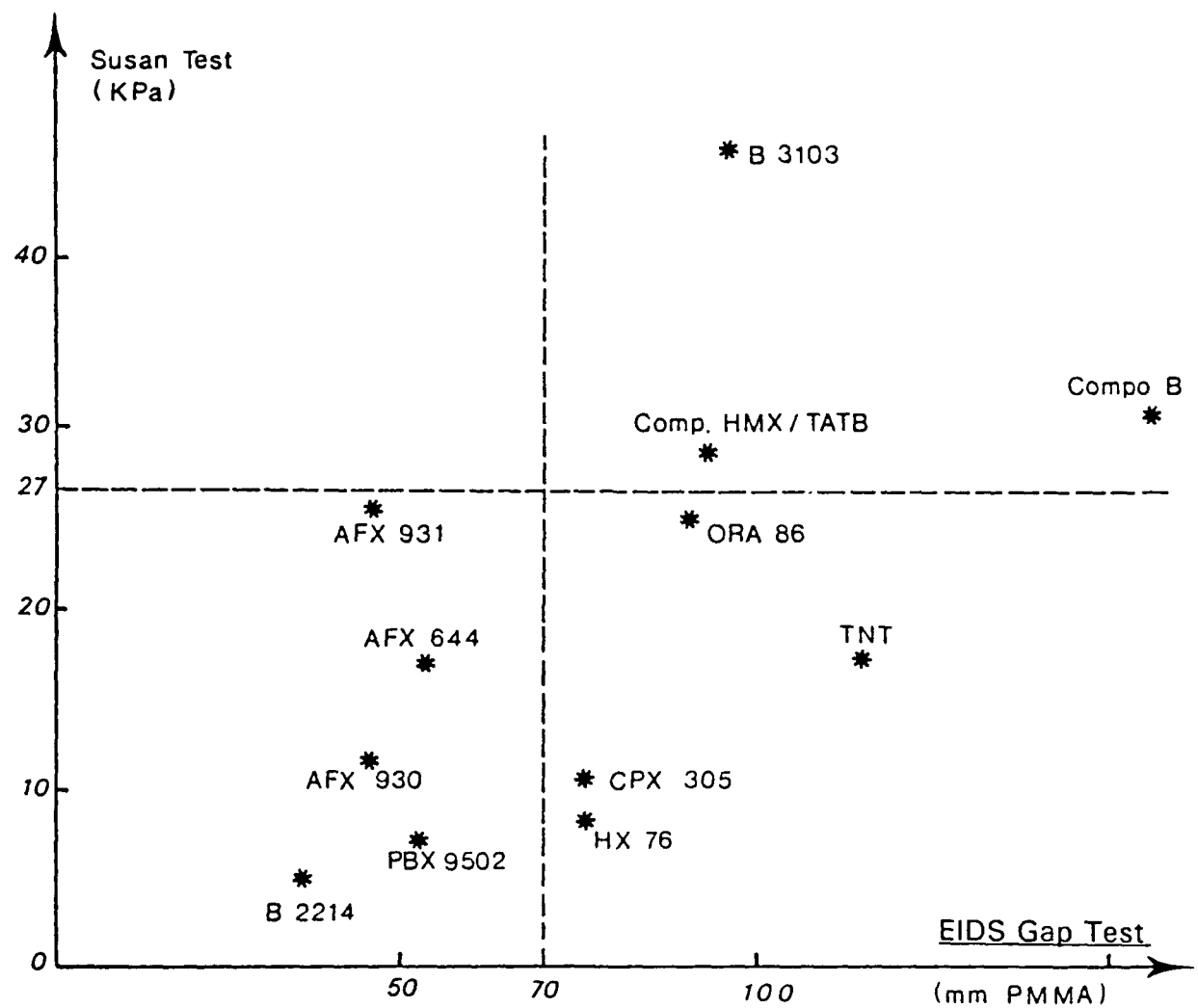
E = violent opening of the case with case fragmentation

DEF = opening of the case by caps ejection

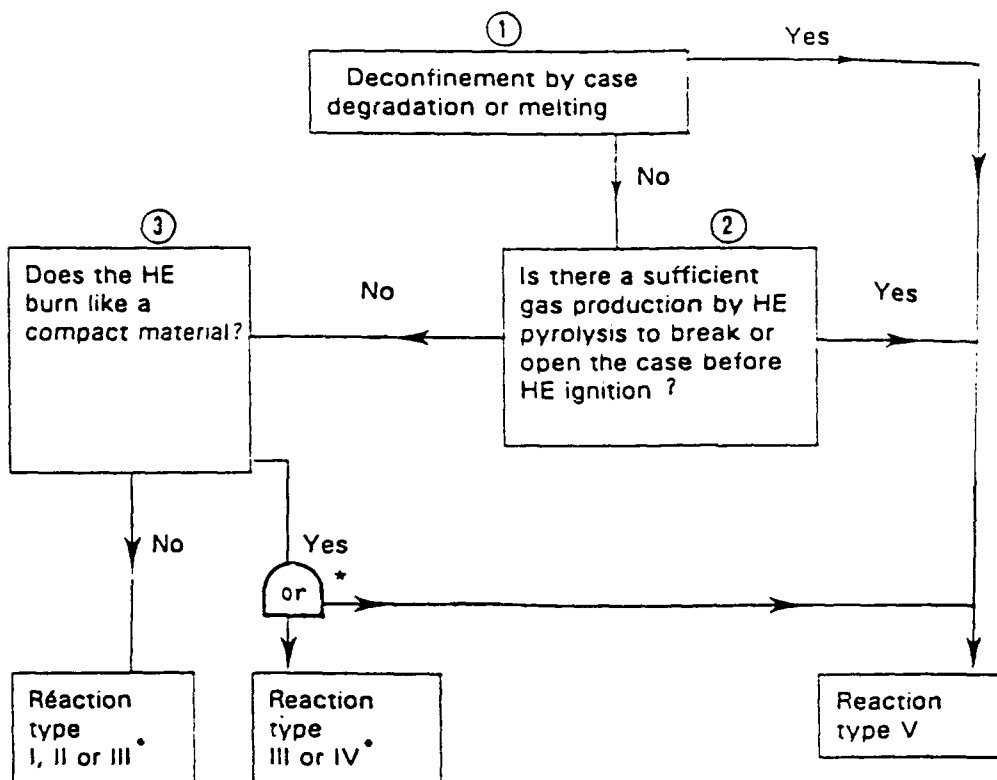
C = combustion without opening of the case

A = absence of reaction

Appendix 5 : Susan Test/Gap Test comparisons



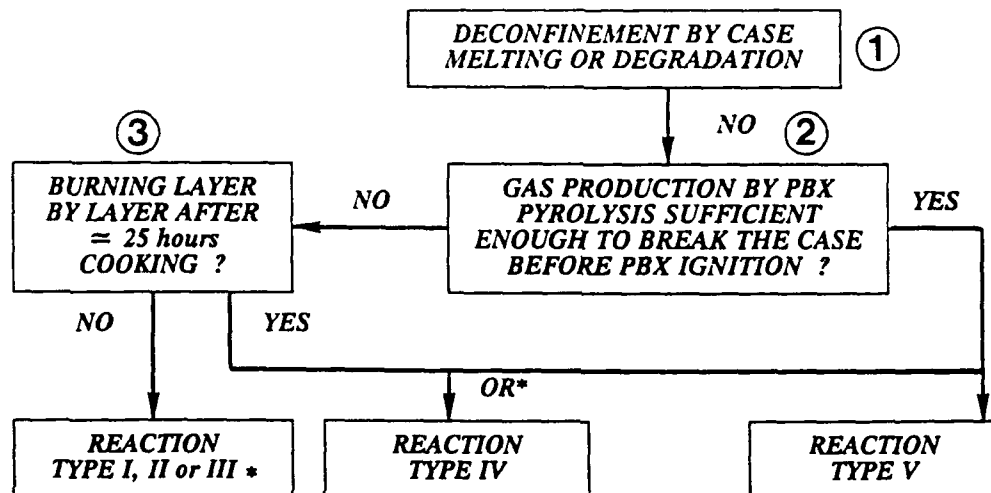
Appendix 6 : Hazard analysis protocol for fuel fire



\* depending on confinement

Type I	:	detonation
Type II	:	partial detonation
Type III	:	explosion
Type IV	:	deflagration
Type V	:	combustion

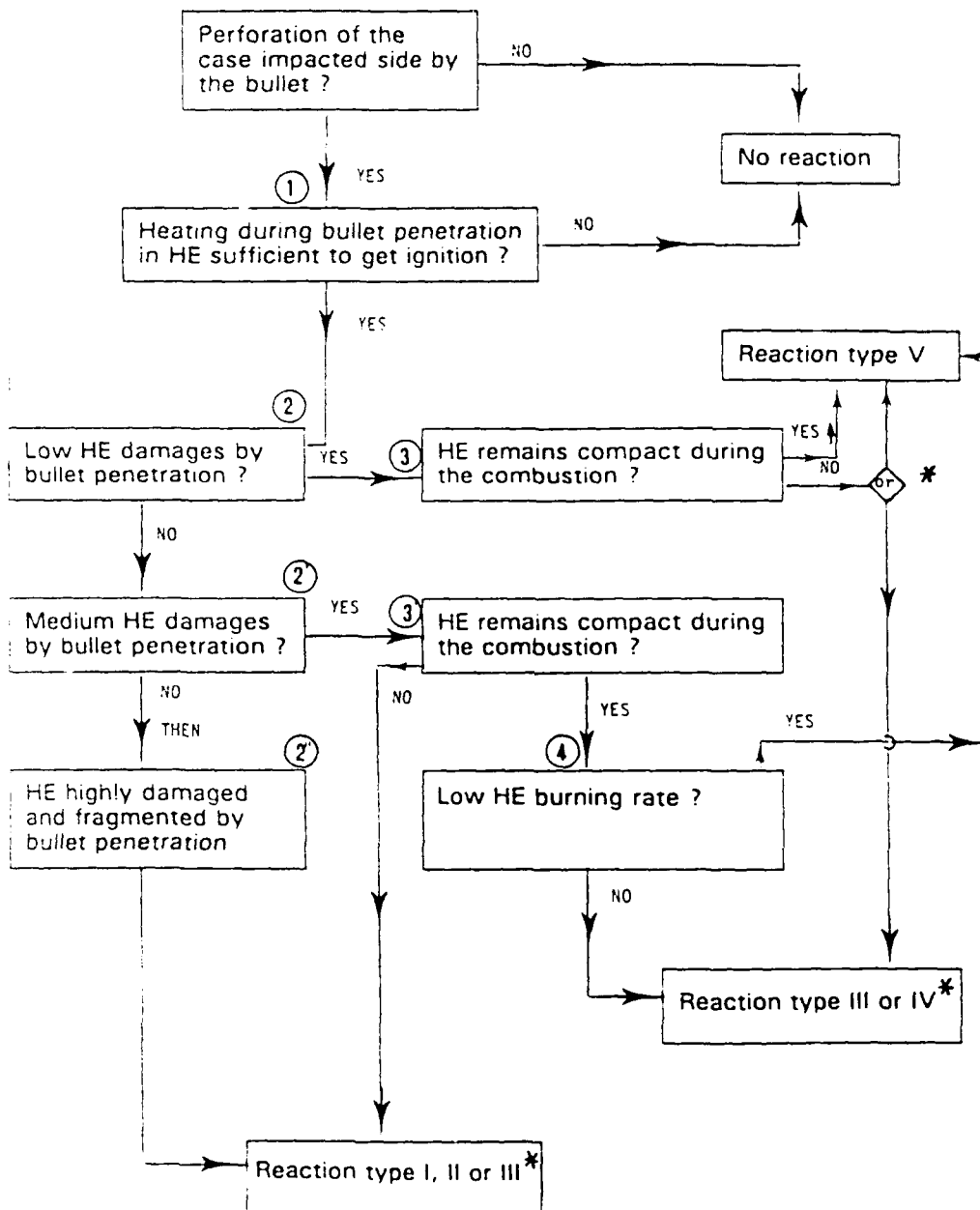
Appendix 7 : Hazard analysis protocol for slow cookoff



- \* : Depending on confinement
- (1) : Very unlikely with SCO
- (2) and (3) : According to 40 mm diameter confined pipe test

Type	I	: detonation
Type	II	: partial detonation
Type	III	: explosion
Type	IV	: deflagration
Type	V	: combustion

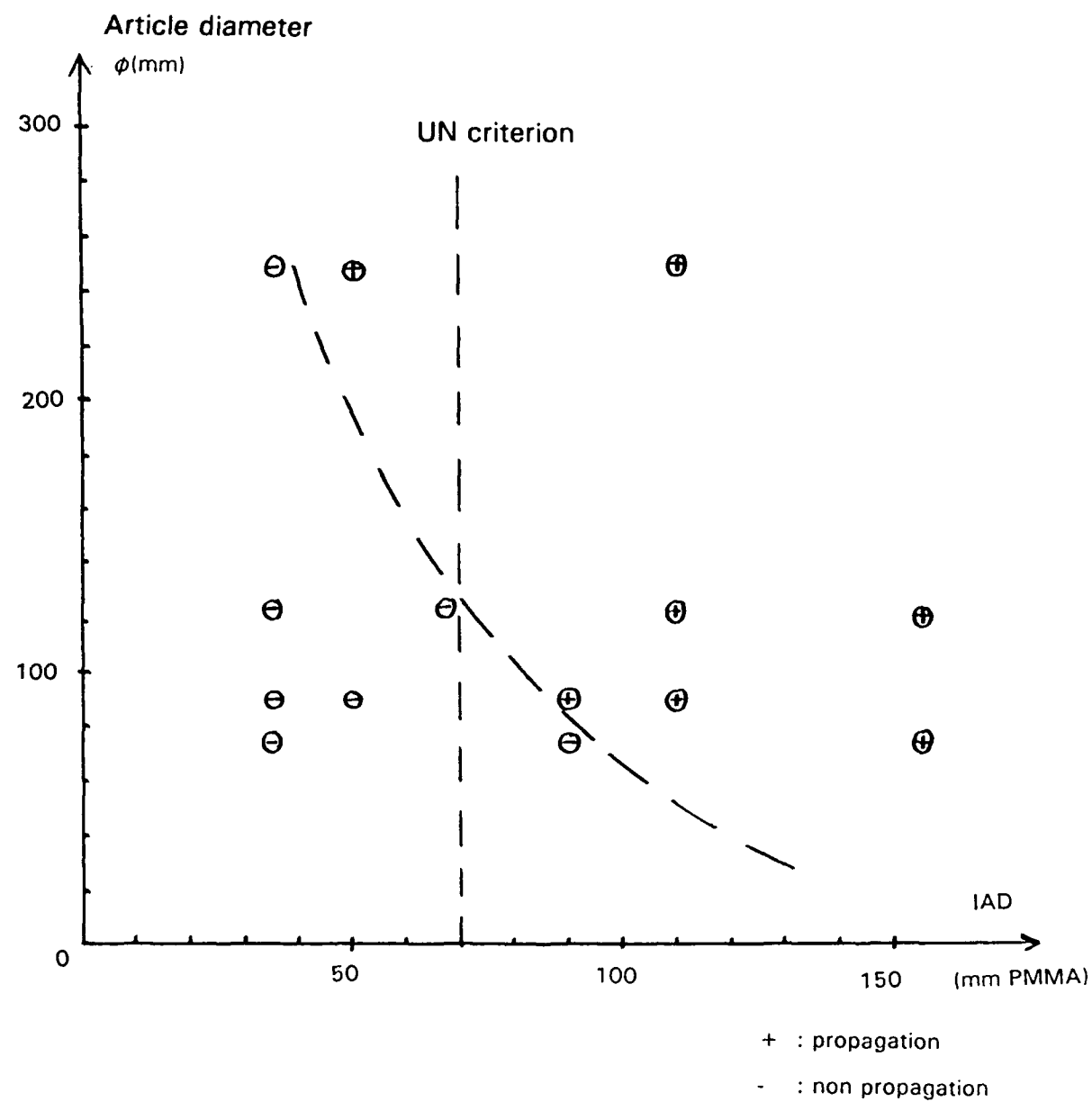
Appendix 8 : Hazard analysis protocol for bullet impact on confined warhead.



- |          |   |                    |
|----------|---|--------------------|
| Type I   | : | detonation         |
| Type II  | : | partial detonation |
| Type III | : | explosion          |
| Type IV  | : | deflagration       |
| Type V   | : | combustion         |

\* depending on confinement

**Appendix 9 : Comparisons between Gap Test and Sympathetic Detonation results in articles with 12.5 mm steel case.**



## **WHAT Q/Ds FOR H.D. 1.6 ?**

prepared by

Jacques C. Besson

French Ministry of Defence  
Délégation Générale pour l'Armement  
Inspection de l'Armement pour les Poudres et Explosifs  
Centre SULLY - B.P. 24 - 92211 SAINT-CLOUD Cedex - FRANCE

### **Abstract**

In 1988 the NATO Working Group AC/258 decided to apply U.N. recommendations for the classification of military ammunition and explosives for transport and storage purposes. This decision had no consequences on what has made the AC/258 Group's reputation , the determination of safety distances to storage magazines, more commonly called the Q/D rules.

In 1989 the United Nations Group of Experts on Transport of Dangerous Goods introduced a new Hazard Division (HD), namely the Hazard Division 1.6. which was immediately adopted by AC/258 with the secret hope that this new division could one day be assigned to future Insensitive Munitions.

The elaboration of the storage rules for this new H.D., Q/D rules and mixed storage rules, has been on the agenda of AC/258 ever since. There are technical difficulties and the stakes are consequent. They are related to safety, of course, but they are also of economical nature.

From the assessment of the most probable accidental event, France has made a proposal on which this paper is based.

## **TABLE OF CONTENTS**

1. Introduction
2. Recall of the definition and classification criteria of Hazard Division 1.6 articles
3. The position of AC/258 Group
4. Consequences of the definition of Hazard Division 1.6 on the "most probable accidental event"
5. Proposed rules for the storage of 1.6N munitions.
  - 5.1. Safety distances
  - 5.2. Compatibility groups mixing
  - 5.3. Hazard divisions mixing
6. Conclusion

**ANNEX : Tests and criteria for Hazard Division 1.6 articles**

**LIST OF REFERENCES**

## ***1. Introduction***

When deciding, in 1989, to introduce, in class 1 of dangerous goods, a sixth Hazard Division (HD) 1.6, the United Nations Committee of Experts on the transport of dangerous goods (UNCOE) satisfied a need expressed already since a few years by some nations. Above all the Committee did take a bet on the future deemed to encourage explosive technology to move towards products safer to transport.

Two years later the aim has not yet been reached : today there is no 1.6 article recognised as such. Therefore there is no statistical data on the behaviour of these articles when stored or transported. The new hazard division remains an empty set which, yet, must be prepared to welcome the future 1.6 articles by providing them with attractive yet safe storage and transport rules.

But researches continue; the aim comes nearer and the move towards products less sensitive to accidental aggressions seems irreversible.

## ***2. Recall of the definition and classification criteria of Hazard Division 1.6 articles***

U.N. Committee has defined HD 1.6 as

"the division which comprises articles which contain only extremely insensitive detonating substances and which demonstrate a negligible probability of accidental initiation or propagation."

The risk from articles of Division 1.6 is limited to the explosion of a single article."

A new compatibility group was created at the same time, namely the group "N"; it can only be used for HD 1.6 articles which then necessarily carry the classification code "1.6N".

The guarantee that the 1.6N articles do have the qualities specified in the definition is obtained through several tests and criteria which are briefly recalled in annex.

More details over these tests can be found in the "Orange Book" published by U. N. O. (cf references 1 and 2).

The tests are regrouped into three tests series:

a) Series 3 tests which are applied to all substances and articles of Class 1.

These tests answer the question : "are the explosive substances contained in the candidate 1.6N ammunition too dangerous to be transported ?"

These tests determine the sensitivity to mechanical stimuli like shock and friction, and to heat and flame .

b) Series 7 tests for substances

Substances contained in the 1.6N munitions are called "Extremely Insensitive Detonating Substances (EIDS)". They must pass five tests to prove their insensitivness.

c) Series 7 tests for articles

The articles, to be classified 1.6N, must pass the four series 7 tests for articles.

It has to be noted that

- a candidate 1.6N must pass 9 specific tests

- articles from other Hazard Divisions, 1.2, 1.3 and 1.4, have also a negligible probability of mass detonation or propagation. But it is the first time that tests on substances are used to complete the guarantee given by the tests on the articles.

### **3. The position of AC/258 Group**

The Terms of Reference of AC/258 NATO Working Party cover all safety aspects of all modes of transportation and storage of military ammunition and explosives within NATO. The Group comprises experts from 14 nations and its 25th anniversary has just been celebrated. The Group, being the only international group dealing with storage safety, is well known for the "Manual on NATO safety principles for the storage of military ammunition and explosives" where the hazard division classification concept was introduced for the first time.

AC/258 Group has decided to take U. N. O. path and to introduce also, in storage, 1.6N classification (cf reference 3 and 5).

Tests and criteria which allow to assign an article (munition) to hazard division 1.6 are the same as those U. N. O. decided to use for transport. This decision fits the general policy of the Group which is to use the same tests and criteria in storage as in transport, since the aggressions encountered in storage and in transport are generally considered not significantly different.

Wheras the classification for transport is mainly used to part articles with different risks, the classification for storage of a munition has very constraining consequences on storage infrastructures due to safety distances in relation with the mass stored (Q/D). Thus, once a new H.D. is defined, it is necessary to be able to have at one's disposal very soon the Q/Ds and mixing rules between different hazard divisions and compatibility groups.

AC/258 Group had to establish these rules before the first 1.6N munitions arrive in stock.

To do this, it was first necessary to determine "the most probable accidental event" liable to happen during the storage of 1.6N ammunition.

The storage rules that will follow must be as simple to apply as possible, and consistent with the rules for the other HD as the hazards are the same. They must be "incitive", which means that, when applied, they lead to a reduction of the constraints on the surrounding of the storage facilities induced by the current penalizing HD, 1.1 and 1.2 rules.

Safety of persons and assets but also environmental and economical factors are at stakes.

It is in this framework that the French proposal was elaborated.

#### **4. Consequences of the definition of Hazard Division 1.6 on the "most probable accidental event"**

Under accidental stimuli a stock of munitions can:

- mass detonate (1.1)
- explode on an intermittent way (1.2)
- burn(1.3)
- have no significant effect (1.4)

The event can spread to the whole stock or stop all by itself, one or a few munitions being concerned.

What about 1.6N ammunition ?

According to the a priori estimation one makes on the efficiency of the classification tests and criteria and because of lack of experimental data, one is tempted to adopt one of the preceding events as the most probable accidental event and therefore to apply to 1.6 the rules of 1.1, 1.2, 1.3 or even 1.4.

Starting from the above mentioned considerations and on the guarantee brought by the tests and the classification criteria, France has made the following proposal:

In a 1.6N ammunition storage, the "most probable accidental event" which may happen is the conjunction of two events :

"There is detonation of a single munition without instant transmission to the other munitions" and/or "there is moderate combustion of the whole set of munitions"

Moreover, when assessing the hazards generated by the detonation of a single munition, it is proposed to take in account only the blast effect (1.1 effect) and to neglect the projection hazard (1.2 effect).

#### Why such a proposal ?

It is the result of the following remarks:

- it would be neither realistic nor "incitive" to consider that a stock of 1.6N munitions would behave in an accident like a stock of 1.1 or 1.2 ammunition. Such a choice would not be consistent with the aims set up for Hazard Division 1.6 and, therefore, it could only be temporary.

- the choice of a type 1.4 accidental behaviour is premature . It must be noted that it is also the solution where it is most difficult to go backwards.

It could be adopted after several years of experience for it leads to an important economical and environmental gain by reducing the areas frozen by the application of the current Q/D rules.

- the projection hazard generated by the detonation of a single article can be neglected for the following reasons:

- the probability to be hit by a missile coming from the detonating munition is much smaller than the probability to be hit by the blast of the same detonation, probability which is negligible by definition.

- the way the Q/D are computed (see below) introduces an inclusive minimum distance which, in the case of Inhabited Building Distance (IBD) is 60m.

Q/D and mixing rules, as given below, are derived from these assumptions.

## **5. Proposed rules for the storage of 1.6N munitions.**

### **5.1. Safety distances**

The safety distances, or Q/D between a potential explosion site and an exposed site, are derived from the above described "most probable accidental event". The assessment of the hazards generated by the detonation of a single article considers only the blast effect and neglects the projection effect.

As a general rule, a given safety distance like the Inhabited Building Distance (IBD), Public Road Distance (PRD), Workshop Distance or Intermagazine Distance, is obtained by taking the largest of two distances:

- the corresponding safety distance which would be determined for the storage of a single article classified 1.1, with only a blast effect. This distance is found in table 1 of part 1 of the AC/258 Storage Manual (reference 3), after extension to small Net Equivalent Quantities expressed in TNT equivalent (NEQ) by using the proper formula

- the corresponding safety distance which would be determined for the storage of the whole stock of ammunition classified 1.3. This distance is found in table 3 of part 1 of the Manual, the minimum distance being maintained.

As an exemple, let us consider a 50000 kg open stack of bombs, each bomb having a NEQ of explosive of 100kg.

The AC/258 Manual gives, as Inhabited Building Distance:

- for a single article classified 1.1: in an open stack

$$D_{13} = 5.5 \times Q^{1/2} = 5.5 \times (100)^{1/2} = 55\text{m}$$

- for the whole stock classified 1.3: in an open stack

$$D_4 = 6.4 \times Q^{1/3} = 6.4 \times (50000)^{1/3} = 235\text{m}$$

The IBD for the stock of bombs classified 1.6 would be at least 235m.

The IBD for the same stock of bombs classified 1.1 would have been 818 m and, if classified 1.2, 480m according to NATO rules.

## **5.2. Compatibility groups mixing**

It must be noted that, due to the fact that Compatibility Group "N" is only used for HD 1.6, mixing 1.6 articles with other hazard divisions articles, is like mixing Compatibility Group "N" with other compatibility groups "A", "B", "C" ... .

By definition, mixing articles of different compatibility groups is forbidden except with Compatibility Group "S" necessarily associated with HD 1.4. However NATO rules allows mixing of munitions of Compatibility Groups "C", "D" and "E".

Thus, by analogy, it is proposed to authorized mixing of 1.6N munitions with Compatibility Groups "S", "C", "D" and "E" munitions.

With "S" the compatibility group of the mixed set would remain "N" (and thus the hazard division 1.6).

With "C", "D" and "E" the compatibility group of the mixed set would become "D" (and the hazard division would no longer be 1.6).

### **5.3. Hazard divisions mixing**

To be consistent with the above mentioned compatibility group mixing rules, one must consider that mixing of 1.6 articles with articles of other hazard divisions is authorized provided that the compatibility groups involved are "C", "D", "E" or "S".

The hazard division of the resulting mixed set is obtained by determining the resulting "most probable accidental event".

This gives the following rules:

A mixed set of H.D. 1.6 articles with

- 1.1 articles belongs to H.D. 1.1,
- 1.2 articles belongs to H.D. 1.2,
- 1.3 articles belongs to H.D. 1.1 except if it has been demonstrated otherwise by test or by analogy,
- 1.4 articles belongs to H.D. 1.6,
- 1.5 articles belongs to H.D. 1.1,
- 1.6 articles of another family belongs to H.D.

1.1 except if it has been demonstrated otherwise by test or by analogy.

In all cases other than a mixed set of 1.6 and 1.4, the NEQ of the resulting mixed set is obtained by aggregation of the two NEQ.

In the case of mixing 1.4 and 1.6 only the 1.6 NEQ is to be considered.

## **6 Conclusion**

The French proposal was welcomed by AC/258 Group when presented at the May 1992 meeting of this group. The odds are good that the final agreement will be reached at the beginning of 1993.

It is close to a similar proposal made by the USA.

The proposed rules meet the requirements : simplicity, "incitativity" , consistency with the rules for other hazard divisions. When adopted, the storage rules for 1.6 will give safety to the surrounding of the storage facilities with a reasonable risk level.

## ANNEX

### TESTS AND CRITERIA FOR HAZARD DIVISION 1.6

#### Test series 7 for substances (EIDS)

7(a)	CAP test	sensitivness to detonation
7(b)	GAP test	sensitivness to shock
7(c)(i) and 7(d)(i)	Susan impact test Bullet impact test	sensitivness to impact
or		
7(c,d)(ii)	Friability test	sensitivness to impact
7(e)	External fire test	reaction to external fire
7(f)	Slow cook off test	reaction to increasing heat

#### Test series 7 for articles

7(g)	External fire test	reaction to fire
7(h)	Slow cook off test	reaction to increasing heat
7(j)	Bullet impact test	sensitivness to impact
7(k)	Stack test	transmission of detonation

#### Criteria:

Several tests of the same kind are made.  
For 7a, 7b, 7d, 7e, 7f, 7g, 7h, 7j there must be no detonation.  
For 7k there must be no propagation.  
For 7c(i) and 7d(ii) it depends on the measurements made.

## **LIST OF REFERENCES**

- 1 U.N. recommendation on the transport of dangerous goods - 7th revised edition 1991
- 2 U.N. recommendation on the transport of dangerous goods - Tests and criteria - 2nd edition 1990
- 3 NATO Publication AASTP 1 "Manual of NATO safety principles for the storage of military ammunition and explosives" (edition May 1992)
- 4 NATO Publication AASTP 2 "Manual of NATO safety principles for the transport of military ammunition and explosives" (edition May 1992)
- 5 NATO STANAG 4123 (2nd revision) on the determination of the classification of military ammunition and explosives. This document is being revised; it will be completed by NATO Publication AASTP 3 "Manual of NATO principles for the hazard classification of military ammunition and explosives"

**SENSITIVITY AND PERFORMANCE  
EVALUATION  
OF A**

**1.6 CANDIDATE EXPLOSIVE**

**AFX-770**

**PRESENTER: LARRY PITTS**

# **CREDITS**

**CO-AUTHORS:**

**MR JOHN CORLEY**

**MR GREG GLENN**

**CAPT ELTON GRISSOM**

**MR STEPHEN STRUCK**

# **CREDITS**

## **ORGANIZATIONS:**

**WRIGHT LABORATORY**

**ARMAMENT DIRECTORATE**

**MUNITIONS DIVISION**

**ENERGETIC MATERIALS BRANCH**

**ATLANTIC RESEARCH CORPORATION**

**VIRGINIA AND ARKANSAS**

**PROPULSION DIVISIONS**

# **BACKGROUND**

## **OBJECTIVE:**

**DEVELOP A HIGH PERFORMANCE PLASTIC  
BONDED 1.6 HAZARD CLASSIFICATION  
EXPLOSIVE FOR MK82, MK84, AND BLU-109**

## **APPROACH:**

- USE FORMULATIONS RESULTING FROM  
PREVIOUS CONTRACT**
- REFORMULATE FOR MK84 AND BLU-109**
- EVALUATE IN SUBSCALE HARDWARE**
- LOAD MK82, MK84, AND BLU-109**

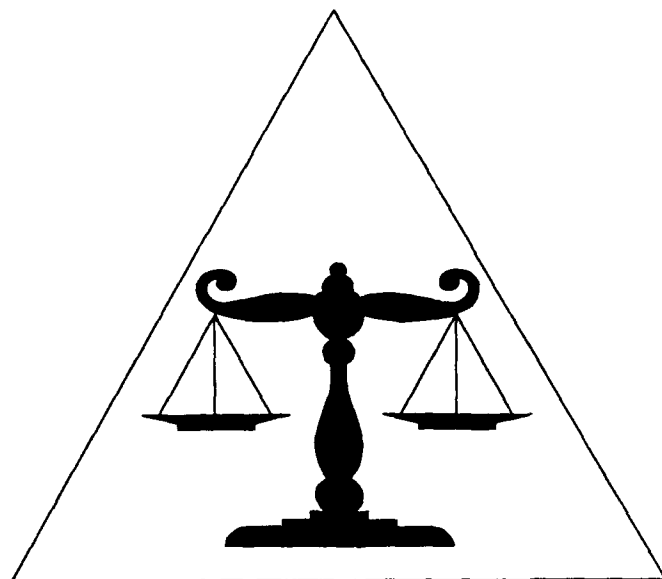
# **UN HAZARD CLASSIFICATION**

<b><u>CLASS</u></b>	<b><u>DESCRIPTION</u></b>
1.1	<b>MASS DETONATION</b>
1.2	<b>NON-MASS DETONATION/FRAG HAZARD</b>
1.3	<b>MASS FIRE</b>
1.4	<b>INDIVIDUAL FIRE</b>
1.5	<b>INSENSITIVE SUBSTANCES</b>
1.6	<b>INSENSITIVE ARTICLES</b>

# **TECHNICAL CHALLENGE**

**INSENSITIVITY**

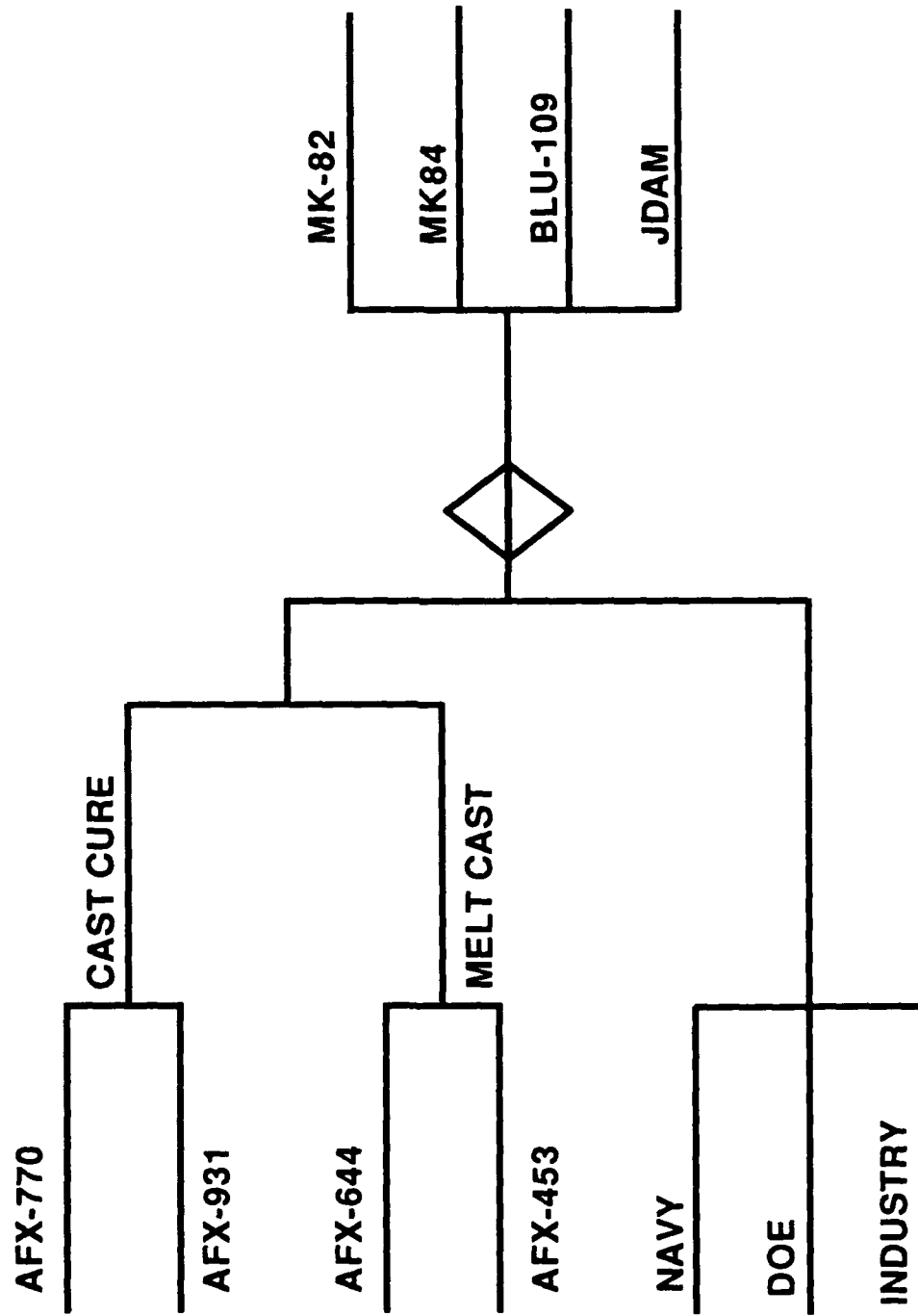
**TO SHOCK**



**ACCEPTABLE  
PERFORMANCE**

**RELIABLE  
INITIATION**

# EXPLOSIVE DEVELOPMENT



# **STARTING FORMULATIONS**

<b><u>INGREDIENT</u></b>	<b>AFX-920</b>	<b>AFX-931</b>
<b>RDX</b>	<b>22%</b>	<b>32%</b>
<b>EDDN</b>	<b>15%</b>	<b>----</b>
<b>HBNQ</b>	<b>33%</b>	<b>----</b>
<b>AP</b>	<b>----</b>	<b>37%</b>
<b>AL</b>	<b>14%</b>	<b>15%</b>
<b>HTPB</b>	<b>16%</b>	<b>16%</b>

# **AFX-920/931 MK82 EXPERIMENTS**

<b><u>TEST</u></b>	<b><u>AFX-920</u></b>	<b><u>AFX-931</u></b>
<b>FAST COOKOFF</b>	<b>BURN</b>	<b>BURN W/PROP</b>
<b>SLOW COOKOFF</b>	<b>BURN</b>	<b>BURN W/VR</b>
<b>BULLET IMPACT</b>	<b>BURN</b>	<b>BURN</b>
<b>SYM DET</b>		
<b>ONE-ON-ONE</b>	<b>PASS</b>	<b>PASS</b>
<b>PALLET</b>	<b>PASS</b>	<b>FAIL</b>
<b>6-PALLET</b>	<b>PASS</b>	<b>NO TEST</b>
<b>AIRBLAST</b>	<b>.85 TRITONAL</b>	<b>1.3 TRITONAL</b>
<b>ARENA</b>	<b>PASS</b>	<b>NO TEST</b>
<b>BOOSTER</b>	<b>NO DET.</b>	<b>DET.</b>

# PBIHE FORMULATIONS

<u>INGREDIENT</u>	<u>AFX-770</u>	<u>AFX-931</u>
RDX	27%	32%
AP	27%	37%
NQ	12%	----
AL	16%	15%
HTPB	18%	16%

# **SHOCK SENSITIVITY OF EXPLOSIVES (ELSGT)**

<b><u>EXPLOSIVE</u></b>	<b>INITIATION <u>PRESSURE (KBAR)</u></b>
TRITONAL	19
PBX-9502	71
AFX-644	74
AFX-770	73
AFX-931	73

# **AFX-770 MK82**

## **EXPERIMENT**

**FAST COOKOFF/2**

**-BURN/MINOR PROPULSION  
-BURN**

**SLOW COOKOFF/2**

**-BURN/PRESSURE RUPTURE  
-BURN**

**SYMPATHETIC  
DETONATION/5**

**-NO DETONATIONS**

**BULLET IMPACT/1**

**-BURN/MINOR PROPULSION**

**BLAST PRESSURE/1**

**-PEAK PRESS=.95 TRITONAL  
-IMPULSE=1.07 TRITONAL**

**FRAG ARENA/1**

**-NO TEST**

## **RESULTS**

# **AFX-770 BLU-109**

## **EXPERIMENT**

**FAST COOKOFF**

**-BURN/PROPULSION**

**SLOW COOKOFF**

**-BURN/PROPULSION**

**BLAST PRESSURE**

**-PEAK PRESS=1.28 TRITONAL**

**-IMPULSE=.95 TRITONAL**

**SLED TRACK**

**-BURN**

# **AFX-931 BLU-109**

## **EXPERIMENT**

## **RESULTS**

**FAST COOKOFF**

**-BURN/PROPULSION**

**SLOW COOKOFF**

**-EXPLOSION**

**SYMPATHETIC  
DETONATION**

**-NO DETONATION**

**SLED TRACK**

**-TBD**

**BLAST PRESSURE**

**-PEAK PRESS=1.25 TRITONAL**

**-IMPULSE=1.14 TRITONAL**

# **CONCLUSION**

**AFX-770 AND AFX-931 MET EIDS**

**SUBSTANCE CRITERIA**

**AFX-770 ARTICLE TESTS RESULTS**

**ENCOURAGING**

**AFX-931 DID NOT SYMPATHETICALLY DETONATE**

**IN BLU-109 - DID SYMPATHETICALLY DETONATE**

**IN MK-82**

**HEAVY WALL PENETRATORS WILL NEED VENT**

**FOR GASES IN COOKOFF**

**SHRAPNEL PROTECTION TESTING IN  
SUPPORT OF THE PROPOSED SITE 300  
CONTAINED FIRING FACILITY**

**C. F. Baker  
J. W. Pastrnak  
L. F. Simmons**

**Lawrence Livermore National Laboratory  
University of California, Livermore, California 94550**

**Abstract**

To prepare for the planned Contained Firing Facility at the LLNL Site 300, we investigated various multilayered shrapnel protection schemes to minimize the amount of material used in shielding. As a result of testing, we found that two pieces of 1-in.-thick mild steel plate provide adequate general-purpose protection from shrapnel generated by normal hydrodynamic and cylinder shots at Bunker 801.

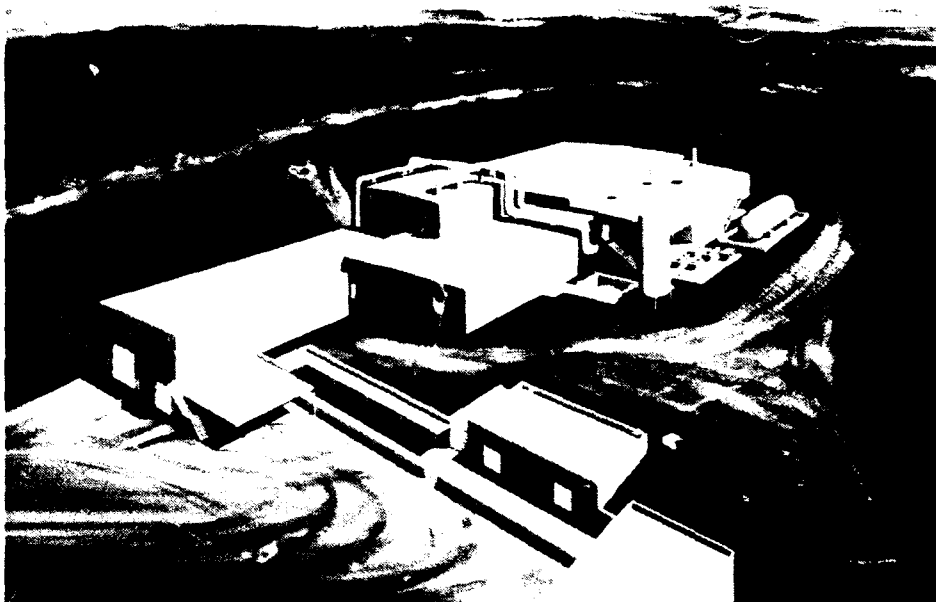


Figure 1. Artist's conception of the planned Contained Firing Facility.

## Introduction

The Contained Firing Facility, which is planned to replace open-air testing at Bunker 801, consists of a large rectangular, reinforced-concrete firing chamber lined with steel plates for shrapnel protection. Figure 1 is an artist's conception of the planned Contained Firing Facility at the LLNL Site 300. The Conceptual Design Report<sup>1</sup> requires that a typical wall section consist of 4 feet of reinforced concrete followed by a 1-in. steel pressure liner and two layers of 2-in.-thick steel armor plate.

The purpose of this testing was to experimentally subject various shrapnel protection schemes to normal types of shrapnel generated by hydrotest experiments at Bunker 801. The philosophy was to start with minimum-thickness mild steel plates and work upward, increasing plate thickness as necessary. Multilayer plate technology was selected that uses air spaces to separate steel plates. Moreover, because it was desired to determine damage caused by shrapnel, the steel plates were positioned to minimize the damage from blast effects and maximize the damage from shrapnel.

To obtain shrapnel with realistic fragment velocities and sizes, the tests were performed as "add on" experiments to actual hydrodynamic and cylinder tests. Because of required diagnostics on these shots, the steel test plates could not always be positioned in the path of worst-case shrapnel, but it is believed that most of the worst-case fragments have been sampled. This report describes nine shrapnel tests, including test configurations, comparisons of measured versus calculated penetration and perforation results, and recommendations for general-purpose shrapnel protection for the planned Contained Firing Facility at Site 300.

## Objectives

To support the proposed Contained Firing Facility, the shrapnel protection scheme must:

- Allow no damage to the pressure liner.
- Minimize fabrication costs.
- Emphasize versatility for installation and use.
- Afford easy repair and low maintenance.

## Test Descriptions

Eight tests were conducted by exposing a large 36 in.  $\times$  36 in. block assembly to various shrapnel environments. Appendix A includes a test record for each shot which shows the block geometry, the number and size of plate perforations, test setup, and damage observations from each test. Additional penetration data (Test No. 9) was obtained by observing damage to the shrapnel protection plate for the gamma ray camera (see Figs. 12, 13, and 14), a new radiographic diagnostic being developed.

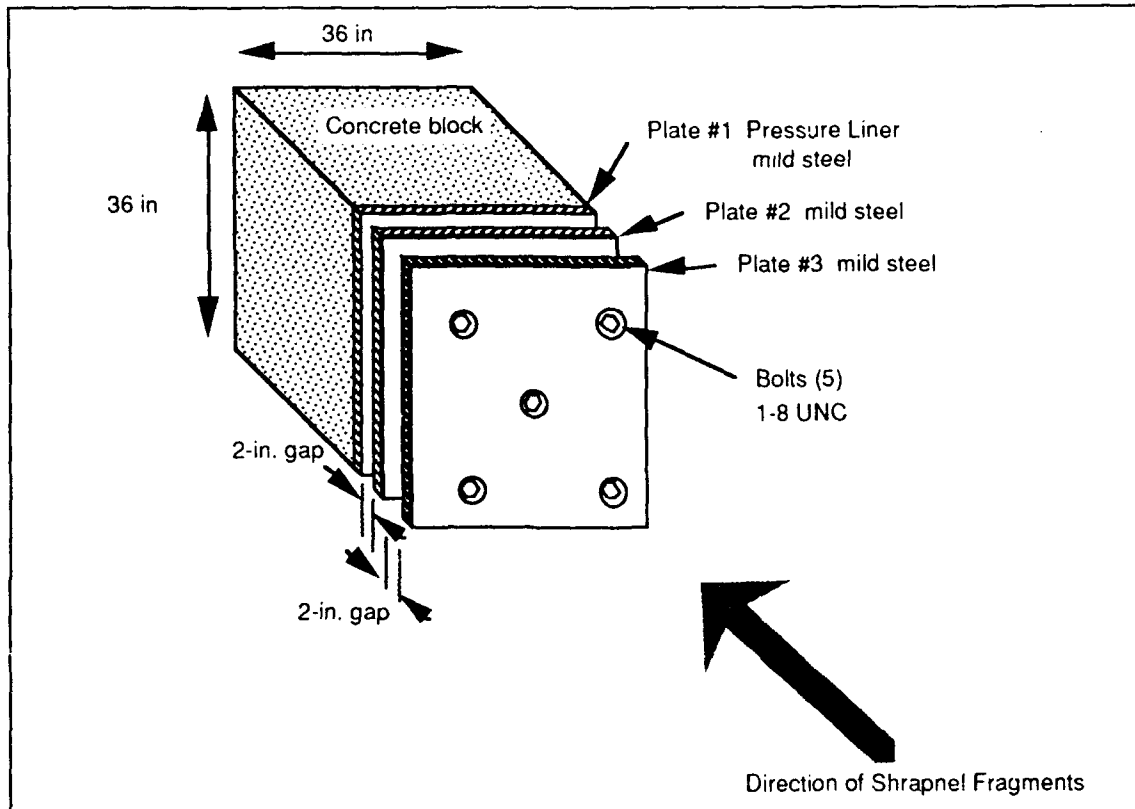
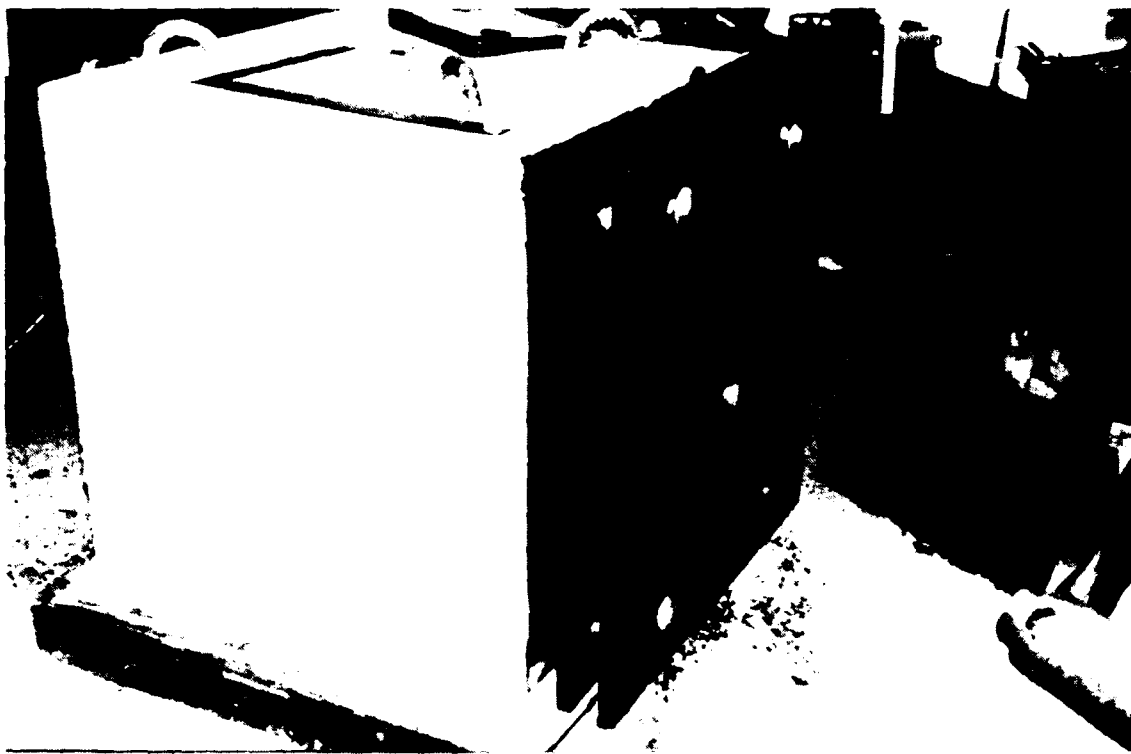


Figure 2. Typical test block.

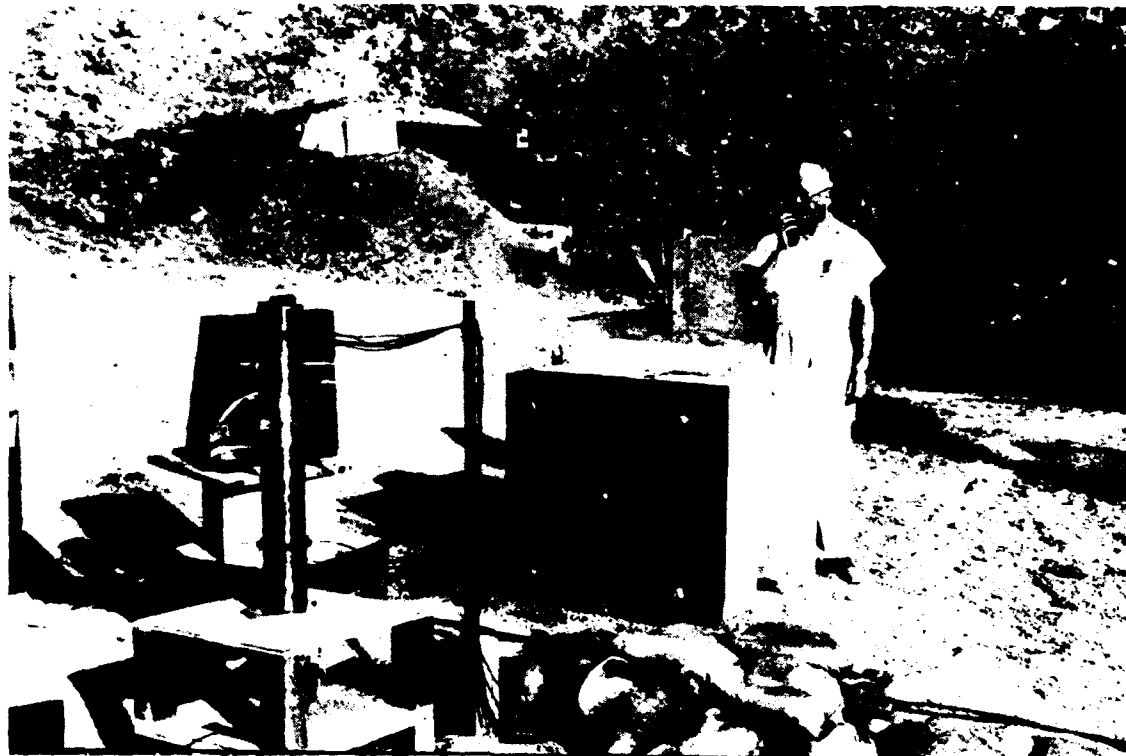
Figure 2, a typical configuration of the test block, shows the large reinforced-concrete block, the pressure liner, and the multilayered shrapnel protection plates. The large reinforced-concrete block was used to simulate the wall of the Contained Firing Chamber and provide backing and support for the steel pressure liner. The shrapnel mitigation plates Nos. 2 and 3 were spaced 2 in. away from the pressure liner and from each other. The spacing or "air-gap" between plates was maintained by welded-on bosses on the pressure liner and on plate No. 2. The plates were then bolted to each other with 1-in. 8UNC A307-grade bolts and torqued to 250 ft-lb. Mild steel was used instead of armor plate for all the tests because it has roughly 85% of the perforation resistance<sup>2</sup> of armor plate at less than half the cost.

Figure 3 depicts the final shrapnel protection test-block design during the final stages of its construction. This configuration consisted of a 0.5-in.-thick pressure liner and two 1.0-in.-thick shrapnel mitigation plates which were all constructed from mild steel.



**Figure 3. Final shrapnel protection scheme (test block) during final stages of construction.**

Most of the shrapnel-producing experiments were from the fragmentation of copper or steel cylinders filled with high explosives. Figure 4 shows a typical cylinder shot (Test No. 4) just before detonating the explosive. The nine tests presented in this report were considered "add on" experiments to the hydrodynamic and cylinder explosive tests. Three of the tests (Nos. 1, 5, and 6) were not simple cylinder shots from a shrapnel generating standpoint, but they produced damage representative of normal hydrodynamic shots that are typically performed at the LLNL Site 300.



**Figure 4.** Test setup for a typical 4-in.cylinder shot with shrapnel protection test block in place (Test No. 4).



**Figure 5.** Workers removing clamping bolts after Test No. 3. Note the plate deformation from blast and pitting from shrapnel for this minimal design.



**Figure 6. Example of excessive deformation and pitting resulting from a cased explosive 5 feet from the test block. (Test No. 2).**

Test No. 6 produced a shaped-charge metal jet that is usually very difficult to protect against with general-purpose shrapnel protection. It was found that local shielding placed near the point of jet formation significantly reduced full development of the jet and its damage potential. Figure 7 shows a large dent in plate No. 3—approximately 1 inch in diameter and 1.25 inches deep—after the shot was shielded locally with plate glass.



**Figure 7. Large dent from the explosively-formed metal jet from Test No. 6. The jet was reduced by passing through a total of 1 inch of glass before the jet hit the target (plate No. 3).**

The methodology for shrapnel protection design was to start with a minimal design (1/2-in. mild steel plates) and increase the plate thickness as necessary. The goal was to achieve a balance between deformation caused by blast and perforation caused by shrapnel versus material cost and ease of handling. By increasing plate thickness, it was found that a reasonable, minimal shrapnel shield consisted of two layers of 1-in. mild steel plate separated by a 2-in. air gap. As shown in Table 1, the final design with this configuration (Tests 3 and 5 to 8) provided good protection because there were no perforations of plate No. 2, and bending deformation caused by the blast was acceptable. Figures 8, 9, and 10 show the effects of copper shrapnel on a test block of the final design.



Figure 8. Penetrations and plate bending from copper shrapnel in Test No. 7.

## Testing Results

Table 1 summarizes the perforation results for the tests.

Table 1. Shield thicknesses and shrapnel perforations.

Test No.	Plate thicknesses (in)			Number of perforations		
	#1 plate pressure liner	#2 plate	#3 plate	#1 plate pressure liner	#2 plate	#3 plate
1	0.5	0.5	none	1	5	
2	0.5	2.0	0.5	0	0	42
3	0.5	1.0	1.0	0	0	1
4	0.5	0.5	0.5	0	2	18
5	0.5	1.0	1.0	0	0	11
6	0.5	1.0	1.0	0	0	0
7	0.5	1.0	1.0	0	0	5
8	0.5	1.0	1.0	0	0	2
9	none	none	4.0			0



**Figure 9. Effects of shrapnel from Test No. 7. Note the destroyed bolt head in the upper-right corner of the plate.**



**Figure 10. Workers removing remnants of a mangled bolt head after being hit by copper shrapnel from Test No. 7.**



**Figure 11. Example of plate No. 3 perforation under worst-case conditions (Test No. 8).**

The worst-case shrapnel came from Test No. 8 which consisted of an 8-in. steel cylinder with a wall thickness of 0.8 in. The maximum fragment weight was calculated to be approximately 1 pound with a velocity of 4200 ft/s. Figure 11 shows perforation damage for the worst-case condition from this fragment type. Note that even though there was a large perforation in plate No. 3, there was almost no damage to the second plate behind it (plate No. 2).

The last shrapnel protection test (No. 9) in this series was an experiment to access the integrity of a protection housing for a new radiographic diagnostic called the gamma ray camera. Figure 12 shows an overall view of the protection housing with a 4-in.-thick mild-steel shrapnel protection plate in front of the assembly. This plate was used as a witness plate, instead of the multilayered test block, to observe the damage to a much thicker shrapnel protection shield.

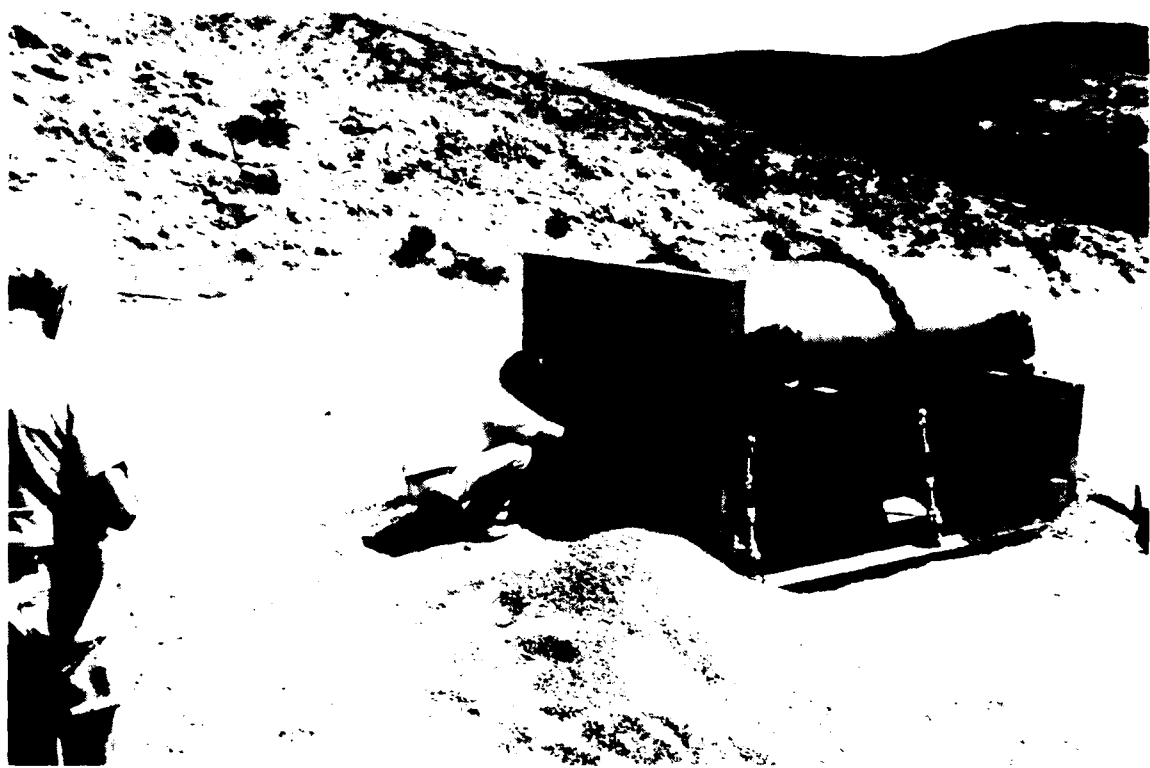


**Figure 12. Physicist inspecting damage to the shrapnel protection plate for the gamma ray camera (Test No. 9).**

The shrapnel-producing charge for Test No. 9 was a C4 explosive, 10-in. in diameter by 13.25 in. long, cased with a 3/8-in.-thick mild steel cylinder. This particular charge was designed to simulate the worst-case blast and shrapnel of close-up hydrodynamic experiments called core punch shots. Figures 13 and 14 show close-ups of the shrapnel patterns and the depth of penetration from Test No. 9.

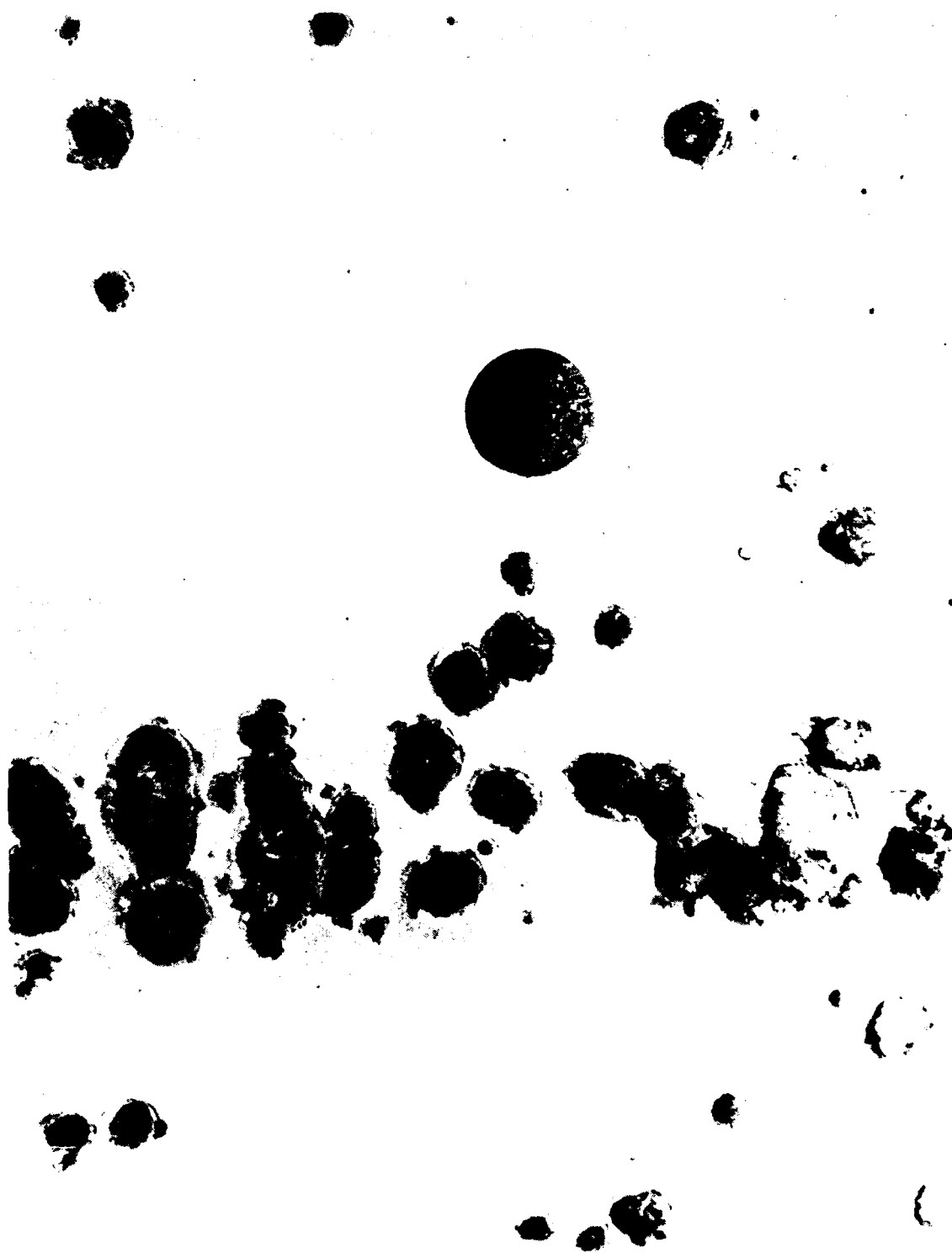


Figure 13. Skewed shrapnel pattern on the shield from Test No. 9. Cased explosive was purposely rotated 10 degrees to prevent most of the shrapnel from hitting the center hole in the protection plate.



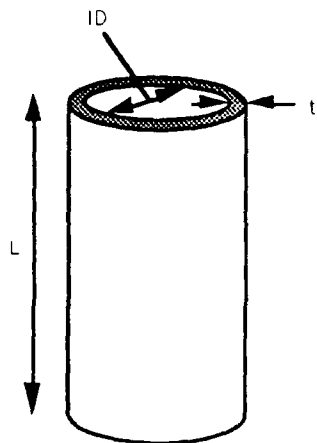
Figure 14. Cratering of 4-in.-thick steel plate surface caused by shrapnel fragments from Test No. 9.

## Calculated Shielding Requirements

In addition to observing the shrapnel perforations, basic shrapnel penetration calculations were performed to compare and to make recommendations for general purpose shrapnel shielding for the Contained Firing Facility. The calculation methodology that was used is demonstrated below using the parameters from a single test (Test #7). The penetration calculations for all of the tests are given in Appendix B and a summary of these results is presented in Table 2.

The penetration calculations were performed as a two step process. First a calculation of the shrapnel mass and velocity was performed. The penetrations were then calculated by using three accepted but different formulas. Due to the fact that penetration formulas are generally empirically based and were derived for differing regimes, three different formulas were used to assure a greater confidence in predicted penetration.

### Sample Calculation (Test No. 7 parameters)



$W$  = charge weight = 30# Lovex explosive

ID = case inside diameter = 4.0 in

$t$  = case thickness = 0.4 in

$L$  = case length = 48 in

$\gamma = \rho g$  = case weight density for copper = 0.323  $\frac{\text{lb}}{\text{in}^3}$

The case weight,  $W_c$ , is given by  $W_c = \gamma \frac{\pi}{4} [(ID + 2t)^2 - ID^2] L$ .

$$W_c = \left( 0.323 \frac{\text{lb}}{\text{in}^3} \right) \frac{\pi}{4} [(4 \text{ in} + 2(0.4) \text{ in})^2 - (4 \text{ in})^2] 48 \text{ in} = 85.7 \text{ lb}$$

The initial velocity,  $V_o$ , of a case fragment is given by the Gurney<sup>3</sup> equation

$$V_o = \sqrt{2E} \sqrt{\frac{W_c}{W} \frac{1 + \frac{W_c}{2W}}{1 + \frac{W_c}{2W}}}$$

where  $\sqrt{2E}$  = Gurney energy constant = 8068 fps for Lovex.<sup>4</sup>

$$V_o = 8068 \frac{\text{ft}}{\text{s}} \sqrt{\frac{85.7 \text{ lb}}{\frac{30 \text{ lb}}{1 + \frac{85.7 \text{ lb}}{2(30 \text{ lb})}}}} = 4403 \text{ fps}$$

The largest case fragment,  $W_f$ , is given by the Mott equation<sup>5</sup> with a fragment distribution factor,  $M_a$ , as:

$$M_a = \frac{5}{B} \left( \frac{t}{ID} \right)^{\frac{1}{3}} \left( 1 + \frac{t}{ID} \right)$$

where

$$B = \text{explosive constant} = 0.22 (\text{oz})^{\frac{1}{2}} (\text{in})^{-\frac{7}{6}}$$

$$M_a = \left( 0.22 (\text{oz})^{\frac{1}{2}} (\text{in})^{-\frac{7}{6}} \right) \left( 0.4 \text{ in} \right)^{\frac{5}{6}} \left( 4 \text{ in} \right)^{\frac{1}{3}} \left( 1 + \frac{0.4 \text{ in}}{4 \text{ in}} \right) = 0.179 (\text{oz})^{\frac{1}{2}}$$

$$W_f = \left[ M_a \left( \ln 8 \frac{W_c}{M_a^2} \right) \right]^2 = \left[ 0.179 \text{ oz}^{\frac{1}{2}} \left( \ln 8 \frac{85.7 \text{ lb}}{(0.179 \text{ oz}^{\frac{1}{2}})^2} \right) \right]^2 = 3.18 \text{ oz}$$

The penetration depth ( $p$ ) of the case fragment into the shrapnel protection plate is calculated by three different methodologies for comparison. The penetration formulas used are:

1. Demarre.
2. THOR equations modified for density.
3. Christman and Gehring.

Method No. 1: Demarre's equation<sup>3</sup>

$$p = c \left( W_f \right)^{\frac{1}{3}} \left( \frac{V_s}{1000} \right)^{\frac{4}{3}}$$

where

$p$  = penetration depth (in.) ,

$c = 0.112 (\text{in})(\text{oz})^{\frac{-1}{3}} \left( \frac{\text{ft}}{\text{s}} \right)^{\frac{4}{3}}$  for mild steel.

$$p = (0.112) (3.18 \text{ oz})^{\frac{1}{3}} \left( \frac{4403 \text{ fps}}{1000} \right)^{\frac{4}{3}} = 1.19 \text{ in.}$$

penetration = 1.19 in

**Method No. 2:** Modified THOR equation

The original THOR<sup>6</sup> equation is given by

$$V_r = V_s - 10^{c1} (hA)^\alpha (7000W_f)^{\beta1} (\sec \theta)^{\gamma1} V_s^{\lambda1}$$

where

- $V_r$  = residual velocity after perforating (fps),
- $V_s$  = striking velocity at the target (fps),
- $h$  = target thickness (in),
- $A$  = fragment cross sectional area ( $\text{in}^2$ ),
- $W_f$  = fragment weight (lb),
- $\theta$  = angle between fragment trajectory and the normal to the target material (deg),
- $\alpha1, \beta1, \gamma1, \lambda1$  = target specific material constants.

By setting residual velocity equal to zero ( $V_r = 0$ ; no perforation) and rearranging terms yields the THOR equation for minimum shield thickness to prevent perforation:

$$h_{\min} = \frac{1}{A} \left[ \frac{V_s}{10^{c1} (7000W_f)^{\beta1} (\sec \theta)^{\gamma1}} \right]^{\frac{1}{\alpha1}}.$$

Because the original THOR equations were for steel projectiles (fragments), the calculated fragment weight,  $W_f$ , was modified by the ratio of the densities of actual fragment material,  $\rho_f$ , to that of steel,  $\rho_s$ :

$$h_{\min} = \frac{1}{A} \left[ \frac{V_s}{10^{c1} \left( 7000 W_f \frac{\rho_f}{\rho_s} \right)^{\beta1} (\sec \theta)^{\gamma1}} \right]^{\frac{1}{\alpha1}}.$$

The target specific material constants for mild steel from Table 6.17<sup>7</sup> are:

- $\alpha1 = 0.906$
- $\beta1 = -0.963$
- $\gamma1 = 1.286$
- $c1 = 6.523$ .

Using Test No. 7 parameters with  $\theta = 0^\circ$ ,

$$A = \frac{W_f}{(\rho_f g)t} = \frac{3.18 \text{ oz}}{\left( 0.323 \frac{\#}{\text{in}^3} \right) (0.4 \text{ in})} \left( \frac{\#}{16 \text{ oz}} \right) = 1.54 \text{ in}^2,$$

$$h_{\min} = \frac{1}{1.54 \text{ in}^2} \left[ \frac{4403 \text{ fps}}{10^{6.523} \left( 7000 (3.18 \text{ oz}) \left( \frac{\#}{16 \text{ oz}} \right) \frac{0.323}{0.283} \right)^{-0.963} (\sec 0)^{1.286}} \right]^{\frac{1}{0.906}} = 1.09 \text{ in.}$$

penetration = 1.09 in

Method No. 3: Christman and Gehring<sup>8</sup>

$$p_c = (L - D) \left( \frac{\rho_f}{\rho_i} \right)^{\frac{1}{2}} + 0.13 \left( \frac{\rho_f}{\rho_i} \right)^{\frac{1}{3}} \left( \frac{E_1}{\beta_{max}} \right)^{\frac{1}{3}}$$

where

- $p_c$  = total penetration depth (in),
- $L$  = length of projectile (in),
- $D$  = diameter of projectile (in),
- $E_1$  = projectile kinetic energy (J),
- $\beta_{max}$  = maximum target hardness after impact Brinell hardness ( $\text{kg}/(\text{mm})^2$ ).

For Test No. 7:

$$L = t = 0.4 \text{ in} ,$$

$$D = \left( \frac{4A}{\pi} \right)^{\frac{1}{2}} = \left( \frac{4(1.54 \text{ in}^2)}{\pi} \right)^{\frac{1}{2}} = 1.4 \text{ in}^2 .$$

Because  $L/D < 1$ , the first term in the penetration equation, associated with long rod penetrators, is insignificant and can be neglected to yield:

$$p_c \approx 0.13 \left( \frac{\rho_f}{\rho_i} \right)^{\frac{1}{3}} \left( \frac{E_1}{\beta_{max}} \right)^{\frac{1}{3}} .$$

The kinetic energy of the fragment  $E_1$  is given by

$$E = \frac{1}{2} \frac{W_f (V_o)^2}{g} .$$

$$E_1 = \frac{1}{2} (3.18 \text{ oz}) \left( \frac{0.454 \text{ kg}}{16 \text{ oz}} \right) \left( \frac{4403 \text{ ft}}{\text{s}} \right) \left( \frac{\text{m}}{3.28 \text{ ft}} \right)^2 = 8.1 \times 10^4 \text{ J} ,$$

which gives a penetration depth of

$$p_t \equiv 0.13 \left( \frac{\rho_f}{\rho_i} \right)^{\frac{1}{3}} \left( \frac{E_i}{\beta_{max}} \right)^{\frac{1}{3}} = 0.13 \left( \frac{0.323}{0.283} \right)^{\frac{1}{3}} \left( \frac{8.1 \times 10^4 \text{ J}}{165 \frac{\text{kg}}{\text{mm}^2}} \right)^{\frac{1}{3}} = 1.07 \text{ in.}$$

penetration = 1.07 in

These calculated depths of penetration compare quite favorably with the values measured and listed in Table 1 for Test No. 7. Test No. 7 had five perforations through the inner plate and small dents less than 1/8 in. in the second plate. These data correspond to a total penetration of approximately 1 in. + ≈1/8 in. ≈ 1.125 in. compared to 1.19 in., 1.09 in., and 1.07 in. calculated above.

Table 2 provides a summary of results using all three calculation methodologies compared to the measured penetration depths. Tests 1, 5, and 6 were jet producing tests and did not produce shrapnel.

**Table 2. Calculated versus measured penetration depths for tests producing shrapnel.**

Test No.	Calculated Depth (in)				
	Demarre	Modified THOR	Gehring and Christman	perforation + penetration	Measured Depth (in)
1	na	na	na	0.5 + 0.5 + ?	1.00 +
2	1.97	1.40	1.45	0.5 + 1.5	2.00
3	0.75	0.55	0.62	0.5 + .125	0.63
4	1.52	1.34	1.21	0.5 + 0.5 + 0.1875	1.19
5	na	na	na	0.5	0.50
6	na	na	na		*
7	1.19	1.09	1.07	1 + 0.125	1.13
8	1.92	2.30	1.78	? + 1	1.50†
9	2.71	1.48	1.60	1.5	1.50

\* Metal jet formed without significant shrapnel..

† Total measured depth could not be determined because the largest fragment struck and shattered a 0.5-in.-thick granite sheet before perforating plate No. 3.

na Not applicable for a calculational method.

## Conclusions and Recommendations

1. These recommendations are good for *general purpose* shrapnel protection and are based on the assumption that local primary shielding is provided on a shot-by-shot basis. This assumption allows for conservatism and redundancy.
2. An analysis of the optimal air gap between plates is not provided. The 2-in. air gap between plates was based on earlier LLNL work.<sup>2</sup>
3. Provide a 1-in. mild-steel intermediate plate (plate No. 2 in Fig. 1) for redundancy and safety. A 2-in. air gap is recommended between all plates (plates 1, 2, and 3).
4. A minimum of 1/2 in. of mild steel should be provided for the pressure liner (plate No. 1) or other weldable, easily installed liner.
5. A 1-in. minimum of mild steel should be used for the innermost chamber plate (plate No 3 of Fig. 1) to prevent bending and minimize penetration and plate replacement.
6. Seal or exclude high-explosive (HE) particles or other contaminated material that might become lodged between the plates, under bolt heads, and in bolt threads. If this precaution is not taken, safety problems could be encountered during disassembly and re-assembly.
7. Measured shrapnel penetration depths compare quite favorably with calculational techniques in common use and provide a reference for shrapnel protection design in a contained chamber. Specifically, the calculational method of Gerhing and Christman provided the best overall match to the measured data for fragment sizes and velocities encountered in the testing.

## Acknowledgments

The authors would like to thank Wayne Conner for coordinating construction of the test blocks as well as measuring and photographing the effects of these experiments. We would also like to acknowledge Michele Doyle for her help in documenting the test results. Our appreciation also to Fred Sator and his Bunker 850 crew for their assistance in the gamma ray camera blast and shrapnel testing.

Work performed under the auspices of the U.S. Department of Energy by the Lawrence Livermore National Laboratory under Contract W-7405-Eng-48.

## DISCLAIMER

This document was prepared as an account of work sponsored by an agency of the United States Government. Neither the United States Government nor the University of California nor any of their employees, makes any warranty, express or implied, or assumes any legal liability or responsibility for the accuracy, completeness, or usefulness of any information, apparatus, product, or process disclosed, or represents that its use would not infringe privately own rights. Reference herein to any specific commercial products, process, or service by trade name, trademark, manufacturer, or otherwise, does not necessarily constitute or imply its endorsement, recommendation, or favoring by the United States Government or the University of California. The views and opinions of authors expressed herein do not necessarily state or reflect those of the United States Government or the University of California, and shall not be used for advertising or product endorsement purposes.

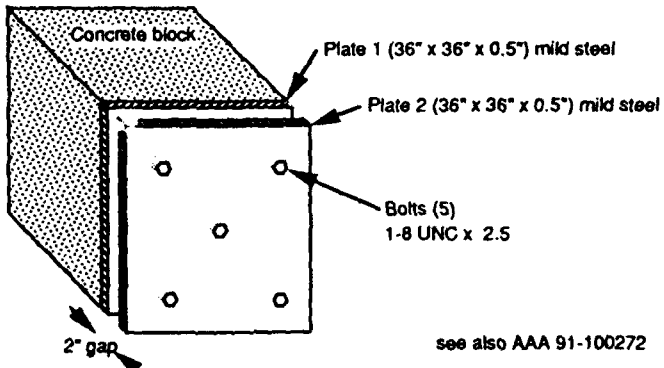
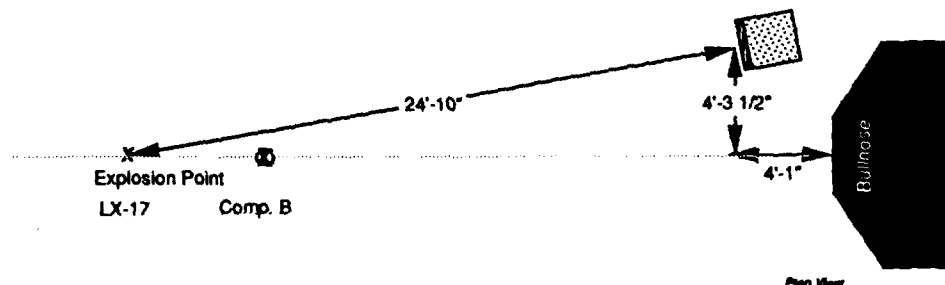
This report has been reproduced  
directly from the best available copy.

Available to DOE and DOE contractors from the  
Office of Scientific and Technical Information  
P.O. Box 62, Oak Ridge, TN 37831  
Prices available from (615) 576-8401, FTS 626-8401

Available to the public from the  
National Technical Information Service  
U.S. Department of Commerce  
5285 Port Royal Rd.,  
Springfield, VA 22161

**Appendix A. Test records, Nos. 1 to 8.****TEST RECORD**Test # 1      B Division Shot # 3113-A      Test Date 12/5/90HE type Comp. B      HE wt. 16#  
LX-17      40#

Fragment Velocity \_\_\_\_\_ Fragment wt. (max) \_\_\_\_\_ Fragment Mat'l \_\_\_\_\_

Test  
AssemblyTest  
SetupResults/Conclusions

Perforations in plate # <u>1</u>	0"-0.25"	0.25"-0.5"	0.5"-0.75"	0.75"-1.0"	Max. hole <u>0.1875"</u>
<u>1</u>	<u>1</u>	<u>0</u>	<u>0</u>	<u>0</u>	<u>0.1875"</u>

Perforations in plate # <u>2</u>	0	2	1	2	.75" x 1"
<u>0</u>	<u>2</u>	<u>1</u>	<u>2</u>	<u>.75" x 1"</u>	

Numerous pits in plate #2, five perforations of plate #2. Because of a single perforation of plate #1, the geometry is unacceptable.

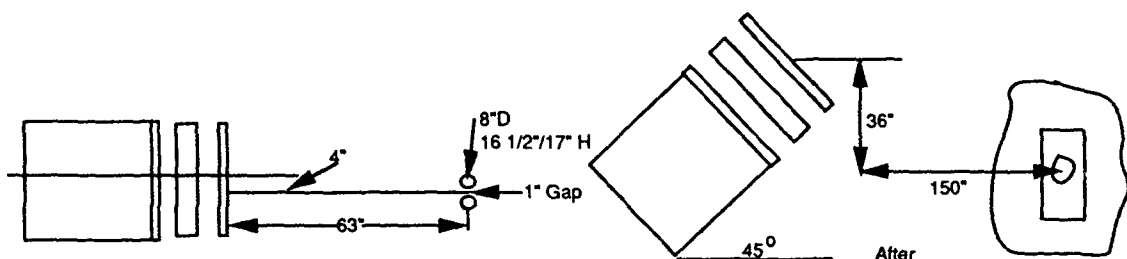
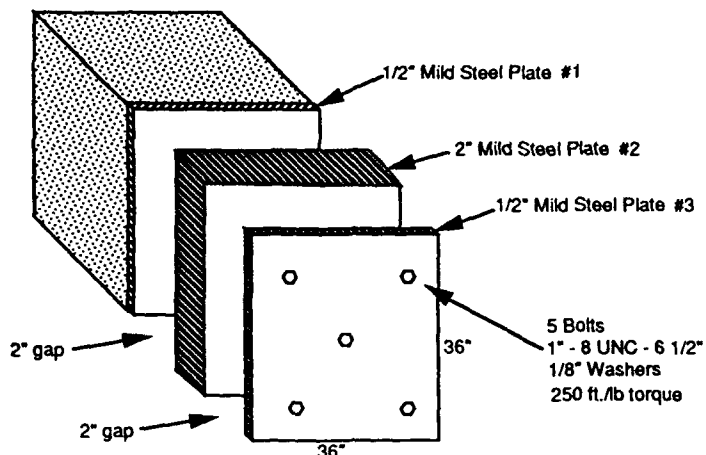
**Test Record No. 1**

## TEST RECORD

Test # 2 B Division Shot #CPLOV-109 Test Date 2/4/91

HE type RX-35-BT

HE wt. 41lb. each - 82 lb. total

Fragment Velocity \_\_\_\_\_ Fragment wt. (max) 128 lb. Fragment Mat'l 1/2" Mild SteelTest Assembly

Perforations in plate # <u>1</u>	<u>0-0.25"</u>	<u>0.25"-0.5"</u>	<u>0.5"-0.75"</u>	<u>0.75"-1.0"</u>	<u>1.0"-1.5"</u>	<u>1.5"-2.0"</u>	<u>2"-3"</u>
Perforations in plate # <u>2</u>	<u>0</u>	<u>0</u>	<u>0</u>	<u>0</u>	<u>0</u>	<u>0</u>	<u>0</u>
Perforations in plate # <u>3</u>	<u>0</u>	<u>0</u>	<u>5</u>	<u>7</u>	<u>14</u>	<u>9</u>	<u>7</u>

Plate #1 - Impacts at edges. Bent plate at corners where concrete broke.

Plate #2 - No perforations. One stand-off loose. Major impacts up to 1 1/2" deep. Thirty impacts. Two-in. bend on edge of plate caused by blast.

Test Engineer - Frank Helm

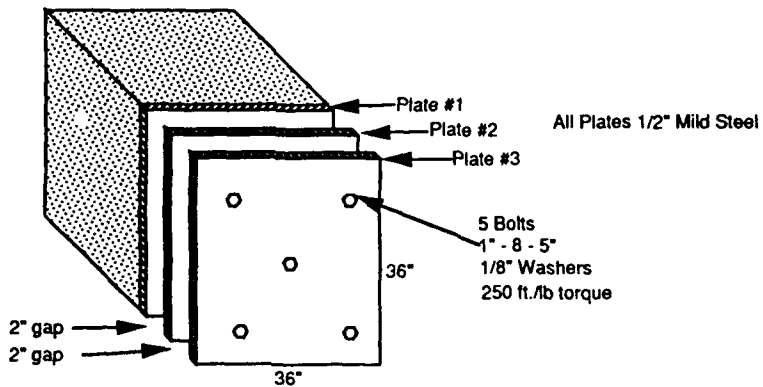
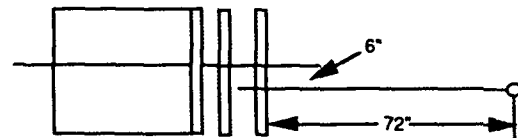
## Test Record No. 2

**TEST RECORD**Test # 3B Division Shot # K260-566Test Date 2/5/91HE type RX-35-BTHE wt. 2 1/2 lb.

Fragment Velocity \_\_\_\_\_

Fragment wt. (max) .5.27 lb.Fragment Matl' Cu. 0.2 Wall Thickness 12" H

Cylinder Shot - 2" I.D.

Test  
AssemblyTest  
SetupResults/ Conclusions

Perforations in plate # <u>3</u>	<u>0</u>	<u>1</u>	<u>0</u>	<u>0</u>	Max. hole <u>1/4" x 3/8"</u>
-------------------------------------	----------	----------	----------	----------	---------------------------------

Numerous pits in plate #3, one perforation of plate #3.

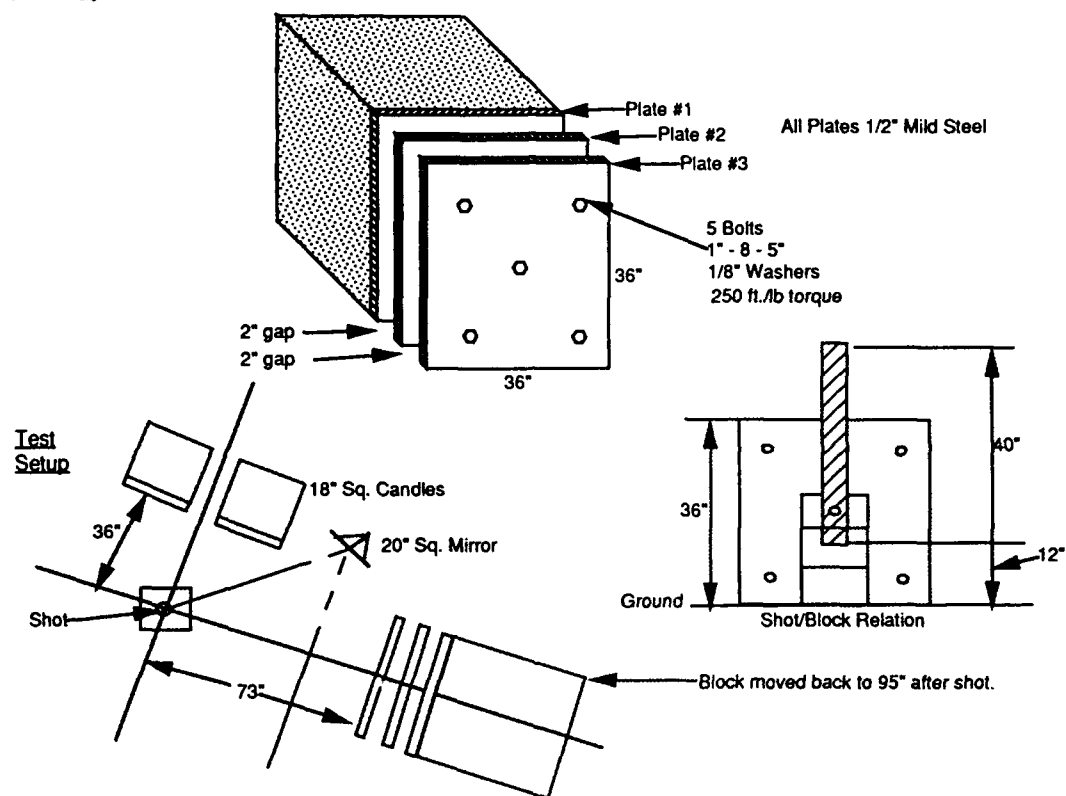
Test Engineer - Don Breithaupt

**Test Record No. 3**

## TEST RECORD

Test # 4B Division Shot # K260-567Test Date 2/6/91HE type RX-35-BTHE wt. 40 lb.Comp. B - 8lb.

Fragment Velocity \_\_\_\_\_

Fragment wt. (max) 70.28 lb.Fragment Matl' Cu. Cylinder Shot 4.8" O.D.Test Assembly

Perforations in plate # <u>2</u>	0-0.25"	0.25"-0.5"	0.5"-0.75"	0.75"-1.0"	1.0"-1.5"	1.5"-2.0"	2"-3"
Perforations in plate # <u>3</u>	0	0	1	1	0	0	0

Two Impacts on plate #1: one is a surface discolor, the other a 1/2" x 3/4" circular depression 3/16" deep.

Sixteen Impacts on plate #2. Cracked weld at standoff.

One damaged area, 5/8" x 3/4" by 1/4" deep.

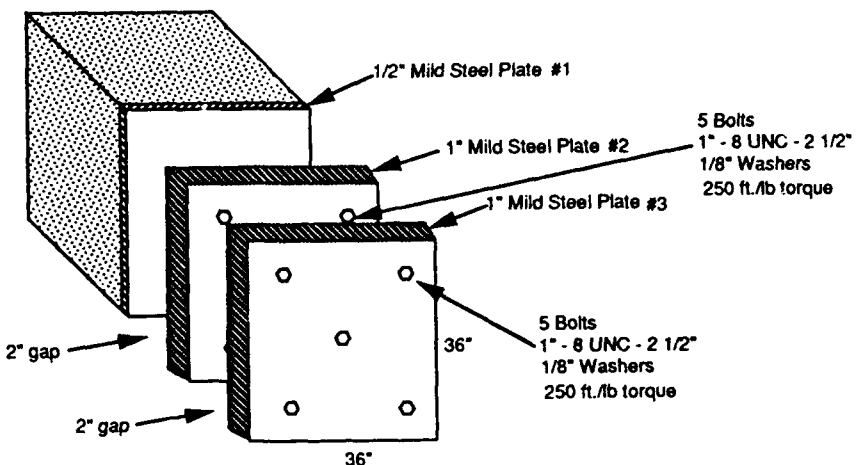
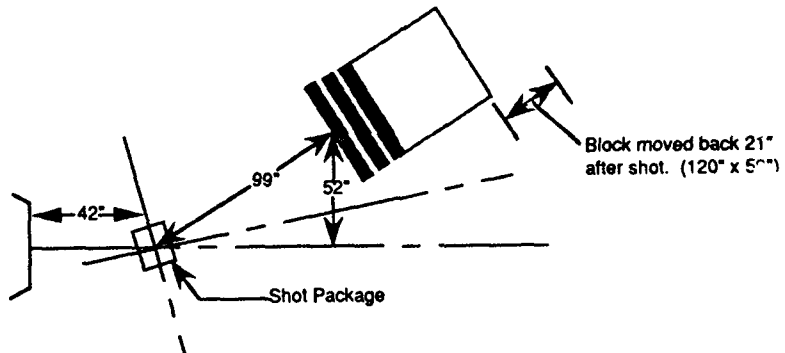
Test Engineer - Don Breithaupt

## Test Record No. 4

## TEST RECORD

Test # 5B Division Shot # 495-ATest Date 4/4/91HE type LX-17HE wt. 50 lb.

Fragment Velocity \_\_\_\_\_

Fragment wt. (max) 25KgFragment Mat'l D-38Test AssemblyTest Setup

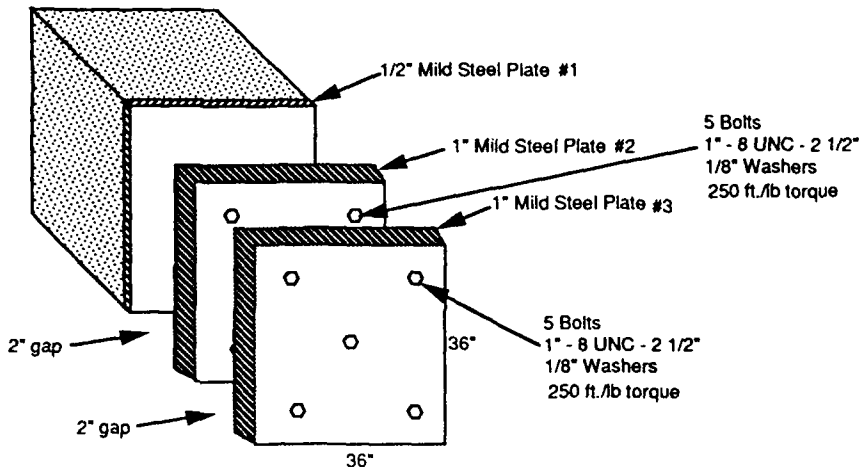
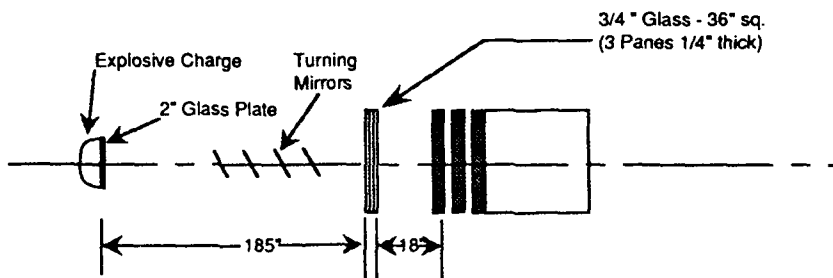
Perforations in plate # 1	0"-0.25"	0.25"-0.5"	0.5"-0.75"	0.75"-1.0"	1.0"-1.25"	Max. Hole
Perforations in plate # 2	0	0	0	0	0	0
Perforations in plate # 3	0	1	3	6	1	1 5/8" x 5/8"

- Numerous minor impacts.
- No perforations.
- Two edge hits on plate #3 - 3/4" and 1".
- Very slight bend in plate #3 caused by blast.
- Assembly would be reusable without changing plates.
- We probably received impacts from the most damaging fragments.
- The assembly may have been partially shielded.
- We may have received fragments from the waste.

## Test Record No. 5

## TEST RECORD

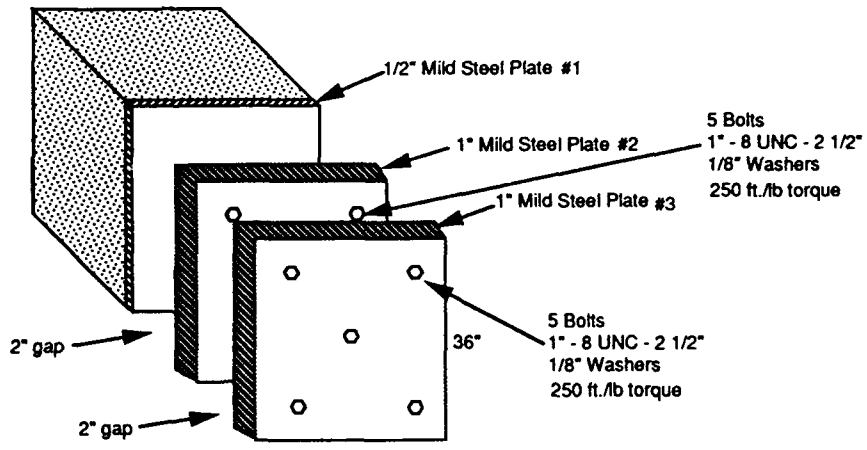
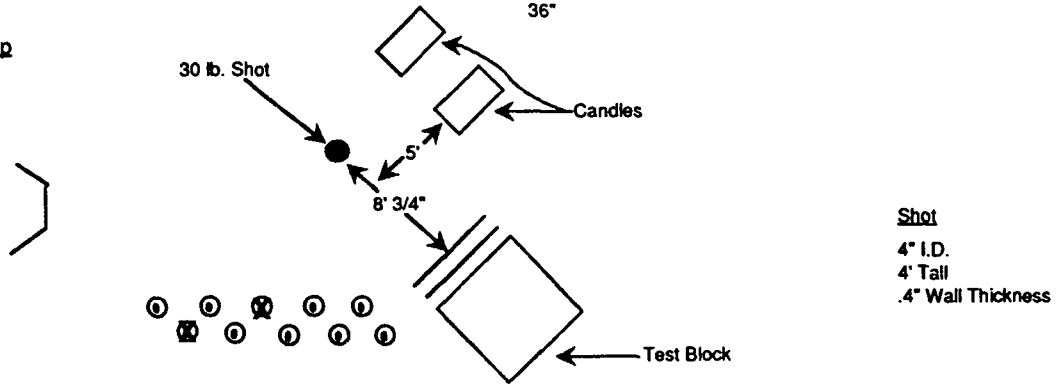
Test # 6      B Division Shot # 417A      Test Date 4/11/91  
 HE type LX-17      HE wt. 10 lb.  
Comp B      18 lb.  
 Fragment Velocity \_\_\_\_\_      Fragment wt. (max) 25Kg      Fragment Mat'l D-38

Test AssemblyTest Setup

- Large dent in plate #3 as if hit by a projectile approximately 1" in diameter. Dent is approximately 1 1/4" deep.
- Did not penetrate 1"-thick plate #3. Plate is deformed on back surface and does have a slight bend.
- No damage to plates #1 or #2.
- Explosive charge was covered with 2" glass plate on surface face of hemisphere. Other turning mirrors may have also attenuated the impact.
- Since the test, we have learned that placing glass close to the explosive charge has a much greater effect on reducing the jet than placing the glass near the block assembly. Therefore, the effect of glass plates near the block assembly alone cannot be determined.
- The explosive charge generated a jet effect and did not produce shrapnel.
- In our experiment, the total effect of the glass (explosive charge face, turning mirrors, and plate glass) successfully protected our block assembly.

## Test Record No. 6

## TEST RECORD

Test # 7      B Division Shot # K260-570      Test Date 5/30/91HE type Lovex  
Comp B      HE wt. 30lb.  
16lb.Fragment Velocity \_\_\_\_\_ Fragment wt. (max) 73 lb.      Fragment Mat'l' CopperTest AssemblyTest Setup

Perforations in plate # <u>1</u>	<u>0-0.25"</u>	<u>0.25"-0.5"</u>	<u>0.5"-0.75"</u>	<u>0.75"-1.0"</u>	Max. hole
Perforations in plate # <u>2</u>	<u>0</u>	<u>0</u>	<u>0</u>	<u>0</u>	<u>0</u>
Perforations in plate # <u>3</u>	<u>0</u>	<u>1</u>	<u>1</u>	<u>1</u>	<u>1 1/2" x 3/4", 1 1/4" x 5/8"</u>

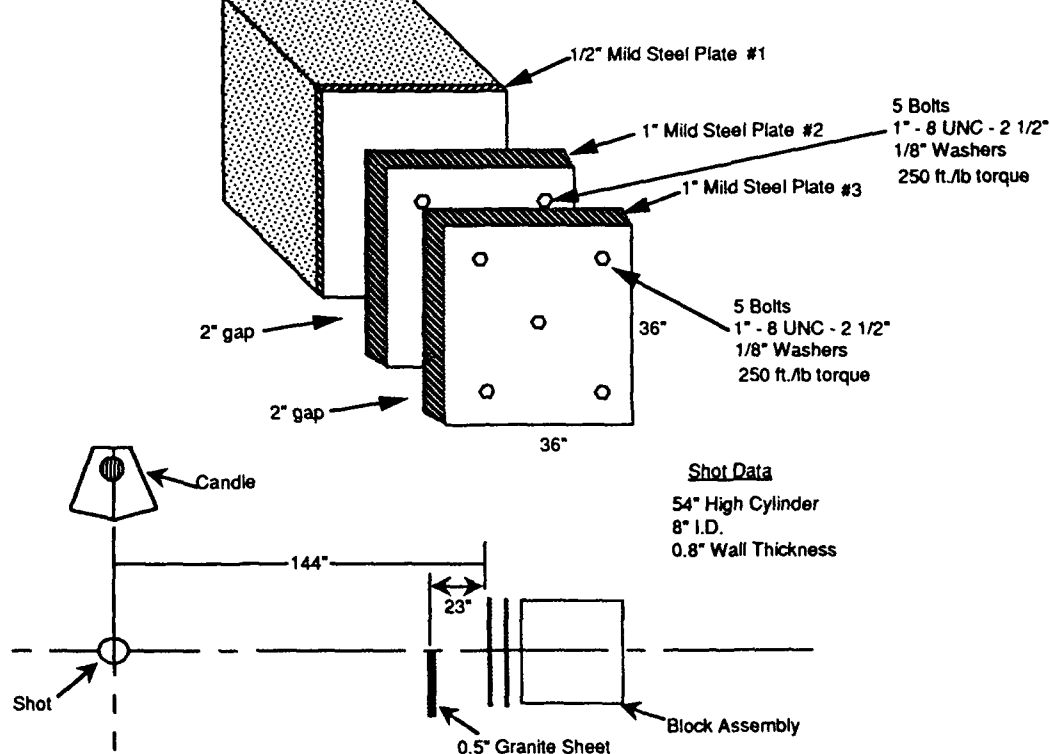
- No impacts on plate #1.
- Five impacts on plate #2. No perforations. Small dents to 1/8" deep, approximately 1/2" diameter.
- Major damage to plate #3. Slight bend in plate. Five perforations.
- Upper-right bolt head destroyed. Had to be removed with hammer, chisel, and channel lock pliers.
- Bolts holding plate #3 were at reduced torque. Damaged bolt was loose.
- Bolts holding plate #2 were still tight but at approximately 200 ft./lb torque. They were retorqued to 250 ft./lb.
- This was a very successful test. Plate #1 received no impacts.
- Plate #3 received impacts from Tests # 5, 6, and 7. It has now been replaced with a new plate.

## Test Record No. 7

## TEST RECORD

Test # 8B Division Shot # K260-572Test Date 6/28/91HE type PBXN-103 - Main Charge  
Comp B - CandleHE wt. 173 lb.  
16 lb.

Fragment Velocity \_\_\_\_\_

Fragment wt. (max) 360 lb.Fragment Mat'l' CuShot Data

54" High Cylinder  
8" I.D.  
0.8" Wall Thickness

Impacts in plate # <u>1</u>	<u>0-1"</u>	<u>1"-2"</u>	<u>2"-3"</u>	Perforations
<u>0</u>	<u>0</u>	<u>0</u>	<u>0</u>	<u>0</u>
Impacts in plate # <u>2</u>	<u>0</u>	<u>0</u>	<u>0</u>	<u>0</u>
Impacts in plate # <u>3</u>	<u>1</u>	<u>6</u>	<u>2</u>	<u>2 (8" x 2.25"), (2.4" x 1.8")</u>

- Plate #1 received no impacts.
- Plate #2 was not perforated. It did receive a large dent when impacted by shrapnel from plate #3. The plate was distorted by 1.1" at the edge and tapered toward center bolt.
- Plate #3 received 20 major impacts; however, only two were perforations. One perforation was quite large and impacted plate #2 severely.
- A 0.5-in.- thick granite sheet was placed 23 in. in front of one-half of the impact block. This action was taken to test the shrapnel mitigation potential of various materials. We are currently considering glass, ceramics, and granite. By chance, that half of the block received the major impacts. The performance of the granite sheet is inconclusive.
- Although the witness block assembly was impacted by large shrapnel pieces, the two 1-in. steel plates successfully protected the one-half-in. pressure liner plate #1 on the block face.

## Test Record No. 8

## Appendix B. Spreadsheet of Penetration Calculations

Test No.	Plate Thicknesses (in)			Number of Perforations		
	#1 plate		#1 plate			
	pressure liner	#2 plate	#3 plate	pressure liner	#2 plate	#3 plate
1	0.5	0.5	none	1	5	
2	0.5	2	0.5	0	0	42
3	0.5	1	1	0	0	1
4	0.5	0.5	0.5	0	2	18
5	0.5	1	1	0	0	11
6	0.5	1	1	0	0	0
7	0.5	1	1	0	0	5
8	0.5	1	1	0	0	2
9	-	-	4	-	-	0

Test No.	Case						Mott Explosive constant "B"
	Charge Wt. (lb)	Case ID (in)	Case Thickness (in)	Length (in)	Case Wt. (lb)	Case density lb/in^3	
1	40		c				
2	41	8	0.5	17	64.23536	0.283	0.22
3	2.5	2	0.2	12	5.357798	0.323	0.22
4	40	4	0.4	40	71.4373	0.323	0.22
5	50		c				
6	10		c				
7	30	4	0.4	48	85.72476	0.323	0.22
8	173	8	0.8	54	385.7614	0.323	0.22
9	60	10	0.375	13.25	45.83229	0.283	0.22

Test No.	Gurney		Calculated	Calculated	Gurney
	Energy Const. (fps)	Mott Constant Ma	Frag. Wt. (lb)	Frag. Wt. (oz)	Frag. velocity (fps)
1					
2	8068	0.262375504	0.342182	5.474909	5612.10101
3	8068	0.07974137	0.030888	0.494201	4962.58001
4	8068	0.179013324	0.191917	3.070678	5336.22557
5					
6					
7	8068	0.179013324	0.199133	3.186128	4403.09836
8	6986	0.401871324	0.980897	15.69436	4228.24739
9	8800	0.217155171	0.236544	3.784704	7827.64662

**Appendix B. Spreadsheet of Penetration Calculations (continued)**

Test No.		Calculated Depth (in)		Measured Depth (in)	
		Modified	Gehring & Christman	Perforation & penetration	Total
		Demarre	THOR		
1					
2	1.96869	1.402139574	1.446696	.5 + 1.5	2
3	0.74954	0.552870682	0.624808	.5 + .125	0.625
4	1.51801	1.343886927	1.205612	0.5+0.5+0.1875	1.1875
5					0.5
6					
7	1.18937	1.08951833	1.073742	1 + 0.125	1.125
8	1.91725	2.303601418	1.778258	1+	
9	2.71271	1.48341677	1.596858	1.5	1.5

## References

1. *Conceptual Design Report—Site 300 Contained Firing Facilities*, Holmes & Narver (April 1990)
2. Private communication with Dr. Calvin D. Wood, LLNL (Nov. 8, 1990.)
3. "Prevention of and Protection Against Accidental Explosion of Munitions, Fuels and Other Hazardous Mixtures," *Annals of the New York Academy of Sciences*, 314–315 (Oct. 28, 1969).
4. Pruneda, Ceasar, *Lovex RX-35-BX: A Low Vulnerability, High Performance Explosive for Main-Charge Applications*, LLNL Report UCRL-UR-110363 (in publication).
5. *Structures to Resist the Accidental Effects of Explosions*, TM5-1300/NAVFAC P-397 /AFR 88-22, p. 2-290 (Nov. 1990).
6. *The Resistance of Various Metallic Materials to Perforation By Steel Fragments; Empirical Relationships, for Fragment Residual Velocity and Residual Weight (U)*, Ballistics Analysis Laboratory/ BRL, Project THOR Technical Report No. 47 (April 1961).
7. *A Manual for the Prediction of Blast and Fragment Loadings on Structures*, United States Department of Energy, DOE/TIC 11268 (November 1980).
8. D. R. Christman and J. W. Gehring, "Analysis of High Velocity Projectile Penetration Mechanics," *J. Appl. Phys.*, 37 (4) (March 15, 1960).

**"FIREBOX"**  
**AN ENVIRONMENTALLY SOUND**  
**TEST ENCLOSURE**

D.W. Erdley  
Combat System Test Activity  
Aberdeen Proving Ground, MD 21005

**ABSTRACT**

The Fire Safety Test Enclosure, Firebox, is a state-of-the-art, environmentally sound, test enclosure designed for full scale fire suppression, live fire, vulnerability, insensitive munitions, blast, and weapons firing tests. The 84 ft diameter dome enclosure is designed to contain a 100 lb TNT equivalent high explosive event. The internal dome design will completely contain and recover all test fluids and gaseous effluents produced during the various types of testing. The liquid effluents, once recovered, are filtered, separated, and disposed of in accordance with environmental regulations or, in the case of fuels, and oils, reused. Gaseous effluents, consisting of unburned hydrocarbon, Halons, propellants combustion products, CO and particulates are drawn from the enclosure top and scrubbed in a multi-stage 60,000 CFM scrubber system. The first stage consists of an oxidizer which completes the combustion of the gaseous effluents. The resulting acidic combustion products and particulates are then passed through a scrubber where the acidic compounds are neutralized via an acid/base reaction. This reaction produces various salt products. The salts are recovered and disposed of in accordance with current environmental regulations. Combustion particulate matter is also captured and appropriately disposed. The remaining gaseous effluents are CO<sub>2</sub> and water vapor which are released out the stack. All captured effluents are separated, and either recycled or disposed of in a method to meet current environmental regulations.

**"FIREBOX"**  
**AN ENVIRONMENTALLY SOUND**  
**TEST ENCLOSURE**

D.W. Erdley  
Combat System Test Activity  
Aberdeen Proving Ground, MD 21005

### INTRODUCTION

Historically fire suppression testing and live fire vulnerability testing for the Army has been conducted by the U.S. Army Combat Systems Test Activity (CSTA), at Aberdeen Proving Ground. As a proactive solution and because of the ever changing environmental regulation an enclosed environmentally sound test facility was envisioned. The original design concept was intended to eliminate the release of Halons and chlorofluorocarbons (CFC) to the atmosphere during fire suppression and live fire vulnerability testing. More recently the design has evolved into being able to capture and scrub other waste effluents which are produced during fire suppression and live fire vulnerability testing.

### LIVE FIRE VULNERABILITY AND FIRE SUPPRESSION TESTING

Vulnerability and lethality testing of major combat systems is mandated by Chapter 139 of title 10, United States Code. Fire suppression testing is a major survivability subcomponent of this requirement. Typically testing of this type has been divided into two separate areas: those fires which occur during peace time and those which result from perforations by overmatching threat munitions during time of war. This distinction is made because peace time fires usually occur in the engine compartment as a result of electrical shorts or fuel line rupture. Crew compartment fires are usually a result of perforating impacts from threat munitions during combat.

Halon 1301 has been the fire suppression agent of choice because of its overwhelming ability to effectively control fires at low concentrations without killing or injuring the crew. Therefore it is widely used in crew occupied spaces of combat vehicles, watercraft, and aircraft. Halon 1301 is also used because of its friendly handling qualities over a broad range of conditions, and its ease of distribution such as in engine compartments. Unfortunately Halon 1301 also has a detrimental affect on the ozone layer, i.e., by being approximately 14 times more destructive than the common household refrigerants like R12. The DoD has classified combat vehicle crew compartments as a critical use of Halon 1301 and will continue to use Halon 1301 in combat vehicle crew compartment until a suitable replacement can be found. Currently no suitable replacement exists for Halon 1301 in crew compartments. There does appear to be some evidence that Hydrochlorofluorocarbon (HCFCs) could be used as a "transitional substances". HCFCs are intended as short term replacements only, because they are also ozone depleting substances and are banned by the Clean Air Act after 2015. They are however less destructive to the ozone layer than Halon and CFCs. No fire suppression agents are currently available which possess the unique performance qualities of Halon 1301 without having an adverse affect on the ozone layer and/or personnel safety. Whatever the substance that is found to replace Halon, it will inevitably be compared to and directly tested against Halon 1301. Thus Halon 1301 will continue to be used for baseline comparison purposes. At least in the near term, 8 to 10 years, substances having some potential to deplete the ozone layer will continue to be used in lifesaving conditions.

## HALON AND CHLOROFLUOROCARBON REGULATIONS

Scientific evidence has indicated that the ozone layer is being depleted by (CFCs) and Halons which have been released into the atmosphere. Most recently the predictions of the rate of depletion have increased to as much as four times that of what was originally thought. This depletion allows an increasing amount of harmful ultraviolet radiation from the sun to reach the earth's surface.

The U.S. Government has responded to such a threat to our environment by enacting several laws to limit the production and release of Halons and CFCs. The government has also entered into international agreement, specifically the Montreal Protocol and its subsequent amendments to limit the production of the ozone depleting chemicals. By law, production will be reduced by 15% in 1991, 50% by 1995, and 100% by the year 2000. President Bush has announced that these reduction schedules will be moved up to a complete phase out by 1995. In addition, the Omnibus Budget Reconciliation Act of 1989 imposes a heavy tax on high ozone depletion potential substances. This tax is designed to incrementally increase through 1994 thus making the purchase of ozone depleting chemicals prohibitively expensive. Additionally the Clean Air Act and its amendments require the quantification of emissions and prohibits venting of CFCs to the atmosphere. The Department of Defence has also issued directives and implemented regulations regarding the use of Halons and CFCs through DoD Directive 6050.9 and AMC Reg. 70-68. However, the regulations provide for the use of Halons in mission critical lifesaving uses, i.e., in the crew compartment of combat vehicles.

The driving issue, however, for CSTA is the National Environmental Policy Act which requires the individual in charge of a test to make an assessment as to whether the test will have a lasting detrimental effect on the environment. When conducting fire suppression testing involving the use of Halon, CSTA will not make the statement "there will be no lasting significant impact on the environment". Therefore an environmental impact statement will have to be prepared prior to conducting the test. This process can take upwards of 18 months to complete with no firm assurance that the testing will be approved. Consequently, this can jeopardize fire suppression and live fire testing which could subsequently affect the survivability of a combat vehicle or aircraft and their crew.

## FIREBOX AN ENVIRONMENTAL SOLUTION

To reduce the release of Halons to the atmosphere and to capture other emissions produced during fire suppression and live fire vulnerability testing, CSTA has developed a test facility concept known as the Fire Safety Test Enclosure, nicknamed Firebox. The facility will be a state-of-the-art, environmentally sound, test enclosure designed for full scale fire suppression tests, and live fire vulnerability testing. It will provide DoD with the means to test and evaluate potential fire suppression agents, used to prevent the loss of life, without adversely effecting the environment.

The Firebox design will be based on the Superbox<sup>1</sup> design and will consist of several major subsystems including the pressure containment vessel, the emissions control system (ECS), and the washdown/asset protection system. However the ECS will differ considerably from that of

---

<sup>1</sup>. Grove, C. A. Live Fire Testing: The Environmentally Safe Way, U.S. Army Combat Systems Test Activity, July 1992.

Suberbox because of the inherent design difference between the two, i.e., Superbox being designed to filter Depleted Uranium particulates and Firebox being designed to filter the test effluent produced during fire suppression testing (DU will not be tested in Firebox).

The pressure containment vessel will consist of a 84 ft diameter hemispherical steel enclosure which is designed to contain the test effluent under the test scenarios described below:

- a) A high explosive blast equivalent to 100 lb TNT detonated in the center of the containment vessel within  $\pm$  2 ft and approximately 12 ft from the center of the floor surface.
- b) Test scenario a) combined with the burning of 650 lb of JA-2 propellant.
- c) Test scenario a) combined with the burning of a maximum of 500 gallons of JP-8 fuel. Maximum fuel consumption is expected to be 200 lb/min for a 15 minute duration. Maximum Halon 1301 discharge is 1000 lbs.
- d) Test with a high explosive blast no greater than the equivalent of 10 lb of TNT
- e) Test scenario d) combined with the burning of a maximum of 500 gallons of diesel fuel.
- f) Test scenario d) combined with the burning of a maximum of 250 gallons of diesel fuel and 500 lb of JA-2 propellant.

The vessel will prevent the direct release of the test effluents to the atmosphere. There will be a plenum chamber at the base of the sphere to provide fresh air to the vessel. The air handling system will be able to completely ventilate the interior of the containment vessel and provide sufficient air to sustain combustion as described in the test scenarios above. The spilled liquid effluent, e.g., diesel, JP-8, hydraulic fluids, etc., will be captured by the washdown/asset protection system and subsequently separated and filtered. The gaseous test effluents will be drawn off the top of the hemisphere and fed to the ECS thought attached duct work.

The 60,000 cfm ECS consist of two major subsystems which will be able to efficiently operate under the input test scenario described above and will be able to operate over intermittent duty cycles of up to several hours. The first stage will consist of an oxidizer which will complete the combustion of the gaseous effluents, i.e., smoke, particulates, volatile organic compounds, unburned hydrocarbons, acidic gases, and unreacted Halons. After passing through the oxidizer the resulting exhaust gases will consist of carbon dioxide, nitrogen dioxide, and halogen acids (HCl, HBr, etc). These exhaust gases will then pass through a heat exchanger where the gases are cooled. The second stage will consist of a spray dryer absorber containing an alkaline mixture. In the spray dryer an acid base reaction will occur resulting in a neutralization reaction, producing solid salts. The acid-base reaction will be optimized to produce the least environmentally offensive products. These will be collected, separated, and deposited in accordance with environmental regulations. It is important to note that wherever possible, captured and separated effluents as well as heat will be recycled. Ultimately, what is released to the atmosphere at the end of the ECS exhaust train will be water vapor and CO<sub>2</sub>.

The following diagram, Fig 1, illustrates the flow of effluent through the proposed concept.

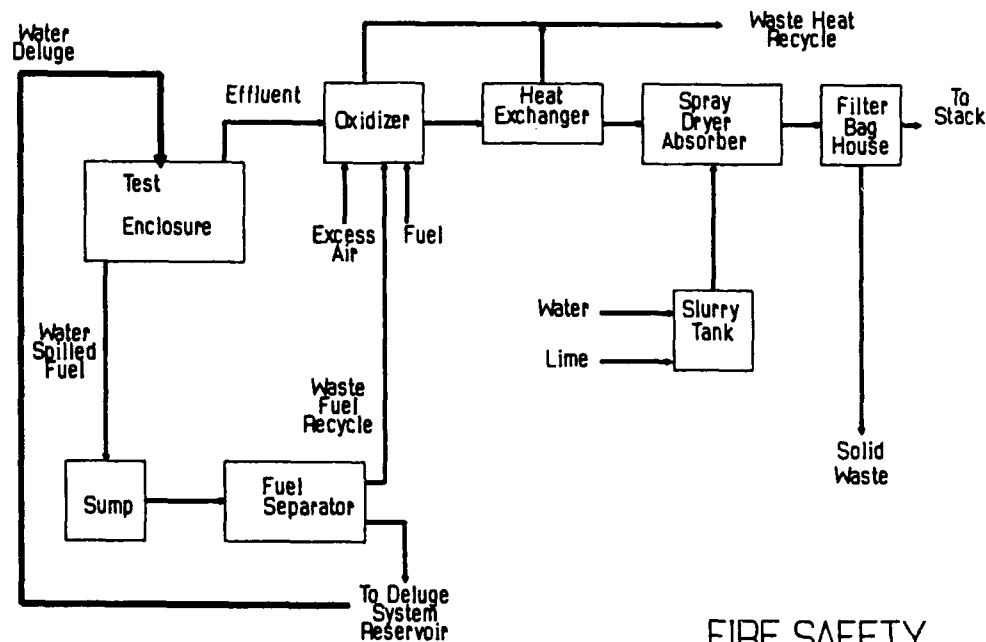


Figure 1

FIRE SAFETY  
TEST ENCLOSURE  
Design Concept  
10 Jul 92

The washdown/asset protection system will be similar in design to the system used in Superbox. It will provide for the ability to fight fires which were not extinguished by the vehicle fire suppression system. It will also provide for a source of cooling for the containment vessel. As part of the washdown/asset protection system, a drainage system will be provided for the removal of liquid effluent waste from within the vessel. The drainage system will be a self contained system to prevent the release of waste effluent to the environment. The waste effluents will be processed through automatic processing equipment to remove and separate oils, fuels, and solid wastes form the water used in the system. The recovered materials, once separated, will be either recycled or disposed of in accordance with state and federal regulations. The water will be returned to the system.

#### SUMMARY

The completed test facility will provide multiple capabilities to include Live Fire Vulnerability Testing, Automatic Fire Extinguishing System (AFES) Test, Flammability tests, DOT Hazard Classification tests, and insensitive munitions test. It will provide the DoD, other government agencies, and private industry with the ability to comply with the various laws, regulations, and international protocols, which address the release of ozone depleting chemicals and the other waste effluents to the atmosphere. The Fire Safety Test Enclosure will be a state-of-the-art environmentally sound test facility designed for the testing of fire suppression agent without adversely affecting the environment.

## ACKNOWLEDGMENTS

I would like to acknowledge and express my appreciation to Mr. Craig Herud, Mr. William Bolt, and Mr. David Grow for their insight as the concept originators and for their input into this paper. I would also like to acknowledge Mr. James Fasig, Director of CSTA's Live Fire Vulnerability Directorate for his environmental insight and in going forward with this concept. I would like to thank Mr. Joseph Ondek, CSTA's Environment Officer, for his personal and his staff's support and help during this project.

## REFERENCES

1. Omnibus Budget Reconciliation Act, 1989.
2. Clean Air Act and Amendments (Title III & VI), 1990.
3. DoD Directive 6050.9, SUBJECT: Chlorofluorocarbons (CFCs) and Halon, 13 February 1989.
4. AMC Reg. 70-68, Elimination of Ozone Depleting Substances, 4 September 1989.
5. National Environmental Protection Act, 1972.
6. Grove, C. A."Live Fire Testing: The Environmentally Safe Way," U.S. Army Combat Systems Test Activity, July 1992.

***Design of the M-9 Firing Facility Containment Vessel  
for Los Alamos National Laboratory***

*by*

Michael A. Polcyn

Edward D. Esparza

Southwest Research Institute

Mark G. Whitney

Wilfred Baker Engineering

**Abstract**

Los Alamos National Laboratory Group M-9 has been performing tests of high explosives at their open facilities. Southwest Research Institute was contracted to design, fabricate, and test a containment vessel which will be installed at the M-9 facility. It is required that the vessel contain blast and fragments from routine explosives tests using charge weights up to 10 kg of TNT equivalent.

The vessel is fabricated from a 11.5 foot diameter steel cylindrical section with 2:1 elliptical ends. The cylinder is made of 1.5 inch thick HY100 steel and the heads are made of 2 inch thick HY100 steel. A 4 inch thick HY100 steel plate door is placed in one head, and seats against a 6 inch thick steel frame. Fragment shields constructed with 0.5 inch thick steel are placed against the cylinder walls. The floor is concrete with steel plates along the surface. Penetrations through the vessel are provided for an air inlet and outlet, electrical and gas penetrations, viewports, and a drain. This paper contains a discussion on the need for a contained firing facility at Los Alamos. The design approach, including loads prediction and dynamic structural response calculations, is presented. Drawings of several details of the vessel are also included.

## **1.0      Introduction**

Los Alamos National Laboratory Group M-9 has been performing routine explosion testing at their outdoor facility. The principal purpose for these tests is to gain technical advantages in advanced experimentation on shocked materials, mainly in detailed investigations of the initiation and detonation of high explosives, and of the reaction rates that govern these processes. The experimental methods presently used include high-speed streak photography, electronic pin-contactor and gauging measurements, and laser velocity interferometry. The possibility exists to add flash x-ray, framing photography, and dynamic spectroscopic measurements.

Utilizing the generous available space at Los Alamos, and following good practice in handling explosives and barricading against blast and shrapnel, the users have developed a long record of very safe practice of open firing. The products of the detonation of high explosives are rather benign, so the program has had relatively little detriment to the environment. There are some modest environmental, health and safety advantages to a contained firing facility, not the least of which is that regulatory zeal in these areas may someday limit tests to contained firing as the only means to continue this type of work. One of the major motives for developing the contained firing facility has been to build an experience base for such a contingency.

There are a number of operational advantages to contained firing. The containment vessel enables greater proximity and multiple access with optical, electronic and electro-optical instrumentation. The greater ability to combine many channels of mixtures of the various diagnostic methods used in each experiment will both enhance the technical efficiency of the program and will allow more definitive experiments when several simultaneous measurements are helpful. Additionally, many of the techniques are improved through the use of shorter signal cables and optical paths than are feasible in open firing.

The work at Los Alamos involves an increasing number of experiments on cryogenic or heated specimens of explosives and other energetic materials. The heated explosives experiments are mainly motivated by weapons safety problems. These tests typically involve several hour cooling or heating cycles, with remote operation of the specimen conditioning system. In open firing, these tests are subject to complications, and occasional aborted procedures, from suddenly varied weather conditions. The conversion to contained firing provides operational advantages by moving the tests indoors, and reduces the amount of supplemental apparatus sacrificed in the current shots.

The new contained firing facility will be located within an easy walking distance to the staff offices and support laboratories, thus providing better access for the users. Also, the new facility will be located adjacent to a long-existing and recently improved gun facility. It is hoped that both facilities will benefit from convenient exchange of instrumentation, hardware, technology, and perhaps personnel.

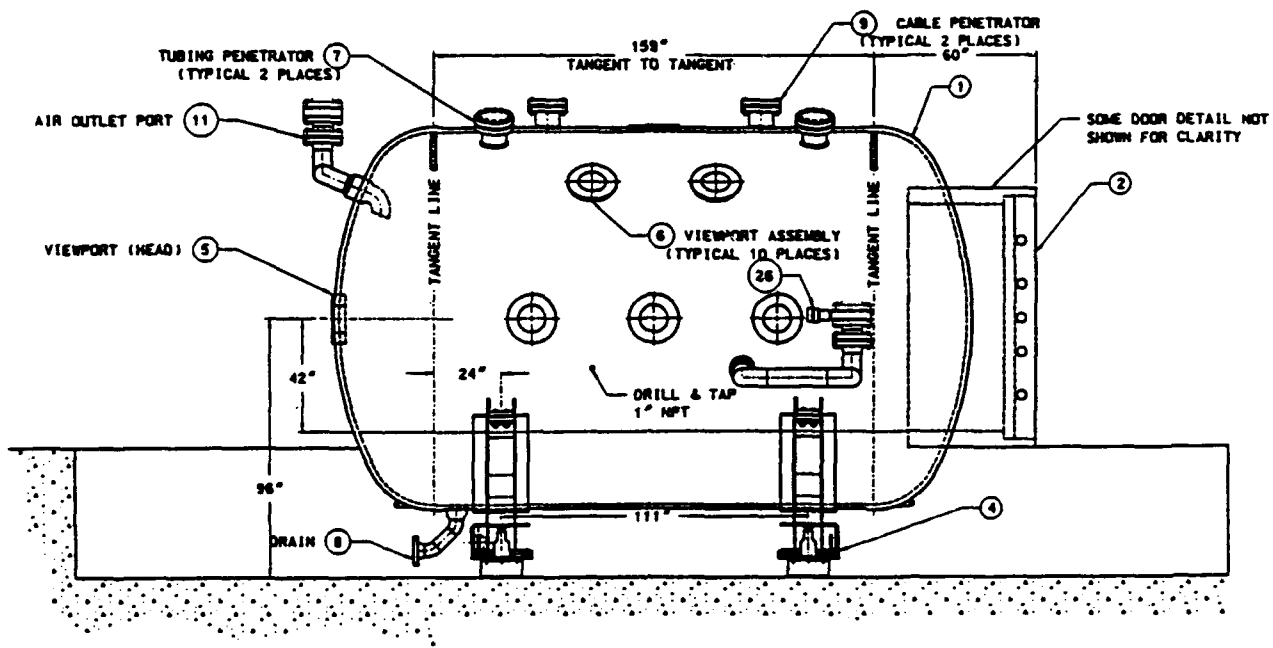
## **2.0 Design Requirements**

Los Alamos National Laboratory contracted Southwest Research Institute to design, fabricate, and test a containment vessel for performance of explosive tests. Figure 1 shows exterior views of the vessel.

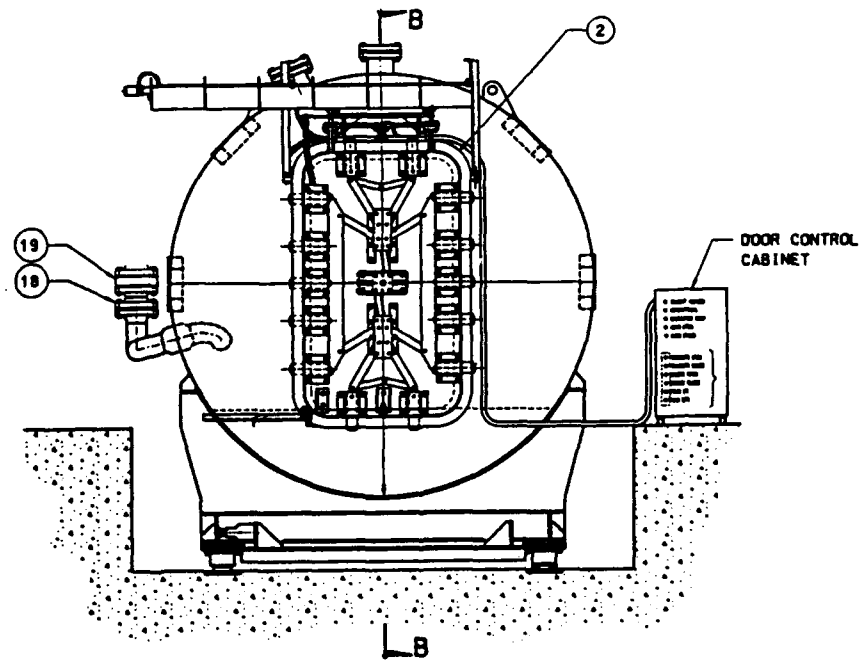
The vessel was designed to contain blast, fragments, and residual gases from repeated detonations of up to 10 kg TNT equivalent centered in the vessel.<sup>(1)</sup> It is also required to provide for the use of smaller charges at off-center locations as determined by analysis.

The vessel was designed to meet the following additional requirements:<sup>(2)</sup>

- The vessel shall have a minimum inner diameter of 11.5 feet and a minimum inner length of 19 feet.
- The weight of the vessel should be minimized and shall not exceed 75 metric tons (165,000 pounds)
- The vessel is to provide a lifetime of 1500 full charge shots or 10 years of installed operational use, whichever comes first. Maintenance and component replacement is acceptable as further specified.
- The vessel shall have a floor located 3.5 feet below the centerline of the vessel. It shall be designed to survive 100 full charge shots without replacement, and allow for easy removal for vessel maintenance.
- The vessel shall be fabricated with a minimum of four roller assemblies to allow the vessel to be rolled into and out of the facility. Also, a jacking mechanism shall be provided to adjust the vessel height and orientation.
- A door, 4 foot by 7 foot minimum, shall be provided in one end of the vessel. The door shall be designed for a cycle life of 100 openings and closings between required lubrication, 1500 openings and closings between major system maintenance, and 1500 shot cycles before door replacement. The door shall be power operated with a manual back-up operating system.
- The vessel shall have one air inlet connection and one air exhaust connection. The fixtures shall be equipped with valves that can maintain the vessel containment requirements during repeated tests with minimum lifetimes of 100 shots between maintenance and 500 shots before replacement.



a) Side View



b) End View

Figure 1. Containment Vessel

- Eleven 10-inch diameter viewports shall be provided in the vessel. The design shall allow for easy protection of the viewports not used during a test, and for easy replacement of the clear material between tests.
- The vessel shall have two cable pass-through fixtures with fragment shields to protect from line-of-site damage from fragments during tests.
- The vessel shall contain pass-through fixtures for gas and vacuum lines.
- A drain shall be provided to remove liquids from the vessel during cleaning.

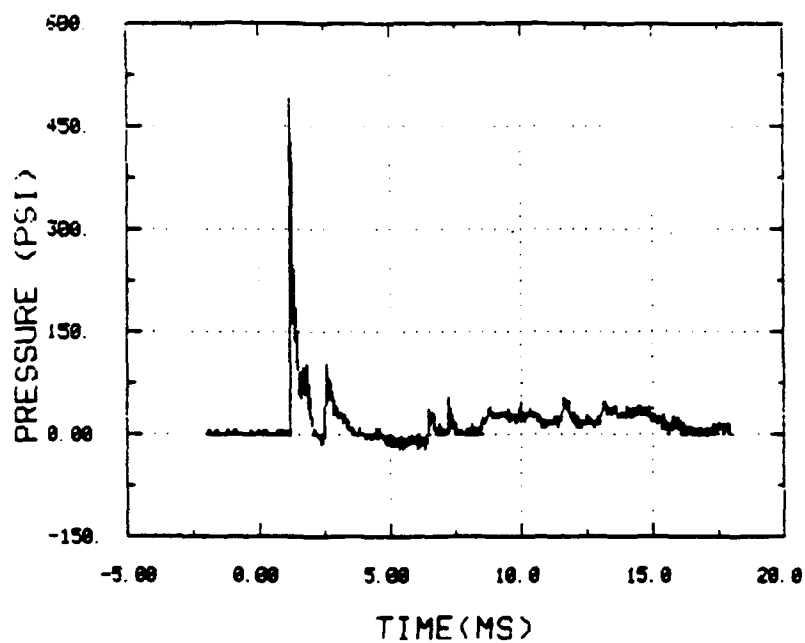
### **3.0 Loads Prediction**

Blast loads in the vessel consist of both a shock loading phase and a quasi-static, gas loading phase. The quasi-static load can be predicted with confidence using empirically based curves which are available from a variety of references. The shock loading is much more difficult to predict due to the reverberation of the shock waves within the chamber.

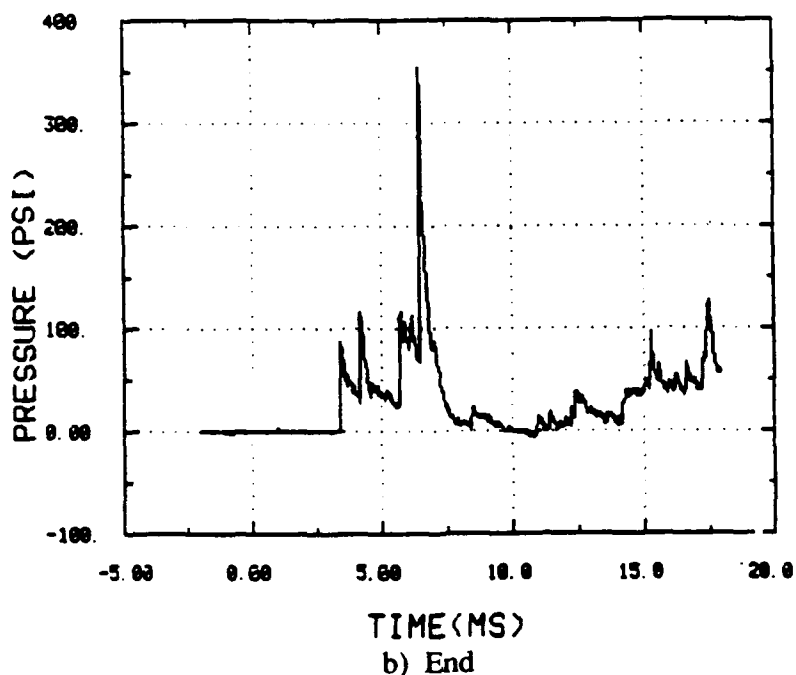
Shock loads were predicted using a combination of blast predictive methodologies and test data from a similar vessel at the DOE Mound Laboratory.<sup>(3)</sup> The approach involved the following steps:

- A close review of the Mound data was made, concentrating on measured loads at the vessel sidewall (center) and at the middle of the elliptical endcap.
- Predictions of these measured loads in the mound vessel were made. Several methods were attempted, including the use of standard airblast curves and the computer code BLASTINW.<sup>(4)</sup>
- Comparisons of the Mound predictions and measurements were made. Adjustments to the predictions were implemented to account for differences, and predictions were repeated.
- Once reasonable correlation between predicted and measured data were obtained for the Mound vessel, the final predictive procedures were repeated for the LANL vessel geometry and charge weight.

Typical blast pressure traces from the Mound tests are shown Figure 2 for locations at the cylinder wall directly adjacent to the charge and at the center of one end. Note that at both locations, the load history is defined by more than one significant pressure pulse. The shock loading phase normally consists of a large initial pulse from the expanding shock wave and later, smaller pulses from the reflection of the shock wave off adjacent surfaces. This type of loading was demonstrated in Figure 2a on the cylindrical shell. However, Figure 2b shows that the loading on the head is



a) Cylinder



b) End

**Figure 2. Typical Mound Test Data**

different. The shock wave expands spherically from the center until it reaches the confining cylinder wall, reflects, then moves toward the center. This reflected wave is not planer. It approaches the cylinder axis and forms a very strong, focused wave which is directed against the endcaps. This strongly focused reflected wave reaches the endcaps after the initial blast wave from the explosion, and the data indicate that this second pulse will have a greater peak pressure and more specific impulse than the first pulse.

Comparisons between the Mound data and several blast predictive methods indicated that a combination of the methods were required. Peak pressures were calculated using standard airblast curves. An equivalent charge weight to account for the confinement provided by the vessel was determined. The total impulse was based on calculations made with BLASTINW for an approximate geometry. The distribution of the impulse in multiple pulses was based on the data from the Mound tests. The times of arrival for each pulse were based on "image" charge methods. Time histories used for design of the LANL vessel are shown in Figure 3.

#### **4.0 Primary Structure**

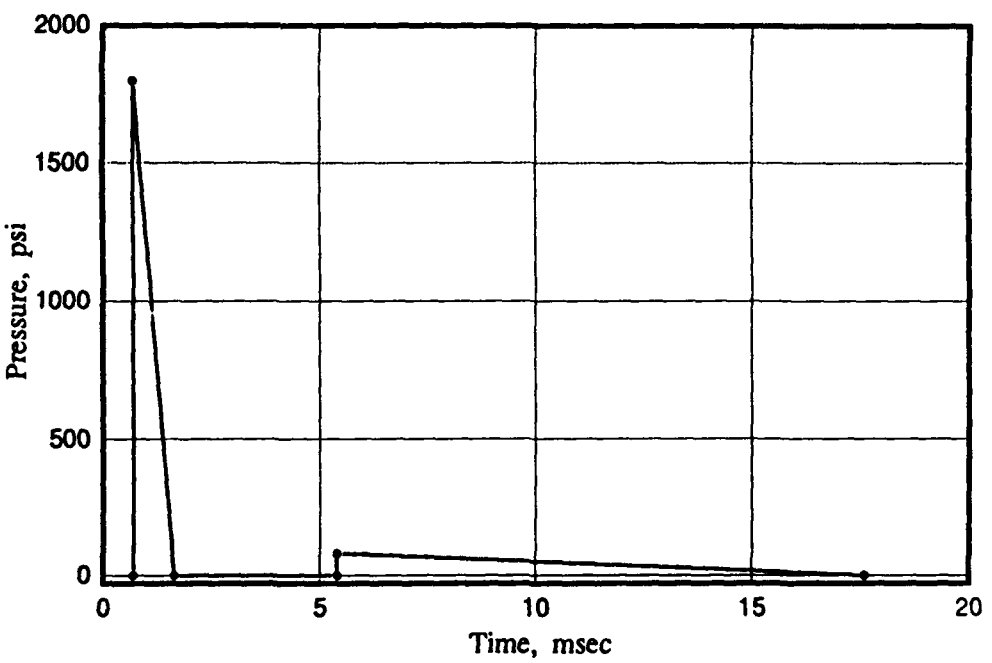
The primary structure consists of the cylindrical shell, the heads, the door, and the door frame. The vessel was designed to be totally elastic. The type of analysis used for each component of the vessel was selected based on the complexity of the component response. Equivalent static load analyses were used to design support components and secondary components such as pins, viewports, viewport frames, etc. Single-degree-of-freedom (SDOF) analyses were used to design the door, the shell, and the head of the vessel without the door. A multiple-degree-of-freedom (MDOF) analysis was used to design the head of the vessel with the door and the door frame. Also, maximum stresses were checked against ASME fatigue design requirements assuming 1500 charge detonations and a conservative damping factor. The following sections contain a description of each of these components and a summary of the design approach.

#### **4.1 Cylindrical Shell**

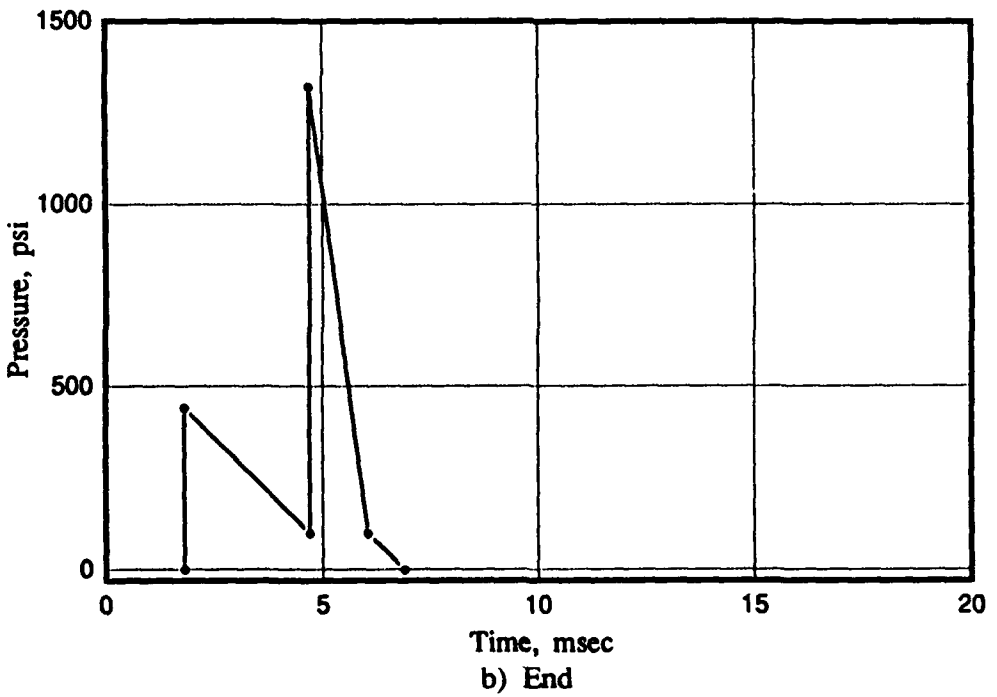
The cylindrical shell was analyzed using SDOF methods to account for the hoop response of the shell. Materials of varying strengths were considered, including A514 Grade 70, A588, HY80 and HY100. One and one-half inch thick HY100 was chosen. Although HY100 is more expensive than the other materials and requires more stringent welding procedures, the high strength ( $f_y = 100$  ksi) allows for thinner material, thus reducing the vessel weight. Also, the thinner material requires smaller welds, somewhat offsetting the increased fabrication costs.

#### **4.2 Head Without Door**

The head opposite the door was analyzed using SDOF methods. A 2:1 elliptical head was chosen for both heads. The stiffness and deformed shape of the head were determined by performing



a) Cylinder



b) End

**Figure 3. LANL Design Loads**

a finite element analysis using ABAQUS.<sup>5)</sup> The analysis showed that a 1-1/2 inch thick HY100 will adequately resist the blast loads. The head was fabricated from 2 inch thick steel to provide resistance to fragments.

#### **4.3 Head with Door Frame and Door**

The head with the door is shown in Figure 4. The head is a 2:1 elliptical head, identical to the head at the opposite head. An opening was cut into the head for the door opening. The sides, top, and bottom of the door frame were fabricated from 6 inch thick A572 Grade 50 plate. The corners were cut from a HY100 forged cylinder.

Initially, static finite element analyses were performed to estimate stresses in the head and door frame. Regions of high stress were identified in the head near the door frame corners. Gussets were added to strengthen the head and reduce the stresses.

The door plate is 4 inch thick HY100 plate. The door opens outward so as not to limit working space inside the vessel when the door is open. Because of this outward opening door, restraining pins were designed to resist the loads from the door reactions due to motion in the direction of the loads. The plate is latched in the closed position by 5 pins on each side of the door and 2 pins on the top and bottom of the door. All pins are 3-1/2 inch diameter, heat treated 4340 alloy steel, and are mounted on the door in pin blocks. Pin insertion into the door frame is accomplished simultaneously by remotely activating a hydraulic rotary actuator and its associated connecting linkage hardware to the pins, all of which are mounted on the door plate as shown in Figure 1. Also shown is the overhead structure containing a carriage-like arrangement which rolls on a track positioned such that the door can translate away from the frame, and then to the left, clear of the door way. Carriage movement is provided by DC motor-driven, rodless cylinders which are remotely operated by a programmable microprocessor based controller.

Final analysis of this head involved a combination of finite element analysis and Multi-Degree-of-Freedom dynamic analysis. Initially, the finite element analysis was used to determine the deformed shape of the head and the stiffness of the components of the head. The head system was modeled as a 3 degree-of-freedom system as shown in Figure 5. This model considered the motion of the vessel in the axial direction by accounting for elongation of the shell, radial motion and bending of the head, and bending of the door plate. The door frame was assumed to be rigid. The peak resistance developed in the springs of the model was used to develop equivalent static pressures for the finite element analysis, which allowed calculation of the stresses in the head.

#### **5.0 Secondary Components**

##### **5.1 Floor System**

Two types of floors were considered for the vessel: a solid floor and a grate floor. The grate floor uses lighter sections which eases removal and replacement of sections. However, debris

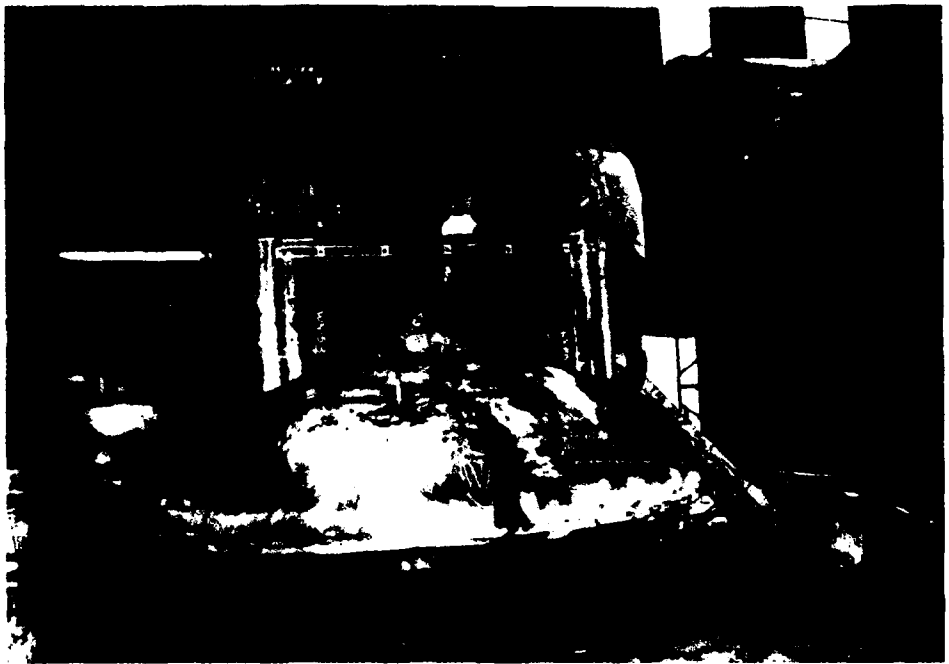
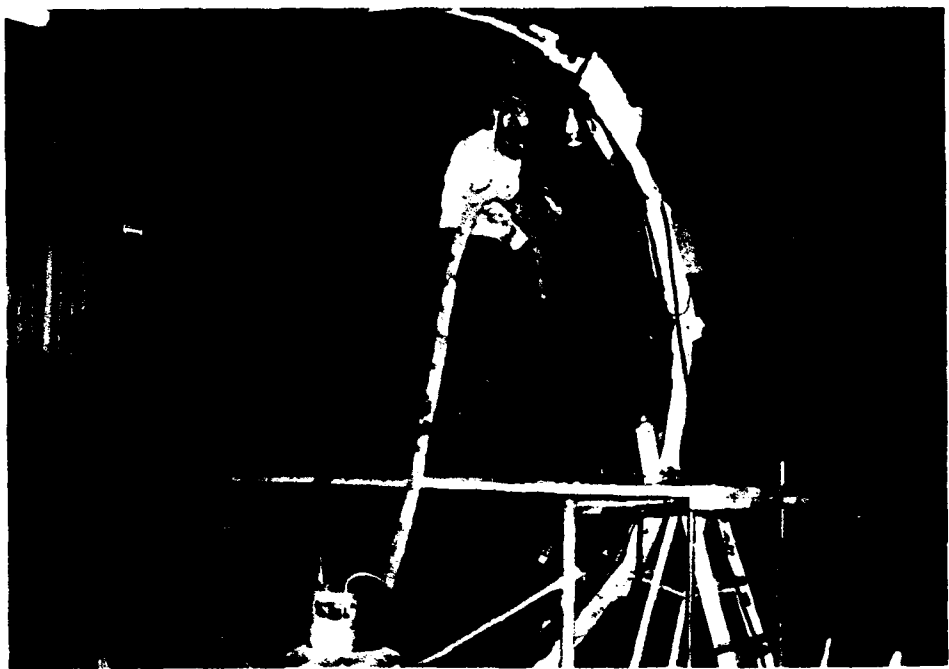
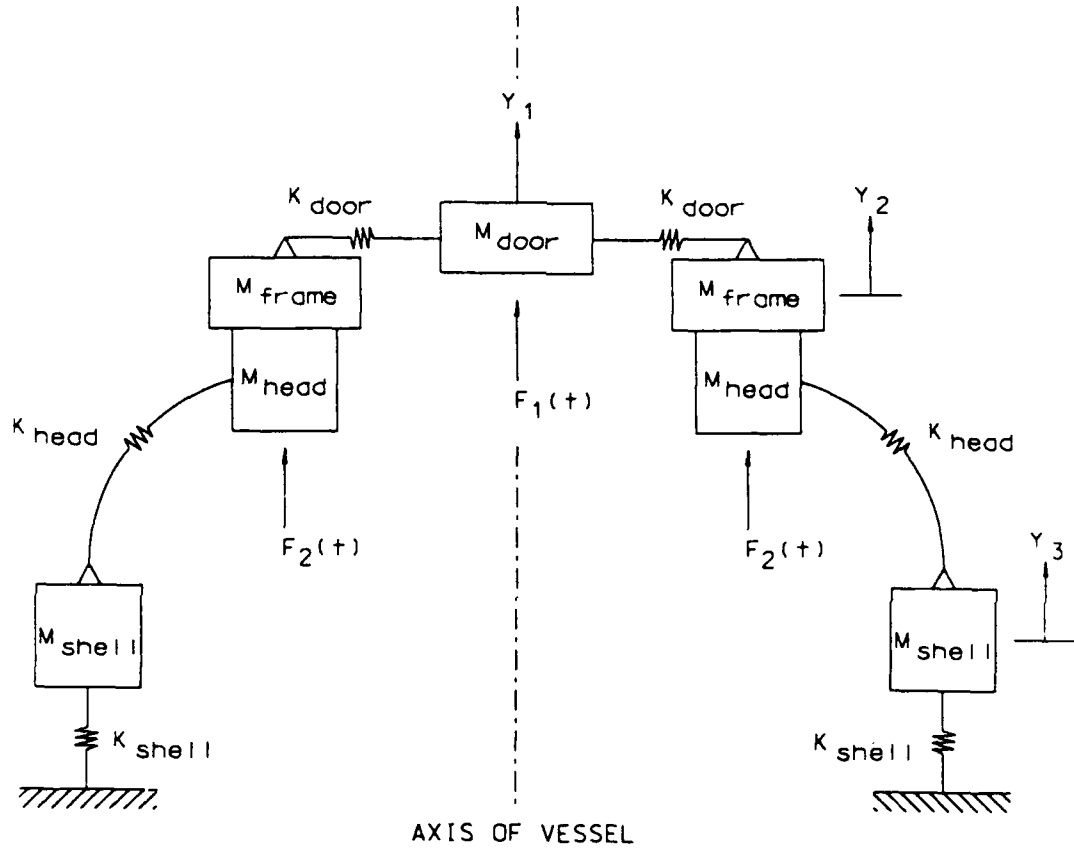


**Figure 4. Head with Door Frame During Fabrication**



$Y_1$  = Door centerpoint displacement

$Y_2$  = Frame displacement

$Y_3$  = Shell displacement @ connection to head

**Figure 5. Three-Degree-of-Freedom Model of the Head with the Door**

from the tests can pass through the openings in the floor which could be a maintenance problem. There was an additional concern that connections could loosen during tests which would require tightening before proceeding with subsequent tests.

A solid floor eliminates these problems and also provides a much smoother work surface inside the vessel. A concrete floor was chosen with steel plates at the surface to provide protection from fragment impacts and local concentrated blast pressures. The system is shown in Figure 6. The plates are placed in two layers of 0.5 inch thick steel, each separated by 1/8 inch neoprene. Two layers are used to simplify replacement by reducing the weight of the sections. The top layer consists of sixteen "tiles" which are plug welded to the lower plates. Smaller tiles are located in the center of the vessel where the larger charge weights will be detonated. The lower layer consists of twelve tiles which are plug welded to embedded structural steel.

## 5.2 Fragment Shields

Most of the shot configurations planned for the vessel use considerable amounts of metal. Internal barricading around the shot will be used to provide protection for the vessel; however, complete protection is not expected. Therefore, fragment shields are provided around the cylinder. The heads and door do not have attached shields and will be protected by the barricades around the shot.

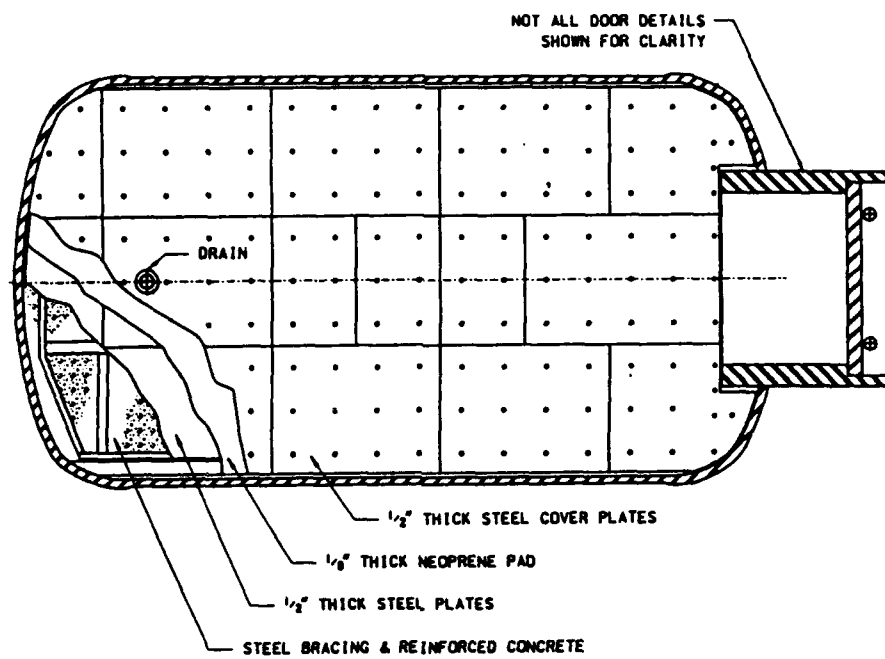
The fragment shields on the cylindrical section are approximately 12 inch by 12 inch square, 1/2 inch thick steel plates backed by 1/8 inch thick neoprene. Each plate is attached to cylinder with four 1 inch threaded studs.

## 5.3 Viewports

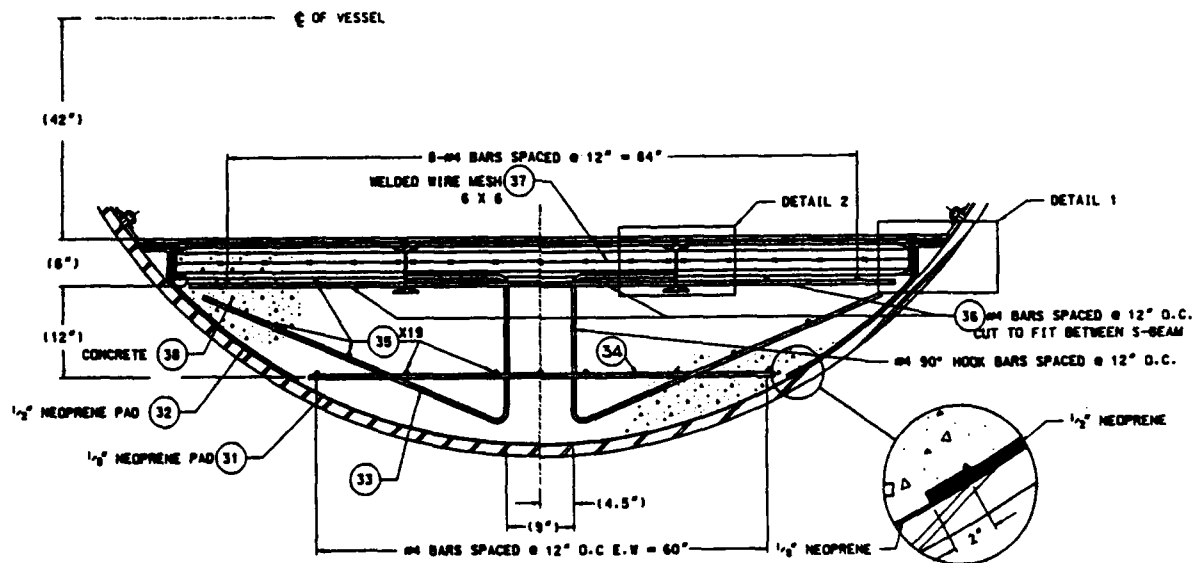
The viewport system is designed to meet three operational requirements:

- Provide a clear window to provide light inside the vessel and for users to look into the vessel before and after the test.
- Provide a high optical quality glass window for photography and other data collection as required for various tests.
- Accept a shield when the windows are not required for the tests.

The viewport system shown in Figures 7 meets these requirements. The frames were machined from HY100 forgings and are designed to accept a circular 3 inch thick thermally tempered glass window or 6061 T651 aluminum plate. Inserts were fabricated to accept 5 inch diameter high optical quality glass. The glass is secured in the insert, and the insert is placed in the viewport frame.



a) Plan



b) Cross Section

Figure 6. Vessel Floor

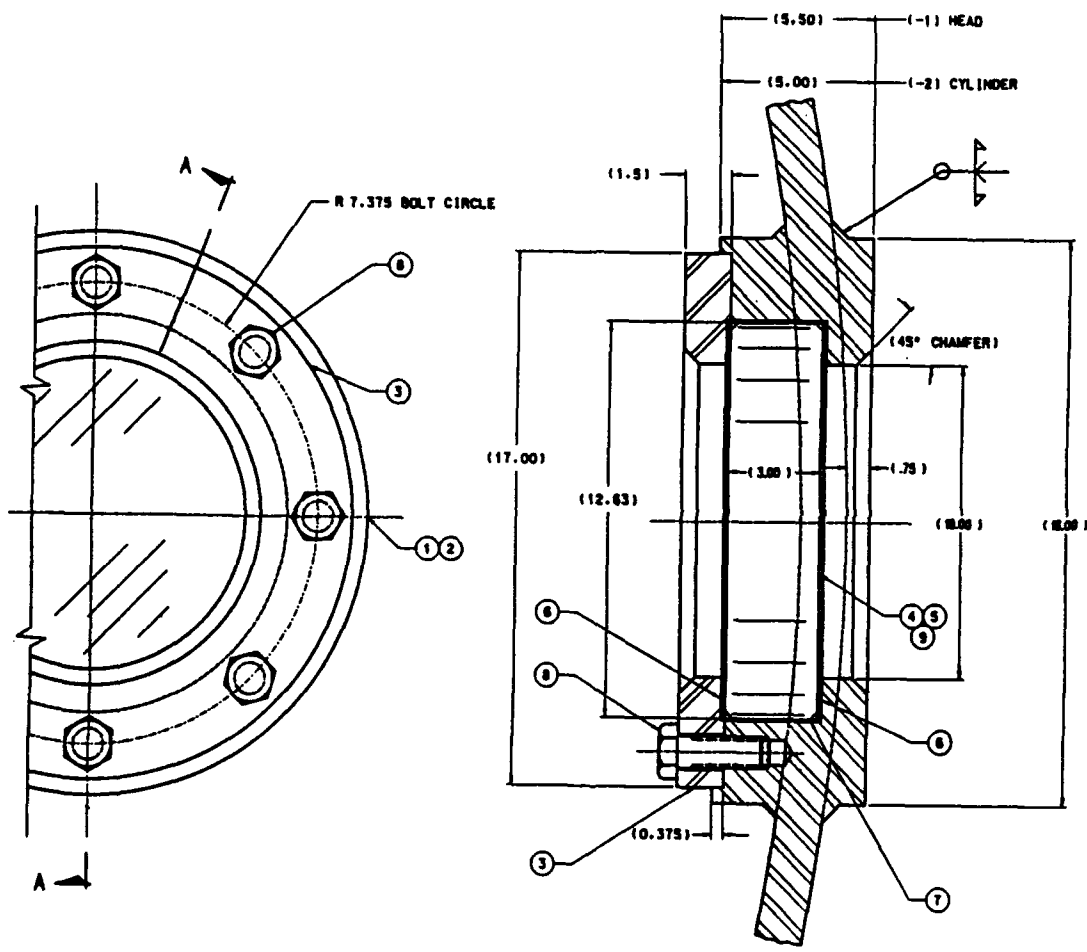


**Figure 7. Viewport**

#### **5.4 Air Inlet and Exhaust**

Following a test, the products from the explosion must be vented from the vessel. The vessel design includes a 6 inch air inlet near the forward end of the vessel and a 6 inch air outlet at the aft end of the vessel. A prefilter and valve is provided at the exterior end of the piping. The valves are 6 inch butterfly valves with pneumatic actuators and position sensors. The valves will be connected to the HVAC system constructed with the building, and will provide protection to the building HVAC system upstream and downstream from the vessel during tests. The prefilter contains a duocel metal foam filter core inside a filter housing. The prefilter will catch larger particles which may be passed through the ventilation system and will reduce shock loads on the valves.

#### **5.5 Other Penetrations**

Additional penetrations through the vessel are required for cable ports, gas and vacuum ports, and a drain. These are shown in Figures 8.

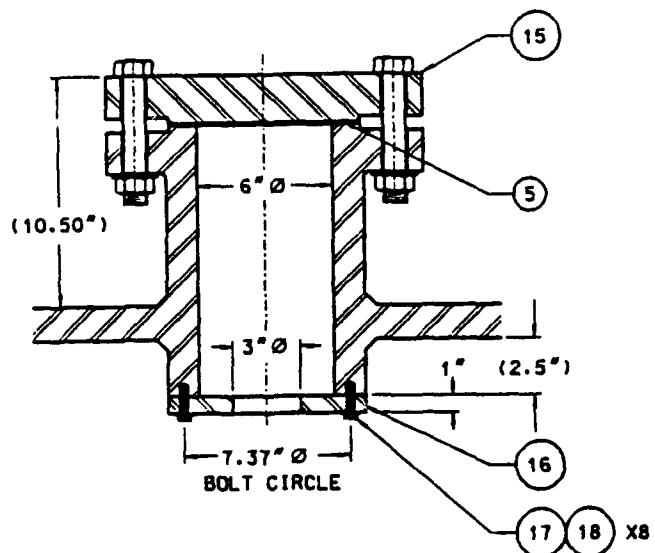
The cable penetration includes a blind flange which the users will drill and tap as necessary to provide for cable pass-throughs. A cover plate will be placed on the inside of the vessel to protect cable connectors from blast and fragments.

The penetrations for gas and vacuum lines are similar to the cable penetrations. The fittings will be attached to the outside of a plate attached to the penetration; therefore, a shield is not needed.

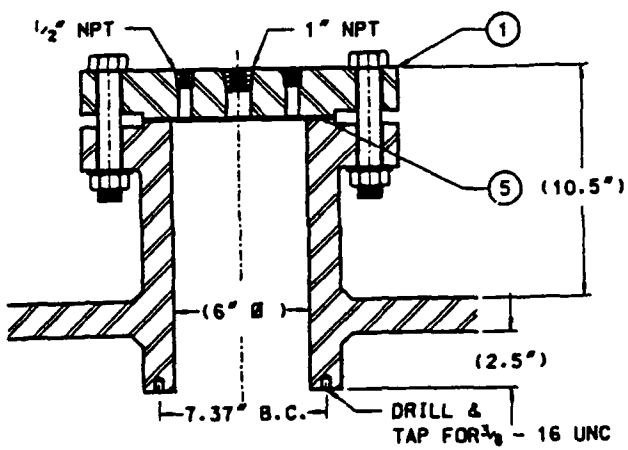
### **6.0 Proof Testing**

Three types of tests are required for proof testing of the vessel: hydrostatic, pneumatic and explosion. The hydrostatic test will confirm the "equivalent" static capacity of the dynamic loads on the vessel. The pneumatic air leak tests will show that the vessel is tight and free of leaks up to 125% of the estimated quasi-static gas pressure generated by the 10 kg TNT equivalent charge. The pneumatic tests will be performed before, during, and after the explosion proof tests. The explosion proof tests will show the performance of the vessel at its rated capacity. A summary of the tests in the order in which they will be performed is as follows:

- 1) Hydrostatic test to an internal pressure of 780 psig. This test will be done prior to the floor being installed in the vessel.
- 2) Air leak test No. 1 will be conducted after the vessel fabrication is completed and before the first explosion test takes place. The test will show that the chamber is tight and free of leaks for 4 hours from the gas pressure rise of the explosive detonations. For the proof test charge weight of 10 kg, the peak gas pressure rise is estimated to be 125 psig. The pressure for the leak tests will be 125% of this value, or 156 psig.

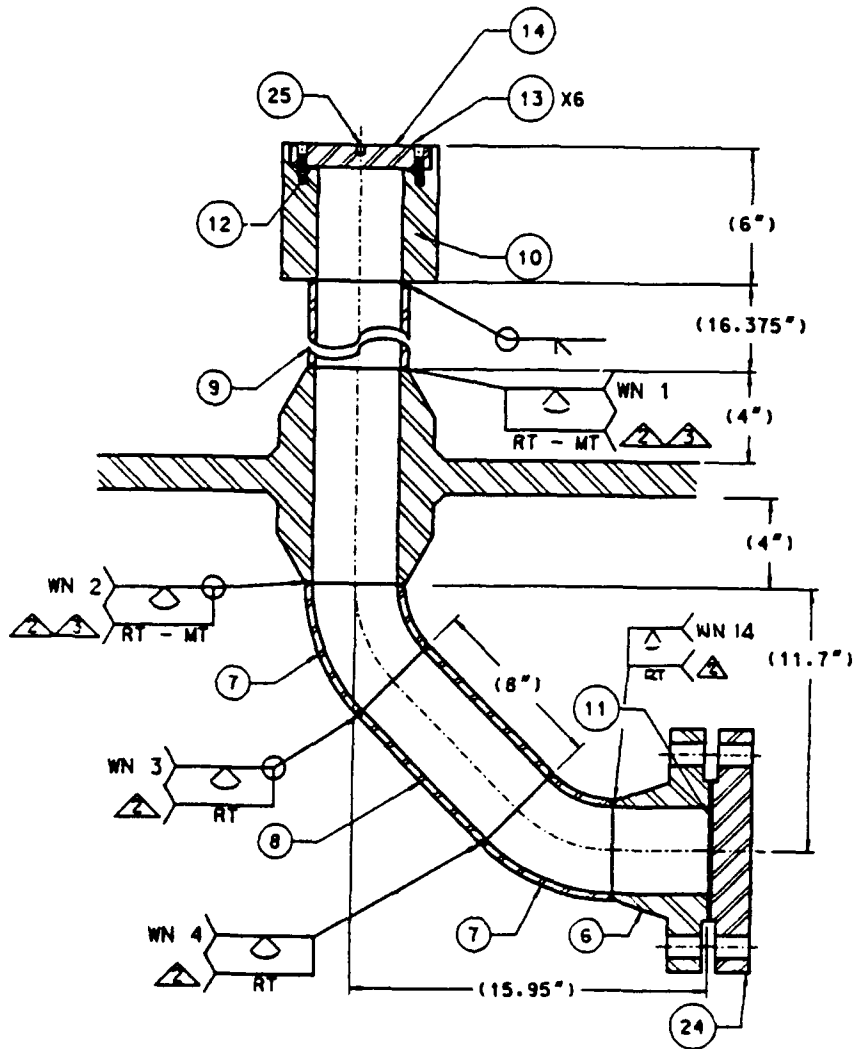


a) Cable Penetration



b) Gas and Vacuum Penetration

Figure 8. Miscellaneous Penetrations



c) Drain

**Figure 8. Miscellaneous Penetrations (Continued)**

- 3) A minimum of 3 preliminary explosion tests will follow leak test No. 1. These preliminary tests will use TNT explosive weights of about 5 and 10 pounds, will serve as operational checks on the measurement systems, and will provide blast load and response data to evaluate the chamber design prior to the explosion proof tests.
- 4) Explosion proof test No. 1 will consist of firing a 10 kg spherical charge after the data from the preliminary tests indicate the expected results. Again, the response of the chamber and the blast pressures generated by the charge will be measured by strain gages and pressure transducers, respectively.
- 5) Air leak test No. 2 will follow the first explosion proof test.
- 6) After completion of the second air leak test, explosion proof test No. 2 will be conducted in a similar manner to the first test.
- 7) Proof testing of the vessel will be completed by performing air leak test No. 3.

Testing of the vessel is scheduled to begin in late September of this year.

### **Acknowledgements**

The authors extend their gratitude to all those individuals at Los Alamos National Laboratory and Southwest Research Institute who contributed to the design, fabrication, and review through the course of the project. Especially noted are Mr. Jerry Wackerle of Los Alamos, who provided review throughout the project and provided information on the use of the vessel and current testing at Los Alamos, and Mr. Wendel Seitz, who was the program manager for Los Alamos. Also Acknowledged are Mr. Francis Caroline, who supervised the fabrication of the vessel at Southwest Research Institute and Ms. Shirley Demel, who prepared this manuscript and processed the records for the project.

## **References**

1. "M-9 Firing Facility Containment Vessel One Hundred Percent Design Basis Document," prepared for Los Alamos National Laboratory Group M-9 under Subcontract 9-L51-D9320-1, August 1991.
2. Statement of Work for the M-9 Contained Firing Facility Containment Vessel, February 2, 1990.
3. Esparza, Edward D. and White, Robert E., "Blast Pressure Measurements in Containment Test Cells," 23rd Department of Defense Explosives Safety Seminar, August 9-11, 1988.
4. Britt, J.R., Drake, J.L., Cobb, M.B., and Mobley, J.P., "BLASTINW User's Manual," ARA 5986-2, Final Report 2, Contract DACA39-86-M-0213, with U.S. Army Waterway Experiment Station, April 1986.
5. "ABAQUS User's manual," Version 4.8, Hibbit, Karlsson & Sorensen, Inc., Copyright 1989.

**DESIGN OF A LARGE DOOR  
FOR AN EXPLOSION-CONTAINMENT STRUCTURE**

by

**David A. Parkes and Harold D. Laverentz**

**Presented at the  
25th DoD Explosives Safety Seminar  
Anaheim, California**

**August 20, 1992**

# **DESIGN OF A LARGE DOOR FOR AN EXPLOSION-CONTAINMENT STRUCTURE**

## **I. BACKGROUND**

### **A. FACILITY DESCRIPTION**

The facility addressed in this paper was built during the 1980's to provide for destructive testing of various types of munitions. These types of munitions include: large caliber, kinetic energy (KE) projectiles of up to 155 mm; advance chemical energy (CE) munitions; self-forging fragment (SFF) munitions; and reactive armors (RA). The principal structures at the facility are a Target Room and a Range Tunnel (See Figure 1).

The Range Tunnel is a 340 feet long reinforced concrete box type structure, 20 feet wide by 16 feet tall. The purpose of the tunnel is to enclose the trajectory of test projectiles between launch and entry into the Target Room. It was designed to remain within the dynamic elastic range when subjected to a muzzle blast loading.

The Target Room, located at the down-range end of the Range Tunnel, is the place of projectile impact. Any one of several types of targets can be located within the room during test firing. The Target Room structure is a vertical truncated cone fabricated from ASTM A572, Grade 60, steel plate. Above this cone is a hemispherical dome, fabricated from ASTM A516, Grade 70, steel plate. The reinforced concrete floor of the Target Room is protected by a cover of armor plate. See Figure 2 for a cross sectional view through the Target Room.

The inside diameter of the conical section at floor level is 59 feet. The clear height inside the Target Room is 29'-6". A three-foot diameter opening in the shell wall adjacent to the Range Tunnel provides for the shot line access. A 14 feet wide by 18 feet high opening was provided in the steel shell for transfer of targets in and out of the room. The original closure for this opening consisted of a horizontally-rolling steel, manually operated door. This original door is now in the process of being replaced, and its replacement is the subject of this paper.

Dust from munitions interactions with the target is controlled by exhaust fans and filters connected to the Target Room. Outside air is introduced through the shot line access opening in the Target Room shell. A high pressure air handling unit forces air and other gases through pre-filters, secondary filters, and high efficiency particulate filters. Blast attenuators, located between the Target Room and filters, minimize sudden pressure differences across the filters. For ease of maintenance, exhaust fans and filters are enclosed in an adjacent structure.

## **B. EQUIPMENT DOOR DEFICIENCIES**

The original door weighed approximately 18,000 pounds. It was designed to operate by rolling laterally across the door opening and then being pulled tight against the shell by a number of peripheral bolts to effect an air seal. Access to these bolts was inconvenient, and tightening the bolts was found to be a time-consuming operation. Over a period of time, the blast pressure impulse on the door and fragment impacts had irreparably damaged the door so that it could no longer be opened and closed manually.

After the door could no longer be manually operated, a fork lift had to be used to position the door before and after each test firing. The time required to move the door by this method, the uncertainty of fork lift availability, and the inconvenience of sealing by a bolted connection all contributed to the decision to investigate possible modifications to the door.

## **II. INITIAL STUDY**

A study was performed to determine the most appropriate action. The study considered economic, reliability, firing range operation, and constructability factors. Criteria for the study were as follows:

- Subsequent repairs to the door would not be required.
- Construction must be phased to coordinate with the range firing schedule.

Two basic options were considered. The first was to modify the existing door and the second was to provide a new door. Eight different variations of the basic options were developed. When all factors were considered, the decision was made that the best course of action would be to replace the door.

## **III. DESIGN OF THE DOOR REPLACEMENT**

### **A. DESIGN OBJECTIVES**

1. Criteria for the original door included provisions for:

- Containment of pressure within the Target Room,
- Containment of explosion fragments,
- Adequate size for passage of targets, and

2. Criteria for the door replacement encompassed all requirements for the original door, plus:
  - Ease of door operation.

## B. ESTABLISHMENT OF THE DOOR CONFIGURATION.

Design of the new door configuration was influenced by several inter-related factors that were considered both individually and in concert. These factors were:

1. Transfer of Blast Pressure at Reaction Points. The original blast door was positioned inside the Target Room and remained within that room during its opening and closing travels. This inside position allowed bearing against the internal faces of its jambs, a rather simple arrangement. However, experience showed that projectiles created during test firings tended to damage operating mechanisms that were exposed to the interior.
2. Direction of Motion. A basic step in design of the door replacement was the definition of its opening and closing motions. Each of twelve singular directions of motion (six ways of translation and six way of rotation) were theoretically possible. By combination of translational and rotational modes, 36 additional travel motions were possible.
3. Support of Gravity Load. The completed door replacement was estimated to weigh about ten tons. Support of this ten-ton weight during its travel and while at its terminal positions was considered in parallel with door motion studies. Several schemes involving suspension devices, underneath rollers, and hinges were studied.
4. Precision of Motion. Because of it requirement for air containment, little tolerance was permitted in fitting of the door replacement to the door opening. The small tolerance permitted by criteria for air-tightness was reduced to an even lower degree when means for locking into place were considered.

After study of these factors, the basic configuration of the door replacement was established to be:

- The door would be positioned outside the Target Room structure.
- The door would be designed to rotate about a vertical axis that was offset from the door opening.
- Weight of the door would be resisted by rigid connection to an overhead truss. The truss, in turn, was to be

supported on one end by a trolley system that travelled on a curved monorail and on the other end by a steel post with a jib-like connection.

- The internal blast load on the door was to be resisted by multiple locking lugs on its exterior surface.

See Figure 3 for the design configuration of the new door.

## C. DETAILS OF DESIGN.

Sizing the door structure to resist an internal blast pressure was straightforward, with the behavior of steel under dynamic loading taken into account. The spring-action rebound of the door after loading was also considered.

The inside plate of the door was designed to be fabricated of Type HY80 steel to provide greater resistance to damage by projectiles emanating from test firings. This type of steel is more normally used for submarine hulls.

A pneumatic hose gasket were designed to seal doors edges for containment of air pressure within the Target Room. This gasket was shielded against damage from projectiles. Accurate fitting of the door to the door frame was made necessary to allow gaskets to function. For this reason, the door replacement was designed for adjustable positioning in horizontal and vertical directions.

The locking mechanism consisted of six latch-bars on both ends of the door; these bars were designed to be electrically inserted and withdrawn (See Figure 4). An annunciator light was designed to prominently display evidence when all latch-bars were not in place, and in this way, prevent test firing while the door was unlocked.

## IV. INSTALLATION OF THE DOOR REPLACEMENT

### A. PROCUREMENT

Drawings and specifications were prepared for the door replacement, stipulating that the supplier must satisfactorily demonstrate operation of the door upon completion of his work. Purchasing documents also required erection work to be performed only during periods of non-testing at the site.

Although much interest was shown by prospective door suppliers during the design period, this interest narrowed when construction bids for the door were sought. Only a few bids were received, and bid amounts were disappointingly high.

## **B. CONSTRUCTION**

Work preparatory to installation of the door replacement is still underway. Construction problems to date have been (1) a need to repair damage to the existing door frame, and (2) coordinating the contractor's work with the facility operations schedule for testing. Onsite construction work is not permitted during test firing at the facility because of the hazards involved.

## **V. CONCLUSIONS**

The Equipment Door, after its replacement, will likely be one of the most complex and most expensive components of the facility. This complexity and expense resulted from a need for custom-design, a need for precision installation, and other factors that normally attend retrofit of an existing and operating facility.

The primary conclusion of this paper is, then, to emphasize the need for convenient operation of large doors in a containment structure, particularly if doors are to be frequently used. Convenient operation is not easy to achieve and can be even more difficult when the construction budget is strained.

A secondary conclusion may be inferred from the primary one. That is, costs for such doors must be recognized and carefully estimated during the planning phase for a containment structure. Thoroughly detailed estimation of costs for large doors is essential because such costs cannot be found simply by consulting a handbook nor by use of rule-of-thumb estimating guides.

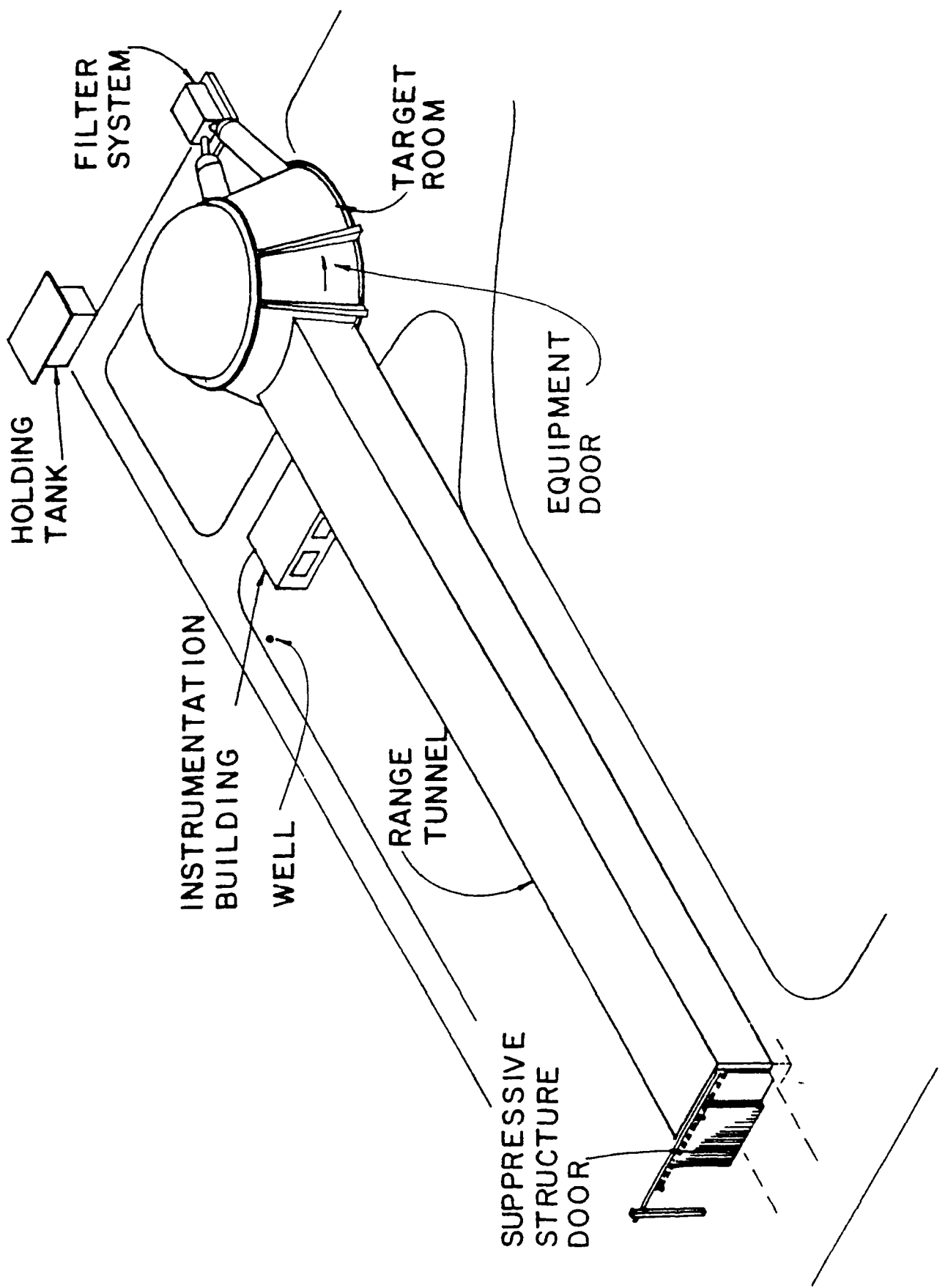
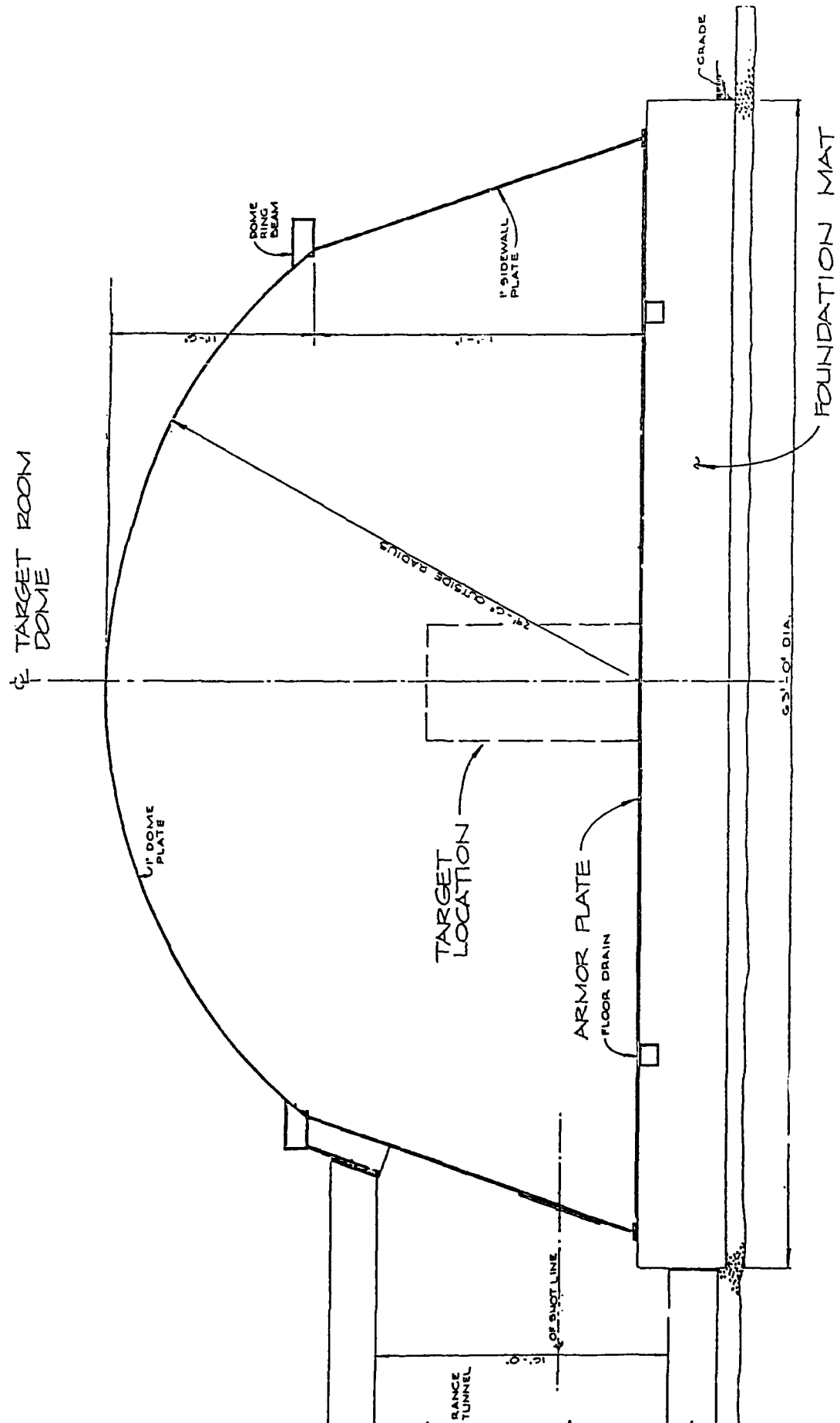


FIGURE 1  
537

## TARGET ROOM CROSS SECTION



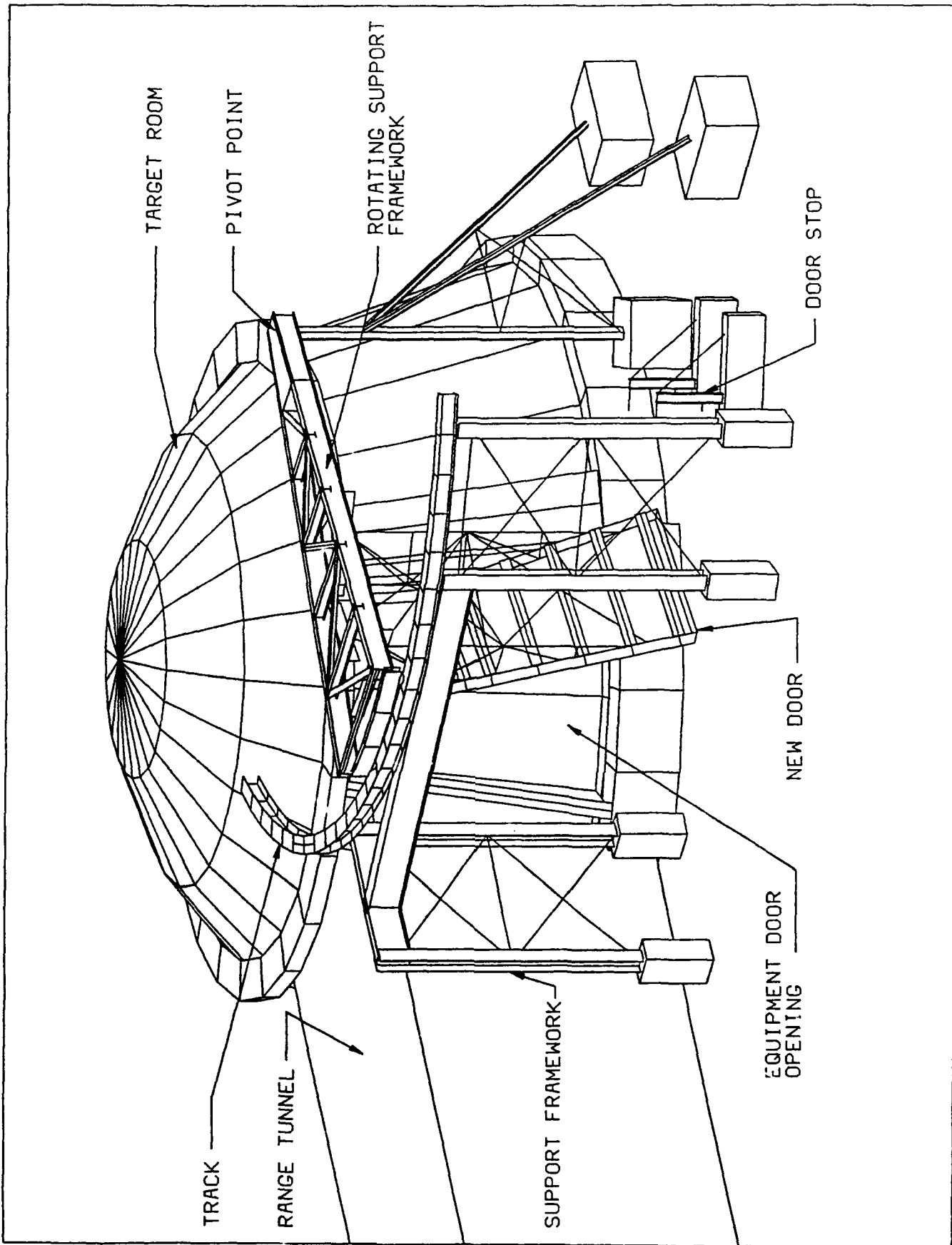
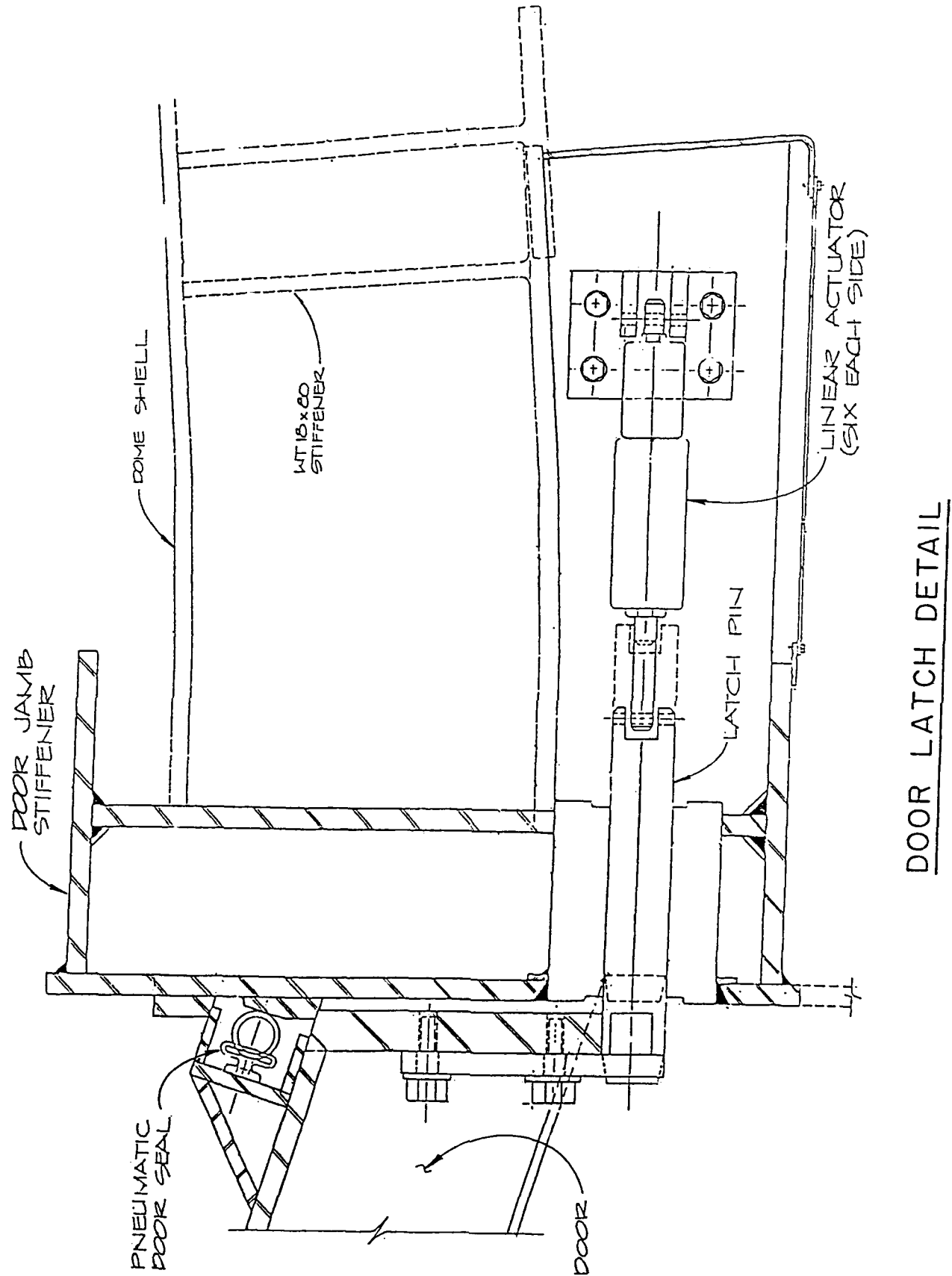


FIGURE 3  
539



## TWENTY FIFTH D.O.D. EXPLOSIVES SAFETY SEMINAR

### REDUCTION OF HAZARD ZONES

### BY UNCOUPLING BETWEEN MUNITIONS

By

Maurice C. CHIZALLET  
GIAT Industries - Ammunition and Pyrotechnics Division  
13, route de la Minière - Satory  
78008 VERSAILLES  
FRANCE

#### Abstract :

For determining the Maximum Credible Event concerning a munitions production or storage facility, it is necessary to take account of the N.E.Q. of all the mass detonating munitions located in the immediate neighbourhood of the donor.

Safety distances which will be determined (Q/D factor) will be those of 1.1 division. This risk division induces highest constraints. Uncoupling between munitions allows to reduce safety distances with important benefits by suppressing sympathetic detonation.

Different means can be used, specially like specific packaging, venting devices, or intrinsic characteristics of insensitive munitions.

This paper shows tests realized by GIAT Industries / Ammunition and Pyrotechnics Division with different types of munitions and main results obtained.

Presented at the 25th Explosives Safety Seminar, August 92 - Los Angeles - California

## **CONTENTS**

**I INTRODUCTION**

**II DETERMINATION OF SAFETY DISTANCES**

**III SEARCH FOR UNIT RISK**

**3.1 Uncoupling tests**

**3.1.1 Tests with rifle grenades**

**3.1.2 Tests with gun ammunition**

**3.1.3 Missiles Warheads**

**3.1.4 Anti-tank rockets**

**3.2 Venting devices**

**3.3 In-sensitive munitions**

**IV CONSEQUENCES ABOUT SAFETY AREAS**

**V CONCLUSION**

**VI LIST OF REFERENCES**

## I INTRODUCTION

Any activity concerning munitions means a risk level. The risk is defined as a notion with two dimensions which are gravity (consequences) and probability. The risk characterizes an inadvertent hazardous event. For any installation of munitions, the inadvertent hazardous event must be located on the basis of the Maximum Credible Event (MCE) : the worst single event that is likely to occur from a given quantity and disposition of ammunition and explosives (Ref 2). Then, it is fitting to estimate the acceptable risk for the individual man, the manufacturer or the Armed Forces, the society.

Today, the public is concerned by safety of persons, property and environment and bring pressure on administration. It induces to obligatory size measures in order to assure safety of munitions facilities at one and the same time for logistical, tactical or operational phasis.

Safety goes by distances between potential explosion seat (P.E.S.) and exposed seat (E.S.). But these distances become less and less compatible with urbanization which is growing up near military installations.

It is necessary to search for all the means allowing to maintain the operational potential and to guarantee the safety of neighbouring installations of P.E.S.

## II DETERMINATION OF SAFETY DISTANCES

The principles allowing to determinate safety distances are harmonized into NATO's countries on the basis of the A/C 258/D 258 manual.

Thereby, there is no important divergence between national regulations (ex D.O.D. 6055.9 for the USA and ministerial order of the 26th September 1980 "rules for determining safe distances of explosive facilities" in France).

Safety of munitions facilities is organized according to the following criteria :

- \* Class/division and compatibility group classification
- \* Possible protections existing to the P.E.S.
- \* Separation distances

Q/D criteria is the minimum distance between a P.E.S. and an E.S. It is based on an acceptable risk to life and property from the effect of a mass fire or an explosion (Ref 1).

At this distance, the exposed seat is normally submitted to an acceptable risk. "Q" means the net quantity of explosive (NEQ) generally expressed in TNT equivalent weight, susceptible to be located into P.E.S., it sizes the M.C.E.

"D" varies according to the class/division, characteristics of the P.E.S., nature of E.S., and the orientation of P.E.S./E.S.

Most of munitions in service into Armed Forces at the present time are classified into the 1.1 class/division because they present a hazard of mass detonation. But the mass detonation is the worst accident which could occur with munitions, what lead to the worst Q/D.

Although this paper be limited to the logistical aspects, it is necessary to speak about tactical and operational phases.

At once, during operational phase, a troop carries explosive munitions, and the carried stock must take account of the attrition rate due to enemy actions.

Indeed, due to mass detonation, if a vehicle is hit by a projectile, the stock it carries, and may be the entire stock carried, will detonate dragging important losses.

Concerning tanks, combats during "Desert Storm" have shown that when a tank is hit by an APFDS or a shaped charge, the initial damages are significantly increased by the ammunition reserve explosion, resulting in the turret being blown off.

It is the same thing for tactical facilities. For example, when a hardened aircraft shelter with airborne ammunition inside is hit by Air to ground attack, munitions mass detonation lead to catastrophic results.

The storage of important quantities of munitions which are capable of mass detonating led NATO's countries to set up safety policy based on earth-covered magazines and distances between magazines or between P.E.S. and E.S. Heavy and costly earth-covered magazines like igloos are utilized primarily to prevent propagation of explosion.

NATO AC 258 manual contains all the dispositions adopted by NATO. Some countries believe these rules severe. But in these NATO's countries where these rules are applied, the accidents are extremely rare into storage facilities.

Specialized review recently talked about two accidents which happened in May 1992 :

First one : Explosion at the Commonwealth of independent states pacific fleet ammunition depot of Vladivostok, five injuries, 16 magazines damaged and may be more extensive damages.

Second one : Explosion at a Lybian ammunition depot near Tripoli, 17 persons killed, about one hundred injured.

Explosive munitions can be classified in division 1.1 or 1.2, as they present or not a mass detonation risk. Constraints due to this risk can be easily measured by the obligatory safety distances between the P.E.S. and the E.S.

Thus, the P.E.S. mass detonation risk prohibits storage of munitions into operational installations.

So, it is necessary to store ammunition into isolated munitions storage area. Generally vulnerable to enemies or terrorists actions, it reduces the operational disponibility of forces, increases the risk, especially for handling and transport operations and increases the operating cost of the munitions storage area.

Also for maintenance or manufacturing operations, the growing of the M.C.E. obliges to lay out installations with heavy and costly structures.

### III SEARCH FOR UNIT RISK

For lowering constraints, the only way consists to decrease the M.C.E. in order to reach an inadvertent hazardous event which could be acceptable. So, it is necessary to prohibit mass detonation of all the munitions which are in the immediate neighbourhood for limiting the M.C.E., according to circumstances of one stack, one box and if possible only one munition.

For this, the munitions designer can :

- \* Define new methods of operating and storage for limiting stimuli level and consequences of an accidental event in logistical phase.
- \* Develop packaging which offer an efficient and immediatly available protection, against mechanical and thermal stimuli.
- \* Incorporate devices allowing to liberate energy.
- \* Use structures and architectures limiting development of phenomenon.
- \* Use explosives acting with satisfactory making against stimuli.

The munitions designer must be the designer of the new packaging which protect munitions against external stimuli, or the designer of shields which prohibit sympathetic detonation.

For many years, studies and tests made in France and in USA have allowed to know better sympathetic detonation conditions according to :

- \* Space between munitions.

- \* Location of munitions inside packaging.
- \* Nature and thickness of shields.

We realized a lot of tests concerning several families of munitions which allow us today to set solutions answering to the users problems.

### 3.1 Uncoupling tests

#### 3.1.1 Tests with rifle grenades

We realized a lot of tests for determining sympathetic detonation conditions with rifle grenades in storage and transport conditions. i.e. in boxes and in palettes with eight boxes. We get a total of two hundred grenades presenting a TNT equivalent weight of 45 Kg.

These tests allowed us to optimize a logistical configuration leading to reduce very much the M.C.E.

With two hundred grenades concerned, only ten maximum are susceptible to detonate presenting an e.TNT < 2.5 Kg, it means 5% of theoretical M.C.E. And then, it allowed us concerning production phase to set up workshops to ensure perfectly operators safety.

#### 3.1.2 Tests with gun ammunition of 35 mm and 40 mm

For illustrating works we make with gun ammunition, example of tests with gun ammunition of 35 mm and 40 mm.

Gun ammunition surrounded by a cardboard tube are located into a screwed covered wood box. The shield between gun ammunition is made of wood with a thickness of 10 mm. The donor gun ammunition is surrounded by four receivers, two of them are fuzeless.

Uncoupling between gun ammunition is effective. Only the donor detonates, what is shown by the metallic sheet located under the box. In these conditions of uncoupling, the M.C.E. is detonation of only one gun ammunition.

#### 3.1.3 Missiles Warheads

Among tests realized in this area, our works concerning uncoupling between ground to Air missiles are significant.

At the time of these explosive charges fabrication, the mass detonation presented an unacceptable risk for the operators located into the workshop and for the neighbouring installations.

We set up a packaging ensuring uncoupling, thus reducing the hazardous event to the detonation of only one warhead. Many shields have been tested made of wood, composite materials, etc...

The positive result concerning these tests allowed us to take simple and effective actions about safety.

Thanks to this, French Authority approved our safety analysis concerning operators and environment safety.

#### **3.1.4 Anti-tank rockets**

We realized tests in order to find the possible best shield between anti-tank rockets. TNT equivalent weight of each rocket is about 2.5 Kg.

The tests concerned sympathetic detonation study with the only launch tube like shield, locating successively rockets in the same way, in opposite way.

At first, we used polyethylene shields with different thicknesses, and finally we used wood shields.

The results of these tests allow us to control non-propagation conditions of detonation in all logistical phase and to set up a packaging limiting to a unit risk.

#### **3.2 Venting devices**

One of the means allowing the munition designer to limit consequences of an accidental event is to fit the warhead or the rocket motor with venting device. For example, we manufacture the venting device of U.S.A.F. Durandal anti-runway bomb. This system is used in the event of an undesired high temperature. The aim is to prevent a normal propulsive thrust of the R.M. These devices are used to prevent such events from occurring in munitions which are in transport or storage.

#### **3.3 Insensitive munitions**

Methods we have just seen present very important advantages :

- a) They allow to avoid mass detonation and reduce constraints, more particularly in storage.
- b) They can be used immediatly.

- c) They don't need long and expensive R and D preserving in the same time initial operational performances.

But they are in use just once and their efficiency cannot be guarantee in case of multiple stimuli.

The insensitive munitions take here all their interest as their intrinsic characteristics limit the effects of an accidental event and delete the mass detonation.

Among in progress programs which reduce munitions vulnerability, we produce gun ammunition, grenades, anti-tank rockets, missiles warheads, bombs, example of land mine shows what it is possible to obtain.

After having tested different high explosives and specially several cast or pressed PBX, a land mine has been developed with insensitive munitions capacities.

This mine is mainly composed with a structure, a pressed PBX charge composed of HMX and TATB with the safety and arming unit.

Two series of vulnerability tests have been realized, 12.7 mm bullet impact and sympathetic detonation. The third test, fast cook-off, will be soon realized.

a) 12.7 mm Bullet Impact

Tests procedures : In a packing corresponding with 1H2 UN classification (rigid plastic drum), 5 mines are located vertically, 3 explosive mines and 2 inert mines.

The central mine surrounded by 2 explosive mines is the target. The mines are vertically located. A steel witness plate is positioned beneath the test item.  
The 12.7 mm are type M2 armor piercing projectile at a velocity of 860 m/s.

Main results : The central mine, hit by the bullet, burns during several seconds after the impact. High explosive burns and the hole created by the bullet acts like a nozzle. The 2 explosive mines in touch with the target do not react. For this test, the passing criteria no reaction more severe than burning is obtained.

b) Sympathetic detonation :

Tests procedures : Two 1H2 UN packages (rigid plastic drum) are located side by side in a natural wood box. The first drum contains 3 explosive mines and 2 inert mines. The second one contains 1 explosive mine and 4 inert mines. The acceptor explosive mine is located in front of the donor mine.

Main results : After the post tests examination, we can note the following results :

- Concerning the 2 neighboring mines, the first one detonates and the second one deflagrates. The acceptor explosive mine located into the neighboring drum has been mechanically broken in small pieces but no explosive reaction or burning occurs.

This land mine presents vulnerability and performances characteristics very interesting due to the HMX/TATB composition.

The tests go on in order to obtain the label "insensitive munitions" in conformity with the Military Standard 2105A and the classification in risk division UN/NATO 1.6.

#### **IV CONSEQUENCES ABOUT SAFETY AREAS**

The interest for the munitions storage area user is to reduce constraints that impose presence of munitions to environment while disposing of maximum storage capacities.

For illustrating the benefit brought by uncoupling between munitions, i.e. the passage from the class division 1.1 to the division 1.2, we can take an example of earth covered magazines like igloos with capacity of 60,000 Kg, on the base of NATO safety distances :

Safety distances to inhabited buildings and public traffic routes :

$$\begin{aligned}1.1 \text{ division} &= 870 \text{ m (22 Q 1/3)} \\1.2 \text{ division} &= 500 \text{ m}\end{aligned}$$

If the existing safety distance separating the P.E.S. from the nearest E.S. is about 500 m, it would be necessary to decrease the igloo capacity from 60,000 Kg to 12,000 Kg in 1.1 division, i.e. divide the storage capacity by 5.

If we take the hypothesis that for 1.6 division, 1.3 division safety distances will be applicable, we obtain for 60,000 Kg :

$$1.3 \text{ or } 1.6 \text{ division} = 255 \text{ m}$$

If the P.E.S./E.S. safety distance is always about 500 m, it is possible to store in this case 250,000 Kg, it means twenty times more than 1.1 division.

Safety distances mentioned above are those advised at the present time by NATO.

American and French national regulations are most strict for detailed application. We can think that M.C.E. reduction, more particularly by the uncoupling mean, should form the

subject of safety analysis for determining the maximum hazardous consequences for a given accident.

In effect, uncoupling can be obtained :

- \* Between stacks. For example, into an igloo containing 60,000 Kg, five stacks uncoupled limit the M.C.E. to 12,000 Kg.
- \* Between boxes, the M.C.E. is reduced to the explosive mass contained into the packaging.
- \* Between munitions, the maximum hazard to take into account would be unitary hazard.

## V CONCLUSION

We can see that particularly important perspectives appear for Armed Forces which must :

- \* Improve combat platforms survivability.
- \* Ensure safety in logistical and tactical phase.
- \* Decrease logistical costs.

But it is really necessary to distinguish between near term and long term. Uncoupling between munitions by packaging and / or adapted shields allow to resolve problems met at the present time and particularly during storage phase when reducing :

- \* Safety distances between P.E.S. and E.S.
- \* Risks due to transport and handling imposed by off-site storage.
- \* Operating costs by reduction of necessary areas, undercontrol areas, number of magazines and resistive structures.

Concerning long term, major programs about R and D are on the way to reach to insensitive munitions, and concerning storage phase to classified munitions in 1.6 class division.

Armed Forces must find here same and if possible best performances and money saving upon possession cost.

The job of the munition manufacturer is to answer to his customer troubles, because he knows the munitions characteristics he manufactures. That's what GIAT Industries wants to propose to his customers.

## **LIST OF ACRONYMS**

<b>M.C.E.</b>	:	Maximum Credible Event
<b>P.E.S.</b>	:	Potential Explosion Site
<b>E.S.</b>	:	Exposed Site
<b>Q/D</b>	:	Quantity Distance
<b>N.E.Q.</b>	:	Net Equivalent Quantity (Kg)
<b>H.A.S.</b>	:	Hardened Aircraft Shelter
<b>I.M.</b>	:	Insensitive Munitions
<b>R.M.</b>	:	Rocket Motor
<b>G.A.</b>	:	Gun Ammunition
<b>C.D.</b>	:	Class Division
<b>e. T.N.T.</b>	:	Equivalent Weight T.N.T.

## **REFERENCES**

- 1) Manual on NATO Safety principles for the storage of ammunition and explosives (AC 258 / D 258).
- 2) Ammunition and explosives safety standards D.O.D. 6055-9.
- 3) Structure to resist the effect of accidental explosions TM 5-1300.
- 4) French ministerial order, rules for determining safe distances of explosives facilities.
- 5) Manual of NATO principles for the hazard classification of military ammunition and explosive - Draft AASTP 3.

SAFE SEPARATION DISTANCE OF 81mm MORTARS  
BY ANALOGY TO THE M374 SERIES TESTING

Joseph P. Caltagirone  
U.S. Army Armament Research, Development  
and Engineering Center  
Picatinny Arsenal, NJ 07806

ABSTRACT

Safety regulations require a safe separation distance between ammunition items to prevent propagation between buildings or between bays when conveyors are used to transport such items. Establishing such a distance usually requires testing to obtain the 50 samples necessary for statistically acceptable data. This paper presents the rationale used to avoid testing the new generation M821E1/M889E1 81mm mortars by comparing the velocities, and fragment weights from arena tests, configurations, and projectile physical parameters with the older M374 Series 81mm mortar. The M374 mortar was extensively tested in several configurations and use of the new 81mm mortar safe separation distance data established by this analogy allows production of the new mortar on existing production lines without conducting testing and expending costly items.

SAFE SEPARATION DISTANCE OF 81mm MORTARS  
BY ANALOGY TO THE M374 SERIES TESTING

BACKGROUND

Ammunition and explosive items, or groups of items that are transported from one operating building to another, or from bay to bay within an operating building shall be separated to preclude the establishment of a path for the propagation of an explosion or fire between the buildings or bays. This requirement is imposed by the Army Material Command regulation AMC-R 385-100. A minimum spacing of intraline distance is to be used unless statistically acceptable testing is conducted to show that the non-propagation distance is less than intraline distance.

An extensive series of tests was conducted in the 1970's and 1980's to determine this reduced non-propagation distance for numerous ammunition items, bulk explosives and explosive components. These tests were conducted under Manufacturing Methods and Technology (MMT) Projects 57X4201, 57X4288 and 58X4288, for the Project Manager for Munitions Production Base Modernization and Expansion as part of their Army-wide facility modernization program.

Under the above programs testing was conducted to determine the minimum safe separation distance of 81mm HE mortar rounds in various configurations. These results were approved by the AMC Field Safety Activity and applied at both Kansas and Milan Army Ammunition Plants. The items tested were the M374 HE Cartridge, M374A1 HE Projectile, and the M374A2E1 HE Projectile.

Recently, new 81mm HE mortar rounds have been developed: the M821E1 and M889E1. These items, which are identical to each other except for the fusing, are very similar to the M374 series, except for a lower explosive weight and a different projectile body material. These rounds were developed to improve the fragmentation (numbers of fragments and pattern) of the 81mm mortar.

Use of intraline distances to separate these items during production is unacceptable if design production rates are to be met. The cost of these new 81mm rounds, which are not yet in production, is high and safe separation distance testing typically requires 25 confirmatory tests for each configuration with a donor and two acceptors to obtain the 50 data points necessary for statistically acceptable distances (i.e., a probability of detonation of less than 10% with a confidence level of at least .95). This is in addition to exploratory testing to establish a starting point for the confirmatory tests. These rounds were being "hand-produced" at the time of this study to fulfill other testing requirements. Waiting for the necessary number of rounds would have necessitated testing at a much later date, possibly impacting set-up of the production lines.

Since these rounds are similar to the older M374 series, a preliminary evaluation of the configurations indicated that the safe separation distance of the M374 series is applicable to the newer M821E1 and M889E1 rounds. A

detailed analysis of applicable parameters is presented in this paper. The previously established M374 series safe separation distances are presented along with drawings and descriptions of the M374, and M821E1/M889E1 rounds. A rationale for using the established safe separation distance for the newer rounds is developed.

A successful analogy and application of previously established distances as adequate for the new rounds will result in a large cost savings by avoiding the testing, test items and hardware, and engineering labor that would have been required. In addition establishing the safe separation distance at this time will avoid a late impact on the production line "design".

#### M374 SERIES SAFE SEPARATION DISTANCES

Previous testing conducted on the M374, M374A1 and M374A2E1 81mm HE mortars in various configurations is detailed in references 1, 2 and 3. The configurations, items as tested, other parameters and results are provided below. Results are summarized in Table 1.

#### M374 HE Cartridge

The projectile body for the M374 cartridge is shown in Figure 1. The projectile body is identical for the M374, M374A1 and M374A2E1. It was tested in the vertical position with and without 2 inch diameter aluminum (6061 T6) interrupter bars (Figure 2). The M374 projectile body is loaded with 2.1 lb of Composition B. The safe separation distance was an 8 inch separation with the 2 inch aluminum bar based on a total of 62 samples (including 22 at a 7 inch spacing) without propagation of detonation. The actual test configuration was conducted without the 2 inch shield; however, for additional safety the 8" distance with the shield was utilized. This corresponds to a probability of detonation of 5.6% at a 95% confidence level.

#### M374A1 Projectile

The M374A1 projectile body as shown in Figure 1 was tested in the single item and 72 projectile pallet configurations. The single projectile configuration simulated the transporting of items in the vertical position on a powered link-belt conveyor (Figure 3). The pallet configuration, with 72 projectiles in a 6 by 12 matrix (with 0.83 inch lateral spacing) simulated transport of the pallets on a power roller conveyor (Figure 4). These configurations were derived from Load, Assemble, and Pack (LAP) areas at Milan AAP. The M374A1 projectile contains 2.1 lb of Composition B.

Results obtained for the single projectile resulted in an approved safe separation distance of 18 inches between items with no shielding and for the 72 projectile pallet configuration a spacing of 30 feet unshielded.

Fifty-three data points were obtained for the "single" projectile and 52 for the pallet configuration, resulting in probabilities of detonation of 6.6 and 6.7 percent, respectively, at a 95% confidence level.

### M374A2E1 Projectile

Figure 1 is a drawing of the M374A2E1 mortar (projectile body). Tests were conducted with the projectiles in a horizontal position in a transfer pallet and two-inch thick aluminum (6061 T6) shields 4 inches high by 14 inches long on a simulated roller conveyor, as shown in Figure 5. This configuration was tested to verify that propagation would not occur on transfer pallets designed by Ingersoll-Rand for use in the Automated Assembly and Packout Line at Kansas AAP. The operations involved were facing of the fuze well, assembly of fuzes, and attaching propelling charges to the fin housing. The M374A2E1 is loaded with 2.1 lb of Composition B.

Since a shielded 8 inch spacing for the M372 cartridge in the vertical position was verified previously, these tests were conducted at an 8.8 inch spacing (the additional 0.8 inch to accommodate the operational heads of the work station equipment). Forty-four tests were conducted, yielding 88 data points. This corresponds to a probability of propagation of 3.9 percent at a 95% confidence level.

### DESCRIPTION OF THE 81mm M821E1 AND M889E1 HE PROJECTILES

The M821E1 and M889E1 projectile body is shown in Figures 6a and 6b. The difference between the two is the M821E1 has the M734 multi-option fuze while the M889E1 has the M935 point detonating fuze. They are designed to be more lethal through the use of high fragmentation steel with an explosive load of 1.72 lb of Composition B. The increased lethality comes from the production of more fragments, even though the fragments do not have increased velocity. Increased fragmentation results in a higher probability of a hit at a given distance.

The physical differences in the M821E1/M889E1 from the M374 series are shown in Table 2. The new rounds, M821E1/M889E1, have a smaller explosive load, slightly thicker casing, and a longer length of explosive. The casing for the M374 is 1340 steel, cold-worked, while the newer rounds are high fragmentation steel known as HF1. The production of more fragments and therefore, increased lethality is due to the casing material and a longer effective warhead length.

### RATIONALE FOR M821E1/M889E1 SAFE SEPARATION DISTANCE

Propagation between cased rounds when separated by an air space is caused primarily by fragment impact. The blast pressure alone will not result in propagation since there is an air space between mortar rounds. This is sufficient to prevent crushing of the item which could initiate the acceptor round. The tests of the M374 series mortar verify this fact. Also, the shield impact on the acceptor did not cause propagation. In the case of the new M821E1/M889E1 mortars propagation will not occur due to shield impact. The lower explosive weight will mean a lower velocity for the shield and the casing of the M821E1/M889E1 is thicker, thus it can absorb more energy before deforming enough to crush the explosive and initiate the explosive.

The rationale presented herein will address the fragments produced by the donor round and will show that since propagation (within acceptable statistical criteria) did not occur for the spacings and configurations of the M374 series, it will not occur for the M821E1/M889E1 with the same spacings and configurations.

Terminal Effects Data for the M374A2 81mm mortar was obtained from the Joint Munitions Effectiveness Manual (JMEM). This data is generated from a series of arena tests, and is the same for the M374, M374A1 and M374A2E1 since the warhead is identical. Terminal Effects Data for the M821E1/M889E1, not yet published, was also obtained. In an arena test, an item is detonated horizontally. Fragments are collected in panels in a 180° arc from the nose to the tail. This arc is divided into polar zones. Fragment weights are recorded and velocities measured. Symmetry of the round is assumed. Data is then entered into an established program which generates the fragment data for the entire item. This data is used to determine an item's effectiveness.

In studying the Terminal Effects Data, it can be seen that the M821E1/M889E1 is indeed more effective. With the use of high fragmentation steel (HF1) more fragments are produced with a smaller explosive fill, 1.72 lb of Composition B versus 2.1 lb for the M374. This greater number of fragments are also produced in zones more likely to result in a hit. This is due to the shape of the new mortar projectile.

The M374 series warhead, which weighs 5.05 lb, produces 30,913 grains, or 4.4 lb, of fragments. The M821E1/M889E1, weighing 5.90 lb, produces 34,322 grains, or 4.9 lb, of fragments. The number of fragments from the M374 is 2,811, while the M821E1/M889E1 produces 6,432. The largest fragment produced by the M374 is 155 grains and for the M821E1/M889E1 it is 143.5 grains, but more importantly the size of the fragments are smaller for the new mortar round. From Table 3 it can be seen that for the M821E1/M889E1 a higher percentage of the fragments are in the smaller size range. Thus, more than twice the number of fragments is produced at the expense of the fragment weights. Since the energy associated with the fragment is  $1/2MV^2$ , smaller fragments have less energy at the same velocity.

The peak velocities of the fragments from the M821E1/M889E1 are lower. The largest velocity for the M374 is 2125 m/s (6,972 fps); for the M821E1/M889E1 it is 1689 m/s (5,540 fps). Higher velocities from a particular round are associated with the smaller fragments. Table 4, velocities of the two new mortar rounds by zone, shows that the new rounds do not produce maximum velocities as high as the M374. The new rounds do have higher velocities at the nose and near the tail of the projectile; however, since propagation of the M374 acceptors did not occur at velocities near 7,000 fps, it will not occur at velocities less than half of that. Also, these fragments are not hitting at normal angles as are those emanating from the center of the round. From the above rationale, it can be seen that the new rounds M821E1/M889E1 produce fragments which are generally smaller in size with lower velocities.

Analyzing the fragment mass distribution from Table 3 shows that for the M821E1/M889E1 98 percent of fragments weigh less than 25 grains. For the M374, 98.5 percent of fragments weigh less than 100 grains. Thus, taking these as the maximum fragment weights, and utilizing the maximum velocities, the associated energies for the M374 and M821E1/M889E1 are 10,802 and 1,705 ft-lb, respectively. This does not happen; therefore, we can say that fragments from the new rounds will have kinetic energies less than the M374.

Since propagation did not occur, within statistically acceptable limits, with the M374 series mortars, the same safe separation distances, with identical configurations/shielding, can be applied to the M821E1/M889E1 mortars.

#### CONCLUSIONS

- The M821E1/M889E1 mortars produce more fragments but with smaller size and generally lower velocities.
- Propagation between M821E1/M889E1 81mm mortar rounds will not occur, within the acceptable statistical limits previously mentioned, when in the same configuration/shielding as the M374 series 81mm mortar.

REFERENCES

1. Anderson, O.F. and Badowski, W.J., Test Report - Propagation of Detonation of Cartridge 81mm, HE, M374 Series, Picatinny Arsenal Laboratory Report, Picatinny Arsenal, NJ, April 1971.
2. Anderson, O.F., et al, Eight-Inch separation Propagation Tests for Cartridge, 81mm, HE, M374A2E1 and Projectile 81mm, HE, M374, Picatinny Arsenal Technical Report 4773, Picatinny Arsenal, NJ, June 1975.
3. Koger, D., and Stirrat, W., Determination of Minimum Non-Propagation Distance of 81mm M374A1 Projectiles, Technical Report ARLCD-TR-78021, U.S. Army Armament Research and Development Command, Picatinny Arsenal, NJ, April 1978.
4. Healy, J., et al, Primary Fragment Characteristics and Impact Effects on Protective Barriers, Picatinny Arsenal Technical Report 4903, Picatinny Arsenal, NJ, December 1975.

TABLE 1. Approved Safe Separation Distance for the  
81mm Mortar

<u>Item</u>	<u>Configuration</u>	<u>Shield</u>	<u>Spacing</u>
M374	Single cartridges in vertical position in holding fixture	2 inch diameter aluminum bars	8 in
M374A1	Single projectiles on simulated link-belt conveyor	None	18 in
M374A1	Transfer pallet with 6 x 12 matrix of 72 projectiles	None	30 ft
M374A2E1	Single projectiles in horizontal position in transfer pallet on conveyor	2 in thick x 4 in high aluminum	8.8 in

TABLE 2. Comparison of 81mm Mortar Projectile  
Design Parameters

	<u>M374</u>	<u>M821/889</u>
Explosive Fill	Composition B	Composition B
Explosive Weight, lb	2.1	1.72
Casing Thickness, in. (at center of round)	0.220	0.260
Maximum Casing Thickness, in.	0.235	0.290
Length of Explosive	8.37	8.87
Fill, in. (approximate)		

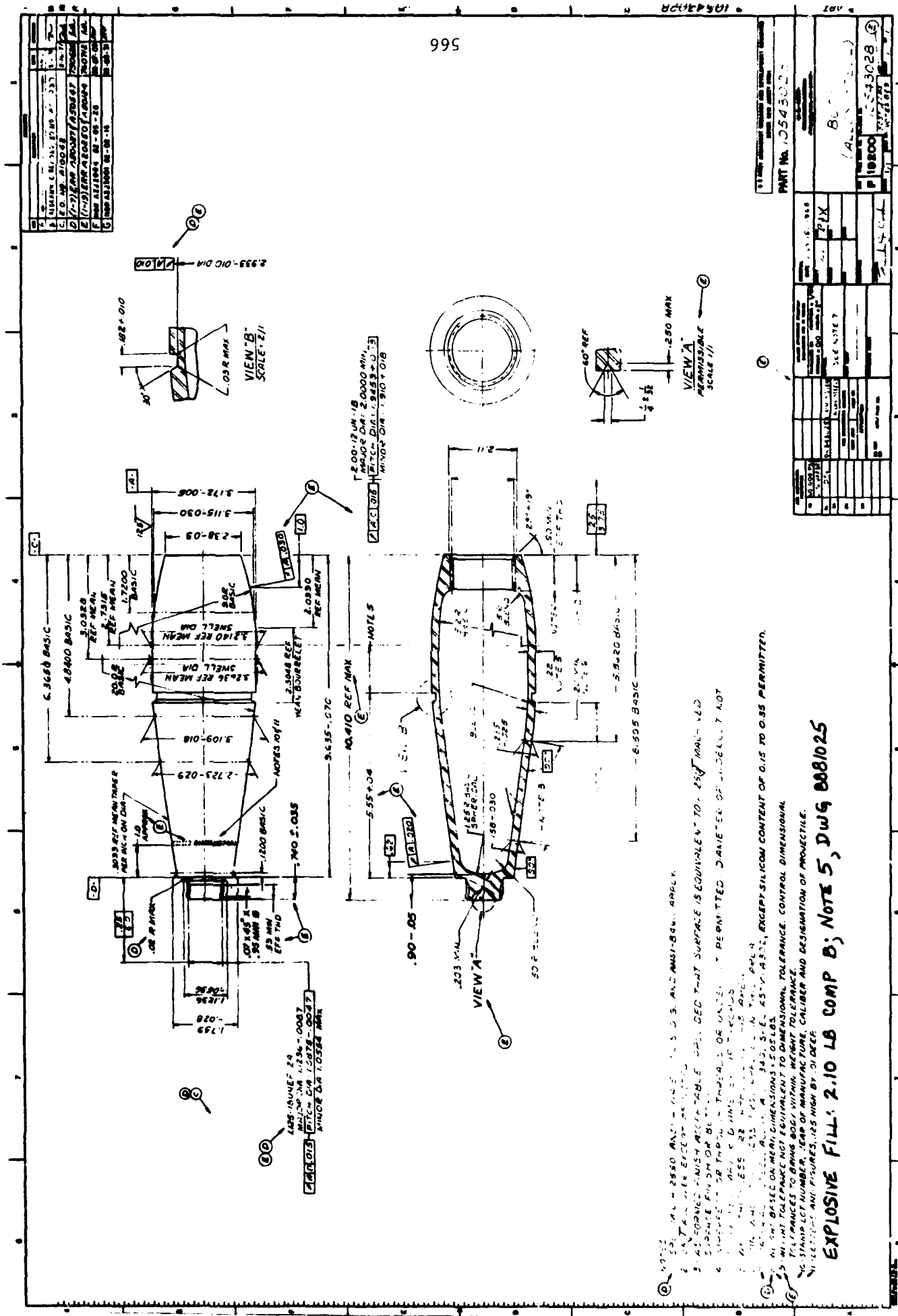
TABLE 3. Fragment Mass Distribution

<u>Mass Interval, grains</u>	M374 <u>Series</u>	Percent of Total <u>Fragments</u>	M821E1/ <u>M889E1</u>	Percent of Total <u>Fragments</u>
0.5 - 1.00	390	14	817	12.5
1.00 - 2.00	552	19.5	1601	25
2.00 - 8.00	964	34.5	2929	45.5
8.00 - 10.00	147	5	363	5.5
10.00 - 25.00	437	15.5	591	9
25.00 - 35.00	127	4.5	65	1
35.00 - 50.00	98	3.5	25	<1
50.00 - 100.00	59	2	14	<1
Over 100.00	37	1.5	27	<1
<hr/>				
TOTAL FRAGMENTS	2811		6432	

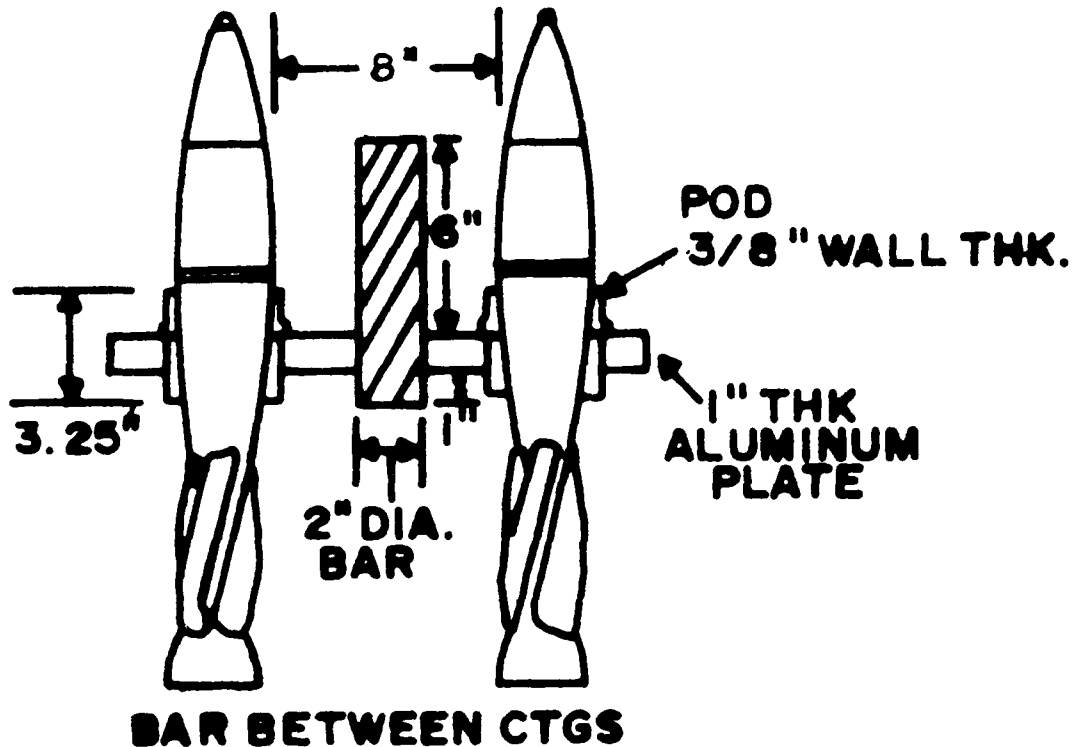
TABLE 4. Velocity,  $V_m$ , of Fragments for 81mm Mortars, fps

<u>ZONE</u>	<u>DEGREES</u>	<u>M374</u>	<u>M821/889</u>
1	0 - 2.5	-	3880
2	2.5 - 7.5	-	3150
3	7.5 - 12.5	-	3070
4	12.5 - 17.5	1326	2250
5	17.5 - 22.5	-	2570
6	22.5 - 27.5	1490	3170
7	27.5 - 32.5	1591	2650
8	32.5 - 37.5	-	2430
9	37.5 - 42.5	2198	3120
10	42.5 - 47.5	2251	2730
11	47.5 - 52.5	2054	3360
12	52.5 - 57.5	2444	3200
13	57.5 - 62.5	3160	4090
14	62.5 - 67.5	4006	4430
15	67.5 - 72.5	4164	4570
16	72.5 - 77.5	4433	4700
17	77.5 - 82.5	4705	4840
18	82.5 - 87.5	4987	5340
19	87.5 - 92.5	5204	5300
20	92.5 - 97.5	5105	5430
21	97.5 - 102.5	5834	5540*
22	102.5 - 107.5	6605	5440
23	107.5 - 112.5	6322	4940
24	112.5 - 117.5	6972*	4650
25	117.5 - 122.5	5732	4310
26	122.5 - 127.5	4210	3480
27	127.5 - 132.5	3543	4150
28	132.5 - 137.5	2795	3650
29	137.5 - 142.5	2247	2310
30	142.5 - 147.5	1578	2430
31	147.5 - 152.5	1716	1510
32	152.5 - 157.5	1755	1870
33	157.5 - 162.5	1601	1530
34	162.5 - 167.5	1545	1420
35	167.5 - 172.5	1440	1370
36	172.5 - 177.5	1263	1210
37	177.5 - 180.0	-	1130

\*Maximum Velocity

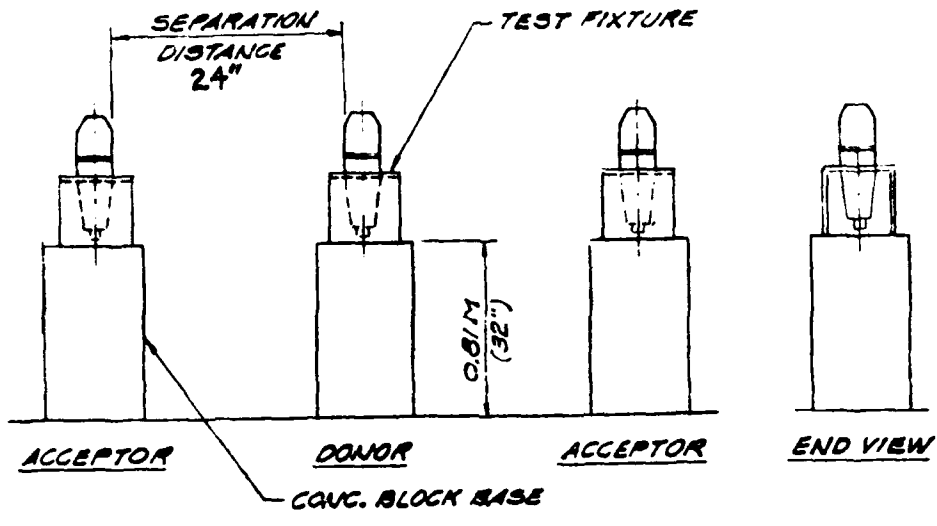


COPIY AVAILABLE TO PCIS MEMBERS ONLY. FULLY LEGIBLE REPRODUCTION

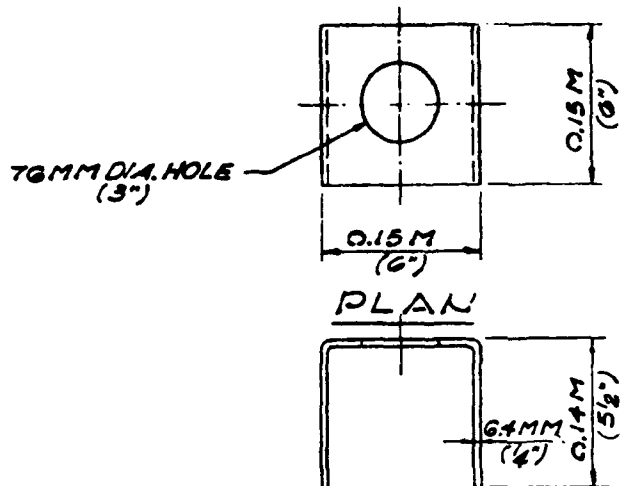


6061 T6 Aluminum

FIGURE 2. Configuration for Safe Separation Distance of 81mm M374 HE (Comp B) Cartridge



ELEVATION



ELEVATION MATL - GOGI-TG AL

FIGURE 3. Safe Separation of Single 81mm M374A1 Projectiles on Simulated Link - Belt Conveyor

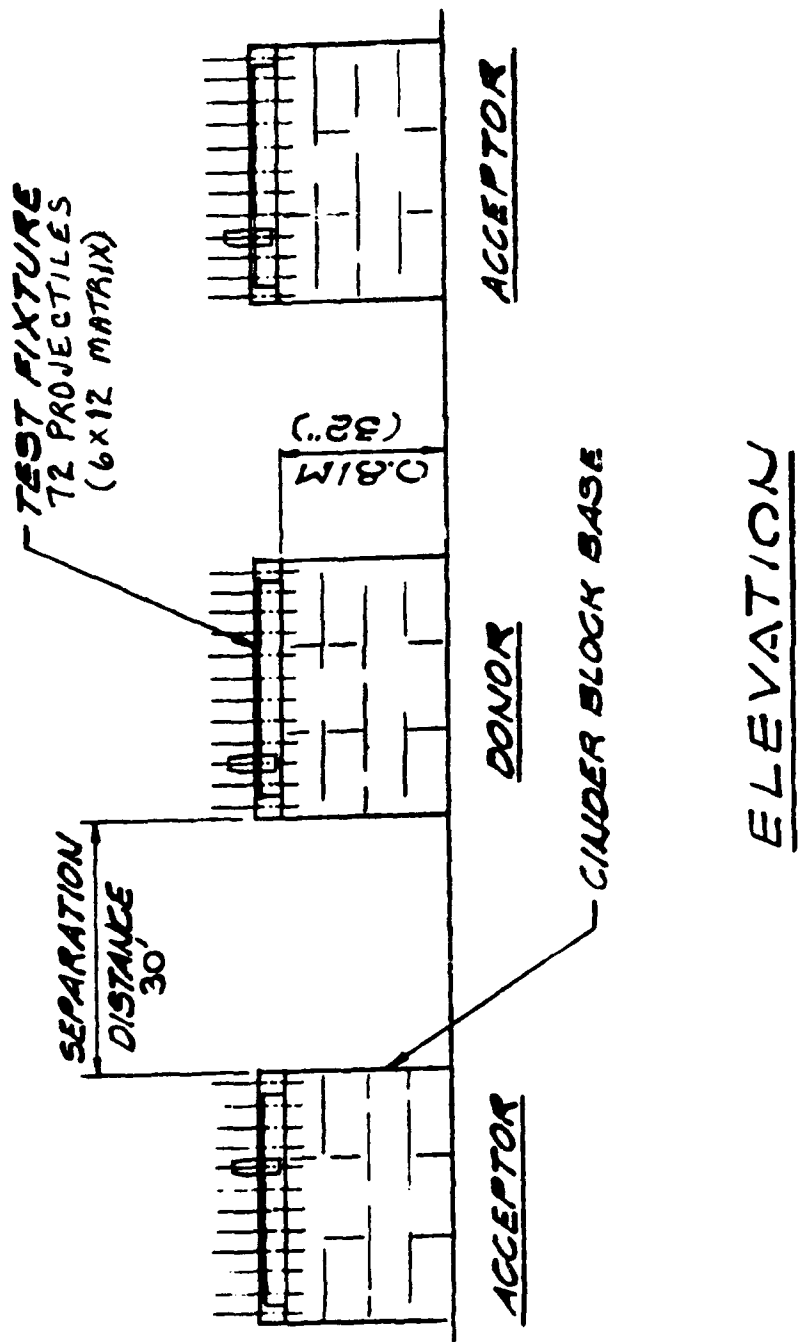


FIGURE 4. Safe Separation of 81mm M374A1 Projectile Pallets on Simulated Power Roller Conveyor.

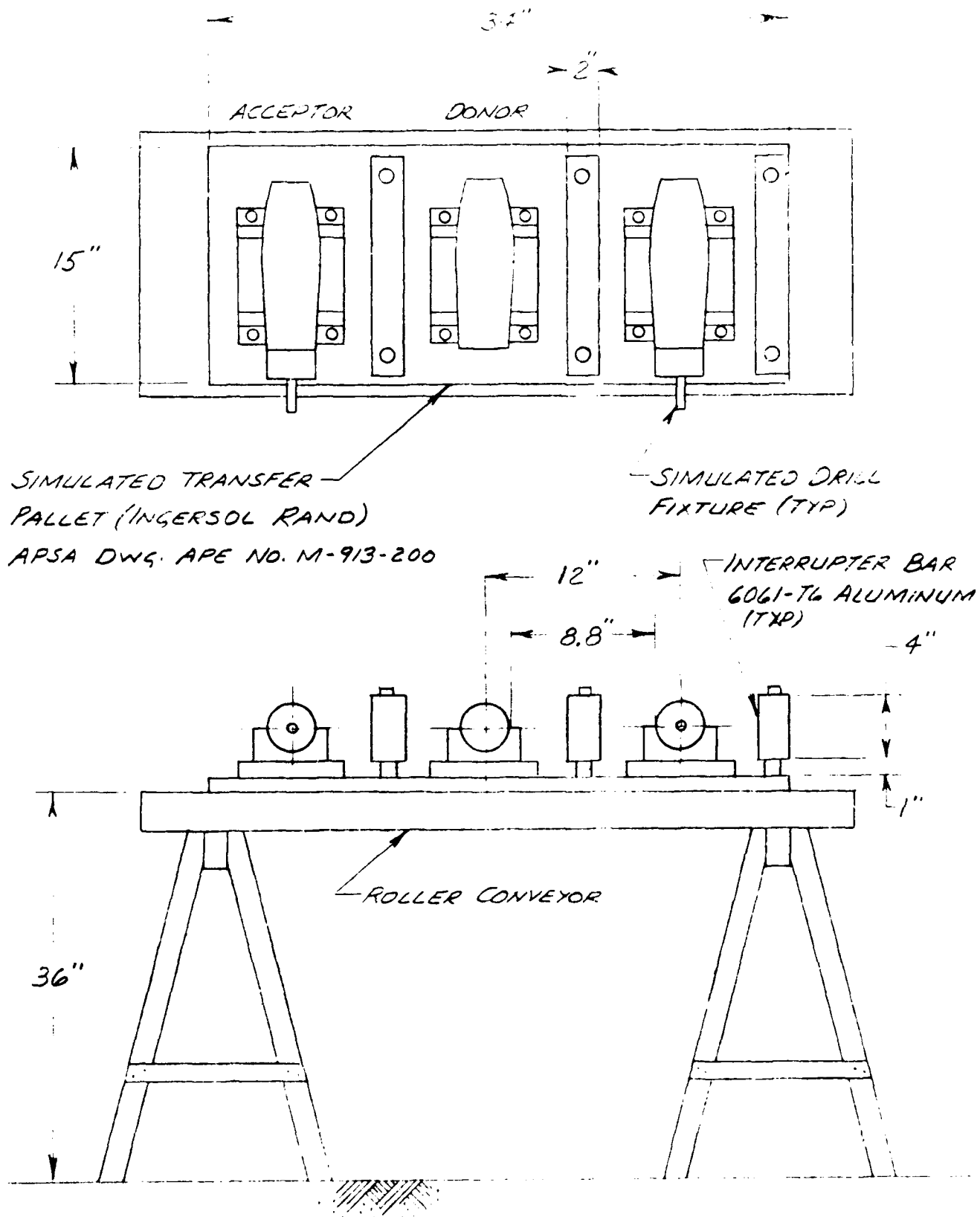
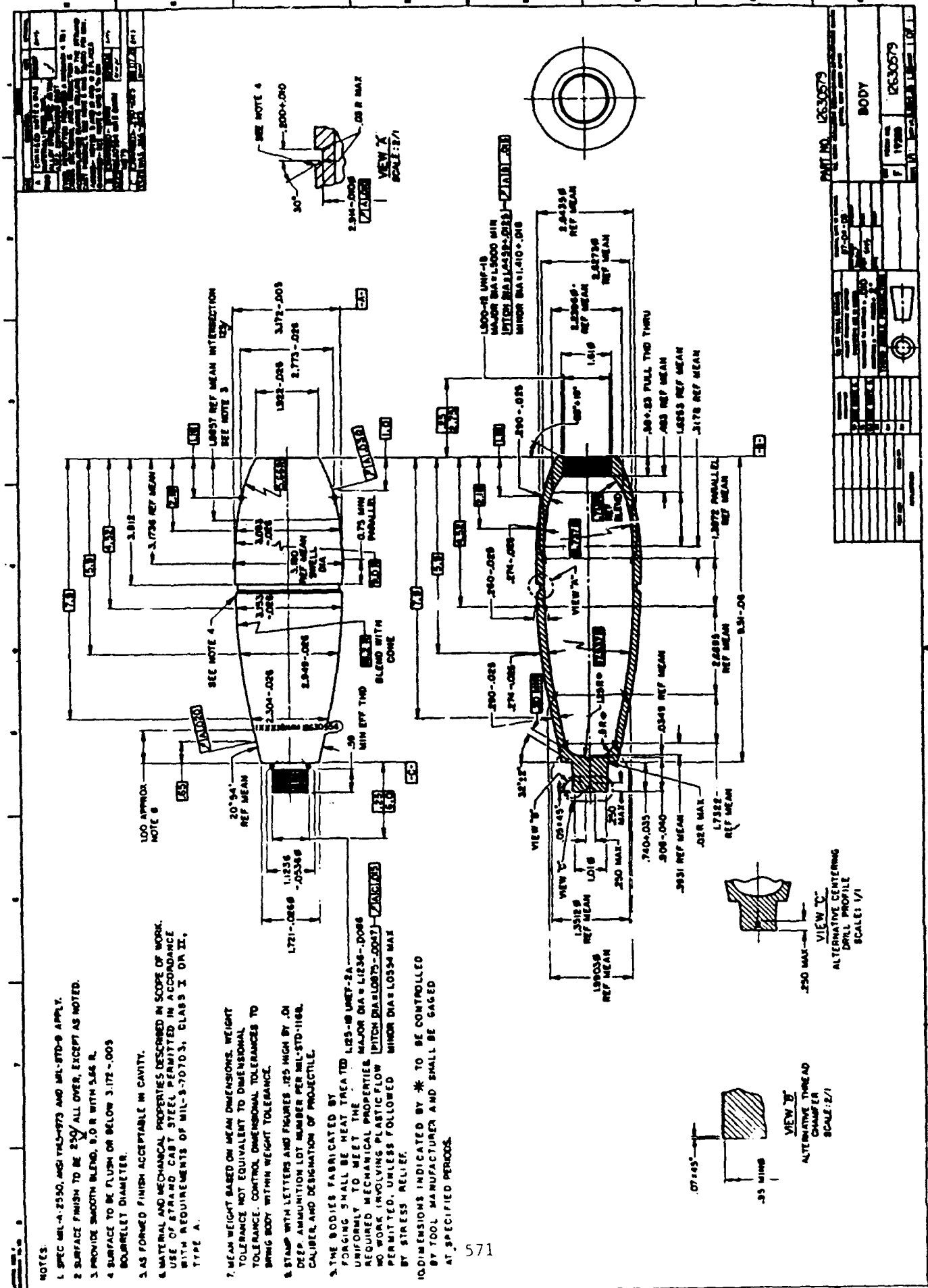


FIGURE 5. Safe Separation of Simm M374A1E1 Projectiles  
on a Simulated Transfer Pallet.



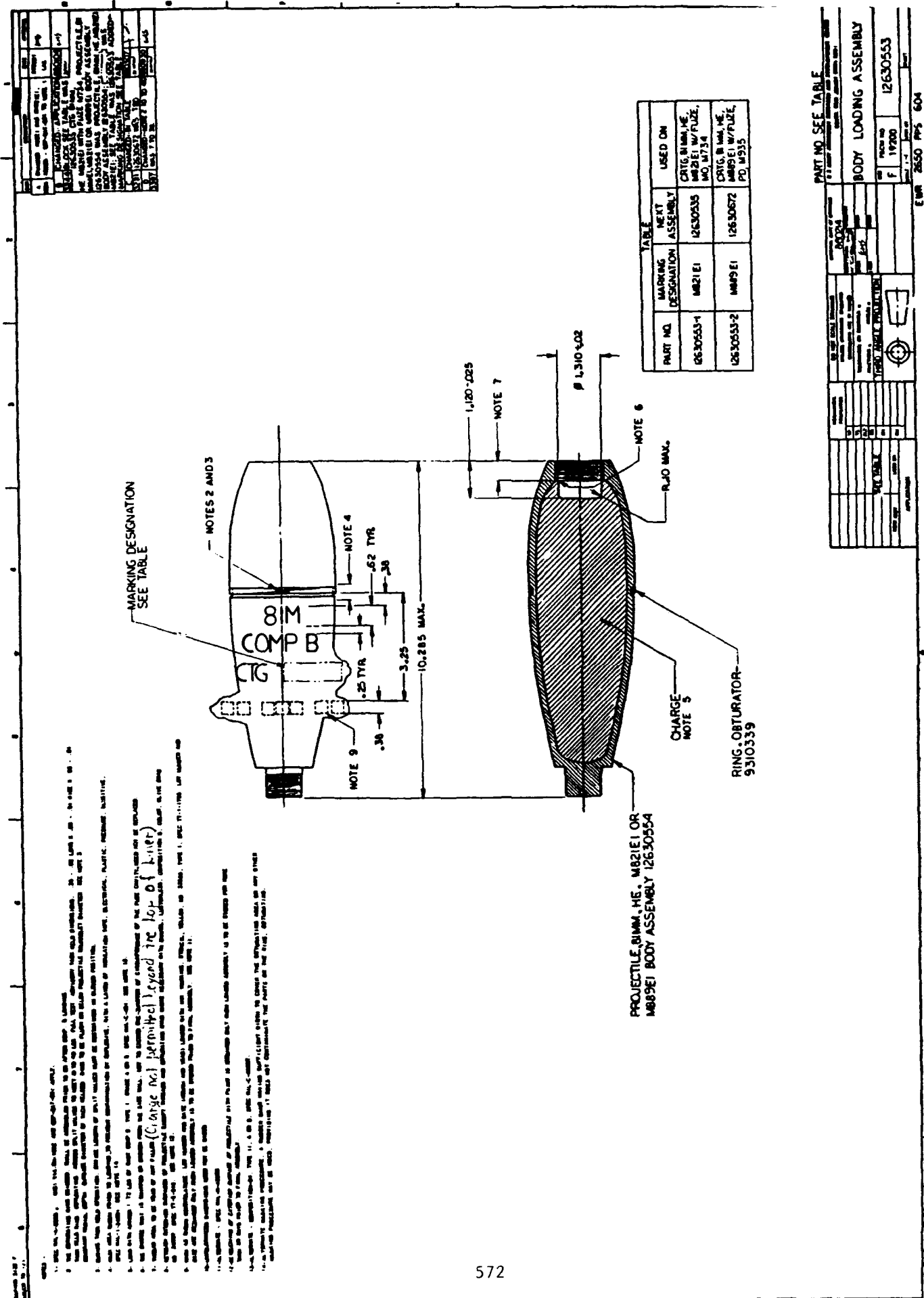


FIGURE 6b. Body Loading Drawing for the 81mm M821E1/M889E1 HE Mortar.

# **AN INNOVATIVE APPROACH TO ASSESS QUANTITY-DISTANCE**

Khosrow Bakhtar  
President, Bakhtar Associates  
Geomechanics, Structures and Mechanics Consultants  
2429 West Coast Highway, Suite 201  
Newport Beach, California 92663  
U. S. A.

## **ABSTRACT**

Protection of personnel, properties, and equipments is the main concern to the Air Force and other DOD agencies for their ammunition storage program. The review of the available reports and standards , documented on assessment of hazards associated with a given situation, lead to identification of five principal effects (DOD 6055.9 STD); namely: (1) blast pressure, (2) primary and secondary fragments, (3) thermal hazards, (4) chemical hazards, and (5) ground shocks. Extensive studies have been performed in the past on hazardous effects of blast pressure, induced thermal and chemical environments, and ground shocks. However, the degree and extent of fragment induced hazards associated with accidental detonation of explosives stored in rock/soil structures (underground chambers) are still not fully verified. The empirical relationships used are too general and do not account for site specific characteristics of the geologic system (rock and/or soil mass) and engineering system (structural components). The results of a recent KLOTZ tunnel explosion test, conducted at China Lake, California confirmed the importance of rock mass characteristics, natural joints, and concrete support (hardness elements) on the generated fragments (Bakhtar, 1989). Based on the limited test conducted, it is clear that additional research is needed to develop more accurate Q-D relationships which accounts for site specific properties of the host media, structure, and the quantity of explosive stored. This paper describes the general formulation of an innovative approach for quantity-distance assessment which accounts for the site specific properties of the underground structure (engineering system) and the characteristics of the geologic formation hosting the subsurface facility. The functional form of a recently developed Q-D criteria is presented along with the procedural details for verification. Finally, applications of physical modeling under normal gravity, with emphasis on modeling tunnel explosion scenario, are discussed which will provide a cost-effective approach for model testing and research in the area of explosive hazard prediction.

## **BACKGROUND**

Studies relative to explosive safety quantity-distance (Q-D) effects from detonations of shallow underground magazines in hard rocks have been underway since early 1970. The overall objectives of the test program are to determine the hazardous effects of; tunnel/chamber blast pressure, free-field air blast, free-field ground motion, and ejecta/debris produced by accidental detonation of explosive magazines which rupture the overhead cover of the underground chamber. Many empirical relationships have been developed, based on data from near surface bursts, to determine the free-field air blast pressure and induced ground motion. However, estimates of the debris thrown and the associated kinetic energy are much harder to make in the absence of detailed information on site specific rock mass characteristics.

In order to study the explosive safety quantity-distance, a shallow underground tunnel/chamber explosion test (KLOTZ Tunnel) was performed at the Naval Weapons Center in China lake, California , on August 24, 1998. The test consisted of a 20,000 kg (44,000 lbs.) -- net explosive weight -- detonation inside a half-scale tunnel/chamber system constructed in highly weathered granitic rock mass. Prior to shotcreting and emplacement of explosives, a detailed rock mass characterization was performed in the tunnel and attached chamber and relevant geologic and geo-engineering information were documented (Bakhtar, 1988).

Based on the pre-blast rock mass characterization, five major joint sets and a single shear zone were identified within the site. The major joint sets were blocky with well defined dip/strike and spacings. The block sizes were generally 0.43 m (17 in) to 0.56 m (22 in) in length. The Q System developed by Barton et al. (1974) was employed for rock mass characterization. Values of 0.65 and 1.3 were obtained for the tunnel and chamber, respectively, which categorized the rock from "very poor" to "poor" on the basis of the Q System. Seismic wave measurements and index test performed in situ indicated that unconfined compressive strength of the rocks was much less than expected because of extensive weathering.

Post-blast analysis of rock mass, reported by Bakhtar (1989), based on visual observation at the site revealed the following:

- - Larger ejecta were from the jointed blocky rocks.
- - The intact rocks with minor random joints were broken into smaller pieces in comparison with those from major joint sets.

- - The majority of pieces (ejecta) observed around the test site with at least one smooth-weathered face (originated from major joint sets) were smaller than 0.43 m x 0.43 m x 0.30 m (17 in x 17 in x 12 in) in size.
- - The majority of pieces (ejecta) observed around the test site from intact rock were less than 0.25 m x 0.25 m x 0.38 m (10 in x 10 in x 15 in) in size.
- - Broken rocks (ejecta) were observed beyond 300 m (982 ft) line from the original location of the portal.
- - Large pieces of concrete (debris) 0.97 m x 0.79 m x 0.38 m (38 in x 31 in x 15 in) thrown more than 61 m (200 ft) from the original portal location.
- - The sizes of ejecta thrown originating from the jointed rocks were larger than those from the intact rocks.
- - Higher kinetic energy associated with ejecta originating from joint sets than those from intact rocks.

The results of above observation indicate the importance of site characterization, identification of major geological features, and an understanding of the basic mechanical/physical properties of rocks hosting the underground explosive structures.

Data obtained from the KLOTZ Tunnel explosion test in China Lake, California, provide a unique opportunity to physically construct a series of scale model experiments to validate a more precise "scaling law" for the current Q-D standards for underground storage of munitions. This paper outlines the results of a recent feasibility study completed on development of a novel approach for assessment of quantity-distance based on an empirical relationship which accounts for the characteristics of the geologic and engineering systems in addition to the chamber loading density. Furthermore, it elaborates on the uniqueness of using scale model testing under normal gravity for validation and verification of the explosive safety standards. The physical modeling approach is particularly attractive because prototype scenario can be modeled at a small scale at a fraction of the cost. Assuming the similitude conditions are preserved, the results from the scale model tests can be used to predict prototype behavior. Additionally, the geologic and engineering systems are physically modeled and test are performed under pre-determined controlled conditions which facilitate the ease of instrumentation and retrieval of maximum information.

## PHYSICAL MODELING CONCEPT

Traditionally, munitions have always been stored in underground structures. Several of the existing US and NATO facilities were built many decades ago and in part have undergone extensive weathering and deteriorations. With the growth of population, personnel safety issues around these facilities are of the main concern to the Air Force and other DOD agencies. Therefore, the need for economical techniques to evaluate the performance, in particular load response resulting from internal detonation, of these structures is growing. The full-scale structures designed in geologic materials can not be tested for their load response. Even if the possibility of such tests existed, i.e., KLOTZ Tunnel explosion test in China Lake, California, it would involve extensive instrumentation scheme, high capital expenditures, in addition to planing and communication difficulties which always exists because of large geographic distances separating the responsible individuals in charge.

The difficulties encountered in testing full scale (prototype) structures warrant the need for scale models in which the linear dimension, or geometry, of the prototype structure is reduced by a certain definite scale. Because the geometry is scale down, the strength-related parameters also need to be scaled down in order to maintain dimensional homogeneity between a prototype structure and its model. The design of synthetic geologic materials, herein called "rock simulant," for scaled model testing therefore needs to be done in such a way that similarity in material behavior (i.e., prototype/model behavior) is conserved and the important dimensionless strength related ratios remain unchanged for the model and prototype.

For geologic materials scaling affects the material behavior, particularly, the overall strength. Other features of the geologic materials that may affect the behavior of full scale structures are discontinuities and unconformities. These need to be accounted for in physical modeling. In general the choice of the model depends on

- - nature of investigation
- - limitation of testing facility
- - economic constraints.

In order to model, within an acceptable approximation, a particular geology with associated discontinuities at the reduced scale, the proper ingredients need to be mixed in appropriate portions to produce low strength "rock-like" materials. Because no standard low-strength rock simulant exist, the method developed by Bakhtar (1984) and described in details by Bakhtar (1986, 1987) may be employed to identify and formulate

low strength synthetic geologic materials which have dimensionless strength related properties similar to those of rocks. It is important to note that feasibility of scale-model testing based on material scaling developed by the author for underground structures have been proven through a decade of research sponsored by the Defense Nuclear Agency (DNA).

In general, tests on reduced scale models are based on the possibility of changing the three scales of length, time, and force (or mass) without altering the equations describing a mechanics phenomenon. The model material should exhibit rock-like behavior beyond elastic limit, i.e., considerations of both linear and non-linear requirements. The model materials should be chosen in such a way that their elastic, inelastic, plastic, and viscous behavior are similar to rock response at reduced scale. Also, density and dilatational wave velocity (characteristic impedance of the medium) are important intrinsic material properties under blast loading conditions and must be accounted for in modeling under normal gravity.

The complete similitude for formulation and fabrication of material model (rock-simulant) would require the following conditions to be satisfied:

$$(\sigma_c/E)_{\text{prototype}} = (\sigma_c/E)_{\text{model}} \quad (1)$$

$$v_{\text{prototype}} = v_{\text{model}} \quad (2)$$

$$\phi_{\text{prototype}} = \phi_{\text{model}} \quad (3)$$

where:

$\sigma_c$  = unconfined compressive strength

$E$  = Young's modulus

$v$  and  $\phi$  = Poisson's ratio and angle of internal friction, respectively.

An extensive report outlining the scaling relationships and applications of scale model testing to underground structures is being prepared (Bakhtar, 1992) and will be submitted to the United States Air Force under SBIR Phase II research program for publication in October. This report elaborates on the scaling laws under normal gravity and provides

a systematic procedure for prediction of the prototype response based on model behavior.

By and large, for static problems only two fundamental quantities are involved: force (F) and linear dimension (d). For dynamic problems, such as blast loading, The scaling laws that govern the dynamic relationship between a model and its prototype depend on the geometric and material properties of the structure and the type of loading. The derivations of these relationship have been presented in a recent report Bakhtar (1991) and are elaborated in detail by Bakhtar (1992, under press). Generally speaking, the dynamics of any structure are governed by an equilibrium balance of the time-dependent external forces that are the product of local mass and acceleration, the resistance forces that are a function of stiffness of the soil and rock/structure in the particular direction in which motion is occurring, and the energy dissipation of the damping forces, whether material or construction related. For the tunnel explosion test scenario, i.e. China Lake KLOTZ Tunnel, following detonation, the blast and gas induced energy go into internally pressuring the chamber and access tunnel and eventually breaking the rock cover and creation of the crater before damping forces are activated.

By far, the most important step in physical modeling of the geologic materials is the identification of the pertinent parameters which need to be accounted for (Bakhtar and DiBona, 1985; Bakhtar and Jones, 1986). For cases of interest to us, these parameters include:

- Elastic properties (Young's modulus and Poisson's ratio)
- Triaxial shear strength
- Unconfined strength characteristics
- Angle of internal friction
- Density
- Impedance characteristics
- Frictional characteristics of joints and discontinuities

## BAKHTAR'S Q-D FORMULATION

### GENERAL

The peak pressure associated with detonation of a partially confined source , i.e, explosives stored in an underground structure is initially extremely high and becomes amplified by reflection within the chamber. In the absence of adequate venting, the explosive induced gases exert additional pressure and the combined effects increase the duration of loading and may result in eventual destruction of the structure. At the beginning of this paper, the five principal effects that are associated with the accidental detonation of a storage magazine were outlined. The thrust of this paper is the rational behind development of an explosive safety criteria by considering the hazards associated with the impact energy of explosion induced fragments.

The Air Force Explosives and Safety Standards (1990) and the Department of Defense Ammunition and Safety Standards (1984) define fragments as primary or secondary depending on their origins. Primary fragments are formed as a result of shattering the explosive casing or container, they are usually small, and travel initially at velocities of the order of thousands of feet per second. Secondary fragments are formed as a result of high blast pressure on the structural components, they are larger in size than primary fragments, and travel initially at velocities in the order of hundreds of feet per second. The DOD Standards further defines a hazard fragment as one having an impact energy of 58 ft-lb (79 joules) or greater.

The damage or injury potential of explosion induced fragments is normally determined by the distance prevailing between the "potential explosion site" (PES) and the "exposed site" (ES), DOD6055.9 STD, and

- i) ability of PES to suppress the blast overpressure;
- ii) ability of ES to resist the explosion effects.

The available Q-D relationships were established for related and unrelated PES and explosives, explosives and nonexplosive ESs. For explosives stored in facilities constructed in rocks, the current Q-D relationships are based on cubic-root expressions having a general form:

$$D = KW^{1/3} \quad (4)$$

where:

- D - distance (ft),
- W - weight of explosives (lb),
- K - risk factor.

The review of available documents on explosive safety and the results of rock mechanics investigation at the tunnel explosion test site (Bakhtar, 1989) reveal the influence of rock mass characteristics, loading density, structural hardness, and venting characteristics of the system, in determination of the quantity-distance and safety criteria for the underground explosive storage structures.

## RATIONALE

The phenomenology of explosive effects in hard rocks, explosive hardening and survivability of shallow tunnels comprising potential explosion sites; such as munitions storage chambers; are very much affected by the hardness or "equivalent stiffness" (overall rock mass deformability modulus) characteristics of the geologic units hosting the structures. The equivalent stiffness characteristics of the geologic units, in turn, are dependent on:

- size of individual rock blocks between joints
- joint roughness and dilation
- extent of weathering
- degree of saturation
- in situ stress field
- physical and mechanical properties of rock mass
- seismic (also called sound) wave velocity.

In developing safety criteria for the explosive storage structures in rocks, all the above parameters should be included in order to realistically account for the overall characteristics of the geologic system. Additionally, the characteristics of the engineering system, i.e., structural components should be accounted for.

The underground explosive storage structures constructed and/or planned for construction by the United States Air Force and other government agencies do not have the benefit of performance monitoring. Safety requirements are nevertheless dictated by the Q-D standards for the allowable quantity of explosives to be stored. In the absence of site specific information on the characteristics of engineering and geologic systems, no matter

what quantity of explosive is stored in an underground chamber, the safety specialists (engineers) will come back to the basic question-- "How much damage is to be expected to the exposed site (ES) in case of accidental detonation of the potential explosion site (PES)?"

At present, the Q-D relationships, similar to Equation 4, are used to determine the safe distance around a potential explosion site. However, as evident from the recent tunnel explosion test in China Lake, the site specific characteristics of the storage structure (engineering system) and the host medium (geologic system) play dominant roles in assessment of hazardous effect of the fragments generated by the explosion. Furthermore, the joints or discontinuities control the propagation of the ground shock and the kinematics of the resulting motion, as observed around many nuclear and high explosive (HE) tests (Bedsun, et.al., 1985). Therefore, an explosive safety criteria which accounts not only for the loading density, but for the pertinent site specific characteristics of the geologic and the engineering components of the storage magazines is required to provide the necessary protection for personnel and property. The Bakhtar's Explosive Safety Criteria was formulated to account for the pertinent and site specific characteristics of ammunition storage structures and may provide much more accurate approach than the available techniques.

## FORMULATION OF EXPLOSIVE SAFETY CRITERIA

As mentioned previously, development of a reliable safety criteria is contingent on the ability to characterize and assess the equivalent stiffness characteristics of the engineering and geologic systems. These requirements present a challenging task for engineering planning. The varied properties of adjacent rocks, both in terms of hydrology and deformability, lend emphasis to the importance of reliable extrapolation procedures.

The site specific features which will provide the principal challenge in the assessment of the equivalent stiffness characteristics of rock mass hosting an explosive storage chamber are:

- extent of discontinuities or simply "joints"
- number of joint sets
- amount of water or degree of saturation
- various adverse features associated with loosening, high stress, squeezing and swelling
- strength of intact rocks
- shear and normal stiffness of joints, or simply shear strength.

Also, important characteristics of the engineering system, i.e., the structural components, which include:

- loading density
- stiffness characteristics
- venting characteristics (number of entrances).

The Bakhtar's formulation of the explosive safety criteria combines the above parameters into a single functional empirical expression with the following general form:

$$D = f(E^a, L^b, R^c, V^d, S^e) \quad (5)$$

where:

- D = distance, m (ft) ;  
E = equivalent stiffness defining characteristics of geologic system, GPa (psi);  
L = loading density, kg/m<sup>3</sup> (lb/ft<sup>3</sup>) ;  
R = equivalent stiffness defining characteristics of engineering system, GPa (psi);  
V = P-wave velocity in geologic system, m/sec (ft/sec);  
S = venting characteristics of the engineering system, m<sup>2</sup> (ft<sup>2</sup>).  
a, b, c, d, e = constants.

The five parameters chosen to describe the Bakhtar's formulation, Equation (5), are easily obtained in the field as briefly described in the following pages. More detailed information on the rock mass characterization can be found by referring to the final report on the China Lake Tunnel Explosion Test (Bakhtar 1988, 1989).

## EQUIVALENT STIFFNESS OF ROCK MASS

The equivalent stiffness, or the overall deformation modulus, of the rock mass is determined based on the Q-system of rock mass classification developed by Barton, et.al., (1974). In the Q-system, six parameters are chosen to describe the rock mass quality in the following way:

$$Q = \left( \frac{RQD}{J_n} \right) \cdot \left( \frac{J_r}{J_a} \right) \cdot \left( \frac{J_w}{SRF} \right) \quad (5)$$

where:

RQD = rock quality designation (Deere, 1963)

$J_n$  = joint set number

$J_r$  = joint roughness number (of least favorable discontinuity or (joint set))

$J_a$  = joint alteration number

$J_w$  = joint water reduction factor

SRF = stress reduction factor

It is important to notice the values  $J_r$  and  $J_a$  relate to that joint set or discontinuity most likely to allow initiation of failure. The important influence of orientation relative to the tunnel axis is implicit.

Detailed descriptions of the six parameters and their numerical ratings are shown in publications by Barton and presented in a recently completed work by Bakhtar (1991) for the United States Air Force under the SBIR Program. The range of possible Q values (approximately 0.001 to 1000) encompasses the whole spectrum of rock mass qualities from heavy squeezing ground to sound unjointed rock. Figure 1 shows how the rock quality and support requirements are determined based on the Q values.

## **RQD (Rock Quality Designation)**

RQD is based on a modified core recovery procedure. This, in turn, is indirectly based on the number of fractures and amount of softening or alteration in the rock mass as observed in the rock cores from a drill hole. Instead of counting the fractures, an indirect measure is obtained by summing up the total lengths of core recovered, but counting only those pieces of core which are 10 cm (4 inches) in length, or longer, and which are hard and sound (Deere, 1963). In the absence of drilled cores, the method is applied directly to the excavated walls.

## **Joint Roughness ( $J_r$ )**

Joint roughness, most commonly found in rocks, ranges from 1.0 to 20, which represent smooth-planar, rough-planar and smooth-undulating surfaces, respectively. Extreme values may consist of discontinuous joints in massive rock and plane slickenside surfaces typically seen in faulted rock and in clay fillings. It is measured using a profile gauge.

## **Joint Alteration ( $J_a$ )**

The joint alteration parameter describes the conditions of joint in fillings. It can describe the unaltered or unweathered joint, or as is most commonly seen, clay minerals of various kinds. Favorable cases include the joints which are healed.

## **Joint Water ( $J_w$ )**

The joints water-reduction factor describes the degree of water inflow and is strongly biased in the direction of "dry excavations or minor inflows" (less than five liters per minute locally).

## **Stress Reduction Factor (SRF)**

The stress reduction factor has 16 classes, which are divided into four broad groups:

- 1) Weakness zones causing loosening or fall-out.
- 2) Rock stress problems in competent rock.
- 3) Squeezing-flow of incompetent rock.
- 4) Swelling chemical effects due to water uptake

Group (1) refers to cases where the infillings are the direct cause of loosening and fall-out.

Rock stress problem arises when the ratio of  $\sigma_c/\sigma_1$  is less than 10.

### **Equivalent Stiffness or Modulus of Deformability**

Estimates for range of deformation modulus are made on the compilation of in situ test data by Barton (1980) and Bieniawski (1974). Large-sale deformation modulus measurements that have been correlated with Bieniawski's (1974) RMR rock mass quality ratings are shown in Figure 2. The relationship between RMR and Q values were obtained by Bieniawski. As shown in the Figure, the approximate lower and upper bond values of modulus are given by [10 logQ] and [40 logQ] for Q values larger than 1. The filled circles in Figure 2 are values that have been correlated with Q values by Barton, et al. (1982).

### **Remarks on Rock Mass characterization**

The pertinent parameters required for determining "Q" using Equation (6) are obtained based on simple index testing in the field. Typical example is the KLOTZ Tunnel rock mass characterization which was reported by Bakhtar (1988, 1989). Tables providing numerical ratings for the various parameters defined in the Equation (6) are available which facilitate the ease of characterization (Barton et al., 1974).

## **LOADING DENSITY**

The loading density is defined as the ratio of net explosive weight to the volume of the chamber. If the overall loading density is required the volume of the access tunnel is added to the chamber volume. In the Bakhtar's formulation, Equation (5), the chamber volume is considered for calculation of the loading density.

## **EQUIVALENT STIFFNESS (CHARACTERISTICS OF ENGINEERING SYSTEM)**

The equivalent stiffness of the engineering system defines the hardness characteristics of the structure and can be determined as the overall deformability modulus. It can be determined in the field using a Schmidt Hammer technique.

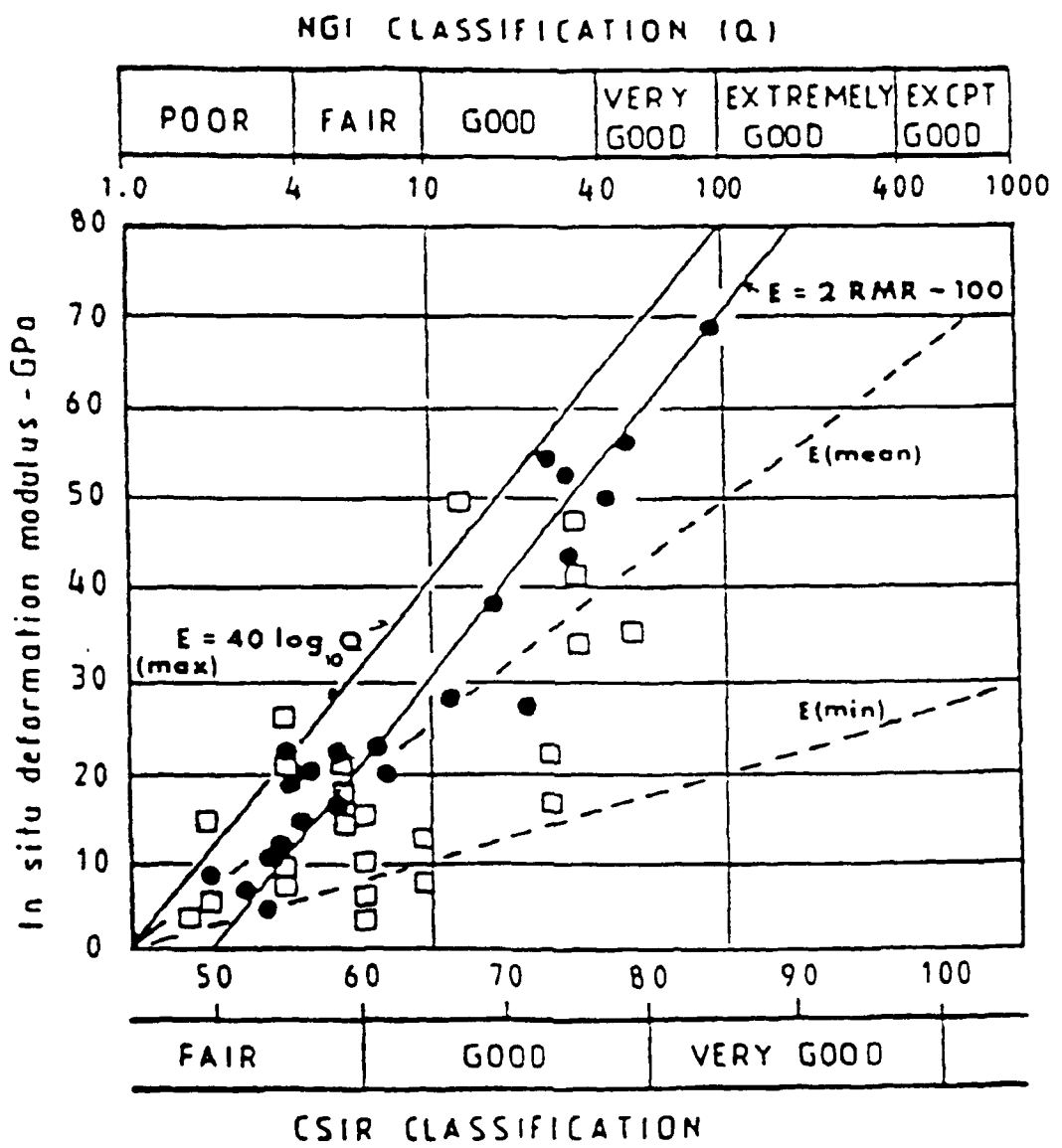


**Figure 2.** Estimation of In Situ Deformation Modulus from Two Classification Methods (Barton, et al., 1982).

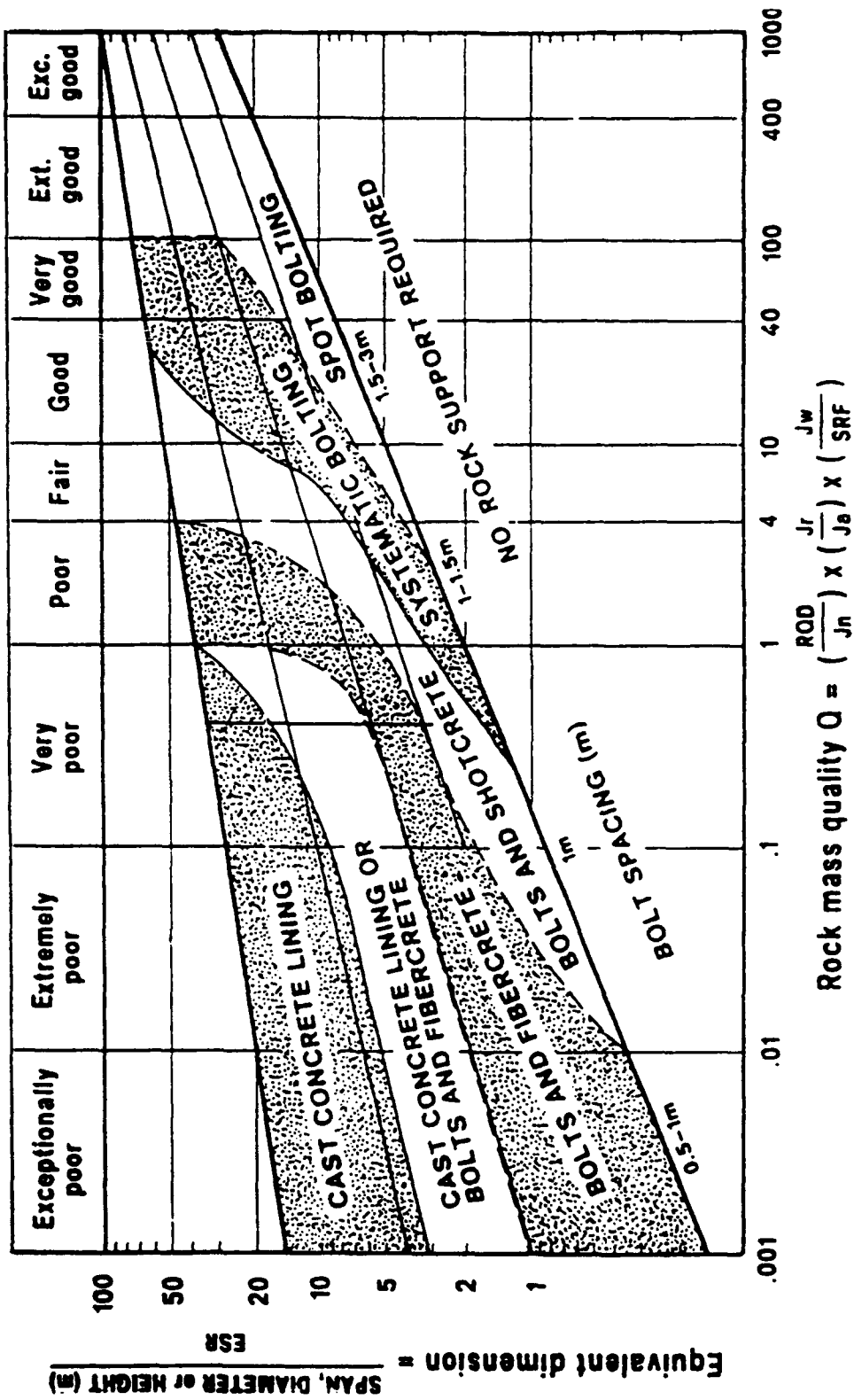


Figure 1. Two Hundred Case Records Plotted in Terms of Rock Quality and Excavation Dimensions. These Cases Form the Basis for Support Selection (Barton, et al., 1974).

## P-WAVE VELOCITY

The P-wave or seismic wave velocity through the geologic formation is the most important intrinsic material property that can be determined in the field which defines the site specific characteristics of the geologic system. The seismic wave velocity can be estimated based on the rock quality (Q) using the relationship developed by Bakhtar (1992) which eliminates the need for the field measurement.

## VENTING CHARACTERISTICS

Venting characteristics refer to the average cross-sectional areas of the openings. For the case of chamber with one access tunnel venting characteristics, the term "S" in Equation (5), represents the average sectional area of the tunnel. Chambers with two or more access tunnels, summation for the average sectional areas representing each single opening should be accounted for.

## DIMENSIONAL ANALYSIS

The functional relationship shown in Equation (5) can be solved using dimensional analysis which yields an expression of the following form:

$$D = g[(E)^{-(0.5 + b)}(L)^b(R)^{0.5}(V)^{2b}(S)^{0.5}] \quad (7)$$

where:  $g$  and  $b$  are constants which can be determined from scale model testing, physical modeling at normal gravity.

It should be noted that the functional relationship shown by the Equation (5) represent the general form of the Bakhtar's explosive Safety Criteria. The terms shown in the expression (5) are the constituent parameters representative of the site conditions and are determined based on index testing. Dimensional analysis was used to determine the possible variations of the Equation (5) and expression shown by the Equation (7) was derived. However, the final form of the Bakhtar's explosive safety criteria for underground structures will be verified following the completion of a series of scale model tests planned (Air Force SBIR Phase II) during the Fiscal Year of 1993.

## PHYSICAL SIMULATION OF TUNNEL EXPLOSION TEST

Applications of numerical and physical modeling for event simulation are commonly practiced in engineering and physics. Physical modeling has the advantage that a correctly constructed dynamic scale model shows a behavioral response which simulate exactly that of the prototype at a smaller scale. Therefore, scale model tests, assuming correctly constructed, in majority of cases can be used to predict the prototype behavior and assist in verification of numerical models. For blast loading, both geometric and kinematic similarity between the model and prototype structures must be satisfied for realistic simulation.

For modeling structures in rock mass (also applies to hardened aircraft shelters), the following basic conditions of similarity must be satisfied:

- **Geometric Similarity** - requires the ratio of distances between any two points in prototype to the corresponding distances in its model to be constant.
- **Kinematic Similarity** - requires that the movement of the particles in the model follow those of its prototype with respect to time and space.

Geometrically and kinematically similar structures are dynamically similar if the ratio of various similar mechanical forces that act on any two corresponding particles in the prototype and its model are constant. Assuming  $F^*$  is the force scale factor (ratio of force in the prototype to that in its model), the above conditions can be mathematically represented by:

$$\frac{(F_g)_m}{(F_g)_p} = \frac{(F_i)_m}{(F_i)_p} = \frac{(F_v)_m}{(F_v)_p} = \frac{(F_e)_m}{(F_e)_p} = \frac{(F_f)_m}{(F_f)_p} = F^*$$

where:

(8)

$F_g$  = gravity force

$F_i$  = inertia force

$F_v$  = viscous force

$F_e$  = elastic forces

$F_f$  = friction force

Subscripts m and p refer to model and prototype, respectively.

The size and material properties of the model, with all the structural components,

can be determined based on the following relationship:

$$\sigma^* = l^* \rho^* \quad (9)$$

where:

$$\sigma^* = \text{stress and/or strength scale factor} = \sigma_p / \sigma_m$$

$$l^* = \text{geometric scale factor} = l_p / l_m$$

$$\rho^* = \text{density scale factor} = \rho_p / \rho_m$$

Using equations (8) and (9) the majority of scale factors needed for model studies can be derived (Bakhtar, 1991, 1992). Several of those scale factors are shown in the Table 1.

In order to verify the explosive safety criteria discussed above for the underground storage structures and the associated Q-D standard, Equation (9) is used to design and fabricate a series of scale model experiments. Figure 3 shows a schematic of a typical test bed which will be embedded within a geologic formation with matched impedance characteristics. The China Lake KLOTZ tunnel explosion scenario is used as the prototype and the results of rock mass characterization performed by Bakhtar (1989) are used to derive the relevant scale factors.

The above mentioned tests provide the necessary data for verification of the scaling relationships developed (Bakhtar, 1992) for internal detonation within a shallow structure and final formulation of the Bakhtar's explosive safety criteria represented by the Equation (5).

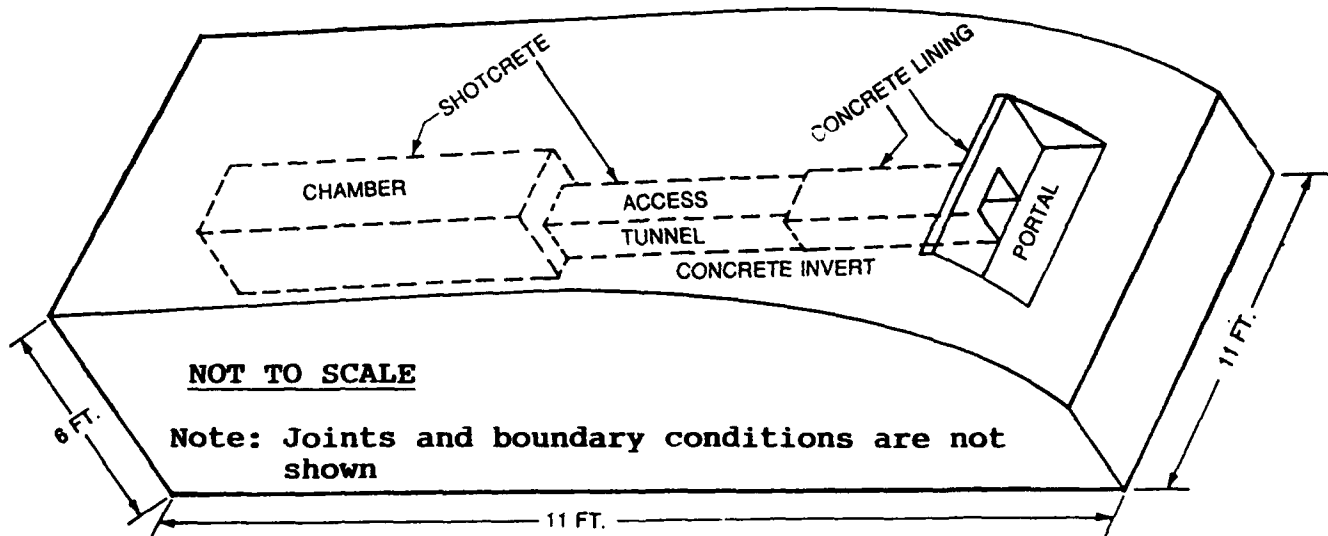


Figure 3. Schematic of a Typical Test Bed

Table 1 - Scale Factors for Mechanical Quantities

Quantity	Dimensional Form	Scale Factor
Linear Dimension	L	1
Area	$L^2$	$l^{*2}$
Volume	$L^3$	$l^{*3}$
Density	$ML^{-3}$	$m^*l^{*-3}$
Time	T	$l^{*1/2}$
Stress	$ML^{-1}T^{-2}$	$m^*l^{*-2} = m^*l^{*-1}t^{*-2}$
Force	$MLT^{-2}$	$m^*l^*t^{*-2} = m^*$
Velocity	$LT^{-1}$	$l^{*1/2}$
Acceleration	$LT^{-2}$	$l^*t^{*-2}$
Angular Velocity	$T^{-1}$	$t^{*-1}$
Mass	M	$\rho^*l^{*3}$
Energy	$MLT^{-2}$	$m^*l^*t^{*-2}$
Impulse	$MLT^{-1}$	$m^*l^*t^{*-1}$
Strain	$LL^{-1}$	1
Friction Angle	$L^0$	1
Poisson's Ratio	$\Delta l_1/L_1/\Delta l_2/L_2$	1
Frequency	$T^{-1}$	$t^{*-1}$
Curvature	$L^{-1}$	$l^{*-1}$

\* - references: Bakhtar 1991 and Bakhtar 1992

The above relationships should be satisfied for any surface or subsurface structures

## REMARKS

It is firmly believed that successful completion of a correctly constructed scale model test program can contribute towards several areas of interest to prediction of hazardous effects of explosives. The finalizing remarks presented in this section highlight several areas which can be covered under the scale model testing.

**Verification and optimization of a more complete Safety Criteria** - properly scaled model structures can be used to verify a well formulated and generalized explosive safety criteria for munitions magazines constructed in geological formations. Equation (5), presented earlier, is an example of such formulation which accounts in addition to the loading density of the explosive storage structure for the site specific characteristics of geologic (rock/soil mass hosting the underground facility) and engineering (structural components) systems. Once the pertinent parameters of interest for scenario verification are identified, the scale models can be constructed and tested at fraction of cost for prototype structures. A series of such tests are planned for the United States Air Force in Fiscal Year 1993 to verify the functional relationship, Equation (5), developed by Bakhtar (1991). The main ingredients for model fabrication consist of barite, bentonite, glass beads, an air entraining agent, Portland Cement Type I and II, and water.

Important applications of the empirical relationship derived by Bakhtar (1991), expected to complete the verification based on scale model testing, for underground explosive storage structures are listed below:

- Verification of a more precise safety criteria which can be introduced into the current Q-D standards.
- Determination of the "optimum load," (unique approach) i.e., the loading density that upon accidental detonation causes localized repairable internal structural damage to the chamber without damaging the structural integrity of the cover rock or the access tunnel.
- Determination of communication between adjacent magazines in case of accidental detonation in one chamber and optimization of loading density.
- Determination of the required depth of cover for a given storage

structure and optimization of loading density.

- Verification of numerical models.
- Site characterization.
- Classification and loading density optimization of existing underground magazines.
- Safe design of next generation magazines.

**Studies related to movement of blast-induced fragments** - a detailed study of the movement of blast-induced fragments based on prototype structures is very difficult to conduct because of the following reason:

- Detonation within geologic formation crushes the soil and rocks into fragments of different sizes, ranging from specks of dust to very large fragments several meters in size. In addition, the shape of the fragments generated differ greatly (Baron, 1960). Because the extent of retarding force in the air depends on the shape and mass of the fragment (ejecta and debris), it becomes very difficult to calculate the air drag for an entire mass of ejecta originating from a prototype explosion because of wide range of fragment breakages and uncertainty of fragment shape. Therefore other simplified means which the characteristics of the test beds, initial conditions, can be determined and defined prior to detonation are needed.
- The initial projection velocity of ejecta can not be determined with adequate accuracy. Although currently fast-frame (still and movie) cameras are used, also, there are formulas available for calculating the initial velocity of projection, they only hold good for the **throw-front**. Velocity of ejecta behind the throw-front vary over a long range. Errors in evaluating the initial velocity leads to wide errors in calculating the quantity-distance. For example, if the initial velocity of projection is known within  $\pm 10\%$  accuracy, it leads to an error of  $\pm 20\%$  in the estimated value of the range of scatter in a case of very large fragments.
- Ejecta moving in the air collide with one another. As a result the

velocity changes drastically in magnitude and direction. Beside interference on the nature of movement is observed when ejecta move in the form of a solid mass. Large perturbations are caused by the bursting out of explosion products which are ejected at a velocity considerably greater than the velocity of individual ejecta. The explosion products impart a very high velocity to the ejecta emerging along with them. As a result a cloud of fast-flying fragments is formed in the front of the main mass of exploded rock. This phenomenon was clearly observed during the KLOTZ Tunnel explosion test in China Lake, California. Therefore, basic understanding of hazardous effects resulting from movement of blast induced fragments can best be achieved if the initial conditions are known and test are conducted under controlled boundary constraints.

- The air between ejecta moving at short distances from each other is also set in motion which considerably changes the initial flying conditions and interaction with the medium and other fragments. In particular, as observed from high-speed photography, a continuous stream of soil is usually divided into a number of cone-shaped jets, some of which move well ahead of the main body of ejecta. A theoretical investigation of this process was first undertaken by Professor Pokrovskii (1959).

Therefore, it is clear that the main problem in determining the constitutive laws of movement of a body, originating from the surface or below the surface, projected in the air (ballistics) can not be formulated without a stagewise division in order to simplify the process of detonation by reducing the yield or net weight of explosive. Clearly, the scale model testing based on physical modeling under 1-g provides an attractive alternative to support such studies.

**Studies to formulate laws of ejecta distribution** - detailed studies on distribution of ejecta resulting from internal detonation within a volume of a rock mass can lead to refinement of the Q-D standards. For hazardous effects prediction, it is very important to know the expected value of a fragment size and the ejecta frequency distribution based on loading density. It is important to develop a localized constitutive law providing the density of distribution of rock in fractions which shows which part of the ejecta belongs to the fraction measuring  $d_f$  per unit volume. Where  $d_f$  is the relative size of the ejecta normalized with respect to the largest fragment. Development of such localized constitutive laws of frequency

distribution is contingent on our ability to completely characterize the rock mass to determine the nature of distribution of discontinuities for the medium which is being fragmented. Since the rock mass characteristics and conditions are not controlled by a definite constitutive relationship and as previously mentioned are site specific, the localized constitutive laws of distribution can only be determined by experiments using scale modeling techniques. For such purposes methods of concentric layers of colored rock-simulants can be employed to cast the model.

In addition, to calculate the differential law of ejecta distribution, i.e., the mathematical expression that predicts the probable maximum and average size of ejecta based on a given loading density, it is necessary to know the localized and site specific or initial PES conditions. The simplest approach for formulating a generalized differential law of distribution is the scale model testing. For such scale model tests it is necessary to use same rock-like materials within which the explosion is conducted and preserving the geometric and kinematic similarity of charges and volume of the material to be blasted.

Based on the discussion presented above it is clear that physical modeling technique, using scaled materials can open a full spectrum of opportunities in studies related to "explosive hazards reduction".

#### **ACKNOWLEDGMENT**

The work presented in this paper was funded under DOD (AF) SBIR Phase I and supervised by the Air Force Operability Systems Management Office , ASD/YQI, at the Eglin Air Force Base. The author would like to extend his thanks to Mr. Joseph Jenus, Jr., Project Manager, for his support and Mr. Paul Price, P.E., for providing technical guidance.

#### **REFERENCES**

Bakhtar, K., "Theory and Practice of Scaling Laws in Physical Modeling at 1-g," Report to be submitted to the US Air Force, October 1992.

Bakhtar, K., "Development of Safety Criteria for Explosive Storage Structures," United States Air Force, Aeronautical Systems Division, ASD-TR-92-1000, SBIR Phase I Final Report, November 1991.

Bakhtar, K. and A.H. Jones. "Scaled Model Testing of Tunnel Intersection and Large Cavity", Defense Nuclear Agency, Strategic Structures Division, Contract DNA 001-84-C-0435, Washington D.C., October 1986.

Bakhtar, K. and G. DiBona. "Dynamic Loading Experiments on Model Underground Structures", Defense Nuclear Agency, Strategic Structures Division, Contract DNA 001-84-C-0144, Washington, D.C., October 1985.

Bakhtar, K. "Derivation of Similitude Conditions Based on Stress Equation of Motion," Report Submitted to Defense Nuclear Agency, Strategic Structures Division, Washington, D.C., March 1984.

Bakhtar, K., "Rock Mechanics at the Tunnel Explosion Test Site", Chief Office of Test and Development, Norwegian Defense Construction Service, Oslo, Norway, January 1989.

Bakhtar, K. "Physical Modeling at Constant G," presented at Second International Conference on Constitutive Laws for Engineering Materials; Theory and Application, University of Arizona, Tucson, January 5-10, 1987.

Bakhtar, K., "Material Modeling", Presentation at Lawrence Livermore National Laboratory on Blasting, May 1986.

Bakhtar, K. "Rock Mass Characterization at Tunnel Explosion Test Site, U.S. Naval Weapons Center," Chief Office of Testing and Development, Norwegian Defense Construction Services, Oslo, Norway, August 16, 1988.

Baron, L. I., "Kuskovatost'i metody ee izmereniya (Lumpiness and Methods of its Measurements). Izd. AN SSSR, Moscow, Russia pp. 124, 1960.

Barton, N., Lien, R. and J. Lunde. Engineering Classification of Rock Masses for the Design of Tunnel Support, Rock Mechanics, Springer Verlag, Volume 6, pp 189-236, 1974.

Barton, N., "Estimation of In Situ Joint Properties, Nasliden Mine", International

Conference on Application of Rock Mechanics to Cut and Fill Mining, Lulea, Sweden, Institution of Mining and Metallurgy, London, 1980.

Barton, N.R., F. Losen, R. Lien and J. Lunde. "Application of the Q-System in Design Decisions Concerning Dimensions and Appropriate Support for Underground Installations", International Conference on Sub-Surface Space, Rockstore, Stockholm, Sub-Surface Space, Vol 2, pp. 553-561, 1982.

Bedsun, D.A., Ristvet, B.L. and E.L. Tremba. "Summary and Evaluation of Techniques to Predict Driven and Triggered Block Motion: A State-of-the Art Assessment", S-Cubed, Albuquerque, NM, Report to Defense Nuclear Agency, DNA-TR-85-249, p 122, June 1985.

Bieniawski, Z.T. Geomechanics Classification of Rock Masses and its Application in Tunneling, Advances in Rock Mechanics, Proceedings of 3rd Congressional of International Society Rock Mechanics, Denver, Colorado, 1974, Vol. II.A, pp 27-32, 1974.

Deere, D.U. Technical Description of Rock Cores for Engineering Purposes, Felsmechanik und Ingenieurgeologie, Vol. 1, No. 1, pp 16-22, 1963.

Department of the Air Force, "Explosive and Safety Standards", AF Regulation 127-100, August 1990.

Department of Defense, "Ammunition and Safety Standards", DOD 6055.9 STD., July 1984.

Miller, R.P. "Engineering Classification and Index Properties for Intact Rock", Ph.D. Thesis, pp 1-332, 1965.

Pokrovskii, G. I., "Novaya forma napravленного действия взрыва (A New Technique of Directional Blasting). In Doklady soveshchaniya po narodnokhozyaistvennomu isopl'zvaniu vzryva. Izd AN SSSR, Novosibirsk, p. 11-17, 1959.

CLOSING REMARKS

by

Captain David K. Wallace  
Chairman  
Department of Defense Explosives Safety Board  
United States Navy

CHAIRMAN, DOD EXPLOSIVES SAFETY BOARD

CLOSING REMARKS

My congratulations to all who participated in this great Seminar. Our attendance was more than 600 people, representing eighteen nations. In particular, I want to single out those of you who dedicated time and effort to present these excellent papers advancing our field of explosives safety and its relationship to the Environment. You make the Seminar happen. We owe you our appreciation and our thanks for a job well done. We are also grateful for the appearances of Mr. McMillan, Mr. Baca, and Rear Admiral Bondi who lent their support to our cause.

As this Seminar draws to a successful end, remember we will be back again for the 26th Seminar somewhere on the East Coast in 1994. We hope to see you then.

Now, it is my pleasure to introduce a most distinguished member of our Community, Dr. Connor, Chairman of the Explosives Storage and Transport Committee in the United Kingdom, who has consented to make a few closing remarks.

CLOSING ADDRESS

by

Dr. John Connor  
Chairman  
Explosives Storage and Transport Committee  
United Kingdom

Thank you, Capt Wallace, for inviting me to make a few remarks with which to conclude this seminar. This is a task which has traditionally fallen to the Chairman of the UK Explosive Storage & Transport Committee, the ESTC, a position which I currently hold. Those of you who keep note of such things will realise that my predecessors in this role have been military officers and today, for the first time, this closing address comes from a civilian. I am not however, the first civilian to be Chairman of the ESTC. That honour fell to my predecessor, known to many of you in the explosives safety community, Dr John Rees. John retired just about a year ago and as some of you may know he is now fighting back from serious illness. I hope, Capt Wallace, you will accept these remarks from a humble civilian!

Before I go any further I think I should, on behalf of everyone here, record our appreciation to you Captain Wallace and to the Department of Defence Explosives Safety Board for sponsoring up this Seminar. Our thanks are also due especially to the staff of the Board, particularly Paul Moran and Donna Barker who have yet again put such sterling work into organising what has clearly been one of the most successful seminars in recent years. In proposing these thanks it would be remiss of me not to acknowledge the overall quality of the presentations; it is a self-evident tribute to the presenters that the sessions were vastly better attended than the pool. Lastly, I would like to thank the hotel staff whom I know from both behind and in front of the scenes have been unfailingly courteous and helpful. Thank you all.

In the keynote address, Assistant Secretary of Defence Mr. McMillan drew attention to the tremendous changes in the world scene which have taken place over the last three or four years. He noted that the collapse of the Warsaw Pact and the break-up of the Soviet Union has dramatically altered defence needs. For Example in the United States and throughout Europe the levels of armed forces are being reduced and defence budgets are being cut. We have to recognize that the explosives safety community is not, and cannot be, protected from these changes.

However, Mr. McMillan identified other pressures which our community faces. As forces are reduced and reconfigured we are confronted with massive demilitarization programmes; vast redeployments of ammunition stocks are under way, bases are being closed and require to be cleaned up. At the same time public expectations are changing. New and more demanding safety and environmental standards are being put in place and Defence Departments are being required to comply. Increasingly too, as Deputy Assistant Secretary Baca made clear, environmental and safety issues are being linked and, for example, traditional methods of disposal of ordnance such as sea-dumping are no longer available to us.

Against this background, the theme of this Seminar, environmental awareness in the safety community, was particularly opposite and most welcome to me. It is encouraging to find that the concerns we have concerning the management of explosives safety in the United Kingdom are widely shared and to see so much positive work being undertaken to provide solutions.

During the various sessions of the Seminar I have attended over the past three days, I have seen enormous expertise being applied to a wide range of practical and theoretical problems. Topics which we have discussed include demilitarization and clean up, small and large scale explosive testing, accidents, magazine design, risk

analysis and insensitive munitions. Throughout these presentation, some common themes have developed and I would like to pick up one or two which have struck me.

The first concerns compliance with legal requirements and mandatory standards. There are problems here because safety and environmental standards become more and more demanding. The public seems less willing to tolerate defence activities as their perception of the threats we face change. But we also have problems because of the wide range of different standards which confront us and because, it has to be said, of the ignorance of the regulators in some technical areas. We have also heard of problems in the US and in Australia where Federal standards may be modified by state authorities and in Europe where European Community Directives are affecting our national laws. So far we as a community have reacted to all this law making and standard setting but perhaps we have been failing to take chances to influence what is happening. I believe the military explosives safety community needs to be more active and effective in dealing with the regulators if we are to avoid being faced with standards which are over bureaucratic, difficult to achieve and which deliver little safety benefit.

A second major theme has been concerned with resource issues. As budgets are cut we need to operate more effectively if we are to do the job in hand and cope with the massive changes now underway. It is likely that the size of the military explosives safety community will fall over the next few years. Do we have methods in place to maintain our corporate skill base? Can we demonstrate convincingly to budget managers that our efforts can save money directly by, for example, cutting out accidents or through less restrictive storage requirements based on safer explosive materials? Do we do enough to sell the benefits of our work to legislators, administrators and the general public?

The third theme which has struck me is the growing recognition that explosives safety has to be seen in a total system context. Time and again, presenters have stressed the need to think about the whole life of, for example, munitions at the design stage; the need to design in safety so that in twenty or thirty years time our successors are not faced with some of the intractable disposal problems that we now have to tackle.

A part of this whole system approach will inevitably involve risk assessment and the analysis of risk. A series of papers delivered this week have described risk based approaches to explosives safety. We have heard about some of the problems in assigning probabilities to very unlikely events and in assessing their consequences. We have also been told something of the difficulties in establishing risk criteria which politicians and public can accept. In this latter context I would draw your attention to the presentations we heard from Switzerland where criteria based on the costs of saving lives have been developed and accepted.

The key feature of the risk based approach to explosives safety is that it imposes on us a logical method for assessing both hazards and proposals to reduce or remove hazards. It provides managers with a tool for the assessment of the cost effectiveness of safety measures, it helps to get resources where they will do most good. Properly applied, it offers the chance of overcoming some of the emotional prejudices which can affect decision makers, providing a rational basis for their decisions.

Increasingly I believe we are seeing explosives safety becoming a management issue in the same way that quality or reliability are management issues. Therefore managers must be made aware of the costs, the benefits and the risks associated with explosives activities. We need to invest time and energy in educating them. We need to develop the culture where safety is designed in, risks

are understood and assessed, benefits identified and costed. We need to push towards safety based on understanding not on costly and potentially ineffective prescriptive regulations.

The message is very clear. Military explosives safety is a complex technical matter and, of course, we need to understand it. However, technical understanding is not enough. The world will no longer simply accept our expert view, if indeed it ever did. We need to assess risks and quantify benefits more clearly than perhaps we have in the past. We have to reach the legislators, the decision makers and influence their thinking. I am encouraged to see the way in which this excellent seminar has moved us forward in that direction. I congratulate the DoD Explosive Safety Board on the timeliness and importance of the theme they selected for the Seminar and I hope and trust that the Board will continue to take the lead in this area in all its dealing within the United States and worldwide.

We live in challenging times and thanks to the Board and to this Seminar I think we can see the way forward just that little bit more clearly. From my discussions with other delegates during the week it is obvious to me that this Seminar is the pre-eminent worldwide military oriented focus on explosive safety. It seems equally obvious, that we need such a focus. While as an outsider it is easy to me to say this, I am sure that we all join together in encouraging the Board to look forward to the 26th DDESB explosives safety seminar in 1994. Captain Wallace, members of the Explosives Safety Board, Ladies and Gentleman, thank you for the honour of being asked to conclude these proceedings and for the privilege of sharing your insights.

Thank you

# TWENTY-FIFTH DDESB EXPLOSIVES SAFETY SEMINAR

## TABLE OF CONTENTS

### VOLUME I

<b>PREFACE .....</b>	iii
<b>OPENING REMARKS AND WELCOMING ADDRESS .....</b>	1
Captain David K. Wallace, U.S. Navy, Chairman, Department of Defense Explosives Safety Board	
<b>INTRODUCTORY SPEECH: SAFETY AND ENVIRONMENT--THE CHALLENGE SHARED .....</b>	3
Mr. Thomas Baca, Deputy Assistant Secretary of Defense for Environment	
<b>KEYNOTE ADDRESS .....</b>	7
Mr. Colin McMillan, Assistant Secretary of Defense for Production and Logistics	
<b>NAVY SAFETY .....</b>	11
Rear Admiral Peter A. Bondi, U.S. Navy, Fleet Supply, CINCPACFLT	

### *ORDNANCE DISPOSAL--I* *Moderator: Ray Fatz*

<b>The Establishment of a Tri-Service Ammunition Demilitarisation Facility by the UK Ministry of Defence .....</b>	13
Alan R. Davis	
<b>Environmentally Acceptable Disposal of Munition and Explosives .....</b>	21
Nico van Ham and Henk Bartelds	
<b>Results of Trial Test Burns on Army Deactivation Furnaces Upgraded to Meet RCRA .....</b>	27
Robert G. Anderson, Jerry R. Miller, and Mark M. Zaugg	
<b>Soil Remediation Methods .....</b>	43
C. James Dahn and Bernadette N. Reyes	

### *ACCIDENTS* *Moderator: Edward Kratovil*

<b>Some Remarks on a 100 Tons Accidental Explosion in Tunnel Systems in 1965 .....</b>	61
Seppo Tuokko	

*ACCIDENTS* (Continued)

<b>MJU-8 IR Flare Mix Fire at Longhorn AAP, 28 September 1991</b>	83
Ralph A. Knape	
<b>The Explosion of the Display Fireworks Assembly Plant "MS VUURWERK" on February 14, Culemborg, The Netherlands</b>	97
W. P. M. Mercx and H. H. Kodde	
<b>Explosive Accident Summary: World War II</b>	113
Edward P. Moran, Jr.	

*SAFELOAD PROGRAM*

*Moderator: Cliff Doyle*

<b>The U.S. Army Safeload Explosives Safety Program</b>	133
Thomas M. Tobin and Robert A. Rossi	
<b>Simulated Large Scale Propagation Test</b>	151
Robert Frey, O. Lyman, and David Collis	
<b>A Safer Method of Storing Ammunition in a Conex Container</b>	163
Anthony E. Finnerty, J. L. Watson, and Philip J. Peregino, II	
<b>Two-Dimensional Simulations of Sand Barrier Motion Induced by The Explosion of an Ammunition Stack Inside the Magazine</b>	183
William Lawrence and John Starkenberg	

*ORDNANCE DISPOSAL--II*

*Moderator: Arlie Adams*

<b>The Mechanisms and Parameters of Abrasive Waterjet (AWJ) Cutting of High-Explosive Projectiles</b>	213
Paul L. Miller	
<b>Cutting of Munitions and Removal of Explosives Through Application of Water Jet Technology</b>	235
George Wilken, Hal Monson, Mark M. Zaugg, and Alan Bailey	
<b>Current Progress on the Use of Waste Energetic Materials as Fuel Supplements for Industrial Combustors</b>	249
Kevin R. Keehan, Timothy S. O'Rourke, and Wayne E. Sisk	
<b>Carbon Dioxide Blast/Vacuum Demilitarization</b>	261
Leonard S. Olson	

*IGLOOS--I*  
*Moderator: Sam Kiger*

<b>Canadian Ammunition Storage Magazines</b> .....	271
H. Vaidyanathan	
<b>Development of a New Rectangular Box-Shaped Standard Ammunition Storage Magazine</b> .....	313
Joseph M. Serena, III	
<b>Small-Scale High Performance Magazine Roof and Soil Cover Feasibility Test Results</b> .....	331
Robert N. Murtha	
<b>AUTODYN 2D Predictions for Small Scale HP Magazine Cell Wall Tests</b> .....	373
Kevin Hager and James Tancreto	

*AIRBLAST--I*  
*Moderator: Wayne Frazier*

<b>Spherical Equivalency of Cylindrical Charges in Free-Air</b> .....	403
Edward D. Esparza	
<b>Air-Blast Characteristics of an Aluminized Explosive</b> .....	429
Jun W. Lee, Jaimin Lee, Jeong H. Kuk, So-Young Song, and Kyung Y. Choi	
<b>Acceptor Loads and Response of an Intervening Sand Wall Barrier from the Simultaneous Detonation of 24 Mk82 Donors</b> .....	453
Robert D. Eisler, A. K. Chatterjee, L. Pietrzak, James Tancreto, and Kevin Hager	
<b>The Reflected Impulse on a Curved Wall Produced by a Spherical Explosion in Air</b> .....	467
Y. Kivity	

*ORDNANCE DISPOSAL--III*  
*Moderator: Clifford Dunseth*

<b>Disposal of Liquid Propellant Rocket Motors</b> .....	479
Meir Savariego	
<b>AEDC Capability to Perform Environmentally Safe Disposal of Solid-Propellant Rocket Motors</b> .....	487
Bryan S. DeHoff and Earl E. Anspach	
<b>Degradable and Hydrolyzable Binder Explosives</b> .....	495
Benjamin Y. S. Lee	

*IGLOOS-II*  
*Moderator: A. G. Papp*

<b>Design and Full Scale Trial of a Large Span Arch Explosive Storehouse .....</b>	507
G. Horoschun	
<b>Assessment of Hazardous Areas When Storing HD 1.1 Ammunition in French "Igloo Type" Magazine .....</b>	525
Michel Roger	
<b>Calculation of Hazardous Soil Debris Throw Distances Around Earth Covered Magazines .....</b>	543
Charles J. Oswald	
<b>Hazards Produced by Explosions Inside Earth-Covered Igloos .....</b>	557
Michael M. Swisdak, Jr.	

*RISK ANALYSIS*  
*Moderator: Glenn Leach*

<b>An Approach to the Safe Management of the Storage of Military Explosives Based on Quantitative Risk Assessment .....</b>	575
John Connor	
<b>An Investigation into the Feasibility of Using Risk Assessment Methodology for Licensing Explosives Handling Ports .....</b>	591
R. Merrifield and P. A. Moreton	
<b>Risks from the Transport of Explosives .....</b>	603
G. E. Williamson	
<b>Risk Analysis for Temporary Storage of Ammunition in Combat Areas .....</b>	615
Max B. Ford	
<b>The Threat Related Attrition (THREAT) System Casualty Estimation Facility Model .....</b>	633
Martin J. Fertal	

*INDEXES*

<b>Table of Contents--Volume II .....</b>	643
<b>Table of Contents--Volume III .....</b>	647
<b>Table of Contents--Volume IV .....</b>	651
<b>Author Index .....</b>	655
<b>Attendee List .....</b>	659

## **TWENTY-FIFTH DDESB EXPLOSIVES SAFETY SEMINAR**

### **TABLE OF CONTENTS**

#### **VOLUME II**

<b>PREFACE .....</b>	iii
----------------------	-----

#### ***ORDNANCE CLEAN UP--I*** *Moderator: Gary Bottjer*

<b>Risk Assessment Methodology to Evaluate Public Risk for Cleanup of Ordnance at Formerly Used Defense Sites .....</b>	1
C. David Douthat	

<b>Operation Desert Sweep--The Restoration of Kuwait .....</b>	19
Fred Dibella	

<b>Ordnance Removal and the Public: Public Affairs at Formerly Used Defense Sites .....</b>	25
Ken Crawford	

#### ***UNDERGROUND STORAGE--I*** *Moderator: Arnfinn Jenssen*

<b>Overview and R&amp;D Test Planning for the Joint U.S./ROK R&amp;D and Test Program for New Underground Ammunition Storage Technologies .....</b>	29
Gary Abrisz	

<b>Effect of Blast Traps on Air-Blast Propagation in Underground Explosive Storages .....</b>	85
So-Young Song, Jaimin Lee, Jae Woon Ahn, Hyung Won Kim, and Jin Soo Choi	

<b>Blast Attenuation Effects of Access Tunnel Configurations for Underground Magazines--A Parameter Study .....</b>	99
Helge Langberg	

#### ***SITE PLAN ANALYSIS*** *Moderator: Wilson Blount*

<b>A Geographic Information System (GIS) for Explosives Facility Sitting Analysis .....</b>	107
Larry D. Becker and Joseph Jenus	

## *SITE PLAN ANALYSIS (Continued)*

<b>Siting of An Explosives Assembly and Storage Operation for Maximum Utilization of Limited Available Area</b> . . . . .	123
Edward W. Soleau	
<b>Uncertainties and Probabilistic Risk Assessment of Explosive Safety</b> . . . . .	129
Lawrence A. Twisdale, R. H. Sues, F. M. Lavelle, and James L. Drake	
<b>Consequences of Pressure Blast--The Probability of Fatality Inside Buildings</b> . . . . .	143
David J. Hewkin	

## *CHEMICAL EXPLOSIVES DISPOSAL* *Moderator: Larry Smith*

<b>The Role of Risk Analysis in Directing the Quality Assurance Program of the U.S. Army Chemical Materiel Destruction Agency</b> . . . . .	159
Thomas Kartachak and John Jardine	
<b>Chemical Warfare Material at Formerly Used Defense Sites</b> . . . . .	169
Charles L. Twing	
<b>Hot Gas Decontamination of Explosives--Contaminated Equipment</b> . . . . .	211
Kevin R. Keehan, Timothy S. O'Rourke, Wayne E. Sisk, and Erik B. Hangeland	
<b>Decontamination of Chemical Agent Contaminated Structures and Equipment</b> . . . . .	219
Kevin R. Keehan, Timothy S. O'Rourke, and Wayne E. Sisk	

## *UNDERGROUND STORAGE--II* *Moderator: Bengt E. Vretblad*

<b>Camp Stanley Underground Magazine Design Validation Test</b> . . . . .	227
Charles E. Joachim	
<b>Hydrocode Calculations for Simulation of 1/3-Scale Munitions Storage Facility Tests</b> . . . . .	257
Lynn W. Kennedy, Joseph E. Crepeau, and Charles E. Needham	
<b>Ground Motions from Detonations in Underground Magazines in Rock</b> . . . . .	277
Gordon W. McMahon	
<b>Brick Model Tests of Shallow Underground Magazine</b> . . . . .	295
Charles E. Joachim	

***EXPLOSIVES SAFETY MANAGEMENT***  
***Moderator: John Byrd***

<b>Measures Proposed to Improve the Safety of Materiel Within the Defence Establishment .....</b>	<b>317</b>
Bo Demin	
<b>Storage Cost--Benefit Analysis in Case of Giving Up 1.1 Munitions .....</b>	<b>325</b>
Jean Goliger, Laurent Allain, Jean Isler, and Jean-Pierre Languy	
<b>How the Safety of the Ammunition and Explosives Storage and Handling is Managed in Switzerland: Part I--Safety Concept, Regulations, and Organisation .....</b>	<b>341</b>
Andreas F. Bienz and Peter O. Kummer	
<b>How the Safety of the Ammunition and Explosives Storage and Handling is Managed in Switzerland: Part II--Risk Analysis of Ammunition Magazines .....</b>	<b>373</b>
Peter O. Kummer and Andreas F. Bienz	

***RISK AND ENVIRONMENT***  
***Moderator: Leslie Kline***

<b>Chemical Warfare Materiel (CWM): Hazardous Waste or Ordnance? When Does is Matter? Who is in Charge? .....</b>	<b>401</b>
Margaret P. Walls	
<b>Mitigative Features for Explosive Containment on the Chemical Stockpile Disposal Program .....</b>	<b>411</b>
Boyce L. Ross	
<b>Australian Policy for the Management of Land Affected by Unexploded Ordnance (UXO) .....</b>	<b>437</b>
Clive W. Badelow and Ken R. Hutchison	
<b>Ranking Combined UXO/CSM/HTW Sites Requiring Restoration: An Initial Protocol .....</b>	<b>445</b>
Joseph Bern, Femi Adeshina, and James P. Pastorick	

***HARDENED AIRCRAFT SHELTERS***  
***Moderator: Paul Price***

<b>Structural Response and Resulting Quantity-Distance Debris Collection Techniques and Results .....</b>	<b>467</b>
Aaron Perea and Bryan S. Austin	
<b>Numerical Calculations of Explosive Charges Inside Scaled Aircraft Shelters .....</b>	<b>509</b>
Robert W. Robey	

## *HARDENED AIRCRAFT SHELTERS* (Continued)

<b>Hardened Aircraft Shelter Test Program .....</b>	527
Michael M. Swisdak, Jr.	
<b>Quantity-Distance Prediction Methodology for Hardened Aircraft Shelters--QDRACS .....</b>	547
Mark G. Whitney, Kathy H. Spivey, and Debra D. Skerhut	

### *AIRBLAST-II* *Moderator: Gerald Meyers*

<b>Airblast Damage to Windows .....</b>	561
Jack W. Reed	
<b>Measured Leakage Pressures from a Test Structure Through Covered and Uncovered Vent Areas .....</b>	569
Charles J. Oswald, Luis M. Vargas, and Edward D. Esparza	
<b>Airblast Attenuation and Flow Loss Performance of Passive Attenuators .....</b>	589
Quentin A. Baker and John P. Harrell	

## *INDEXES*

<b>Table of Contents--Volume I .....</b>	611
<b>Table of Contents--Volume III .....</b>	615
<b>Table of Contents--Volume IV .....</b>	619
<b>Author Index .....</b>	623
<b>Attendee List .....</b>	627

# TWENTY-FIFTH DDESB EXPLOSIVES SAFETY SEMINAR

## TABLE OF CONTENTS

### VOLUME III

PREFACE .....	iii
---------------	-----

#### *ORDNANCE CLEAN UP--II*

*Moderator: David Douthat*

Raritan Arsenal--Unexploded Ordnance Removal Project, Edison, New Jersey .....	1
Robert Nore	

The Decontamination of the Royal Naval Armament Depot, Milford Haven .....	11
L. H. Armstrong	

Explosive Ordnance Engineering .....	17
Rob Wilcox	

Reactivity of Explosive--Contaminated Soils to Flame and Shock Stimuli .....	47
Thomas W. Ewing and F. T. Kristoff	

#### *ELECTROSTATIC HAZARDS AND LIGHTNING PROTECTION*

*Moderator: Ignacio Cruz*

Electrostatic Hazards of Explosive, Propellant, and Pyrotechnic Powders .....	89
C. James Dahn and Bernadette N. Reyes	

Development of RF-Insensitive Electric Primers .....	103
John L. Bean	

Evaluation of Lightning Protection Systems for Explosives .....	139
Richard S. Collier, Rodney A. Perala, and Frederick J. Eriksen	

Application of Lightning Detection and Warning Systems Within the Explosives and Blasting Environment .....	161
William C. Geitz and Jack McGuinness	

#### *POSTER SESSION*

*Moderator: Jerry Ward*

Radon Testing at Radford Army Ammunition Plant .....	173
John M. Crable	

*POSTER SESSION* (Continued)

<b>Explosives Safety Training for the 1990s .....</b>	181
David W. Foulk	
<b>Development of an On-Line Text-Based Retrieval System for the DDESB Seminars Abstracts .....</b>	235
Paul N. Myers and Harry J. Hoffman	
<b>The Effects of Ultrahigh-Pressure Waterjet Impact on High Explosives .....</b>	247
Paul L. Miller	
<b>Advanced Field Data Acquisition Techniques for Contaminated Site Characterization .....</b>	259
J. W. Sharp and C. Flynn	
<b>High Explosive Damage Assessment Model Advanced Industrial Version (HEXDAM-D+)</b> .....	273
Frank B. Tatom, Mark D. Roberts, John W. Tatom, and Bart A. Miller	
<b>Investigation of Igniter Composition Fire, Bay 9 Building G-11, Lonestar Army Ammunition Plant, 15 May 1991 .....</b>	299
Robert A. Loyd	
<b>Low Cost, Combination RF and Electrostatic Ferrite Device Protection for Electroexplosive Devices .....</b>	327
Robert L. Dow	
<b>Operation Desert Sweep--The Restoration of Kuwait .....</b>	335
Fred Dibella	
<b>A Brief History of Lightning Protection .....</b>	341
Norman L. Fowler	
<b>A Geographic Information System (GIS) for Explosives Facility Sitting Analysis .....</b>	347
Larry D. Becker and Joseph Jenus	
<b>Automated Site Planning--Explosive Ordnance Land Use Planning Aid (EOPA)</b> .....	363
Tom Yonkman	

*EXPLOSIVES AND AMMUNITION SAFETY TESTS*  
*Moderator: Pete Yutmeyer*

<b>The Interrelationships Between Qualification, Insensitive Munitions, and Hazard Classification Testing of Explosives (High Explosives, Propellants, and Pyrotechnics)</b> .....	373
Richard E. Bowen, Jerry M. Ward, and Edward A. Daugherty	

## *EXPLOSIVES AND AMMUNITION SAFETY TESTS (Continued)*

<b>Explosive Charges Safety Tests</b> .....	385
Zhang Yinliang, Zhang Jikang, Mi Litian, and Lin Ying	
<b>The Explosive Component Water Gap Test</b> .....	399
Alan J. Morley	
<b>High Temperature/Solar Effects Testing on Various Munitions</b> .....	407
Gary P. Appel	

## *PERSONNEL PROTECTION DESIGN CONSIDERATIONS*

*Moderator: Roger Goldie*

<b>Inhabited Building Distance Criteria and Modern Construction</b> .....	415
Paul M. Lahoud and William H. Zehrt, Jr.	
<b>Evaluation of Operator Protection from Remote Operations in Existing Buildings with 12-Inch Substantial Dividing Walls (SDWs)</b> .....	437
Adib R. Farsoun	
<b>A New Processing Facility for the Prins Maurits Laboratory TNO</b> .....	453
Jan J. Meulenbrugge	
<b>Lacing and Stirrups in One-Way Slabs</b> .....	457
Stanley C. Woodson	

## *DEBRIS*

*Moderator: Fred Krach*

<b>Practical Use of the Building Debris Hazard Prediction Model, DISPRE</b> .....	475
Patricia Moseley Bowles	
<b>Assessment of Secondary Fragment Threats from Conventional DoD Building Construction</b> .....	497
James P. Manthey	
<b>Comparison of Debris Trajectory Models for Explosive Safety Hazard Analysis</b> .....	513
Lawrence A. Twisdale and P. J. Vickery	
<b>Pressure Vessel Burst Test Program: Progress Paper No. 3</b> .....	527
Maurice R. Cain and Douglas E. Sharp	

## *INDEXES*

<b>Table of Contents--Volume I</b> .....	543
<b>Table of Contents--Volume II</b> .....	547
<b>Table of Contents--Volume IV</b> .....	551
<b>Author Index</b> .....	555
<b>Attendee List</b> .....	559

## AUTHOR INDEX

Abriss, Gary	II-29	Défourneaux, Marc	IV-1
Adeshina, Femi	II-445	DeHoff, Bryan S.	I-487
Ahn, Jae Woon	II-85	Demin, Bo	II-317
Allain, Laurent	II-325	Dibella, Fred	II-19, III-335
Anderson, Robert G.	I-27	Douthat, C. David	II-1
Anspach, Earl E.	I-487	Dow, Robert L.	III-327
Appel, Gary P.	III-407	Drake, James L.	II-129
Armstrong, L. H.	III-11	Eckhardt, William T.	IV-341
Austin, Bryan S.	II-467	Eisler, Robert D.	I-453
Baca, Thomas	I-3	Erdley, Derek W.	IV-505
Badelow, Clive W.	II-437	Eriksen, Frederick J.	III-139
Bailey, Alan	I-235	Esparza, Edward D.	I-403, II-569, IV-511
Baker, Charles F.	IV-471	Ewing, Thomas W.	III-47
Baker, Quentin A.	II-589	Farsoun, Adib R.	III-437
Bakhtar, Khosrow	IV-573	Ferritto, John	IV-111
Barker, Darrell D.	IV-299	Fertal, Martin J.	I-633
Bartelds, Henk	I-21	Finnerty, Anthony E.	I-163
Bean, John L.	III-103	Flynn, C.	III-259
Becker, Larry D.	II-107, III-347	Ford, Max B.	I-615
Berkbigler, Larry W.	IV-81	Foulk, David W.	III-181
Bern, Joseph	II-445	Fowler, Norman L.	III-341
Besson, Jacques C.	IV-443	Frey, Robert	I-151
Bienz, Andreas F.	II-341, II-373	Gardner, Janet S.	IV-77
Bolton, B. Louise	IV-81	Geitz, William C.	III-161
Bondi, Peter A.	I-11	Glenn, Greg	IV-455
Bowen, Richard E.	III-373	Goliger, Jean	II-325
Bowles, Patricia Moseley	III-475	Gould, Michael J.	IV-179
Browning, Richard V.	IV-81	Graham, Kenneth J.	IV-409
Bussell, T. J.	IV-203	Grissom, Elton	IV-455
Cain, Maurice R.	III-527	Guerke, Gerhard H.	IV-161
Caltagirone, Joseph P.	IV-555	Hager, Kevin	I-373, I-453
Chatterjee, A. K.	I-453	Halsey, Carl C.	IV-341
Chick, M.	IV-203	Hangeland, Erik B.	II-211
Chizallet, Maurice C.	IV-541	Harrell, John P.	II-589
Choi, Jin Soo	II-85	Hay, J. Edmund	IV-233
Choi, Kyung Y.	I-429	Hewkin, David J.	II-143
Collier, Richard S.	III-139	Hoffman, Harry J.	III-235
Collis, David	I-151	Hoffman, Robin M.	IV-341
Connor, John	I-575, IV-601	Holland, T. J.	IV-133
Corley, John	IV-455	Horoschun, G.	I-507
Crable, John M.	III-173	Houchins, W. D.	IV-179
Crawford, Ken	II-25	Hutchison, Ken R.	II-437
Crepeau, Joseph E.	II-257	Isler, Jean	II-325, IV-419
Dahn, C. James	I-43, III-89	Jardine, John	II-159
Daugherty, Edward A.	III-373	Jenus, Joseph	II-107, III-347
Davis, Alan R.	I-13	Jikang, Zhang	III-385
Davis, L. Kim	IV-63, IV-375	Joachim, Charles E.	II-227, II-295

Kartachak, Thomas	II-159	O'Rourke, Timothy S.	I-249, II-211, II-219
Keegan, Kevin R.	I-249, II-211, II-219	Olson, Leonard S.	I-261
Keenan, William A.	IV-311	Oswald, Charles J.	I-543, II-569, IV-111
Kennedy, Lynn W.	II-257	Parkes, David A.	IV-531
Kernen, Patrick	IV-1	Pastorick, James P.	II-445
Kim, Hyung Won	II-85	Pastrnak, John W.	IV-471
Kivity, Y.	I-467	Perala, Rodney A.	III-139
Knape, Ralph A.	I-83	Perea, Aaron	II-467
Kodde, H. H.	I-97	Peregrino, II, Philip J.	I-163
Kristoff, F. T.	III-47	Pietrzak, L.	I-453
Kuk, Jeong H.	I-429	Pitts, Larry	IV-455
Kummer, Peter O.	II-341, II-373	Polcyn, Michael A.	IV-511
LaHoud, Paul M.	III-415, IV-281	Reed, Jack W.	II-561
Langberg, Helge	II-99	Reyes, Bernadette N.	I-43, III-89
Languy, Jean-Pierre	II-325	Roberts, Mark D.	III-273
Lavelle, F. M.	II-129	Robey, Robert W.	II-509
Laverentz, Harold D.	IV-531	Roger, Michel	I-525
Lawrence, William	I-183	Ross, Boyce L.	II-411
Lee, Benjamin Y. S.	I-495	Rossi, Robert A.	I-133
Lee, Jaimin	I-429, II-85	Salzman, Paul K.	IV-269
Lee, Jun W.	I-429	Savariego, Meir	I-479
Litian, Mi	III-385	Serena, III, Joseph M.	I-313
Loyd, Robert A.	III-299	Sharp, Douglas E.	III-527
Lyman, O.	I-151	Sharp, J. W.	III-259
Malvar, L. J.	IV-133	Shugar, T. A.	IV-133
Manthey, James P.	III-497	Simmons, Larry F.	IV-471
Marchand, Kirk A.	IV-111	Sisk, Wayne E.	I-249, II-211, II-219
McCleskey, Frank	IV-217	Skerhut, Debra D.	II-547
McGuinness, Jack	III-161	Soleau, Edward W.	II-123
McMahon, Gordon W.	II-277	Song, So-Young	I-429, II-85
McMillan, Colin	I-7	Spivey, Kathy H.	II-547
McQueen, D.	IV-203	Starkenberg, John	I-183
McVay, L.	IV-203	Struck, Stephen	IV-455
Mercx, W. P. M.	I-97	Sues, R. H.	II-129
Merrifield, R.	I-591	Swisdak, Jr., Michael M.	I-557, II-527,
Merrill, Claude	IV-225		IV-351, IV-391
Meulenbrugge, Jan J.	III-453	Tancreto, James	I-373, I-453
Miller, Bart A.	III-273	Tatom, Frank B.	III-273
Miller, Jerry R.	I-27	Tatom, John W.	III-273
Miller, Paul L.	I-213, III-247	Tobin, Thomas M.	I-133
Monson, Hal	I-235	Tuokko, Seppo	I-61
Montanaro, Paul E.	IV-391	Twing, Charles L.	II-169
Moran, Jr., Edward P.	I-113	Twisdale, Lawrence A.	II-129, III-513
Moreton, P. A.	I-591	Vaidyanathan, H.	I-271
Morley, Alan J.	III-399	van Ham, Nico	I-21
Murtha, Robert N.	I-331	Vargas, Luis M.	II-569
Myers, Paul N.	III-235	Vickery, P. J.	III-513
Nebuda, Dale	IV-111	Victor, Andrew C.	IV-19
Needham, Charles E.	II-257	Wager, Phillip C.	IV-311
Nore, Robert	III-1	Wallace, David K.	I-1, IV-599

Walls, Margaret P.	II-401
Ward, Jerry M.	III-373
Watson, Jerry L.	I-163
Watson, R. W.	IV-233
Whitney, Mark G.	II-547, IV-299, IV-511
Wilcox, Rob	III-17
Wilken, George	I-235
Williamson, G. E.	I-603
Woodson, Stanley C.	III-457
Ying, Lin	III-385
Yinliang, Zhang	III-385
Yonkman, Tom	III-363
Zaugg, Mark M.	I-27, I-235
Zehrt, Jr., William H.	III-415

# TWENTY-FIFTH DDESB EXPLOSIVES SAFETY SEMINAR

## ATTENDEE LIST

MR.	ADAMS	ARLIE	AIR FORCE MATERIEL COMMAND
MR.	ADAMS	RICHART	NAVAL SEA SYSTEMS COMMAND
LCDR	ADAMS	GREGORY	U.S. COAST GUARD
MR.	ADAMS	ROBERT	THE BOEING COMPANY
CAPTAIN	ADOLF	DAVID	HQ, PACAF/SEW
MR.	ALBIN	RICHARD	COMMANDER, US ARMY
MSGT	ALT	JEFF	3246 EQUIPMENT MAINTENANCE SQUADRON
LTCOL	ALTMAN	DERRALL	HQ, AFIA
MR.	AMMERMAN	DON	NAVAL SURFACE WARFARE CENTER
MR.	ANDERSEN	EARL	UNITED TECHNOLOGIES/CHEMICAL
MR.	ANDREASSEN	MARK	TRACOR AEROSPACE, INC.
MR.	ANKESHEILN	WADE	30TH SPACE WING/SEV
MR.	ANSPACH	EARL	SVERDRUP TECHNOLOGY, INC.
MR.	APPEL	GARY	COMBAT SYSTEMS TEST ACTIVITY
MR.	ARMBRESTER	BRANSCOMB	WRIGHT LABORATORY
MR.	ARMSTRONG	L. H.	MOD(N), DST (AS), ST 64A
MR.	ARNOLD	JAMES	U.S. ARMY TOXIC & HAZARDOUS MATERIALS
MR.	ATHEY	RONALD	HERCULES INCORPORATED
MR.	AUSTIN	BRYAN	PL/W5B
MR.	AUTEN	STEPHEN	U.S. ARMY YUMA PROVING GROUND
LTC	BADELOW	CLIVE	DEPARTMENT OF DEFENCE-LOGISTICS
MR.	BAGGETT	ALBERT	QUANTIC INDUSTRIES, INC.
MR.	BAHL	DAVID	DCMAO VAN NUYS
MR.	BAJPAYEE	T.	US BUREAU OF MINES
MR.	BAKER	CHARLES	UNIVERSITY OF CALIFORNIA
MR.	BAKER	QUENTIN	WILFRED BAKER ENGINEERING, INC.
DR.	BAKHTAR	KHOSROW	BAKHTAR ASSOCIATES
MR.	BANNING	DOUG	MARTIN MARIETTA ASTRONAUTICS
CAPTAIN	BARATTA	GARY	HAWTHORNE ARMY AMMUNITION PLANT
MR.	BARBERO	LUIS	CLAUDIO COELLO, 124
MR.	BARNETTE	JERRY	MARINE CORPS SYSTEMS COMMAND
MR.	BARR	MICHAEL	LOS ALAMOS NATIONAL LABORATORY
SMSGT	BARTIS	JAMES	103D FIGHTER GROUP
MR.	BAUERMEISTER	DONALD	PUEBLE DEPOT ACTIVITY
MR.	BECK	MERVIN	UMATILLA DEPOT ACTIVITY
MR.	BELL	KENNETH	NEW MEXICO ENGINEERING RESEARCH LAB
MR.	BELLING	DAN	NATIONAL TECHNICAL SYSTEMS

LTCOL	BEN-BASSAT	ELI	ATTISTANT MILITARY ATTACHE
MR.	BERN	JOSEPH	IT CORPORATION
MS.	BERRY	SHARON	NAVAL AIR WARFARE CENTER
ICA	BESSON	JACUES	Inspection de l'Armenent pour les
MR	BIBLE	WILLIAM	MARTIN MARIETTA ORDNANCE SYSTEMS, INC.
MR.	BIENZ	ANDREAS	BIENZ, KUMMER & PARTNER LTD
MR.	BILLINGSLEY	LARON	THIOKOL CORPORATION
MR.	BISCOTTE	MICHAEL	HAYES, SEAY, MATTERN & MATTERN, INC.
MS.	BISHOP	NANCY	EXPLOSIVES SAFETY TEAM (ARMAMENT DIV)
MR.	BISHOP	STEPHEN	USBI, P&W, UTC
MR.	BISHOP	DAVID	62 AIRLIFT WING
MR.	BLAIR	DOUGLAS	HQ, USAREUR/7A
MR.	BLAYLOCK	NEIL	SOUTHWEST RESEARCH INSTITUTE
MR.	BLOOM	THOMAS	QUANTIC INDUSTRIES, INC.
MR.	BLOSE	THOMAS	NAWCWPNS
MR.	BOAZ	GROSMAN	
MR.	BOBIS	JOHN	AEROJET PROPULSION DIVISION
LTC	BOCHAN	DOV	ASSISTANT MILITARY ATTACHE
MR.	BOHIS	JOHN	AEROJET PROPULSION DIVISION
MR.	BOHLMAN	P.	LOCKHEED MISSILE & SPACE COMPANY
MR.	BOIMEL	ARIE	I.M.I. INDUSTRIES
MS.	BOLTON	LOUISE	LOS ALAMOS NATIONAL LABORATORY
MR.	BONSON	LLOYD	EXPLOSIVE PROJECTS & DIAGNOSTICS DEPT.
MR.	BORGARDT	FRANK	LOCKHEED MISSILES & SPACE COMPANY
MR.	BOURENANE	MICHAEL	AEROJET ORDNANCE COMPANY
MR.	BOVENSCHEN	WILLIAM	NAVAL SURFACE WARFARE CENTER
MR.	BOWEN	RICHARD	NAVAL SEA SYSTEM COMMAND
MS	BOWLES	PATRICIA	SOUTHWEST RESEARCH INSTITUTE
LCDR	BOYDEN	JOHN	UXB INTERNATIONAL, INC.
MR.	BRADFORD	W	Olin Corporation
SGT	BRINDLEY	PATRICK	EOD MALS-13
MR.	BRODERICK	CHARLES	LAWRENCE LIVERMORE NATIONAL LABORATORY
MR.	BROOKS	JESSIE	KAO
MR.	BROWER	JAMES	US ARMY TECH ESCORT-UNIT

MR	BROWN	WARREN	OLIN CORPORATION
MR.	BROWN	NICHOLAS	PUEBLO DEPOT ACTIVITY
MR.	BROWN	MICHAEL	NAVAL SURFACE WARFARE CENTER
MR.	BROWN	LARRY	DENVER RESEARCH INSTITUTE
MR.	BRUNO	FRED	MCDONNELL DOUGLAS MISSILE SYSTEM CO.
MR.	BRUNTY	JOE	FEDERAL/OSHA
SMSGT	BRYANT	JAMES	102ND FW/SE
MR	BUEHLER	KURT	6510 TW/DORH
MR.	BUMMER	GLENN	CALIFORNIA INSTITUTE OF TECHNOLOGY
MR.	BURCH	V.	NAVAL SURFACE WARFARE CENTER
M/SGT	BURCHETT	STEPHEN	2701 EXPLOSIVES ORD SQUADRON
MR.	BUTLER	FENOY	GEO-CENTERS, INC.
MR.	BUTLER		US ARMY YUMA PROVING GROUND
SSGT	CACIOPPU	BEN	EOD 7E5B 1ESSG
MR.	CAIN	MAURICE	GENERAL PHYSICS SERVICE CORP.
MR.	CALHOUN	JAMES	ATLANTIC RESEARCH CORPORATION
MR.	CALTAGIRONE	JOSEPH	U.S. ARMY ARMAMENT R&D CENTER
MR	CAMPBELL	JAMES	BMO/SE
MR.	CAMPBELL	DEAN	BRISTOL AEROSPACE LIMITED
CR.	CANADA	CHESTER	
MR	CANNON	PAUL	THIOKOL CORPORATION
COLONEL	CARLSSON	BERNDT-IVAN	DEFENCE MATERIEL ADMINISTRATION
CAPTAIN	CARROLL	JAMES	HEADQUARTERS, USAFE
CAPTAIN	CARTER	JOHN	11 AF/SEW
MR.	CATES	CHARLES	
MR.	CENTENNIAL	CARL	SOUTHWEST RESEARCH INSTITUTE
MR.	CHANDLER	ERNEST	RED RIVER ARMY DEPOT
MSGT	CHARON	ROBERT	388 FIGHTER WING
MR.	CHASE	RONALD	542D CPTS/FMFP
MR.	CHIA	CAKE HAN	LANDS & ESTATES ORGANIZATION, LEOMINDEF
MR.	CHING	REGINALD	OLAC PHILLIPS LABORATORY
MR.	CHIZALLET	MAURICE	GIAT INDUSTRIES - B.M.P.
MR.	CHRISTENSON	ALAN	MCDONNELL DOUGLAS SPACE AND
MS.	CINNAMON	CYNTHIA	DEFENSE CONTRACT MGMT
MR.	CLAFFY	JOHN	DISTRICT WEST LOCKHEED ENGINEERING & SCIENCES COMPANY
MR.	CLAPP	ROBERT	MARTIN MARIETTA MISSILE SYSTEMS

MR.	CLARK	RONALD	CRANE ARMY AMMUNITION ACTIVITY
MR.	CLARK	EUGENE	DDESB
MR.	CLIFFORD	LIM KONG	EXPLOMO TECHNICAL SERVICES PTE LTD
MR.	CLINTON	STEPHEN	HAYES, SEAY, MATTERN & MATTERN, INC.
MR.	CLOONAN	JAMES	SM-ALC/SEW
MR.	COBB	WILLIAM	436 AW/SEW
MR.	COLBERG	MELVIN	U.S. ARMY DEFENSE AMMUNITION CENTER
MR.	COLLIER	RICHARD	Electro Magnetic Applications
MR.	COLLIS	DAVID	NEW MEXICO INSTITUTE OF MINING
MR.	COLTON	JAMES	SRI INTERNATIONAL-POULTER LABORATORY
MR.	CONNOR	J	Naval Surface Weapons Center
MR.	CONNOR	JOHN	CHIEF OF SAFETY
MR.	CONSTANTINO	LARRY	PACIFIC SCIENTIFIC
MR.	COONFARE	GREGORY	445 AW/SEG
MR.	COULSON	JOHN	COULSON CONSULTING CORPORATION
MR.	CRAVEN	JEFFERY	REDSTONE TECHNICAL TEST CENTER
MR.	CRAWFORD	KENNETH	US ARMY CORPS OF ENGINEERS
MR.	CREVECOEUR	RONALD	HQ, ARMY MATERIEL COMMAND
LTCOL	CROWE	STEWART	DIRECTORATE OF LAND SERVICE AMMUNITION
MR.	CRUFF	DELBERT	Lawrence Livermore National Laboratory
MR.	CUMMINGS	BRUCE	SRS TECHNOLOGIES
MR.	DAHN	CARL	SAFETY CONSULTING ENGINEERS, INC.
LT COL	DANIELSON	WILLIAM	DIRECTOR OF NUCLEAR SURETY
MR	DAVIS	KIM	WATERWAYS EXPERIMENT STATION
MAJOR	DAVIS	ALAN	DIRECTORATE OF LAND SERVICES AMMUNITION
MR.	DAY	ROBERT	DEFENSE CONTRACT MGMT
MR.	DAY	KEVIN	DISTRICT WEST
MR.	DAYE	JAMES	NAVAL SURFACE WARFARE CENTER CRANE
MR.	DAYWALT	RAYMOND	NAVSEACENLANT
MAJOR	DEHOFF	BRYAN	NAVAL SURFACE WARFARE CENTER
MR.	DEMERSION	ELISHA	AEDC DOPR
			DEPARTMENT OF ENERGY

MR.	DEMIN	B.	DEFENCE MATERIEL ADMINISTRATION
MR.	DENISON	THOMAS	ALLIANT TECHSYSTEMS, INC.
MR.	DESCHAMBault	ERIC	NAVAL SURFACE WARFARE CENTER
MR. MSGT	DESSAIX	LOUIS	GROUPE EPC
	DEUTSCH	KENT	EOD MALS-16 MAG-16 3RD MAW
MR.	DIBELLA	FRED	CONVENTIONAL MUNITIONS SYSTEMS, INC.
MR.	DICKINSON	PAUL	DCMAO DENVER
MR.	DILLARD	DONALD	OLIN CORPORATION
MR.	DILLEHAY	DAVID	THIOKOL CORPORATION - LONGHORN DIVISION
MR.	DILTS	CHARLES	MCDONNELL DOUGLAS MISSILE SYSTEMS CO.
MR.	DITTMAN	HARRY	DCMD MID-ATLANTIC
MR.	DIVINE	KIRBY	CRANE DIV NAVAL SURFACE WARFARE CENTER
MR.	DODGEN	JAMES	DODGEN ENGINEERING COMPANY
MR.	DONALD	DILLARD	OLIN CORPORATION
MR.	DOOLITTLE	CRAIG	NAVAL SURFACE WARFARE CENTER
MR.	DOTTS	JAMES	SANDIA NATIONAL LABORATORIES
MR.	DOUTHAT	C.	U.S. ARMY CORPS OF ENGINEERS
MR.	DOW	ROBERT	ATTENUATION TECHNOLOGY INC.
MR	DOWLING	THOMAS	INSTITUTE OF MAKERS OF EXPLOSIVES
MR	DRAKE	JAMES	APPLIED RESEARCH ASSOC. INC.
MR.	DRAKE	RICHARD	FLUOR DANIEL
MR.	DRURY	CHUCK	SHAMROCK SERVICES
MR.	DUA	BALBIR	DAY & ZIMMERMANN, INC.
MR.	DUCHOCK	JEFF	
MR.	DUDLEY	MICHAEL	DEFENSE LOGISTICS AGENCY
MR.	DUNAND	MAURICE	ENAA/4 B
MAJOR	DUNCAN	KENDAL	US ARMY ARMAMENT, MUNITIONS,
MR.	DUNHAM	C	US ARMY JEFFERSON PROVING GROUND
CWO-2	DUNN	JOSEPH	MALS-13 EOD TEAM
MR.	DUNSETH	CLIFFORD	U.S. ARMY SAFETY CENTER
MR.	EDDY	JOHN	Defense Nuclear Agency
MR.	EIFF	ARTHUR	HEIERLI CONSULTING ENGINEERS
MR.	EINERTH	BENGT	NATIONAL INSPECTORATE OF EXPLOSIVES

MR.	EISLER	ROBERT	MISSION RESEARCH CORPORATION
MR	ELLEDGE	JAMES	UNITED TECHNOLOGIES/CHEMICAL
MR	ELLIOTT	JAMES	US ARMY RESEARC
MR.	ELLIOTT	MARTIN	DEVELOPMENT AND US ARMY TOXIC & HAZARDOUS MATERIALS
CWO2	ELLIS	JUDITH	MARINE CORPS SYSTEMS COMMAND
MR. MSGT	ELMSHAEUSER	KARL	AEROJET ORDNANCE
MR.	EMERTON	SHERWOOD	9AF, ATTN: SEW
MR.	ERDLEY		US ARMY COMBAT SYSTEMS TEST ACTIVITY
CAPTAIN	ERIKSEN	STEINAR	ROYAL NORWEGIAN NAVY
MR.	ERNESTO	VIGIL	MATERIAL COMMAND
MR.	ESCRICHE	GABRIEL	LOS ALAMOS NATIONAL LABORATORY
MR.	ESPARZA	EDWARD	UNION ESPANOLA DEEXPLOSIVOS
MR.	EWING	THOMAS	SOUTHWEST RESEARCH INSTITUTE
MR.	EYTAN	REUBEN	HERCULES, INC.
COLONEL	FABRE	JACQUES	EYTAN BUILDING DESIGN, LTD
COL	FAHL	ROBERT	FRENCH LIAISON OFFICER
MR.	FALLON	JOHN	ACCUDYNE CORPORATION
MR.	FANNIN	GERALD	DEFENSE LOGISTICS AGENCY
MR.	FARRAR	STEPHEN	NATIONAL TECHNICAL SYSTEMS
MR.	FARSOUN	A.	U.S. ARMY ENGINEERING DIVISION
DR.	FELLER	SHAUL	RAFAEL-ISRAEL ARMAMENT DEVELOPMENT
MR.	FELTEN	PHILIP	HERCULES INCORPORATED
MR.	FENNESSY	RICHARD	MILSEARCH PROPRIETARY LIMITED
LT	FENTON	WILLIAM	EODMU TWO DET NEWPORT
MR.	FERNANDEZ	HERBERT	NEW MEXICO INSTITUTE OF MINING
CAPTAIN	FICK	RUDI	FEDERAL MINISTRY OF DEFENCE
MR.	FLEMING	PAUL	SANDIA NATIONAL LABORATORIES
MR	FLORY	ROBERT	APPLIED RESEARCH ASSOC. INC.
MR.	FOGLIETTA	JAMES	WYLE LABORATORIES
MR.	FORDHAM	THOMAS	TRW SS/M
MR.	FORSYTHE	FRANKLIN	UNIROYAL CHEMICAL COMPANY, INC.

1LT	FORSYTHE	MICHELLE	51 WING/SEW
MR.	FOULK	DAVID	U.S. ARMY DEFENSE AMMUNITION CENTER
MR.	FOWLER	NORM	HQ AFESC/DEMM
MR.	FRAY	ROBERT	BALLISTIC RESEARCH LABORATORY
MR.	FREIMANIS	ALVIS	KNIGHT ARCHITECTS ENGINEERS
CAPTAIN	FREITAS	ANTONIO	COMANDO OPERATIONAL DA FORCA AEREA
MR.	FUENTES	FERNANDO	US ARMY STRICOM (AMSTI-S)
MR.	GALLAGHER	RICHARD	DEFENSE CONTRACT MANAGEMENT DISTRICT
MR.	GARRETT	GERALD	LONGHORN ARMY AMMUNITION PLANT
MR.	GARRISON	JOHN	US MARINE CORPS AIR STATION
MR.	GATELY	R.	E.O.D. WORLD SERVICES, INC.
MR.	GEISLER	ROBERT	RESEARCH TRIANGLE INSTITUTE
MR.	GENEST	RON	ORBITAL SCIENCE CORPORATION
MAJOR	GERDES	GREGORY	DASC/RS
MR.	GESSLER	JOHNSON	NAVAL SURFACE WARFARE CENTER
MR.	GILL	RANDOLPH	US ARMY COMBAT SYSTEMS TEST
MR.	GLAD	THOMAS	GENCORP AEROJET
MR.	GLAZNER	FRED	US ARMY - PATRIOT
MR.	GODDARD	FRANCIS	NAVAL WEAPONS STATION
MAJOR	GOH	YONG KIAT	AIR LOGISTICS DEPARTMENT - HQ RSAF
MR.	GOLDIE	ROGER	LOS ALAMOS NATIONAL LABORATORY
MR.	GOOLD	JOHN	INSTITUTE OF EXPLOSIVES ENGINEERS
MR.	GORDON	D.	IRECO, INC.
MR.	GORDON	WALT	STRATEGIC WEAPONS FACILITY, ATLANTIC
MR.	GORDON	REX	SUPPRESSION SYSTEMS ENGINEERING, INC.
MR.	GOSSELIN	HENRY	DYNAMICS RESEARCH CORPORATION
MR.	GOULD	MICHAEL	MINISTRY OF DEFENCE
MR.	GRACE	PAUL	AEROJET PROPULSION DIVISION
PROFESSOR	GRAHAM	K.	JUDSON CONSULTING SERVICE
MAJOR	GRANT	GLORIA	HQ, USAF/SEP
MR.	GRAY	WALT	SOUTHWEST RESEARCH INSTITUTE

MR.	GREGORY	O.	USA CHEMICAL RESEARCH COMMAND
MR.	GRILLS,	JAMES	NAVAL WEAPONS STATION
MR.	GROSMAN	BOAZ	I.M.I LTD - SYSTEMS GROUP
MR.	GUARIENTI	RICHARD	LAWRENCE LIVERMORE NATIONAL LABORATORY
MR.	GUENNEL	RANDOLPH	380TH AIR REFUELING WING
MR.	GUERKE	GERHARD	ERNST INSTITUT
MR.	HAGER	KEVIN	NAVAL CIVIL ENGINEERING LAB
MR.	HAGGARD	PAUL	MASON & HANGER ENGINEERING INC.
MR.	HAINES	ROBERT	IOWA ARMY AMMUNITION PLANT
MR.	HAINS	DAN	NAVEODTECHCEN
MR.	HALL	JACK	SUNFLOWER ARMY AMMUNITION PLANT
MR.	HALL	THOMAS	BATTELLE PANTEX
MR.	HALSEY	CARL	NAVAL AIR WARFARE CENTER
MR.	HAMILTON	JERRY	VITRO CORPORATION
MR.	HAMMEL-MUELLER	JUERGEN	HQ USAFE, PLANS & PROGRAMMING DIVISION
MR.	HAMPTON	ROBERT	NORTHROP CORPORATION-AIRCRAFT DIVISION
GMC(SW)	HAMPTON	LEON	NAVAL STATION PASCAGOULA
MR.	HAMRICK	MICHAEL	BATTELLE-PANTEX
LT	HANEWICH	STEVEN	U.S. COAST GUARD
MR.	HANLEY	PETER	CANADA, EXPLOSIVES DIVISION
MR.	HARDIN	ROBERT	MISSISSIPPI ARMY AMMUNITION PLANT
MS.	HARKER	JESSICA	NAVY SURFACE WARFARE CENTER
MR.	HARVEY	HARRY	HERCULES AEROSPACE COMPANY
MR.	HASAN	NAJMUL	THE RALPH M. PARSONS COMPANY
MR.	HASH	HARMON	USA COMBAT SYSTEMS ACTIVITY
MR.	HAWKINS	JERRY	CENTRAL AMMO MGMT OFFICE-PACIFIC
MR. SQNLDR	HAY HAYDEN	EDMOND ANDREW	BUREAU OF MINES RAAF TECHNICAL LISISON
MR	HAYES	JACK	OFFICE NAVAIR US ARMY CONSTRUCTION ENGINEER
MSGT	HAYES	ROBERT	EOD, RMD, SOMS
MR	HEATH	C.	DIRECTOR, SAFETY & ENVIRONMENTAL AFFAIR
MSGT	HEISE	DEAN	HQ AFSPAECOM

MR	HELLE	CHARLES	C/O CIA, BRASILEIRA-
MR	HENDERSON	JON	MINISTRY OF DEFENCE
MR.	HENDERSON	JIMI	DEFENSE CONTRACT MGMT
			DISTRICT WEST
MR.	HENDERSON	WILLIAM	NAVAL SURFACE WARFARE
			CENTER
MR.	HERRBACH	ALLAN	US DEPARTMENT OF ENERGY
MR.	HERRON	ROGER	U.S. ARMY BALLISTIC
			RESEARCH LABORATORY
DR.	HEWKIN	DAVID	MOD (UK) ESTC
MR.	HOFER	HERBERT	MINISTRY OF DEFENSE
MR	HOFFMAN	NORMAN	TECHNICAL ORDNANCE INC.
MR.	HOFFMAN	ROBIN	NAVAL AIR WARFARE CENTER
MR.	HOFFMAN	WILLIAM	NAVAL SURFACE WEAPONS
			CENTER
MR.	HOFFMAN	HARRY	JHU-CPIA
MR.	HOLLAND	LAURENCE	LOS ALAMOS NATIONAL
			LABORATORY
MR.	HOLLOWAY	BOBBY	VOLUNTEER ARMY AMMUNITION
			PLANT
MR.	HOWE	PHILIP	LOS ALAMOS NATIONAL
			LABORATORY
MR.	HUDSON	MELVIN	NAVAL SURFACE WARFARE
			CENTER
LT.COL	HUEHN	WILFRIED	GERMAN ARMY OFFICE
LTCOL	HUMPHREY	JAMES	US ARMY ARMAMENT,
			MUNITIONS,
MR.	HUNT	EDDIE	USASDC
MR.	HUNTER	DENNIS	NEW MEXICO INSTITUTE OF
			MINING
MR.	HUSCHKA	HOWARD	DEFENSE CONTRACT
			MANAGEMENT DISTRICT
COLONEL	HUTCHINSON	ALAN	PRESIDENT, AUSTRALIAN
			ORDNANCE COUNCIL
MR.	HUTCHISON	KEN	WESTERN AUSTRALIA POLICE
MR.	HUTCHISON	VERL	US ARMY WHITE SANDS
			MISSILE RANGE
MR.	ISBELL	JOHNNY	ICI EXPLOSIVES,
			ENVIRONMENTAL
MR.	IWANCIOW	BERNARD	STONE ENGINEERING
MR.	JACOBS	EDWARD	INTEGRATED SYSTEMS
			ANALYSTS, INC.
MR.	JACOBSSON	LARS-OLOF	ROYAL SWEDISH
			FORTIFICATIONS
MR.	JAMIN	PIERRE	FRENCH MOD/DGA
MR	JENSSEN	ARNFINN	CHIEF, OF OFFICE TEST &
			DEVELOPMENT
MR	JENUS	J.	EXPLOSIVES HAZARD
			REDUCTION DIRECTORATE
MR.	JOACHIM	CHARLES	U.S. ARMY ENGINEER
			WATERWAYS

DR. LTCOL	JOHN JONASSEN	CONNOR KIELL	MINISTRY OF DEFENCE NORWEGIAN DEFENSE CONSTRUCTION SERVICE
MR.	JONES	STEVE	U.S. ARMY MATERIEL COMMAND
MS.	JONES	KATHRYN	LOS ALAMOS NATIONAL LABORATORY
MS.	JONES	PATRICIA	SENECA ARMY DEPOT
MR.	JONES	DONOVAN	TALLEY DEFENSE SYSTEMS, INC.
MR.	JORGENSEN		US ARMY DUGWAY PROVING GROUND
MR.	JOSEPHSON	LARRY	NAVAL AIR WARFARE CENTER
MR.	JOYNER	TAYLOR	TERA GROUP
MR.	KATSANIS	DAVID	SHIELDING TECHNOLOGIES, INC.
MR.	KEENAN	WILLIAM	NAVAL CIVIL ENGINEERING LABORATORY
MR. GYSGT	KELLEY KELLY	PHILIP JOHN	BATTELLE PANTEX EXPLOSIVE ORDNANCE DISPOSAL
DR.	KENNEDY	LYNN	S-CUBED, A DIVISION OF MAXWELL LABS
MR.	KERNEN	PATRICK	ORGANIZATION DUE TRAITE DE L'ATLANTIQUE
MR.	KERR	SCOTT	TALLEY DEFENSE SYSTEMS, INC.
MAJOR	KIEHN	ERNEST	2701 EXPLOSIVE ORDNANCE DISPOSAL SQDN
MR.	KIGER	SAM	WEST VIRGINIA UNIVERSITY
MR.	KING	JAMES	LOS ALAMOS LABORATORY, M-6
MR.	KINNISON	ROBERT	DCMAO DENVER
MR.	KLAPMEIER	KENNETH	DETECTOR ELECTRONICS CORP
	KLINE	LESLIE	U.S. ARMY CHEMICAL MATERIEL DESTRUCTION
MR	KNAPE	RALPH	U.S. ARMY ARMAMENT, MUNITIONS &
COLONEL	KNIGHT	JOHN	HQ AFSA/SEW
MR.	KOBAN	G	EODMU TWO DETACHMENT DAHLGREN
MR. LTC	KODDE KONGEHL	HERMAN H. F.	VITRO CORPORATION Bundesministerium der Verteidigung
MR.	KRACH	FRED	EG&G MOUND APPLIED TECHNOLOGIES
MR.	KRAKE	JAMES	NAVAL SURFACE WARFARE CENTER
MR.	KRATOVIL	EDWARD	NAVAL SEA SYSTEMS COMMAND
MR.	KRAUSE	WILLIAM	UNITED TECHNOLOGIES-ASD
MR.	KRAUTHAMMER	THEODOR	PENN STATE UNIVERSITY

MR.	KRIETZ	TERRY	DEPARTMENT OF ENERGY
MR.	KRISTOFF	F	Hercules Inc.
MR.	KUMMER	PETER	BIENZ, KUMMER & PARTNER LTD
SMSGT MAJOR	KUNKLE LAMBRECHT	RONALD MICHAEL	HQ AFOTEC/SE FIELD COMMAND DEFENSE NUCLEAR AGENCY
MR.	LAMY	PATRICK	FRENCH MOD/DGA
MR.	LANGBERG	HELGE	ESTABLISHMENT
MR.	LAVERENTZ	HAROLD	BLACK AND VEATCH
MR.	LAVERTU	ROGER	DEFENCE RESEARCH
MR	LAWRENCE	WILLIAM	ESTABLISHMENT BALLISTICS RES. LABORATORY
MR.	LEACH	GLENN	HQ AMCCOM, SAFETY OFFICE
MR.	LEANDER	RICHARD	THIKOL CORPORATION
MR.	LEATHAM	SCOTT	DEFENSE CONTRACT
MR.	LEDERER	JOHN	MANAGEMENT COMMAND DIRECTORATE OF NUCLEAR SYSTEMS
MR.	LEE	J.	AGENCY FOR DEFENSE DEVELOPMENT/KOREA
MR. CAPTAIN	LEE	BENJAMIN	NAVAL AIR WARFARE CENTER
CAPTAIN	LEE	DIANA	VANDENBERG AFB
MR.	LEGALUPPI	TIONG HUA	HQ SUPPLY & TRANSPORT
		MARCO	WHITNEY, BAILEY, COX & MAGNANI
MS.	LEGALUPPI	CRYSTAL	PM CHEMICAL DEMILITARIZATION
MR.	LEK	HUAT LEE	CHARTERED INDUSTRIES OF SINGAPORE
MR.	LEROUZES	GILLES	ICI EXPLOSIVES CANADA
MR.	LEWIS	BUD	KANSAS ARMY AMMUNITION PLANT
MR.	LIBERMAN	PAUL	NATIONAL TECHNICAL SYSTEMS
MR.	LIM	CLIFFORD	EXPLOMO TECHNICAL SERVICES, LTD
MR.	LIM	KONG HING	NO.80, GENTING LANE
MR.	LIN	JACK	NATIONAL TECHNICAL SYSTEMS, INC.
MR.	LIND	LARRY	WESTNAVFACENGCOM
MR.	LINDELL	CARL	KDI PRECISION PRODUCTS, INC.
MR.	LIPP	CURTIS	AEROJET PROPULSION DIVISION
MR.	LITTLE	THOMAS	COUNTY OF LOS ANGELES FIRE DEPT.
MR.	LOCKARD	MICHAEL	RED RIVER ARMY DEPOT
MR.	LONG	EVERETT	NAVAL AIR WARFARE CENTER
MR.	LOWE	ALONZO	NAVAL SEA SUPPORT CENTER, ATLANTIC

MR.	LOYD	ROBERT	US ARMY ARMAMENT, MUNITIONS &
MS	MACINTYRE	ANNETTE	LAWRENCE LIVERMORE NATIONAL LABORATORY
MR.	MACKENZIE	GERALD	STONE ENGINEERING COMPANY
MR.	MAGNANI	RICHARD	WHITNEY, BAILEY, COX & MAGNANI
MR.	MAHANEY	KENNETH	MOTSU (META-SU-SAS)
MR.	MAIRANTZ	BENNY	B. MAIRANTZ CONSULTING ENGINEERS
MS.	MALONE	DOROTHY	MCALESTER ARMY AMMUNITION PLANT
MR.	MANNSHRECK	WILLIAM	NAVAL SAFETY CENTER
MR	MANTHEY	J.	US ARMY CORPS OF ENGINEERS
MR.	MAPLE	GARY	900 E. CAMINITO MADRIGAL
SMSGT	MARSH	JOHN	3246 EQUIPMENT MAINTENANCE SQUADRON
MS.	MARTIN	SUSAN	ATLANTIC RESEARCH CORPORATION
CAPTAIN	MARTIN	MARK	HQ, AIR COMBAT COMMAND
MR.	MARTIN	ELLIOTT	US ARMY TOXIC & HAZARDOUS MATERIALS
MS.	MASSIE	JOYCE	EG&G MOUND APPLIED TECHNOLOGIES, INC.
CAPTAIN	MATTERN	STEVEN	ASC/NA
DR.	MAURITS	WILLIAM	
MS.	MCBRIDE	CLAIR	US ARMY DUGWAY PROVING GROUND
MR.	MCCLELLAN	JAY	NAWC WEAPONS DIVISION
MR.	MCCLESKEY	FRANCIS	BOOZE, ALLEN & HAMILTON
MR.	MCCLURE	GERALD	AEROJET ELECTRONIC SYSTEMS DIVISION
MR.	MCCORMICK	BILL	LOS ALAMOS NATIONAL LABORATORY
MR.	MCDANIELS	E.	E.O.D. WORLD SERVICES, INC.
MR.	MCDONALD	JACK	DCMAO SAN ANTONIO
MR.	MCENTEE	ROGER	NAVAL WEAPONS CENTER
MR.	MCFALL	LARRY	U.S. ARMY LABORATORY COMMAND
MR.	MCGRAW	R.	ENSIGN BICKFORD AEROSPACE COMPANY
MR.	MCINTOSH	ALVIN	OO-ALC/SEW
MR.	MCKENZIE	ALLAN	UNITED
MR.	MCLAIN	JOHN	TECHNOLOGIES/CHEMICAL NEW MEXICO INSTITUTE OF MINING
MR.	MCNEIL	DOYLE	AEROJET PROPULSION DIVISION
MS.	MCNULTY	SUZANNE	MENDES & MOUNT

MR.	MCPHERSON	DARREL	U.S. DEPARTMENT OF ENERGY
MR.	MCQUEEN	JERRY	MOTOROLA INC.
MR.	MELSER	CHARLES	DEFENSE CONTRACT MGMT
DR	MERRIFIELD	R.	DISTRICT WEST
MR	MERRILL	CLAUDE	TECHNOLOGY DIVISION
LTCOL	MEYER	WALLACE	OL-AC PL/RKCP
MR	MEYERS	GERALD	825 BRENTWOOD PLACE
MR.	MIKASA	GLENN	US DEPARTMENT OF ENERGY
MR.	MIKOЛЕIT	KURT	NAVAL WEAPONS STATION
			NAVAL SURFACE WARFARE
			CENTER
MR.	MIKULA	JAMES	U.S. ARMY ARDEC
MR.	MILLER	STEVE	UNIVERSAL PROPULSION
MR.	MILLER	STEPHEN	CO. & INC
MR.	MILLER	PAUL	UNIVERSAL PROPULSION
CAPTAIN	MITTELMAN	GREG	COMPANY, INC.
MR.	MIXTER	HENRY	ALLIANT TECHSYSTEMS
CAPTAIN	MONTANA	SCOTT	AFMC, NUCLEAR SUPPORT
MR.	MONTANARO	PAUL	OFFICE
MR.	MONTELEONE	PAUL	E.O.D. WORLD SERVICES,
MS.	MONTROSS	JAN	INC.
COMMANDER	MOODY	DEWITT	351 MW/SEP
MR.	MOOI	KOK HEONG	NAVAL SURFACE WARFARE
MR.	MOONEY	R.	CENTER
MR.	MOORE	HAROLD	USARDEC
MR.	MORAN	EDWARD	SAFETY ENGINEERING
MR.	MORCOS	MICHAEL	LANDS AND ESTATES
DR.	MORETON	P.	ORGANIZATION
MR.	MORGAN	CHARLES	TALLEY DEFENSE SYSTEMS,
LTC	MORLEY	ALAN	INC.
MR.	MORRIS	TODD	TECHNICAL ANALYSIS, INC
MR.	MOXLEY	ROBERT	DDES
1LT	MUHL	GERALD	NAWC-WEAPONS
MSGT	MULDROW	JEFFERY	SRD
MR.	MURPHY	DAVID	NAVAL UNDERSEA WARFARE
MR.	MURPHY	THOMAS	UK ORDNANCE BOARD
MR.	MURTHA	ROBERT	U.S. ARMY SYSTEMS TEST
MR.	MYERS	PAUL-REGIS	FACILITY
			SAN ANTONIO AIR LOGISTICS
			CENTER/SEW
			ESCORT & DISPOSAL DET
			96TH WING WEAPONS SAFETY
			OFFICE
			LOCKHEED MISSILES & SPACE
			COMPANY, INC.
			DEFENSE CONTRACT MGMT
			DISTRICT WEST
			NAVAL CIVIL ENGINEERING
			LABORATORY
			JOHN HOPKINS UNIVERSITY

MR.	NANCE	WILLIAM	NANCE & ASSOCIATES
MS.	NAPADENSKY	HYLA	NAPADENSKY ENERGETICS, INC.
MR.	NARVER		999 TOWN & COUNTRY ROAD
MR.	NASH	JOHN	OFFICE OF ASST SECRETARY OF ARMY
MSGT	NASH	KEITH	ARNOLD AFB
MR.	NEEDHAM	CHARLES	S-CUBED, A DIVISION OF MAXWELL LABS
MR.	NEFF	RONALD	MILAN ARMY AMMUNITION PLANT
MR.	NEIDERBERGER	GARY	NAVAL WEAPONS STATION
MR.	NEIGHBORS	WILLIAM	GENCORP AEROJET ELECTRONIC SYSTEMS
CWO4	NEILL	STEPHEN	EODMU TWO DET YORKTOWN
MR.	NEWBURN	ROBERT	
MAJOR	NEYRINCK	RONNY	ARSENAAL MATERIEEL&MUNITIE
MR.	NICKERSON	HOWARD	NAVAL FACILITIES
MR.	NICOL	WILLIAM	ENGINEERING COMMAND
MR.	NOEL	THOMAS	CHIEF OF NAVAL OPERATIONS
MR.	NOEL	LLOYD	MASON & HANGER SILAS MASON CO., INC.
MR.	NORTUNEN	LARRY	NAVAL WAPONS STATION, SEAL BEACH
MR.	O'Bleness	ROBERT	US ARMY DEFENSE AMMO CENTER & SCHOOL
MR.	O.	GREGORY	BERGSTROM AFB USA CHEMICAL RESEARCH COMMAND
MR.	ODELLO	ROBERT	NAVAL CIVIL ENGINEERING LABORATORY
LT.COL	ODENBRING	TOR	SWEDISH DEFENCE MATERIAL ADMINISTRATION
MR.	OEI	SU CHEOK	DEFENCE MATERIALS ORGANIZATION
MR.	OHLSON	JOHNNY	DYNASAFE AB
MR.	OIOM	HANS	ARMY MATERIEL COMMAND
MAJOR	OLSON	LEONARD	CRANE ARMY AMMUNITION ACTIVITY
MR.	OPEL	ALAN	ALPHEUS CLEANING TECHNOLOGIES
MR.	OSWALD	CHARLES	SOUTHWEST RESEARCH INSTITUTE
MR.	OWENS		ATTN: FKSF, UNIT #15230
MR.	PACQUING	LEONARD	DEFENSE CONTRACT MGMT DISTRICT WEST
MR.	PAPE	RONALD	IIT Research Institute
MR.	PAPP	A.	BATTELLE PANTEX
MR.	PARK	LUINDE	LAKE CITY AAP
MR.	PARKES	DAVID	BLACK & VEATCH

MS.	PASCAL	SYLVIANE	AEROSPATIALE
LCDR	PASTORICK	JAMES	IT CORPORATION
MR.	PASTRNAK	JOHN	LAWRENCE LIVERMORE NATIONAL LABORATORY
MR.	PATRICK	GWYN	US ARMY TEST & EVALUATION COMMAND
MR.	PELTIER	MICHAEL	DCMAO TWIN CITIES
MR.	PEREA	AARON	ATTN: PL/WSB
MR.	PEREGINO	PHILIP	BALLISTIC RESEARCH LABORATORY
MR.	PEREZ	ANTHONY	DAY & ZIMMERMANN
MR.	PESKO	MICHAEL	STRESAU LABORATORY, INC.
MR.	PETERS	CHARLES	US ARMY, ARDEC
MR.	PETERSON		DEMEX
MR.	PEZESHK	ALI	THE RALPH M. PARSONS COMPANY
MS.	PH-THEODULE	HELEN	US ARMY MATERIAL TECHNOLOGY LABORATORY
MR.	PHILLIPS	HERMAN	US DEPARTMENT OF ENERGY
CAPTAIN	PHILLIPS	PETER	DEPARTMENT OF DEFENSE
MR.	PHILLIPS	GEORGE	MARINE CORPS SYSTEMS COMMAND
MR.	PIER	DAVID	MP ASSOCIATES, INC.
CAPT	PINHEIRO	JOSE	COMANDO LOGISTICO E ADMINISTRATIVO
MR.	PIPER	CHARLES	QUANTIC INDUSTRIES
MR.	PITTS	LARRY	WRIGHT LABORATORY/ARMAMENT DIRECTORATE
MR.	POJMANN	DAVID	OLIN CORPORATION
MR.	POLCYN	MICHAEL	SOUTHWEST RESEARCH INSTITUTE
LCDR	POLIZZI	JOHN	NAVAL AIR WEAPONS STATION
MR.	PONSONBY	MRAK	ATLAS ENVIRONMENTAL SERVICES
MR.	POPE	ALVIN	MASON & HANGER ENGINEERING INC.
MR.	POULAIN		COMMISSARIAT A L ENERGIE
MR.	PRATT	WILLIAM	MISSILE TARGETS
MR.	PRESTON	H.	STRATEGIC WEAPONS FACILITY PACIFIC
MR.	PRICE	WILLIAM	VITRO CORPORATION
MR.	PROPER	KENNETH	US ARMY DEFENSE AMMO CTR & SCHOOL
MR.	PUDENZ	PAUL	NAVAL WEAPONS STATION
MR.	PURVIS	JAMES	80 SPACE WING 30 SPW/SES
MR.	QUINN	KEITH	SSI SERVICES, INC.
MS.	QUINTANA	ROXANNE	NAVAL AIR WARFARE CENTER
MR.	RABUS	HEINRICH	- ARMEE MATERIAL OFFICE, GERMANY

MR.	RADFORD	C	Military Traffic Management Command
MR.	RAGAN	ELMER	906 FG 906/SEW
CWO3	RAMSEY	EDWARD	NAVAL AIR WEAPONS STATION
MR.	RANKIN	JOHN	US ARMY MATERIEL COMMAND
MR.	REBBY	RAYMOND	ATLANTIC DIVISION - NAVAL FACILITIES
MR.	REDMOND	BEN	EODT SERVICES, INC
MR.	REED	JACK	JWR, INC.
MR.	REEVES	HARRY	NEW MEXICO INSTITUTE OF MINING
MR.	REEVES	JOHN	WEAPONS STATION CONCORD
MR.	REILLY	WILLIAM	ASC/YQI
MR.	RENTER	LAVERN	DEFENSE CONTRACT MGMT DISTRICT WEST
MS.	REYES	BERNADETTE	SAFETY CONSULTING ENGINEERS, INC.
MR.	REYNOLDS	SKIP	IWGERSOLL RANO WATERJET
MR.	RHEA	RICHARD	OLIN CORPORATION
MR.	RHODES	JOHN	THIOKOL CORPORATION
MR.	RICH	MAX	SAFETY ENGINEERING
MR.	RICHARDSON	DAVID	HERCULES, INC.
MR.	RIEF	GEORGE	AIR FORCE FLIGHT TEST CENTER
MR.	RILEY	WILLIAM	30 SPACE WING
MR.	RINARD	GEORGE	GR ASSOCIATES
MR.	RISE	RONALD	NATIONAL TECHNICAL SYSTEMS
MR.	RISING	MERRILL	TECHNICAL ANALYSIS, INC.
MR.	RIVERS	DOUG	3M
MR.	ROBB	DAVID	HQ AFRES/SEV
MR.	ROBEY	ROBERT	NEW MEXICO ENGINEERING RESEARCH LAB
MR.	ROBINSON	RALPH	FIELD COMMAND
MR.	ROBSON	WILLIAM	AEROJET ASRM DIVISION
LTCOL	ROGER	MICHEL	KINISTERE DE LA DEFENSE-DCG-STBFT
MR.	ROLLINS	CHARLES	OLIN ORDNANCE
MR.	ROMAN	BOBBY	AEROJET ELECTRONIC SYSTEMS DIVISION
MR.	ROSADO	ROBERTO	OLIN ORDNANCE
MR.	ROSBERG	ALT	THE NATIONAL INSPECTORATE OF
MS.	ROSENBERG	DIANE	DEFENSE CONTRACT MGMT DISTRICT WEST
MR.	ROSENOW	JOHN	Sandia National Laboratories
MR.	ROSSI	ROBERT	PROJECT MANAGER- AMMO LOGISTICS
MR.	ROUZES	GILLES LE	ICI MCMASTERVILLE
MR.	RYTZ	HANSJOERG	MOD, DEFENSE TECHNOLOGY & PROCUREMENT

MR.	SACI	AVIGDOR	ISRAEL MILITARY INDUSTRIES LTD (IMI)
MR.	SAGE	THOMAS	CORPS OF ENGINEERS
MR.	SALZMAN	PAUL	TRW SPACE & DEFENSE
MR.	SAM NGOOI	YIM SANG	EXPLOMO TECHNICAL SERVICES PTE LTD.
MR.	SAMS	DOUG	AEROJET ASRM DIVISION
MR.	SANTA CRUZ	LAVION	WYLE LABORATORIES
MR.	SAUARIEGO	MEIR	IEOD ENGINEERING LTD.
MR.	SAWYER	RAY	DDESB
MR.	SAYLORS	JAMES	FERRO - SAYLORS, INC
MS.	SCHAFF	MICHELE	ACCUDYNE CORPORATION
LTCOL	SCHAICH	EBERHARD	MATERIALAMT DER BUNDESWEHR IV 1
MR.	SCHIPMAN	JOSEPH	NAVAL WEAPONS STATION
MR.	SCHMIDT	JOHN	US ARMY MISSILE COMMAND
MR.	SCHNEIDER	GILBERT	NAVAL SURFACE WARFARE CENTER
MR.	SCHOOLER	JAMES	RED RIVER ARMY DEPOT
MR.	SCHUM	ROBERT	DCMAO TWIN CITIES
MR.	SCOTT	JOHN	TEXAS INSTRUMENTS, INC.
MR.	SCOTT	RICHARD	ALLIED SIGNAL
MR.	SEIWELL	ROBERT	WEBB, MURRAY & ASSOCIATES, INC.
MR.	SERENA	J.	U.S. ARMY ENGINEERING DIVISION
COL	SEXSTONE	P.	SECRETARY ESTC
MR.	SHAH	DINESH	R.M. PARSONS COMPANY
MR.	SHANHOLTZ	ERIC	542 SG/MST
MR.	SHATTUCK	MILTON	US ARMY YUMA PROVING GROUND
MR.	SHAW	DOUGLAS	DEFENSE CONTRACT MANAGEMENT AREA
MAJOR	SHEEHAN	CHARLES	103D FIGHTER GROUP
MR.	SHOPHER	KENNETH	
MR.	SHRIVER	JERRY	DEFENSE CONTRACT MANAGEMENT DISTRICT
MS.	SICHON	ALBERTA	
MR.	SIMMONS	LARRY	LAWRENCE LIVERMORE NATIONAL LABORATORY
MGYSGT	SIMMONS	FRANKLIN	EOD SECTION, HQS & SERVICE COMPANY
MR.	SINGH	ASHOK	CRSS ARCHITECTS, INC.
MR.	SMITH	LAWRENCE	US ARMY ARMAMENT
MR.	SMITH	KENNETH	MUNITIONS &
MR.	SMITH	SAMUEL	STRESAU LABORATORY, INC.
MR.	SMITH	DENNIS	ALLIANT TECHSYSTEMS, INC.
MR.	SMITH	ROGER	MARTIN MARIETTA AEROSPACE
MR.	SMITH	DAVID	FIELD COMMAND, DEFENSE NUCLEAR AGENCY
			DEPARTMENT OF ENVIRONMENT UK

MR.	SMITH	STEVEN	US ARMY MISSILE COMMAND
MR.	SNOW	RANDY	THE RICHWAY GROUP
MR	SOLEAU	EDWARD	LTV AEROSPACE & DEFENSE COMPANY
MR.	SONG	SO-YOUNG	AGENCY FOR DEFENSE DEVELOPMENT/KOREA
MR.	SORENSEN	HENRIK	NAVAL MATERIEL COMMAND, DENMARK
MR.	SORRENTINO	LEONARD	HQ AIR MOBILITY COMMAND
LCL	SOUCHET	GILBERT	FRENCH AIR FORCE
MR.	SPAHN	LARRY	MARTIN MARIETTA MISSILE SYSTEMS
MR.	SPEER	HAROLD	NORTHROP
MR.	SPENCE	JOHN	OLIN ORDNANCE CORPORATION
CWO2	SPENCER	PAUL	EOD MALS-16 MAG-16
MR.	SNAMEK	CARL	HOLMES & NARVER, INC.
MR.	STANLEY	GEORGE	OLIN CORPORATION
MR.	STANLEY	CHARLES	NAVAL AIR WEAPONS STATION
MR.	STARTZELL	GREG	THIOKOL CORPORATION
MR.	STAYTON	LEROY	NAVAL AIR WARFARE CENTER WEAPONS DIV
MS.	STERANKA	PAT	PUEBLO DEPOT ACTIVITY
MR.	STEVENSON	RANDY	NORTHROP CORPORATION
TSgt	STEWART	DANIEL	314 AW/SEW
MR.	STINCIC	THOMAS	SENECA ARMY DEPOT
MR	STRATMAN	GEORGE	OGDEN AIR LOGISTICS CENTER (AFLC)
MS.	STUCKEY	BEVERLY	LONE STAR ARMY AMMUNITION PLANT
MR.	STUDDERT	WILLIAM	U.S. ARMY MATERIEL COMMAND
MR.	SUMMERS	RICHARD	DEFENSE CONTRACT MGMT DISTRICT WEST
MR	SUTHERLAND	JOHN	MARTIN MARIETTA ASTRON. GROUP
MR.	SWANEY	DANIEL	THIOKOL CORPORATION
MR	SWANSON	NORMAN	HURLBURT FIELD
MR.	SWANSON	KEITH	834 AIR BASE WING/SEW
MR.	SWINDALL	TERRELL	U.S. ARMY MISSILE COMMAND
MR	SWISDAK	MIKE	NAVAL SURFACE WARFARE CENTER
GROUP	SYMONDS	PETER	DEPUTY DIRECTOR
CAPT			
MR.	TALLEY	GARY	THIOKOL CORPORATION
MR.	TANCRETO	JAMES	NAVAL CIVIL ENGINEERING LABORATORY
MR	TATOM	FRANK	ENGINEERING ANALYSIS INC.
MR.	TAYLOR	JOYNER	NEW MEXICO INSTITUTE OF MINING
MR.	TEO	KIAN	CDC CONSTRUCTION & DEVELOPMENT PTE LTD

MR.	THOMAS	JOSEPH	HAWTHORNE ARMY AMMUNITION PLANT
MR.	THOMPSON	JOSEPH	THIOKOL CORPORATION
MR.	THOMPSON	N.	21ST SPACE WING
MR.	THOMPSON	LEROY	U.S. DEPARTMENT OF ENERGY
SFC	THORSON	DONALD	ESCORT & DISPOSAL DETACHMENT
MR.	TIBBITS	WILLIAM	JET PROPULSION LABORATORY
MR.	TINKLER	WILLIAM	W.S.N. TINKLER
MR.	TOMINACK	JOHN	NAVAL SURFACE WARFARE CENTER
MR.	TOMLIN	MAX	US ARMY STRATEGIC DEFENSE COMMAND
MR.	TORMA	STEVEN	OLIN ORDNANCE
MR.	TRIPP	BRIAN	351 MW/SEP
MR.	TSCHRITTER	KEN	SANDIA NATIONAL LABORATORY
MS.	TUCKER	BARBARA	DEFENSE PLANT REPRESENTATIVE OFFICE
MR.	TUOKKO	SEPO	MINISTRY OF DEFENSE
MR.	TWING	CHARLES	U.S. ARMY CORPS OF ENGINEERS
MR.	TWISDALE	LAWRENCE	APPLIED RESEARCH ASSOCIATES, INC.
CAPTAIN	ULSHAFER	MICHAEL	PHILLIPS LABORATORY
MR.	URSERY	ALBERT	DPRO HERCULES
MR.	USKIEVICH	RAY	NAVAL FACILITIES ENGINEERING COMMAND
MR.	VAIDYANATHAN	H.	DEPARTMENT OF NATIONAL DEFENSE
MR.	VAN EVERDINK	LEO	MTMC EUROPE
MR.	VAN EVERY	DESHA	NORTHROP CORPORATION
MR.	VAN Riper	ED	U.S. ARMY BALLISTIC RESEARCH LABORATORY
MR.	VASELICH	RAYMOND	NASA
MR.	VEZINA	REMI	SNC INDUSTRIAL TECHNOLOGIES, INC.
MR.	VICK	C.	ATLANTIC RESEARCH CORPORATION
MR.	VICKERS	MARVIN	NAVAL SEA SUPPORT CENTER, PACIFIC
MR.	VICTOR	ANDREW	VICTOR TECHNOLOGY
MS.	VINEY	FRAN	DEFENSE CONTRACT MGMT DISTRICT WEST
DR	VRETBALAD	BENGT	FORT F - ROYAL SWEDISH -
MR.	WAGER	PHILLIP	NAVAL CIVIL ENGINIERING LABORATORY
MR.	WAGMAN	JAMES	PL/SEW
MR.	WAGNER	WILLIAM	HERCULES INC.
MR.	WALDMAN	BENJAMIN	US ARMY PRODUCTION BASE
CMSGT	WALKER	JOHN	919 SOW/MAEWM

CAPTAIN	WALLACE	DAVID	CHAIRMAN, DOD EXPLOSIVES SAFETY BOARD
MR	WALSH	JAMES	NAVAL ORD MISSILE TEST STATION
MR.	WALTERS	JAMES	US ARMY NUCLEAR AND CHEMICAL AGENCY
MR.	WANCZYK	GLEN	PMOSSP
DR.	WARD	JERRY	DDESB
MR.	WARSHAUR	KEN	MARTIN MARIETTA ELECTRONIC
MR.	WARWICK	WAYNE	LOCKHEED MSD
MR.	WATANABE	WALLACE	US ARMY CORPS OF ENGINEERS
MR.	WEBSTER	LARRY	DDESB
MR.	WEE	TERRY	CHARTERED INDUSTRIES
MR.	WENDEL	CLIFFORD	AMXRM-SHE
MR.	WHEELER	RONALD	SSI SERVICES, INC.
MR.	WHITE	CHARLES	HQ AFSOC/SEW
MAJOR	WIJDEMANS	JAN	MOD/R. NETHERLANDS AIR FORCE
MR.	WILCOX	ROBERT	HUNTSVILLE DIVISION, CORPS OF
MR.	WILLIAMS	GEORGE	HERCULES, INC.
MR.	WILLIAMSON	G.	HEALTH & SAFETY EXECUTIVE
MR.	WILLIS	RICHARD	NORTHROP CORPORATION
MR.	WILSON	NATHANIEL	ARMAMENT RESEARCH, DEVELOPMENT AND
MR.	WINDSOR	MARVIN	NAVAL AIR WARFARE CENTER
MR.	WINGATE	MARK	OLIN CORPORATION
CAPTAIN	WINTLE	FREDERICK	FIELD COMMAND, DEFENSE NUCLEAR AGENCY
MR.	WISE	DANIEL	U.S. ARMY CHEMICAL RESEARCH DEVELOPMENT
MR.	WITIAK	R.	DCMDS-GBQS
MR.	WOFFORD	KENT	SIERRA ARMY DEPOT
MR.	WOLFGANG	GARY	OLIN ORDNANCE
MR.	WOOD	RANDALL	EG&G MOUND APPLIED TECHNOLOGIES
MR.	WOOD	SCOTT	NAVAL WEAPONS STATION - SEAL BEACH
MR.	WOODSON	STANLEY	U.S. ARMY ENGINEER WATERWAYS
CAPTAIN	WORKMAN	RICKEY	HQ USAF WPNS & TACTICAL CENTER
MR.	WU	DA-LIH	BECHTEL NATIONAL
MR.	WYLIE	ALISTAIR	AUSTRALIAN DEFENCE INDUSTRIES, LTD.
LT COL	WYSOWSKI	JOHN	HQ, AIR COMBAT COMMAND
MR.	YAN HAM	NICK	TNO - DEFENSIEONDERZOEK
MR.	YONKMAN	THOMAS	
MR.	YOUNG	MARVIN	GENCORP AEROJET

MR.	YUHAS	JOHN	TECHNICAL ORDNANCE, INC.
MR.	YUN	CHAD	DEFENSE CONTRACT MGMT
MR.	YUTMEYER	WILLIAM	DISTRICT WEST
COL	ZAKRZEWSKI	STEPHEN	AMC FIELD SAFETY ACTIVITY
MR.	ZAUGG	MARK	TOOELE ARMY DEPOT
MR.	ZEHRT	W.	U.S. ARMY ENGINEERING
PROFESSOR	ZHANG	YINLIANG	DIVISION
			XIAN MODERN CHEMISTRY
MR.	ZOGHBY	DAVID	RESEARCH
MR.	ZUCKERWISE	JEFFREY	ICI EXPLOSIVES
			ENVIRONMENTAL
			DCMAO, SPRINGFIELD